

**Mechanistic Investigations of the Direct Arylation of
Pyridine *N*-oxides with Bromoarenes**

and

**Structure-Reactivity Relationship of Aryl Palladium Complexes
in Transmetalations with Organoboron Compounds**

INAUGURAL-DISSERTATION

to obtain the academic degree

Doctor rerum naturalium (Dr. rer. nat.)

submitted to the Department of Biology, Chemistry and Pharmacy of Freie Universität Berlin

by

EMMA SVENSSON AKUSJÄRVI

from Uppsala, Sweden

2018

1st reviewer: Prof. Dr. C. Christoph Tzschucke

2nd reviewer: Prof. Dr. Christian Müller

Date of defense: 07.06.2018

The described work was carried out between October 2013 and January 2018 under the supervision of Prof. Dr. C. Christoph Tzschucke at the Institut für Chemie und Biochemie of Freie Universität Berlin.

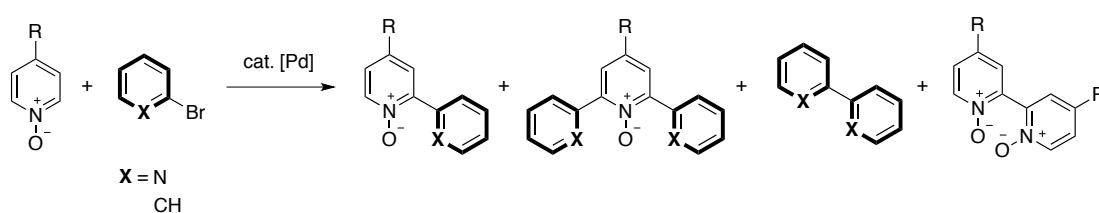
“This could really be a good life”

Massimo Rigo

Abstract

Reaction Rates of the Catalytic Reaction Between Pyridine *N*-oxides and Bromoarenes

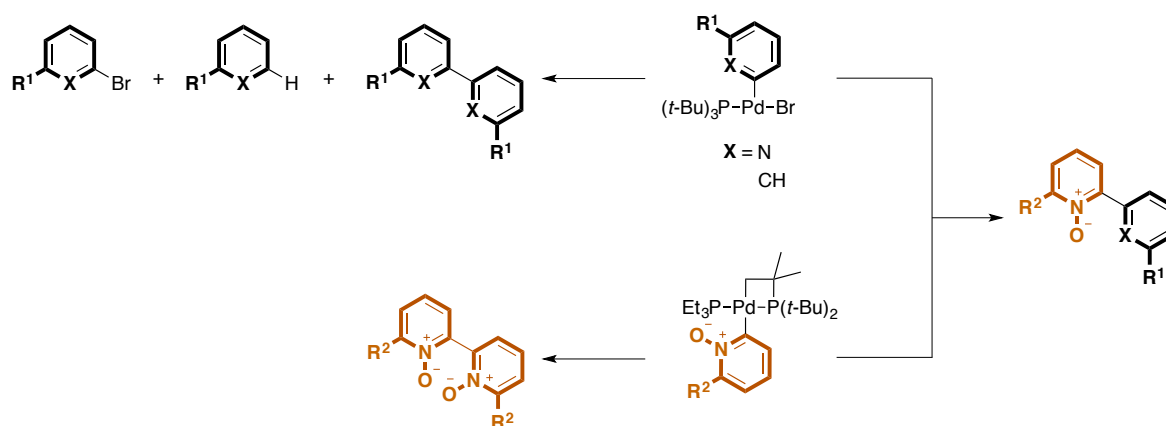
The direct arylation of 4-substituted pyridine *N*-oxides with bromobenzene provides arylpyridine *N*-oxide products in high yields of 70-80%. However, the analogous arylation reaction between 2-bromopyridine and pyridine *N*-oxides bearing electron-donating substituents results in the cross-coupled product in lower yields of 23-49%. Yet, arylation of pyridine *N*-oxides bearing electron-withdrawing substituents with 2-bromopyridine forms the bipyridine *N*-oxide product in ~70% yield. Previous reports on the mechanism do not explain this substrate dependence and, therefore substrate consumption and product formation rates for the reaction of five 4-substituted pyridine *N*-oxides with 2-bromopyridine and bromobenzene were determined. Reactions with both aryl halides showed that electron-poor pyridine *N*-oxides exhibit a higher reactivity towards C–H activation and form the cross-coupled products faster than electron-rich *N*-oxides. A competing homocoupling side reaction of the aryl halide substrate was identified, forming 2,2'-bipyridine and biphenyl, respectively. Where the yield of cross-coupled product was low, homocoupling of 2-bromopyridine resulted in bipyridine in up to 35% yield. Homocoupling of bromobenzene to biphenyl was obtained in significantly lower yields of <10%. A faster consumption rate of 2-bromopyridine in comparison to bromobenzene was observed and its origin assigned to the competing homocoupling pathway. As additional side reaction, the homocoupling of pyridine *N*-oxide substrate to bipyridine *N,N'*-dioxide was quantified. Aryl halide and pyridine *N*-oxide homocoupling products were obtained in similar yields from each reaction, suggesting that the two side reactions proceed by linked redox cycles.



Potential inhibitory effects by nitrogen-containing compounds present in the reaction mixture were studied. With the addition of pyridine, bipyridine or bipyridine *N*-oxide, slower cross-coupled product formation rates were observed. However, the yields did not significantly decrease, ruling out that substrate or product inhibition is responsible for the drop in yield in reactions with 2-bromopyridine.

Synthesis and Reactivity of Aryl Palladium Complexes in the Direct Arylation of Pyridine *N*-oxides

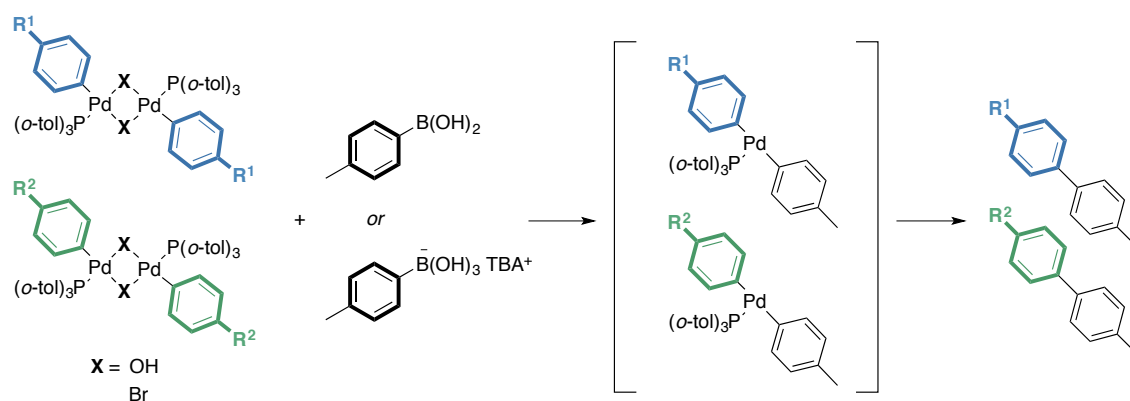
To investigate the reactivity of the aryl palladium complexes in the direct arylation of pyridine *N*-oxides, the proposed intermediates were synthesized. A 6-*tert*-butyl-2-pyridyl palladium(II) bromide complex bearing one P(*t*-Bu)₃ ligand was synthesized and characterized via X-ray analysis, revealing an unusual η^2 -C,N-binding mode of the pyridyl ligand. For comparison, a 3-methyl-phenyl palladium(II) complex ligated by one P(*t*-Bu)₃ ligand was synthesized. Upon heating, the pyridyl complex formed bipyridine homocoupling product almost quantitatively whereas the phenyl complex resulted in biphenyl homocoupling product as well as proto-demetalated arene and reductively eliminated aryl halide (ratio 3:4:1). The phenyl complex exhibited an exponential decay of starting material ($t_{1/2}$ = 15 minutes at 80 °C), whereas the decomposition of pyridyl complex occurred only after an induction period, where formation of an anionic 2-pyridyl palladate species was observed. Independent synthesis of the anionic species and investigation on its influence on the reaction suggested that it catalyzes the decomposition reaction.



A 2-pyridyl *N*-oxide palladium(II) complex ligated by one cyclometalated phosphine ligand and one stabilizing PEt₃ ligand was synthesized with a methyl or a trifluoromethyl substituent on the pyridyl *N*-oxide ligand. The complexes reacted with a 2-pyridyl or phenyl palladium complex at room temperature or below, forming cross-coupled arylpyridine *N*-oxide products. Formation of bipyridine *N,N'*-dioxides via homocoupling of the pyridyl *N*-oxide complexes was observed, however only at elevated temperatures. Homocoupling of aryl palladium complexes and pyridyl *N*-oxide palladium complexes were significantly slower than a cross-coupling reaction between the complexes.

Transmetalation Between Aryl Palladium Complexes and Organoboron Compounds

In Suzuki-Miyaura cross-coupling reactions, the transmetalation step is suggested to take place either between an anionic boronate species and a halide-ligated palladium complex (boronate pathway) or a neutral organoboron species and a hydroxide-ligated palladium complex (oxo-palladium pathway). To investigate the transmetalation, a set of dimeric bromide-bridging $P(o\text{-tol})_3$ palladium(II) complexes bearing 4-substituted aryl ligands was synthesized and obtained in good yields. Displacement of the bromide with a hydroxide provided the analogous hydroxide-bridged aryl palladium(II) dimers. Investigations on the transmetalation step are often limited by the solubility of the anionic organoboronate species. An anionic boronate species bearing a tetrabutylammonium counter ion was formed and demonstrated sufficient solubility in organic solvents such as THF and DCM.

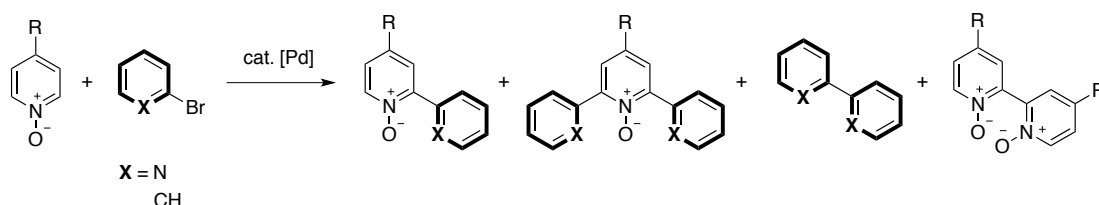


Initial experiments investigating the transmetalation step were performed by competition experiments between eight 4-substituted aryl palladium complexes and an organoboron species. The relative reaction rates of each substituted complex were determined for the boronate and the oxo-palladium pathway. Linear Hammett correlations resulted in $\rho = +0.81$ for the reaction between bromide-bridged palladium complexes and an anionic boronate and $\rho = +0.52$ for the reaction between hydroxide-bridged palladium complexes and a neutral boronic acid. A positive reaction constant signifies an increase in reactivity of more electrophilic aryl palladium complexes. Comparison of the ρ -values indicates that bromide-ligated aryl palladium complexes are slightly more sensitive towards substitution pattern than a hydroxide-ligated aryl palladium complex.

Zusammenfassung

Reaktionsgeschwindigkeiten der katalytischen Reaktionen zwischen Pyridin-*N*-oxiden und Bromaromaten

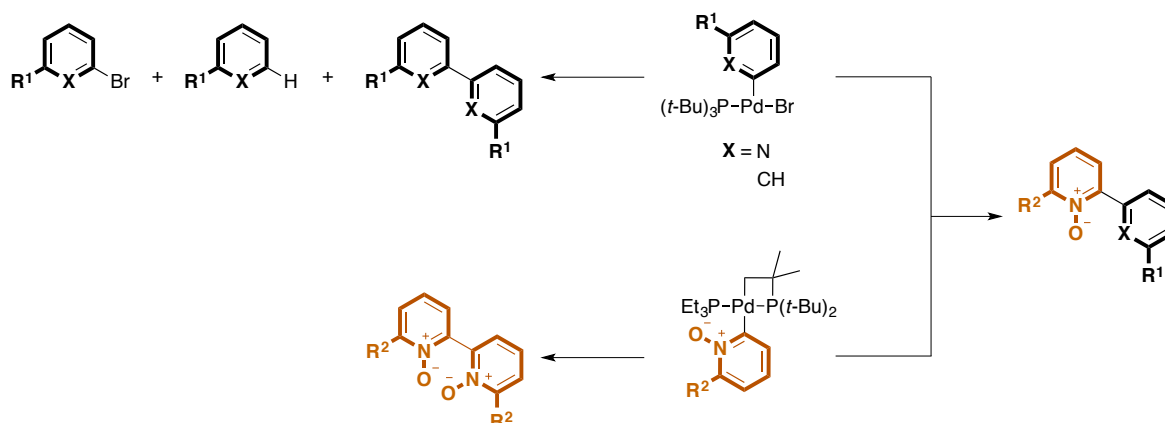
Die direkte Arylierung von 4-substituierten Pyridin-*N*-oxiden mit Bromaromaten ergibt Arylpyridin-*N*-oxide in Ausbeuten von 70-80%. Jedoch ergeben analoge Arylierungsreaktionen zwischen 2-Brompyridinen und Pyridin-*N*-oxiden, welche elektronschiebende Substituenten tragen, Kreuzkupplungsprodukte in niedrigeren Ausbeuten von 23-49%. Hingegen bilden Arylierungen von Pyridin-*N*-oxiden, welche elektronziehende Substituenten tragen, mit 2-Brompyridinen die Pyridin-*N*-oxidprodukte in 70% Ausbeute. Frühere Berichte über den Mechanismus erklären nicht diese Substratabhängigkeit, weshalb die Geschwindigkeiten der Substratverbräuche und Produktbildungen für die Reaktionen von fünf 4-substituierten Pyridin-*N*-oxiden mit 2-Brompyridin und Brombenzol bestimmt wurden. Die Reaktionen mit beiden Arylhalogeniden zeigten, dass elektronarme Pyridin-*N*-oxide eine höhere Reaktivität gegenüber C-H-Aktivierung aufweisen und bilden das Kreuzkupplungsprodukt schneller als elektronreiche *N*-oxide. Als Nebenreaktion wurde eine konkurrierende Homokupplung des Arylhalogenids identifiziert, wodurch 2,2'-Bipyridin bzw. Biphenyl gebildet wird. Wo die Ausbeute des Kreuzkupplungsprodukts niedrig war, ergab die Homokupplung des 2-Brompyridins Bipyridin in bis zu 35% Ausbeute. Die Homokupplung von Brombenzol zu Biphenyl wurde in signifikant niedrigeren Ausbeuten von <10% beobachtet. Im Vergleich zum Brombenzol, wurde eine schnellere Verbrauchsrate mit 2-Brompyridin beobachtet und dessen Ursprung dem konkurrierenden Homokupplungsmechanismus zugeschrieben. Als zusätzliche Nebenreaktion wurde die Homokupplung des Pyridin-*N*-oxidsubstrats identifiziert. Homokupplungsprodukte des Arylhalogenids und des Pyridin-*N*-oxids wurden in jeder Reaktionen in ähnlichen Ausbeuten erhalten, was darauf hindeutet, dass beide Nebenreaktionen durch miteinander verbundene Redoxzyklen ablaufen.



Potentiell inhibierende Effekte durch die stickstoffhaltigen Verbindungen, welche in der Reaktionsmischung vorhanden sind, wurden untersucht. Mit der Zugabe von Pyridin, Bipyridin oder Bipyridin-*N*-oxid wurden langsamere Bildungsgeschwindigkeiten der Kreuzkupplungsprodukte beobachtet. Jedoch sanken die Ausbeuten nicht signifikant, was ausschließt, dass die Inhibierung durch das Substrat oder durch das Produkt für das Absenken der Ausbeuten in Reaktionen mit 2-Brompyridin verantwortlich ist.

Synthese und Reaktivität von Arylpalladiumkomplexen in der direkten Arylierung von Pyridin-*N*-oxiden

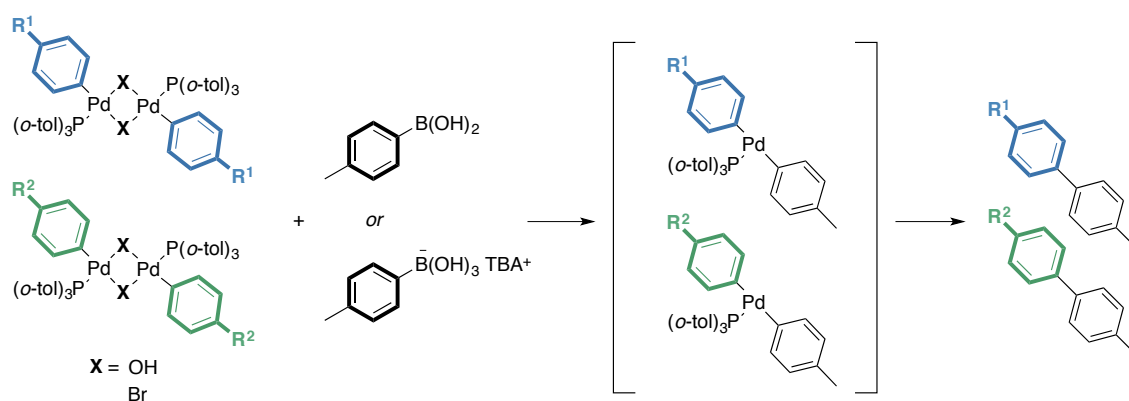
Um die Reaktivität von Arylpalladiumkomplexen in der direkten Arylierung von Pyridin-*N*-oxiden zu untersuchen, wurden die vorgeschlagenen Intermediate synthetisiert. Ein 6-*tert*-Butyl-2-pyridylpalladium(II)bromidkomplex, welcher ein $P(t\text{-Bu})_3$ -Ligand trägt, wurde synthetisiert und mittels Röntgenstrukturanalyse charakterisiert, was einen ungewöhnlichen $\eta^2\text{-C,N}$ -Bindungsmodus des Pyridylliganden aufdeckte. Zum Vergleich wurde ein 3-Methylphenylpalladium(II)komplex, an dem $P(t\text{-Bu})_3$ gebunden ist, synthetisiert. Nach dem Erhitzen bildete der Pyridylkomplex das Bipyridinhomokupplungsprodukt nahezu quantitativ, wohingegen der Phenylkomplex das Biphenylhomokupplungsprodukt, sowie den protodemetallierten Aromaten und das reduktiv eliminierte Arylhalogenid (Verhältnis 3:4:1) ergab. Der Phenylkomplex wies einen exponentiellen Zerfall des Startmaterials auf ($t_{1/2} = 15$ Minuten bei $80\text{ }^\circ\text{C}$), wohingegen die Zersetzung des Pyridylkomplexes erst nach einer Induktionsperiode, bei der die Bildung einer anionischen 2-Pyridylpalladatspezies beobachtet wurde, auftrat. Die unabhängige Synthese der anionischen Spezies und die Bestimmung dessen Einfluss auf die Reaktion deuteten an, dass es die Zerfallsreaktion katalysiert.



Ein 2-Pyridyl-*N*-oxidpalladium(II)komplex, bei dem ein zyklometallierter Phosphinligand und ein stabilisierender PEt_3 -Ligand gebunden sind, wurde mit einem Methyl- oder einem Trifluoromethylsubstituenten am Pyridyl-*N*-oxidliganden synthetisiert. Die Komplexe reagierten mit einem 2-Pyridyl- oder Phenylpalladiumkomplex bei Raumtemperatur oder niedriger und bildeten kreuzgekuppelte Arylpyridin-*N*-oxidprodukte. Die Bildung des Bipyridin- N,N' -dioxids über Homokupplung des Pyridyl-*N*-oxidkomplexes wurde zwar beobachtet, jedoch aber nur bei höheren Temperaturen. Die Homokupplungen der Arylpalladiumkomplexe und Pyridyl-*N*-oxidpalladiumkomplexe waren signifikant langsamer als eine Kreuzkupplungsreaktion zwischen den Komplexen.

Transmetallierung zwischen Arylpalladiumkomplexen und Organoborverbindungen

In Suzuki-Miyaura-Kreuzkupplungsreaktionen wird angenommen, dass der Transmetallierungsschritt entweder zwischen einer anionischen Boronatspezies und einem Palladiumkomplex mit einem Halogenidliganden (Borolat-Mechanismus) oder zwischen einer neutralen Organoborspezies und einem hydroxidgebundenem Palladiumkomplex (Oxo-Palladium-Mechanismus) stattfindet. Um die Transmetallierung zu untersuchen, wurde ein Satz von dimeren bromidverbrückten $P(o\text{-tol})_3$ -palladium(II)komplexen, welche 4-substituierte Arylliganden tragen, synthetisiert und in guten Ausbeuten erhalten. Der Austausch des Bromids mit Hydroxid lieferte die analogen hydroxidgebundenen Arylpalladium(II)dimere. Untersuchungen des Transmetallierungsschritts sind oft auf Grund der Löslichkeit der anionischen Organoboronatspezies eingeschränkt. Eine anionische Boronatspezies, welche als Gegenion Tetrabutylammonium tragen, wurde hergestellt und zeigte eine ausreichende Löslichkeit in organischen Lösungsmitteln, wie THF und DCM.



Erste Experimente, welche den Transmetallierungsschritt untersuchen, wurden durchgeführt anhand von Konkurrenzexperimenten zwischen acht 4-substituierten Arylpalladiumkomplexen und einer Organoborspezies. Die relativen Reaktionsgeschwindigkeiten der substituierten Palladiumkomplexe wurden für den Borolat- und den Oxo-Palladiummechanismus bestimmt. Lineare Hammett-Korrelationen ergaben $\rho = +0.81$ für die Reaktionen zwischen bromidverbrückten Palladiumkomplexen und einem anionischen Borolat, und $\rho = +0.52$ für die Reaktion zwischen hydroxidverbrückten Palladiumkomplexen und einer neutralen Boronsäure. Eine positive Reaktionskonstante kennzeichnet einen Anstieg in der Reaktivität der elektrophileren Arylpalladiumkomplexe. Der Vergleich der ρ -Werte zeigt an, dass bromidgebundene Arylpalladiumkomplexe leicht empfindlicher gegenüber Substitutionsmuster sind als ein hydroxidgebundener Arylpalladiumkomplex.

Table of Contents

1 Reaction Rates of the Catalytic Reaction Between Pyridine <i>N</i>-oxides and Bromoarenes	1
1.1 Motivation	1
1.2 Background	3
1.2.1 Palladium-catalyzed C–H bond functionalization of nonactivated arenes	4
1.2.2 Direct arylation of pyridine <i>N</i> -oxides with halobenzenes	5
1.2.3 Direct arylation of pyridine <i>N</i> -oxides with heteroaryl halides	7
1.2.4 Previous mechanistic studies on the direct arylation of pyridine <i>N</i> -oxides	9
1.2.5 Mechanistic background for direct arylations with bromopyridines	15
1.3 Results and discussion	17
1.3.1 Substrate consumption and product and side-product formation	17
1.3.2 Inhibition of active catalyst	25
1.3.3 Quantification of homocoupling products	29
1.3.4 Independent synthesis of bipyridine <i>N,N'</i> -dioxide by oxidative coupling	34
1.4 Conclusion	36
2 Synthesis and Reactivity of Aryl Palladium Complexes in the Direct Arylation of Pyridine <i>N</i>-oxides	39
2.1 Motivation	39
2.2 Background	41
2.2.1 Phenyl palladium complexes	41
2.2.2 Pyridyl palladium complexes	43
2.2.3 2-Metalated pyridine <i>N</i> -oxides	45
2.2.4 Oxidative addition and reductive elimination	47
2.2.5 Transmetalation reactions	49

2.2.6	Homocoupling product formation	50
2.3	Results and discussion	52
2.3.1	Synthesis of aryl palladium complexes	52
2.3.2	Displacement of ligands	57
2.3.3	Decomposition of aryl palladium complexes	63
2.3.4	Synthesis of a pyridyl <i>N</i> -oxide intermediate	80
2.3.5	Pyridyl <i>N</i> -oxide complex with a nitrogen-containing ligand	85
2.3.6	Decomposition of pyridyl <i>N</i> -oxide palladium complexes	86
2.3.7	Transmetalation between (hetero)aryl palladium complexes	89
2.4	Conclusion	98
3	Transmetalation Between Aryl Palladium Complexes and Organoboron Compounds	101
3.1	Motivation	101
3.2	Background	103
3.2.1	Synthesis of proposed catalytically active intermediates	106
3.2.2	Previous mechanistic investigations	107
3.2.3	Hammett correlations for determining sensitivity to substituents.....	111
3.3	Results and discussion	114
3.3.1	Organoboron reagents	114
3.3.2	Halide-ligated palladium complexes	115
3.3.3	Hydroxide-ligated palladium complexes	116
3.3.4	Screening of transmetalation conditions	122
3.3.5	Competition experiments with $[(\text{Ar})\text{Pd}(\mu\text{-X})(\text{P}(o\text{-tol})_3)_2]$	124
3.4	Conclusion	127
4	Experimental Section.....	129
4.1	General procedures and instrumentation	129

4.2	Starting materials and reference compounds	130
4.2.1	Oxidations	130
4.2.2	Substituted pyridines	137
4.3	Catalysts, ligands and precursors	139
4.3.1	Ligands	139
4.3.2	Palladium precursors and catalysts	143
4.3.3	Cyclometalated catalysts	148
4.3.4	Organometallic reagents.....	152
4.4	Palladium-catalyzed direct arylation of pyridine <i>N</i>-oxides	152
4.4.1	Direct arylation with bromopyridines	152
4.4.2	Direct arylation with bromobenzenes	158
4.4.3	Deoxygenation of cross-coupling products.....	161
4.5	Homocoupling products	162
4.6	Kinetic measurements of direct arylations.....	166
4.6.1	Reactions with bromopyridine	167
4.6.2	Reactions with bromobenzene	177
4.6.3	Hammett plot.....	186
4.6.4	Inhibition reactions.....	186
4.7	Quantification of homocoupling products 8c, 9a, 10.....	195
4.8	Oxidative coupling of pyridine <i>N</i>-oxides	197
4.8.1	Screening of catalytic conditions	197
4.8.2	Control experiments	198
4.9	Aryl palladium intermediates from the direct arylation reaction	199
4.9.1	(6- <i>tert</i> -Bu-2-pyridyl)Pd(Br)(P(<i>t</i> -Bu) ₃) (12a).....	199
4.9.2	(6- <i>tert</i> -Bu-2-pyridyl)Pd(OAc)(P(<i>t</i> -Bu) ₃) (13a)	199
4.9.3	[(μ -(6- <i>tert</i> -Bu-2-pyridyl)-C ² ,N)Pd(Br)(py)] ₂ (17).....	200
4.9.4	(6- <i>tert</i> -Bu-2-pyridyl)Pd(Br)(bipy) (18).....	201
4.9.5	(6- <i>tert</i> -Bu-2-pyridyl)Pd(Br)(dppf) (19)	202
4.9.6	(6- <i>tert</i> -Bu-2-pyridyl)Pd(Br)(dcpe) (20)	202

4.9.7	[(6- <i>tert</i> -Bu-2-pyridinium)Pd(Br) ₃][HP(<i>t</i> -Bu) ₃] (30).....	202
4.9.8	(6- <i>tert</i> -Bu-2-pyridyl)Pd(Br)(PEt ₃) ₂ (23).....	203
4.9.9	(3-tolyl)Pd(Br)(P(<i>t</i> -Bu) ₃) (14a)	204
4.9.10	(2-tolyl)Pd(Br)(P(<i>t</i> -Bu) ₃) (14b).....	204
4.9.11	(3-tolyl)Pd(OAc)(P(<i>t</i> -Bu) ₃) (15a)	205
4.9.12	(3-tolyl)Pd(Br)(PEt ₃) ₂ (24)	205
4.9.13	(6-Me-2-pyridyl <i>N</i> -oxide)Pd(<i>tert</i> -Bu ₂ PC(CH ₃) ₂ CH ₂)(PEt ₃) (21)	206
4.9.14	(6-CF ₃ -2-pyridyl <i>N</i> -oxide)Pd(<i>tert</i> -Bu ₂ PC(CH ₃) ₂ CH ₂)(PEt ₃) (22)	207
4.9.15	Attempted synthesis of a pyridine-ligated pyridyl <i>N</i> -oxide complex	207
4.9.16	Attempted synthesis of an anionic phenyl dimer 29d	208
4.10	Decomposition of aryl palladium complexes	209
4.10.1	Pyridyl palladium bromide complex 12a	209
4.10.2	Phenyl palladium bromide complex 14a	222
4.10.3	Pyridyl palladium acetate complex 13a	227
4.10.4	Phenyl palladium acetate complex 15a	227
4.10.5	Decomposition of other aryl palladium complexes	227
4.10.6	Methyl pyridyl <i>N</i> -oxide palladium complex 21	228
4.10.7	Trifluoromethyl pyridyl <i>N</i> -oxide palladium complex 22	229
4.10.8	Control experiments	230
4.11	Transmetalation between aryl palladium complexes	232
4.11.1	Transmetalation with methyl pyridyl <i>N</i> -oxide complex 21	233
4.11.2	Transmetalation with trifluoromethyl pyridyl <i>N</i> -oxide complex 22	235
4.11.3	Yields of transmetalations	239
4.11.4	Transmetalation between other aryl palladium complexes	240
4.12	Intermediates in Suzuki-Miyaura cross-coupling reactions	243
4.12.1	(Pseudo)halogen-ligated palladium complexes.....	243
4.12.2	Hydroxide-ligated palladium complexes	250
4.12.3	Attempted direct displacement of halogen ligand.....	256
4.12.4	Organoboron compounds	257

4.13	Transmetalation reactions of the Suzuki-Miyaura reaction.....	259
4.13.1	Non-competitive transmetalation reactions.....	260
4.13.2	Competitive transmetalation reactions.....	261
5	Crystallographic Data	265
6	References.....	277
	Curriculum vitae	284
	Acknowledgements.....	285

Abbreviations

Ac	acetyl
Ad	adamantyl
aq.	aqueous
Ar	aryl
calc.	calculated
cat.	catalytic
CMD	concerted metalation-deprotonation
conc.	concentrated
conv.	conversion
Cy	cyclohexyl
dba	dibenzylideneacetone
DCM	dichloromethane
decomp.	decomposition
DFT	density functional theory
DMA	<i>N,N</i> -dimethylacetamide
DMF	<i>N,N</i> -dimethylformamide
DMSO	dimethylsulfoxide
dppe	1,2-bis(diphenylphosphino)ethane
dppf	1,1'-bis(diphenylphosphino)ferrocene
EDG	electron-donating group
eq.	equation
equiv.	equivalents
ESI	electrospray ionization
EWG	electron-withdrawing group
FID	flame ionization detector
GC	gas chromatography
IR	infrared
KIE	kinetic isotope effect
L	ligand
LDA	lithium diisopropylamide
LiHMDS	lithium bis(trimethylsilyl)amide
<i>m</i> -	<i>meta</i> -
M	molar

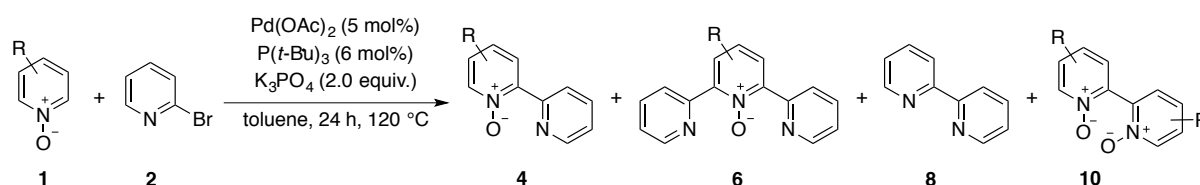
<i>m</i> -CPBA	<i>meta</i> -chloroperoxybenzoic acid
Me	methyl
MEK	methyl ethyl ketone
m.p.	melting point
MS	mass spectrometry
NHC	N-heterocyclic carbene
NMR	nuclear magnetic resonance
<i>o</i> -	<i>ortho</i> -
ORTEP	Oak Ridge Thermal Ellipsoid Plot Program
<i>p</i> -	<i>para</i> -
Ph	phenyl
Piv	pivalyl
ppm	parts per million
py	pyridine
quant.	quantitative
R	aliphatic group
RDS	rate-determining step
r.t.	room temperature
<i>t</i>	time
temp.	temperature
THF	tetrahydrofuran
TLC	thin layer chromatography
TMB	1,3,5-trimethoxybenzene
tmeda	<i>N,N,N',N'</i> -tetramethylethane-1,2-diamine
TMP	2,2,6,6-tetramethylpiperidine
TMS	trimethylsilyl
X	(pseudo)halogen

1 Reaction Rates of the Catalytic Reaction Between Pyridine *N*-oxides and Bromoarenes

1.1 Motivation

Transition metal-catalyzed activation and functionalization of C–H bond has over the last 20 years emerged as an attractive route to creating new carbon-carbon or carbon-heteroatom bonds. A path circumventing a pre-functionalized substrate is desirable, both due to the cost aspect as well as to avoid side-product formation. A large challenge regarding C–H activation reactions is the abundance of C–H bonds in organic molecules and the need for specificity of the metal catalyst. This problem has been addressed in numerous reports and often solved by directing groups which coordinate to the metal that subsequently cleaves a proximal C–H bond.¹ Functionalization of nitrogen-containing molecules such as pyridines is challenging due to the coordinating ability of the nitrogen to the metal catalyst. This difficulty has been overcome by masking the pyridine nitrogen by oxidation. Fagnou and co-workers developed a direct arylation protocol of pyridine *N*-oxides **1** with bromobenzenes **3** in the presence of Pd(OAc)₂, P(*t*-Bu)₃·HBF₄ and a base, yielding cross-coupling arylpyridine *N*-oxide products **5** in high yields.² The *N*-oxide moiety does not only prevent coordination of the nitrogen atom but also acts as an activating group to the C–H bond *ortho* to the nitrogen.

Since the direct arylation of pyridine *N*-oxides is a convenient alternative to cross-coupling of pre-formed pyridyl organometallics with aryl halides, our group extended the reaction to also include arylation with bromopyridines **2** (scheme 1.1).³ The reaction proceeded readily under similar conditions to the reported reaction, yielding a number of substituted bipyridine *N*-oxides **4**. Due to the presence of two polarized C–H bonds, also the terpyridine *N*-oxide products **6** were formed.



Scheme 1.1. Products obtained from the direct arylation of pyridine *N*-oxides **1** with bromopyridines **2**.

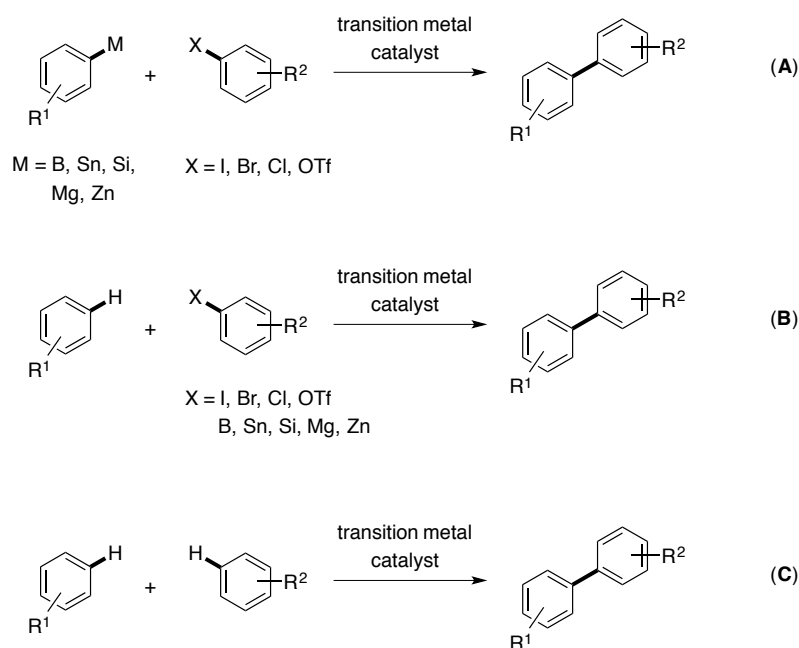
Fagnou and co-workers observed high yields of cross-coupling product when employing both electron-rich and electron-poor pyridine *N*-oxides **1** in the arylation with bromobenzenes **3**.² However, a large difference in yield was observed with differently substituted pyridine *N*-oxides in the arylation with bromopyridines **2**. When applying electron-poor 4-CO₂Et substituted *N*-oxide **1d**, cross-coupling

product **4d** was obtained in 67%, whereas applying the electron-rich unsubstituted pyridine *N*-oxide **1c**, the yield of cross-coupling product **4c** dropped drastically to 23%.³ It was later observed by our group that in addition to the cross-coupling products, bipyridine **8** was formed by homocoupling of bromopyridine **2**. The analogous homocoupling of bromobenzenes to biphenyl **9** has not been reported as a competing pathway.² Furthermore, a homocoupling pathway of the pyridine *N*-oxide substrate forming bipyridine *N,N'*-dioxide **10** was observed. This pathway has not previously been identified nor quantified as a side reaction in the direct arylation of pyridine *N*-oxides **1**.

The most recent mechanistic proposal suggests a cooperative catalytic cycle with two palladium centers.⁴ A first order-dependence on pyridine *N*-oxide **1** was observed, suggesting that the rate-determining step of the reaction is the C–H bond cleavage.^{4,5} The aryl halide substrate does not influence the rate-determining step of the reaction and therefore, it is expected that the nature of the aryl halide should not influence the yield of cross-coupling product. Possibly, the homocoupling product bipyridine **8** could decrease the reactivity of the proposed active palladium intermediates due to its coordination ability. Furthermore, other nitrogen-containing compounds present, such as bromopyridine substrate **2** or cross-coupling products **4** and **6**, could also bind to a palladium complex and lower its reactivity. Because the mechanistic proposal does not explain our observation of a lower yield of cross-coupling product when employing bromopyridines **2** in the reaction with electron-rich pyridine *N*-oxides **1**, mechanistic studies of the reactivity of pyridine *N*-oxides **1** towards an electrophilic coupling partner were performed.

1.2 Background

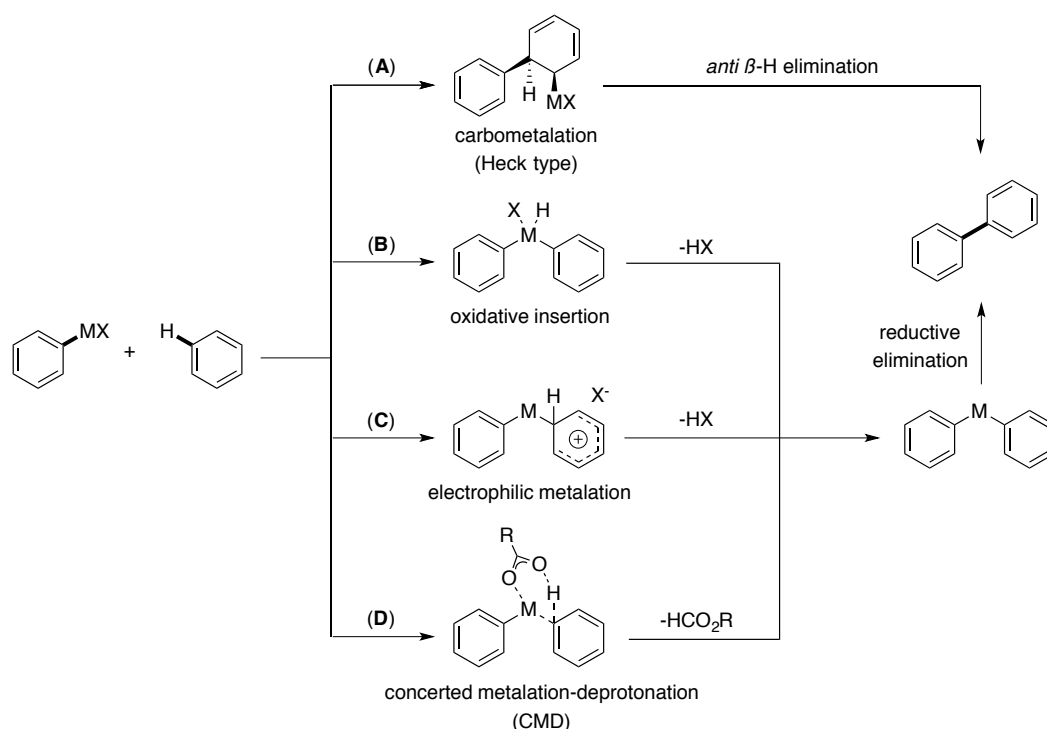
Biaryls are structural motifs present in various important compounds such as pharmaceuticals,⁶ natural products⁷ and functional materials.^{8,9} Particularly, bipyridines and terpyridines are widely applied as ligands for metal ions forming catalytically active complexes. Over the last century, transition metal-catalyzed reactions forming biaryls have been explored and great progress has been made. Initial protocols employed stoichiometric amounts of metal, leading to the need for separation of metal-containing by-products during purification. Great development of metal-catalyzed biaryl forming reactions has been made since the first reported Ullman reaction in 1901. An array of transition-metal catalyzed reactions has been described, such as the Suzuki-Miyaura, Negishi, Stille and Kumada cross-coupling protocol. Using a catalytic amount of transition metal complex together with an organometallic reagent and an aryl (pseudo)halide has become a standard approach to the synthesis of simple and more complex biaryl compounds (scheme 1.2, A). Although these cross-coupling reactions are very selective and useful, they require pre-functionalization of both substrates. A less wasteful pathway would be desirable to decrease the reaction steps and by-products. One very attractive alternative are direct arylations where one activated substrate such as a (pseudo)halide or organometallic reagent is coupled with a non-activated substrate by breaking a C–H bond (scheme 1.2, B). Another alternative is oxidative couplings where a C–C bond between two nonactivated substrates is formed by breaking C–H bonds (scheme 1.2, C). The latter is an attractive pathway because it produces less by-products and employs cheaper starting materials, however costs are dependent on the oxidant used. Furthermore, regioselectivity among the ubiquitous C–H bonds of the substrates is still challenging.



Scheme 1.2. Methods of transition metal-catalyzed cross-coupling reactions.

1.2.1 Palladium-catalyzed C–H bond functionalization of nonactivated arenes

In biaryl formation via direct arylation of a C–H bond with an electrophilic coupling partner, the C–H bond cleavage of the arene is a key step in the catalytic cycle. In cross-coupling reactions with one non-activated coupling partner, the C–H bond cleavage step is often proposed to proceed via reaction of a palladium(II) complex formed after oxidative addition. Different mechanisms for breaking the C–H bond are usually considered (scheme 1.3): a Heck type carbometalation (**A**),¹⁰ oxidative addition of the C–H bond to the palladium complex (**B**),¹¹ electrophilic aromatic substitution (**C**),^{12,13} and a concerted metalation-deprotonation (CMD) mechanism with the aid of a base (**D**).^{5,14–16} The exact mechanism of C–H bond cleavage depends heavily on substrate, metal and the reaction conditions.¹⁷



Scheme 1.3. Proposed pathways for the metal-catalyzed C–H bond cleavage of an arene.

The Heck type pathway **A** proceeds via a *syn*-addition of a metal-carbon bond across a double bond of the arene coupling partner. Either the carbometalated intermediate undergoes a high-energy *anti*- β -hydride reductive elimination, or isomerization takes place to form the *syn* complex, which subsequently undergoes a *syn*- β -hydride elimination. The rate-limiting step of the reaction would be the carbometalation and the subsequent reductive elimination is proposed to be fast.¹⁸ Similar pathways have been proposed for the palladium-catalyzed arylation of furan derivatives.¹⁰

Pathway **B** is an oxidative insertion of a metal species into a C–H bond. Such bond cleavage has been proposed as an intermediate step, taking place after carbopalladation of a vinylic substrate. The

vinylpalladium(II) species is proposed to form a hydridopalladium(IV) by oxidative C–H insertion of a proximal C–H bond and subsequent reductive elimination.¹⁹ Other examples of oxidative insertions of C–H bonds have been suggested. In the palladium-catalyzed synthesis of fused polycycles, a 1,4-shift of a palladium(II) species through the oxidative addition of a C–H bond to form a hydridopalladium(IV) is proposed.¹¹ Opposed to the Heck type pathway **A**, a C–H bond oxidative addition mechanism to the metal would exhibit a KIE > 1.

An electrophilic aromatic substitution ($S_{\text{E}}\text{Ar}$) type pathway **C** is often suggested as the mode of C–H bond cleavage of aromatics. An $S_{\text{E}}\text{Ar}$ type pathway would favor electron-rich over electron-poor substrates due to their increase in nucleophilicity. A Hammett plot of the substrates reaction rates under an $S_{\text{E}}\text{Ar}$ mechanism would give a negative ρ -value due to that a positive charge is built up under the course of the reaction.¹² An $S_{\text{E}}\text{Ar}$ pathway would also manifest itself in the typical *ortho-para* selectivity of the metalation.¹³ Typically, the rate-limiting step is the metalation step forming the intermediate electrophile-arene complex. Subsequent abstraction of the proton to regain aromaticity is a fast process. Thus, the C–H bond cleavage would not yield an observable KIE. However, the formation of the electrophile-arene complex is reversible and if the decomplexation reaction (k_{-1}) is much larger than the deprotonation (k_2), a steady-state approximation of the complex can be made and the deprotonation can become kinetically significant, i.e. the reaction would exhibit a KIE > 1.¹²

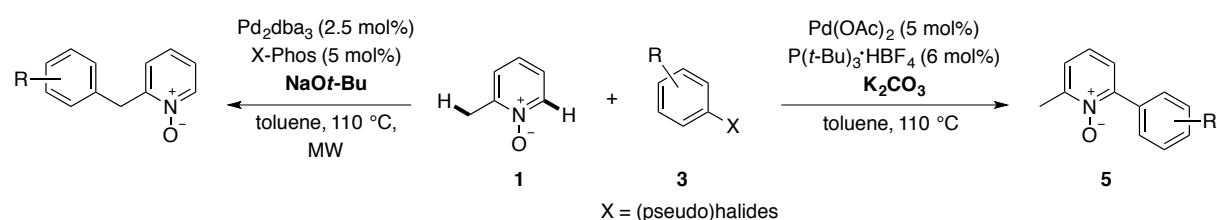
The CMD mechanism **D** is a σ -bond metathesis type of C–H bond cleavage promoted by a base where the C–H bond is cleaved simultaneously as the new M–C bond is formed. This would give rise to a KIE > 1 and can therefore be distinguished from an $S_{\text{E}}\text{Ar}$ mechanism. Furthermore, a more electron-deficient substrate would react faster than an electron-rich substrate due to the increase in acidity of the C–H bond broken. Opposed to an $S_{\text{E}}\text{Ar}$ pathway, a Hammett correlation would exhibit a positive ρ -value. In the arylation of fluorine-containing arenes¹⁴ and the intramolecular cyclization of tethered aromatics,¹⁵ both features were observed, compatible with a C–H bond cleavage by a concerted metalation-deprotonation mechanism.

1.2.2 Direct arylation of pyridine *N*-oxides with halobenzenes

In formation of 2-arylpyridines by means of traditional cross-coupling reactions (see above, scheme 1.2, **A**), an organometallic species has to be synthesized and subsequently coupled with an aryl (pseudo)halide. However, organometallic species with a nitrogen atom adjacent to a metal can be demanding to synthesize. Depending on the nature of the metal, the electron-withdrawing nitrogen results in instability of the compound and tendency for decomposition under the reaction conditions. Furthermore, due to the free electron pair of nitrogen-containing heterocycles, substrate coordination

and deactivation of the active catalyst could pose as a problem.²⁰ To circumvent these issues, the pyridine nitrogen can be oxidized to form bench-stable pyridine *N*-oxides **1**. These substrates can be employed in reactions with aryl (pseudo)halides (see above, scheme 1.2, **B**), reacting via a direct arylation of a C–H bond *ortho* to the *N*-oxide. In addition to increasing the reactivity and selectivity by oxidation of the nitrogen, an *N*-oxide moiety also decreases substrate coordination and deactivation of the catalyst.

Fagnou and co-workers first reported the use of pyridine *N*-oxides **1** as a pyridine surrogate. Employing bromobenzenes **3** as electrophile and 5 mol% Pd(OAc)₂, P(*t*-Bu)₃·HBF₄ as catalytic system in addition to K₂CO₃ as base, the protocol gave excellent yields of C2 arylated pyridine *N*-oxides (scheme 1.4). Both electron-deficient and electron-rich pyridine *N*-oxides substrates as well as substituted bromobenzenes gave high yields of the 2-arylated pyridine products.² The selectivity could be changed by applying Pd₂dba₃, X-Phos and NaOt-Bu as base, which led to the sp³-carbon of 2-picoline *N*-oxide **1f** being arylated, even in the presence of a sp²-C–H bond in 6-position on the pyridine *N*-oxide substrate. It was shown that the benzylic sp³ carbon undergoes the fastest H/D exchange with D₂O under basic conditions. However, the conditions optimized for sp²-carbon arylation did not give rise to any arylation in benzylic position.²¹ The sp²/sp³ selectivity depends on the base, where NaOt-Bu is a strong enough base to deprotonate the benzylic position but K₂CO₃ is not. In addition to preventing nitrogen binding of the substrate to the catalyst, oxidation of the nitrogen atom polarizes the C–H bonds the most in 2- and 4-position, and to a smaller extent in 3-position of the pyridine *N*-oxide substrate.¹⁶ In most cases, the *N*-oxide moiety stays intact over the course of the reaction, presenting the possibility of further functionalization after the first arylation reaction.²²



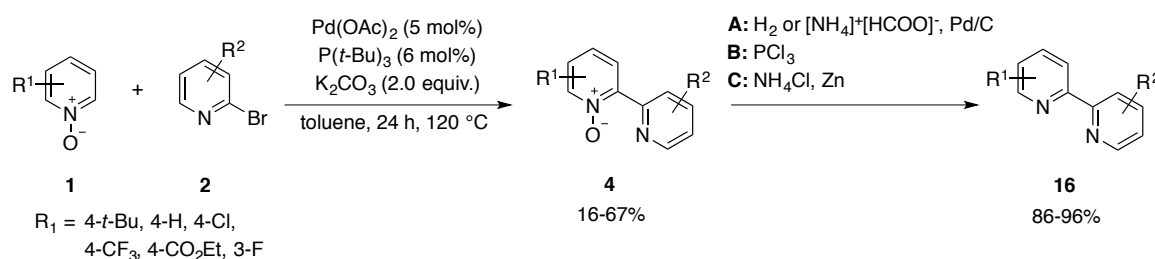
Scheme 1.4. Direct arylation of pyridine *N*-oxides **1** with bromobenzenes **3**.

Subsequent reports have shown that the *N*-oxide directing functionality is useful for other heterocyclic substrates as well. Under similar conditions, 6-membered diazine compounds such as pyrazine, pyrimidine and pyridazine *N*-oxides and fused heterocycles such as quinoxaline *N*-oxide can be arylated in 2-position to the *N*-oxide bond.²³ Also, 6- and 7-azaindoles,²⁴ thiazole and imidazole *N*-oxides²² were readily arylated. Additionally to chlorides, bromides and iodides, aryl triflates,²⁵ tosylates and mesylates²⁶ were applied as electrophiles in similar direct arylation reactions.

1.2.3 Direct arylation of pyridine *N*-oxides with heteroaryl halides

2,2'-Bipyridines are structural motifs with a wide variety of applications, such as ligands for catalysis,²⁷ in photovoltaics²⁸ or in supramolecular structures.^{9,29} Several multi-step syntheses to yield substituted 2,2'-bipyridines have been reported. For example, the Kröhnke synthesis is based on the Michael addition of a pyridinium methyl ketone to an α,β -unsaturated carbonyl compounds in the presence of ammonia and results in highly functionalized bipyridines.³⁰ Another pathway was developed by Reissig and co-workers, employing an activated picolinic acid and an enaminone to yield bipyridines and related oligoaryls such as terpyridines.³¹ However, the yield is often highly dependent on the substitution pattern of the reactants. Alternatively, traditional palladium-catalyzed cross-couplings such as Stille,³² Negishi³³ and Suzuki-Miyaura³⁴ cross-couplings forming 2,2'-bipyridines have also been described. Such reactions are however limited by instability, toxicity and availability of the organometallic reagent. Also, potential bipyridine product inhibition caused by coordination to the palladium catalyst could lower the reactivity of an active catalytic species.

By our group, it was shown that the direct arylation of pyridine *N*-oxides **1** as described by Fagnou and co-workers could be extended to substituted 2-bromopyridines **2** as electrophilic coupling partner (scheme 1.5). Similar reaction conditions to the previously reported protocol with bromobenzenes **3** were applied and lowering the amount of *N*-oxide **1** from 4 equivalents to 2 equivalents still gave satisfactory yields.³

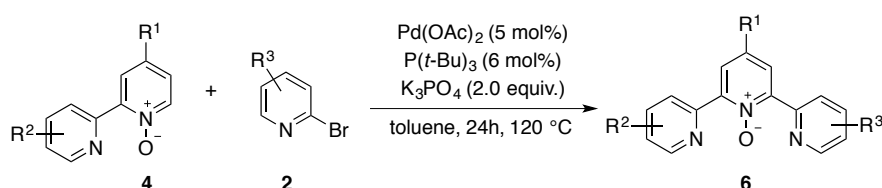


Scheme 1.5. Direct arylation of pyridine *N*-oxides **1** with bromopyridines **2**.

Other (pseudo)halides were tested with the 4-ethyl ester substituted pyridine *N*-oxide **1d** as model substrate. 2-Chloropyridine resulted in cross-coupling product **4d** in 57% yield but with 2-iodopyridine or pyridylsulfonates, the yield was significantly lower. Screening of the reaction conditions showed that the highest yield could be obtained with 2 equivalents **1d** and 1 equivalent 2-bromopyridine **2a**, yielding the CO_2Et substituted 2,2'-bipyridine *N*-oxide **4d** in 67% yield. Also substituted bromopyridines gave cross-coupled bipyridine *N*-oxide **4** in moderate yields.³ After the cross-coupling reaction, deoxygenation of the *N*-oxide products can be performed by different protocols. The *N*-oxide can be selectively deoxygenated by a Pd/C-catalyzed reduction with either H_2

or $[\text{NH}_4]^+[\text{HCOO}]^-/\text{NH}_4\text{Cl}$ as H source.^{3,35} Also, trivalent phosphorus compounds such as PCl_3 ³⁶ or PBr_3 ³⁷ or zinc dust in ammonium chloride has been employed.³⁸

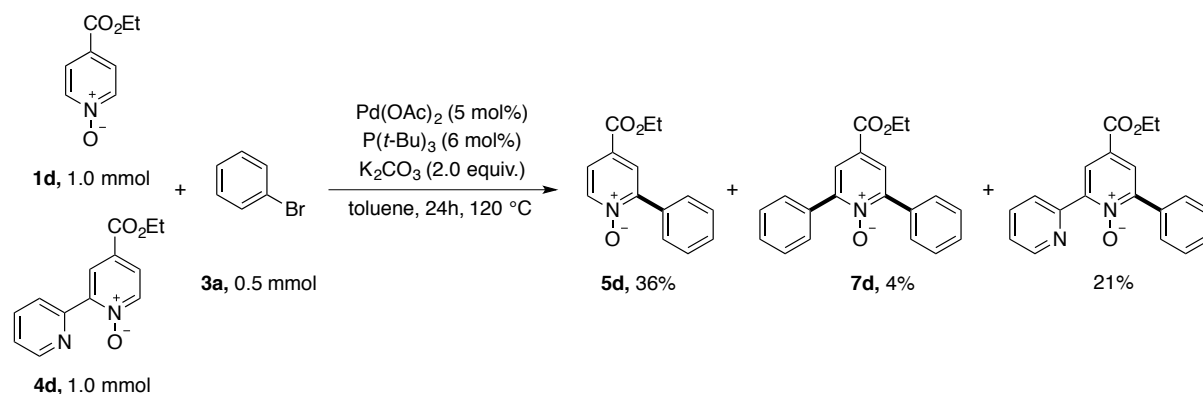
Due to the presence of two C–H bond *ortho* to the *N*-oxide moiety, the biarylated terpyridine *N*-oxide product **6** was also obtained. Optimization of the reaction conditions by increasing the amount of aryl halide from 1 equivalent to 2.4 equivalents consumed all of **1** and increased the yield of symmetrically substituted **6**. Using substituted monoarylated bipyridine *N*-oxide **4** as starting material for the second arylation yielded asymmetrically substituted terpyridine *N*-oxides (scheme 1.6). With the pyridine *N*-oxide **1** as limiting reagent and the presence of only one activated C–H bond on the substrate, the ratio of starting materials was changed to 1 equivalent of **4** and 1.2 equivalents of bromopyridine **2**.³⁹



Scheme 1.6. Direct arylation of bipyridine *N*-oxides **4** with bromopyridines **2**.

The limitation of the arylation reaction is the substitution pattern of pyridine *N*-oxide substrate **1**. In the arylation of *N*-oxides **1** with bromopyridine **2a**, electron-withdrawing groups such as an ester, cyano or trifluoromethyl substituent in 4-position resulted in yields of 56-67% of the arylated bipyridine *N*-oxide product **4**. However, electron-donating groups such as *tert*-butyl or the unsubstituted *N*-oxide only gave product **4** in 16% and 23%, respectively. A fluoro substituent in 3-position activated the C–H bond in 2-position further, resulting in a yield of 51% of bipyridine *N*-oxide product.³ The increased reactivity of electron-poor *N*-oxides is in agreement with the C–H bond cleavage via a CMD mechanism. An electron-withdrawing substituent would polarize the C–H bond, facilitating metalation of the substrate.⁵ However, the yield of arylations of electron-rich *N*-oxides with bromopyridines **2** is surprisingly low. For comparison, Fagnou and co-workers reported a yields of 78-80% of arylated product when employing both electron-rich 4-methoxy pyridine *N*-oxide and electron-poor 4-nitro pyridine *N*-oxide.²

A competition experiment between equimolar amounts of pyridine *N*-oxide **1d** and bipyridine *N*-oxide **4d** with bromobenzene **3a** gave arylpyridine *N*-oxide **5d** and teraryl *N*-oxide **7d** arising from arylation of **1d**. Also, the mixed teraryl *N*-oxide, arising from the arylation of bipyridine *N*-oxide **4d** with bromobenzene **3a**, in a ratio of 2:1 was obtained (scheme 1.7). This implies that the C–H bonds of both pyridine *N*-oxide **1d** and bipyridine *N*-oxide **4d** exhibit the same reactivity towards palladium-catalyzed C–H bond activation.³⁹

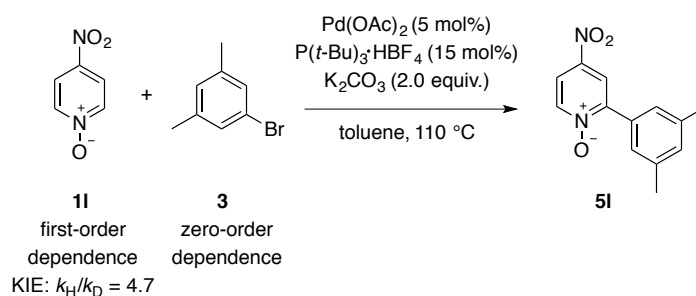


Scheme 1.7. Competition experiment between pyridine *N*-oxide **1d** and bipyridine *N*-oxide **4d**.

In the monoarylation reaction of pyridine *N*-oxides **1**, the competing pathway of bromopyridine **2a** forming homocoupling product 2,2'-bipyridine **8c** was observed, however was not quantified for different substrates. In contrast, the analogous homocoupling of bromobenzenes **3** to the biphenyl product **9a** has not been reported as a competing pathway in the direct arylation of pyridine *N*-oxides **1**.² So far, no systematic survey on the side reactions of the direct arylation reaction has been reported.

1.2.4 Previous mechanistic studies on the direct arylation of pyridine *N*-oxides

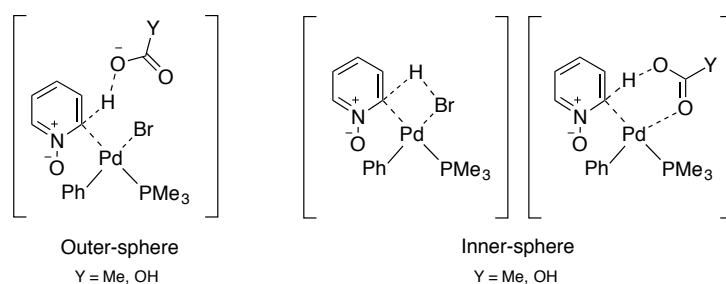
The group of Fagnou reported an extensive mechanistic study of the direct arylation of pyridine *N*-oxides with bromobenzenes including experimental data on the reaction rates of the substrates as well as DFT calculations of potential transition states.⁵ As model reaction, 4-nitro pyridine *N*-oxide **11** and 5-bromo-*m*-xylene with 5 mol% Pd(OAc)₂ catalyst and K₂CO₃ as base was employed. Varying the aryl bromide concentration from 0.2 M to 0.6 M did not change the rate of product formation; however increasing the concentration of *N*-oxide **11** from 0.1 M to 0.8 M increased the product formation rate. This is suggesting a zero-order dependence on the aryl halide and a first-order dependence on **11**, indicating that one *N*-oxide molecule is involved in the rate-determining step of the reaction (scheme 1.8). Arguably, the C–H bond cleavage or the reductive elimination can be the RDS of the reaction.⁵ A one-pot competition experiments between pyridine *N*-oxide and pyridine-*d*₅ *N*-oxide gave a significant KIE ($k_H/k_D = 4.7$),² implying that the reductive elimination is not the rate-limiting step. Furthermore, a partial order dependence on catalyst was determined. Partial order dependence has previously been suggested for systems where the active catalyst is a monomer and the catalyst exists in an oligomeric resting state.⁵



Scheme 1.8. Order of dependence on the reactants investigated by Fagnou and co-workers.

As illustrated above in scheme 1.3, different modes of C–H bond cleavage have been proposed. Under the assumption that the initial step of reaction is the oxidative addition of **3** to a palladium(0) species, the C–H bond activation step is presumed to be performed by an aryl palladium(II) bromide complex **14** or acetate complex **15**. The transition states of the C–H activation of unsubstituted pyridine *N*-oxide **1c** performed by an aryl palladium(II) complex bearing a bromide, carbonate or acetate anionic ligand was calculated with the $\text{P}(t\text{-Bu})_3$ ligand approximated with PMe_3 .⁵

A Heck-type pathway and an oxidative insertion of the C–H bond were calculated to proceed via high-energy transition states of $\Delta G^\ddagger = 56.6$ kcal/mol and 53.4 kcal/mol, respectively. For the often proposed electrophilic palladation pathway, no complex with a cationic character could be located, suggesting that an $\text{S}_{\text{E}}\text{Ar}$ pathway is also unlikely. Therefore, the most plausible mode of C–H bond cleavage would be a concerted metalation-deprotonation. A CMD mechanism can proceed via an outer-sphere or an inner-sphere mechanism, as depicted in scheme 1.9. Furthermore, a bromide from the starting material or a carbonate or acetate originating from the inorganic base or Pd(OAc)_2 can act as deprotonating agent.



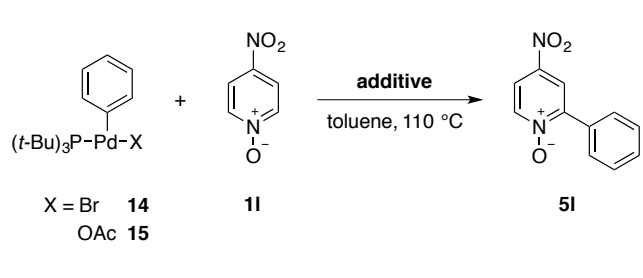
Scheme 1.9. Proposed types of C–H bond cleavage via a concerted metalation-deprotonation (CMD) mechanism.

In an outer-sphere mechanism, the base cleaving the C–H bond is not bound to the palladium complex (left), whereas, in the inner-sphere pathway, the base deprotonating the substrate is bound to the metal center (right). For carbonate as base, transition state energies of $\Delta G^\ddagger = 40.3$ kcal/mol for the outer-sphere mechanism and $\Delta G^\ddagger = 32.4$ kcal/mol for the inner-sphere mechanism were calculated. The analogous calculation with acetate as the base revealed the same trend, with $\Delta G^\ddagger = 37.2$ kcal/mol and

26.9 kcal/mol for the outer-sphere and the inner-sphere transition states, respectively. With bromide as base, there was no thermodynamic barrier, however, the formed biaryl complex product with HBr was distinctively higher in energy than the analogous HOAc complex ($\Delta G = 36.8$ versus 6.1 kcal/mol).⁵

The ability of an aryl palladium(II) complex to activate a pyridine *N*-oxide C–H bond was also experimentally investigated by stoichiometric reactions of the isolated phenyl palladium complexes bearing either a bromide **14** or acetate **15** ligand (table 1.1). Bromide palladium complex **14** in the reaction with *N*-oxide **11** gave no arylpyridine *N*-oxide **51** in the absence of K_2CO_3 /KOPiv and only low yield in the presence of K_2CO_3 alone. With the addition of KOPiv or KOPiv/ K_2CO_3 , the yield increased to approximately 30%. The analogous reaction between acetate palladium complex **15** and *N*-oxide **11** with and without K_2CO_3 gave yields of 49% and 48% of arylpyridine *N*-oxide product **51**, respectively.⁵ This is suggesting that both pivalate or acetate and K_2CO_3 are required for the reaction to take place.

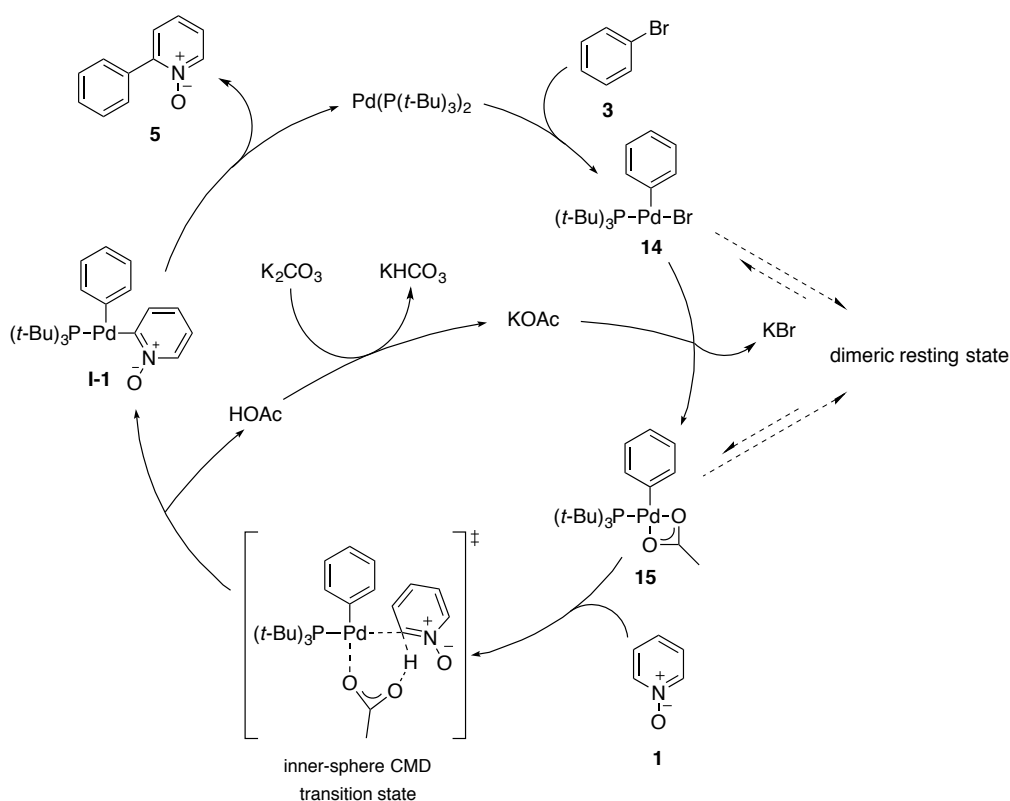
Table 1.1. Additives influencing the reaction between an isolated aryl palladium(II) complex and pyridine *N*-oxide **11**.

	<table border="1" style="border-collapse: collapse; width: 100%;"> <thead> <tr> <th style="text-align: center;">entry</th> <th style="text-align: center;">X</th> <th style="text-align: center;">additive</th> <th style="text-align: center;">yield 51</th> </tr> </thead> <tbody> <tr> <td style="text-align: center;">1</td> <td style="text-align: center;">Br</td> <td style="text-align: center;">none</td> <td style="text-align: center;">0%</td> </tr> <tr> <td style="text-align: center;">2</td> <td style="text-align: center;">Br</td> <td style="text-align: center;">K_2CO_3</td> <td style="text-align: center;">5%</td> </tr> <tr> <td style="text-align: center;">3</td> <td style="text-align: center;">Br</td> <td style="text-align: center;">KOPiv</td> <td style="text-align: center;">29%</td> </tr> <tr> <td style="text-align: center;">4</td> <td style="text-align: center;">Br</td> <td style="text-align: center;">K_2CO_3/ KOPiv</td> <td style="text-align: center;">31%</td> </tr> <tr> <td style="text-align: center;">5</td> <td style="text-align: center;">OAc</td> <td style="text-align: center;">none</td> <td style="text-align: center;">48%</td> </tr> <tr> <td style="text-align: center;">6</td> <td style="text-align: center;">OAc</td> <td style="text-align: center;">K_2CO_3</td> <td style="text-align: center;">49%</td> </tr> </tbody> </table>	entry	X	additive	yield 51	1	Br	none	0%	2	Br	K_2CO_3	5%	3	Br	KOPiv	29%	4	Br	K_2CO_3 / KOPiv	31%	5	OAc	none	48%	6	OAc	K_2CO_3	49%
entry	X	additive	yield 51																										
1	Br	none	0%																										
2	Br	K_2CO_3	5%																										
3	Br	KOPiv	29%																										
4	Br	K_2CO_3 / KOPiv	31%																										
5	OAc	none	48%																										
6	OAc	K_2CO_3	49%																										

The catalytic reaction starting from $Pd(OAc)_2$ did not require addition of a pivalate additive, whereas using $Pd(P(t-Bu)_3)_2$ as palladium source and K_2CO_3 as base exhibited low reactivity without pivalate additive. Although a low-energy transition-state has been found computationally with carbonate as the base, the above observations indicate that an acetate or pivalate anion is crucial for the CMD step of the reaction and that the C–H bond cleavage is not performed by a bromide palladium(II) complex **14** alone. However, the yield of the stoichiometric reaction between acetate palladium complex **15** and *N*-oxide **11** resulted in approximately 50% yield of arylpyridine *N*-oxide **51**, being lower than catalytic reaction of *N*-oxide **11** and bromobenzene **3a**, where **51** was obtained in 62% yield.⁵ This observation suggests that another catalytic species bearing an acetate might be formed and subsequently performs the C–H bond cleavage.

A Hammett correlation of the reaction rates of 4-substituted *N*-oxides versus their σ_{meta} -values resulted in a reaction constant of $\rho = +1.53$, indicating an increase in reaction rate with more electron-withdrawing character of the substituent. An electron-withdrawing group would stabilize the negative charge formed during the CMD step of the reaction. Thus, a positive ρ -value is arguing against an

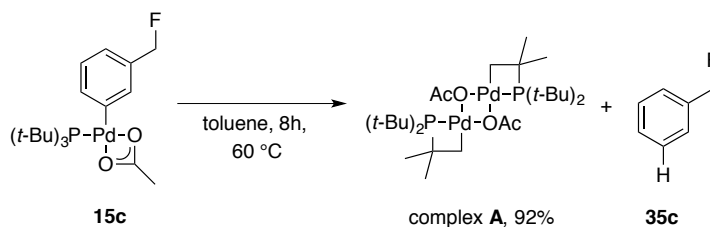
$S_{\text{E}}\text{Ar}$ mechanism.⁵ From these experimental and computational data, a mechanism for the direct arylation of *N*-oxides **1** with bromobenzenes **3** was proposed (scheme 1.10). Initially, the aryl halide **3** undergoes a fast oxidative addition to a palladium(0) species forming palladium(II) complex **14**. An acetate anion can displace the bromide to form the κ^2 -acetate complex **15**. From the results described above, it was concluded that an acetate is likely to deprotonate the C–H bond and the CMD step is proposed to take place with **15**. The inner-sphere C–H bond cleavage proceeds via a 6-membered transition state forming biaryl palladium **I-1**, which undergoes fast reductive elimination to release arylated product **5** and regenerate the palladium(0) catalyst. The formed acetic acid is deprotonated by the inorganic base and re-enters the catalytic cycle. Crystallization of aryl palladium(II) complexes bearing a bulky $\text{P}(t\text{-Bu})_3$ ligand has revealed that the complexes often exist as monomeric species due to the steric demand of the ligand.⁴⁰ The partial order dependence on catalyst is therefore not explained by the reported calculation and experiments.



Scheme 1.10. Mechanistic proposal for the direct arylation of pyridine *N*-oxides **1** by Fagnou and co-workers.

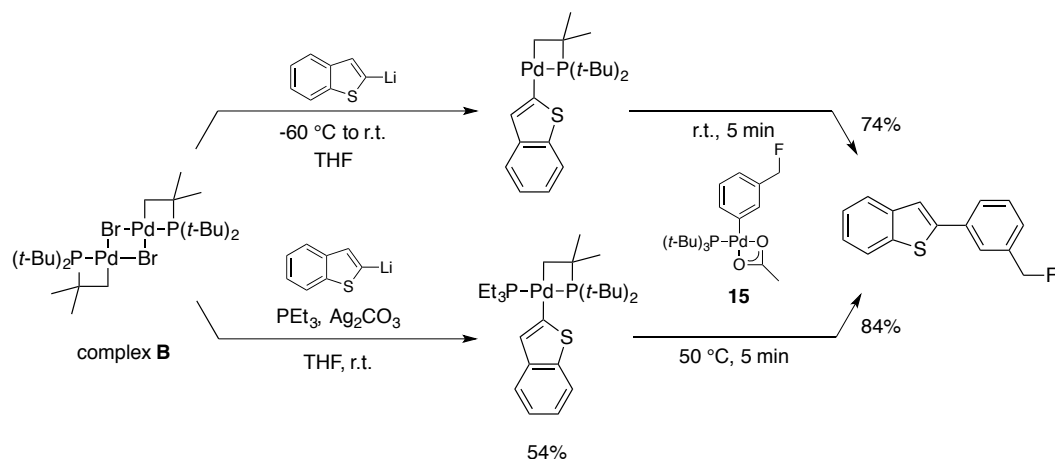
Later, Hartwig and co-workers further investigated the direct arylation reaction. Employing 3-(fluoromethyl)phenyl iodide and pyridine *N*-oxide **1c** with 5 mol% $\text{Pd}(\text{OAc})_2$ and $\text{P}(t\text{-Bu})_3$ as model reaction, it was shown that the catalytic reaction resulted in cross-coupled arylpyridine *N*-oxide product **5** in 77% yield. However, reaction of an isolated palladium acetate complex $(3\text{-CH}_2\text{FC}_6\text{H}_4)\text{PdOAc}(\text{P}(t\text{-Bu})_3)$ **15c** with stoichiometric amount of *N*-oxide **1c** provided arylpyridine *N*-oxide product **5** in only 52% yield. Monitoring of the consumption of complex **15** by ^{19}F NMR in the presence of **1c** and K_2CO_3 at 60 °C showed an induction period of approximately 30 minutes

during which <1% of product **5** was formed. Instead, formation of the dimeric cyclometalated complex **A** together with 3-fluoromethylbenzene **35c** was observed (scheme 1.11).⁴ Complex **A** has previously been detected in the α -arylation of silylnitriles with aryl halides where it was observed as a catalytic precursor.⁴¹ Testing the decomposition of complex **15** in the absence of *N*-oxide **1c** at 60 °C in toluene gave complex **A** in 92% yield.



Scheme 1.11. Decomposition of acetate complex **15** to palladium complex **A** and free arene.

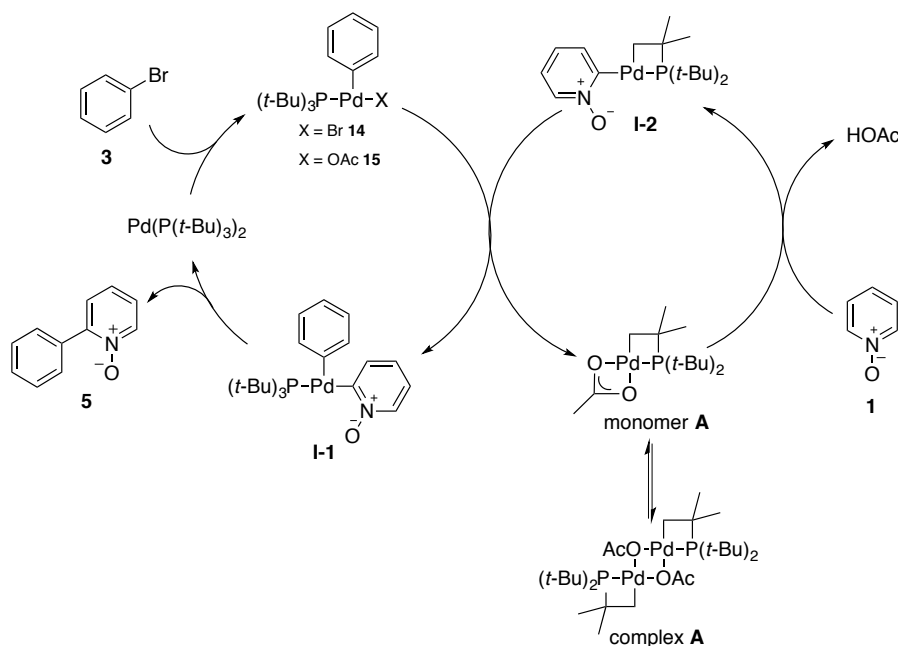
Addition of complex **A** to the reaction between complex **15** and *N*-oxide **1c** resulted in a zero-order decay of **15** without induction period, indicating that the aryl acetate complex does not take part in the rate-determining step of the reaction. Product **5** was obtained in 84% yield, which is similar to 77% yield in the catalytic reaction. A partial order of dependence was determined for complex **A**, indicating an equilibrium between the dimeric **A** and a monomeric species that is taking part in the rate-determining step. These results are suggesting that the monomeric form of complex **A** is performing the C–H bond cleavage of pyridine *N*-oxide **1**. No deuterium incorporation in the $\text{P}(\text{t-Bu})_3$ ligand was observed in the reaction between complex **A** and *N*-oxide **1c-d**₅, indicating that the C–H bond cleavage is not performed by the palladium-bound cyclometalated phosphine ligand. Cleavage of the C–H bond by the acetate of monomer **A** would result in a 2-pyridyl *N*-oxide palladium(II) intermediate **I-2** bearing an intact cyclometalated phosphine ligand. To further elucidate the intermediacy of such species, the synthesis of a 2-pyridyl *N*-oxide intermediate formed after C–H bond activation was sought. However, such a complex was deemed too complicated to synthesize and a cyclometalated benzothiophenyl palladium complex was used as a surrogate for the proposed intermediate. It was formed by lithiation of benzothiophene and subsequent reaction with cyclometalated bromide bridged complex **B** (scheme 1.12). The benzothiophenyl complex and acetate complex **15** reacted within 5 minutes at room temperature to the arylated benzothiophene product in 74% yield. Furthermore, stabilization of the heteroaryl complex with a PEt_3 ligand produced a more stable 2-heteroaryl palladium(II) complex, however only characterized via ¹H and ³¹P NMR. The PEt_3 complex reacted with acetate complex **15** to form the arylated benzothiophene product in 84% yield within 5 minutes at 50 °C.



Scheme 1.12. Reaction of an *in situ* formed (above) or PEt₃-stabilized (below) benzothieryl palladium complex with aryl palladium(II) complex **15**.

Since the reactivity of the benzothieryl palladium(II) complex with acetate complex **15** was fast, it was concluded that such a complex is a kinetically competent species in the catalytic cycle.⁴ However, due to the difference in electronic nature of benzothiophene and pyridine *N*-oxide, the reactivity cannot be directly translated to the direct arylation reaction of pyridine *N*-oxides. Furthermore, the benzothieryl palladium(II) complex does not provide any information of potential side reactions of the nucleophilic coupling partner employed in the reaction.

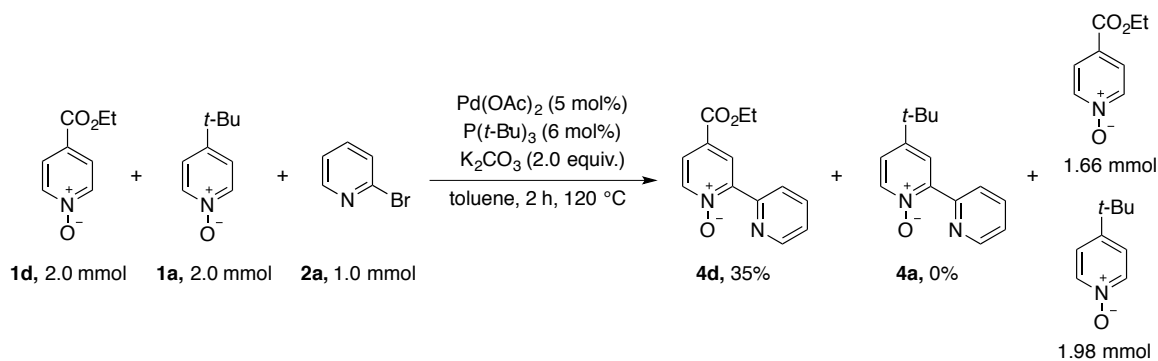
The above experimental data led to a revised mechanistic proposal of the direct arylation of pyridine *N*-oxides **1** (scheme 1.13). Two cooperating palladium cycles are suggested in which the left one begins with a fast oxidative addition of the aryl halide substrate **3** to a palladium(0) species, yielding aryl palladium(II) complex **14**. Displacement of the bromide anion by acetate would give complex **15**. The right-hand cycle comprises of the rate-determining C–H bond cleavage of the pyridine *N*-oxide **1** by the monomer of complex **A**, forming cyclometalated 2-pyridyl *N*-oxide intermediate **I-2**. In turn, this species undergoes transmetalation with acetate complex **15** and subsequent fast reductive elimination of the biaryl palladium species **I-1** results in the cross-coupling product **5** and regenerates a palladium(0) complex. No information on how the initial palladium(II) species is reduced to a palladium(0) species required for oxidative addition was reported.



Scheme 1.13. Updated mechanistic proposal for the direct arylation of pyridine *N*-oxides **1** by Hartwig and co-workers.

1.2.5 Mechanistic background for direct arylations with bromopyridines

A brief investigation of the reactivity of pyridine *N*-oxides towards bromopyridine **2a** has been performed by our group.³⁹ The reaction between equimolar amounts of 4-CO₂Et pyridine *N*-oxide **1d** and 4-*tert*-butyl pyridine *N*-oxide **1a** with 2-bromopyridine **2a** gave only the cross-coupled 4-CO₂Et bipyridine *N*-oxide **4d** product and 4-*tert*-butyl pyridine *N*-oxide **1a** was recovered after the reaction (scheme 1.14). This is in agreement with the observation of Fagnou and co-workers, which is that electron-poor pyridine *N*-oxides should undergo faster C–H cleavage due to the polarization of the bond.⁵



Scheme 1.14. Competition reaction between an electron-poor pyridine *N*-oxide **1d** and an electron-rich pyridine *N*-oxide **1a** towards bromopyridine **2a**.

Furthermore, no inhibition of the rate-limiting step by nitrogen-containing starting material or product for the arylation was observed when employing electron-poor pyridine *N*-oxides. In the reaction of *N*-oxide **1d** with either bromopyridine **2a** or bromobenzene **3a**, the aryl halide substrates were consumed with a similar constant rate. Catalyst inhibition by bromopyridine starting material **2a** would have resulted in a slower consumption of **2a** in comparison to the consumption of bromobenzene **3a**. Bipyridine *N*-oxide product **4d** inhibition would have given a decrease in the rate of consumption of **2a** over time as more product **4** was formed. However, all of the aryl halide starting material in both reactions was consumed within 4 h, indicating that no inhibition by **4d** was present.³⁹ Also, the linear decay of both **2a** and **3a** is in agreement with the zero-order dependence proposed for the aryl halide.⁵ However, these results only account for the reaction of an electron-poor pyridine *N*-oxide in the reaction with the two electrophiles. Until now, no survey of the reactivity of electron-rich pyridine *N*-oxides in the reaction with bromopyridines and bromobenzenes has been performed.

1.3 Results and discussion

The observed reactivity in direct arylations of pyridine *N*-oxides **1** with bromopyridine **2a** is that electron-poor CO₂Et substituted *N*-oxide **1d** gives cross-coupling product **4d** in 67% yield and unsubstituted electron-rich pyridine *N*-oxide **1c** gives product **4c** in only 23% yield.³ Although the yield can be increased to 44% by drying the hygroscopic *N*-oxide starting material **1c**,⁴² there is still an unexplained difference in yield between the electron-rich and electron-poor substrates. One explanation for the decrease in yield is the presence of competing decomposition pathways. Our group has previously observed homocoupling of bromopyridine **2a** substrate to 2,2'-bipyridine **8c** as a side product formed under the catalytic conditions. This competing pathway consuming the limiting starting material will obviously lower the yield of cross-coupling product. Furthermore, coordination of bipyridine **8c** could influence the active catalyst and lead to incomplete conversion of starting materials by inhibition or faster deactivation of the catalyst.

To investigate how the substitution pattern of pyridine *N*-oxides influence substrate consumption and product and side-product formation, pyridine *N*-oxides **1a-e** bearing substituents ranging from electron-rich *tert*-butyl to electron-poor CF₃ in 4-position were chosen for the following mechanistic survey. The substrates consumption rates and the product formation rates were monitored for *N*-oxides **1a-e** in the reactions with bromopyridine **2a** and bromobenzene **3a**. Also, the rate of side products formed via competing homocoupling pathways was monitored and the side products quantified. If bromopyridine starting material or (side)products influence an active catalytic species, a difference in rate of formation should be observed for bipyridine *N*-oxide **4** in comparison to arylpyridine *N*-oxide **5**. Also, comparing consumption rates of **2a** and **3a** to product formation rates of **4** and **5** rates should reveal the influence of competing side reactions. If no side reactions are present, the consumption of **2a** or **3a** should be identical to formation of **4** or **5**.

1.3.1 Substrate consumption and product and side-product formation

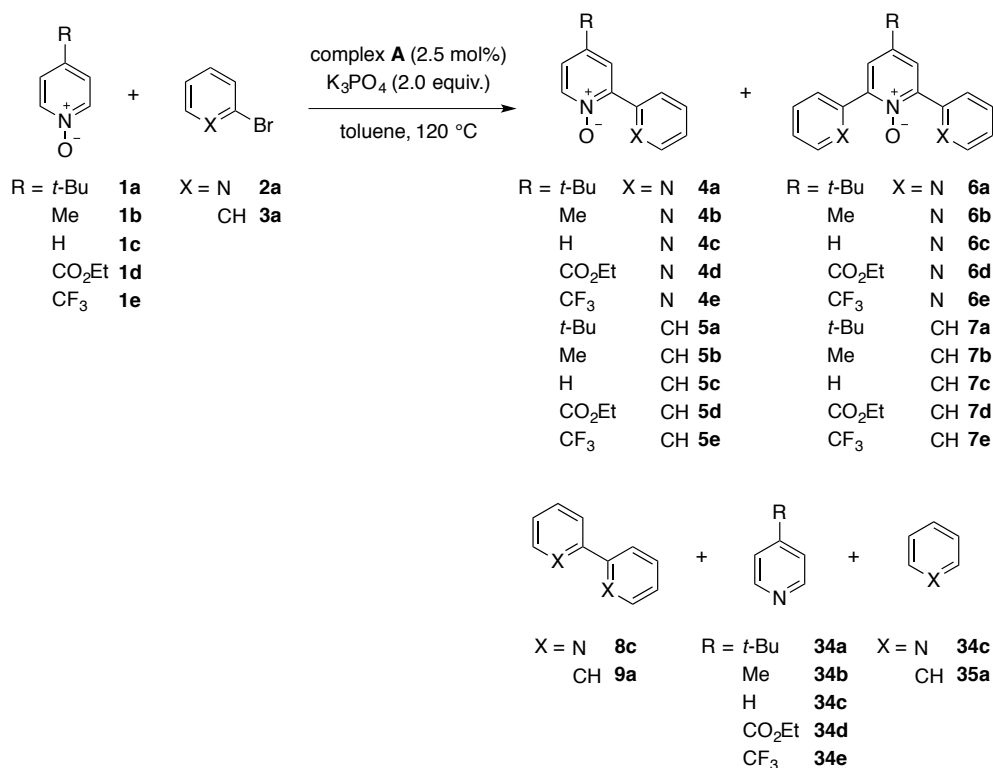
For the kinetic measurements, reaction conditions identical to the reported conditions were applied.³ However, due to the decomposition of P(*t*-Bu)₃ in air, the cyclometalated dimeric complex **A** was used instead. Complex **A** is suggested to be the catalyst resting state⁴ and it is readily formed from Pd(OAc)₂ and P(*t*-Bu)₃ in toluene after 30 minutes at 90 °C,^{39,43} indicating that it would be rapidly formed under the arylation reaction conditions as well.

The formation rates of cross-coupling products **4** and **5** were determined via ¹H NMR with CDCl₃ as solvent. To avoid signal overlap in spectrum, the consumption rates of aryl halides **2a** and **3a** were

determined via GC-FID. Due to the volatility of **2a** and **3a**, they can be easily removed by evaporation prior to recording an ^1H NMR spectrum. The reactions were set up in a glovebox and subjected to a pre-heated oil-bath at 120 °C. One sample was withdrawn at 10 minutes interval for 1 hour and thereafter a sample after 2 hours. Each sample was analyzed via both GC-FID and ^1H NMR. Pyridine *N*-oxide substrates **1b** and **1e** exhibit low solubility at room temperature in CDCl_3 and therefore the consumption rate of **1** could not be determined in these reactions. Rates were calculated as averages of duplicate reactions. Due to the C–H bond cleavage being the RDS of the reaction, a first-order dependence on **1** and consequently an exponential decay would be expected.⁴⁴ However, *N*-oxide **1** is added in two-fold excess to aryl halide **2a** or **3a** and therefore limits the consumption to a maximum of 50%. To distinguish between a linear or exponential decay, consumption over at least three-half lives of the substrate is required,⁴⁴ precluding any conclusions to be drawn on order in substrate from these individual kinetic measurements. All reaction rates shown below are the formation and consumption rates until $t = 120$ minutes, or where a linear correlation was observed. For some reactions, an initial induction period was observed and therefore the rates were calculated with the data points after the induction period.

Table 1.2 shows the initial formation rate of monoarylated *N*-oxide product **4** and **5** and the corresponding substrate consumption of aryl halide **2a** and **3a**. For the sequential reaction forming teraryl *N*-oxide **6** and **7**, a low initial concentration of the products was observed and they could only be detected after approximately 40 minutes into the reaction. Furthermore, due to peak overlap in the ^1H NMR spectrum, quantification of teraryl *N*-oxide **6** and **7** proved difficult. In addition to cross-coupling products, quantification of homocoupling products 2,2'-bipyridine **8c** or biphenyl **9a** was performed. Using GC-FID, the yield and rate of formation of **8c** or **9a** was monitored simultaneously with cross-coupling product yield and rate. Also dehalogenation of starting material **2a** or **3a** to pyridine **34c** or benzene **35a**, respectively, and deoxygenation of *N*-oxide **1** to substituted pyridines **34** took place under the reaction conditions. The dehalogenation side reaction is likely due to a proto-demetalation process of the aryl palladium(II) complex formed after oxidative addition by a proton donor.⁵ In addition to a competing homocoupling side reaction, for *N*-oxides undergoing slow C–H activation, the absence of sufficient pyridyl *N*-oxide **I-2** could lead to competing proto-demetalation of the aryl palladium(II) complex. For the observed deoxygenation products **34**, a potential pathway would be concomitant oxidation of phosphine ligand. Deoxygenation of *N*-oxides is often carried out by trivalent phosphorus compounds as reducing agent at elevated temperatures.³⁶ However, no oxidation of the $\text{P}(t\text{-Bu})_3$ ligand took place when subjected to the reaction conditions the absence of complex **A**,⁴² indicating that the deoxygenation is a catalyzed process. In addition to deoxygenation of *N*-oxides **1**, deoxygenation of cross-coupled products **4** and **5** has also been observed.⁴² In all reactions between *N*-oxide **1a-e** and aryl halide **2a** and **3a**, less than 5% of **34** and **35** was obtained (see Experimental section, 4.6).

Table 1.2. Initial formation rate and yield of cross-coupled product **4-7** and homocoupling product **8c** and **9a** and consumption rate of **1**, **2a**, **3a**. Formation rate of **9a** in the reaction between **1c** and **3a** not determined due to signal overlap in ¹H NMR spectrum. Pyridine *N*-oxide 7.0 mmol, aryl halide 3.5 mmol.



entry	R	<i>N</i> -oxide	aryl halide	k_{obs}	k_{obs}	k_{obs}	k_{obs}	yield	yield	yield
				1 [mM/min]	2a, 3a [mM/min]	4, 5 [mM/min]	8c, 9a [mM/min]	4, 5 [%]	6, 7 [%]	8c, 9a [%]
1	<i>t</i> -Bu	1a	2a	-2.3	-3.5	+1.2	+0.74	23	5	35
2	<i>t</i> -Bu	1a	3a	-4.6	-3.8	+2.5	+0.17	63	16	18
3	Me	1b	2a	-	-4.8	+2.2	+0.45	49	14	28
4	Me	1b	3a	-	-2.2	+1.6	+0.074	83	21	7
5	H	1c	2a	-3.9	-4.5	+2.5	+0.94	40	6	31
6	H	1c	3a	-2.1	-2.0	+1.2	-	76	20	3
7	CO ₂ Et	1d	2a	-3.0	-3.6	+2.4	+0.24	68	13	8
8	CO ₂ Et	1d	3a	-2.3	-2.6	+1.9	+0.074	71	26	4
9	CF ₃	1e	2a	-	-5.2	+3.5	+0.33	70	37	10
10	CF ₃	1e	3a	-	-4.5	+3.7	+0.089	83	24	3

Comparing the product formation rates for all reactions of bromopyridine **2a**, an increase in rate from $k_{\text{obs}} = 1.2$ mM/min for electron-rich *tert*-butyl-substituted *N*-oxide **4a** to $k_{\text{obs}} = 3.5$ mM/min for electron-poor CF₃-substituted **4e** was observed as expected. The same trend is not as obvious in the reactions with bromobenzene **3a**. As anticipated, the product formation rate increases from unsubstituted **5c** with a formation rate of $k_{\text{obs}} = 1.2$ mM/min to electron-poor **5e** with a rate of $k_{\text{obs}} = 3.7$ mM/min.

Notably, the reaction of electron-rich **1a** forming the product **5a** proceeded with a fast rate of $k_{\text{obs}} = 2.5$ mM/min, being comparable to the rate of electron-poorer *N*-oxides. The origin of fast product formation is not clear. Due to incomplete oxidation in the formation of starting material **1a**, pyridine **34a** was already present in the initial sample and could possibly play a role (see below, section 1.3.2). The CF₃-substituted product **4e** was formed with $k_{\text{obs}} = 3.5$ mM/min and product **5e** with $k_{\text{obs}} = 3.7$ mM/min. A similar product formation rate for aryl halide **2a** and **3a** is supporting the observation of the similar yields obtained for **4e** and **5e**, indicating that potential competing side reactions are not substantially influencing the arylation of electron-poor *N*-oxide **1e**. Surprisingly, the product formation rates were faster in the reactions between bromopyridine **2a** and *N*-oxide **1b**, **1c** and **1d** than the same reactions with bromobenzene **3a**. The absence of rate inhibition by the nitrogen-containing substrate indicates that bromopyridine **2a** does not inhibit the catalyst. On the contrary, **2a** might facilitate formation of an active catalytic species from complex **A**, increasing the rate of C–H activation. However, the structure of such an intermediate remains unknown.

The general trend for the aryl halide consumption is that bromobenzene **3a** is consumed considerably slower than bromopyridine **2a**. Comparing the consumption rate of bromobenzene **3a** to the formation of product **5** in the reaction with *N*-oxide **1a**, bromobenzene **3a** is consumed 1.5 times as fast as product **5a** is formed. In comparison, in the analogous reaction between *N*-oxide **1a** and bromopyridine **2a**, the consumption rate of bromopyridine **2a** is consumed 2.9 times faster than **4a** is formed. In addition to the lower yields of biaryl *N*-oxide and teraryl *N*-oxide in reaction **1a-c** with bromopyridine **2a** in comparison to bromobenzene **3a**, this further indicates a side reaction consuming bromopyridine **2a**.

Regarding *N*-oxide substrate consumption, CO₂Et substituted *N*-oxide **1d** in the reactions with **2a** and **3a** showed that the *N*-oxide substrate consumption was only slightly slower than the aryl halide consumption ($k_{\text{obs}} = 3.0$ mM/min versus 3.6 mM/min for **2a** and $k_{\text{obs}} = 2.3$ mM/min versus 2.6 mM/min for **3a**). The same holds true for the reaction of unsubstituted *N*-oxide **1c** with **2a**, where **2a** is consumed with a slightly faster rate of $k_{\text{obs}} = 4.5$ mM/min compared to $k_{\text{obs}} = 3.9$ mM/min for **1c**. In the reaction of **1c** with **3a**, both substrates exhibit a virtually identical consumption rate, where **1c** is consumed at $k_{\text{obs}} = 2.1$ mM/min and **3a** at $k_{\text{obs}} = 2.0$ mM/min.

The formation of homocoupling product strongly depends on the substituent of pyridine *N*-oxide **1** starting material. In reactions with bromobenzene **2a**, *N*-oxides with electron-rich substituents gave relatively large amounts of homocoupling product and low yields of cross-coupling products whereas *N*-oxides with electron-poor substituents exhibited the opposite trend of low yield of homocoupling product and relatively high yield of cross-coupling product. A homocoupling pathway was also present in reactions with bromobenzene **3a**, however the reactions gave an overall high yield of cross-

coupling product and consistently low yield of homocoupling product **9a**. The only exception is the reaction of *tert*-butyl *N*-oxide **1a** with bromobenzene **3a**, where homocoupling product biphenyl **9a** was obtained in 18% yield. This deviation could be due to the presence of coordinating **34a**, which is a contaminant of the *N*-oxide starting material (see below). Comparing the formation rates of **8c** and **9a** show that for all reactions, bipyridine homocoupling product **8c** forms approximately 4 times as fast as biphenyl homocoupling product **9a**. The hypothesis is that the increase in rate of homocoupling product formation is due to a decrease in stability of a pyridyl palladium complex in comparison to a phenyl palladium complex (see Chapter 2). If the hypothesis holds true, an increase in bipyridine **8c** formation would be observed when homocoupling becomes competing with cross-coupling, i.e. for less reactive pyridine *N*-oxides **1**.

Comparison of the yield of cross-coupled arylpyridine *N*-oxide product **5** formed from reaction between *N*-oxide **1a-e** and bromobenzene **3a** shows that similar yields for product **5a-e** were obtained, analogous to previous reports.² In stark contrast, the yield in reactions of *N*-oxide **1a-e** with bromopyridine **2a** shows a clear increase in yield from 23% of cross-coupling product for *tert*-butyl-substituted **1a** to 70% for CF₃-substituted **1e**. The reactions of electron-poor *N*-oxides **1d** and **1e** with both aryl halides gave the corresponding arylpyridine *N*-oxides **4d, e** and **5d, e** in similar yields (68-83%). A comparison of the yield of cross-coupling products versus the σ -value of the substituent is shown in figure 1.1.

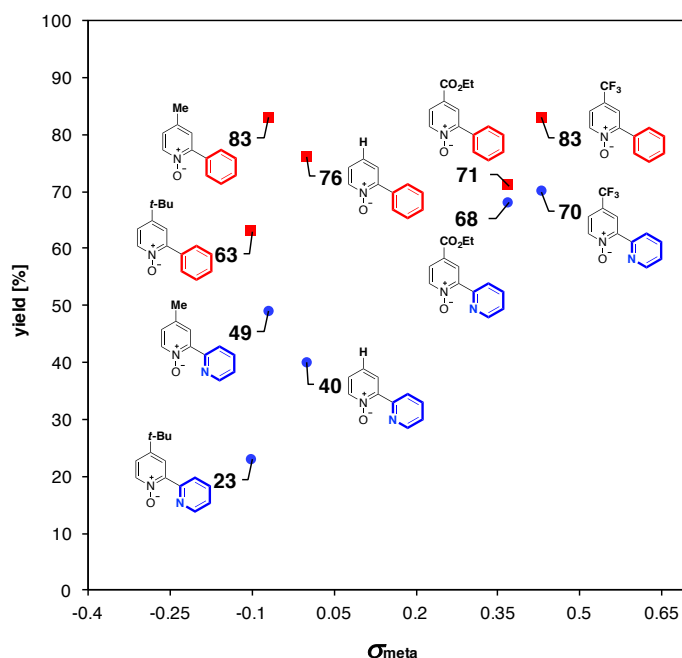


Figure 1.1. Yield of arylpyridine *N*-oxide **4** and **5** from the direct arylation of pyridine *N*-oxide **1a-e** with bromopyridine **2a** or bromobenzene **3a** versus the σ_{meta} -value of substituents.

The trend in yield for teraryl *N*-oxide products **6** and **7** was similar to what observed for monoarylated product **4** and **5**. Teraryl *N*-oxide **7** formed from the double arylation of *N*-oxide **1** with bromobenzene

3a was in the range of 16-26%. In contrast, terpyridine *N*-oxide **6** formed from the reaction of *N*-oxide **1** with bromopyridine **2a** gave **6a** in 5% and **6e** in 37%. Due to signal overlap in the ¹H NMR spectrum *N*-oxide **1e**, the sum of calculated yields of arylated products exceeds 100%.

A previous report by Fagnou and co-workers showed the Hammett correlation between five 4-substituted pyridine *N*-oxides **1** in the reaction with a 5-bromo-*m*-xylene substrate **3**. A linear correlation with $\rho = +1.53$ ($R^2 = 0.97$) for the formation of product **5** was reported.⁵ Further analysis of their data however indicate that the data points used between $t = 0$ minutes and up to $t = 300$ minutes for the product formation rate show a weak linear correlation. Particularly, a deviation was observed for the electron-rich 4-methoxy substituted *N*-oxide, where a significantly slower formation rate is obtained using the initial reaction rates in comparison to the reported rate. For the reaction between *N*-oxides **1a-e** and bromopyridine **2a** or bromobenzene **3a**, the obtained Hammett plot does not show a linear correlation of reaction rate versus σ -value (see Experimental section, 4.6.3). A nonlinear Hammett correlation can indicate that a change in mechanism for different substituents is present.⁴⁵ However, in the direct arylation of *N*-oxides **1**, it is feasible that the formation of side-products influence an active catalytic species and therefore affecting the obtained reaction constant.

Comparison of the product formation graphs for the reaction of *N*-oxides **1a-e** reveals a difference in the shape of the formation curves. In the reaction between electron-poor *N*-oxides **1d** and **1e** and **2a**, product formation is linear until $t = 120$ minutes. Linearity was also observed for the analogous reaction between **1d** and **1e** with bromobenzene **3a** (see Experimental section 4.6 for detailed plots). For reactions with **1a-c** with **2a** and **3a**, there is a pronounced difference in the product formations (figure 1.2, left). Reactions with bromopyridine **2a** exhibit a sigmoidal graph for the formation of bipyridine *N*-oxide **4**. A slight induction period was observed prior to a constant formation between approximately $t = 20$ minutes to $t = 60$ minutes. Afterwards, the formation rate decreased and after $t = 120$ minutes until the last sample was withdrawn after 24 h, less than 10% of product was formed. In contrast, no decrease in formation rate was observed after 120 minutes for arylation of **1d**, **e** with bromopyridine **2a** (not shown). A sigmoidal shape is often associated with an autocatalytic behavior of the reaction.⁴⁴ However, later experiments (see section 1.3.3) showed that addition of independently prepared side products did not increase the rate of bipyridine *N*-oxide **4** formation, deeming autocatalysis unlikely. In comparison, arylations with bromobenzene **3a** exhibited an almost linear formation of product **5** for reactions with **1a-c** (figure 1.2, right). Between $t = 120$ minutes and 24 h, 30-50% of arylpyridine *N*-oxide product **5** was formed.

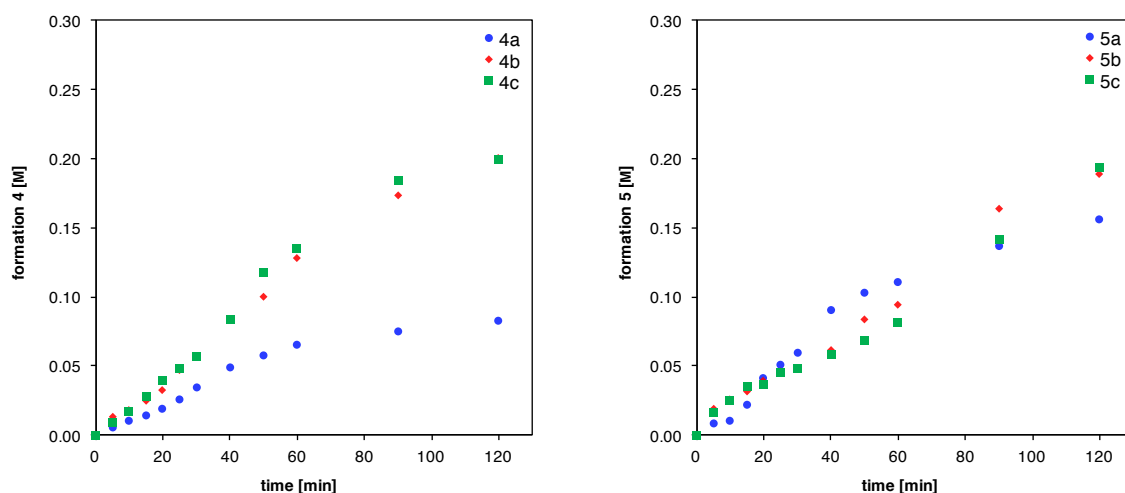


Figure 1.2. Graphs of initial formation rates of cross-coupled product **4a-c** (left) and **5a-c** (right) until $t = 120$ minutes.

These results indicate a catalyst inhibition or deactivation process associated with bromopyridine **2a**. As the analogous reaction with bromobenzene **3a** does not exhibit the same behavior, it is likely due to a coordination or deactivation initiated by a nitrogen-containing substrate or (side)product. After 24 h of reaction, the aryl halide was completely consumed in all arylation reactions, with the exception of the reaction between *N*-oxide **1a** and **2a**. This indicates that an inhibition of the active catalyst by **2a** does not prevent the complete consumption of aryl halide. Monitoring the ratios of phosphorus species formed over the course of the reaction between *N*-oxide **1c**, **1d** and **2a** or **3a** has previously been performed by Sina Zucker.⁴² Multiple reactions were set up in NMR tubes simultaneously and quenched by cooling down at pre-determined time intervals. This gave an overview of the dominating phosphorus species at different time points of the reaction. In all four reactions, a main phosphorus species with a shift of $\delta = -9.2$ ppm was observed. The peak was assigned to a cyclometalated complex **B**, analogous to complex **A** but with bridging bromides instead of acetates. In reactions between unsubstituted *N*-oxide **1c** and CO₂Et-substituted *N*-oxide **1d** with bromobenzene **3a**, the species at $\delta = -9.2$ ppm was the predominant species up until 120 minutes. In comparison, in the analogous reaction between *N*-oxide **1c** or **1d** and bromopyridine **2a**, the cyclometalated species was consumed after 30 minutes for **1c** and after 60 minutes for **1d**. In general, new unidentified phosphorus containing species were formed in the reactions with bromopyridine **2a** that were not found in reactions with bromobenzene **3a**.⁴² The extended presence of a potential catalytically active species in reactions with bromobenzene **3a** supports the hypothesis of a faster decomposition of the active catalyst in reactions with bromopyridine **2a**. Decomposition could mean formation of palladium black or other inert palladium species or an irreversible binding of an unknown nitrogen ligand, preventing further reaction with a substrate or preventing transmetalation of with **I-2**.

Formation graphs of bipyridine **8c** show that in reactions with *N*-oxides **1a-c**, the reaction is initially fast and subsequently decelerates with the decrease in concentration of **2a** (figure 1.3, left). The initially fast formation rate of bipyridine **8c** is suggesting that the homocoupling of bromopyridine **2a** to bipyridine **8c** is initially competing with transmetalation of pyridyl *N*-oxide palladium intermediate **I-2**. In reactions of *N*-oxide **1d** and **1e**, homocoupling is initially competing with cross-coupling, however, already after 15 minutes the homocoupling rate of **8c** decelerates. A faster C–H bond cleavage of the more reactive *N*-oxides **1d** and **1e** results in a more efficient competition with a homocoupling pathway.

An opposite trend was observed for the formation of biphenyl **9a** (figure 1.3, right). During the initial 30 minutes of reaction, a formation rate close to zero was observed. Subsequently, homocoupling product **9a** forms with a constant reaction rate. Phenyl palladium complexes **14** bearing a bulky $P(t\text{-Bu})_3$ ligand have previously been shown to undergo homocoupling to the biphenyl product as a side reaction in a palladium-catalyzed arylation reaction of α -silyl nitriles with substituted bromobenzenes.⁴¹ Also subjecting phenyl palladium complexes **14** to heat promotes decomposition to homocoupling product **9**.⁴⁶ However, under the direct arylation conditions of pyridine *N*-oxides, even in reactions where the C–H bond activation is slow, the cross-coupling reaction efficiently competes with the homocoupling reaction.

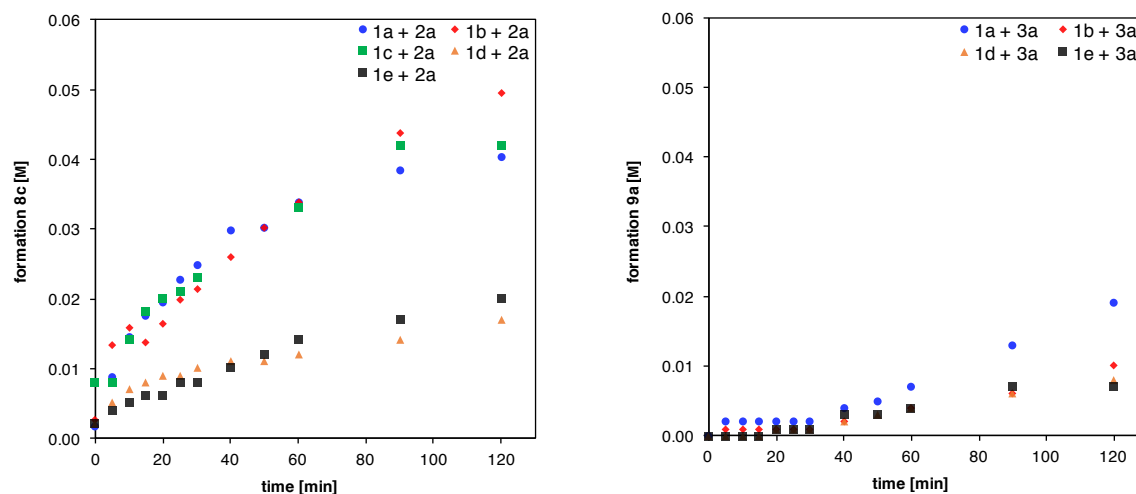


Figure 1.3. Graphs of initial formation rates of bipyridine homocoupling product **8c** (left) and biphenyl homocoupling product **9a** (right). **9a** in the reaction of **1c** + **3a** not determined due to signal overlap.

To test if the homocoupling of bromopyridine **2a** to bipyridine **8c** is a catalyzed process, a reaction between pyridine *N*-oxide **1c** and bromopyridine **2a** in the absence of palladium catalyst was set up (figure 1.4). After 24 h, no change in concentration of either starting material **1c** or **2a** was observed, clearly showing that the formation of bipyridine **8c** is a palladium-catalyzed process.

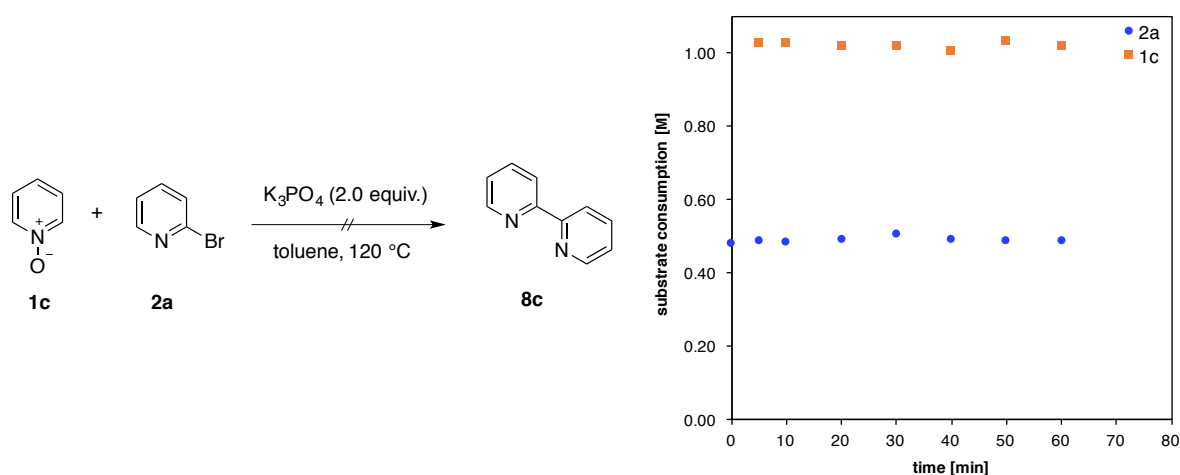
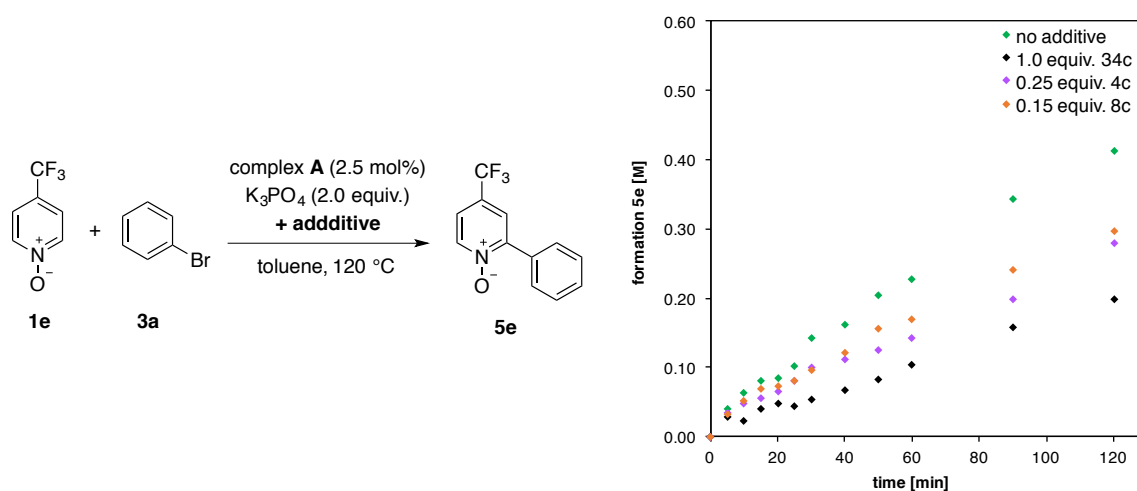


Figure 1.4. Kinetic measurement of the reaction between *N*-oxide **1c** and bromopyridine **2a** in the absence of palladium complex **A**. Pyridine *N*-oxide 7.0 mmol, aryl halide 3.5 mmol.

1.3.2 Inhibition of active catalyst

To obtain further insight into the influence of products and side products on the reaction rates, independent inhibition experiments were set up. In the reaction of CO₂Et-substituted *N*-oxide **1d** with aryl halide **2a** and **3a**, experiments showed that the electrophile does not influence the reaction rate.³⁹ However, only the consumption rate of aryl halide was monitored and no product or side-product formation rate was determined. Bromopyridine starting material **2a**, direct arylation bipyridine *N*-oxide product **4** or two-fold arylated product **6** as well as bipyridine homocoupling product **8c** all contain Lewis-basic nitrogen atoms that could coordinate to the catalyst, forming pyridine or bipyridine palladium complexes. Palladium complexes with bipyridine ligands are well known catalyst for various cross-coupling reactions,⁴⁷ however might not be active catalysts in the C–H activation of pyridine *N*-oxides **1**.

As model reaction, the reaction between CF₃-substituted *N*-oxide **1e** and bromobenzene **3a** was chosen. The yield of arylated pyridine *N*-oxide **5e** in the non-inhibited reaction was 80% and only a small amount of side products were obtained. The substrate consumption and product formation rates were monitored via ¹H NMR analogously to the previous kinetic experiments. Due to the reactivity of **2a**, pyridine **34c** was chosen as a surrogate to investigate the potential starting material inhibition. Furthermore, unsubstituted bipyridine *N*-oxide **4c** and 2,2'-bipyridine **8c** were chosen as inhibiting agents and added in sub-stoichiometric amounts to mimic the catalytic reaction conditions (figure 1.5).



additive	yield 5e	k_{obs}	inhibition
	[%]	[mM/min]	[mM/(min·equiv.)]
none	83	3.7	-
34c (1.0 equiv.)	76	1.6	2.3
4c (0.25 equiv.)	79	2.2	6.7
8c (0.15 equiv.)	75	2.7	9.1

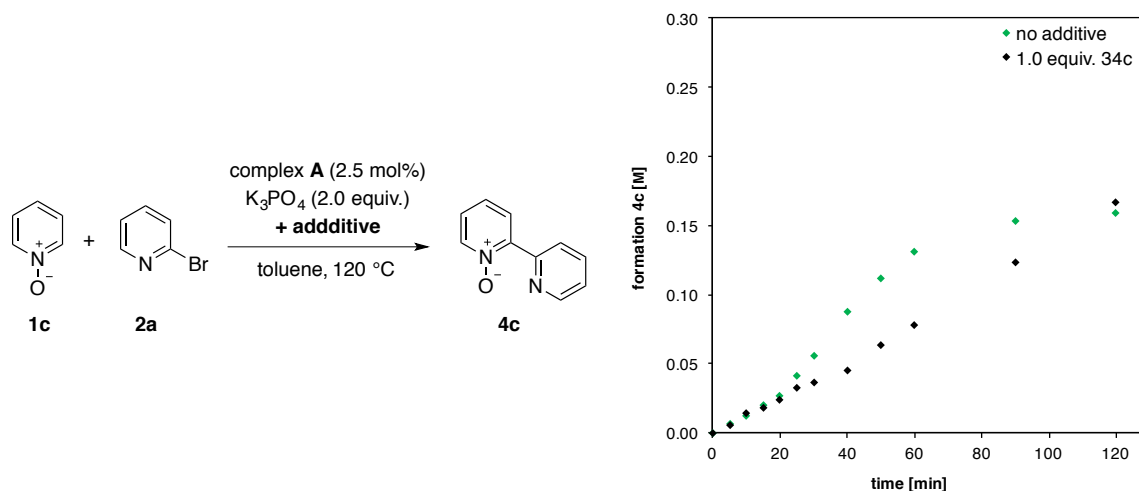
Figure 1.5. Kinetic measurement of arylation of pyridine *N*-oxide **1e** with bromobenzene **3a** and coordinating additives. Pyridine *N*-oxide 7.0 mmol, aryl halide 3.5 mmol.

All nitrogen-containing compounds inhibited the reaction rate. The largest effect was observed in the reaction where 1.0 equivalent of pyridine **34c** was added, where the formation rate of **5e** decreased from $k_{\text{obs}} = 3.7$ mM/min to $k_{\text{obs}} = 1.6$ mM/min. Addition of 0.25 equivalents of bipyridine *N*-oxide **4c** and 0.15 equivalents of 2,2'-bipyridine **8c** both decreased formation rate of **5e** to $k_{\text{obs}} = 2.2$ mM/min and $k_{\text{obs}} = 2.7$ mM/min, respectively. However, extrapolating the rate with **4c** and **8c** added to 1.0 equivalent indicates that the largest inhibition is in fact exerted by bipyridine **8c**. Although slower formation rates were observed, the yield of cross-coupled product **5e** was only slightly affected by the inhibiting agents. As expected, the consumption rate of **3a** also decreased with the addition of inhibitor. The rate of consumption and rate of formation changes linearly with additives, indicating that the binding of nitrogen heterocycles does not lead to a faster formation of side products. Accordingly, all three inhibitors decreased the formation of **9a** to less than half of the rate for the reaction with no additive (see Experimental section, 4.6.4).

It is known that pyridine **34c** reacts with an aryl palladium(II) complexes by displacing a ligand to give a monomeric complex bearing two pyridine ligands.^{42,48,49} However, an analogous reaction with a pyridyl palladium(II) complex **12** and pyridine **34c** results in a dimeric complex with a bridging

$\mu\text{-C}^2\text{,N}$ ligand (see Chapter 2). Conceivably, these two different species formed with an inhibiting agent exhibit different reactivity in a homocoupling or transmetalation pathway.

To further test the inhibitory effects, an experiment between the electron-rich *N*-oxide **1c** and bromopyridine **2a** and 1 equivalent of pyridine **34c** was set up (figure 1.6).



additive	yield 4c [%]	k_{obs} [mM/min]	inhibition [mM/(min·equiv.)]
none	40	2.5	-
34c (1.0 equiv.)	38	1.1	2.4

Figure 1.6. Kinetic measurement of arylation of pyridine *N*-oxide **1c** with bromopyridine **2a** and coordinating additive. Pyridine *N*-oxide 7.0 mmol, aryl halide 3.5 mmol.

Pyridine as an inhibiting agent showed to slow down the formation of product **4c** from $k_{\text{obs}} = 2.5$ mM/min for the non-inhibited reaction to $k_{\text{obs}} = 1.1$ mM/min with the addition of **34c**. As expected, the consumption of **2a** is approximately twice as fast for the non-inhibited reaction in comparison to addition of **34c** (see Experimental section 4.6.4). Regarding the yield of bipyridine *N*-oxide **4c**, very similar yields were obtained in the non-inhibited reaction and with pyridine **34c** added (38% and 40%, respectively). The inhibitory effect of pyridine **34c** was approximately the same for the reaction between *N*-oxide **1e** and bromobenzene **3a** as for the reaction between *N*-oxide **1c** and bromopyridine **2a**. In both inhibition experiments, the rate of formation of product **4c** and **5e** slowed down to approximately 40% of the non-inhibited rate.

Interestingly, the previously observed sigmoidal curve for product formation of **4c** disappeared with addition of pyridine **34c**. The induction period and decrease in rate after 1 h reaction time previously observed is apparently influenced by the addition of a coordinating pyridine compound. However, if

an autocatalytic mechanism was operating, an increase in formation rate of product **4** is to be expected.⁴⁴ Due to that the rate decreased to less than half of the rate with the addition of **34c**, catalysis by dehalogenation product can be ruled out. As shown in Chapter 2, both pyridine **34c** and bipyridine **8c** can displace the P(*t*-Bu)₃ ligand of a pyridyl palladium(II) complex **12**, resulting in a dimeric or monomeric species. Both complexes exhibit higher stability in air and in solution than the parent palladium complex bearing a P(*t*-Bu)₃ ligand. Arguably, the displacement of P(*t*-Bu)₃ by a nitrogen-containing ligand forms a complex which undergoes slower C–H bond activation or slower transmetalation.

Noteworthy, in the initial sample in the reaction of 4-*tert*-butylpyridine *N*-oxide **1a**, reduced 4-*tert*-butylpyridine **34a** was present in approximately 40 mM concentration. This corresponds to approximately 0.1 equivalent in regard to aryl halide and it is stemming from incomplete oxidation in the preparation of the starting material. The arylation of *N*-oxide **1a** exhibited a slower product formation rate of bipyridine *N*-oxide **4a** in comparison to arylpyridine *N*-oxide **5a** (see above, table 1.2). Generally, a faster formation of bipyridine *N*-oxide **4** in comparison to arylpyridine *N*-oxide **5** was observed. The deviation of reactions with *N*-oxide **1a** from this trend might be due to the presence of coordinating **34a**. In the other reactions, such high concentrations of pyridines **34** are only reached after 120 minutes of reaction.

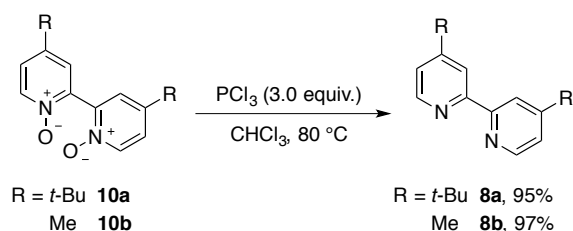
The inhibition experiments show that coordinating starting material or (side)products influence rates of product formation and substrate consumption. Since almost no change in cross-coupled yield was observed with and without inhibitor, nitrogen-containing ligands must either bind reversibly or pyridine or bipyridine-ligated palladium complexes must be catalytically active. Furthermore, pyridine **34c** could also bind to the cyclometalated complex **A**, forming an air stable pyridine-stabilized monomeric species.⁵⁰ Isolation of the side products formed in the reaction of *N*-oxide **1c** and bromopyridine **2a** revealed that in addition to homocoupling products, a bipyridine-coordinated monomeric cyclometalated species was obtained.⁴² Since the monomeric form of complex **A** is proposed to be the active catalytic species undergoing the C–H bond cleavage, binding of pyridine **34c** or bipyridine **8c** would block the free coordination site of monomer **A**. Due to that an open coordination site is required for C–H bond cleavage to take place, a decrease in reactivity of complex **A** would be expected. The fact alone that this complex was isolated by column chromatography indicates its very high stability. If the binding of a pyridine or bipyridine ligand is much faster than the reversible dissociation, the reactivity towards C–H bond cleavage might be influenced.

1.3.3 Quantification of homocoupling products

As outlined above shown, homocoupling products **8c** and **9a** were obtained in yields exceeding the catalyst loading, indicating that the decomposition is a catalyzed process. Because the homocoupling of the aryl halide is an overall reduction, a complementary oxidative process must also take place. In reactions with the electron-poor CO₂Et substituted pyridine *N*-oxide **1d** and bromopyridine **2a**, it has been shown by our group that a homocoupling pathway of pyridine *N*-oxide **1** takes place.⁴² This pathway formed the bipyridine *N,N'*-dioxide product **10d** in 3% yield based on the *N*-oxide starting material. Formation of bipyridine *N,N'*-dioxides **10** from pyridine *N*-oxide **1** via an initial C–H activation and subsequent decomposition of the pyridyl *N*-oxide palladium complex is an overall oxidative process. Homocoupling product **10** could plausibly be formed by the disproportionation of the cyclometalated pyridyl *N*-oxide intermediate **I-2** into a palladium(II) and a palladium(0) complex. This decomposition pathway of **I-2** could explain how the starting palladium(II) species is reduced to the catalytically active palladium(0) in the mechanistic proposal (section 1.2.4, scheme 1.13). The assumption is that the yield of the homocoupling products **8c**, **9a** and **10** is the same, if they are formed by linked redox cycles.

For *N,N'*-dioxide **10d**, isolation by column chromatography with polar solvent proved effective. However, isolation of *N,N'*-dioxides **10a-c** bearing electron-rich substituents was more complicated. Due to the increase in basicity of **10** with electron-donating groups, the products tended to bind strongly to the slightly acidic silica gel.⁴² Quantification of *N,N'*-dioxide **10** via ¹H NMR under the catalytic reaction conditions is also complicated due to the low concentration of **10** in comparison to cross-coupling products **4** and **5**. Additionally, the ¹H NMR signals of *N,N'*-dioxide **10** tend to overlap with those of the starting materials of the reaction. Since quantification of bipyridines **8c** from homocoupling of bromopyridines was straightforward via GC-FID, it was envisioned that converting the *N,N'*-dioxide products **10** into the corresponding bipyridines **8** would open up for quantification via GC-FID. As shown in section 1.2.3, various protocols to deoxygenate the *N*-oxide moiety have been described. Since for quantification purposes, the procedure for deoxygenating **10** to the bipyridine derivative **8** must be easily reproducible and reliably give complete conversion, different conditions were screened. 4-*tert*-Butyl and 4-methyl-substituted 2,2'-bipyridines **8a** and **8b** were oxidized with H₂O₂ in AcOH to the corresponding *N,N'*-dioxide compounds **10a** and **10b** in high yields.⁵¹ First, reduction with H₂ or HCOONH₄ with Pd/C as heterogeneous catalyst was tested, however did not give reproducible yields of bipyridine **8**. The variance in yield was found to be due to the adsorption of **8** on the palladium surface, deeming Pd/C a poor choice of method. Reduction with PCl₃ in a chlorinated solvent is described to readily reduces mono or dioxidized bipyridine substrates **4** and **10**.³⁶ Applying 3 equivalents of PCl₃ in CHCl₃ at 80 °C with the dioxides **10a** and **10b** gave almost quantitative yield of

bipyridines **8a** and **8b**, respectively (scheme 1.15), deeming a PCl_3 deoxygenation method as useful for the quantification experiments.



Scheme 1.15. Reduction of bipyridine *N,N*-dioxide **10a** and **10b** with PCl_3 .

Aryl halide and pyridine *N*-oxide homocoupling products **8c**, **9a** and **10** were quantified simultaneously from the same substrate pairs as for the kinetic analysis. Cross-coupling of the formed *N,N'*-dioxide via a second C–H activation forming terpyridine *N,N'*-dioxides or quarterpyridine *N',N''*-dioxides has previously been observed.⁴² However, the yield of such species should be low and is hence disregarded. The direct arylation reactions were set up under the same conditions as shown above. After 24 h, the toluene mixture was diluted with CHCl_3 and filtered through a glass frit to remove potentially interfering base residues. Decane as an internal standard and PCl_3 (3 equiv.) were added. After heating until no *N,N'*-dioxide **10** was observed by TLC, a short workup consisting of quenching with aqueous base, followed by extraction with a minimum amount of DCM was performed. The yield of homocoupling products **8c**, **9a** and **10** was quantified by GC-FID. The yield of cross-coupled product was not determined in these experiments. An overview of the homocoupling yields of **8c**, **9a** and **10** is shown side-by-side figure 1.7. Because 2 equivalents of **1a–e** and 1 equivalent of **2a** and **3a** are employed, no percentage yield based on starting material is calculated but amounts are given in μmol . In the reaction between pyridine *N*-oxide **1c** and bromopyridine **2a**, the aryl halide homocoupling product **8c**, reduced *N,N'*-dioxide **10c** and reduced cross-coupled product **4c** are the same compound. To get an approximate yield of all products, the yield of aryl halide homocoupling product **8c** was determined prior to reduction. After reduction, the yield of **8c** and the yield of cross-coupled product **4c** was subtracted from the amount obtained from the GC-FID measurement, result in an estimation of the yield of *N,N'*-dioxide **10c**.

As stated above, the homocoupling of aryl halide and pyridine *N*-oxide are expected to give the same amount of respective homocoupling product **8c**, **9a** and **10**. For the arylation reactions with bromopyridine **2a**, the amount of *N*-oxide homocoupling product **10** is similar to that of the homocoupling bipyridine **8c** formed from the bromopyridine substrate. Reactions with electron-rich **1a–c** produced lower yield of **10a–c** in comparison to aryl halide homocoupling **8c** whereas the rest of the reactions give nearly matching yields of **8c** and **10** (figure 1.7, left).

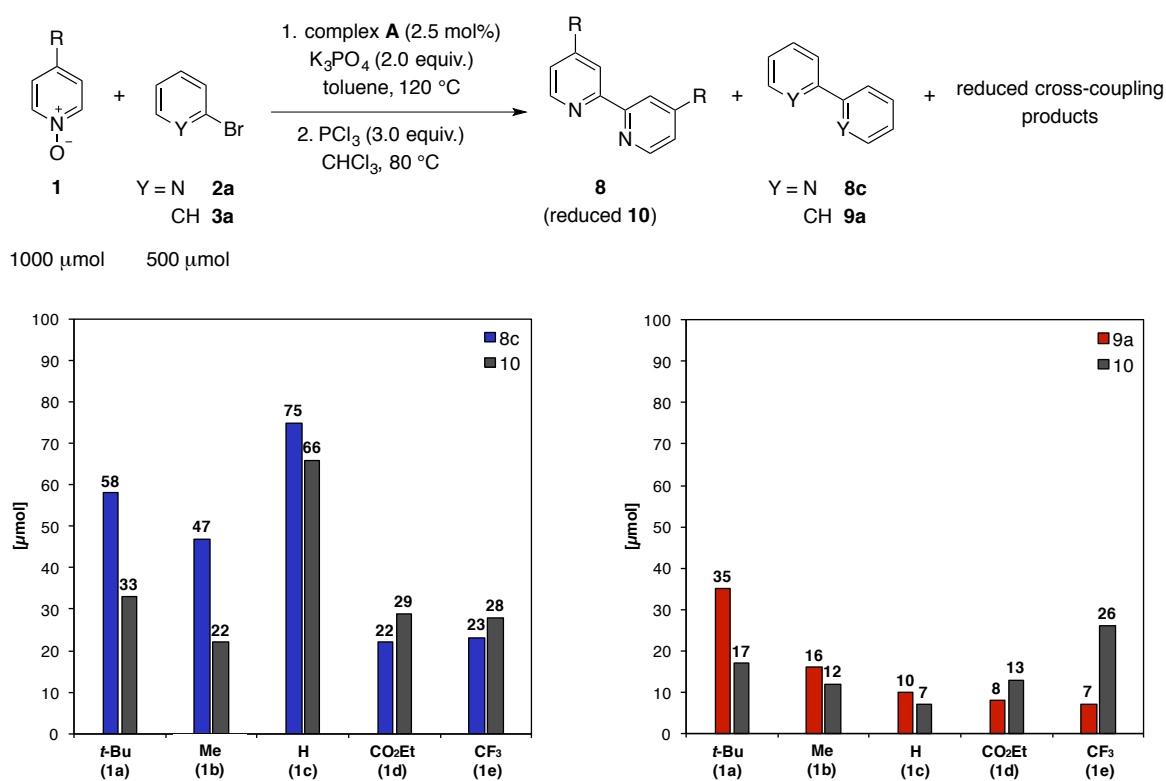


Figure 1.7. Quantification of homocoupling products **8c**, **9a** and **10** from catalytic reactions. *N,N'*-dioxide **10** was reduced to bipyridine **8** and yield of homocoupling products determined by GC-FID with decane as internal standard. *N,N'*-dioxide homocoupling product **10** and aryl halide homocoupling product **8c** and **9a** plotted side-by-side for comparison.

For the arylation reactions with bromobenzene **3a**, similar yields of both homocoupling products **9a** and **10** were obtained in the reaction with *N*-oxides **1b-d** (figure 1.7, right). However, for *N*-oxide **1a** and **1e**, a difference in homocoupling products was observed. The origin of the error was not thoroughly investigated. Even though the independent reduction of isolated **10a** and **10b** gives almost quantitative conversion to **8a** and **8b**, it can be envisioned that catalyst or base residues in the crude reaction mixture might influence the reduction. Arguably, the differences observed arise from limitations in the deoxygenation protocol rather than reflecting a significant deviation of the two homocoupling reactions.

Due to that the homocoupling product yields in the reaction between *N*-oxide **1c** and bromopyridine **2a** are determined via subtraction, an additional experiment was performed. Instead of bromopyridine, 2-bromo-4-methylpyridine was used as substrate in the reaction with pyridine *N*-oxide **1c** and the reaction mixture subsequently subjected to the deoxygenation protocol. The yield of bipyridine product **8c** arising from the homocoupling of *N*-oxide **1c** after deoxygenation and bipyridine **8b** arising from the homocoupling of the aryl halide was determined via GC-FID (figure 1.8).

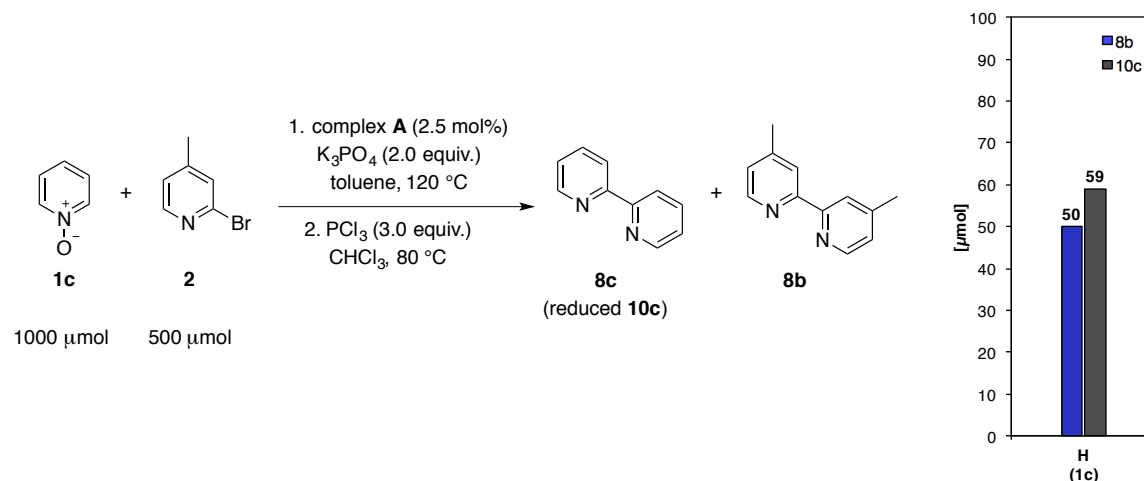
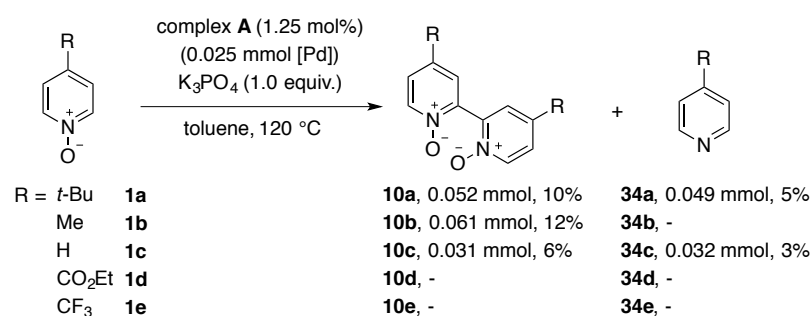


Figure 1.8. Homocoupling products formed from the reaction between pyridine *N*-oxide **1c** and 2-bromo-4-methylpyridine. Yields determined by GC-FID.

Expectedly, the both homocoupling products were obtained in similar yields (59 μ mol versus 50 μ mol). This observation is in accordance with the hypothesis that the homocoupling reactions of *N*-oxide and aryl halide are linked redox-reactions. For all above-shown quantifications of homocoupling product, no determination of formation rate or at what stage of reaction *N,N'*-dioxide **10** is formed was performed. However, it is feasible that the initial step of the catalyst activation is C–H bond cleavage followed by the homocoupling of **I-2** to generate an active palladium(0) species required for oxidative addition.

Homocoupling of the pyridine *N*-oxide substrate **1** has not previously been reported as a side-product in the direct arylations of *N*-oxides **1**. To test if the pyridine *N*-oxide homocoupling pathway also takes place in absence of aryl halide, control experiments were performed (scheme 1.16). The reactions were set up like the analogous kinetic reactions and the ratio of products after 24 h was determined via 1H NMR spectroscopy. In addition to *N,N'*-dioxide **10**, deoxygenation of the starting material **1** to the pyridine analogue **34** was observed. No reduction of *N,N'*-dioxide **10** to bipyridine **8** was detected.



Scheme 1.16. Reaction of pyridine *N*-oxide **1** (1.0 mmol) forming bipyridine *N,N'*-dioxide **10** and reduced starting material **34**.

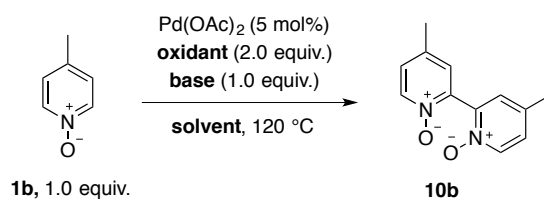
In the reactions with electron rich pyridine *N*-oxide **1a-c**, homocoupling to the *N,N'*-dioxide **10** was observed in around 10% yield. Since the amount of **10** exceeds the amount of palladium complex, it can be deduced that the homocoupling pathway is a catalyzed process and not only a decomposition of the pre-catalyst. For the electron-poor pyridine *N*-oxides **1d** and **1e**, no homocoupling product was observed. From this experiment, it can be concluded that the formed intermediate **I-2** with a *t*-Bu, Me or H substituted pyridyl *N*-oxide ligand are more prone to undergo homocoupling with another **I-2** species than a palladium intermediate with a CO₂Et or CF₃ substituted pyridyl *N*-oxide ligand. The absence of **10d** and **10e** in the control experiments indicates that an additive might induce the decomposition pathway to **10**. Since coordinating bipyridine **8c** is present in the reactions of electron-rich *N*-oxides **1** to a larger extent than in reactions with electron-poor *N*-oxides **1**, it can be envisioned that **8c** promotes decomposition of **I-2**. Furthermore, the presence of dehalogenated or deoxygenated starting material **34** or the bromopyridine substrate itself **2a** might also play a role in the decomposition of the pyridyl *N*-oxide complex. This would further explain the observation that more homocoupling product is formed in the reactions with electron-rich *N*-oxides **1**.

Since *N,N'*-dioxide **10** is formed in amounts exceeding the amount of initial palladium(II) despite the absence of homocoupling of aryl halide, another oxidation process must be present. Possibly, the deoxygenation of *N*-oxide **1** to the pyridine analogue **34** provides the required oxidizing equivalents. In the reactions with *N*-oxides **1a** and **1c** in scheme 1.16, reduced starting material **34a** and **34c** was observed in approximately the same amount as homocoupling product **10**. The phosphine ligand is a potential reducing agent that could deoxygenate *N*-oxide **1**. However, no simultaneous reduction of **10** and oxidation of P(*t*-Bu)₃ was observed in the control experiments (see Experimental section, 4.10.8), indicating that the reduction is a process involving more species than dioxide **10** and complex **A**. In the reaction of *N*-oxide **1b**, reduced **34b** was not observed. The reason is likely signal overlap of the deoxygenation product with the signals of homocoupling product or starting material in the ¹H NMR spectrum. In an experiment in the absence of complex **A**, no homocoupling product **10** was detected, ruling out a metal-free base-catalyzed pathway.⁵²

1.3.4 Independent synthesis of bipyridine *N,N'*-dioxide by oxidative coupling

Dehydrogenative cross-couplings between an *N*-oxide substrate and other (hetero)cycles or the coupling between two substrates containing an *N*-oxide moiety via dual C–H/C–H bond activation have been reported.⁵³ A protocol from our group describes the oxidative coupling of *N*-oxides **1** with pyrroles where Cu(II) or Ag(I) additives play a role as both co-catalyst and terminal oxidant.⁵⁴ In the homocoupling of quinoline *N*-oxides catalyzed by a Pd(II) species, the silver additive played a role additionally to being an oxidant of the formed Pd(0) species.⁵⁵ Sanford and co-workers showed by NMR spectroscopy that for the homocoupling of 2-alkylthiophenes, an initial Ag-aryl species is formed as a product of C–H bond cleavage, which would subsequently transmetalate with a Pd(II) species.⁵⁶ Applying O₂ as the terminal oxidant, copper-catalyzed coupling of benzoxazoles and *N*-substituted (benz)imidazoles have been reported.⁵⁷ Other first-row metals such as Mn, Co and Ni can catalyze dimerization of thiazoles and substituted benzene derivatives.⁵⁸ using a directing group as an internal oxidant.⁵⁹ In C–H bond activation reactions, oxime esters⁶⁰ or *N*-oxides⁶¹ can both act as a directing group for the metal catalyst to a proximal C–H bond, as well as an oxidant of the catalyst. This obviates the need for addition of a Ag(I) salt or other oxidant and would simultaneously reduce the *N*-oxide moiety. Kuang and co-workers described the dehydrogenative cross-coupling of *N*-oxides **1** with 2-aryl-1,2,3-triazole *N*-oxides, Pd(OAc)₂ (5 mol%) as catalyst in dioxane and where Ag(I) salts (2 equiv.) were used as oxidants.⁶² Additionally to the unsymmetrical cross-coupled product, homocoupling of the 2-substituted 1,2,3-triazole *N*-oxide was reported in a yield of 30% under the catalytic conditions. Addition of 1 equivalent of pyridine to the reaction mixture increased the amount of homocoupled triazole to 69%, even in the presence of *N*-oxide **1** substrate. Furthermore, the addition of pyridine also resulted in the homocoupling of 2-picoline *N*-oxide **1f** to the *N,N*-dioxide **10f** in 58% yield.⁶² It was later shown that employing the strong KO*t*-Bu as base also resulted in the homocoupling of 2-substituted 1,2,3-triazole *N*-oxides in high yields.^{52,63}

Inspired by the report by Kuang and co-workers,⁶² a short survey of the homocoupling of 4-methyl pyridine *N*-oxide **1b** was attempted (table 1.3, see Experimental section 4.8 for full table). The reactions were set up under argon, employing 1 equivalent of pyridine *N*-oxide **1b** and 5 mol% of Pd(OAc)₂ catalyst. Applying the reaction conditions similar to the reported conditions resulted in a yield of 22% of *N,N'*-dioxide **10b** (entry 1). Compared to the reported yield of 58% for the homocoupling of 2-methyl pyridine *N*-oxide **1f** to *N,N'*-dioxide **10f**,⁶² the yield is surprisingly low. A similar yield was obtained under the direct arylation reaction conditions with the exception that Ag₂CO₃ is used as oxidant instead of an aryl halide (entry 2). Other Ag(I) oxidants did not increase the yield (entry 6-7) Although other oxidative couplings have employed air or O₂ as the terminal oxidant,^{52,64} reactions performed without exclusion of air gave lower yields of **10b** (entry 7-10).

Table 1.3. Screening of conditions for oxidative coupling of pyridine *N*-oxide **1b** to bipyridine *N,N'*-dioxide **10b**.

entry	oxidant	additive/base	solvent	10b [%]
1	Ag ₂ CO ₃	pyridine (34c)	dioxane	22
2 ^a	Ag ₂ CO ₃	K ₃ PO ₄	toluene	21
3	Ag ₂ CO ₃	2,2'-bipyridine (8c)	dioxane	28
4	Ag ₂ CO ₃	4-methyl pyridine (34b)	dioxane	23
5	Cu(OAc) ₂	pyridine (34c)	dioxane	-
6	AgOPiv	pyridine (34c)	dioxane	traces
7 ^b	AgOAc	pyridine (34c)	dioxane	15
8 ^{b,c}	Ag ₂ CO ₃	pyridine (34c)	DMSO	10
9 ^{b,c}	PhI(OAc) ₂	K ₃ PO ₄	DMSO	traces
10 ^{b,c}	Oxone	K ₃ PO ₄	DMSO	traces
11	BQ	K ₃ PO ₄	DMSO	-

^acomplex **A** used as catalyst. ^breaction performed in air. ^ctemperature = 140 °C. Yields calculated by ¹H NMR.

Alternatives to metal oxidants were briefly investigated, however, the organic oxidants applied did not successfully convert *N*-oxide **1b** to *N,N'*-dioxide **10b** (entry 9-11). The highest yield was obtained when adding the coordinating 2,2'-bipyridine ligand **8c**, however, even then only 28% yield of **10b** was obtained. Additionally, the problem with isolation of **10** remained. Electron-rich *N,N'*-dioxide **10b** proved difficult to elute from a silica gel column due to the binding to the slightly acidic silica gel. Furthermore, basic aluminum oxide did not give a desired separation of starting material **1b** and product **10b**. Due to the low yield of *N,N'*-dioxides **10** via an oxidative coupling pathway in addition to the difficulty in isolation, no further attempts on a development of the homocoupling reaction were performed.

1.4 Conclusion

Kinetic investigations on the direct arylation of five different 4-substituted pyridine *N*-oxides **1a-e** with 2-bromopyridine **2a** exhibited a clear trend in yield of the cross-coupling bipyridine *N*-oxide product **4**. Reactions between electron-rich *N*-oxides **1a-c** bearing a *tert*-butyl, methyl or no substituent and bromopyridine **2a** gave the bipyridine *N*-oxide products **4a-c** in low yields of 23-49%. In contrast, reactions with *N*-oxides **1d, e** bearing an electron-withdrawing ethyl ester or trifluoromethyl substituent resulted in cross-coupling product **4d, e** in yields around 70%. The analogous reaction between *N*-oxides **1a-e** and bromobenzene **3a** did not exhibit the same trend. Arylpyridine *N*-oxide products **5a-e** were obtained in consequently good yields of 63-83%. Monitoring of the product formation rate of cross-coupling products **4** and **5** showed that no decrease in rate occurred in the presence nitrogen-containing bipyridine *N*-oxide product **4**, indicating that no inhibition by product **4** is present. In contrast, formation of bipyridine *N*-oxide product **4** exhibited a slightly faster formation rate than the formation of arylpyridine *N*-oxide product **5**, suggesting a faster formation of an active catalytic species.

Under the reaction conditions, homocoupling of the aryl halide substrate **2a** and **3a** was found as a competing side reaction. The influence of this alternative reaction pathway was significant in reactions between electron-rich pyridine *N*-oxides and bromopyridine **2a**. In the reactions of *N*-oxides **1a-c**, the yield of homocoupling of **2a** to give 2,2'-bipyridine **8c** significantly exceeded the catalyst loading. The amount of homocoupling product **8c** is directly related to the substituent on *N*-oxide **1**, increasing in amount where the yield of cross-coupling product **4** is low. Additionally, homocoupling of bromobenzene **3a** resulting in biphenyl **9a** was detected, however, to a much smaller extent than homocoupling of bromopyridine. A faster consumption of bromopyridine **2a** in comparison to bromobenzene **3a** was observed. In all reactions, the aryl halide consumption rate was faster than the product formation rate. The established homocoupling pathway is a plausible explanation for the increase in consumption rate of aryl halide in comparison to product formation rate of biaryl *N*-oxide.

As the homocoupling of aryl halide is a reductive process, a linked oxidative process must occur simultaneously. Identification of additional side products in the direct arylation reaction revealed that homocoupling of pyridine *N*-oxide **1** resulted in a significant amount of *N,N'*-dioxide homocoupling product **10**. *N,N'*-Dioxide **10** is likely produced by the decomposition of a pyridyl *N*-oxide intermediate **I-2**. Homocoupling products **8c**, **9a** and **10** were obtained in roughly the same yield in each reaction, explaining how the active catalyst is regenerated after a homocoupling reaction. The higher yield of bipyridine **8c** than biphenyl **9a** is suggested to be due to the lower stability of a pyridyl palladium complex **12** formed after oxidative addition than the analogous phenyl palladium complex **14**. Combining the lower stability of **12** with a slower C–H bond activation of electron-rich *N*-oxides

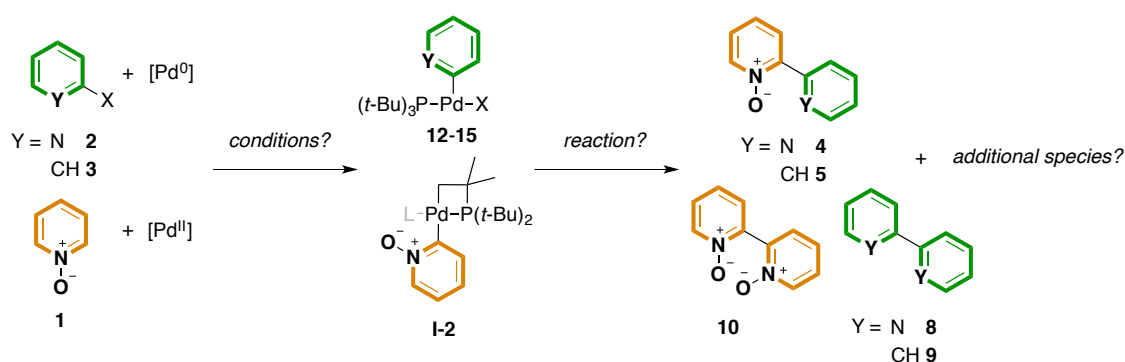
is assumed to lead to an increase in formation of bipyridine **8c** in reactions of *N*-oxides **1a-c**. The mechanistic hypothesis is that the monomeric species formed by dimeric complex **A** undergoes C–H bond cleavage to form a pyridyl *N*-oxide intermediate **I-2**, which subsequently undergoes disproportionation into a palladium(II) and a palladium(0) species and forming the homocoupling product **10**. Subsequently, oxidative addition of aryl halide **2a** or **3a** could take place and an aryl palladium(II) complex would form that can undergo transmetalation with **I-2**.

As a potential explanation for the lower yield of bipyridine *N*-oxide product **4** in comparison to arylpyridine *N*-oxide product **5**, inhibition by nitrogen-containing (side)products was investigated. To the reaction of CF₃-pyridine *N*-oxide **1e** and bromobenzene **3a**, pyridine **34c**, homocoupling product 2,2'-bipyridine **8c** and unsubstituted bipyridine *N*-oxide **4c** were added. All compounds decreased the rate of reaction but none had a significant influence on the yield. An analogous reaction between unsubstituted pyridine *N*-oxide **1c** and bromopyridine **2a** with pyridine **34c** added gave similar results in that the reaction rate was diminished but not the yield. Even though the influence of nitrogen-containing additives has been established, substrate or (side)product inhibition can be excluded as reason for the observed lower yields in the reactions with bromopyridines.

2 Synthesis and Reactivity of Aryl Palladium Complexes in the Direct Arylation of Pyridine *N*-oxides

2.1 Motivation

Three-coordinated aryl palladium(II) complexes bearing only one phosphine ligand have been proposed to form via oxidative addition of an aryl halide to a palladium(0) species prior to transmetalation with an organometallic reagent.⁶⁵ In the direct arylation of pyridine *N*-oxides **1** with bromobenzenes **3**, an unsaturated phenyl palladium(II) complex bearing either a bromide or an acetate ligand undergoes transmetalation with a cyclometalated pyridyl *N*-oxide intermediate **I-2**.^{4,5} In a similar manner, a 2-pyridyl palladium(II) complex is anticipated to form when employing bromopyridines **2a** in the direct arylation of pyridine *N*-oxides **1**. A few examples of 2-pyridyl palladium(II) complexes have been reported,⁶⁶⁻⁶⁹ however no monomeric complex with only one phosphine ligand is described. Therefore, a synthesis forming an unsaturated palladium(II) complex is desirable, not only for the mechanistic studies on the direct arylation of pyridine *N*-oxides, but for other cross-coupling reactions as well. For palladium, an unexplored class of complexes is the pyridyl *N*-oxide-ligated species formed after a C–H activation process. Similar complexes exist for more electropositive metals such as thorium and uranium,⁷⁰⁻⁷² for which the *N*-oxide moiety acts as an additional electron-donating ligand to the metal center to stabilize the complex. A similar stabilization by the *N*-oxide functionality on a palladium(II) center has been calculated,^{5,73} however if it translates to enough stabilization for isolation of the complex is not described. To increase stability of a pyridyl *N*-oxide palladium intermediate **I-2**, an additional ligand L can be added (scheme 2.1).



Scheme 2.1. Outline of the proposed aryl palladium(II) intermediates formed in the direct arylation of pyridine *N*-oxides **1** with bromopyridines **2** and bromobenzenes **3**.

The observation of homocoupling products **8-10** in the direct arylation reaction described in Chapter 1 suggests that both aryl palladium(II) complexes formed after oxidative addition (**12-15**) and C–H activation (**I-2**) undergo homocoupling reactions. Synthesis of the proposed intermediates would allow investigation of their reactivity towards both a transmetalation and a homocoupling pathway. As shown in Chapter 1, direct arylation reactions of pyridine *N*-oxides **1** with bromopyridines **2** resulted in lower yield of cross-coupled product and higher yield of homocoupling product **8** and **10** in comparison to the analogous reaction with bromobenzenes **3**. To probe the differences in reactivity towards decomposition under catalytic reaction conditions, independent thermolysis of the isolated complexes would give information on stability. Furthermore, transmetalation between a pyridyl palladium(II) complexes bearing either a bromide or an acetate anion **12, 13** and a pyridyl *N*-oxide intermediate **I-2** would reveal if there is a difference in reactivity in comparison to the reaction between a phenyl palladium(II) complexes **14, 15** and intermediate **I-2**.

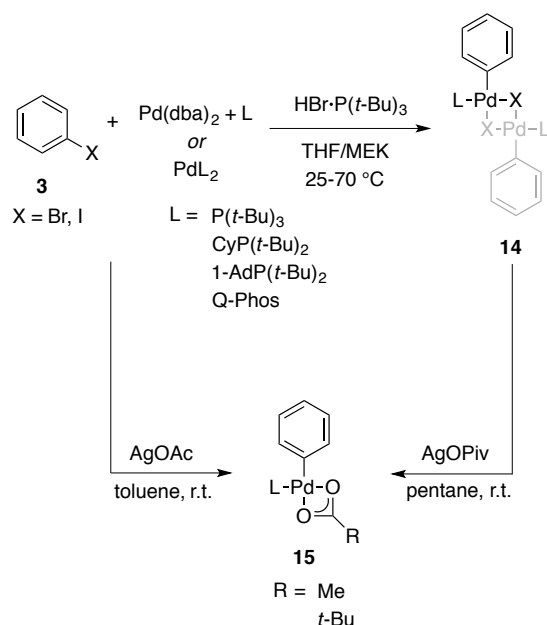
Synthesis of all palladium intermediates proposed in the catalytic cycle would give an overview of how the reactivity changes with substitution pattern and changes depending on the (hetero)aryl ligand. Formation of catalytically active decomposition products has been reported to play a role in the oxidative addition of aryl halides to a palladium(0) complex.⁷⁴ Arguably, similar additives could play a role in a homocoupling reaction as well. Addition of potential catalysts will give further information on the reaction pathways of the palladium complexes.

2.2 Background

2.2.1 Phenyl palladium complexes

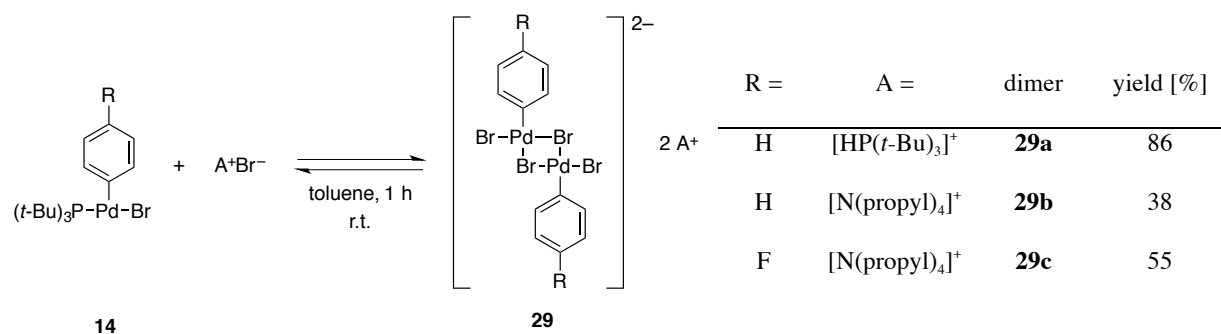
As described in Chapter 1, formation of an aryl palladium(II) complex bearing a bulky $P(t\text{-Bu})_3$ ligand is the initial step in the proposed catalytic cycle of the direct arylation of pyridine *N*-oxides **1**.^{4,5} Furthermore, it has been shown that 14-electron three-ligated palladium complexes are likely intermediates in numerous other cross-coupling reactions as well.⁴⁰ Formation of such complexes is achieved by established procedures. Oxidative addition of an aryl halide species to a phosphine-ligated palladium(0) complex or to a palladium(0) species bearing sacrificial ligands in the presence of the relevant phosphine ligand are the strategies of choice. Substituted aryl halides have been employed and complexes bearing both electron-rich and electron-poor groups have been reported.^{40,42,75}

The first X-ray structure of a monomeric palladium complex bearing one dative phosphine ligand was reported by Hartwig and co-workers.⁴⁰ Oxidative addition of an excess of phenyl halide to $\text{Pd}_2(\text{dba})_3$ was performed, employing 1 equivalent of the sterically demanding phosphine ligand $P(t\text{-Bu})_3$ or 1-AdP(*t*-Bu)₂ (scheme 2.2). Due to an observed Heck-type side reaction of the dba ligand, the reaction conditions were modified employing bisphosphine palladium(0) complex $\text{Pd}(P(t\text{-Bu})_3)_2$ **32** instead. Heating the reactants to 70 °C in the presence of $\text{HBr}\cdot P(t\text{-Bu})_3$ resulted in the 14-electron phenyl palladium(II) complex **14**. Addition of $\text{HBr}\cdot P(t\text{-Bu})_3$ is suggested to promote the oxidative addition (see below). Single crystal X-ray analysis of bromide and iodide-ligated complexes revealed a three-coordinated T-shaped structure without a coordinated solvent or additional ligand. The strongest *trans* donor ligand is the phenyl group and was observed to be opposite to the open coordination site. This leaves the most sterically demanding alkyl phosphine ligand at the least hindered position. An agostic interaction between the metal and a C–H from the phosphine ligands results in a square planar geometry of the complex.⁴⁰ Also, complexes with other hindered phosphine ligands such as 2-AdP(*t*-Bu)₂ or Q-Phos were synthesized in the same manner and exhibited T-shaped structures.⁶⁵ However, dimerization has been observed for aryl palladium(II) complexes with chloride and bromide anions bearing $P(t\text{-Bu})_3$, CyP(*t*-Bu)₂ and 1-AdP(*t*-Bu)₂ ligands. Dimeric structures were observed in the solid-state but molecular weight determination via the Signer method indicated that the complexes were monomeric in solution.⁷⁶ In comparison, palladium complexes with an aryl phosphine ligand such as $P(o\text{-tol})_3$ preferentially adopt dimeric structures with one phosphine-ligated to each palladium center.⁷⁷ As explanation, it has been put forward that the palladium-halide bond of the bridging ligand is stronger than the agostic C–H bond interaction with the methyl group of the *ortho*-tolyl ligand.⁷⁸ A less sterically demanding ligand such as PPh_3 gives a monomeric species with two phosphines *trans* to each other on each palladium atom.⁷⁹



Scheme 2.2. Oxidative addition of an aryl halide to a palladium(0) species to generate aryl palladium(II) bromide complex **14** and displacement of bromide generating acetate/pivalate complex **15**.

Acetate-ligated aryl palladium(II) complexes have been synthesized in a similar manner (scheme 2.2). A one-pot reaction with AgOAc added results in the displacement of bromide anion *in situ*, yielding κ^2 -acetate phenyl complex **15**.⁴ Formation of **15** can also be achieved by displacement of the bromide anion from the isolated phenyl complex **14**.⁸⁰ Furthermore, displacement of the phosphine ligand can take place by the addition of a halide source. Hartwig and co-workers reported that addition of trialkylphosphonium halide or tetraalkylammonium halide to an isolated aryl palladium(II) complex **14** bearing an aryl ligand resulted in the fast formation of a dianionic dimeric $[(\text{Ph})\text{Pd}(\text{Br})_2]_2^{2-}$ complex **29** (scheme 2.3).^{80,81} The anionic phenyl complex **29** existed in equilibrium with the neutral starting phenyl complex **14** with a small equilibrium constant K_{eq} . Isolation of anionic complex **29** was promoted by the precipitation of the complex from a nonpolar solvent. X-ray analysis on the solid-state of unsubstituted anionic phenyl dimer **29a** with two $[\text{HP}(t\text{-Bu})_3]^+$ counterions adopt a *trans* orientation of the phenyl groups.⁸¹

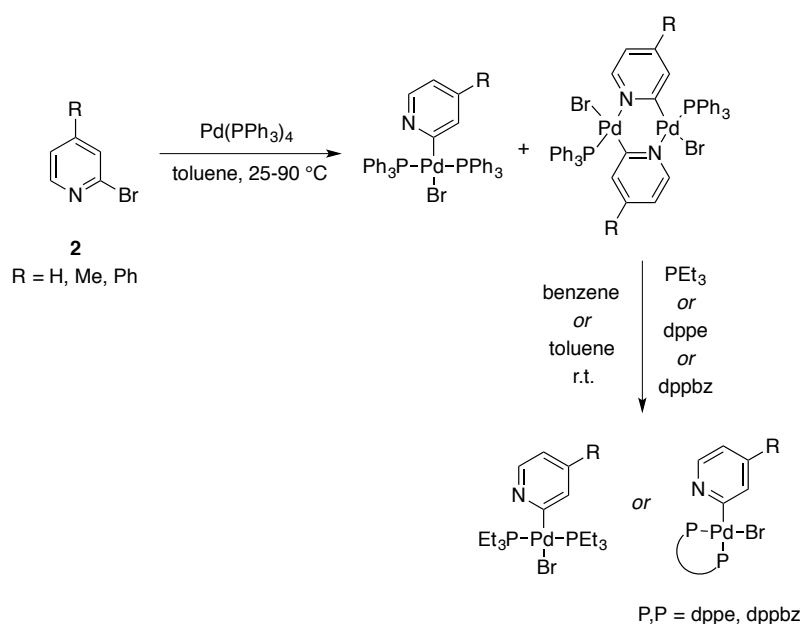


Scheme 2.3. Formation of a dimeric dianionic phenyl palladium(II) complex by displacement of phosphine ligand by a bromide anion.

Anionic aryl complexes have been identified as active catalytic species in Heck reactions,⁸¹⁻⁸³ where coordination or insertion of an alkene would be favored by a “ligandless” complex due to it being less hindered. Furthermore, anionic complexes have been proposed as active intermediates in Suzuki-Miyaura coupling reactions when employing polar additives. Due to an increase in nucleophilicity of an anionic palladium complex, oxidative addition towards an aryl (pseudo)halide would be accelerated.⁸⁴ In fact, anionic phenyl complex **29** is suggested to activate the C–H bonds of benzene faster than a neutral aryl palladium acetate complex **15** bearing a hindered P(*t*-Bu)₃ phosphine ligand.⁸⁰

2.2.2 Pyridyl palladium complexes

As opposed to palladium(II) complexes with phenyl substituents, reports on 2-pyridyl palladium(II) complexes are sparse. Cid and co-workers reported a reaction between 2-bromo-4-phenylpyridine and Pd(PPh₃)₄ in toluene at 25 °C which resulted in a monomeric 2-pyridyl palladium complex bearing two PPh₃ ligands *trans* to each other (scheme 2.4).⁶⁹ The palladium atom in (2-pyridyl)Pd(Br)(PPh₃)₂ adopt a square planar configuration where the carbon of the pyridyl group is located *trans* to the bromide.^{66,67} However, the oxidative addition product was obtained as a mixture of the monomeric complex and a dimeric species formed by the coordination of the pyridyl nitrogen to a second palladium center with the concomitant displacement of one PPh₃ ligand. This results in a pyridyl μ -C²,N-bridging complex, which has previously been reported by similar oxidative addition reactions of substituted bromopyridines to Pd(PPh₃)₄.^{66,67,68} It has also been shown that a dimeric structure forms from a monomeric species if left over time in solution. The resulting dimeric complexes exhibit low solubility in organic solvents.^{66,85}

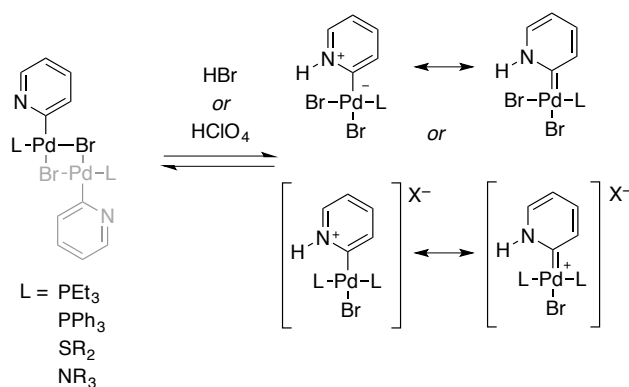


Scheme 2.4. Formation of monomeric or dimeric 2-pyridyl palladium(II) complexes with mono- or bidentate ligands.

Displacement of the PPh_3 ligand from the dimeric complex can be performed by prolonged stirring with an excess of monodentate phosphine ligand such as PEt_3 ,⁶⁸ or bidentate phosphine ligand such as dppe ⁸⁶ or dppbz ⁸⁷ (scheme 2.4). These reports all result in four-coordinated pyridyl palladium(II) complexes. Attempts to isolate a monomeric three-coordinated 2-pyridyl palladium(II) complex **12** with a $\text{P}(t\text{-Bu})_3$ ligand by oxidative addition of 2-bromo-3-methylpyridine to palladium(0) complex **32** resulted in a phosphine-free pyridyl $\mu\text{-C}^2,\text{N}$ -bridging dimer.⁴² Arguably, the monomeric species **12** is initially formed, however undergoes dimerization by coordination of the basic pyridyl nitrogen to a second palladium center in a similar manner as for the PPh_3 -ligated complexes.

For more electropositive metals, examples of monomeric 2-pyridyl palladium complexes are reported. A group of complexes performing C–H activation on pyridines are bent metallocene complexes of group 4 metals, and also lanthanides or actinides. Expectedly, more electropositive metals can better stabilize an electron-withdrawing 2-pyridyl moiety. Thorium and uranium metallocene complexes have been reported to undergo C–H activation of pyridine and forming 2-pyridyl-ligated complexes.^{71,88} Also zirconium or titanium metallocene complexes with Cp or Cp* undergo C–H activation reactions with pyridines to form 2-pyridyl complexes.⁸⁹ These 2-pyridyl complexes often exhibit an η^2 -binding of the pyridyl C,N-atoms to the metal. Likely, the free electron pair of the pyridyl nitrogen stabilizes the metal complex via binding as a dative ligand. A few complexes lacking the metallocene motifs can form similar η^2 -coordinated pyridines, such as mono-Cp* lutetium complexes,⁹⁰ rhenium-PNP hydride complexes⁹¹ or bulky alkoxide or siloxide tantalum complexes.⁹² Although a similar η^2 -binding has been suggested for 2-pyridyl or 2-heteroaryl palladium(II) complexes,^{66,85,93} this binding mode has not previously been reported.

Addition of a bromide nucleophile to a 2-pyridyl palladium(II) complex results in a different outcome in comparison to the phenyl palladium(II) complex **14**. With the addition of HBr, no dianionic dimeric μ -bromide complex was formed, but protonation of the pyridyl nitrogen atom took place, resulting in a carbene-type pyridylidene binding of the pyridyl ligand (scheme 2.5).⁹⁴



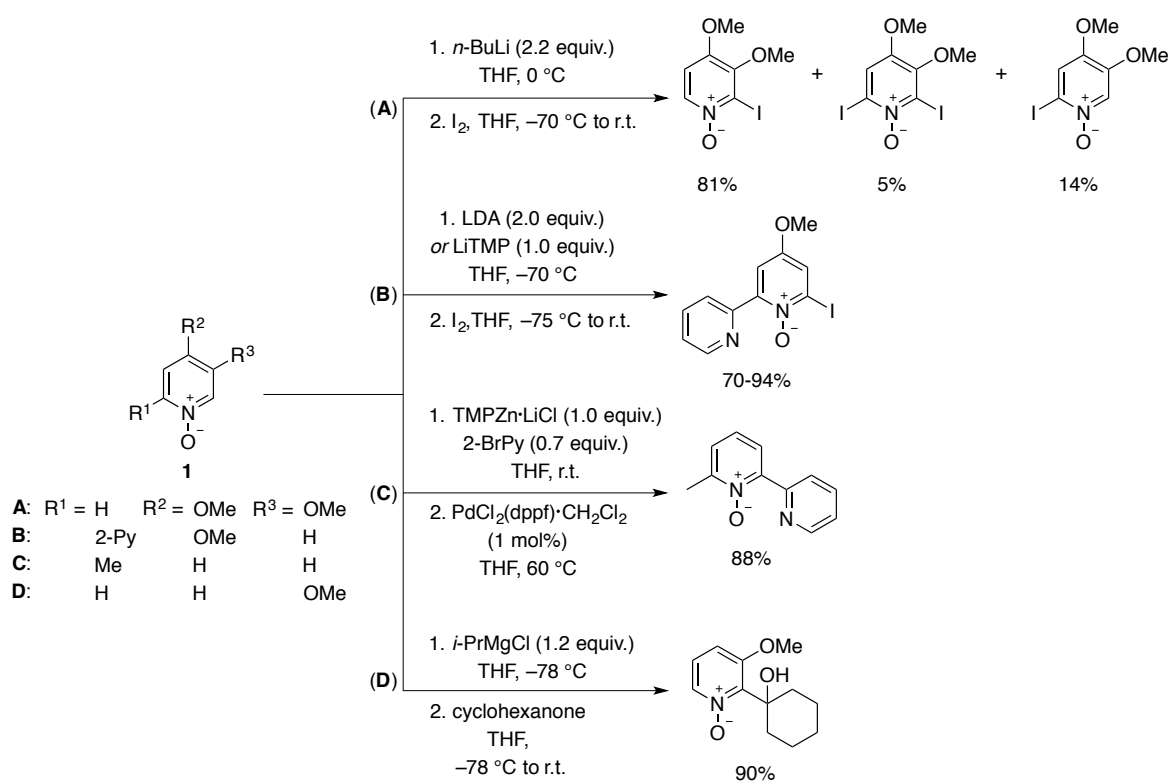
Scheme 2.5. Reaction between a 2-pyridyl palladium(II) complex and an acid inducing a carbene-type binding.

Crociani and co-workers reported that protonation of 2-pyridyl palladium complexes with other Brønsted acids resulted in similar pyridylidene complexes. Protonation of the monomeric complexes (2-pyridyl)Pd(Cl)(PEt₃)₂ or (2-pyridyl)Pd(Cl)(PPh₃)₂ with HClO₄ gave the cationic species (2-pyH)Pd(Cl)(L)₂ with ClO₄ as a counterion.^{68,95} Alternatively, pyridylidene palladium complexes can also be obtained by methylation of the pyridyl nitrogen.⁹⁶⁻⁹⁸ Due to substantial electron donation from the metal center to the pyridyl nitrogen, the basicity of a (2-pyridyl)Pd(Br)(PEt₃) **23** complex has been reported to increase 4 orders of magnitude by metal coordination in comparison to free pyridine.⁶⁸ Quaternization of the pyridyl nitrogen drastically changes the characteristics of the palladium complex. The metal-carbon bond is typically shortened due to more double bond character and a downfield shift of the metal-bound carbon is observed due to decreased electron-density.⁹⁷ This carbene-type bonding of a heterocycle containing only one nitrogen adjacent to the metal-carbon bond has been proposed as a transient intermediate in the rhodium(I)-catalyzed alkylation of a pyridine or quinoline substrate.⁹⁹ Similarly, employing protonated or methylated tetra-coordinated 2-, 3- or 4-pyridyl palladium(II) pre-catalysts showed an increase in activity in Suzuki-Miyaura cross-coupling reactions.^{96,100}

2.2.3 2-Metalated pyridine *N*-oxides

Pyridyl *N*-oxide complexes with metals such as thorium and uranium have been formed via C–H activation reactions,⁷⁰⁻⁷² where the *N*-oxide functional group provide additional stability of the complex by coordination of the free electron pair to the metal. As shown in Chapter 1, the best attempts to investigate the transmetalation between a 2-palladated pyridine *N*-oxide substrate and a three-coordinated aryl palladium complex was performed with the 2-benzothieryl surrogate for intermediate **I-2**. A selective *ortho*-lithiation of benzothiophene was achieved with 1.1 equivalents of *n*-BuLi and subsequent reaction with the cyclometalated palladium complex **B** and PEt₃ yielded the cyclometalated benzothieryl palladium(II) complex stabilized with an additional PEt₃ ligand (see Chapter 1, scheme 1.12).⁴ Arguably, a similar protocol could be employed for the *ortho*-metalation of pyridine *N*-oxides **1** to form a pyridyl *N*-oxide intermediate **I-2** or a phosphine-stabilized species.

Reports on *ortho*-metalation of pyridine *N*-oxides **1** describe a few procedures to yield the 2-metalated species. Similar to electrophilic aromatic substitution, a directing group facilitates either deprotonation by a strong base or stabilization of a 2-metalated species for subsequent reaction with an electrophile. For example, the free electron pair of an *N*-oxide functional group can act as a directing group for a Lewis acidic lithium, a feature that has been proven useful in *ortho*-metalation reactions.¹⁰¹ Deprotonation of unsubstituted *N*-oxides **1** would be favored in 2- or 6-position due to the enhanced acidity of the C–H bonds adjacent to the electron-withdrawing *N*-oxide moiety.¹⁰²



Scheme 2.6. Different protocols for the metalation in 2-position of pyridine *N*-oxides **1**.

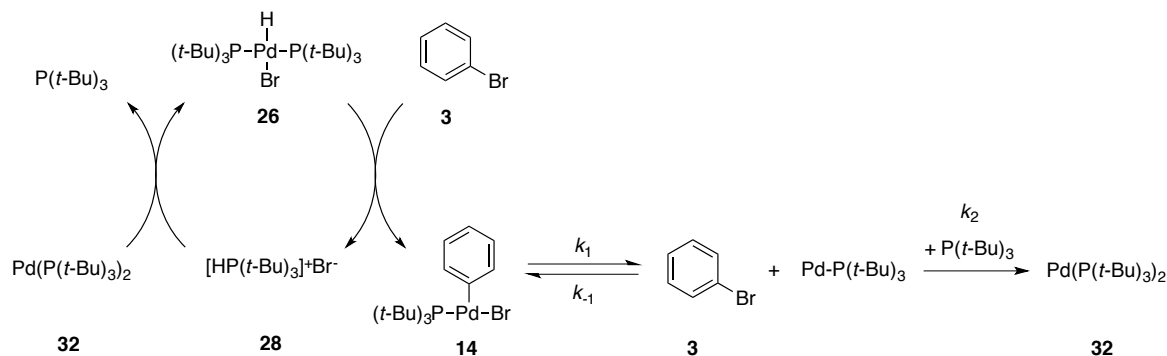
Quéguiner and co-workers showed that 3,4-dimethoxy pyridine *N*-oxide can be deprotonated using 2.2 equivalents of *n*-BuLi at -75 °C. Quenching the lithiated species with I₂ resulted in a mixture of the 2- and 6-iodated products. Due to the directing methoxy group in 3-position, the 2-substituted product was obtained in the highest yield of 81%, whereas the 6-substituted product in a lower yield of 14% (scheme 2.6, **A**).¹⁰¹ In the reported synthesis of Caerulomycins, 4-methoxy 2,2'-bipyridines were deprotonated by 1-2 equivalents of lithium diisopropylamide (LDA) or lithium tetramethylpiperidide (LiTMP) at -70 °C and quenched with I₂. Due to the pyridyl group in 2-position of the substrate, a selective lithiation and subsequent iodation in the desired 6-position was achieved, yielding the 6-iodo bipyridine *N*-oxide in 70-94% (scheme 2.6, **B**).¹⁰³ When employing alkyl substituted pyridine *N*-oxides and strong alkali bases, deprotonation of the benzylic position could also occur.¹⁰⁴ To limit benzylic deprotonation, larger metal reactants such as zinc or magnesium bases have been employed. Gosselin and co-workers applied TMPZnCl·LiCl in THF at room temperature to achieve metalation in 6-position of 2-methyl substituted *N*-oxides as intermediate in the formation of bipyridine *N*-oxides. Following zincation, a palladium-catalyzed Negishi coupling with 2-bromopyridine **2a** in THF at 60 °C furnished the corresponding bipyridine *N*-oxide in 88%. No deprotonation of the benzylic C-H bonds was observed (scheme 2.6, **C**).¹⁰⁵ The procedure was also applicable for zincation of other heteroaromatics such as pyridines, pyrazines and pyrimidines.¹⁰⁶ Additional to the zinc bases, also Grignard reagents have been used for the deprotonation of pyridine *N*-oxides. Almqvist and co-workers reported that 3-, 4-, and 5-substituted pyridine *N*-oxides could be deprotonated in 2-position with 1.2 equivalents of *i*-PrMgCl in THF at -78 °C. 3-Methoxy pyridine *N*-oxide was deprotonated

with the base and the metalated intermediate was quenched by cyclohexanone, yielding the functionalized product in 90% (scheme 2.6, **D**).¹⁰⁷ Furthermore, halogen-lithium exchange with strong lithium bases¹⁰⁸ or *i*-PrMgCl·LiCl Grignard reagents¹⁰⁹ have also been reported for heteroaromatics. A disadvantage is that the reaction of a lithium base with a halogenated aromatic system can induce halogen migration in addition to halogen-lithium exchange.¹¹⁰ Additionally, if a subsequent reaction with an electrophilic palladium(II) center is desired, the presence of alkyl bromides in the reaction mixture might interfere. Although *ortho*-metalation or halogen-metal exchange pathways of (halo)pyridine *N*-oxides have been described, no subsequent reaction with a cyclometalated palladium(II) complex has been reported.

2.2.4 Oxidative addition and reductive elimination

Oxidative addition of an aryl halide to a palladium(0) species is often the initial step of cross-coupling reactions. The rate is dependent on the Ar–X bond strength, implying a faster oxidative addition of an aryl iodide than an aryl chloride.⁴⁶ As shown above, formation of aryl palladium(II) complexes with one bulky P(*t*-Bu)₃ ligand has been reported by oxidative addition of an aryl halide to the Pd(P(*t*-Bu)₃)₂ complex **32** at elevated temperatures. For such complexes, the rate of oxidative addition is dependent on the dissociation of one phosphine ligand prior to oxidative addition when applying aryl chlorides. However, reactions with aryl iodides were suggested to take place directly with the Pd(P(*t*-Bu)₃)₂ **32** species and subsequent dissociation of one ligand.⁷⁶ Anionic additives are proposed to increase the oxidative addition of less reactive aryl halide substrates.⁸² For example, amination of chloroarenes catalyzed by bisphosphine palladium(0) complex **32** is proposed to take place via either oxidative addition to a monoligated Pd(P(*t*-Bu)₃) species or via an anionic [Pd(P(*t*-Bu)₃)(X)][−] species, where X = halide or alkoxide.¹¹¹ A similar result was obtained for the oxidative addition of aryl bromides to palladium(0) complex **32**, where an anionic complex was proposed to undergo reaction with aryl bromide **3** faster than the palladium(0) complex **32** (scheme 2.7). Monitoring the consumption of a 0.040 M solution of **32** with an excess of aryl bromide **3** in toluene at 70 °C resulted in a sigmoidal decay of palladium(0) complex **32** and an autocatalytic reaction mechanism was proposed.⁷⁴ It was shown that oxidative addition of aryl bromide **3** to complex **32** resulted in not only the phenyl complex **14**, but also in the phosphorus-containing decomposition species hydridopalladium bromide complex (H)Pd(Br)(P(*t*-Bu)₃)₂ **26**, palladium(I)-dimer [(P(*t*-Bu)₃)Pd(μ-Br)]₂ **27**, cyclometalated palladium complex **B** and phosphonium salt HBr·P(*t*-Bu)₃ **28**. Addition of 1 equivalent each of the formed phosphorus decomposition species to the oxidative addition reaction revealed that all additives except complex **B** accelerated the consumption of **32**, with hydridopalladium bromide complex **26** exerting the largest effect. Weak bases such as NEt₃ did not quench the autocatalysis, however the strong phosphazene base BTPP significantly decreased the reaction rate. The reaction mechanism was

proposed to involve reversible reductive elimination from hydridopalladium complex **26** resulting in anionic $[\text{Pd}(\text{P}(t\text{-Bu})_3)(\text{Br})][\text{HP}(t\text{-Bu})_3]^+$, which undergoes fast oxidative addition of aryl bromide **3**. The autocatalysis is initiated by the thermal decomposition of phenyl complex **14** to palladium(I)-dimer **27**, which subsequently degrades to complex **26** concomitant with cyclometalation of the phosphine ligand forming complex **B**.⁷⁴



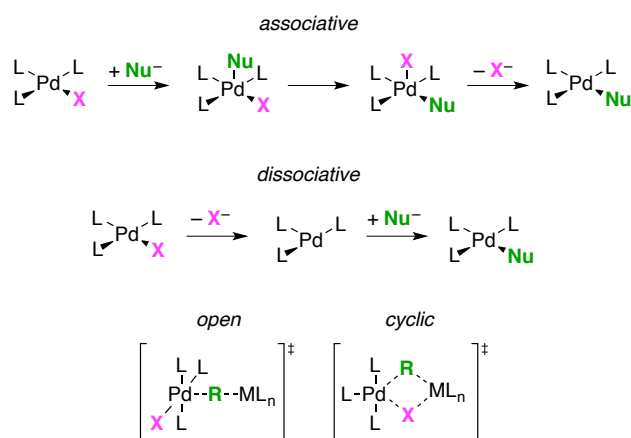
Scheme 2.7. Formation of a T-shaped aryl palladium(II) complex **14** by the reaction between an aryl bromide **3** and hydridopalladium complex **26**. Reductive elimination from complex **14** induced by the addition of $\text{P}(t\text{-Bu})_3$ ligand.

Reductive elimination of aryl halides readily takes place from metal centers in higher oxidation states such as platinum(IV) and palladium(IV).¹¹² The similar process for aryl palladium(II) complexes can be promoted by the addition of a bulky phosphine ligand. Addition of $\text{P}(t\text{-Bu})_3$ to phenyl complex **14** at 70 °C resulted in reductively eliminated aryl bromide **3** from the starting material (scheme 2.7). A first-order dependence on $\text{P}(t\text{-Bu})_3$ and an inverse dependence on aryl bromide was observed. A pathway involving reversible reductive elimination forming the aryl halide **3** and a monoligated $\text{Pd}-\text{P}(t\text{-Bu})_3$ and subsequent trapping of the palladium intermediate by irreversible binding of an additional $\text{P}(t\text{-Bu})_3$ ligand was proposed for the reductive elimination step.⁴⁶ Similarly, the dimeric $[(\text{phenyl})\text{Pd}(\mu\text{-X})(\text{P}(o\text{-tol})_3)]_2$ where $X = \text{halide}$ underwent reductive elimination of haloarene upon addition of $\text{P}(t\text{-Bu})_3$, likely via a two-step process involving ligand exchange forming a monomeric palladium(II) complex and subsequent elimination of aryl halide.⁷⁸ Addition of 15 equivalents of $\text{P}(t\text{-Bu})_3$ converted >95% of the starting dimer **46** to aryl halide **3** and palladium(0) complex **32**. A smaller excess of ligand was required for palladium dimers bearing chlorides in comparison to iodides, indicating that the stronger the C–X bond, the more thermodynamically favorable the reductive elimination.⁷⁸ No reductive elimination was observed from dimer **46** in the absence of added $\text{P}(t\text{-Bu})_3$. The overall yield of reductively eliminated aryl halide **3** was higher in the reaction of monomeric T-shaped aryl palladium(II) complex **14** than the dimeric $[(\text{phenyl})\text{Pd}(\mu\text{-X})(\text{P}(o\text{-tol})_3)]_2$ complex **46**, further supporting the hypothesis that reductive elimination takes place from a three-ligated complex with an open coordination site.^{46,78} Addition of other bulky phosphine ligands such as $\text{PCy}(t\text{-Bu})_2$, 1-AdP($t\text{-Bu}$)₂ and Q-Phos also induced reductive elimination of aryl halide, whereas less bulky ligands such as JohnPhos ((2-biphenyl)di-*tert*-butylphosphine) or an N-heterocyclic carbene did not.⁷⁸

Electron-donating ligands such as $P(t\text{-Bu})_3$ usually favor oxidative addition and electron-withdrawing ligands favor reductive elimination. Therefore, the observation of an increase in reductive elimination product with the addition of bulky alkyl phosphine ligand must be dependent on the sterically demanding nature of trialkylphosphines rather than the electron-donation ability.¹¹³

2.2.5 Transmetalation reactions

Aryl palladium(II) complexes with a d^8 -electron configuration often adopt a $16e^-$ tetra-coordinated square planar geometry. Ligand substitution usually takes place via two different mechanisms, namely an associative or dissociative mechanism.¹¹⁴ In an associative process, an $18e^-$ penta-coordinated complex is formed by attack of the new ligand and subsequent Berry pseudo rotation results in a new species with the X-ligand in apical position. Subsequent release of X^- regenerates a $16e^-$ square planar species. In a dissociative pathway, the metal-ligand bond breaks prior to formation of a metal-nucleophile bond, resulting in a $14e^-$ intermediate. An associate pathway is often favored for palladium(II) complexes due to the instability of such an unsaturated $14e^-$ species. While this pathway is viable for anionic nucleophiles, organometallic species such as organic fragments bound to Mg, B, Si, Sn or Zn typically react with a palladium center via a more complicated ligand transfer process. The ligand exchange is usually described as an electrophilic substitution on carbon and can proceed via an (open) or an (cyclic) transition state (scheme 2.8).¹¹⁵ However, the mechanism can vary greatly depending on the organic group, temperature or solvent. Commonly, the cyclic transition state is proposed when bridging ligands that can induce dimerization are present.



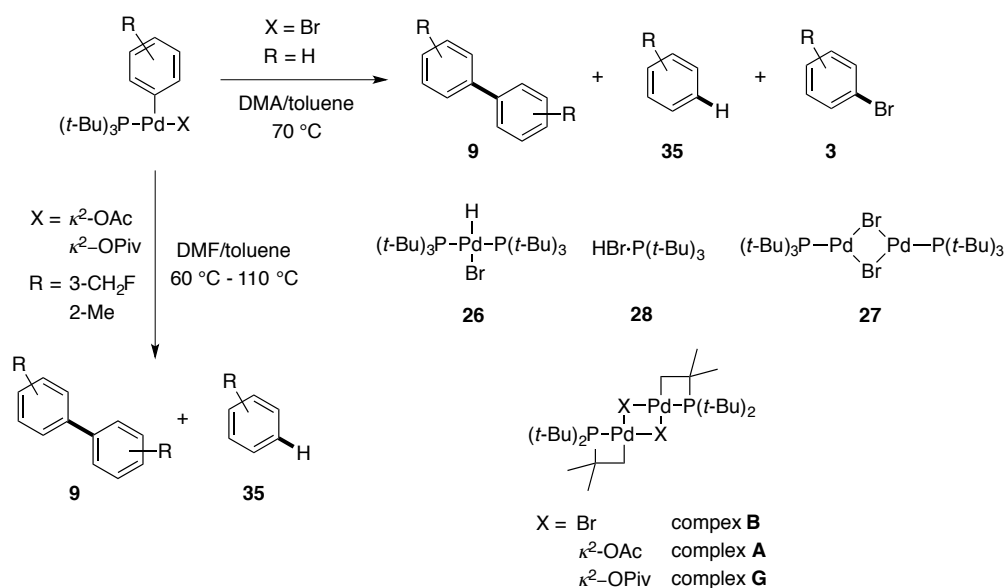
Scheme 2.8. Attack of a nucleophile on a palladium(II) species via an associative (top) or dissociative (middle) pathway. Ligand exchange between an organometallic fragment and a palladium(II) species in an electrophilic substitution via an open or cyclic transition state (bottom).

Although aryl palladium(II) complexes bearing one bulky phosphine ligand have been suggested to undergo transmetalation with an organometallic fragment in traditional cross-coupling reactions,¹¹⁶ studies on the mechanism of the transmetalation step are few. Denmark and co-workers investigated the mechanism of the transmetalation between an unsaturated aryl palladium(II) complex with a $P(t\text{-Bu})_3$ ligand and an organosilanolate. An oxygen-bridged palladium-silanolate intermediate formed prior to transmetalation was identified and characterized. It also revealed the presence of two competing transmetalation pathways, one being a thermal reaction of the intermediate and the other one an anionic intramolecular transmetalation.^{75,117} Similar oxygen-bridged pre-transmetalation intermediates with a boron species have also been observed in the Suzuki-Miyaura cross-coupling reaction (Chapter 3).^{118,119}

2.2.6 Homocoupling product formation

Apart from the investigations on the reductive elimination of aryl halide **3** shown above, few examples of the reactivity of isolated a three-coordinated aryl palladium(II) complexes **14** or **15** in the absence of a cross-coupling partner have been reported. Although not described in the direct arylation of pyridine *N*-oxides **1** with bromobenzenes **3**, thermal decomposition of a phenyl palladium(II) complex **14** forming homocoupling product **9** and proto-demetalation product **35** in addition to the reductive elimination of aryl halide substrate **3** is reported.^{41,74,78} The overall yield of **9** and **35** increase with the decrease of reductively eliminated **3**, indicating the homocoupling and proto-demetalation are competing thermal decomposition pathways at elevated temperatures.⁷⁸ The role of the decomposition phosphorus species formed from phenyl palladium(II) complex **14** has been established, however an influence on the formation of biphenyl **9** or protonated arene **35** has not previously been described.

In the reaction between an isolated (phenyl)Pd(Br)($P(t\text{-Bu})_3$) complex **14c** and an α -silylnitrile at 70 °C in DMF, homocoupling product **9a** was obtained in 31% in addition to 66% α -arylated nitrile. Decomposition of complex **14** without other reactants or additives over 1.5 h at 70 °C resulted in 55% of homocoupling product **9a** (scheme 2.9).⁴¹ Thermolysis of the same phenyl palladium complex **14** in toluene as solvent at 70 °C in the absence of nucleophilic reactant showed that biphenyl **9a** was the major decomposition product, and that minor amounts of benzene **35b** and bromobenzene **3a** were formed. However, no yield of products after complete consumption of **14** was determined.⁷⁴ The phosphorus species observed from the decomposition were hydridopalladium bromide complex **26**, palladium(I)-dimer **27**, cyclometalated complex **B** and a protonated phosphine species with an NMR inactive counterion, it likely being a bromide (compound **28**).⁷⁴



Scheme 2.9. Thermal decomposition pathways of aryl palladium(II) complexes bearing a bromide anion **14** or acetate/pivalate anion **15**. No yields after complete consumption of starting material were reported.

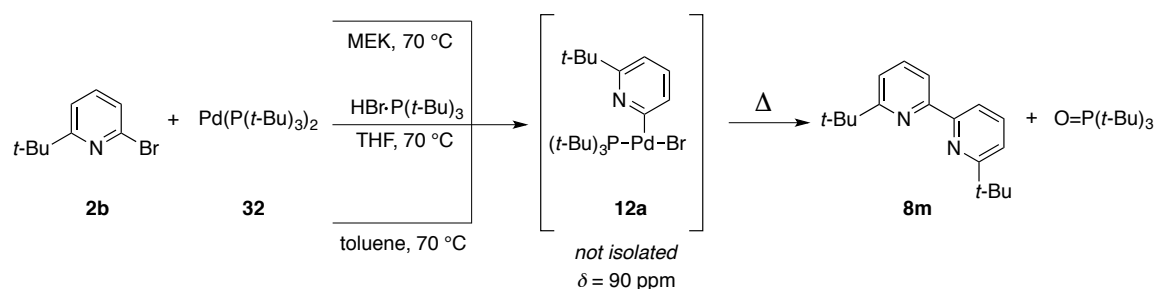
Noteworthy, the analogous acetate-ligated 3-CH₂F-phenyl complex **15c** in toluene at 60 °C underwent neither homocoupling to biphenyl **9**, nor reductive elimination of aryl halide **3**, but when subjected to heating converted completely to fluoromethylbenzene **35c** in addition to cyclometalated acetate complex **A** (scheme 2.9).⁴ Decomposition of a pivalate-ligated 2-tolyl palladium complex in DMA at 110 °C yielded toluene **35b** and biphenyl **9** in roughly equimolar amounts. Additionally, the cyclometalated phosphine complex **G** with a bridging pivalate anion was obtained as the major phosphorus species.⁸⁰

As shown in Chapter 1, roughly equimolar amounts of homocoupled aryl bromide forming bipyridine or biphenyl product **8**, **9** and homocoupled pyridine *N*-oxide yielding bipyridine *N,N'*-dioxide **10** were obtained. Due to the few reports on pyridyl palladium(II) complexes, no reaction rates on the decomposition of an isolated pyridyl palladium complex are reported. However, it has been shown that oxidative addition of bromopyridine **2a** to Pd(P(*t*-Bu)₃)₂ **32** in benzene at 100 °C results in bipyridine **8c** product, in addition to the cyclometalated palladium complex **B**. The reaction was not dependent on base, taking place both with and without K₃PO₄.⁴² Disproportionation of a heteroaryl palladium(II) complexes resulting in homocoupling products has previously been suggested as mechanism for an aryl group transfer.¹²⁰ However, no investigations on the mechanism of isolated palladium complexes have previously been performed.

2.3 Results and discussion

2.3.1 Synthesis of aryl palladium complexes

To investigate the observed differences in reactivity of phenyl and pyridyl intermediates proposed in the direct arylation catalytic cycle, a method for preparation of a novel three-ligated 2-pyridyl palladium species **12** was required. Since no isolation of a 2-pyridyl palladium(II) complex **12** was possible by oxidative addition of 2-bromopyridine **2a** to Pd(P(*t*-Bu)₃)₂ **32**, it was envisioned that a substituent on the bromopyridine might stabilize a three-coordinated intermediate. An electron-rich *tert*-butyl group in 6-position of the bromopyridine starting material **2** was envisioned to increase stability via its steric bulk and electron-donation. 6-*tert*-Butyl-2-bromopyridine **2b** was obtained via a Grignard reaction of *tert*-BuMgCl and 2,6-dibromopyridine,¹²¹ and attempts to form a pyridyl palladium complex **12a** with bromopyridine **2b** via reported procedures are outlined in scheme 2.10.^{46,65,75}

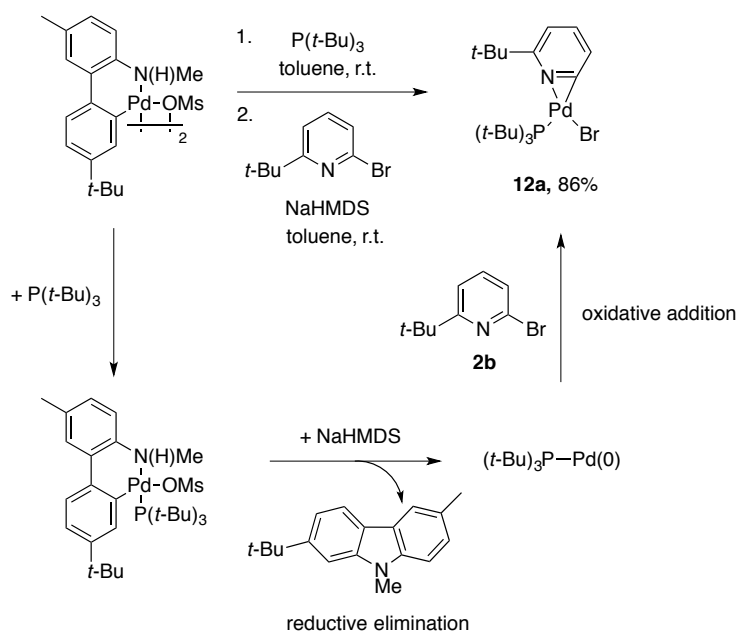


Scheme 2.10. Attempted synthesis of pyridyl palladium(II) complex **12a** by oxidative addition of bromopyridine **2b** (10-40 equiv.) to palladium(0) complex **32**.

Monitoring the reaction between bromopyridine **2b** and palladium(0) complex **32** by ³¹P NMR in THF or MEK with or without HBr·P(*t*-Bu)₃ catalyst resulted in the formation of a new singlet peak with a chemical shift of $\delta = 89.7$ ppm. However, after heating for 1.5 h, starting material **32** was still present. Attempted workup by removal of solvent and precipitation to isolate the new compound resulted in a red solid with a ³¹P shift of $\delta = 66$ ppm.¹²² The signal was assigned to oxidized phosphine ligand O=P(*t*-Bu)₃. A test reaction where acetic acid or H₂O was added to O=P(*t*-Bu)₃ showed that the phosphorus shift of oxidized phosphine could vary up to 5 ppm depending on the presence of coordinating oxygen-containing compounds. Alkyl phosphine ligands can be readily oxidized by oxygen-containing species such as acetates and hydroxides in the presence of a palladium complex.¹²³ The process can be either an initial step converting a palladium(II) species to a reactive palladium(0) species or, as likely here, as a complex decomposition pathway. In addition to oxidized phosphine ligand, bipyridine homocoupling product **8m** was obtained. Unsurprisingly, prolonged heating of

pyridyl complex **12a** results in decomposition. No oxidative addition of bromopyridine **2b** to complex **32** was taking place at room temperature. One attempt was made employing non-coordinating toluene as solvent, however, after 1.5 h at 70 °C, only ~50% of **32** was converted to complex **12a** with the concomitant decomposition to bipyridine **8m**.

An alternative synthesis obviating the need for heating was sought. Buchwald and co-workers have reported the *in situ* formation of a monoligated palladium(0) species generated from a 2-aminobiphenyl palladium mesylate (Buchwald pre-catalyst G3) by addition of a strong base in the presence of phosphine ligand (scheme 2.11).¹²⁴ Initially employing an unsubstituted amine, the reductively eliminated carbazole contaminated the products and the pre-catalyst was altered by methylation of the amine moiety (Buchwald pre-catalyst G4).¹²⁵ Strong bases such as alkoxides or silazides readily deprotonate the *N*-methyl amine-ligand, forming a reactive palladium amido species that undergoes fast C–N reductive elimination of the carbazole. This results in a monoligated palladium(0) Pd–L complex which rapidly undergoes oxidative addition of an aryl halide. The Buchwald pre-catalyst G4 has been used in C–C and C–N cross-coupling reactions, as well as a palladium source for isolation of thermally instable palladium complexes.⁴²



Scheme 2.11. Synthesis of 2-pyridyl palladium(II) complex **12a** via oxidative addition of **2b** (10 equiv.) to a Buchwald type pre-catalyst (1 equiv.) in the presence of $P(t\text{-Bu})_3$ (2.1 equiv.) and NaHMDS (2.1 equiv.).

Application of the Buchwald pre-catalyst G4 under the reported conditions in the presence of $P(t\text{-Bu})_3$ ligand converted the starting material to the new phosphorus species with a ^{31}P shift of $\delta = 89.7$ ppm. Precipitation of the product revealed that the 2-pyridyl palladium(II) complex **12a** was formed, however, the carbazole from the pre-catalyst exhibited low solubility in the solvents used for precipitation and could therefore not be separated from complex **12a**. To circumvent precipitation of

the *N*-methyl carbazole, an alternative Buchwald type precursor was designed. A more lipophilic biphenyl moiety was synthesized via a reported Suzuki-Miyaura cross-coupling of the substituted boronic acid and a bromoaniline.¹²⁶ The amine was methylated by conversion into to ethyl carbamate and subsequent reduction with LiAlH₄.¹²⁷ Formation of the complex precursor was done by addition of Pd(OAc)₂ and MsOH in THF, as previously described by Buchwald and co-workers.¹²⁵

Oxidative addition of **2b** to the monoligated palladium(0) species readily took place at room temperature and the 2-pyridyl palladium(II) complex **12a** was obtained in 86% yield as a yellow solid. The reductively eliminated substituted *N*-methyl carbazole was soluble in pentane and could be readily separated from the palladium complex product. Single crystals of pyridyl complex **12a** were obtained by cooling of a toluene/pentane solution of **12a** to -25 °C. Interestingly, the X-ray analysis revealed that the expected T-shaped complex previously reported for phenyl palladium complexes **14** was not obtained.⁶⁵ Instead, an η^2 -C,N coordination mode of the pyridyl moiety to the metal center was observed (figure 2.1).

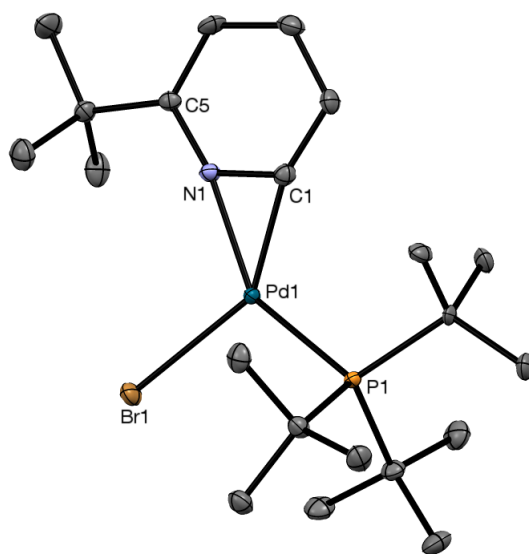
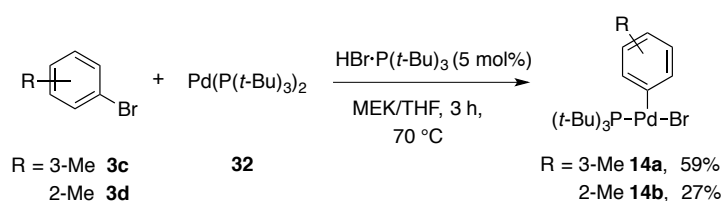


Figure 2.1. ORTEP drawing of complex **12a**. Thermal ellipsoids are drawn at 50% probability level. Hydrogen atoms are omitted for clarity. Selected bond distances (Å) and angles (°): Pd1–N1 2.106, Pd1–C1 1.972, Pd1–P1 2.295, Pd1–Br1 2.527, C1–N1 1.316, C1–N1–C5 124.88, N1–Pd1–C1 37.48, C1–Pd1–P1 110.56, Br1–Pd1–N1 105.67, P1–Pd1–Br1 105.97.

The Pd–C(1) distance of the aryl group was 1.97 Å for pyridyl complex **12a**, which is similar to the analogous unsubstituted phenyl complex **14** where a bond length of 1.98 Å was observed.⁶⁵ Complex **12a** exhibits an almost perfect planar structure. Due to the strained coordination, a Pd–N distance of 2.11 Å in **12a** was observed, being longer than the Pd–N distance of datively coordinated pyridine or bipyridine ligands. A *trans*-dipyridine palladium(II) bromide complex bearing an ester substituted phenyl ligand was reported to exhibit Pd–N bonds of 2.03 Å.⁴² In addition, the analogous

(phenyl)Pd(I)(bipy) complex exhibited Pd–N bond lengths of 2.07 Å and 2.14 Å.¹²⁸ Furthermore, the η^2 -C,N binding mode of the pyridyl moiety results in a slight shortening of the C(1)–N bond to 1.32 Å in comparison to a C–N bond of free pyridine of 1.34 Å,¹²⁹ or a C–N bond of a palladium complex with a datively bound pyridine ligand of 1.35 Å (see below in figure 2.4). Moreover, a C–N–C bond angle of 125° was observed for complex **12a**. For free pyridine, an angle of 117° has been reported,¹²⁹ indicating a significant increase of the angle accompanied with the η^2 -C,N binding of the pyridyl ligand of complex **12a**. For palladium complexes, the η^2 -C,N binding mode of a pyridyl ligand is unprecedented. The N–Pd–C angle of the pyridyl ligand in complex **12a** was 37.5°. For other transition metal complexes adopting an η^2 -C,N binding of a pyridine ligand, similar bite angles of the C–M–N bond were observed, ranging from 29.2° to 37.1°.^{71,91} Arguably, the observed downfield shift of $\delta = 89.7$ ppm is a result of the coordination of the lone pair of the pyridyl nitrogen to the palladium center. In comparison to shifts around $\delta = 65$ ppm for similar three-coordinated phenyl palladium complexes **14**,^{42,46} it can be envisioned that electron-donation from palladium to a π^* orbital of the pyridine ring shifts the ³¹P signal downfield.

For comparison, an analogous phenyl palladium complex was synthesized. Initial attempts were made employing 3-*tert*-butylbromobenzene **3b** under the reported conditions.^{74,75} However, isolation of the formed complex **14d** proved difficult. Likely, the lipophilic *tert*-butyl group results in very high solubility of complex **14d** and limits precipitation from even very nonpolar solvents such as TMS. As an alternative substrate, bromotoluene **3c** and **3d** were employed. The synthesis was performed according to the reported procedure with aryl halide in 40 equivalents to palladium(0) complex **32** and HBr·P(*t*-Bu)₃ in catalytic amounts (scheme 2.12).



Scheme 2.12. Synthesis of phenyl palladium(II) complex **14a**, **14b** by oxidative addition bromotoluene **3** (40 equiv.) to palladium complex **32**.

Phenyl complexes **14a** and **14b** exhibited ³¹P shifts of $\delta = 63.4$ and $\delta = 64.9$ ppm, respectively. For the 2-tolyl complex **14b**, a singlet at $\delta = 64.4$ ppm has been reported.⁴⁶ 3-Tolyl complex **14a** has not previously been described. 2-Tolyl complex **14b** exhibited low solubility in organic solvents whereas 3-tolyl complex **14a** was readily soluble in common organic solvents and addition of nonpolar TMS as solvent was required to precipitate complex **14a** from a pentane solution. Crystals of 3-tolyl complex **14a** could be grown by slow diffusion of pentane into a concentrated DCM solution. Due to the steric bulk of the phosphine ligand, a T-shaped arrangement of ligands similar to unsubstituted

(phenyl)Pd(Br)P(*t*-Bu)₃ **14c** was anticipated.⁶⁵ However, an X-ray analysis indicated a dimeric structure of phenyl complex **14a**, as shown in figure 2.2. Dimerization of T-shaped aryl palladium(II) complexes has previously been observed in the solid-state.⁷⁶ X-ray analysis of a 2-CF₃-phenyl palladium(II) complex showed a dimeric structure with bridging μ -Cl ligands and one P(*t*-Bu)₃ per palladium atom in the solid-state. Similarly, a CyP(*t*-Bu)₂-ligated phenyl palladium complex with a bromide anion also exhibited a dimeric structure determined by X-ray analysis. Based on molecular weight measurements by the Signer method and the similarity in ³¹P shifts to reported T-shaped complexes, it was concluded that the dimers were monomeric in solution but dimeric in the solid-state.⁷⁶ Arguably, complex **14a** adopts a dimeric structure in the solid-state but is expected to be monomeric in solution. However, no molecular weight experiments were performed to determine its nuclearity.

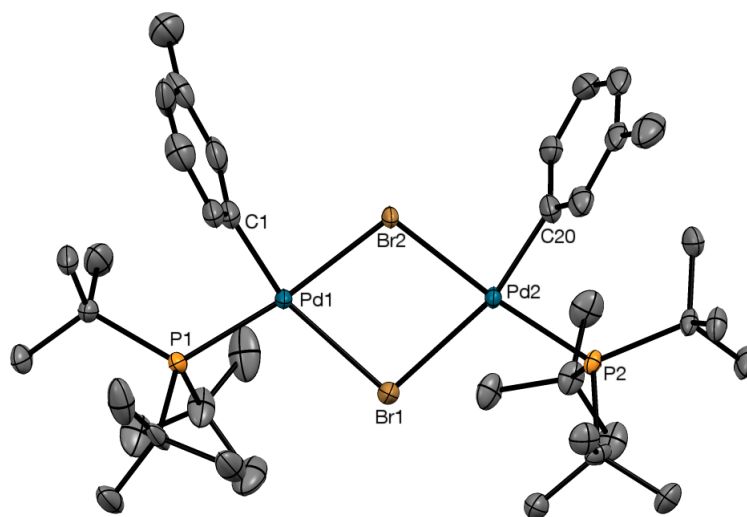


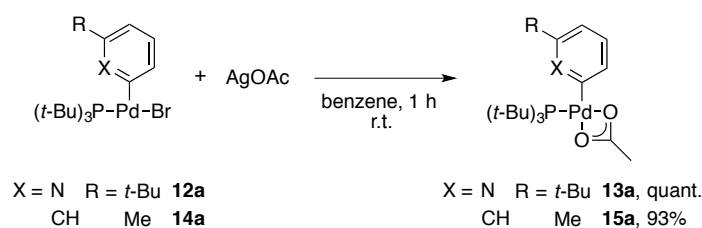
Figure 2.2. ORTEP drawing of complex **14a**. Thermal ellipsoids are drawn at 50% probability level. Hydrogen atoms are omitted for clarity. Selected bond distances (Å) and angles (°): Pd1–C1 1.979, Pd1–Br2 2.509, Pd1–Br1 2.608, Pd1–P1 2.364, Pd2–C20 1.985, Pd2–P2 2.361, Pd2–Br1 2.619, Pd2–Br2 2.511, C1–Pd1–Br2 82.30, Br2–Pd1–Br1 80.26, Br1–Pd1–P1 105.10, P1–Pd1–C1 93.97, Br2–Pd2–C20 82.12, C20–Pd2–P2 94.31, P2–Pd2–Br1 104.37, Br1–Pd1–Br2 80.03.

Similar to [(phenyl)Pd(Br)(CyP(*t*-Bu)₂)₂]₂, the *cis* isomer of phenyl complex **14a** was observed in the crystal structure. Both P(*t*-Bu)₃ and CyP(*t*-Bu)₃ are sterically hindered ligands and it can therefore be anticipated that similar bond lengths are present for the dimers. A Pd(1)–Pd(2) distance of 3.78 Å was reported for [(phenyl)Pd(Br)(CyP(*t*-Bu)₂)₂]₂, similar to the Pd(1)–Pd(2) distance of 3.88 Å in **14a**. Both Br–Pd–Br angles of **14a** are strained, exhibiting angles of 80.0° and 80.3°, respectively. The reported dimeric CyP(*t*-Bu)₂-ligated complex exhibited similar angles of 82.8° and 82.5°. The bond distances of the reported complex reveals Pd–Br bonds of 2.51 Å and 2.60 Å, respectively.⁷⁶ An elongation of the bond opposite the phenyl ligand with the largest *trans* influence is as expected. The same is observed for phenyl complex **14a**, exhibiting almost identical Pd–Br bonds of 2.51 Å for Pd(1)–Br(2)

and Pd(2)–Br(2), and 2.60 Å and for Pd(1)–Br(1) and 2.61 Å for Pd(2)–Br(1). Alike the reported monomeric species (phenyl)Pd(Br)(P(*t*-Bu)₃) **14c**, the phenyl ligands are oriented almost perfectly perpendicular to the palladium-bromide plane. The Pd–C_{ipso} bonds were 1.97 Å and 1.98 Å, respectively, which is alike to the Pd–C_{ipso} bond length of 1.98 Å for the monomeric species reported.⁶⁵

2.3.2 Displacement of ligands

Under the direct arylation conditions, the presence of acetate anions might influence the bromide complexes **12** or **14** by halide displacement. Due to the three-ligated structure of the palladium complexes, displacement of the monodentate bromide anion by acetate would likely form an aryl palladium(II) complex with a κ^2 -bound acetate to the palladium center. Due to the bidentate binding mode, an acetate complex would exhibit a higher stability than the analogous bromide complexes. The reported synthesis of (phenyl)Pd(OAc)(P(*t*-Bu)₃) complexes consists of an oxidative addition of aryl halide **3** to palladium(0) complex **32** in the presence of AgOAc under sonication.⁴ It was envisioned that a 2-pyridyl palladium complex bearing a κ^2 -acetate anion would be stable enough isolate by a similar procedure. However, attempts using bromopyridine **2b** only resulted in palladium black formation. Alternatively, the acetate analogues can be formed by displacement of ligand on the isolated bromide complexes **14**.⁸⁰ Pyridyl complex **13a** and phenyl complex **15a** were readily formed by stirring **12a** or **14a** with AgOAc in benzene for 1 h (scheme 2.13). The formed AgBr is not soluble in benzene and could be filtered off without need for further workup.



Scheme 2.13. Formation of acetate complexes **13a** and **15a** by addition of AgOAc (5 equiv.) to bromide complexes **12a** and **14a**.

Both complex **13a** and **15a** were isolated as yellow solids in excellent yields and exhibited high solubility in organic solvents. The ³¹P NMR spectra revealed sharp singlets at $\delta = 76.6$ ppm and $\delta = 77.9$ ppm for pyridyl complex **13a** and phenyl complex **15a**, respectively, being analogous to the reported (3-CF₃-phenyl)Pd(OAc)(P(*t*-Bu)₃) complex ($\delta = 78.4$ ppm),⁴ or the pivalate analogue (2-tolyl)Pd(OPiv)(P(*t*-Bu)₃) ($\delta = 77.3$ ppm).⁸⁰ Single crystals suitable for X-ray analysis of phenyl complex **15a** were formed by slow diffusion of TMS into a saturated toluene solution (figure 2.3).

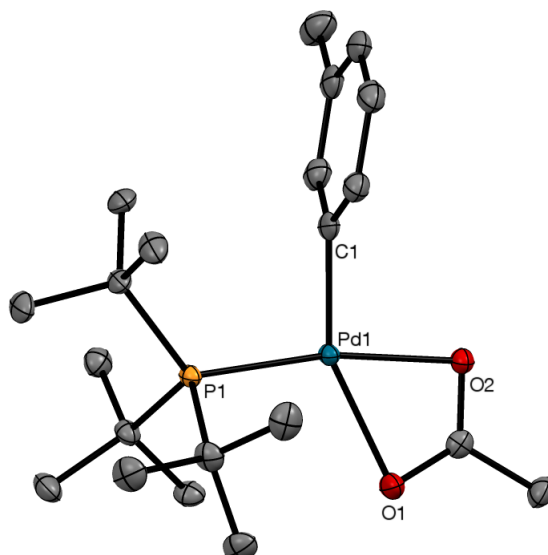


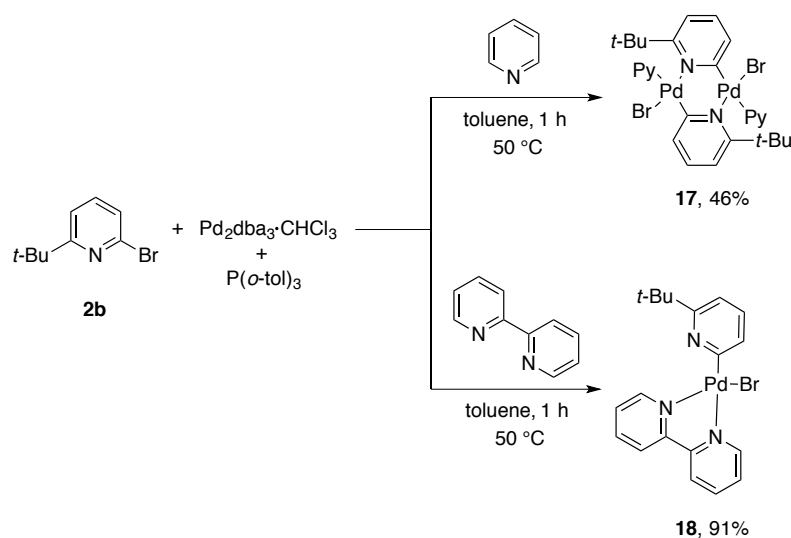
Figure 2.3. ORTEP drawing of complex **15a**. Thermal ellipsoids are drawn at 50% probability level. Hydrogen atoms are omitted for clarity. Selected bond distances (Å) and angles (°): Pd1–C1 1.968, Pd1–O2 2.153, Pd1–O1 2.273, Pd1–P1 2.284, C1–Pd1–O2 94.50, O1–Pd1–P1 110.01, O2–Pd1–O1 59.44, P1–Pd1–C1 95.98.

Complex **15a** exhibited a slightly distorted square planar geometry with the anticipated κ^2 -binding mode of the acetate. The bite angle of the acetate ligand in phenyl complex **15a** was 59.4°, which is almost identical to the pivalate bite angle of 59.2° in the reported (2-tolyl)Pd(OPiv)(P(*t*-Bu)₃) complex.⁸⁰ A shorter Pd–O(1) bond of 2.15 Å *trans* to the phosphine ligand was observed, whereas the Pd–O(2) bond opposite to the stronger *trans* influencing phenyl ligand was 2.27 Å. Both Pd–O bonds are shorter than a Pd–Br of phenyl complex **14a** bond due to the smaller size of the oxygen atoms. Similar to the monomeric T-shaped bromide complexes as well as the dimeric solid-state structure of phenyl bromide complex **14a**, the phenyl ligand is oriented perpendicular to the palladium-acetate plane.

Unfortunately, no single crystals could be obtained of pyridyl acetate complex **13a**. Due to the lipophilic *tert*-butyl substituent on the pyridyl ligand, the complex exhibited a very high solubility in common organic solvents. However, a similar structure is anticipated for pyridyl complex **13a**. Comparing the ³¹P shifts of pyridyl bromide complex **12a** and phenyl bromide complex **14a**, a drastic downfield shift for the pyridyl complex in comparison to the phenyl complex was observed (89.7 ppm versus 63.4 ppm). As stated above, this is likely due to the η^2 -C,N binding of the pyridyl group. However, pyridyl acetate complex **13a** and phenyl acetate complex **15a** exhibit similar chemical shifts, implying that similar electronic environment around the phosphorus ligand is present. Therefore, it is suggested that the acetate ligand of pyridyl complex **13a** binds in a κ^2 -manner forming a monomeric complex analogous to phenyl complex **15a**.

In Chapter 1, it was shown that with addition of bipyridine **8c** or pyridine **34c** to the direct arylation reaction of *N*-oxides, the product formation rate was decreased. This was suggested to be due to the displacement of phosphine ligand by a nitrogen-containing ligand. Although an influence has been identified, isolation of phosphine-free 2-pyridyl palladium complexes would give information on their stability and reactivity.

To investigate the reactivity of a phosphine-free complex, pyridyl complex **12a** was subjected to nitrogen-containing ligands. Addition of pyridine **34c** to complex **12a** resulted in a dimeric pyridyl complex **17**, containing one pyridine ligand per palladium atom. For the synthesis of larger amounts of the phosphine-free complex **17**, an alternative route was sought to circumvent employing pyridyl complex **12a**. Oxidative addition of an aryl halide to Pd₂dba₃·CHCl₃ in the presence of P(*o*-tol)₃ results in dimeric palladium complexes **46** with one phosphine ligand coordinated to each palladium.^{77,130} The phosphine ligand can subsequently be displaced by addition of excess of pyridine.⁴² However, no isolation of the intermediate palladium dimer **46** is required prior to displacement of the phosphine ligand. A similar procedure was applied starting from bromopyridine **2b**, Pd₂dba₃·CHCl₃ and P(*o*-tol)₃, where a one-pot reaction with 15 equivalents of pyridine **34c** resulted in pyridyl dimer **17** as an orange solid in 46% yield (scheme 2.14). No experiment without the sacrificial P(*o*-tol)₃ was performed, however, it is expected that the phosphine is crucial for forming an electron-rich palladium complex on which the oxidative addition occurs.



Scheme 2.14. Oxidative addition of **2b** (15 equiv.) to Pd₂dba₃·CHCl₃ (1 equiv.) in the presence of P(*o*-tol)₃ (1 equiv.) and either pyridine **34c** (15 equiv.) or bipyridine **8c** (5 equiv.) yielding pyridine dimer **17** and bipyridine complex **18**.

The identical protocol can be used in the synthesis of a pyridyl palladium complex with a 2,2'-bipyridine ligand **18**. Again, the oxidative addition takes place on an electron-rich $P(o\text{-tol})_3$ palladium(0) species formed by addition of sacrificial phosphine ligand. Due to the low volatility of bipyridine, only 5 equivalents were added, simplifying the removal of excess bipyridine ligand from the product. Bipyridine pyridyl complex **18** was obtained as a yellow solid in 91% yield.

Single crystals of pyridyl dimer **17** was obtained by crystallization from a benzene/THF mixture at $-25\text{ }^\circ\text{C}$. X-ray analysis showed a phosphine-free dimeric complex with two bridging $\mu\text{-C}^2\text{,N}$ -pyridyl ligands (figure 2.4).

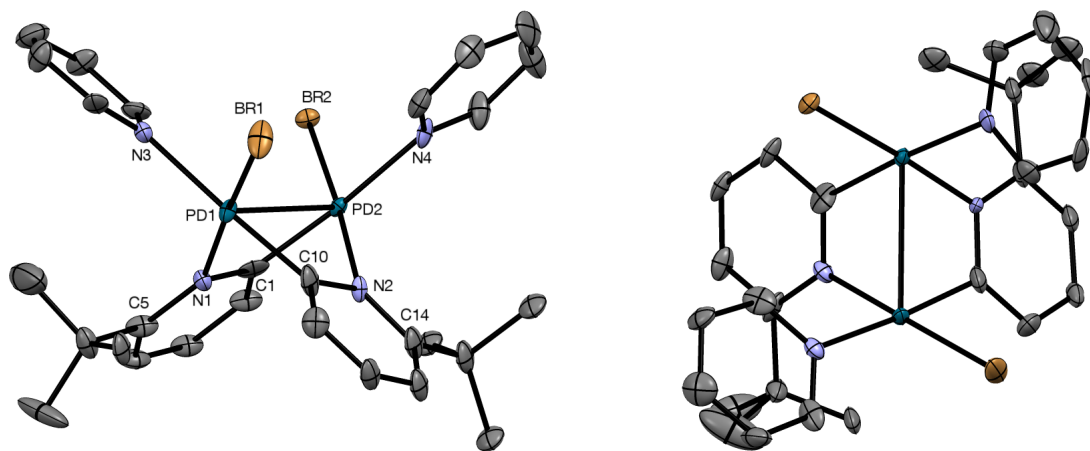


Figure 2.4. ORTEP drawing of pyridyl dimer **17** from side (left) and from above (right). Thermal ellipsoids are drawn at 50% probability level. Disorder on *tert*-butyl group and hydrogen atoms are omitted for clarity. Selected bond distances (\AA) and angles ($^\circ$): Pd1–N3 2.155, Pd1–Br1 2.435, Pd1–N1 2.106, Pd1–C10 1.975, Pd2–Br2 2.428, Pd2–N4 2.153, Pd2–N2, 2.104, Pd2–C1 1.970, Pd1–Pd2 2.875, N3–Pd1–N1 92.34, N3–Pd1–Br1 91.55, Br1–Pd1–C10 89.87, C10–Pd1–N1 86.40, Br2–Pd2–N4 89.11, N4–Pd2–N2 95.14, N2–Pd2–C1 85.56, C1–Pd2–Br2 90.24.

Similar to the reported PPh_3 -ligated 4-phenylpyridyl dimer $[\{\mu\text{-}(4\text{-Ph-pyridyl})\text{-C}^2\text{,N}\}\text{Pd}(\text{Br})(\text{PPh}_3)]_2$,⁶⁹ and the 4-picoline dimer $[\{\mu\text{-}(4\text{-Me-pyridyl})\text{-C}^2\text{,N}\}\text{Pd}(\text{Br})(\text{PPh}_3)]_2$,⁶⁶ complex **17** exhibits a slightly distorted square planar geometry around both palladium atoms and with the bromides *trans* to the nitrogens of the bridging pyridyl groups. The interatomic Pd(1)–Pd(2) distance of pyridyl dimer **17** was 2.88 \AA , being notably shorter than the PPh_3 dimeric structure, which exhibits a Pd(1)–Pd(2) distance of 3.23 \AA .⁶⁶ A *trans* influence of the pyridyl opposite the datively bound pyridine ligand is manifested by the elongation of the Pd(1)–N(3) bond of 2.16 \AA and the Pd(2)–N(4) bond of 2.15 \AA , similar to the reported dimer formed by $\text{P}(t\text{-Bu})_3$ displacement by 2-bromo-3-methyl pyridine.⁴²

Single crystals of pyridyl bipyridine complex **18** were obtained by slow diffusion of pentane to a saturated DCM solution. X-ray analysis of the solid-state revealed a monomeric structure with a distorted square planar configuration around the palladium center (figure 2.5).

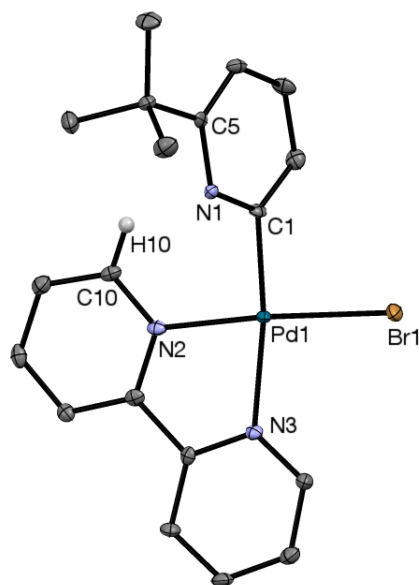
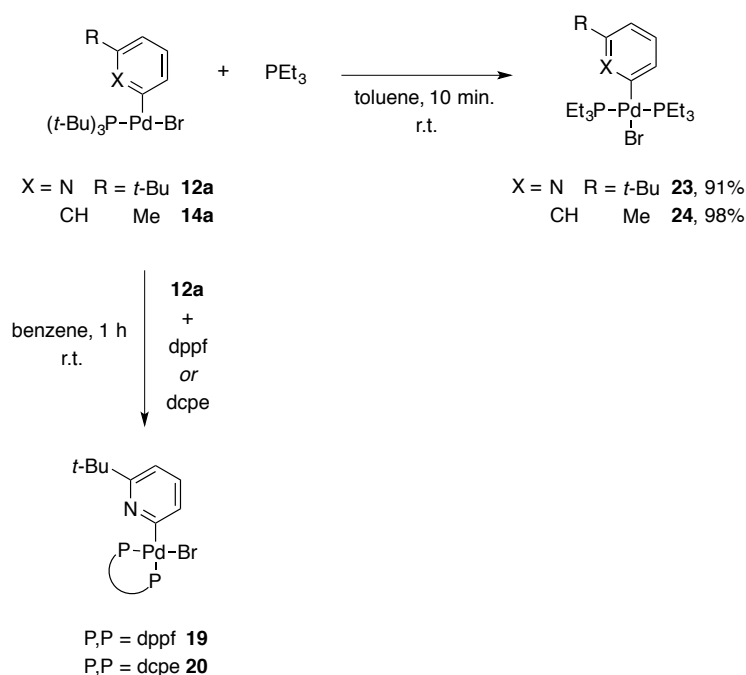


Figure 2.5. ORTEP drawing of pyridyl complex **18**. Thermal ellipsoids are drawn at 50% probability level. Selected hydrogen atoms are shown. Selected bond distances (Å) and angles (°): Pd1–C1 1.975, Pd1–N2 2.068, Pd1–N3 2.136, Pd1–Br1 2.433, C1–Pd1–N2 95.32, N2–Pd1–N3 78.54, N3–Pd1–Br1 97.13, Br1–Pd1–C1 90.03.

A N(1)–C(1)–Pd(1)–N(2) torsion angle of 64.4° was observed, deviating from the almost perpendicular orientation of the aryl group of phenyl complexes **14a** and **15a**. Arguably, an interaction between the basic pyridyl nitrogen and a hydrogen atom on C(10) with a distance of 2.64 Å twists the conformation. The torsion angle for similar tmeda or bipyridine-ligated phenyl complexes deviate less from a 90° perpendicular plane (largest deviation 14.3°),¹²⁸ further supporting the nitrogen lone pair interaction hypothesis. A C–N–C angle 119° of the pyridyl ligand was observed, being similar to the angle of free pyridine of 117° .¹²⁹ Pd–N(2) and Pd–N(3) bond lengths of 2.07 Å and 2.14 Å were observed, being similar to the bond lengths for the analogous square planar (phenyl)Pd(Cl)(bipy) complex (Pd–N(2) = 2.06 Å and Pd–N(3) = 2.12 Å).¹³¹

As opposed to the dimeric structure of pyridyl complex **17**, displacement of P(*t*-Bu)₃ from phenyl complex **14a** with 120 equivalents of pyridine in benzene indicated the formation of a phosphine-free monomeric species with two pyridine ligands per palladium atom. This has previously been proposed a favorable configuration after oxidative addition of an aryl halide to a palladium(0) species in the presence of excess pyridine.^{42,48,49} However, the phenyl complex could not be completely separated from the starting materials and the spectrum obtained exhibited pyridine traces. Arguably, the observation of different nuclearity of the complexes formed by ligand displacement of pyridyl complex **12a** and phenyl complex **14a** is supporting the hypothesis of a difference in reactivity as suggested in Chapter 1.

Attempts to displace the $P(t\text{-Bu})_3$ ligand with other phosphine ligands were also performed. As seen below, PEt_3 readily displaces $P(t\text{-Bu})_3$ from pyridyl complex **12a** and phenyl complex **14a** when present in a reaction mixture. 2-Pyridyl palladium complexes bearing two PEt_3 ligands in a *trans*-configuration have previously been synthesized by the displacement of two PPh_3 ligands from a $\mu\text{-C}^2\text{,N}$ -bridging palladium dimer at $60\text{ }^\circ\text{C}$.⁹⁵ As shown in scheme 2.15, 2 equivalents of PEt_3 readily displace the phosphine ligand of pyridyl complex **12a**, yielding the novel pyridyl complex **23** in 91% yield. Furthermore, the analogous PEt_3 phenyl complex **24** with a 3-tolyl moiety could be obtained in 98% yield from phenyl complex **14a**. Also bidentate phosphine ligands can displace the bulky $P(t\text{-Bu})_3$ ligand. The two phosphine ligands 1,1'-bis(diphenylphosphino)ferrocene (dppf) and 1,2-bis(dicyclohexylphosphino)-ethane (dcpe) were tested under similar reaction conditions (scheme 2.15). Pyridyl complexes **19** and **20** were formed by stirring pyridyl complex **12a** in benzene for 1 h in the presence of 1 equivalent of bidentate phosphine ligand and identified via ^{31}P NMR. No yield was determined.



Scheme 2.15. Displacement of $P(t\text{-Bu})_3$ ligand from pyridyl complex **12a** and phenyl complex **14a** with addition of monodentate ligand (2 equiv.) or bidentate ligand (1 equiv.) forming phosphine-ligated complexes **19**, **20**, **23**, **24**.

Due to the four-ligated configuration, the complexes exhibited high stability towards air and moisture. Pyridyl complex **23** and phenyl complex **24** both gave rise to sharp singlet peaks in the ^{31}P NMR with shifts of $\delta = 12.8$ ppm. The previously described *trans*-(2-pyridyl) $\text{Pd}(\text{Cl})(\text{PEt}_3)_2$ exhibits a very similar singlet with a shift of $\delta = 12.4$ ppm.⁹⁵ Furthermore, a *trans*-(4-tolyl) $\text{Pd}(\text{Br})(\text{PEt}_3)_2$ was reported to have a ^{31}P shift of $\delta = 11.3$ ppm.¹³² The ^{31}P spectra for pyridyl complexes **19** and **20** exhibited two doublets each of $\delta = 26.3$ and 7.35 ppm for complex **19** and $\delta = 67.8$ and 56.9 ppm for complex **20**, similar to

reported bidentate phosphine-ligated palladium(II) complexes.⁴² Due to the bidentate binding of the phosphine ligand, an increase in stability was also observed for pyridyl complexes **19** and **20**. It was envisioned that bidentate phosphine complexes could be synthesized via oxidative addition of bromopyridine **2b** to Pd₂dba₃·CHCl₃ in presence of P(*o*-tol)₃ and relevant bidentate ligand in a similar manner as pyridine pyridyl dimer **17** and bipyridine pyridyl complex **18**. However, such synthesis pathways were not further investigated.

2.3.3 Decomposition of aryl palladium complexes

The yield of homocoupling products obtained in the direct arylation reaction is suggesting that a lower stability and/or an increase in reactivity towards a decomposition pathway of a pyridyl palladium(II) complex **12** in comparison to a phenyl palladium(II) complex **14** is present. To investigate the differences in the decomposition pathways of the intermediate complexes, independent thermal decomposition experiments were performed. From the synthesis of bromide complexes **12a**, **14a** and acetate complexes **13a**, **15a**, an initial notion on the stability was obtained. Bromide-ligated complexes **12a** and **14a** started decomposing after a few days in a C₆D₆ solution. Pyridyl complex **12a** exhibited a slightly higher stability than the phenyl complex **14a**, likely due to the η^2 -C,N binding of the pyridyl ligand. However, no exact decomposition rate was determined at room temperature. Employing coordinating MeCN-*d*₃ as solvent resulted in prolonged stability, and only 10% of the pyridyl complex **12a** was decomposed after 2 weeks. Unsurprisingly, the acetate-ligated complexes **13a** and **15a** exhibited an increase in stability and no decomposition products were observed within 2 weeks in a C₆D₆ solution. Therefore, decomposition of the bromide complexes **12a** and **14a** was expected to be faster at elevated temperatures. Initial screening of the decomposition of **12a** and **14a** in C₆D₆ showed that both complexes were consumed within 2 h at 80 °C. Independent synthesis of biaryl products 6,6'-di-*tert*-butyl-2,2'-bipyridine **8m** and 3,3'-dimethyl-1,1'-biphenyl **9c** was performed by nickel or iron-catalyzed reductive homocoupling of the parent aryl halide substrates **2b** and **3c** according to literature procedures.^{133,134}

Thermolysis of the pyridyl complex **12a** and phenyl complex **14a** was monitored via NMR. Ideally, monitoring the reaction via ³¹P NMR and determining the phosphorus species distribution over time would give easily interpretable spectra. Unfortunately, the chemical shift of pyridyl complex **12a** (δ = 89.7 ppm) is very close to the shift of bisphosphine palladium(0) complex **32** (δ = 85.5 ppm), hydridopalladium(II) bromide (H)Pd(Br)(P(*t*-Bu)₃)₂ complex **26** (δ = 83.6 ppm) and palladium(I)-dimer [(P(*t*-Bu)₃)Pd(μ -Br)]₂ **27** (δ = 86.8 ppm), all of which were formed in the decomposition reaction. Initial decomposition kinetics monitored via ³¹P NMR revealed that the peaks cannot be separated at 80 °C. Therefore, ¹H NMR was chosen for determining the decomposition profile of

pyridyl complex **12a**. For phenyl complex **14a**, the decomposition was also determined via ^1H NMR. The same limitation of peak overlap is not present for the phenyl palladium(II) complex **14a** and one experiment was monitored via ^{31}P NMR to obtain information on the pathway of the phosphorus species.

Initially, phenyl complex **14a** was weighed in an NMR tube with a J Young valve and dissolved in C_6D_6 ($c = 0.045\text{ M}$) in the glovebox. Prior to placing the NMR tube in the spectrometer, the mixture was cooled in an ice bath, in the hopes of preventing any reaction to take place before the first spectrum was recorded. One ^1H NMR spectrum was recorded every 2 minutes over the course of 3 hours and the methyl group signals were integrated for starting material and products. The decay of **14a** and product formation of biphenyl **9c**, toluene **35b** and bromotoluene **3c** is shown in figure 2.6, top. One experiment monitoring the same reaction via ^{31}P NMR was performed and the decay of **14a** and formation of cyclometalated complex **B**, hydridopalladium(II) bromide complex **26**, palladium(I)-dimer **27**, phosphonium salt $\text{HBr}\cdot\text{P}(t\text{-Bu})_3$ **28**, $\text{P}(t\text{-Bu})_3$ ligand and palladium(0) complex **32** is shown in figure 2.6, bottom. An apparent first-order decay of phenyl palladium complex **14a** was observed. Plotting $\ln[\mathbf{14a}]$ versus time gives $k_{\text{obs}} = -0.045\text{ min}^{-1}$ with a half life of $t_{1/2} = 15$ minutes for the consumption determined via ^1H NMR. A similar rate constant was observed for the decay determined via ^{31}P NMR measurement, where $k_{\text{obs}} = -0.042\text{ min}^{-1}$ with $t_{1/2} = 17$ minutes was obtained. Complete consumption of phenyl complex **14a** required approximately 80 minutes at $80\text{ }^\circ\text{C}$. The species obtained from the thermolysis reaction were biphenyl homocoupling product **9c** (37%), toluene **35b** (49%) and bromotoluene **3c** (11%). The formation of homocoupling product **9c** is initially fast, however a maximum concentration of biphenyl **9c** is reached after approximately 40 minutes. At the same time point, only 10% of phenyl complex **14a** was remaining. Formation of toluene **35b** likely takes place via a proto-demetalation process from the reaction between a phenyl palladium(II) complex **14a** and an HBr source. HBr in turn is formed from the cyclometalation of $\text{P}(t\text{-Bu})_3$ ligand yielding complex **B**. As seen from the bottom plot in figure 2.6, complex **B** forms with a constant rate starting at $t = 0$ until complete consumption of **14a**. It has previously been shown that a buildup of Brønsted acid in the cross-coupling reaction of 4-nitropyridine *N*-oxide **11** and an aryl halide **3** diminishes the cross-coupling product due to a proto-demetalation pathway.⁵ A constant formation rate of toluene **35b** was observed until $t = 60$ min. Already in the first spectrum recorded, complex **14a** was converted to bromotoluene **3c** (4%). After 4 minutes, a maximum concentration of 19% of bromotoluene **3c** was reached and which subsequently was consumed over the course of the reaction.

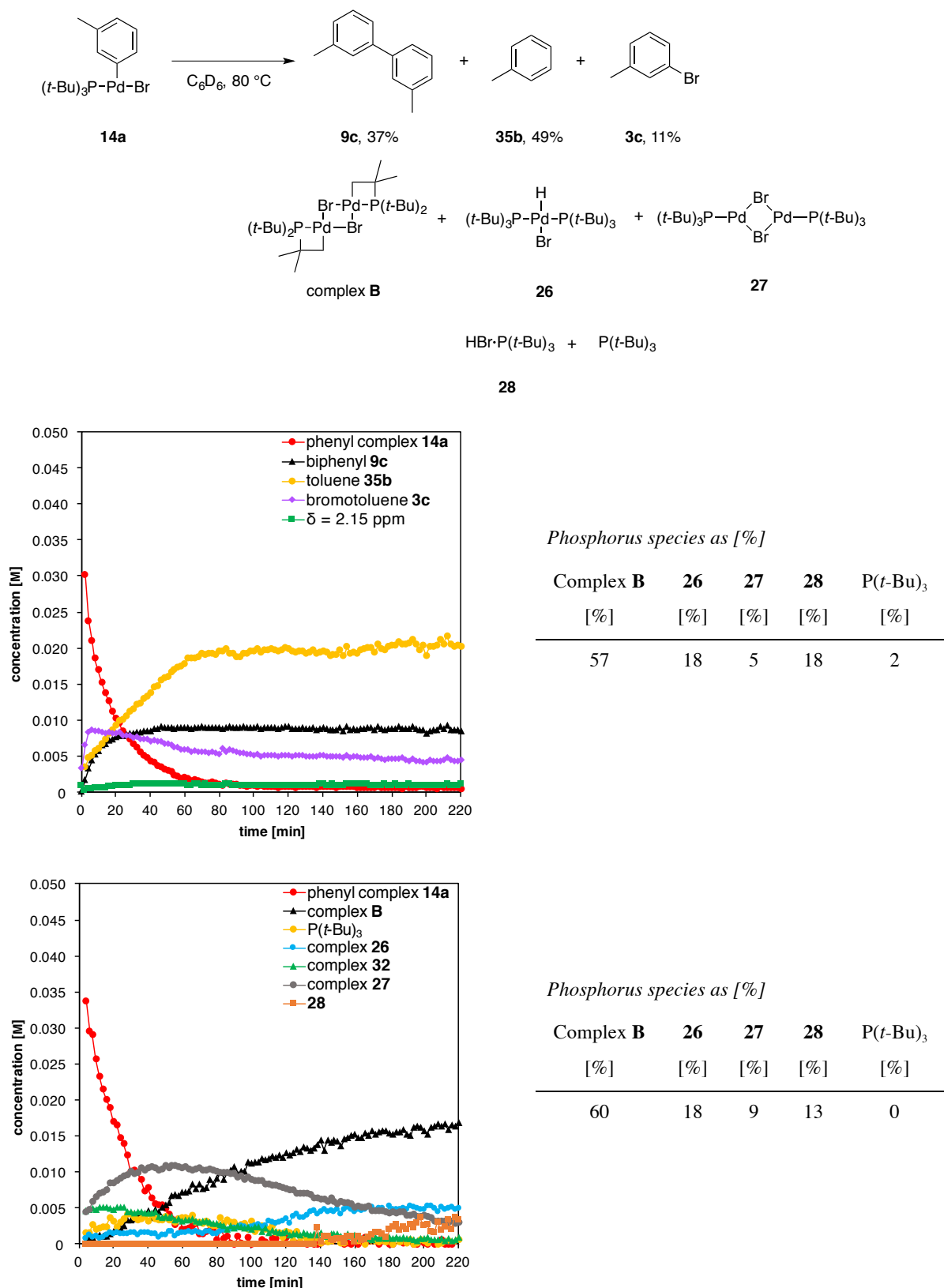


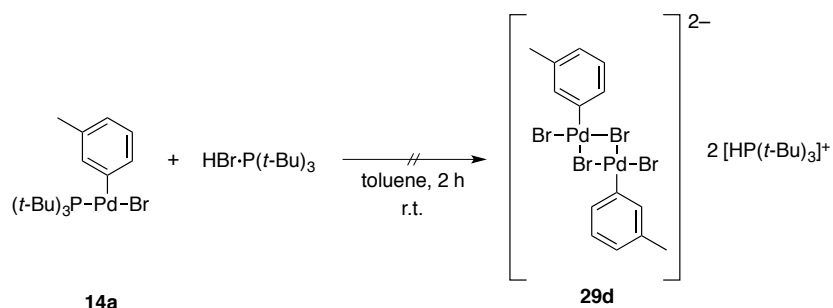
Figure 2.6. Consumption of phenyl complex **14a** ($c_0 = 0.045$ M) and product formation of homocoupling product **9c**, toluene **35b**, 3-bromotoluene **3c** and an unidentified species at $\delta = 2.15$ ppm monitored by ^1H NMR (top) and consumption of **14a** ($c_0 = 0.045$ M) monitored by ^{31}P NMR (bottom). Ratio of P species after 4 hours of reaction.

After the decomposition reaction, the ratio of phosphorus species formed from **14a** was determined via ^{31}P NMR. No internal standard was used and the values shown in figure 2.6 are the ratio of the observed species. Similar to the decomposition of complex (phenyl) $\text{Pd}(\text{Br})(\text{P}(t\text{-Bu})_3)$ **14c** reported by Hartwig and co-workers,⁷⁴ hydridopalladium(II) bromide **26**, palladium(I) dimer **27**, cyclometalated complex **B** and a phosphonium salt **28** were obtained. Independent synthesis of the decomposition products was performed according to reported procedures; hydridopalladium(II) bromide complex **26** is formed by the oxidative addition of HBr to palladium(0) complex **32**,¹³⁵ palladium(I)-dimer **27** by a one-electron-oxidation of **32** with CuBr_2 ¹³⁶ and $\text{HBr}\cdot\text{P}(t\text{-Bu})_3$ by addition of $\text{Py}\cdot\text{HBr}$ to the $\text{P}(t\text{-Bu})_3$ ligand.⁷⁴

As seen from the bottom plot in figure 2.6, the initial phosphorus containing complex formed was palladium(I)-dimer **27** (grey). After disproportionation of **14a**, one palladium(II) species, likely being PdBr_2 and one palladium(0) species, likely being bisphosphine complex **32** (green) are formed. Dimer **27** is a comproportionation product of one palladium(0) species and one PdBr_2 .¹³⁶ An initial fast formation of complex **32** was visible, however the species was consumed fast with the formation of dimer **27**. After a maximum concentration of dimer **27** after $t = 40$ minutes, the complex was consumed and the concentration of hydridopalladium(II) bromide complex **26** (blue) increased. Formation of complex **26** takes place within 10 minutes at room temperature when combining palladium(0) complex **32** and a $\text{Py}\cdot\text{HBr}$.¹³⁵ HBr is formed from the cyclometalation of phosphine ligand forming complex **B** (black) and the presence of HBr is proposed to induce a fast reaction with palladium(0) complex **32** at $80\text{ }^\circ\text{C}$ forming hydridopalladium complex **26**. The concentration of palladium(0) complex **32** and free $\text{P}(t\text{-Bu})_3$ ligand (yellow) decreased as the reaction proceeded and the main phosphorus-containing species after 2 hours was the cyclometalated palladium complex **B** (black).

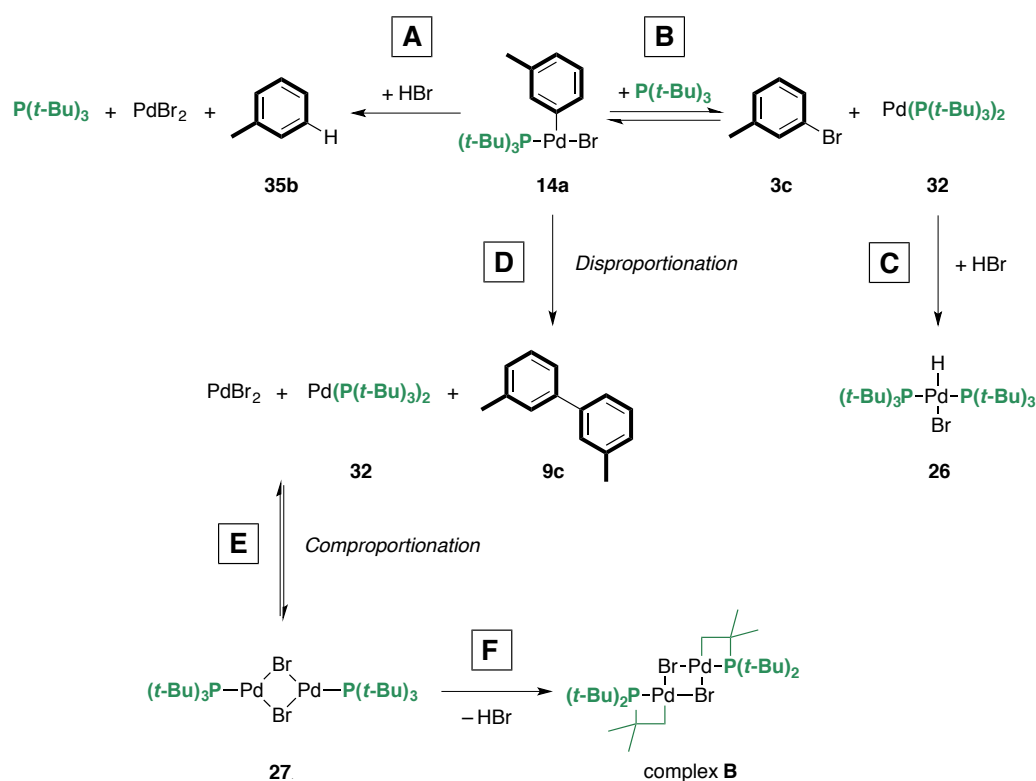
In the decomposition experiment, an unidentified species with a chemical shift of $\delta = 2.15$ ppm was observed in the ^1H NMR. The signal is suggested to belong to the methyl group of a 3-tolyl anionic phenyl dimer **29d**, which can be formed by nucleophilic attack of a bromide on a phenyl palladium complex **14a**.^{80,81,137} Attempts to synthesize anionic dimer **29d** with either a $[\text{HP}(t\text{-Bu})_3]^+$ or $[\text{NR}_4]^+$ counter ion according to reported procedure gave unclear results (scheme 2.16). Addition of $\text{HBr}\cdot\text{P}(t\text{-Bu})_3$ **28** to a solution of phenyl complex **14a** in toluene resulted in a new set of signals in the ^1H NMR spectrum that were upfield shifted from the starting material **14a**. However, additional unidentified decomposition species were also obtained. An equilibrium between aryl palladium complex **14** and the anionic dimer **29** has been proposed¹³⁷ and isolation of the dianionic dimer **29** has been reported by precipitation of the insoluble product from the solvent used in the reaction. However, no precipitation of dimer **29d** was observed. An increase in solubility was assumed as cause, similar to the high solubility of phenyl complex **14a** in nonpolar solvents. Furthermore, a small K_{eq} was

determined for the equilibrium between **14** and **29**, indicating that the equilibrium lies on the starting material side.¹³⁷ Monitoring the formation of the new species in the decomposition reaction shown above gave an initial fast formation over 40 minutes and subsequently, almost no change in concentration was observed. Likely, an equilibrium is present, however only observable at elevated temperatures.



Scheme 2.16. Attempted synthesis on anionic dimeric phenyl complex **29d** by addition of phosphonium salt **28** (0.5 equiv.) to phenyl complex **14a**.

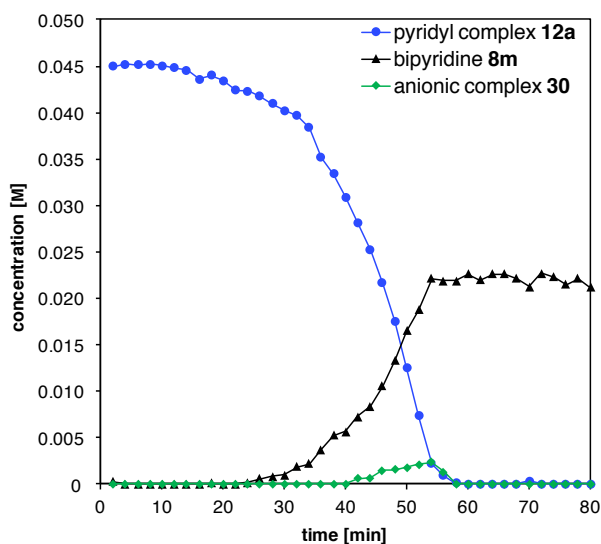
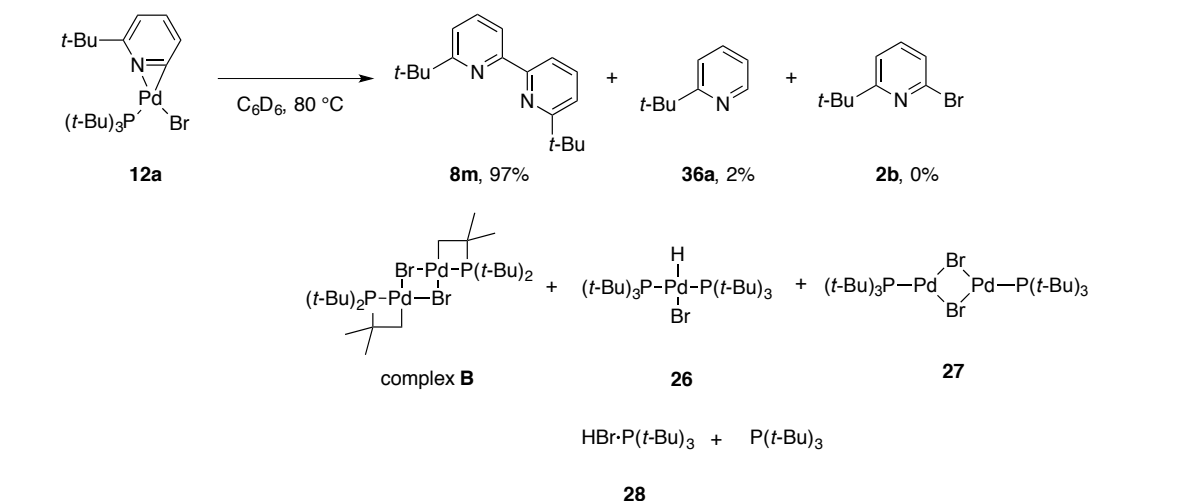
An overview of the consumption pathways for the phosphorus ligand of phenyl complex **14a** is outlined in scheme 2.17. In the presence of a proton source, irreversible proto-demetalation of complex **14a** takes place forming toluene **35b**, a PdBr₂ species and free P(*t*-Bu)₃ (step **A**). Furthermore, complex **14a** exists in an equilibrium with bromotoluene **3c** and palladium(0) complex **32** in the presence of P(*t*-Bu)₃ (step **B**).⁴⁶ Palladium(0) complex **32** is described to readily react with an HBr source forming hydridopalladium complex **26** by oxidative addition (step **C**).¹³⁵ Two phenyl complexes **14a** can undergo a disproportionation reaction forming biphenyl **9c**, palladium(II) complex PdBr₂ and palladium(0) complex **32** (step **D**). The apparent first-order decay of **14a** indicates a dependence on one phenyl complex **14a** in the rate-determining step. Therefore, step **D** likely entails the rate-limiting step with a reaction between one complex **14a** and another phenyl palladium species, presumably anionic dimer **29d**. Arguably, the increased nucleophilicity of **29d** increase the reactivity towards electrophilic phenyl complex **14a**. The palladium complexes formed after biphenyl **9c** formation can undergo comproportionation, forming palladium(I)-dimer **27** (step **E**). Likely, the comproportionation product **27** exists in equilibrium with PdBr₂ and complex **32**. An independent decomposition experiment of dimer **27** heated at 80 °C for 2 h revealed that the major decomposition products formed was cyclometalated complex **B** (step **F**). Additionally, phosphonium salt **28** and free P(*t*-Bu)₃ ligand was observed (see Experimental section 4.10.5). Complex **B** is stable towards thermal decomposition. In the above shown decomposition experiments, no palladium(0) complex **32** or free P(*t*-Bu)₃ ligand was observed after complete consumption of complex **14a**, arguably due to the fast reaction with HBr via oxidative addition to complex **32** (step **C**) or formation of phosphonium salt **28** by the reaction with free P(*t*-Bu)₃ ligand (not shown).



Scheme 2.17. Decomposition pathways of phenyl palladium(II) complex **14a**.

Unfortunately, the regioisomeric complex (2-tolyl)Pd(Br)(P(*t*-Bu)₃) **14b** exhibited low solubility in C₆D₆ and therefore, no monitoring of the thermolysis reaction was performed. However, it has been shown that a substituent *ortho* to the Pd–C bond of a palladium complex increases the reductive elimination of aryl halide.⁷⁸ 2-Tolyl complex **14b** was heated for 4 hours in C₆D₆, which completely dissolved and consumed the starting material. A significant difference in product distribution was observed in comparison to decomposition of 3-tolyl complex **14a**. The major product was reductively eliminated 2-bromotoluene product **3d**, which was observed in 44%. This is in accordance with the proposal that a *ortho*-substitution increases reductive elimination.⁷⁸ Biphenyl **9d** was obtained in 31% and toluene was obtained in 25%. In comparison, the major species from the 3-tolyl palladium complex **14a** was the toluene product **35b** (49%), followed by biphenyl **9c** (37%) and bromotoluene **3c** (11%). Arguably, if reductive elimination and homocoupling are slower, arene formation becomes more significant, as observed for 3-tolyl complex **14a**.

Decomposition experiments were also performed with pyridyl complex **12a**. Dissolving **12a** in C₆D₆ (*c* = 0.045 M) and heating at 80 °C with an ¹H NMR spectrum recorded every 2 minutes resulted in a reaction profile as shown in figure 2.7. The aromatic signals of starting material **12a** and bipyridine product **8m** were integrated. As above stated, the phosphorus species were not monitored due to signal overlap.



Phosphorus species as [%]

Complex B	26	27	28	P(<i>t</i> -Bu) ₃
[%]	[%]	[%]	[%]	[%]
45	25	8	14	8

Figure 2.7. Consumption of aryl palladium complex **12a** ($c_0 = 0.045$ M) and formation of homocoupling product **8m** monitored by ^1H NMR. Ratio of P species after 3 hours of reaction.

A clear difference in consumption profile of pyridyl complex **12a** in comparison to phenyl complex **14a** was observed. Decay of complex **12a** exhibited an induction period until $t = 35$ minutes where only 15% of starting material was consumed. This is in stark contrast to 90% consumption of phenyl complex **14a** during the same time interval. After the induction period, the starting material was converted within 25 minutes to bipyridine homocoupling product **8m** (97%). Additionally, *tert*-butyl pyridine **36a** was obtained in 2% yield. No formation rate of pyridine **36a** could be determined due to signal overlap with the starting material. Reductive elimination of the bromopyridine **2b** did not take place. As proposed for the reductive elimination of aryl halides from a palladium(II) species, the C–X bond strength influences the reductive elimination process. For a weaker C–I bond, reductive elimination forming phenyl iodide took place to a smaller extent than reductive elimination of a C–Br bond of phenyl bromide.⁷⁸ Since the C–Br bond is weaker for a bromopyridine substrate¹³⁸ than for an analogous bromobenzene substrate, it could be argued that reductive elimination of a bromopyridine

substrate is thermodynamically disfavored. Determination of the ratio of phosphorus species after the reaction was performed by ^{31}P NMR. Similarly to the decomposition of phenyl complex **14a**, the major species formed was the cyclometalated complex **B**. In general, the ratio of observed phosphorus species proved similar to the ratio obtained for phenyl complex **14a**.

After the induction period, the decomposition of pyridyl complex **12a** exhibited an apparent zero-order decomposition. An initial slow reaction and subsequent increase in rate is often indicative of an autocatalytic reaction.⁴⁴ During the reaction, an additional transient species was observed via ^1H NMR. A doublet at $\delta = 6.0$ ppm was detected and is suggested to belong to a transient intermediate of the reaction. The species was not present after complete decomposition of pyridyl complex **12a** and could therefore not be detected by NMR after the reaction. Similar to the formation of anionic dimer **29**, pyridyl complex **12a** and $\text{HBr}\cdot\text{P}(t\text{-Bu})_3$ **28** were combined for 1 h at room temperature (figure 2.8). Displacement of the phosphine ligand readily took place from pyridyl complex **12a** and anionic pyridyl complex **30** was isolated in a yield of 68%.

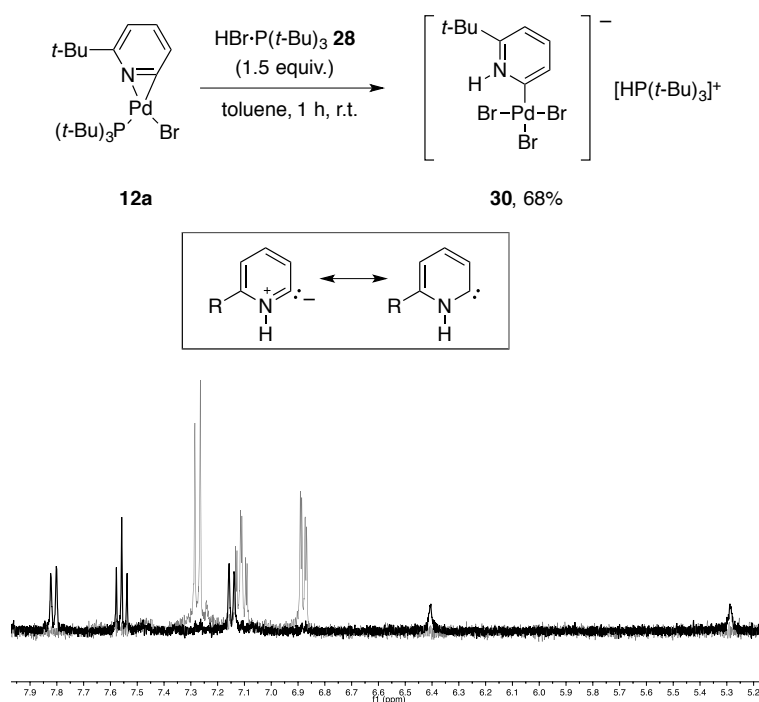


Figure 2.8. Nucleophilic displacement of phosphine ligand on pyridyl complex **12a** (1 equiv.) with phosphonium salt **28** (1.5 equiv.) yielding anionic complex **30**. Resonance structures contributing to the binding of the 2-pyridyl ligand in **30** being mesoionic (left) or carbene binding (right). ^1H NMR spectra of anionic complex **30** (black) and pyridyl complex **12a** (grey) in $\text{MeCN-}d_3$.

Complex **30** exhibited a ^{31}P NMR shift of $\delta = 53$ ppm in $\text{MeCN-}d_3$. The chemical shift is similar to the reported phosphonium ion $[\text{HP}(t\text{-Bu})_3]^+$, for which a ^{31}P shift of $\delta = 51$ ppm was observed.⁷⁴ A very limited solubility of complex **30** in benzene was observed. However, an ^1H NMR recorded in C_6D_6

verified the presence of a doublet at $\delta = 6.0$ ppm, suggesting that complex **30** could be the intermediate formed during the decomposition reaction of complex **12a**.

The obtained ^1H NMR spectrum of **30** indicated a pyridyl ligand and a phosphonium counterion in ratio 1:1, suggesting a monoionic palladium complex. A large coupling constant of $^1J_{\text{P-H}} = 450$ Hz was exhibited by the $[\text{HP}(t\text{-Bu})_3]^+$ proton.¹³⁹ A similar coupling constant $^1J_{\text{P-H}} = 446$ Hz is reported for the phosphonium cation in anionic dimer **29**.⁸¹ Additionally, a broad singlet at $\delta = 11.9$ ppm was observed, indicating an acidic proton (not in figure). The downfield shifted proton at $\delta = 11.9$ ppm disappeared with the addition of D_2O . Due to the 4-fold increase in basicity for a 2-palladated pyridyl species,⁶⁸ addition of a Brønsted acid can protonate the pyridyl nitrogen, which could result in a carbene-type pyridylidene binding of the ligand.⁹⁴ The NMR spectra shown in figure 2.8 reveals a downfield shift of the aromatic signals for anionic complex **30** in comparison to pyridyl complex **12a**. Similar deshielding has previously been reported for protonated 2-pyridyl species.^{68,95} Another indication of a carbene type binding can be seen by comparison of the chemical shift of the metalated carbon. Downfield shifts up to $\delta = 194$ ppm has been reported for 2-, 3- and 4-pyridylidene complexes with nickel or palladium metals.⁹⁶ However, anionic complex **30** only exhibited a small downfield ^{13}C chemical shift of $\delta = 170$ ppm in comparison to the parent pyridyl complex **12a** with a shift of $\delta = 164$ ppm. Similarly to anionic dimer **29**, the formation of anionic complex **30** is likely an equilibrium between the product and the starting aryl complex.¹³⁷ Product formation is driven by the precipitation of anionic complex **30** due to low solubility in nonpolar organic solvents.

Single crystals of complex **30** were obtained by slow diffusion of hexane into a MeCN/benzene solution and the X-ray analysis is shown in figure 2.9. The crystal structure of palladium complex **30** revealed a monomeric palladium(II) species with a protonated $[\text{HP}(t\text{-Bu})_3]^+$ cation as counterion. The ligands around the palladium center exhibit an almost perfect square planar conformation. A Pd–C(1) bond of 1.97 Å was found, identical to the Pd–C(1) bond of parent pyridyl complex **12a**. An N–H proton was calculated at a distance of 0.91 Å, resulting in an overall neutral palladium(II) complex. The Pd–Br(3) bond was longer than the Pd–Br(1) and Pd–Br(2) bonds, consistent with the larger *trans* influence of the 2-pyridyl ligand. The C–N–C bond angle of the pyridyl ligand was 127 Å. Protonation of pyridine has been reported to increase the C–N–C bond angle from 117° to 123° for the pyridinium species.¹²⁹ A similar iridium(III) complex bearing a protonated pyridyl ligand exhibited a C–N–C angle of 128 Å.¹⁴⁰ The distance between the nitrogen-bound hydrogen and the neighboring bromide was 2.58 Å, indicating an interaction. A similar interaction has previously been proposed for a cyclometalated 2-pyridylidene palladium(II) complex.⁹⁴

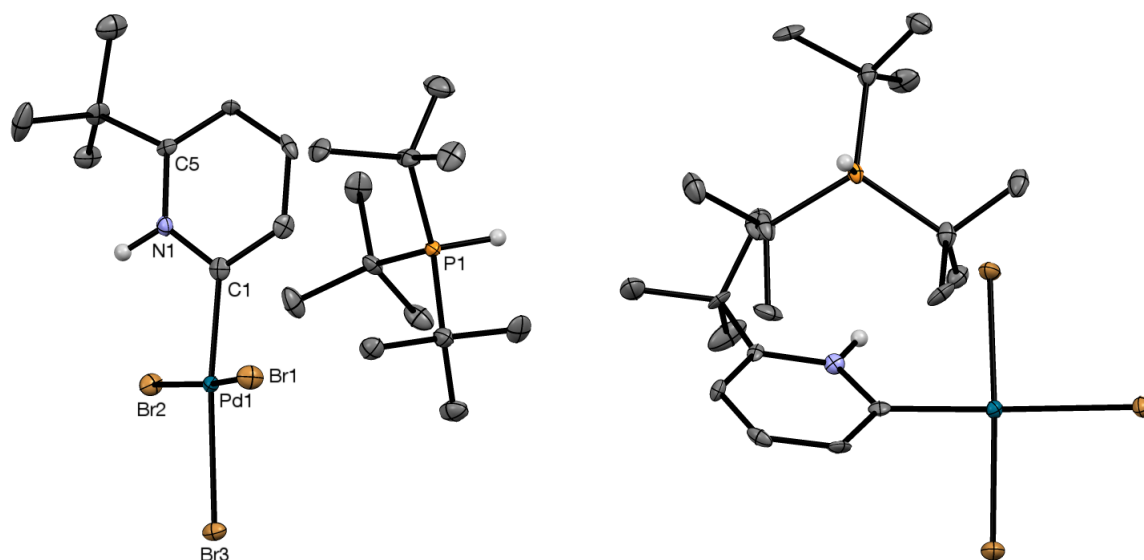
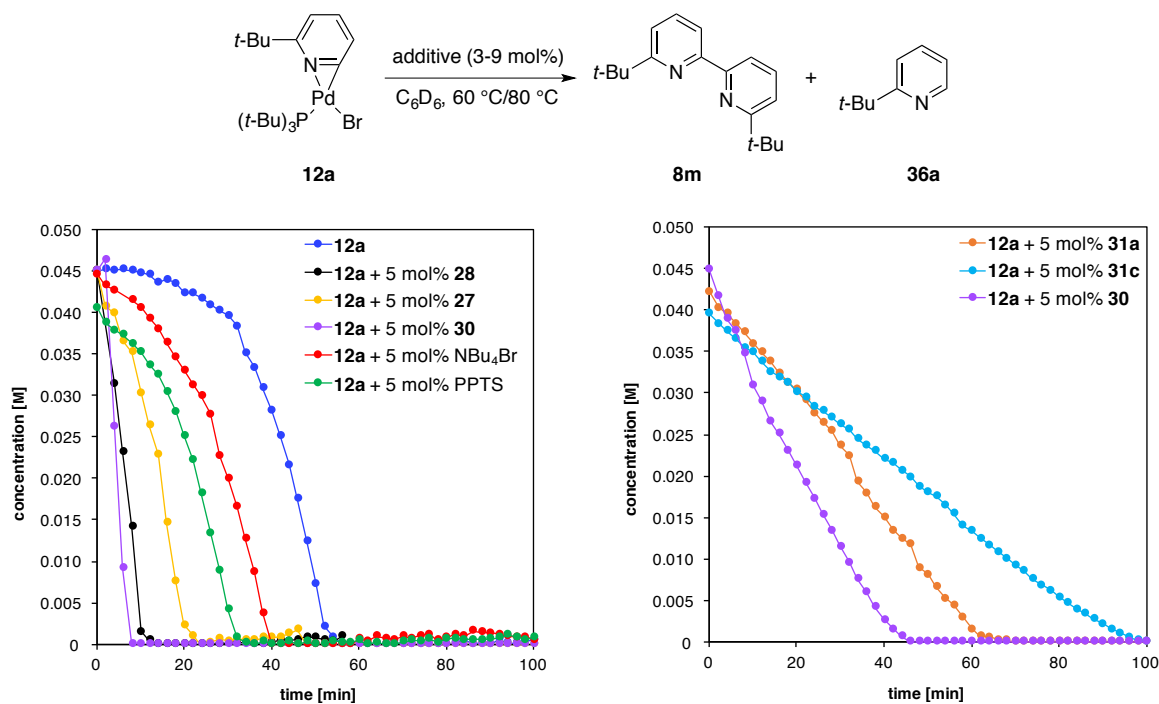


Figure 2.9. ORTEP drawing of **30**. Thermal ellipsoids are drawn at 50% probability level. Selected hydrogen atoms are shown. Selected bond distances (Å) and angles (°): Pd1–C1 1.974, Pd1–Br1 2.438, Pd1–Br2 2.452, Pd1–Br3 2.521, C1–Pd1–Br1 89.07, C1–Pd1–Br2 89.31, C1–Pd1–Br3 173.70.

With an increased carbenic binding, an elongation of the C–N bonds of the pyridyl ring would be expected. Anionic complex **30** exhibited a C(1)–N bond of 1.36 Å, being slightly longer than 1.34 Å observed in free pyridine or 1.35 Å observed for the bipyridine-ligated pyridyl complex **18** shown above. A shortening of the M–C bond for carbenic binding ligands due to a more double bond character has been observed.^{97,141} However, the Pd–C bond of complex **30** was 1.97 Å, being almost identical to the Pd–C bond of bipyridine pyridyl complex **18** of 1.98 Å. The above observations could indicate a slight carbenic character of the pyridyl ligand, however are ambiguous.

Due to the low solubility of complex **30** in benzene, the synthesis of a complex bearing a more lipophilic counterion was attempted. However, reaction between [NR₄]Br compounds and complex **12a** did not result in another anionic pyridyl complex. Instead, addition of potentially catalytic compounds to the decomposition reaction of **12a** was investigated. Palladium(I)-dimer **27**, phosphonium salt **28** and the two palladate complexes (HP(*t*-Bu)₃)₂[PdBr₄] **31a** and (NOct₄)₂[PdBr₄] **31c** were employed due to their formation under the reaction conditions or their proposed reactivity towards aryl palladium(II) complexes.⁷⁴ To investigate influence of acid or bromide anions, two reactions were performed with PPTS (pyridinium *para*-toluenesulfonate) and tetrabutylammonium bromide (NBu₄Br). Also, the influence of anionic complex **30** was investigated. Complex **12a** (*c* = 0.045 M) and additive (3–9 mol%) were dissolved in C₆D₆ and heated to 60–80 °C. Consumption of pyridyl complex **12a** and formation of bipyridine **8m** and anionic complex **30** were monitored via ¹H NMR and is shown in table 2.1.

Table 2.1. Decomposition rate of **12a** ($c_0 = 0.045$ M) in C_6D_6 and formation rate of **8m** with additives at different temperatures. Plot of decomposition of **12a** at 80 °C (left) and 60 °C (right). Yields determined via 1H NMR with 1,3,5-trimethoxybenzene as standard.



entry	additive [mol%]	temperature [°C]	k_{obs}	k_{obs}	yield	yield
			12a [mM/min]	8m [mM/min]	8m [%]	36a [%]
1	no additive	80 °C	-1.8	+0.97	97	2
2	27 (5 mol%)	80 °C	-2.9	+1.6	92	2
3	28 (5 mol%)	80 °C	-4.3	+2.2	90	3
4	30 (5 mol%)	80 °C	-7.8	+4.5	94	4
5	NBu_4Br (5 mol%)	80 °C	-1.9	+0.88	84	2
6	PPTS (5 mol%)	80 °C	-1.9	+1.0	89	-
7	28 (9 mol%)	80 °C	-3.6	+1.8	94	3
8	31c (3 mol%)	80 °C	-3.8	+1.9	108	0
9	31a (5 mol%)	60 °C	-0.69	+0.40	82	0
10	31c (5 mol%)	60 °C	-0.42	+0.20	92	0
11	30 (5 mol%)	60 °C	-1.0	+0.49	95	0
12	31c (3 mol%)	60 °C	-0.33	+0.17	94	0
13	30 (9 mol%)	60 °C	-1.0	+0.55	97	0
14	31c (3 mol%)	50 °C	-0.13	+0.075	101	0
15	30 (9 mol%)	50 °C	-0.68	+0.31	100	0
16	30 (9 mol%)	25 °C	-0.086	+0.048	98	0

The main aromatic product from all decomposition reactions was the bipyridine homocoupling product **8m**. In reactions performed at 80 °C, also the proto-demetalation product *tert*-butyl pyridine **36a** was formed; however **36a** was not detected at lower temperatures. Detailed plots of each reaction is shown in Experimental section 4.10.

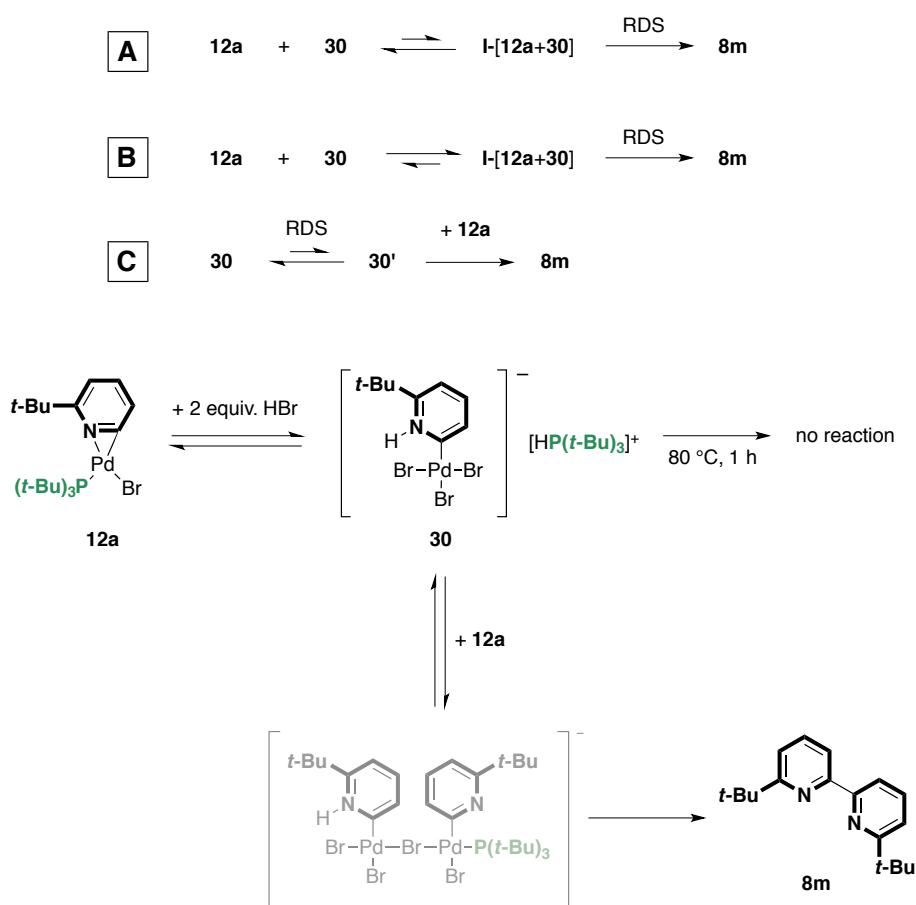
A comparison of potential catalysts added in 5 mol% at 80 °C is shown in table 2.1, left (entry 1-6). The non-catalyzed decomposition of pyridyl complex **12a** (blue) shows the apparent autocatalytic behavior. With the addition of NBu₄Br (red) and PPTS (green), an increase in decomposition rate of **12a** was observed. However, an induction period of 15-20 minutes was still present. A slight induction period was also present with the addition of palladium(I)-dimer **27** (yellow). This is indicative of that the autocatalysis is not driven by only a Brønsted acid, a bromide anion or a palladium(I) species. However, dimer **27** decomposes fast to phosphonium salt **28**, hydridopalladium complex **26**, complex **B** and free P(*t*-Bu)₃ ligand at 80 °C (see Experimental section 4.10.5), of which one or more could act as a catalyst. In comparison, the addition of phosphonium salt **28** and anionic complex **30** resulted in a fast linear decay of pyridyl complex **12a**, with the complex being completely consumed within 15 minutes. The increase in rate at 80 °C follows the trend **30** > **28** > **27** > PPTS > NBu₄Br.

A set of decomposition experiments at 60 °C was also performed as shown in table 2.1, right (entry 9-13). Anionic complex **30** (purple), palladate complexes **31a** (orange) and palladate complex **31c** (blue) added in 5 mol% (entry 9-11) resulted in a clear linear consumption rate of pyridyl complex **12a**. The increase in reaction rate followed **30** > **31a** > **31c**. The change in decay of complex **12a** is indicating that an ionic species plays an important role in the decomposition reaction. Arguably, the increase in rate with all above additives is due to formation of anionic complex **30**. As shown above, phosphonium salt **28** together with **12a** forms anionic complex **30** fast at room temperature. Dianionic palladate complexes **31a** and **31c** can release phosphonium or ammonium bromide that can form an anionic complex. In the initial samples of the reactions with palladates **31a** and **31c**, 5-10% of pyridyl complex **12a** was already converted to the anionic pyridyl complex **30**, indicating its fast formation at room temperature.

Decomposition of **12a** in the presence of tetraoctylammonium palladate **31c** (3 mol%) was performed at 50 °C, 60 °C and 80 °C (entry 8, 12, 14). All reactions exhibited an apparent zero-order decay of pyridyl complex **12a** without induction period. At 80 °C, pyridyl complex **12a** was consumed with a rate of $k_{\text{obs}} = -3.8$ mM/min and complete within 10 minutes. Lowering the temperature to 60 °C gave a consumption rate of $k_{\text{obs}} = -0.33$ mM/min and at 50 °C, a consumption rate of $k_{\text{obs}} = -0.13$ mM/min was observed. After 4 hours of reaction at 50 °C, only 60% of pyridyl complex **12a** was consumed. Not enough data is available to determine the dependence on the catalyst **31c**. However, increasing the loading from 3 mol% to 5 mol% at 60 °C showed to increase the reaction rate of approximately 20%

(entry 10 and 12). Comparison of the reactions with 5 mol% and 9 mol% anionic complex **30** at 60 °C (entry 11 and 13) showed that no increase in consumption rate of pyridyl complex **12a** was detectable with higher concentration of **30**. Both reactions resulted in a consumption rate of $k_{\text{obs}} = -1.0$ mM/min of complex **12a**. Potentially, the low solubility of anionic complex **30** in benzene could result in only a low concentration of **30** present at each time point of the reaction. A similar explanation is suggested for the addition of phosphonium salt **28**. Addition of 5 mol% of **28** at 80 °C resulted in a fast linear decay of $k_{\text{obs}} = -4.3$ mM/min without an induction period (entry 3). Increasing the loading to 9 mol% of **28** at the same temperature did not increase the consumption rate of complex **12a** but a rate of $k_{\text{obs}} = -3.6$ mM/min (entry 7) was obtained. Phosphonium salt **28** also exhibits a low solubility in nonpolar solvents, which is a possible reason for the absence of rate increase. Furthermore, an increased concentration of P(*t*-Bu)₃ ligand could play a role. If the reactivity is dependent on the displacement of P(*t*-Bu)₃ to yield anionic complex **30**, the equilibrium could be shifted to the starting material side with a higher ligand concentration. In all reactions, no complex **30** was detected in the last sample when pyridyl complex **12a** was completely consumed. Yet, this could be due to the low solubility of **30** in benzene. It needs to be noted that the counterion of **30** not necessarily is [HP(*t*-Bu)₃]⁺. With the addition of NBu₄Br or (NOct₄)₂[PdBr₄] palladate **31c**, the cation could be [NR₄]⁺ as well. Concomitant with cyclometalation of **27** forming complex **B** (see above, scheme 2.17), HBr would form which would provide a proton for the pyridyl ring of **30**.

In contrast to phenyl complex **14a**, pyridyl complex **12a** exhibited an induction period prior to consumption. With additives that could promote formation of anionic complex **30**, a zero-order dependence on **12a** was observed, indicating that **12a** does not participate in the rate-determining step. Scheme 2.18 shows an overview of plausible scenarios which could explain the observed kinetic behavior for the homocoupling reaction of **12a**. **A** and **B** show an equilibrium between **12a** and **30** and an unidentified intermediate **I-[12a+30]**. This intermediate would undergo the irreversible rate-determining aryl transfer and fast reductive elimination forming homocoupling product **8m**. However, if the equilibrium lies on the left side (**A**), the concentration of **12a** would be present in the rate law because the concentration of **I-[12a+30]** would be proportional to **12a**. Therefore, the observed kinetic rules out the scenario in **A**. If the equilibrium lies far on the side of **I-[12a+30]** (**B**), almost all **30** would be immediately converted to the intermediate and its concentration would become essentially independent of the concentration of **12a**. Overall a zero-order dependence on pyridyl complex **12a** would be observed. Another possible scenario is a unimolecular reaction of anionic complex **30** in a rate-determining step to an unidentified intermediate **30'** (**C**), which subsequently reacts with **12a** in a fast aryl transfer step. In this case, the dependence on pyridyl complex **12a** would be zero-order. However, no new species that could belong to an intermediate **30'** were observed when heating anionic dimer **30** for 80 °C in the absence of pyridyl complex **12a**. The high stability of complex **30** makes the formation of another intermediate less likely.



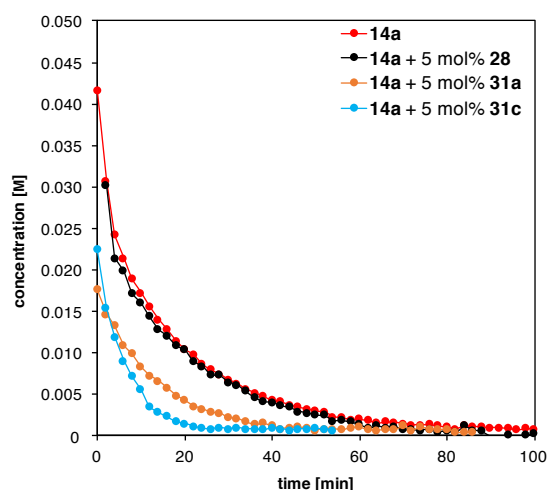
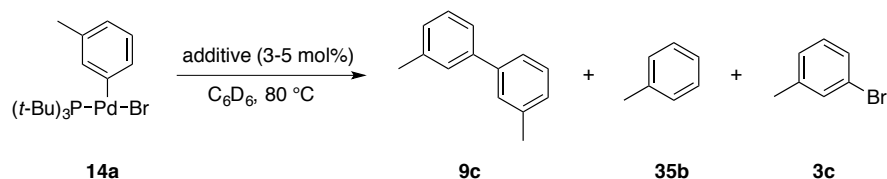
Scheme 2.18. Potential reaction pathways of pyridyl complex **12a** and anionic complex **30**.

Therefore, the pathway suggested in **B** is favored. A plausible structure for **I-[12a+30]** is shown in scheme 2.18. The intermediate is envisioned as a binuclear palladium complex with a bridging bromide ligand, and one protonated pyridyl ligand. Loss of $P(t\text{-Bu})_3$ ligand would result in an open coordination site and allow for rate-determining aryl transfer and subsequent reductive elimination forming bipyridine **8m**. Although no signals in the ^1H NMR could be assigned to such an intermediate, it seems plausible that the intermediate exhibits similar shifts to the reacting complexes because of its structural similarity and therefore, remains unidentified.

Interestingly, the addition of 2 equivalents of K_3PO_4 to a solution of pyridyl complex **12a** in C_6D_6 substantially decreased the decomposition rate. No graph of the decay was determined but after 2 hours of heating at $80\text{ }^\circ\text{C}$, only 5% of pyridyl complex **12a** was converted to bipyridine **8m**. Compared to the reaction without base added where all of **12a** was consumed within 1 hour at $80\text{ }^\circ\text{C}$, a significant increase in stability of **12a** was obtained with the addition of base. Likely, a base removes the HBr required for the formation of complex **30**. As the basicity of 2-pyridyl palladium complexes increase in comparison to free pyridine,⁶⁸ the presence of basic bipyridine **8m** should not influence the formation of anionic complex **30**.

The stability of phosphine-free pyridyl palladium(II) complexes **17** and **18** was also investigated. If a complex with bipyridine product would influence the decomposition, a 2,2'-bipyridine type complex **18** would be formed as shown above in scheme 2.14. Complex **18** was added to an NMR tube with C₆D₆ and heated at 80 °C five days, after which approximately 40% of **18** was converted to homocoupling product **8m**. The slow decomposition could however partially be due to the low solubility of **18** in C₆D₆. Heating of pyridine-ligated pyridyl dimer **17** in C₆D₆ at 80 °C also resulted in a slow formation of bipyridine homocoupling product **8m**. After heating for five days, 60% of dimer **17** was converted to bipyridine **8m**. An additional unidentified species was observed, potentially arising from coordination of **8m** to a palladium species. However, the observed stability of complex **17** and **18** rules out their intermediacy in the homocoupling reaction.

An analogous investigation of additives on the decomposition reaction was performed for phenyl complex **14a**. Although anionic dimer **29d** could not be isolated, formation of such a species could take place *in situ* by the combination of phenyl complex **14a** and phosphonium salt **28** or palladate complexes **31a** or **31c**. The consumption rates of phenyl complex **14a** and the first-order rate constant with additives at 80 °C are summarized in table 2.2. With all additives, an exponential decay of phenyl complex **14a** was observed. Even in the first spectrum measured, ~50% of **14a** was consumed, which indicates that a fast decomposition takes place already at room temperature. However, no decomposition reactions at lower temperature were performed. As can be seen from the consumption graphs in table 2.2, an increase in rate with additives following the trend **31c** >> **31a** > **28** was observed. Anionic palladate **31c** increased the consumption rate of phenyl complex **14a** the most. Likely, the superior solubility of **31c** in comparison to **31a** in benzene is responsible for the increase. In comparison, the opposite trend was observed for pyridyl complex **12a**, where the decomposition rate was increased by anionic [HP(*t*-Bu)₃]⁺ palladate **31a** to a larger extent than [NOct₄]⁺ palladate **31c**. It might be expected that palladate **31a** containing an acidic proton will favor the formation of protonated anionic complex **30**, which is not required for the formation of phenyl palladate **29d**.

Table 2.2. Decomposition rates of **14a** ($c_0 = 0.045$ M) in C_6D_6 at 80 °C with additives. Yields determined via 1H NMR with 1,3,5-trimethoxybenzene as standard.

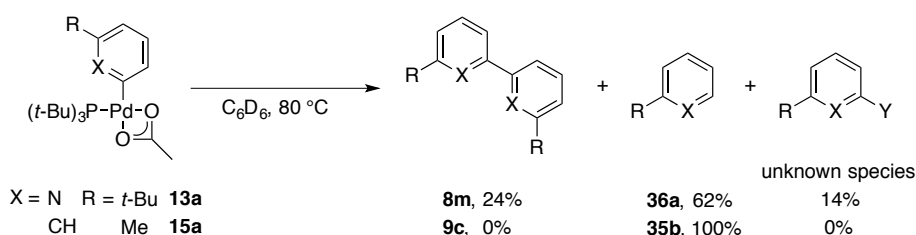
entry	additive [mol%]	temperature [°C]	k_{obs}	yield	yield	yield
			14a [min ⁻¹]	9c [%]	35b [%]	3c [%]
1	no additive	80 °C	-0.045	26	42	11
2	28 (5 mol%)	80 °C	-0.050	27	46	10
3	31a (5 mol%)	80 °C	-0.066	32	35	10
4	31c (3 mol%)	80 °C	-0.13	51	26	3

The putative dianionic dimer **29d** with a chemical shift $\delta = 2.15$ ppm was observed in all decomposition reactions. In the reaction without additive (red) and the reaction with phosphonium salt **28** (black), an initial fast formation rate of the putative dimer **29d** until $t = 40$ minutes was observed. Thereafter, an equilibrium was reached. In contrast, the reactions with palladate complexes **31a** and **31c** (orange and blue), dimer **29d** was already present in the initial sample and the concentration was close to constant throughout the reaction (see Experimental section 4.10.2). Comparing the products formed after decomposition revealed similar yields of biphenyl homocoupling product **9c** in the reaction without additive in comparison to with **28** and **31a** added. With palladate **31c**, a large increase in consumption rate of phenyl complex **14a** also resulted in an increase in biphenyl **9c** yield and a decrease in formation of toluene product **35b**. The hypothesis is that palladate **31c** results in a faster formation of an anionic dimer **29d** and that transmetalation takes place between a phenyl complex **14a** and an anionic species. Due to the smaller steric hindrance, reductive elimination from anionic **29d**

would be less favored, suggesting an explanation why bromotoluene **3c** was obtained in lower amount with **31c** (3%) in comparison to the other reactions (10-11%).

As stated above, the κ^2 -bound acetate complexes **13a** and **15a** exhibited a high stability in solution. Heating at 80 °C in C₆D₆ required several hours to completely consume both complexes. Therefore, no monitoring of the decomposition was performed. To probe the dependence on aryl substituent, the product ratios were determined after complete consumption of the complexes. Heating phenyl palladium complex **15a** in for 4 h C₆D₆ at 80 °C converted ~80% of **15a** and heating overnight resulted in the formation of palladium(0) complex **32**, oxidized phosphine O=P(*t*-Bu)₃ and cyclometalated acetate complex **A** (table 2.3). Heating pyridyl palladium complex **13a** overnight in C₆D₆ at 80 °C only resulted in ~10% conversion of **13a**. Further heating for 2 days resulted in complete conversion of **13a** and formation of palladium(0) species **32**, free phosphine ligand and a phosphorus species with a downfield shift of $\delta = 116$ ppm.

Table 2.3. Decomposition of acetate complexes **13a**, **15a** and ratio of products formed after decomposition.



entry	aryl complex	time [h]	13a/15a [%]	complex A [%]	32 [%]	P(<i>t</i> -Bu) ₃ [%]	O=P(<i>t</i> -Bu) ₃ [%]	116 ppm [%]
1	13a	2	100	0	0	0	-	0
		18	75	17	5	0	-	3
		80	0	0	27	24	-	49
2	15a	2	54	45	1	-	0	-
		4	18	74	1	-	7	-
		18	0	80	6	-	14	-

In stark contrast to the decomposition of the analogous bromide-ligated complexes **12a** and **14a**, palladium(0) species **32** was obtained for both pyridyl palladium complex **13a** and phenyl palladium complex **15a**, indicating that HOAc does not consume complex **32** in the same manner as HBr. Homocoupling of phenyl complex **15a** to biphenyl product **9c** did not take place. Only toluene product **35b** was observed via ¹H NMR in combination with complex **A** (80%). This observation is analogous to the reported decomposition of (3-CH₂F-phenyl)Pd(OAc)(P(*t*-Bu)₃) **15c**, where after heating for 8 hours at 60 °C, cyclometalated complex **A** and fluoromethylbenzene **35c** was obtained.⁴ Arguably, an intramolecular deprotonation via the coordinated acetate takes place on the phosphine ligand,⁴¹

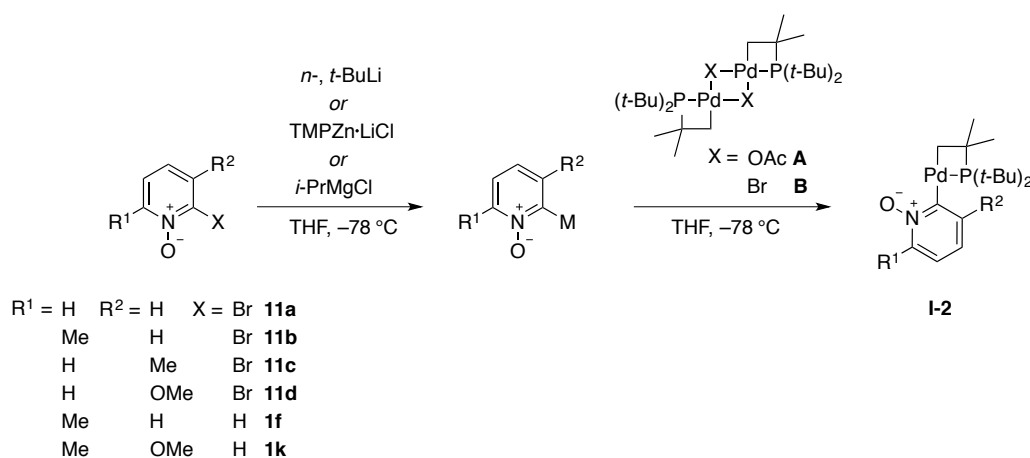
forming a cyclometalated functionality and HOAc subsequently acts as an acid to donate a proton to the C–Pd bond, forming toluene **35b**. Apart from complex **A**, only small amount of oxidized phosphine and complex **32** were obtained after heating over night, which is expected since no homocoupling product was formed. As previously reported, decomposition of complex **A** in benzene results in a small amount of complex **32** and P(*t*-Bu)₃ ligand.⁴² A comproportionation process analogous to the formation of palladium(I)-dimer **27** or a hydridopalladium species analogous to complex **26** was not found in the decomposition of complex **15a**.

In contrast, decomposition of pyridyl complex **13a** resulted in bipyridine homocoupling product **8m** in addition to 2-*tert*-butyl pyridine **36a**. Cyclometalated complex **A** (17%) was observed after 18 hours of heating when pyridyl complex **13a** (75%) was still present. Subsequently, complex **A** was consumed completely with the formation of palladium(0) **32** (27%) and an unidentified species with ³¹P NMR signal at $\delta = 116$ ppm (49%). The signal at $\delta = 116$ ppm has neither been observed in the ³¹P NMR monitoring of the catalytic reaction between *N*-oxide **1** and bromopyridine **2**,⁴² nor in a transmetalation reaction between pyridyl palladium acetate complex **13a** and an cyclometalated pyridyl *N*-oxide palladium complex **21**, **22** (see below, section 2.3.7). Furthermore, independent decomposition of complex **A** resulted in unidentified species with downfield shifted signals at $\delta = 124$ and $\delta = 133$ ppm, however no signal at $\delta = 116$ ppm was observed.⁴² The signal does not necessarily correspond to a palladium complex, but could belong to a metal-free phosphorus compound. By ¹H NMR, another unidentified species with three aromatic signals in similar yield as bipyridine homocoupling product **8m** was observed. Independent synthesis of a 2-acetoxypyridine and 2-hydroxypyridine showed that none of the two compounds were formed during the decomposition reaction. A plausible origin of the signal could be protonated homocoupling product. Due to the basicity of bipyridines ($pK_a \sim 4.3$), the formation of AcOH could lead to a bipyridinium species. The high coordination potential of bipyridines could result in coordination of **8m** to a palladium(II) species. However, no further analysis on the unidentified decomposition products was performed.

2.3.4 Synthesis of a pyridyl *N*-oxide intermediate

For the formation of a 2-pyridyl *N*-oxide intermediate, the assumption is that the reaction between a metalated pyridine *N*-oxide and cyclometalated palladium complex **A** or **B** at low temperatures will form intermediate **I-2**. As shown in Chapter 1, the kinetic experiments were performed with 4-substituted pyridine *N*-oxides. Ideally, employing 4-substituted pyridine *N*-oxides for the formation of a cyclometalated pyridyl *N*-oxide intermediate **I-2** would be desirable. However, the presence of two C–H bonds *ortho* to the *N*-oxide moiety is likely to cause mixed products. To circumvent the need

for separation of two or more complexes, attempts to form intermediate **I-2** were performed with 2-brominated *N*-oxides **11** or 2-substituted *N*-oxides **1f-k**, as outlined in scheme 2.19.

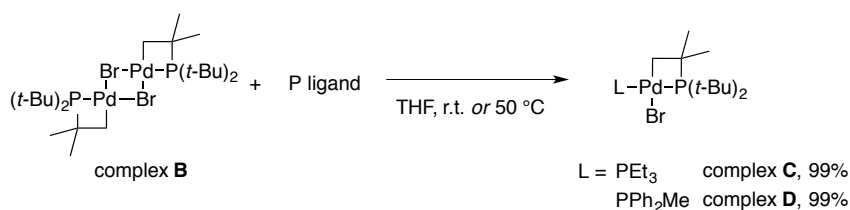


Scheme 2.19. Approaches to synthesize pyridyl *N*-oxide palladium intermediate **I-2**.

Initially, lithium-bromide exchange on 2-bromopyridine *N*-oxides **11** was tested to achieve metalation *ortho* to the *N*-oxide. Subsequently, the metalated species was quenched with *para*-chlorobenzaldehyde to quantify the lithium-bromide exchange. Unsubstituted 2-bromopyridine *N*-oxide **11a**, 2-bromo-3-methyl pyridine *N*-oxide **11c** and 2-bromo-3-methoxy pyridine *N*-oxide **11d** can easily be prepared by oxidation of the 2-bromopyridine derivative by either *m*-CPBA or H₂O₂ in acetic acid. The substrates **11** were treated with 1-2 equivalents *n*-BuLi or *t*-BuLi in THF at -78 °C. However, in addition to bromide-lithium exchange, deprotonation of the acidic proton in 6-position was observed. Even when applying only 1 equivalent of the lithium reagent, a mixture of products was obtained. The methoxy substrate **11d** was superior in reactivity in comparison to the methyl substrate **11c**, where in the former only two products were observed and the latter yielded a mixture of products. The superiority of a 3-methoxy substrate **11d** is likely due to the chelating potential of the lithium by the *N*-oxide moiety and the 3-methoxy group.¹⁰¹ However, **11d** exhibited a low solubility at -78 °C. Increasing the temperature to -45 °C dissolved the starting material, however, also increased side reactions. Alternatively, a 6-substituted bromopyridine *N*-oxide was applied. 2-Bromo-6-methyl pyridine *N*-oxide **11b** was treated in the identical manner with *n*-BuLi and by quenching with *para*-chlorobenzaldehyde, complete conversion to monobenzylic alcohol product was obtained. However, exchanging the electrophile to cyclometalated acetate complex **A** or bromide complex **B** in the reaction with lithiated 6-methyl pyridine *N*-oxide resulted in re-isolation of starting material or unidentified phosphorus species. A cyclometalated complex of the type **I-2** is expected to have a ³¹P shift around or shifted upfield from 0 ppm,⁴³ however no such species were observed. Likely, a reaction of lithium base with the palladium substrate or an influence of the formed butyl bromide is present.

As an alternative to lithium-bromide exchange, a direct *ortho* metalation approach was applied on 2-picoline *N*-oxide **1f** and 5-methoxy-2-methyl pyridine *N*-oxide **1k** (scheme 2.19). Due to the presence of a substituent in 2-position, selective deprotonation of the 6-position *ortho* to the *N*-oxide, should take place. Metalation was carried out with 1-2 equivalents of *n*-BuLi. However, incomplete conversion to the benzylic alcohol was observed when quenching the lithiated *N*-oxide with *para*-chlorobenzaldehyde. Similar results were obtained in the direct *ortho* metalation of pyridine *N*-oxides **1f** and **1k** with 1.2 equivalents of TMPZnCl·LiCl¹⁰⁵ or *i*-PrMgCl in THF.¹⁰⁷ Reaction of the metalated *N*-oxides with palladium complex **B** resulted in multiple unidentified species detected by ³¹P NMR. Likely, the putative Pd–O interaction is too weak to stabilize intermediate **I-2** enough for isolation.

Attempts to stabilize intermediate **I-2** by an additional ligand were made. Ideally, a stabilizing ligand should be basic enough to be not displaced by the alkali base used for deprotonation but labile enough to not inhibit transmetalation with aryl palladium complexes **12-15**. Stambuli and co-workers reported the synthesis of a cyclometalated P(*t*-Bu)₃ acetate complex with an additional P(*t*-Bu)₃ ligand. However, that complex exists in equilibrium with the dimeric complex **A** formed by dissociation of the phosphine.⁴³ The large steric bulk of P(*t*-Bu)₃ (cone angle 182°) might favor dissociation of the ligand to form the dimeric complex **A**. Instead, smaller phosphine ligands were employed. PEt₃ and PPh₂Me both have distinctively smaller cone angles of 132° and 136°, respectively.¹⁴² Both cyclometalated PEt₃ and PPh₂Me complexes **C** and **D** could be prepared starting from the cyclometalated complex **B** and 2 equivalents of phosphine ligand (scheme 2.20). The monomeric complexes (CMe₂CH₂P(*t*-Bu)₂)Pd(Br)(L) **C** and **D** were obtained in almost quantitative yields.



Scheme 2.20. Formation of PEt₃ or PPh₂Me-stabilized monomeric palladium precursors **C** and **D** by addition of phosphine ligand (2 equiv.) to palladium complex **B**.

Complex **C** exhibited two doublets in the ³¹P NMR at $\delta = 12.6$ and $\delta = -10.7$ ppm with a coupling constant of $J_{\text{P-P}} = 426$ Hz. Only the *trans* isomer was obtained. Similarly, complex **D** gave rise to two doublets at $\delta = 6.89$ and $\delta = -13.7$ ppm with $J_{\text{P-P}} = 437$ Hz. Both complexes have similar chemical shifts in comparison to the reported PEt₃-ligated cyclometalated monomeric palladium(II) complex with a chloride ligand.⁵⁰ Single crystals of complex **C** could be obtained by slow crystallization in pentane and the structure from X-ray analysis is shown in figure 2.10.

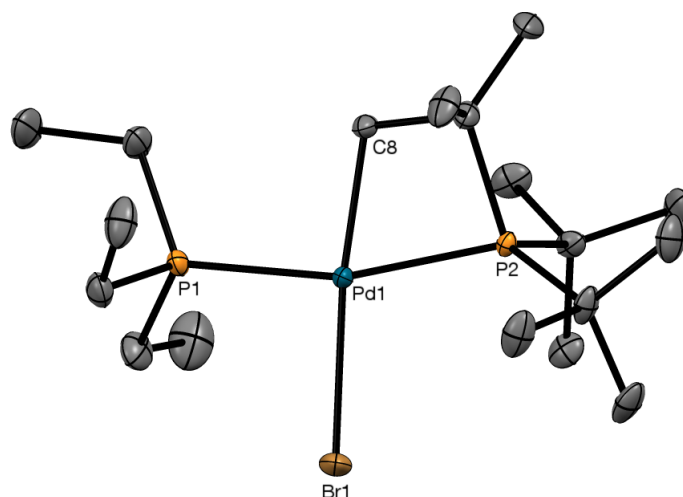
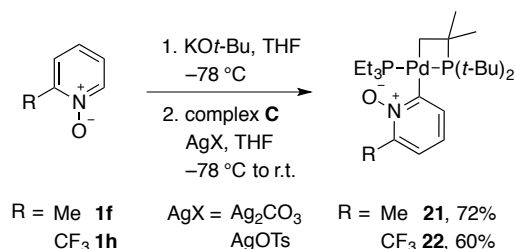


Figure 2.10. ORTEP drawing of complex **C**. Thermal ellipsoids are drawn at 50% probability level. Hydrogen atoms are omitted for clarity. Selected bond distances (Å) and angles (°): Pd1–P1 2.303, Pd1–C8 2.064, Pd1–P2 2.283, Pd1–Br1 2.534, C8–Pd1–P2 69.90, P1–Pd1–P2 163.14, C8–Pd1–Br1 172.55.

A slightly distorted square planar geometry around the palladium(II) metal was observed. The bond lengths of cyclometalated Pd–P(2) and Pd–C(8) are 2.28 Å and 2.06 Å, respectively. These are in the same range as the acetate monomer with a P(*t*-Bu)₃ ligand instead of a PEt₃, where Pd–P bonds of 2.28 Å and Pd–C 2.07 Å were observed.⁴³ The bite angle of the cyclometalated phosphine ligand is 69.9°, comparable to the analogous acetate monomer with a bite angle of 68.3°.⁴³

Due to the side reactions observed with alkyl lithium bases, reactions with another alkali base were performed. Alkoxide bases such as KO*t*-Bu or LiO*t*-Bu have been shown to deprotonate substituted quinoline and bipyridine *N*-oxides in *ortho*-position, which subsequently undergo homocoupling to the dimeric compounds.¹⁴³ KO*t*-Bu is a bulky, non-nucleophilic base and might be less prone to react with an electrophilic palladium species. To form a more electrophilic palladium species and facilitate nucleophilic attack of a metalated pyridine *N*-oxide on palladium complex **C**, Ag₂CO₃ was added. Silver salts can displace halides on palladium complexes and were previously used by Hartwig and co-workers to form a similar cyclometalated benzothienyl complex.⁴ KO*t*-Bu was added to 2-picoline *N*-oxide **1f** at –78 °C and after stirring for 20 minutes, complex **C** and Ag₂CO₃ were added (scheme 2.21). After warming to room temperature, the solid AgBr and palladium black were filtered off and the solvent removed, resulting in methyl pyridyl *N*-oxide complex **21** in 72% yield. However, complex **21** exhibited a high solubility in nonpolar solvents, complicating precipitation. Therefore, a complete conversion of starting complex **C** was required in order to allow isolation for **21**. With the aim of obtaining one electron-rich and one electron-poor pyridyl *N*-oxide complex, an analogous reaction was performed on 2-trifluoromethyl pyridine *N*-oxide **1h**. However, applying identical conditions to *N*-oxide **1h** resulted in a mixture of trifluoromethyl pyridyl *N*-oxide complex **22** and starting complex **C**. As for the methyl *N*-oxide complex **21**, a very high solubility of complex **22** was observed and no

precipitation was possible to separate the starting material from product. To increase the electrophilicity of complex **C** for reaction with the less nucleophilic trifluoromethyl *N*-oxide **1h**, Ag₂CO₃ was replaced with AgOTs. Bromide displacement by tosylate and precipitation of AgBr results in a cationic palladium intermediate, facilitating the reaction with trifluoromethyl *N*-oxide **1h** (scheme 2.21). Trifluoromethyl pyridyl *N*-oxide complex **22** was obtained as an orange solid in 60% yield.



Scheme 2.21. Synthesis of methyl pyridyl *N*-oxide complex **21** and trifluoromethyl pyridyl *N*-oxide complex **22** from pyridine *N*-oxide **1f/1h** (1 equiv.) and KO*t*-Bu (1.2 equiv.), palladium complex **C** (0.8 equiv.) and silver salt (1.6 equiv.).

The spectrum of complex **21** exhibited two doublets at $\delta = 16.6$ ppm and $\delta = 4.66$ ppm with a coupling constant of $J_{\text{P-P}} = 402$ Hz. Similar ³¹P shifts were observed for complex **22** where two doublets at $\delta = 16.6$ ppm and $\delta = 3.33$ ppm with a coupling constant of $J_{\text{P-P}} = 397$ Hz were obtained. Crystallization of methyl *N*-oxide complex **21** and trifluoromethyl *N*-oxide complex **22** was performed by slow evaporation in pentane at -25° or diffusion of TMS into a pentane solution. Single crystals suitable for X-ray analysis were obtained and the solid-state structures are shown in figure 2.11.

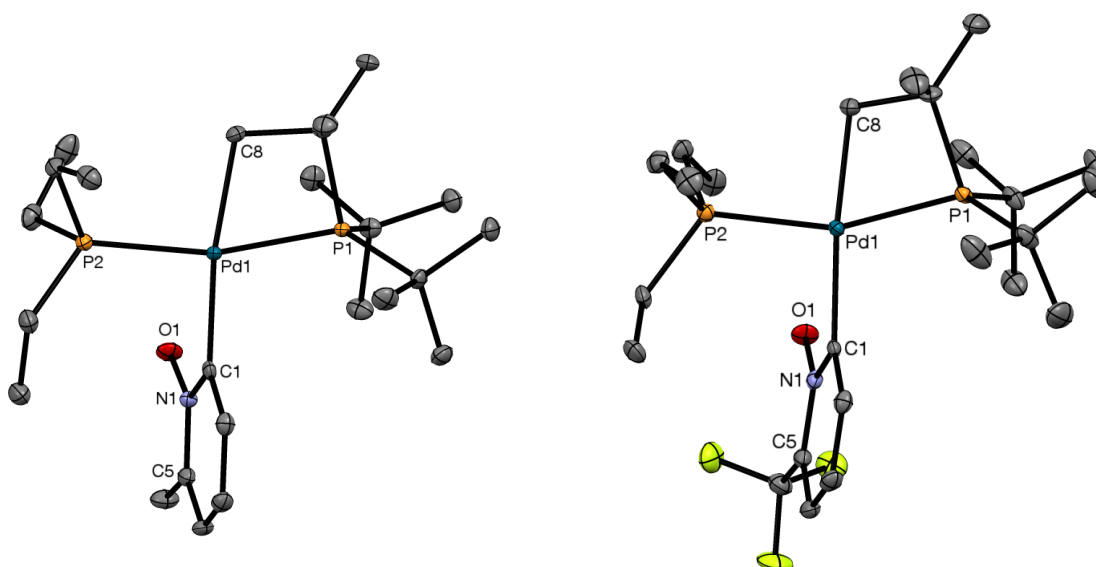


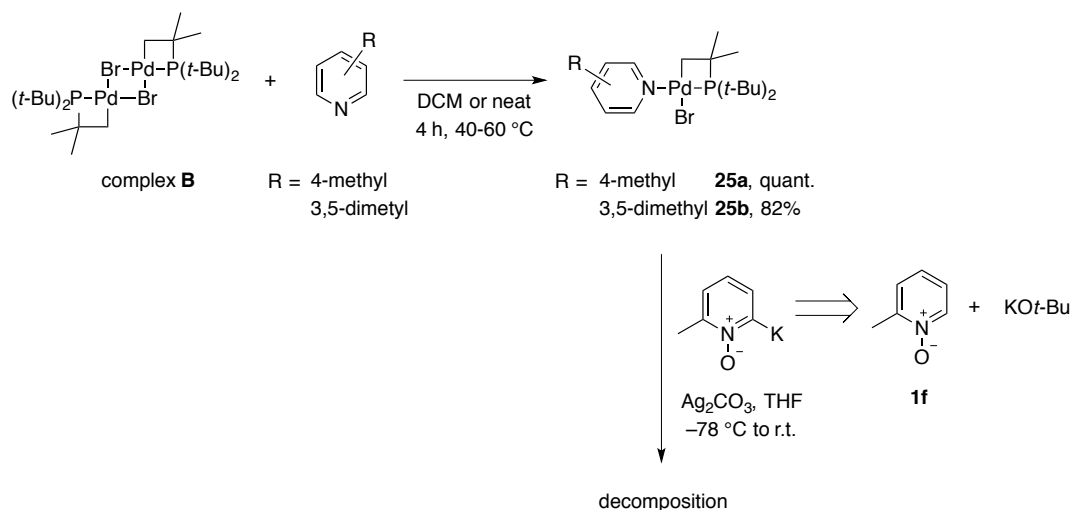
Figure 2.11. ORTEP drawing of methyl pyridyl *N*-oxide complex **21** (left) and trifluoromethyl pyridyl *N*-oxide complex **22** (right). Thermal ellipsoids are drawn at 50% probability level. Hydrogen atoms are omitted for clarity. Selected bond distances (Å) and angles (°) for **21**: Pd1–C1 2.064, Pd1–P2 2.298, Pd1–C8 2.122, Pd1–P1 2.286, C8–Pd1–P1 69.35, P2–Pd1–P1 164.47, C8–Pd1–C1 171.29, **22**: Pd1–C1 2.079, Pd1–P2 2.294, Pd1–C8 2.109, Pd1–P1 2.286, C8–Pd1–P1 69.01, P2–Pd1–P1 158.73, C8–Pd1–C1 174.34.

Both methyl *N*-oxide complex **21** and trifluoromethyl *N*-oxide complex **22** exhibit a distorted square planar geometry around the palladium center with the two phosphine ligands oriented *trans* to each other. The bite angle of the cyclometalated phosphine ligand was 69.3° for complex **21** and 69.0° for complex **22**, being very similar to the bite angle observed in starting complex **C**. Both pyridyl *N*-oxide ligands are oriented almost perfectly perpendicular to the palladium-phosphine plane. Pd–C(1) bond lengths for the pyridyl *N*-oxide ligand were 2.06 Å for methyl pyridyl *N*-oxide complex **21** and 2.08 Å for trifluoromethyl pyridyl *N*-oxide complex **22**. The C(1)–N–C(5) bond angle of the pyridyl *N*-oxide ligand was 122.5° for **21** and 121.9° for **22**, similar to the increased C–N–C bond angle observed for the protonated pyridyl ligand of anionic complex **30** (see above). No complex with a pyridyl *N*-oxide ligand on a palladium(II) metal center has been reported. Similar thallium and uranium complexes with a pyridyl *N*-oxide ligand are described, however both exhibit an *N*-oxide oxygen binding to the metal center,^{70,71} which is not present in complex **21** and **22**.

2.3.5 Pyridyl *N*-oxide complex with a nitrogen-containing ligand

To mimic the reaction conditions, a pyridyl *N*-oxide complex bearing a ligand present under the reaction conditions would be desirable. Since PEt₃ does not fulfill the requirements, attempts to synthesize a pyridine-stabilized pyridyl *N*-oxide complex were performed. A cyclometalated phosphine complex similar to complex **C** but with an unsubstituted pyridine ligand has previously been described, however bearing a chloride instead of bromide ligand.⁵⁰ The weaker binding of a pyridine ligand to a palladium(II) species in comparison to PEt₃ would promote dissociation prior to decomposition or transmetalation. Furthermore, a ligand oxidation side reaction pathway could be circumvented.

Starting from palladium complex **B**, a monomeric species with a substituted pyridine was readily formed by heating the starting complex in either neat pyridine or DCM. Neither 2,6-lutidine nor 2,4,6-collidine completely converted complex **B** to the desired complex, likely due to the steric hindrance exerted by the methyl groups adjacent to the coordinating nitrogen. However, the less sterically hindered 4-picoline and 3,5-lutidine converted complex **B** into monomeric pyridine-ligated complex **25a** and **25b** (scheme 2.24). Both complexes exhibit sharp singlets of $\delta = -11.1$ and $\delta = -10.7$ ppm in the ³¹P NMR. For comparison, the two cyclometalated complexes **A** and **B** exhibit shifts of $\delta = -8.7$ ppm and $\delta = -8.8$ ppm, respectively. Subsequently, the pyridine-ligated precursors **25a** and **25b** were treated with metalated pyridine *N*-oxide **1f** under the identical reaction conditions as for the PEt₃-stabilized complex (scheme 2.24). Unfortunately, the reaction resulted in re-isolation of starting pyridine *N*-oxide **1f** and free pyridine ligand.



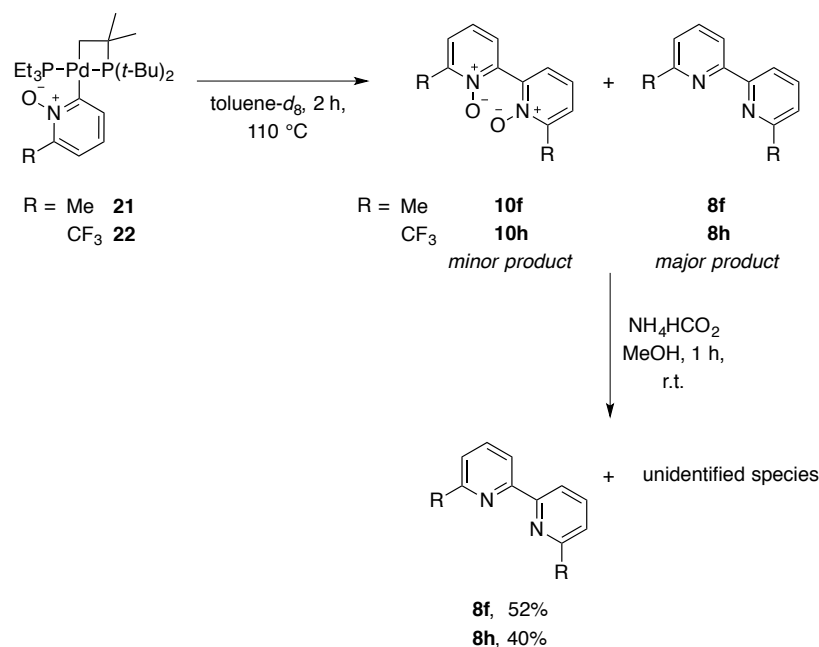
Scheme 2.24. Formation of pyridine-stabilized palladium precursor **25a** and **25b** by addition of substituted pyridine (2.5 mL) to complex **B**. To complex **25** (1 equiv.), addition of metalated pyridine *N*-oxide (1.2 equiv.) and Ag_2CO_3 (2.0 equiv.) in THF resulted in re-isolation of *N*-oxide **1f** and pyridine ligand.

In the ^{31}P NMR, no cyclometalated starting complex **25** was observed but unidentified species around 0 ppm were obtained. Also, palladium(0) complex **32** and free $\text{P}(t\text{-Bu})_3$ ligand were obtained as minor species. Alkoxide bases together with tertiary amines have shown to promote the reduction of palladium(II) to palladium(0).⁴³ The absence of reaction between pyridine precursor **25** and a metalated pyridyl *N*-oxide **1f** species might be due to the weaker binding of a pyridine ligand compared to a phosphine ligand, resulting in an instable pyridyl *N*-oxide complex. Further attempts to isolate a pyridine pyridyl *N*-oxide palladium complex were not performed.

2.3.6 Decomposition of pyridyl *N*-oxide palladium complexes

Prior to oxidative addition of an aryl halide under the catalytic conditions, an initial reaction must be present that can reduce the palladium(II) complex **A** or $\text{Pd}(\text{OAc})_2$ to palladium(0). Often proposed for palladium-catalyzed reactions, the phosphine ligand acts as a reducing agent forming an active palladium(0) species.¹⁴⁴ However, in the reaction between pyridine *N*-oxide **1** and bromopyridine **2**, oxidized phosphine ligand $\text{O}=\text{P}(t\text{-Bu})_3$ was only observed 30-60 minutes into the reaction. In the reaction between bromobenzene **3** and *N*-oxide **1**, no $\text{O}=\text{P}(t\text{-Bu})_3$ was observed at all.⁴² This observation indicates that there must be another reducing agent for the palladium(II) species, possibly via an initial homocoupling of the pyridine *N*-oxide substrate **1** to product *N,N'*-dioxide **10**. A disproportionation process of two pyridyl *N*-oxide palladium intermediates would form one palladium(II) and one palladium(0) species, where the latter could undergo oxidative addition of an aryl halide.

Initial decomposition experiments of pyridyl *N*-oxide complexes **21** and **22** revealed a high stability of both complexes in solution at room temperature. No decomposition products of either complex were observed after weeks when dissolved in benzene. Likely, the additional PEt_3 ligand causes an increase in stability compared to a pyridyl *N*-oxide intermediate **I-2** with an open coordination site. At elevated temperatures, decomposition of pyridyl *N*-oxide complexes **21** and **22** took place. A slow reaction was observed at 80 °C and the reaction temperature was increased to 110 °C. After 2 hours in toluene, both complexes were completely consumed as judged by ^{31}P NMR. Via ^1H NMR, *N,N'*-dioxide homocoupling product **10** was observed as the minor product, whereas deoxygenated bipyridine **8** was obtained as the major product. Due to the very low solubility of *N,N'*-dioxides **10** in organic solvents, quantification of the homocoupling product was performed by deoxygenation of the crude reaction mixture with ammonium formate (scheme 2.22).

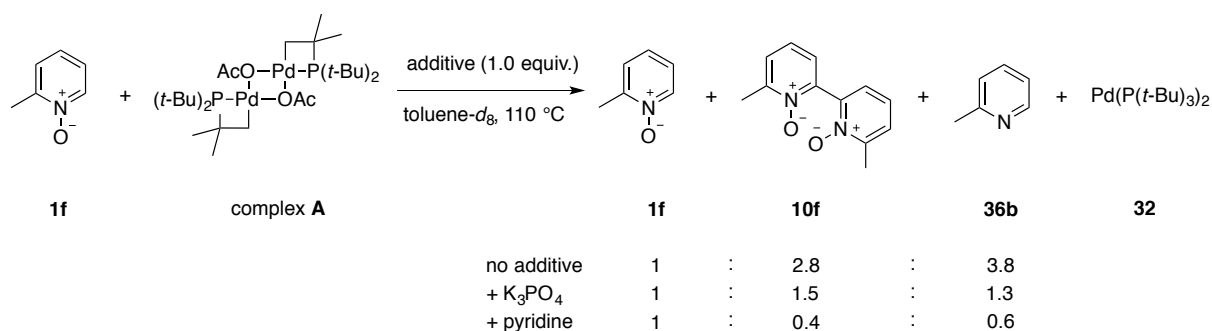


Scheme 2.22. Decomposition of pyridyl *N*-oxide complex **21** and **22** ($c_0 = 0.050$ M) in $\text{toluene-}d_8$ at 110 °C for 2 h and subsequent deoxygenation of formed *N,N'*-dioxide homocoupling product **10** with NH_4HCO_2 in $\text{MeOH}/\text{toluene}$. Yields of bipyridine **8f** and **8h** were determined via ^1H NMR.

Reduced bipyridine product **8f** was obtained in 52% yield from pyridyl *N*-oxide complex **21**. No pyridine *N*-oxide **1f** or 2-methyl pyridine **36b** was observed, however, three additional minor aromatic species were present in the reaction mixture. Similar results were obtained from the decomposition of pyridyl *N*-oxide complex **22**, where reduced bipyridine **8h** was obtained in 40% yield in addition to unidentified aromatic signals. Possibly, the signals arise from coordination of a pyridine or bipyridine ligand to a palladium(II) species, as previously suggested above for bipyridine **8m**. Furthermore, complexation of a pyridine *N*-oxide and a palladium(II) species forming a stable complex with the *N*-oxide moiety acting as a L type ligand could be formed.¹⁴⁵ Also, nickel(II) complexes bearing

N,N'-dioxide **10** ligands have been reported.¹⁴⁶ However, such complexes have not been isolated with the substrates or products from the direct arylation reaction. Whereas such complexes would be stable towards reduction remains unknown. A higher yield of methyl bipyridine **8f** was obtained in comparison to trifluoromethyl bipyridine **8h**. Due to the unidentified signals from the decomposition reaction, no conclusions were drawn from the difference in yield. With the exception of oxidized PEt_3 ligand, the phosphorus species formed after decomposition remain unidentified (see Experimental section 4.10). All formed phosphorus species were stable towards reduction with NH_4HCO_2 . If a palladium(0) species is formed via disproportionation, it likely undergoes oxidation to palladium(II) under the reaction conditions. An oxidation pathway could be concomitant with deoxygenation of *N,N'*-dioxide **10**, as suggested considering the formation of reduced bipyridine **8** as the major decomposition product. However, deoxygenation of *N,N'*-dioxide **10** could also be effected by the PEt_3 ligand.³⁶ A few test reactions were performed to test the deoxygenation. Bipyridine *N,N'*-dioxide **10f** and 2 equivalents of PEt_3 revealed that only $\sim 3\%$ of the PEt_3 ligand was converted to the $\text{O}=\text{PEt}_3$ analogue after 24 h. Reaction between *N,N'*-dioxide **10f** and cyclometalated palladium(II) complex **C** also showed no conversion to phosphine oxide or reduced bipyridine product. Addition of palladium(0) complex **32** to *N,N'*-dioxide **10f** only resulted in re-isolation of starting material **10f**. However, these test reactions were performed at 80°C .

Decomposition without the additional PEt_3 ligand was performed by reacting *N*-oxide substrate **1f** with equimolar palladium complex **A** and complex **B** with and without a base additive. The substrates were heated to 110°C for 15 minutes and subsequently over night and the products identified via ^1H and ^{31}P NMR (scheme 2.23). Reaction with complex **B** only resulted in re-isolation of the starting material **1f** (not shown), which is in agreement with the previously described requirement of an acetate base to carry out the C–H activation.



Scheme 2.23. Reaction between *N*-oxide substrate **1f** (1 equiv.) and palladium complex **A** (0.5 equiv.) forming *N,N'*-dioxide **10f** and reduced pyridine **36b**. Due to signal overlap, ratios were estimated via ^1H NMR.

In the reaction with complex **A**, no new species was observed after 15 minutes as judged via ^1H NMR. ^{31}P spectroscopy revealed that the major species present was cyclometalated complex **A** in the reaction without additive and with pyridine added. In comparison, the reaction with K_3PO_4 showed no starting

complex **A** but new unidentified phosphorus species were observed (see Experimental section 4.10.8 for table). After 18 hours of reaction, complex **A** was consumed in all reactions and palladium black was macroscopically observed. As expected, palladium(0) complex **32** was formed, albeit only in less than 10%. The major species formed in all reactions was a signal at $\delta = 124$ ppm, which has previously been observed as a decomposition product of palladium complex **A**.⁴² Free $P(t\text{-Bu})_3$ ligand was obtained in all reactions, indicating that proto-demetalation of the ligand takes place. Due to peak overlap of *N,N'*-dioxide **10f** and pyridine **36b**, the yield of the products could only be estimated from the ¹H NMR by subtraction of the starting material integral from the product integrals. A maximum conversion of *N*-oxide **1f** to *N,N'*-dioxide **10f** and pyridine **36b** was observed in the reaction without an additive. Addition of both K_3PO_4 and pyridine as base decreased the homocoupling reaction, with the latter exerting the largest inhibitory effect. No reduced homocoupling product **8f** was obtained. Comparison of the phosphorus species formed from decomposition of isolated pyridyl *N*-oxide complex **21** and **22** with the homocoupling of **1f** in the absence of PEt_3 shows that only the peak at $\delta = 124$ ppm was observed in both reactions. Arguably, an additional phosphine ligand promotes the formation of new palladium complexes with mixed ligands.

2.3.7 Transmetalation between (hetero)aryl palladium complexes

With all the putative palladium intermediates proposed in the catalytic cycle at hand, their reactivity in transmetalation reactions was investigated. Due to the observed higher reactivity of bromide-ligated complexes **12a**, **14a**, they were initially employed in the transmetalation experiments with pyridyl *N*-oxide complexes **21**, **22**. The species consumed and formed over the course of the transmetalation was monitored via ³¹P NMR. To imitate the catalytic reaction conditions, all transmetalation experiments were run in toluene-*d*₈ and at a concentration of $c = 0.045$ M in each palladium complex.

With electron-poor trifluoromethyl pyridyl *N*-oxide complex **22**, an initial test reaction with pyridyl complex **12a** at 5 °C showed a slow reaction where only 25% of **12a** was consumed after 3 hours. Increasing the temperature to 25 °C increased the reaction rate to a suitable time frame for monitoring via NMR. Complex **22** was dissolved in toluene-*d*₈ in an NMR tube and cooled to -78 °C. Subsequently, an equimolar amount of pyridyl palladium complex **12a** or phenyl palladium complex **14a** in toluene-*d*₈ was added through a septum. The NMR tube was kept at -78 °C until inserted into the NMR spectrometer. One ³¹P NMR spectrum was recorded every 2 minutes over a period of 3 h. No internal standard was used and consumption and formation are shown as a percentage of the initial phosphorus species (figure 2.12).

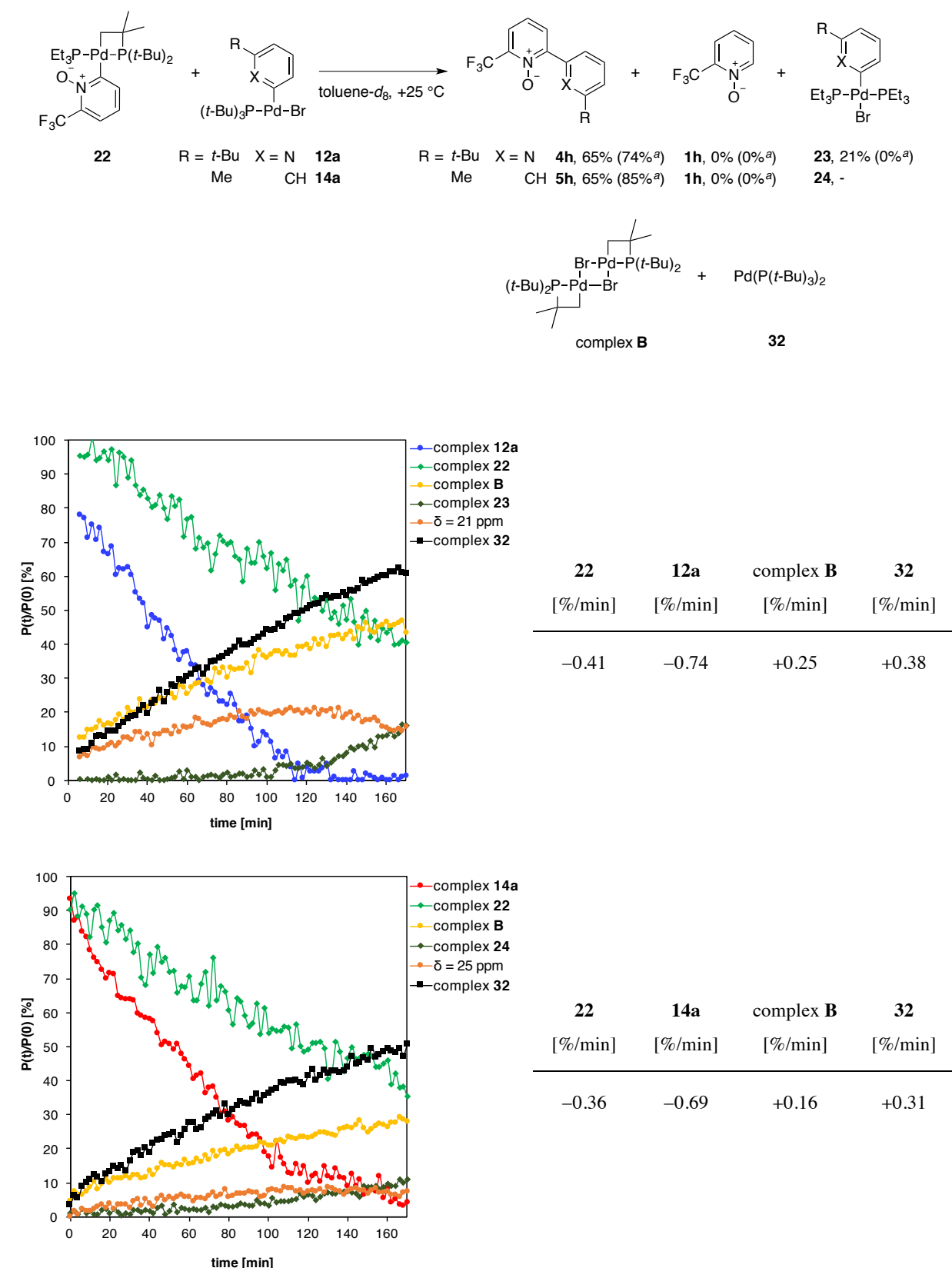


Figure 2.12. Consumption and formation rates of phosphorus species monitored by ³¹P NMR in the transmetalation between trifluoromethyl pyridyl *N*-oxide palladium complex **22** (*c*₀ = 0.045 M) and aryl palladium(II) complex **12a** (*c*₀ = 0.045 M, top) or **14a** (*c*₀ = 0.045 M, bottom) in toluene-*d*₈ at 25 °C for 3 h. ^aYields after 18 h of reaction.

In both transmetalation reactions, pyridyl complex **12a** (blue, top) and phenyl complex **14a** (red, bottom) exhibited an approximately twice as fast consumption rate as pyridyl *N*-oxide complex **22** (green). The rate of decay for pyridyl complex **12a** and phenyl complex **14a** were similar, with a slightly faster consumption rate of pyridyl complex **12a**. The transmetalation step would produce one palladium(II) species and one palladium(0) species formed after reductive elimination of arylpyridine *N*-oxide product. Likely, the species are complex **32** (black) and palladium complex **B** (yellow). In the reaction with pyridyl complex **12a**, a conversion of 20% was observed in the initial spectrum recorded. Concomitantly, a transient species exhibiting a singlet with a shift of $\delta = 21$ ppm (orange) was formed together with free $P(t\text{-Bu})_3$ ligand (not shown). An analogous species with a singlet at $\delta = 25$ ppm (orange) was observed in the reaction with phenyl complex **14a**, however at a lower concentration and concomitant with lower amount of $P(t\text{-Bu})_3$. Both species were formed fast during the first 100 minutes. Thereafter, (pyridyl)Pd(Br)(PEt₃)₂ **23** (dark green) and (phenyl)Pd(Br)(PEt₃)₂ **24** (dark green), respectively, were formed. From the independent ligand displacement reaction shown above, it was already known that displacement of a $P(t\text{-Bu})_3$ ligand by PEt₃ on complex **12a** or **14a** occurs fast (see above, scheme 2.15). Both bisphosphine complexes **23**, **24** exhibited singlets with a chemical shift of $\delta = 12$ ppm. The formation of complex **23**, **24** with the concomitant decay of the transient species at $\delta = 21$ and $\delta = 25$ ppm, respectively leads to the hypothesis that the unidentified species belongs to a dimeric μ -Br aryl palladium(II) complex [(Ar)Pd(Br)(PEt₃)₂]₂ **I-3** bearing one PEt₃ ligand per palladium atom. This is supported by the observation that no free PEt₃ ligand and no PEt₃-containing complex **C** was formed. The presence of only one peak in the ³¹P NMR spectrum in the reaction of *N*-oxide complex **21** and aryl complex **12a** and **14a** rules out a bisphosphine type complex bearing both a PEt₃ and $P(t\text{-Bu})_3$ ligand.

A dimeric pyridyl complex with a PEt₃ ligand has not been described so far, however, for a μ -Cl phenyl dimer [(phenyl)Pd(Cl)(PEt₃)₂]₂, a ³¹P shift of $\delta = 27$ ppm was reported.¹⁴⁷ The peaks at $\delta = 21$ and $\delta = 25$ ppm gave rise to sharp singlets, indicating that only one isomer is present or that a *cis/trans* equilibrium is fast. Attempts to isolate the putative dimeric complex by displacing $P(t\text{-Bu})_3$ of an aryl complex **12a** or **14a** with 1 equivalent of PEt₃ resulted in a singlet with a chemical shift of $\delta = 26$ ppm, however as a mixture with palladium(0) complex **32** and bisphosphine complex **23**, **24**. In the initial stages of the transmetalation, one equivalent of PEt₃ relative to aryl palladium complex **12a** or **14a** would be present. Displacing the $P(t\text{-Bu})_3$ would give rise to a three-coordinated complex with the considerably smaller and less electron-rich PEt₃ ligand. To stabilize such a complex, dimerization likely occurs.

Surprisingly, both pyridyl *N*-oxide complex **22** and aryl palladium complexes **12a**, **14a** exhibited zero-order decays. Pyridyl *N*-oxide complex **22** is coordinatively saturated and therefore unlikely to directly react with aryl palladium complex **12a** or **14a**. Dissociation of PEt₃ would result in intermediate **I-2**

with an open coordination site. The zero-order dependence on the complexes is suggesting that a rate-determining step does not involve the starting complexes, but likely takes place from a sequentially formed species. A twice as fast decay of **12a** and **14a** in comparison to **22** is suggesting that the aryl palladium complexes are undergoing another reaction in addition to transmetalation with *N*-oxide complex **22**. Because no homocoupling or other decomposition of **12a** and **14a** was observed, formation of a transient PEt_3 intermediate **I-3** is suggested and that transmetalation takes place from the monomeric species of the dimer (see below, scheme 2.25).

Both complex **12a** and complex **14a** were completely consumed within 3 hours. In contrast, only 60% of complex **22** was consumed during the same time. In the transmetalation between *N*-oxide complex **22** and pyridyl complex **12a**, 65% of bipyridine *N*-oxide **4h** and 21% of the PEt_3 bisphosphine pyridyl complex **23** were calculated after 3 hours of reaction. The reaction between *N*-oxide complex **22** and phenyl complex **14a** resulted in 65% of arylpyridine *N*-oxide. Due to peak overlap, no yield of the PEt_3 bisphosphine phenyl complex **24** could be determined. No pyridine *N*-oxide **1h** was obtained in either reaction. To achieve full consumption of complexes, a prolonged reaction time of 18 h was required, resulting in complete conversion of complex **22** and complex **23**, **24**.

The electron-rich methyl pyridyl *N*-oxide complex **21** and aryl complexes **12a** and **14a** were subjected to the same transmetalation protocol. Initial screening of appropriate reaction temperature showed that complete consumption of aryl complex **12a** and **14a** was obtained within 3 hours at 5 °C. The transmetalation reactions were set up in an identical manner as shown above and one ^{31}P spectrum was recorded every 2 minutes for 3 hours (figure 2.13). A clear difference in rate was observed in the transmetalation between pyridyl *N*-oxide complex **21** and pyridyl complex **12a** in comparison to phenyl complex **14a**. In the reaction with complex **12a**, *N*-oxide complex **21** (green) and pyridyl complex **12a** (blue) were consumed within 60 minutes. During this period, the same putative dimeric species **I-3** with a chemical shift of $\delta = 21$ ppm (orange) as observed above was formed fast and also consumed fast. With its consumption, bisphosphine complex **23** (dark green) was formed. In addition, palladium(0) complex **32** (black), palladium complex **B** (yellow) and complex **C** (purple) was formed, for which the concentration remained almost constant after $t = 60$ minutes. In the reaction between *N*-oxide complex **21** (green) and phenyl complex **14a** (red), a complete consumption of **14a** within 2 hours was observed. However, after the same time, 30% of *N*-oxide complex **21** was still present. Also the putative dimeric intermediate **I-3** with a shift of $\delta = 25$ ppm (orange) was detected. Similar to the reaction with trifluoromethyl *N*-oxide complex **22**, aryl complexes **12a** and **14a** were consumed with approximately twice the rate as methyl *N*-oxide complex **21**. Intermediate **I-3** was accumulated until complete consumption of complex **12a** or **14a**, and thereafter, bisphosphine complex **23** or **24** was formed.

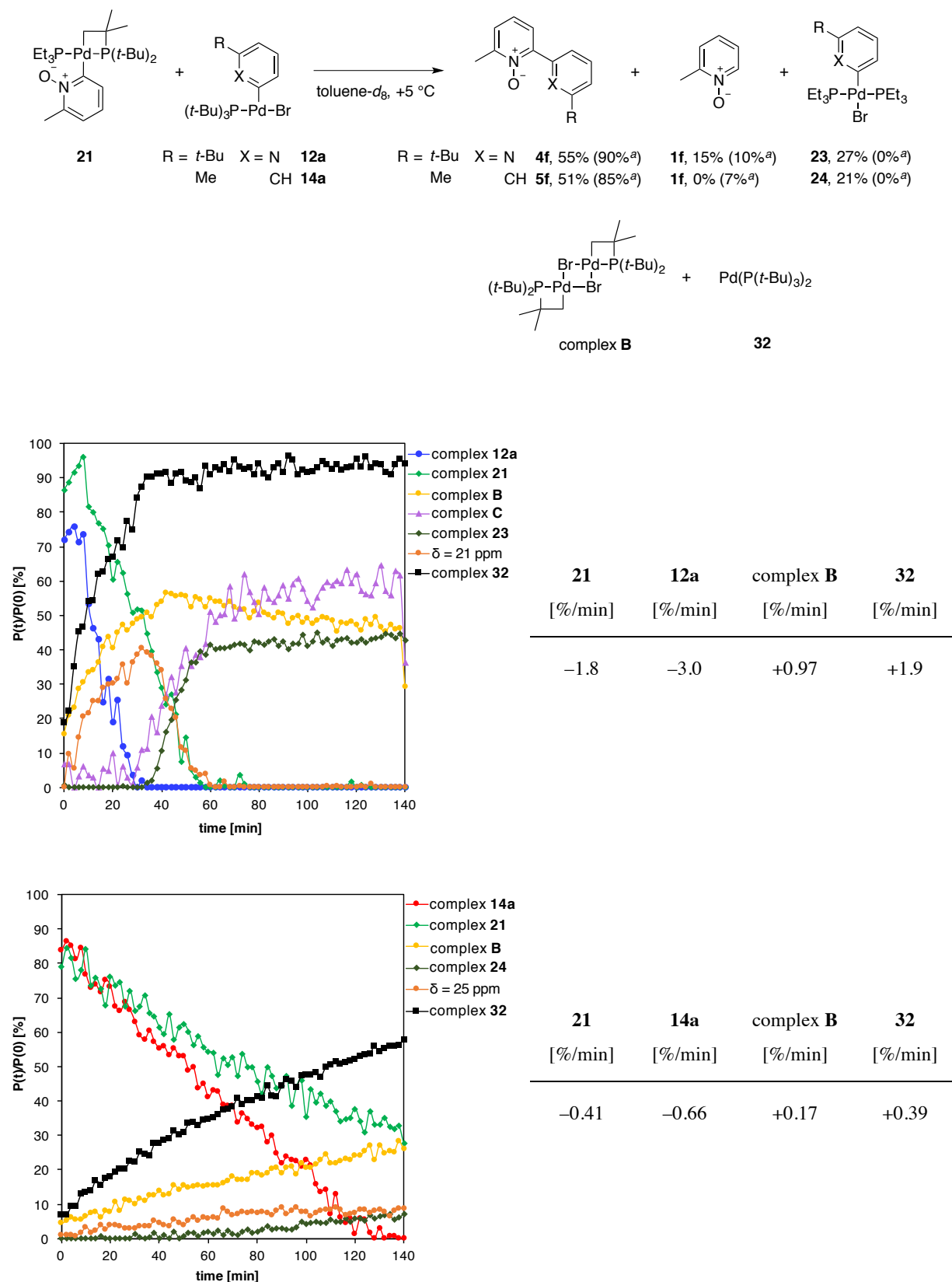


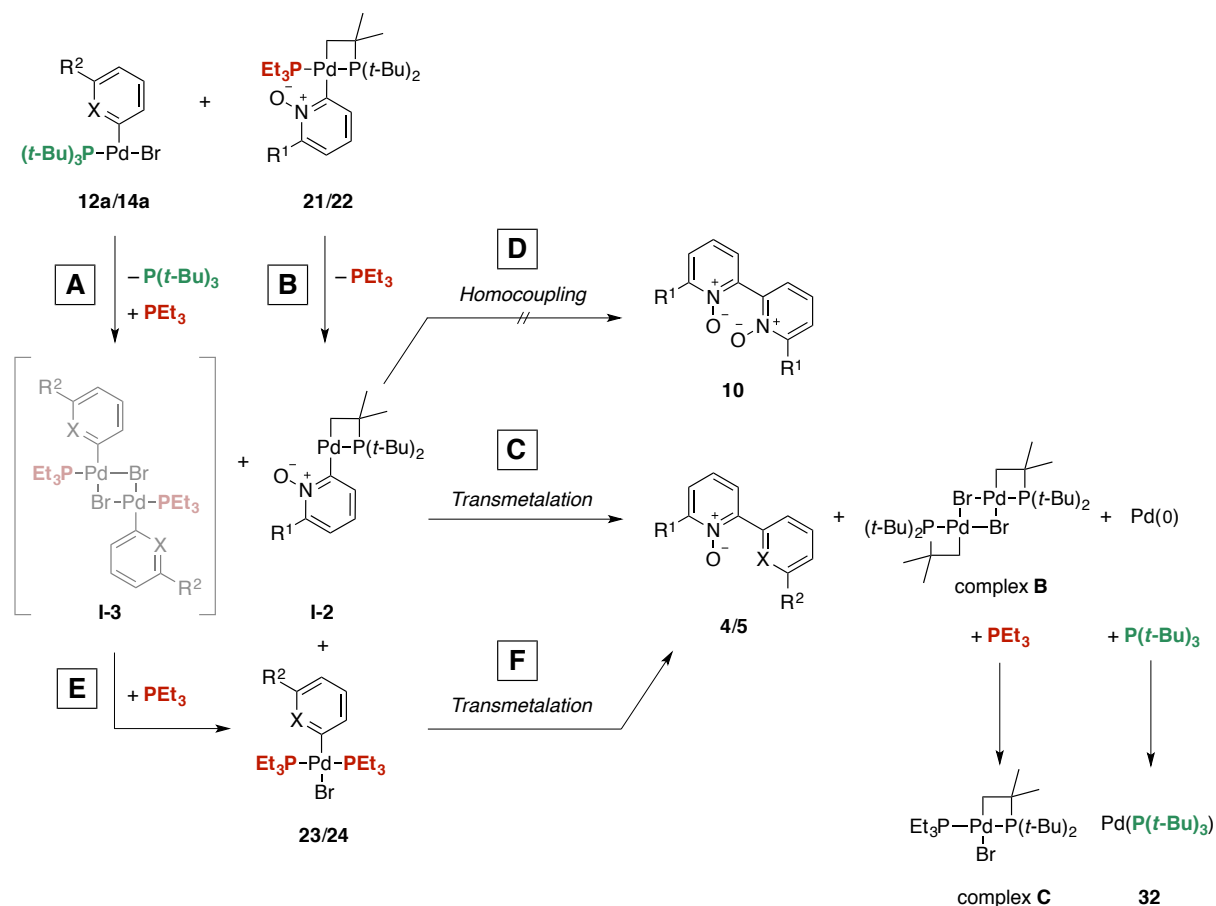
Figure 2.13. Consumption and formation rates of phosphorus species monitored by ^{31}P NMR in the transmetalation between methyl pyridyl *N*-oxide palladium complex **21** ($c_0 = 0.045$ M) and aryl palladium(II) complex **12a** ($c_0 = 0.045$ M, top) or **14a** ($c_0 = 0.045$ M, bottom) in toluene- d_8 at 5°C for 3 h. ^aYields after 18 h of reaction.

After 3 hours of reaction between complex **21** and complex **12a**, a yield of cross-coupled bipyridine *N*-oxide **4f** of 55% was obtained. In addition, bisphosphine pyridyl complex **23** was observed in 27% and pyridine *N*-oxide **1f** in 15% as determined via ¹H NMR. Although the origin of the proton required to form pyridine *N*-oxide **1f** from pyridyl *N*-oxide complex **21** is not known, it is likely a result from cyclometalation of a P(*t*-Bu)₃ ligand. After 18 hours of reaction at room temperature, 90% yield of bipyridine *N*-oxide **4f** and 10% of pyridine *N*-oxide **1f** was obtained. No bisphosphine complex **23** was present. After 3 hours of reaction between *N*-oxide complex **21** and phenyl complex **14a**, a yield of arylpyridine *N*-oxide **5f** of 51% was observed, in addition to bisphosphine complex **24** in 21% yield. Extending the reaction time to 18 hours resulted in complete consumption of complex **24** and the cross-coupled product **5f** was obtained in 85% in addition to pyridine *N*-oxide **1f** in 7%. The absence of homocoupling products shows that a transmetalation reaction is significantly faster than a homocoupling reaction at room temperature.

Comparing the rates of transmetalation reactions with **12a** or **14a** with *N*-oxide complex **21** reveals a significant rate difference. Pyridyl palladium complex **12a** was consumed over four times as fast as the analogous phenyl palladium complex **14a**. This is in stark contrast to the rate difference in the above-described transmetalation with trifluoromethyl *N*-oxide complex **22**, where only a slightly faster rate was observed with pyridyl complex **12a**. This could indicate an alternative pathway unique for the combination methyl pyridyl *N*-oxide complex **21** and pyridyl complex **12a**. Due to the more electron-rich methyl substituent, an increase in nucleophilicity of complex **21** in comparison to complex **22** is to be expected. This could result in that a PEt₃ ligand is more readily displaced from methyl *N*-oxide complex **21** and forming another complex with electrophilic pyridyl complex **12a**. Alternatively, datively binding of an *N*-oxide oxygen to pyridyl complex **12a** could form a pre-transmetalation intermediate. Similar oxygen-bridged species have been suggested with a silanolate substrate in Hiyama-Denmark couplings or a boronate substrate in Suzuki-Miyaura couplings (see Chapter 3).^{69,117,118} Such pre-transmetalation intermediates are proposed to promote phosphine or aryl ligand exchange. Similarly to the reaction of complex **22**, a zero-order decay of both reacting complexes was obtained, suggesting that a rate-determining aryl transfer step takes place from another intermediate formed from the starting complexes.

From these experiments between *N*-oxide complexes **21**, **22** and aryl complexes **12a**, **14a**, an overview of reaction pathways is proposed in scheme 2.25. No free PEt₃ was observed in any of the reactions. Therefore, the formation of the putative dimeric PEt₃ dimer **I-3** is likely a fast step (step **A**) with the loss of PEt₃ from *N*-oxide complex **21** or **22**, forming **I-2** (step **B**). Intermediate **I-2** reacts in a transmetalation reaction with the monomeric version of intermediate **I-3** resulting in the cross-coupled product **4** or **5** (step **C**). Due to that a high yield of cross-coupled product was obtained, a homocoupling pathway yielding *N,N'*-dioxide **10** is not taking place (step **D**). With the complete

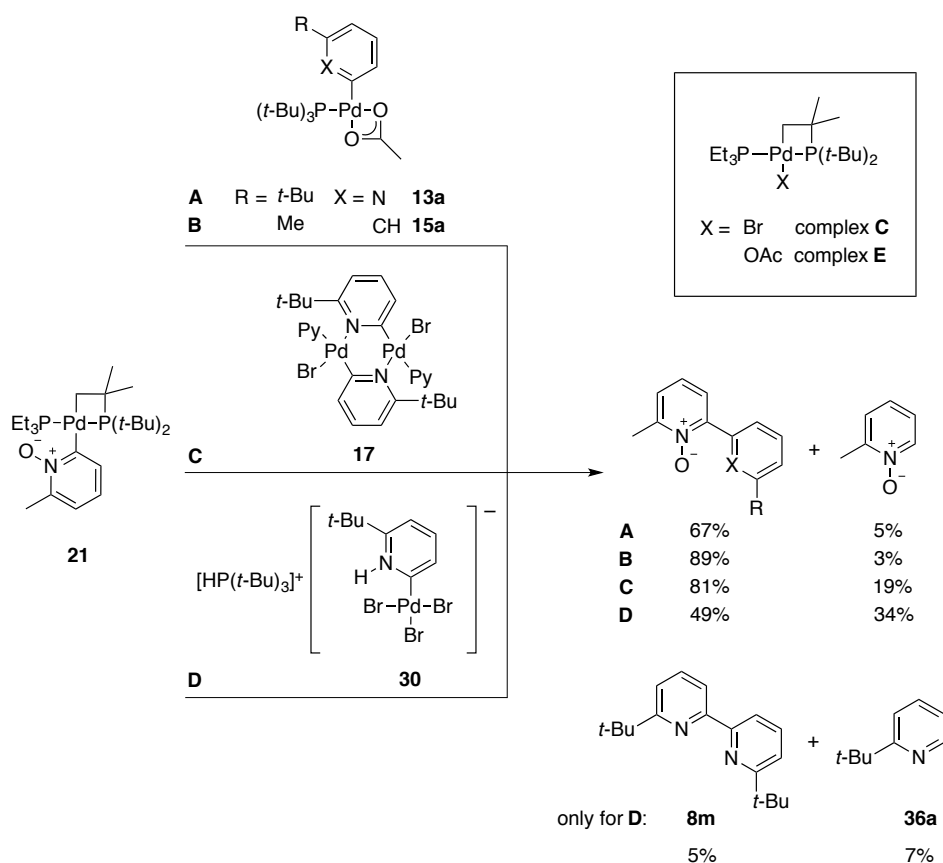
consumption of complex **12a** or **14a**, the liberated PEt_3 ligand convert intermediate **I-3** to bisphosphine complex **23** and **24** (step **E**), which subsequently transmetalates with **I-2** (step **F**). However, bisphosphine complex **23** and **24** exhibit a high stability and an extended period of time is required for complete consumption (18 h). In all four reactions, the major phosphorus species present after 18 h was complex **C** (~70%) in addition to palladium(0) complex **32** (~20%).



Scheme 2.25. Decomposition pathways in the transmetalation between aryl palladium complexes **12a**, **14a** and pyridyl *N*-oxide complexes **21**, **22**.

Aryl palladium complexes **13a**, **15a** bearing acetate ligands were also subjected to the transmetalation protocol. However, no NMR monitoring of starting material or products was performed. Complex **21** and complex **13a** or **15a** were stirred in the glovebox for 30 minutes in C_6D_6 and a ^{31}P NMR of the reaction revealed the complete consumption of starting materials (scheme 2.26, **A** and **B**). In the reaction with pyridyl complex **13a**, the phosphorus species observed were palladium(0) complex **32** (38%), cyclometalated PEt_3 -ligated monomer **E** (24%), cyclometalated complex **A** (18%) and a peak at $\delta = 13$ ppm (20%) which likely belongs to a bisphosphine-ligated pyridyl acetate palladium complex analogous to complex **23**. A yield of bipyridine *N*-oxide **4f** of 67% and pyridine *N*-oxide **1f** of 5% was obtained. In the reaction between *N*-oxide complex **21** and phenyl complex **15a**, palladium(0) complex **32** (32%), cyclometalated PEt_3 -ligated monomer **E** (55%), cyclometalated

complex **A** (7%) and a peak at $\delta = 13$ ppm (6%) were obtained. A yield of arylpyridine *N*-oxide **5f** of 89% and pyridine *N*-oxide **1f** of 3% was observed. Arguably, a similar process takes place in the transmetalation with the acetate analogues as for the bromide analogue, where an aryl PEt_3 complex is accumulated in the reaction and giving rise to a signal at $\delta = 13$ ppm. However, no independent synthesis of such acetate complex was performed and therefore, no yield was determined. Also in the transmetalation of acetate complexes, no homocoupling products were observed.



Scheme 2.26. Transmetalation between pyridyl *N*-oxide complex **21** ($c_0 = 0.030$ M) and acetate-ligated aryl complex **13a** ($c_0 = 0.030$ M) or **15a** ($c_0 = 0.030$ M) at room temperature for 30 min, pyridine pyridyl dimer **17** ($c_0 = 0.015$ M) at 80 °C for 1 h or anionic pyridyl complex **30** ($c_0 = 0.030$ M) at 80 °C for 50 min. All reactions performed in C_6D_6 and products given as ratio determined by ^1H NMR.

Transmetalation between pyridine-ligated pyridyl dimer **17** and *N*-oxide complex **21** was performed in an identical manner (scheme 2.26, **C**). After 10 minutes at room temperature, 80% of the starting *N*-oxide complex **21** was consumed as verified by ^{31}P NMR. The reaction was heated to 80 °C for 1 hour and the ratio of aromatic species was determined via ^1H NMR, showing a 4:1 ratio of cross-coupled product **4f** to pyridine *N*-oxide **1f**. The phosphorus distribution after the course of the reaction was palladium(0) complex **32** (7%), cyclometalated PEt_3 monomer **C** (80%) and $\text{P}(t\text{-Bu})_3$ ligand (13%). Formation of free $\text{P}(t\text{-Bu})_3$ ligand and complex **32** is suggesting that a proto-demetalation of the cyclometalated phosphine ligand takes place. Furthermore, anionic complex **30** was tested in a

transmetalation reaction with complex **21** (scheme 2.26, **D**). A high stability of complex **30** has been observed in solution at room temperature and at elevated temperatures. After heating the NMR tube at 80 °C for 50 minutes, all complex was dissolved and the major species identified by ³¹P NMR were hydridopalladium bromide complex **26** (30%), palladium complex **B** (25%), complex **C** (5%) and a singlet at $\delta = 15$ ppm (34%). The peak at 15 ppm has not previously been observed in any transmetalation reaction. Likely, it belongs to a complex bearing one or more PEt₃ ligands. A palladium(II) complex of the type (PEt₃)₂PdCl₂ has been reported having a ³¹P chemical shift of $\delta = 17.6$ ppm,¹⁴⁸ and a similar bromide-complex can be envisioned. Cross-coupled bipyridine *N*-oxide product **4f** was obtained in 49%, pyridine *N*-oxide **1f** in 34%, bipyridine homocoupling product **8m** in 5% and 2-*tert*-butyl pyridine **36a** in 8%. Arguably, proto-demetalation is occurring assisted by HBr released from anionic complex **30**. This experiments show that even in the presence of a catalyst for homocoupling, transmetalation with a pyridyl *N*-oxide complex **21** is favored over a homocoupling pathway.

2.4 Conclusion

A 6-*tert*-butyl-2-pyridyl palladium(II) complex **12a** bearing a bromide and a bulky P(*t*-Bu)₃ ligand was synthesized by employing a Buchwald-type pre-catalyst that forms a reactive monoligated Pd-P(*t*-Bu)₃ species *in situ*. X-ray analysis of the solid-state structure of pyridyl complex **12a** showed a novel η^2 -C,N binding mode of the pyridyl ligand to the palladium center. The bulky phosphine ligand could be readily displaced by addition of smaller PEt₃ ligands, as well as by nitrogen-containing pyridine or 2,2'-bipyridine ligands. X-ray analysis of a pyridine-ligated pyridyl complex **17** showed a dimeric structure with μ -C²,N-pyridyl ligands bridging the two palladium centers, whereas a 2,2'-bipyridine-ligated pyridyl palladium complex **18** existed as a monomeric square planar complex. For comparison of stability and reactivity, a 3-tolyl palladium(II) complex **14a**, similarly bearing a bromide and a P(*t*-Bu)₃ ligand, was synthesized according to reported procedures.⁷⁵ Displacement of the bromide ligand on pyridyl complex **12a** and phenyl complex **14a** was achieved by addition of AgOAc, resulting in a novel pyridyl palladium acetate complex **13a** and the analogous phenyl palladium acetate complex **15a**.

The stability of complexes **12a-15a** was determined at room temperature as well as at elevated temperatures. Bromide-ligated complexes **12a** and **14a** decomposed to their respective homocoupling products bipyridine **8m** and biphenyl **9c** within a few days at room temperature. Acetate complexes **13a** and **15a** exhibited a stability for 2 weeks in solution at room temperature, arguably due to the κ^2 -binding of the acetate ligand. At 80 °C, up to 2 days were required to decompose acetate complexes **13a** and **15a**. Coordinatively saturated pyridine- and 2,2'-bipyridine-ligated complexes **17** and **18** were stable in solution and in air and decomposition to bipyridine homocoupling product **8m** was only observed after heating for five days. Solubility of 2,2'-bipyridine pyridyl complex **18** proved limited in nonpolar organic solvents used in the arylation reaction of pyridine *N*-oxides **1**, suggesting that formation of a bipyridine complex by phosphine displacement under the catalytic conditions leads to catalyst deactivation.

Bromide complexes **12a** and **14a** decomposed within 100 minutes at 80 °C. Decomposition of pyridyl complex **12a** exhibited an induction period of 35 minutes during which only 15% of **12a** was consumed. Subsequently, a constant consumption rate of pyridyl complex **12a** was observed. A transient pyridyl species was identified, formed by displacement of the phosphine ligand by two bromide nucleophiles and protonation of the pyridyl nitrogen. This anionic complex **30** was independently synthesized by addition of HBr·P(*t*-Bu)₃ to **12a** and X-ray analysis confirmed a square planar palladium(II) complex where the protonated pyridyl moiety likely binds in a carbene-like manner to the palladium center. The decomposition rate of pyridyl complex **12a** was increased by addition of ionic compounds. Addition of 5 mol% of complex **30** to pyridyl complex **12a** at 80 °C

completely consumed the starting complex in less than 10 minutes, as opposed to a complete consumption in 60 minutes in the absence of added **30**. Also, the addition of anionic complex **30** resulted in the absence of induction period and an apparent zero-order decay of pyridyl complex **12a**. The rate-determining step of the decomposition reaction likely involves an intermediate formed by the combination of anionic complex **30** and pyridyl complex **12a**. To not be dependent on the concentration of **12a**, an equilibrium between **12a** and **30** and the intermediate must be shifted to the right side, and that a rate-determining aryl transfer takes place from the intermediate. Decomposition of phenyl complex **14a** exhibited an apparent first-order decay. Addition of ionic compounds containing bromide anions increased the decomposition rate, however the first-order dependence remained. An unidentified transient species in the decomposition of phenyl complex **14a** was observed and is suggested to belong to an anionic phenyl dimer **29d**. Unfortunately, isolation of the anionic dimer was not possible. Arguably, formation of an anionic complex would increase the nucleophilicity and increase the rate of transmetalation forming the homocoupling product **9c**.

Comparison of the products obtained from the decomposition reactions showed that pyridyl complex **12a** was almost completely converted to the bipyridine homocoupling product **8m**. In all reactions, less than 5% of the proto-demetalation product 2-*tert*-butylpyridine **36a** was obtained. Decomposition of phenyl complex **14a** also resulted in decomposition to the biphenyl homocoupling product **9c**. In addition, proto-demetalation product toluene **35b** and reductively eliminated bromobenzene **3c** were obtained. These results show that a pyridyl palladium complex is more prone to undergo a homocoupling pathway in comparison to a phenyl palladium complex under the same reaction conditions.

Two palladium(II) complexes bearing a methyl pyridyl *N*-oxide ligand **21** and a trifluoromethyl pyridyl *N*-oxide ligand **22** were synthesized. For stabilization, an additional PEt_3 ligand was added. X-ray analysis of **21** and **22** confirmed a square planar geometry around the palladium center with the two phosphorus ligands *trans* to each other. The hypothesis is that in the direct arylation of pyridine *N*-oxides, a pyridyl *N*-oxide intermediate **I-2** forms fast and undergoes disproportionation to the *N,N'*-dioxide homocoupling product **10** to initiate the reaction. Independent decomposition of methyl *N*-oxide complex **21** and trifluoromethyl *N*-oxide complex **22** resulted in ~50% conversion to the homocoupling products, confirming that the initiation pathway is plausible. However, a high stability of *N*-oxide complex **21**, **22** was observed, and was assigned to the additional PEt_3 ligand. Transmetalation reactions between pyridyl *N*-oxide complexes **21**, **22** and aryl palladium complexes **12a**, **14a** were performed. In the reaction with trifluoromethyl *N*-oxide complex **22**, similar consumption rates of complex **12a**, **14a** were observed. In the transmetalation reaction between a methyl pyridyl *N*-oxide complex **21** and pyridyl complex **12a**, a 4 times faster consumption rate of **12a** was observed in comparison to the analogous reaction with phenyl complex **14a**. Arguably, the

nucleophilic nature of methyl *N*-oxide complex **21** in combination with the electrophilic character of pyridyl complex **12a** promotes a fast reaction. Possibly, an oxygen-bridged intermediate is formed by nucleophilic attack of **21** on the open coordination site of **12a**, promoting a ligand transfer reaction. All complexes in the transmetalation reactions exhibited a zero-order decay. Therefore, it is suggested that an intermediate is formed prior to a rate-determining transmetalation. In all four combinations, an influence of the stabilizing PEt_3 ligand was detected. Loss of one ligand from **21** or **22** to create an open coordination site is required prior to reaction with an aryl palladium complex. With the release of PEt_3 , a fast displacement of the $\text{P}(t\text{-Bu})_3$ ligand on **12a**, **14a** was observed, forming a PEt_3 or $(\text{PEt}_3)_2$ -ligated aryl palladium(II) complex. Coordinatively saturated PEt_3 bisphosphine pyridyl complex **23** and phenyl complex **24** were independently synthesized and identified as a species formed in the transmetalation reaction. The bisphosphine complexes reacted slowly with a pyridyl *N*-oxide complex. Comparing the decomposition rates to the transmetalation rates indicated that a significantly faster transmetalation between a pyridyl *N*-oxide complex **21**, **22** and an aryl palladium complex **12a**, **14a** takes place in comparison to a homocoupling pathway of each complex at room temperature. This leads to the conclusion that a decomposition pathway of aryl palladium complexes only becomes competing with a transmetalation pathway in the absence of a pyridyl *N*-oxide intermediate **I-2** transmetalation partner.

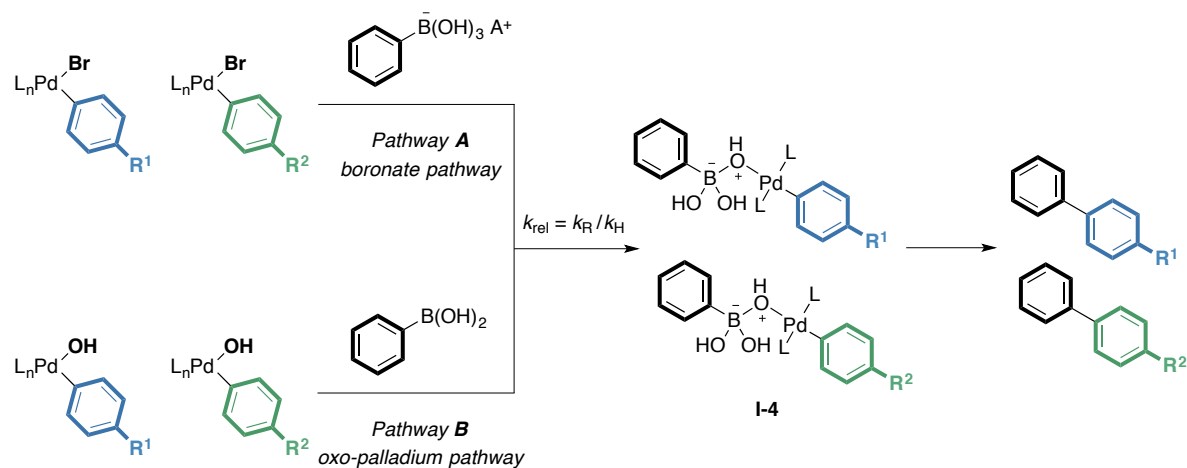
3 Transmetalation Between Aryl Palladium Complexes and Organoboron Compounds

3.1 Motivation

The generally accepted catalytic cycle for palladium-catalyzed cross-coupling reactions of an organometallic reagent and a (pseudo)halide substrate consists of (i) oxidative addition of substrate to a low-valent metal center, (ii) transmetalation of the formed metal complex intermediate with an organometallic species, and (iii) reductive elimination of the product forming a new C–C bond. Oxidative addition and reductive elimination have been well studied and the steps are often similar for different palladium-catalyzed cross-coupling reactions. However, the transmetalation step is highly dependent on the nature of the organometallic reagent and therefore, differs between different types of reactions.

For the Suzuki-Miyaura cross-coupling of organic (pseudo)halides and an organoboron species, two different pathways for the transmetalation step have been proposed, namely a boronate pathway (scheme 3.1, Pathway **A**) or an oxo-palladium pathway (scheme 3.1, Pathway **B**). In both pathways, Pd–O–B linked intermediate **I-4** would initially be formed. Qualitative kinetic experiments and DFT calculations have been published providing evidence that both mechanisms are operating depending on the reaction conditions.¹⁴⁹⁻¹⁵¹ Pre-transmetalation intermediates with a Pd–O–B bond motif have been characterized *in situ* and shown to be kinetically competent to undergo ligand transfer. These transient intermediates could be formed via reaction of a bromide palladium complex with an aryl boronate (Pathway **A**) or a hydroxide palladium complex with an aryl boronic acid (Pathway **B**).^{118,119} No reports on the influence of substituents on the aryl ligand on the reacting palladium complex in Suzuki-Miyaura cross-couplings have been published.

To probe the influence of the electronic character of the aryl ligand in the transmetalation step, the reactivity of substituted aryl palladium(II) complexes towards an organoboron species via either Pathway **A** or Pathway **B** would provide information about the transmetalation step. Assuming that reductive elimination is irreversible, the relative reaction rate k_{rel} of two substituted palladium complexes can be derived from the product ratio and plotted as a function of the σ values of the substituent in a Hammett plot.

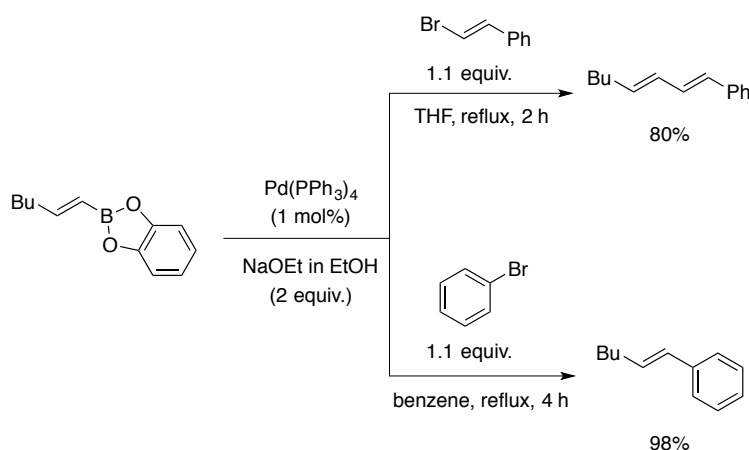


Scheme 3.1. Competition experiments between aryl palladium complexes bearing either a bromide or hydroxide ligand with an organoboron species via a boronate pathway or an oxo-palladium pathway.

The previous mechanistic studies on the transmetalation step of the Suzuki-Miyaura coupling have been heavily dependent on the solubility of the hydroxide-ligated palladium complexes and particularly the solubility of a boronate species. Often, mixed solvent systems and phase transfer additives are employed. Furthermore, few stable hydroxide palladium complexes bearing aryl ligands with different substitution pattern have been reported. A general procedure for the synthesis of stable hydroxide-ligated palladium complexes is therefore desirable. Recent reports on the formation of anionic boronate species involve the addition of an alkali base to a boronic acid, resulting in a water-soluble organoboronate species. Unfortunately, these boronate species exhibit very limited solubility in organic solvents. An alternative boronate species with a lipophilic tetrabutylammonium counterion would increase the solubility in organic solvents typically used for Suzuki-Miyaura cross-couplings and allow for mechanistic studies in a monophasic solvent system.

3.2 Background

Of the known cross-coupling protocols, the Suzuki-Miyaura cross-coupling is one of the most commonly employed reactions for forming new C–C bonds. Since it was first reported in 1979, it has been extensively used in organic synthesis,¹⁵² material science¹⁵³ and pharmaceutical chemistry¹⁵⁴ to name a few areas. The initial protocol described the stereospecific reaction between alkenyl/alkynyl/aryl halides and an alkenylboronic ester catalyzed by Pd(PPh₃)₄ in the presence of a strong alkoxide base, which resulted in *E,E*-dienes (scheme 3.2).¹⁵⁵ Later reported for other (pseudo)halides and organoboron species as well, the Suzuki-Miyaura cross-coupling reaction is a relatively non-toxic and robust protocol for C–C bond formations. Due to that no anhydrous conditions are required, the reactions are often carried out in water-mixtures. The retention of stereochemistry of the initially investigated alkenes opens up for the sp²-sp² or sp²-sp cross-couplings in a selective manner. As an alternative to homogenous cross-coupling reaction conditions employing Pd(PPh₃)₄, PdCl₂ or Pd(OAc)₂ in combination with phosphine ligands,¹⁵⁶ heterogeneous catalysts such as Pd/C¹⁵⁷ or palladium nanoparticles supported on silica¹⁵⁸ have also been employed.



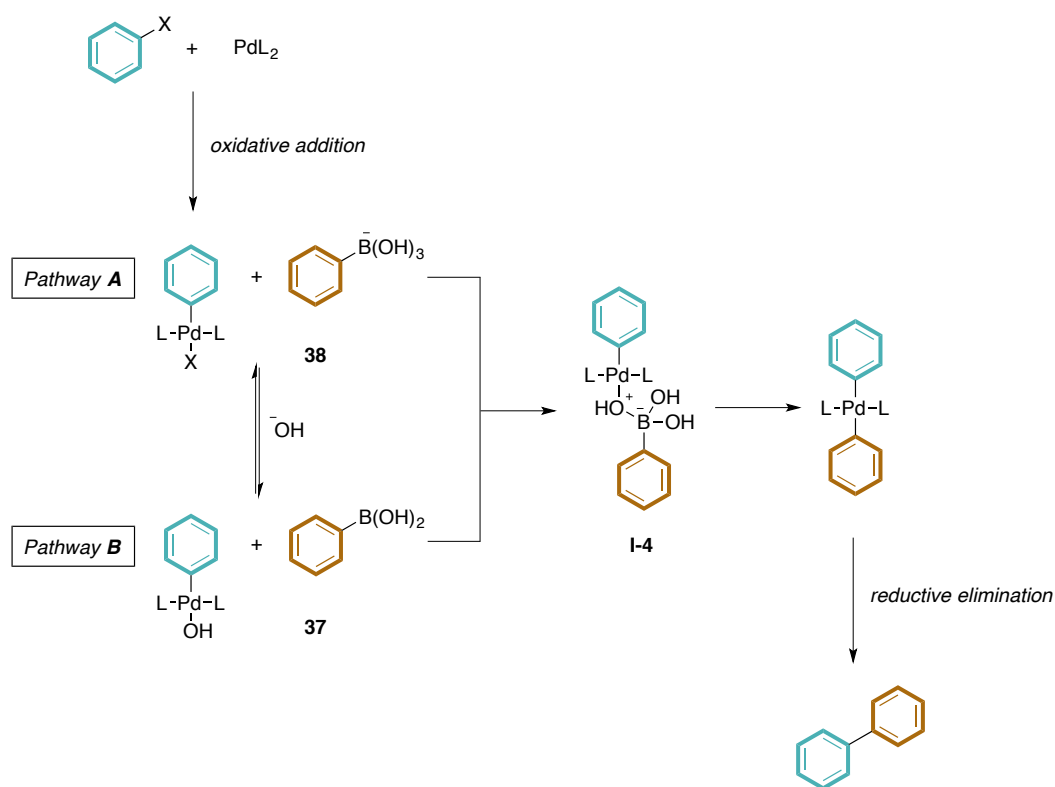
Scheme 3.2. First palladium-catalyzed cross-coupling between an alkenylboronic ester and an alkenyl or aryl halide reported by Suzuki and Miyaura.

Palladium-catalyzed cross-coupling reactions all share similar elemental steps of the catalytic cycle. Initially, oxidative addition of a substrate to a low valent palladium species takes place, followed by transmetalation with an organometallic reactant, and subsequently reductive elimination of the product. Oxidative addition and reductive elimination are two well-studied steps for cross-coupling reactions; however, the transmetalation step is not as well described and it is often unique to each cross-coupling protocol. Due to the concerted nature of oxidative addition reactions, the process will form a *cis* complex by the reaction between an organic (pseudo)halide and a palladium(0) complex. Depending on the rate of transmetalation with an organometallic species, the kinetically formed *cis* intermediate can undergo isomerization to the thermodynamic *trans* product complex.^{159,160} Organotin

species employed in Stille reactions are usually air and moisture stable due to the low polarity of the Sn–C bond and therefore the transmetalation step is slow. Similarly, organoboron species in Suzuki-Miyaura couplings or organosilicon reagents in Hiyama-Denmark couplings also exhibit a high stability and therefore, a slower transmetalation rate is often observed. In contrast, Grignard reagents or zinc species employed in Kumada and Negishi cross-couplings, respectively often present a higher reactivity due to the increased polarity of the C–M bond.¹⁶⁰ For Suzuki-Miyaura cross-couplings, the transmetalation step is often considered being the rate-determining step when employing iodide and bromide reagents.¹⁶¹ However, in reactions with less reactive chloride substrates, it has been suggested that the oxidative addition becomes the rate-determining step instead.¹⁶²

Because of their commercial availability, boronic acids have been extensively employed in Suzuki-Miyaura couplings. However, boronic acids often form dimeric or cyclic trimeric anhydrides by loss of H₂O, which limits reactivity. As initially reported, boronic esters are also reactive towards the cross-coupling protocol. Due to their preferred monomeric structure, the stoichiometry can be accurately determined. However, the increase in stability also results in a lower reactivity of boronic ester substrates in comparison to boronic acids. An observed competing pathway to cross-coupling is homocoupling of the organoboron reactant.^{163,164,165} Homocoupling of the nucleophilic boronic acid has been suggested to take place when an oxidant such as O₂ is present in reaction mixture.¹⁶⁵ A peroxo (η^2 -O₂)Pd(PPh₃)₂ intermediate complex is suggested to form by oxidation of Pd(PPh₃)₂ by O₂. The peroxo complex subsequently reacts with a boronic acid, forming a hydroxide-ligated palladium complex after hydrolysis. This monomeric species thereafter undergoes reaction with an additional boronic acid, yielding the homocoupling product after reductive elimination.¹⁶⁵ Suppression of the homocoupling pathway can be achieved by exclusion of oxygen or the addition of a weak reductant such as potassium formate, which limits the amount of palladium(II) in the reaction mixture and therefore decreases the homocoupling reaction with the boronic acid.¹⁶⁶ Another competing pathway is metal-catalyzed protodeboronation resulting in arene formation from the organoboron species.¹⁵³ Particularly, electron-deficient boronic acids tend to undergo a protodeboronation reaction,¹⁶⁷ and the decomposition pathway is often induced by heat in the presence of H₂O and base.¹⁶⁸ Boronic acids also undergo oxidation to the corresponding phenol in the presence of a palladium source.^{153,163} An alternative to boronic acids are organotrifluoroborates bearing an alkali metal counter cation. Such reactants undergo less side reactions under Suzuki-Miyaura cross-coupling reaction conditions.^{169,170} The organotrifluoroborates hydrolyze in the presence of H₂O, acting as a slow-releasing source of boronic acid, which prevents accumulation of boronic acid and therefore limits side reactions.¹⁷¹ However, a limited solubility of organotrifluoroborates in nonpolar organic solvents is often observed, and polar solvents such as MeCN or H₂O at elevated temperatures are required. Displacing the alkali metal cation with a more lipophilic tetraalkylammonium cation such as tetrabutylammonium (TBA) increases solubility in nonpolar organic solvents.^{170,172}

From the initial report of the Suzuki-Miyaura cross-coupling, it was shown that a strong base is required for product formation to take place.¹⁵⁵ Typically, Suzuki-Miyaura reactions are carried out in the presence of an inorganic base such as alkoxides, hydroxides, carbonates or fluorides in mixed organic/H₂O solvent systems.¹⁷³ Weaker Lewis bases such as NEt₃ do not result in cross-coupling product formation. The inorganic base has been deduced to play an important role in the transmetalation step. Transfer of the organic fragment from the organoboron species to a palladium intermediate has been suggested to proceed via one of two mechanisms. Either, the base undergoes a nucleophilic attack on a Lewis acidic organoboron reactant **37**, forming an anionic boronate species **38**, which subsequently reacts with an organopalladium intermediate forming intermediate **I-4**. This Pd–O–B linked intermediate then undergoes ligand transfer from boron to palladium and subsequent reductive elimination (scheme 3.3, Pathway A).^{15,161,174,175} Alternatively, a hydroxide initially displaces a halide ligand on the aryl palladium complex, resulting in a hydroxide palladium species that reacts with a neutral organoboron species **37** to yield the same Pd–O–B intermediate **I-4** (scheme 3.3, Pathway B).^{149,176,177}



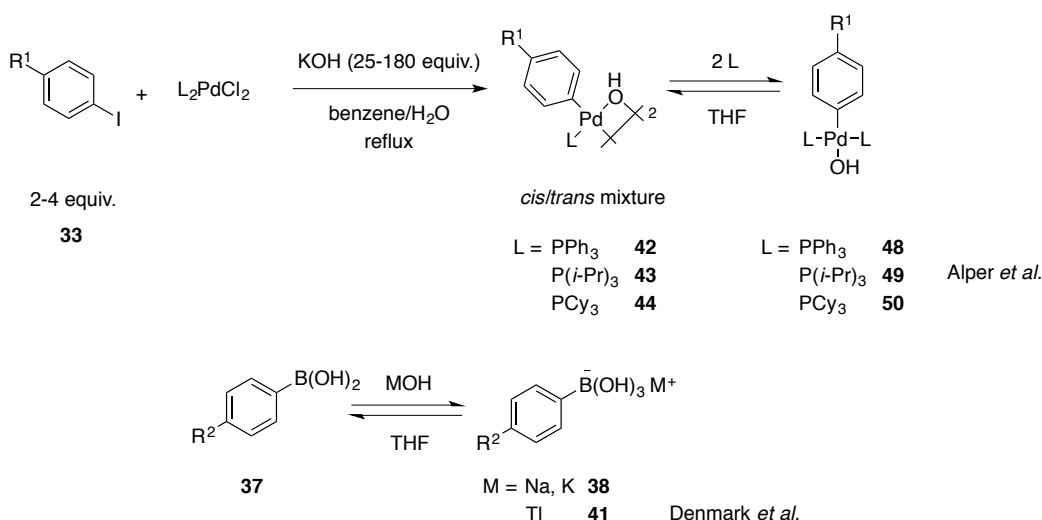
Scheme 3.3. Proposed pathways of the transmetalation in Suzuki-Miyaura cross-couplings.

Both pathways have been proposed to operate under certain reaction conditions. The influence of the electronic properties on the organoboron reagent has been studied, however, the analogous study of substitution pattern of the aryl halide reagent are scarce.¹⁷⁸ Of the studies performed, it has been concluded that the outcome of the reaction is heavily dependent on the reaction conditions such as solvent, base and catalyst.

3.2.1 Synthesis of proposed catalytically active intermediates

In addition to intermediates in the Suzuki-Miyaura cross-coupling, palladium hydroxide species have been detected as intermediates in oxidative palladium-catalyzed reactions, such as the Wacker process^{179,180} or when molecular O₂ is used as oxidant.^{181,182} Synthesis of palladium hydroxide intermediates is limited by the frequent instability of the complexes.¹⁸³ Of the reported hydroxide palladium complexes, anionic dimers with two μ -OH ligands bearing electron-poor pentafluorophenyl groups on the palladium atom were early reported.¹⁸⁴ Monomeric hydroxide complexes bearing electron-deficient aryl or alkenyl ligands have been synthesized by addition of NaOMe to the organopalladium halide complex, forming an alkoxide palladium(II) species that subsequently can be hydrolyzed to the hydroxide complex.¹⁸⁰ Isolation of hydroxide palladium complexes bearing PCP ligands formed by displacement of NO₃ from a PCP palladium(II) complex with KOH or NaOH has also been reported.¹⁸⁵ Alternatively, insertion of O₂ into a Pd-H bond of a PNP palladium(II) hydride complex formed a hydroperoxo complex that subsequently decomposed to the hydroxide species.¹⁸²

Alper and co-workers described the first synthesis of a neutral aryl palladium(II) hydroxide dimer bearing one monodentate phosphine ligand per palladium. The complex was formed from L₂PdCl₂, KOH and phenyl iodide **33** where L = PPh₃, P(*i*-Pr)₃ or PCy₃ in a biphasic H₂O/benzene solvent mixture (scheme 3.4, top).^{186,187} Addition of 18-crown-6 as a phase transfer agent facilitated complex formation in the biphasic solvent system.¹⁸⁸ It is proposed that the palladium(II) complex is initially reduced by the phosphine to a palladium(0) species, which subsequently undergoes oxidative addition of the phenyl iodide **33**. X-ray analysis of the palladium complex showed a μ -OH dimeric species, resulting in a mixture of *cis* and *trans* isomer of complex **42-44**. The dimers could be converted to the monomers by addition of excess ligand.^{118,187} Although the monomers **48-50** were stable in the solid-state, an equilibrium between monomer and dimer was observed in solution. Furthermore, monomeric complex **49** bearing an P(*i*-Pr)₃ ligand also slowly dimerized in the crystalline state,¹⁸⁷ limiting determination of stoichiometry. The formation of oxidized phosphine ligand is a disadvantage of the procedure. The solubility of O=PPh₃ is low in organic solvents, which results in a tedious purification of the formed complex. Hydroxide complexes **42-44** and **48-50** were initially used in carbonylation reactions studies.^{186,188} Recently, both monomers and dimers were employed in mechanistic investigations on the Suzuki-Miyaura cross-coupling.^{118,119,151}



Scheme 3.4. Isolated intermediates of the Suzuki-Miyaura cross-coupling reaction.

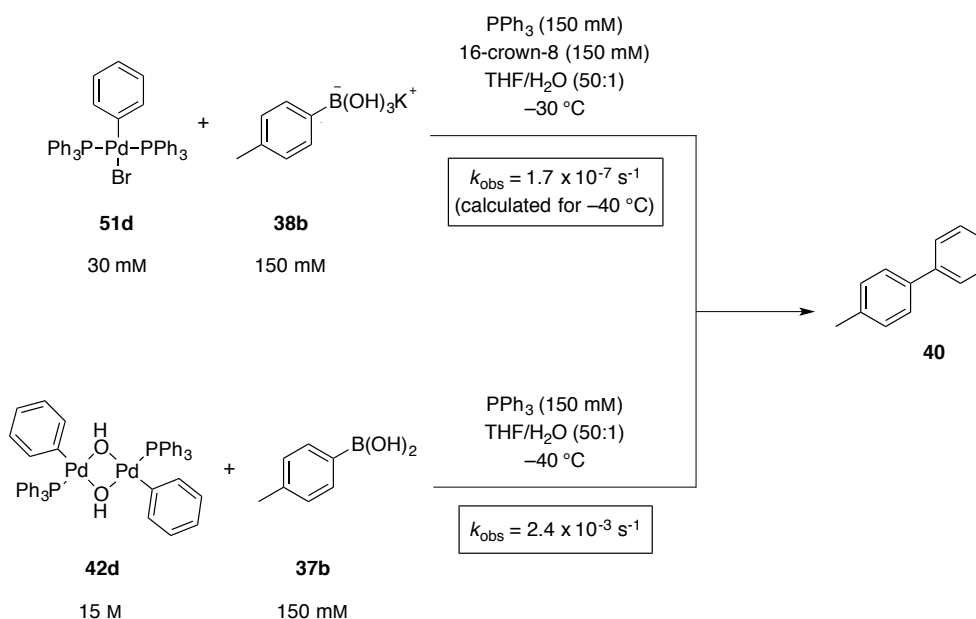
Boronic acids **37** can be readily converted to the boronate species **38** with an alkali cation such as Na⁺ or K⁺ by addition of an aqueous solution of NaOH or KOH to the boronic acid substrate (scheme 3.4, bottom).^{151,189,190} As an alternative for the alkali metal, the softer Lewis acid thallium(I) has been employed as counterion. TlOH readily reacts with 4-fluorophenylboronic acid **37c**, forming a thallium boronate species **41c**, which exhibited an increased solubility in THF and was used for studies of the transmetalation step.¹¹⁹ Thallium(I) hydroxides or carbonates have previously been used as base in Suzuki-Miyaura cross-couplings,¹⁹¹ however, due to the extreme toxicity of thallium, other alternatives are preferred.

3.2.2 Previous mechanistic investigations

Investigations on the operating transmetalation pathway have been performed via both experimental and computational methods. Maseras and co-workers performed DFT calculations on the energy barriers for Pathway **A** and Pathway **B**, using a phenyl palladium(II) bromide complex with two *trans* PH₃ ligands and a phenylboronic acid as model reaction. A large energy barrier of $\Delta G = 48.7$ kcal/mol was found in the absence of a hydroxide base. In the presence of base, the most accessible pathway was calculated to be Pathway **A**, where the hydroxide initially reacts with a boronic acid **37** forming a boronate species **38**, which subsequently reacts with the aryl palladium halide intermediate with an energy barrier of $\Delta G = 10.8$ kcal/mol. No direct displacement of halide with hydroxide on the palladium intermediate via Pathway **B** was calculated to take place in the system.¹⁹² Similar results were obtained for calculation of the reaction between a vinyl palladium(II) complex and a vinylboronic acid, where the lowest energy barrier of $\Delta G = 4.2$ kcal/mol was the reaction of a halide palladium complex and a boronate species via Pathway **A**.¹⁹³ Canary and co-workers performed

electron-spray ionization experiments on the reaction between 3-bromopyridine and phenylboronic acid in the presence of Pd(PPh₃)₄ and a carbonate base. By mass spectroscopy, the oxidative addition product [(PyH)Pd(Br)(PPh₃)₂]⁺ and a post-transmetalation species [(PyH)Pd(Ph)(PPh₃)₂]⁺ were detected. No hydroxide or alkoxide palladium species was observed, which was suggested to support that the transmetalation takes place via Pathway A.¹⁷⁴

Opposing observations were presented by Jutand and Amatore, who investigated the role of the base in the reaction between (phenyl)Pd(OH)(PPh₃)₂ **48** and an arylboronic acid **37** in DMF. No reaction took place in the absence of added base. With base, biaryl formation was observed in the reaction between complex **48** and arylboronic acid **37**. For comparison, the reaction between (phenyl)Pd(Br)(PPh₃)₂ **51** and arylboronate **38** in the presence of excess bromide anions, no biaryl product was observed.¹⁹⁴ Hartwig and co-workers carried out a study comparing the relative reaction rates between stoichiometric amounts of a hydroxide palladium complex and a boronic acid or a halide palladium complex and a boronate species. The hydroxide palladium complex employed was dimeric [(phenyl)Pd(μ-OH)(PPh₃)₂] **42d** in the presence of PPh₃ ligand and for comparison of reactivity, monomeric bromide analogue (phenyl)Pd(Br)(PPh₃)₂ **51d** was used. Due to the low solubility of potassium boronate **38** in THF, 18-crown-6 was added (scheme 3.5). At room temperature, the reaction between equimolar amounts of hydroxide complex **42d** and methyl boronic acid **37b** or bromide complex **51d** and potassium boronate **38b** in THF/H₂O was complete within minutes. The catalytic reaction of iodobenzene **33** and methyl boronic acid **37b** in the presence of Pd(PPh₃)₄ (1 mol%) and K₂CO₃ in the same solvent mixture required heating to 80 °C for 3 hours for complete conversion of starting materials, showing that the stoichiometric reaction is significantly faster and likely is reflecting the transmetalation step.¹⁵¹ Comparison of the relative reaction rates of hydroxide complex **42d** and boronic acid **37b** in the presence of excess PPh₃ and in a THF/H₂O mixture (50:1) at -40 °C occurred with an observed rate constant of $k_{\text{obs}} = 2.4 \times 10^{-3} \text{ s}^{-1}$ as monitored via low-temperature ³¹P NMR. In contrast, the reaction between bromide complex **51d** and tolyl boronate **38b** in the presence of excess 18-crown-6 and PPh₃ did not react after the same time interval of 25 minutes. A rate constant of $k_{\text{obs}} = 1.7 \times 10^{-7} \text{ s}^{-1}$ was extrapolated from an Arrhenius plot. The rate is 1.4×10^4 times smaller than for the reaction between hydroxide palladium complex **42d** and methyl boronic acid **37b**. A similar difference in rate was obtained when comparing the reaction of PCy₃-ligated hydroxide complex **50d** and boronic acid **37b** to the reaction of PCy₃-ligated bromide complex **54d** and tolyl boronate **38b**. From these results, it was concluded that the transmetalation step likely takes place between a hydroxide complex and a boronic acid species via Pathway B.¹⁵¹ However, the influence of the crown ether on the reaction was not determined.

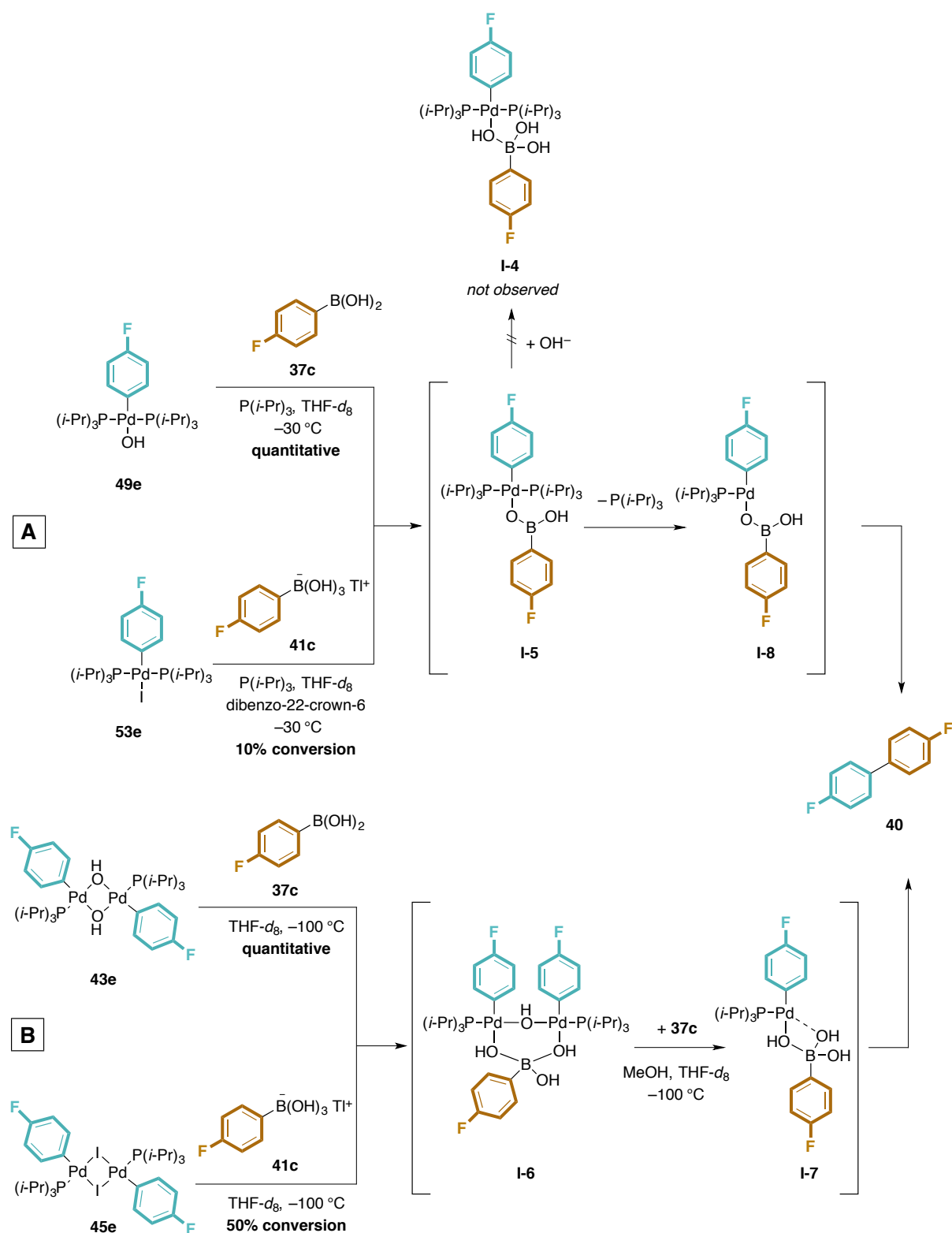


Scheme 3.5. Determination of relative reaction rates for the proposed Pathway **A** and Pathway **B** by Hartwig *et al.*

The equilibrium between the boronic acid and the boronate species was determined for 4-fluorophenylboronic acid **37c** and 4-fluoro potassium boronate **38c**. Both organoboron species existed in approximately equimolar amounts with added K₂CO₃ in an acetone/H₂O solution (1:1).¹⁵¹ Although this equilibrium holds true for weaker bases, a shift towards the boronate side would be expected with a stronger base. Dimeric hydroxide complex **42d** in the presence of tetrabutylammonium bromide also existed in an equilibrium with bromide complex **51d**. However, the equilibrium is more complicated to determine due to the concurrent equilibrium with the monomeric OH complex **48d**.¹⁵¹

The Pd–O–B linked intermediate **I-4** is proposed to be a transient species formed prior to transmetalation.¹⁹⁵ An intermediate with a chemical shift of $\delta = 20.1$ ppm formed in the reaction between hydroxide complex **42d** and boronic acid **37b** was reported by Hartwig and co-workers and proposed to belong to a Pd–O–B linked species.¹³⁷ An intermediate with a similar shift of $\delta = 22.7$ ppm has previously been observed in the reaction between 2-bromopyridine derivatives and phenylboronic acid in the presence of Pd(PPh₃)₄. DFT calculations suggested that it belonged to a (2-pyridyl)Pd(B(OH)₃)(PR₃)₂ intermediate formed by nucleophilic attack of a boronate on a palladium halide complex and where the boronate hydroxide bridge between the palladium and boron.⁶⁹

Denmark and co-workers recently reported an extensive investigation on the transient intermediates formed in the reaction between aryl palladium complexes and organoboron species. One tricoordinated boron species **I-5** and two tetracoordinated boron species **I-6** and **I-7** were detected and characterized *in situ* via low-temperature two-dimensional NMR (scheme 3.6).^{118,119}



Scheme 3.6. Pd–O–B linked intermediates observed in Suzuki–Miyaura couplings by Denmark *et al.*

Reactions between monomeric (4-fluorophenyl) $\text{Pd}(\text{OH})(\text{P}(i\text{-Pr})_3)_2$ **49e** and 4-fluorophenylboronic acid **37c** in $\text{THF-}d_8$ at -30°C $\text{THF-}d_8$ resulted in a quantitative conversion of starting materials to the tricoordinated boron species **I-5** bearing two phosphine ligands on the palladium atom (scheme 3.6, A). Reaction between monomeric (4-fluorophenyl) $\text{Pd}(\text{I})(\text{P}(i\text{-Pr})_3)_2$ **53e** and thallium

4-fluorophenylboronate **41c** at $-30\text{ }^{\circ}\text{C}$ in THF- d_8 resulted in 10% conversion to intermediate **I-5**, in addition to biaryl product **40**, indicating that **I-5** also can be formed in the absence of hydroxide palladium complex.¹¹⁸ However, no reaction between iodide palladium complex **53e** and potassium boronate **38c** was observed, likely to low solubility or potassium boronates in THF.¹¹⁹ Intermediate **I-5** was suggested to form by loss of H_2O from the previously proposed tetracoordinated boron intermediate **I-4**. Addition of H_2O or $\text{CsOH}\cdot\text{H}_2\text{O}$ to **I-5** did not shift the equilibrium to **I-4**, suggesting a high stability of the tricoordinated boron intermediate, arguably due to the steric demand of the $\text{P}(i\text{-Pr})_3$ ligand.¹¹⁸ To circumvent the steric hindrance, reactions with a palladium complex bearing only one phosphine ligand per palladium atom were performed. Dimeric $[(4\text{-fluorophenyl})\text{Pd}(\mu\text{-OH})(\text{P}(i\text{-Pr})_3)_2]_2$ **43e** and boronic acid **37c** at $-100\text{ }^{\circ}\text{C}$ in THF- d_8 resulted in the quantitative formation of intermediate **I-6**, (scheme 3.6, **B**). The intermediate exhibited a 1:2 boron to palladium stoichiometry. The same intermediate was observed in the reaction between iodide dimer **45e** and thallium boronate **41c** under the same conditions, however only in 50% yield. Addition of 1 equivalent of boronic acid **37c** and MeOH to intermediate **I-6** resulted in quantitative formation of the new intermediate **I-7** exhibiting a 1:1 boron to palladium stoichiometry. Noteworthy, similar intermediates were detected employing 4-fluorophenyl palladium(II) complexes bearing PPh_3 , $\text{P}(t\text{-Bu})_3$ and dppf ligands.¹¹⁹ Intermediates **I-5**, **I-6** and **I-7** all decomposed to the biaryl product **40** over time.¹¹⁸ Intermediate **I-6** and **I-7** underwent a fast reaction to the biaryl product, forming **40** within 1 hour at $-30\text{ }^{\circ}\text{C}$.¹¹⁸ However, tricoordinated **I-5** was stable over 12 hours at $-30\text{ }^{\circ}\text{C}$ in the presence of excess $\text{P}(i\text{-Pr})_3$ ligand. Warming the solution and monitoring biaryl **40** formation at $20\text{ }^{\circ}\text{C}$ over 12 hours resulted in an S-shaped formation curve of **40**, indicating an autocatalytic reaction where k_{obs} increase over time. Loss of $\text{P}(i\text{-Pr})_3$ ligand was suggested to form the 14-electron palladium intermediate **I-8**, however it could not be detected. The origin of the apparent autocatalytic behavior was determined to be depending on the presence of H_2O , which together with $\text{P}(i\text{-Pr})_3$ favors the formation of the resting state intermediate **I-5**. An inverse dependence on $\text{P}(i\text{-Pr})_3$ was determined, supporting this hypothesis.^{118,119} An inverse dependence on phosphine ligand has previously been determined for the reaction between a monomeric PPh_3 -ligated aryl palladium complex **51d** and potassium boronate **38b**, indicating that a free coordination site on the aryl palladium complex is required prior to transmetalation.¹³⁷

3.2.3 Hammett correlations for determining sensitivity to substituents

The Hammett correlation is a useful tool for determining the electronic influence of substituents on a reaction, describing how the reaction rate changes with *meta* or *para* substituents on a reactant. The relationship is described by the equation $\log(k_{\text{R}}/k_{\text{H}}) = \rho\sigma$,¹⁹⁶ where $k_{\text{R}}/k_{\text{H}}$ is the relative reaction rate of a substituted substrate to the unsubstituted substrate. The σ -value is a substituent dependent constant¹⁹⁷

and ρ is a reaction dependent constant. A linear Hammett correlation with a positive reaction constant ρ indicates that the reaction is faster for an electron-poor substrates and a negative ρ indicates a faster reaction for an electron-rich reactants. Non-linear Hammett plots can indicate that a change in mechanism is present for different substituents.⁴⁵ However, the reaction constant ρ does not take pre-equilibriums or more than one intermediate into account.

Few reports on quantitative kinetic investigations of isolated aryl palladium intermediates in cross-coupling reactions have been published.^{42,75,198} For Suzuki-Miyaura cross-couplings, one study investigating the transmetalation between a sulfur-containing cyclopalladated complex and a boronic acid has been reported, however, the reaction is possibly catalyzed by heterogeneous palladium nanoparticles.¹⁷⁸ Our group recently reported a thorough study on the electronic influence on the transmetalation step of aryl palladium complexes ligated by dppe with arylzinc reagents in Negishi cross-couplings. Varying the *para*-substituent on the aryl ligand on a palladium(II) complex resulted in a Hammett plot with a negative ρ -value. An electron-withdrawing group often is suggested to increase the rate of transmetalation due to the increase in electrophilicity on the palladium center and therefore, additional DFT calculations of potential transition states were performed. A halide-bridged intermediate was identified, and it was concluded that ligand transfer is not one concerted step but rather takes place over at least one intermediate. The plausible intermediate exhibits a zinc-halide interaction, which is favored for by electron-rich aryl palladium(II) complexes.⁴²

For Hiyama-Denmark couplings, an investigation on the influence of substitution pattern of P(*t*-Bu)₃-ligated aryl palladium complexes **14** towards an arylsilanolate (KOSiMe₂Ar) reactant has been reported. Electron-withdrawing substituents on the aryl ligand facilitate transmetalation, as indicated by an observed positive ρ -value. The reaction of 4-methoxy potassium silanolate and *para*-substituted P(*t*-Bu)₃ complexes **14** was monitored via ³¹P NMR and a reaction constant of $\rho = +0.49$ was obtained, indicating that transmetalation is faster the more electron-deficient the aryl ligand on the palladium complex is. Also, the influence on the substitution of arylsilanolate reagent was investigated and $\rho = -0.50$ was obtained, indicating that transmetalation is faster with more electron-rich silanolate substrates.⁷⁵ A transient intermediate species was formed by the reaction of P(*t*-Bu)₃ complex **14** and arylsilanolates. The intermediate exhibited an oxygen-bridge between palladium and silicon, similar to **I-5** formed between an organoboron species and an aryl palladium complex in Suzuki-Miyaura cross-couplings (see above, scheme 3.6). Addition of a second equivalent of arylsilanolate formed the cross-coupled product. A pre-equilibrium between the silanolate-bridged intermediate and an intermediate containing two linked silanolate groups, forming an anionic intermediate, was supposed to influence the ρ -value. Measurement of the reaction rate at saturated silanolate concentration resulted in a reaction constant of larger magnitude ($\rho = -0.80$), indicating the presence of a pre-equilibrium.^{75,117}

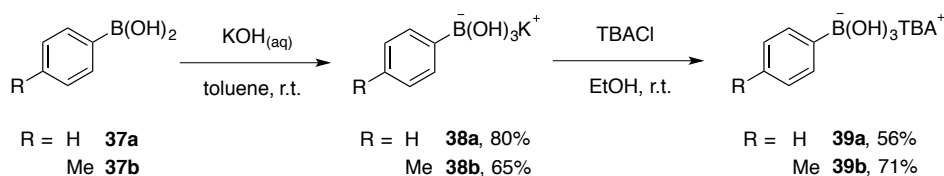
For the Suzuki-Miyaura cross-coupling, quantitative reaction rate measurements to determine the electronic influence of a substituted organoboron species on the reaction between *para*-substituted arylboronic esters and propargylic carbonates were performed by Suzuki and Miyaura. With Pd(PPh₃)₄ as catalyst in THF at room temperature, a decarboxylative coupling takes place, forming a substituted phenylallene product. No base was required because the electrophilic carbonate substrate forms an alkoxide palladium complex *in situ*. For the substituted phenylboronic esters, a reaction constant of $\rho = +0.73$ was obtained. It was suggested that the transmetalation takes place between the alkoxide palladium complex and the organoboronic ester via Pathway **B** under these reaction conditions.¹⁷⁷ A similar investigation on *para*-substituted phenylboronic acid derivatives was performed by Monteiro and co-workers. The reactivity of the organoboron species in the transmetalation with vinyl bromides in the presence of Pd(OAc)₂, PPh₃ and KOH in MeOH at 100 °C was investigated. A reaction constant of $\rho = -1.26$ was obtained, indicating that transfer of the aryl group is promoted by electron-rich boronic acids.¹⁵⁰ A subsequent report from the same group describes the Hammett correlation for the reaction between *para*-substituted phenylboronic acids and (*E*)-bromostilbene under the same catalytic conditions. A reaction constant of $\rho = -0.71$ was obtained, indicating that more electron-rich and less Lewis acidic boronic acids react faster.¹⁷⁵ Because a more electron-rich anionic boronate reagent undergoes faster reaction with an electrophilic palladium species, these results indicate that Pathway **A** is operating under the reaction conditions. These Hammett correlations on the electronic influence of organoboron reactant are based on competition experiments of the catalytic reaction. Therefore, all steps prior to the irreversible ligand transfer are affecting the ρ -value.

As can be seen from the above-described mechanistic investigations, the reaction conditions play a crucial role on the mechanism of the transmetalation step. Results from experiments performed in monophasic organic solvents might not be applicable to biphasic mixtures of organic solvent and aqueous base. Furthermore, the influence on the sterics of phosphine ligand has been calculated and it was proposed that the ligand plays a large role in the transmetalation step, with more sterically demanding ligands increasing the energy barrier for ligand transfer.¹⁹⁹

3.3 Results and discussion

3.3.1 Organoboron reagents

To investigate the reactivity of substituted aryl palladium complexes in the Suzuki-Miyaura cross-coupling, organoboron species exhibiting high solubility in an organic solvent are required. Boronic acids commonly employed in Suzuki-Miyaura cross-coupling reactions are readily available, either from commercial sources or by reaction of an organometallic reagent bearing the relevant organic substituent and a borate ester. Reports show that a saturated aqueous solution of NaOH and a boronic acid **37** in toluene readily forms a sodium boronate species **38** that can be isolated by filtration due to its low solubility in toluene.^{190,200} A similar protocol was employed for unsubstituted boronic acid **37a** and 4-tolylboronic acid **37b**, yielding the corresponding potassium boronates **38a** and **38b** in 80% and 65% yield, respectively (scheme 3.7). No complete solubility was observed in organic solvents and H₂O was required to completely dissolve boronates **38**. A patent procedure reports the reaction between an arylboronic acid **37** and an aqueous solution of tetrabutylammonium hydroxide to form the TBA boronate species **39**.²⁰¹ Employing a similar protocol resulted in the TBA boronate, however, separation of product and starting material proved complicated. Instead, cation exchange by addition of TBACl in EtOH was chosen as method for forming a more lipophilic boronate species. Potassium boronates **38** were converted to TBA boronates **39** by facile reaction at room temperature and subsequent removal of the formed KCl by filtration. Boronates **39** proved very hygroscopic and removal of H₂O was achieved by lyophilization, resulting in boronate **39a** and **39b** in a yield of 59% and 71%, respectively.



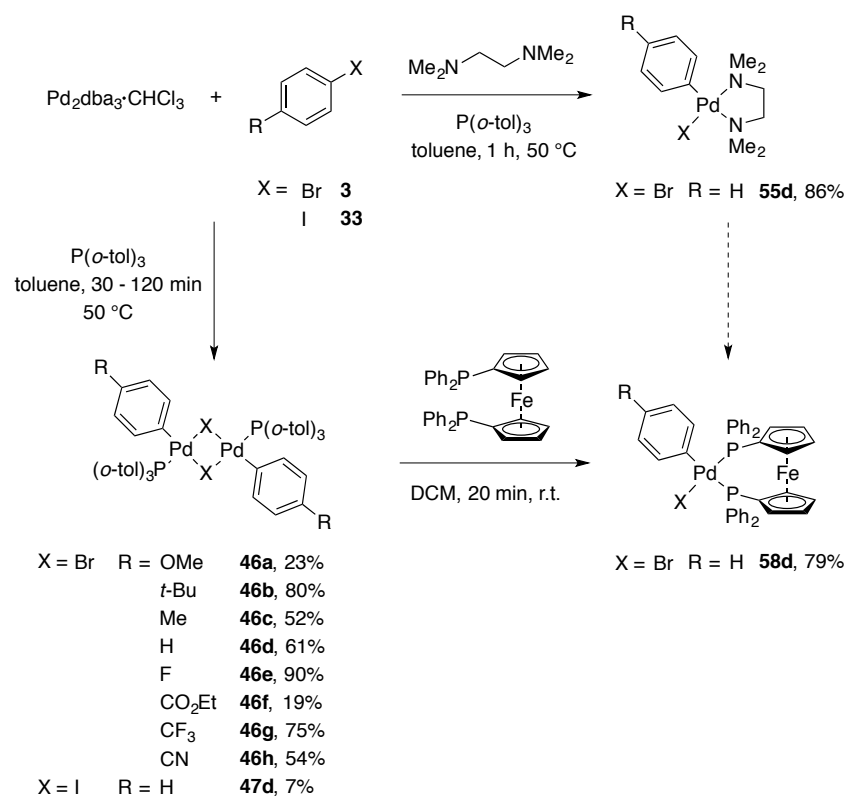
Scheme 3.7. Formation of potassium boronates **38** by addition of saturated KOH to arylboronic acid **37**. Cation exchange by addition of TBACl (0.95 equiv.) forming TBA boronates **39**.

Potassium boronate **38a** and **38b** exhibited ¹¹B shifts of $\delta = 3.34$ ppm and $\delta = 1.87$ ppm, respectively. An upfield shift of $\delta = -5.52$ ppm and $\delta = -4.64$ ppm was observed with the displacement of the potassium cation for a more electron-rich TBA counterion in boronate **39a** and **39b**. Both TBA boronates exhibited high stability and solubility in common organic solvents, deeming them viable substrates for investigations of the reactivity of anionic organoboron reagents towards aryl palladium complexes.

3.3.2 Halide-ligated palladium complexes

For quantitative kinetic investigations of substituted aryl palladium complexes bearing a halide ligand, a general synthesis applicable for substituted aryl halides is desirable. Furthermore, synthesis of the analogous hydroxide complexes should be possible, preferably by direct displacement of halide ligand. Synthesis of a palladium(II) precursor bearing a tmeda ligand can be performed by oxidative addition of relevant aryl iodide **33** to Pd₂dba₃·CHCl₃ in presence of tmeda.¹²⁸ A similar *trans*-dipyridine-ligated complex can be formed by employing pyridine as solvent under otherwise similar reaction conditions.⁴⁸ Oxidative addition of aryl bromides **3** to Pd₂dba₃·CHCl₃ in the presence of only nitrogen-containing ligands form the aryl palladium(II) complexes in lower yields than the reaction with aryl iodides.¹²⁸ However, addition of catalytic amounts of P(*o*-tol)₃ to the aryl bromide reaction increase oxidative addition of the substrate, forming nitrogen-ligated precursor complexes.⁷⁶ Employing this protocol for bromobenzene **3a** and Pd₂dba₃·CHCl₃ resulted in the tmeda-ligated bromide complex **55d** in 86% yield (scheme 3.8). Subsequent displacement of the tmeda ligand with a phosphine ligand is a facile process that takes place within minutes at room temperature.²⁰² Oxidative addition of an aryl halide to either Pd₂dba₃·CHCl₃ in the presence of P(*o*-tol)₃, or to complex Pd(P(*o*-tol)₃)₂ gives aryl palladium(II) dimers with a μ -Br **46** or μ -I **47** ligands.^{77,130} Both complexes adopt halide-bridged dimeric structures in the solid-state as well as in solution.⁷⁷ Complexes **46** with different *para*-substituents of the aryl ligand were obtained in 19-90% yield by oxidative addition of aryl halide to Pd₂dba₃·CHCl₃ in the presence of excess P(*o*-tol)₃ (scheme 3.8). Excess P(*o*-tol)₃ ligand were removed by precipitation of the complex from Et₂O. A lower yield was obtained with methoxy and ester-substituted bromoarenes **3ea** and **3ef**. The decrease in yield might be due to an increase in solubility of dimer **46a** and **46f** in toluene, preventing precipitation. Although the reactions were performed in toluene, complexes **46** proved virtually impossible to re-dissolve after precipitation. The solubility of **46** also proved limited in THF or dioxane, however dissolution could be achieved in halogenated solvents such as DCM and CHCl₃ after 15 minutes of rapid stirring.

All dimeric complexes **46** shown have been previously synthesized and characterized and employed as precursors to monomeric aryl palladium(II) complexes.⁴² The ³¹P spectra of **46a-h** exhibited broad singlets at $\delta = 28$ -29 ppm, arising from a fast *cis/trans* equilibrium of the dimeric species. Due to the equilibrium, no assignment of the *cis* and *trans* isomer in the ¹H NMR could be performed. However, separation of the signals has been reported by lowering the temperature to below 0 °C.⁷⁷ Due to the low solubility of bromide-bridging palladium dimers **46** in non-halogenated organic solvents, the corresponding iodide dimer **47d** was formed. However, the solubility of iodide dimer **47d** in THF or toluene was even lower than bromide dimer **46** and no other iodide dimers **47** were synthesized.



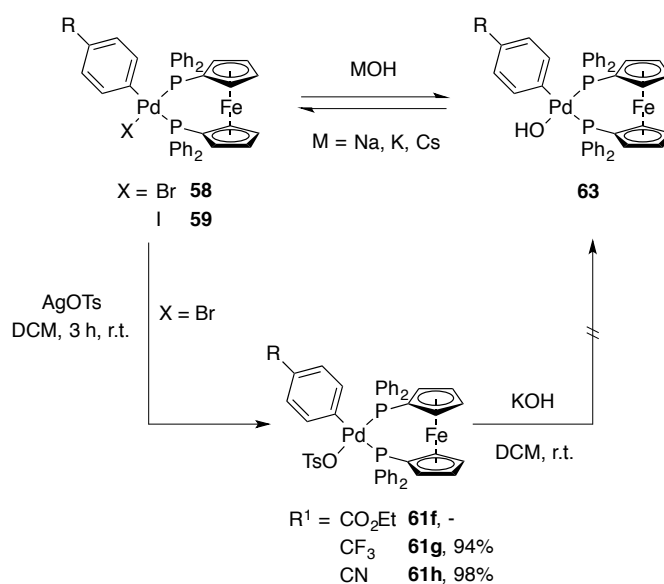
Scheme 3.8. Oxidative addition of aryl halides to $\text{Pd}_2\text{dba}_3 \cdot \text{CHCl}_3$ in the presence excess tmeda forming complex **55** or excess $\text{P}(o\text{-tol})_3$ resulting in dimer **46**. Displacement of $\text{P}(o\text{-tol})_3$ on **46d** by addition of dppf (2 equiv.) forming monomeric complex **58d**.

The $\text{P}(o\text{-tol})_3$ can be readily displaced by other phosphine ligands, demonstrating that dimeric complexes **46** are valuable precursors to other aryl palladium complexes. Displacement of $\text{P}(o\text{-tol})_3$ by bidentate dppf can be achieved by stirring in DCM.⁴² Dimer **46d** was converted to dppf-ligated monomer **58d** in 79% yield and employed in halide displacement test reactions shown below.

3.3.3 Hydroxide-ligated palladium complexes

A general route for the synthesis of aryl palladium hydroxide complexes with a clear stoichiometry is lacking among the protocols shown above. Attempted synthesis according to the reported procedure by reaction of phenyl iodide **33a** and $(\text{PPh}_3)_2\text{PdCl}_2$ in the presence of KOH resulted in a 3:2 *cis/trans* mixture of $\mu\text{-OH}$ dimer **42d**, in addition to $\text{O}=\text{PPh}_3$ (see Experimental section 4.12.2). Synthesis of the analogous complex bearing a 4-tolyl ligand was attempted by an identical procedure, however the formed $\text{O}=\text{PPh}_3$ could not be separated from the hydroxide complex **42c**. Therefore, a procedure obviating the initial reduction of palladium and oxidation of phosphine ligand was sought. Direct displacement of a halide ligand from a monomeric aryl palladium(II) complex was initially investigated. Both dppe- and dppf-ligated bromide and iodide complexes **57-60** were subjected to the

basic reaction conditions. The unsubstituted phenyl dppf complex **58d** was synthesized as shown above and the iodide-ligated dppf and dppe complexes **59-60** were previously formed in a similar manner in another project by the working group.⁴² However, stirring monomeric iodide complexes **59** or **60** with NaOH, KOH or CsOH at room temperature or at elevated temperatures did not result in ligand exchange and either the starting complex was re-isolated or oxidized phosphine ligand was obtained. Solvents such as DCM, THF or benzene were employed. Prolonged heating and particularly in THF as solvent increased the decomposition to oxidized phosphorus species. After stirring dppf phenyl complex **58d** bearing a bromide ligand with KOH in DCM, two new doublets were observed via ³¹P NMR (scheme 3.9). However, a ratio of 3:2 of starting material:product was obtained. Arguably, an equilibrium between the bromide and hydroxide complex exists. Attempts to favor hydroxide complex formation by exchanging the solvent or increasing the temperature did not significantly increase product formation. Similar results were obtained with 4-tolyl and 4-fluorophenyl palladium complexes **58c** and **58e** bearing dppf ligands. Due to similar solubility of starting material and product, separation by precipitation proved unsuccessful. As an alternative, displacement of the bromide ligand on a tmeda-ligated palladium(II) complex **55** and subsequent displacement with a phosphine ligand was tested. However, addition of KOH or CsOH to tmeda-ligated complex **55d** only resulted in re-isolation of starting material.

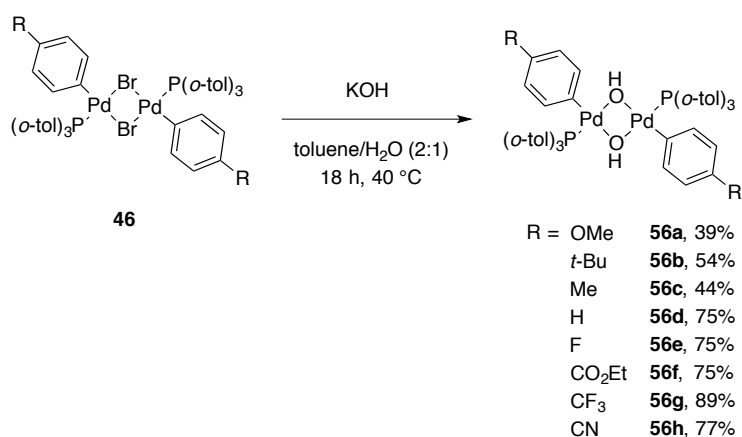


Scheme 3.9. Attempts to displace a halide ligand on monomeric palladium(II) complexes **58**, **59** with MOH (5-50 equiv.) or AgOTs (2 equiv.). No yield of complex **61f** was determined.

It was envisioned that a more electrophilic tosylate palladium(II) complex²⁰³ might react more easily with an inorganic hydroxide base. Addition of AgOTs to the dppf-ligated bromide complexes **58-59** with a CO₂Et, CF₃ and CN substituent readily displaced the bromide ligand forming the tosylate complexes **61**. Complexes **61** were identified via ³¹P NMR and subsequently treated with KOH.

However, no hydroxide complex could be isolated, likely due to fast decomposition of hydroxide complexes in solution.¹⁸³ Furthermore, employing dppf halide complexes **58-59** with electron-donating substituents only resulted in decomposition when AgOTs was added. Therefore, the tosylate approach was abandoned.

As an alternative to direct halogen displacement on monomeric aryl palladium(II) complexes **58-59**, the hydroxide ligands were introduced on the dimeric $P(o\text{-tol})_3$ complexes **46a-h** (scheme 3.10). Dimeric complexes **46** exhibit high stability and no decomposition was detected after prolonged heating in organic solvents. Therefore, it was assumed that anionic ligand exchange could be performed at elevated temperatures. Complex **46** and KOH were dissolved in a biphasic solution of toluene/ H_2O in a ratio of 2:1 was rapidly stirred over night at 40 °C. Only a small amount of $O=P(o\text{-tol})_3$ as decomposition product was obtained after the reaction. Due to the increased solubility of $O=P(o\text{-tol})_3$ in comparison to $O=PPh_3$, precipitation of the products from Et_2O resulted in the analytically pure $\mu\text{-OH}$ complexes **56a-h** in 39-89% yield. The complexes were soluble in halogenated solvents as well as dioxane. However, hydroxide complex **56** decomposed completely to $O=P(o\text{-tol})_3$ within minutes in THF. A similar oxidation of the phosphine ligand occurred in dioxane, however, only 10% of hydroxide complex **56** was decomposed after 48 h.



Scheme 3.10. Displacement of $\mu\text{-Br}$ on dimeric palladium(II) complexes **46** with KOH (180 equiv.) forming dimeric $\mu\text{-OH}$ complexes **56**.

Complexes **56a-h** exhibited ^{31}P shifts of $\delta = 29\text{-}30$ ppm, very similar to the $\mu\text{-Br}$ complexes **46a-h**. Similar to the bromide complexes, no clear assignment of signals could be performed via ^1H NMR due to a fast *cis/trans* isomerization.¹⁸⁶ Therefore, the composition of all hydroxide complexes **56** was established by elemental analysis. Single crystals suitable for X-ray analysis were obtained of complex **56c**, **56d** and **56e** by slow diffusion of Et_2O into a saturated $CHCl_3$ solution. The solid-state structures of the complexes are shown in figure 3.1. All three complexes co-crystallized with a $CHCl_3$ solvent molecule (not shown).

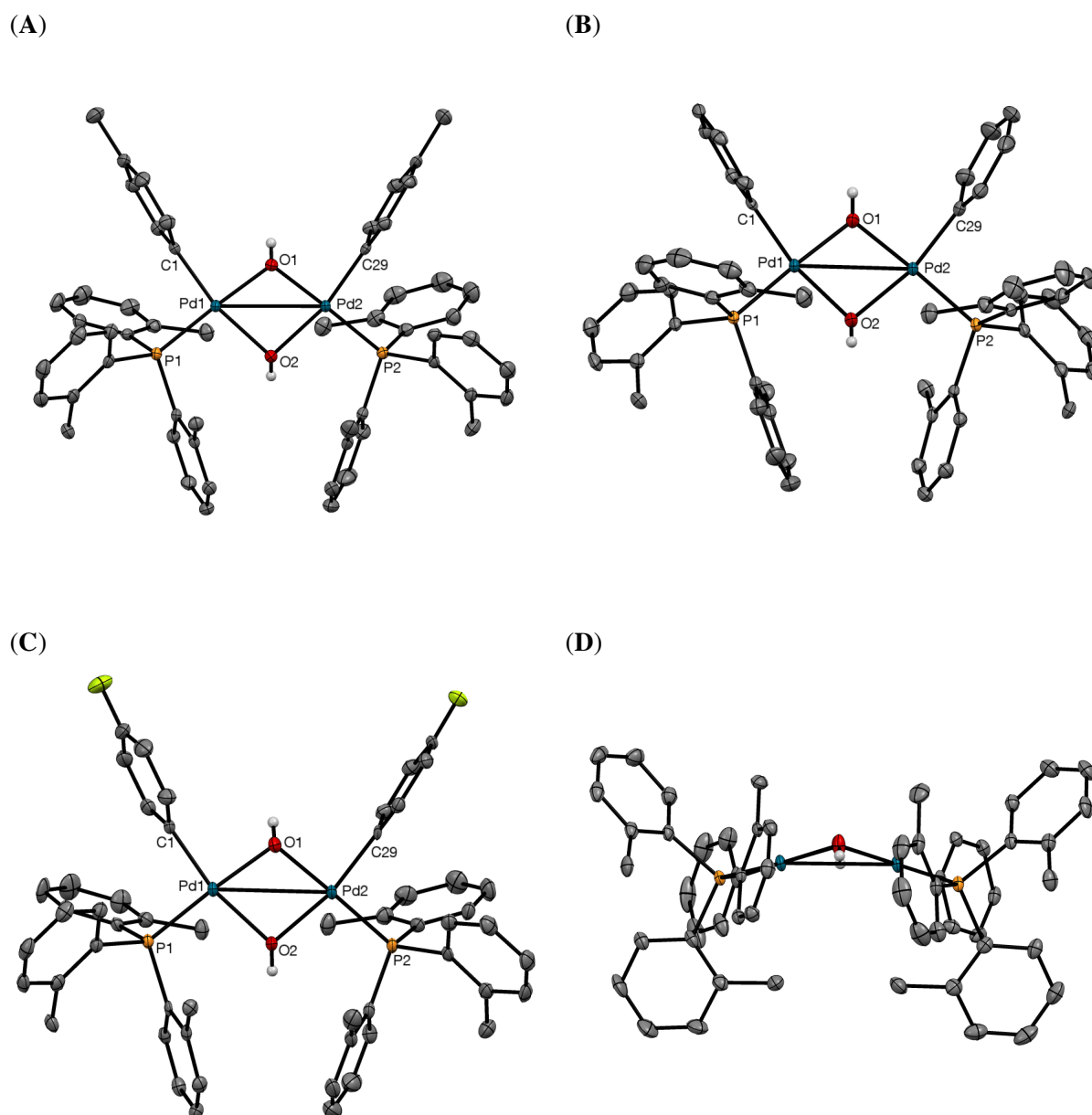


Figure 3.1. ORTEP drawing of μ -OH bridged dimers **56c** (A), **56d** (B) and **56e** (C). Thermal ellipsoids are drawn at 50% probability level. Selected hydrogen atoms are shown. Co-crystallized CHCl_3 was omitted for clarity. (D) shows structure of μ -OH bridge of complex **56d**. Angles between planes: **56c** (A) = 37.9° , **56d** (B) = 34.8° and **56e** (C) = 34.3° .

X-ray analysis of complexes **56** shows a *cis* orientation of the two aryl groups. Between the *cis* oriented *o*-tolyl groups of the phosphine ligands, a distance between 2.49-2.98 Å was observed, indicating a steric strain. The ligands are oriented in a perfect square planar configuration around each palladium center. However, the μ -OH results in a non-planar overall geometry of the two palladium atoms (figure 3.1, D), with angles between the planes were in the range of 34.3 - 37.9° . The analogous PPh_3 -ligated hydroxide dimer **42d** with an unsubstituted phenyl ligand exhibited a larger plane angle of 49.5° ,¹⁸⁶ likely due to the smaller steric demand of the PPh_3 ligands compared to $\text{P}(o\text{-tol})_3$ (cone

angle 145° versus 194°).¹⁴² Dimeric PPh_3 -ligated hydroxide complex **42d** exhibited a *trans* geometry of the phosphine ligands on the palladium centers, further relieving the steric strain between the ligands. In comparison, the analogous μ -Br complex exhibited a plane angle of 9.5° between the two palladium centers.¹³² Selected bond distances and angles of complexes **56c-e** are listed in table 3.1.

Table 3.1. Selected bond distances (Å) and angles ($^\circ$) of μ -OH bridged dimer **56c-e**.

	56c	56d	56e
Pd1–P1	2.235	2.239	2.232
Pd1–C1	2.001	1.997	1.999
Pd1–O1	2.068	2.079	2.070
Pd1–O2	2.119	2.124	2.110
Pd2–P2	2.245	2.239	2.239
Pd2–C29	1.991	2.003	2.001
Pd2–O1	2.074	2.079	2.073
Pd2–O2	2.115	2.124	2.116
O1–Pd1–O2	77.09	76.88	77.26
C1–Pd1–O2	167.31	167.88	167.14
O1–Pd2–O2	77.04	77.31	77.07
C28–Pd2–O2	167.38	167.17	168.01

A Pd(1)–Pd(2) distance between 3.10–3.13 Å was observed, being longer than the Pd(1)–Pd(2) distance of 2.98 Å for the reported PPh_3 -ligated hydroxide dimer **42d**.¹⁸⁶ A larger distance between the two palladium atoms is suggested to be due to the more sterically demanding $\text{P}(o\text{-tol})_3$ ligand in a *cis* configuration. The *trans* influence of the phenyl substituents gives rise to an elongation of the Pd–O(2) of 0.04–0.05 Å in comparison to the Pd–O(1) bonds. In all complexes, an interaction between the H-atom of the CHCl_3 solvent and the oxygen of the hydroxide bridge were found, ranging between 2.25–2.81 Å. Hydrogens of the bridging hydroxides were calculated at 0.66–0.85 Å distance, with the distance being affected by the additional solvent coordination by the oxygen ligand. This feature has also previously been observed for PPh_3 -ligated hydroxide complex **42d**, where the OH bond was 1.10 Å and interacted with the H-atom of a co-crystallized CHCl_3 molecule with a distance of 2.00 Å.¹⁸⁶ For the mixed bridging ligand complex $(\text{phenyl})_2\text{Pd}_2(\mu\text{-OH})(\mu\text{-NH-}t\text{-Bu})(\text{PPh}_3)_2$ formed by reaction of hydroxide dimer **42d** and a primary amine, no solvent interaction was observed and the O–H bond was calculated to be 0.80 Å.²⁰⁴ A similar angle between O(1)–Pd–O(2) of $76.9\text{--}77.3^\circ$ was observed for **56c-e** in comparison to the reported PPh_3 -ligated complex **42d** with a O(1)–Pd–O(2) of $76.6\text{--}77.0^\circ$.¹⁸⁶ Very similar bond lengths and angles of the differently substituted complexes **56c-e** were obtained, indicating that the substituent does not influence the solid-state structure substantially. Pd–C_{ipso} bond distances of 1.99 Å to 2.02 Å were observed, being almost identical to the Pd–C_{ipso} bonds of 2.01–2.02 Å reported μ -Br complexes **46**.^{77,132}

Due to the low solubility of bromide dimers **46** and decomposition of hydroxide dimers **56** in typical solvents used for Suzuki-Miyaura couplings, other palladium complex would be desirable for mechanistic investigations. Since displacement of a bromide with a hydroxide anion directly from the phenyl palladium complex **58d** resulted in a mixture of starting material and product **63d** (see above, scheme 3.9), a different approach was sought. Since $P(o\text{-tol})_3$ is readily displaced from an aryl palladium dimer **46** by the addition of a bidentate phosphine ligand, 4-methyl phenyl $\mu\text{-OH}$ bridging palladium dimer **56c** was treated with dppf or dppe (figure 3.2). Because of the observed instability of hydroxide palladium complexes, displacement of the $P(o\text{-tol})_3$ ligand was performed in the glovebox with dry solvents. Dppe complex **62c** and dppf complex **63c** were isolated as yellow solids.

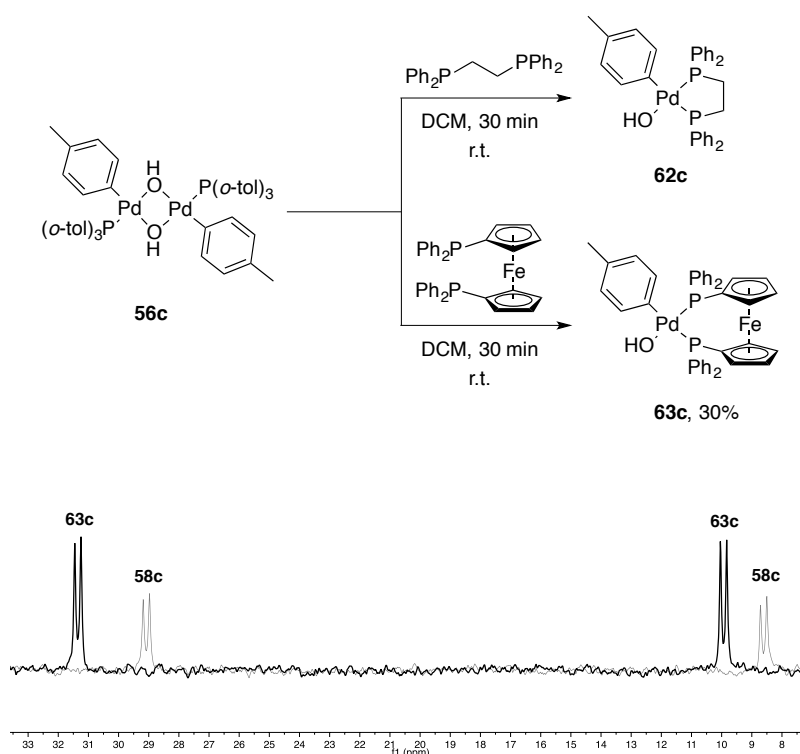


Figure 3.2. Displacement of $P(o\text{-tol})_3$ ligand on hydroxide complex **56c** (1 equiv.) by addition of dppe (2 equiv.) or dppf (2 equiv.). No yield of **62c** was determined. Comparison of ^{31}P shifts for hydroxide dppf complex **63c** (black) and bromide dppf complex **58c** (grey). Reference ^{31}P NMR spectrum of **58c** from Sina Zucker.⁴²

Complex **63c** bearing a dppf ligand gave rise to two doublets with shifts of $\delta = 31.4$ and 9.93 ppm with a coupling constant of $J = 32$ Hz, shifted slightly downfield in comparison to the bromide complex **58c**. The similar dppf-ligated hydroxide complex bearing a 4-fluorophenyl substituent has been reported to give rise to two doublets at $\delta = 28.4$ and $\delta = 9.0$ ppm with a $J = 30$ Hz.¹¹⁹ Complex **62c** bearing a dppe ligand exhibited two doublets in the ^{31}P NMR with chemical shifts of $\delta = 51.6$ and 31.4 ppm with a coupling constant of $J = 27$ Hz (not shown). The analogous bromide dppe complex **57c** has not been reported. Hydroxide complexes **62c** and **63c** exhibited a limited stability in a DCM/ CHCl_3 solution, decomposing within 24 hours to a mixture of unidentified products. In benzene,

stability for up to 12 hours was observed. No further analysis of the bidentate phosphine complexes was performed. Arguably, displacement of a P(*o*-tol)₃ ligand from the palladium dimer **46** bearing other substituted phenyl groups might be possible with a variety of phosphine ligands, facilitating tuning of solubility and stability of hydroxide palladium(II) complexes.

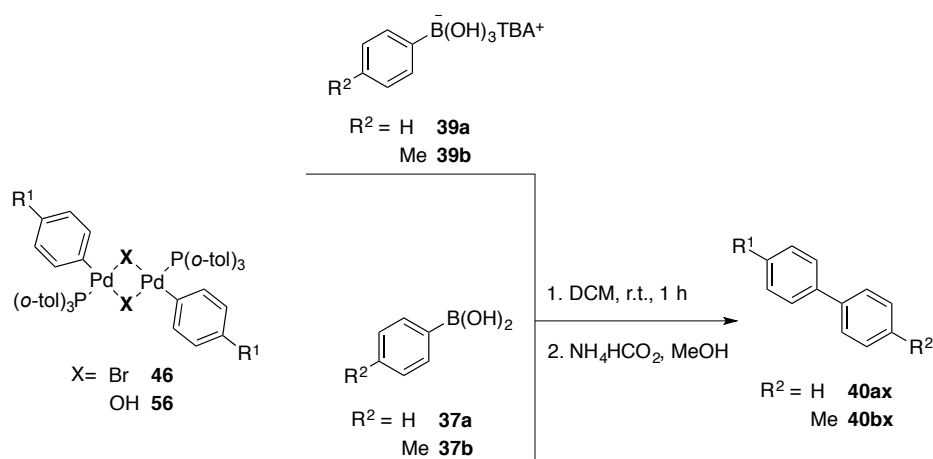
3.3.4 Screening of transmetalation conditions

Investigation on the electronic influence of differently substituted aryl palladium complexes towards an organoboron reactant requires that all reactants exhibit satisfactory solubility in the solvent employed. The solubility of hydroxide bridged P(*o*-tol)₃ complexes **56** in halogenated solvents such as DCM and CHCl₃ was sufficient, with the exception of methyl substituted complex **56c**. In dioxane, slow decomposition of **56** was observed only after days, suggesting that the ethereal solvent could be used for competition experiments between hydroxide complexes **56** and a boronic acid **37**. However, the corresponding bromide and iodide aryl palladium P(*o*-tol)₃ complexes **46** and **47** were only sparsely soluble in dioxane. Boronic acids **37** are completely soluble in most organic solvents. Due to the lipophilic tetrabutylammonium counterion, TBA boronate **39** was soluble in both dioxane and DCM. Due to the solubility limitation of bromide complex **46**, the competition experiments were performed in DCM. To avoid a potentially irreproducible influence of trace amounts of water, a defined amount (0.20%) was added to the solvent. A setup for competition experiments for the investigation of the transmetalation between substituted aryl palladium(II) complexes **60** bearing dppe ligands and substituted aryl zinc reagents has previously been described by the group.⁴² Therefore, all authentic biaryl products **40** were available in the group inventory. A similar setup as reported was employed to investigate the electronic influence on reactivity of substituted aryl P(*o*-tol)₃ dimers **46** and **56** with boronic acids **37** and boronates **39**. Initially, the reactivity of the synthesized palladium(II) complexes **46** and **56** towards an organoboron reagent was investigated. Combination of equimolar amounts of hydroxide complex **56** and boronic acid **37** in DCM at room temperature in the absence of additives resulted in complete consumption of palladium dimer **56** within 1 h. Within the same time frame, bromide complex **46** was completely consumed in the reaction with equimolar amount of TBA boronate **39**. Free P(*o*-tol)₃ and O=P(*o*-tol)₃ was observed by ³¹P NMR. No yield of cross-coupling product was determined.

Under the competition reaction conditions, an excess of palladium dimer **46** or **56** relative to organoboron reagent is employed. To avoid side reactions or homocoupling of non-consumed aryl palladium complex, a quenching protocol for the excess palladium complex was required. Ideally, a reducing agent that completely converts palladium complex **46** and **56** to the free arene is desirable. Ammonium formate has previously been employed as reducing agent for the aryl palladium complexes investigated in the Negishi cross-coupling reaction,⁴² and an analogous procedure was

therefore attempted for aryl dimers **46** and **56**. As model substrates for the quenching, palladium dimers **46a** and **56a** bearing a methoxy substituent and **46h** and **56h** bearing a cyano substituent were chosen. Addition of one spatula tip NH_4HCO_2 to a DCM/methanolic solution of complex **46** and **56** at room temperature and subsequent quantification of arene product via GC-FID resulted in almost quantitative yields of free arene (see Experimental section, 4.13). As internal standard, 1,3,5-trimethoxybenzene was employed. No homocoupling of palladium complex **46** or **56** was observed. Furthermore, the formed arenes are volatile enough that no overlap with the signals of the cross-coupling biaryl products **40** occurs. To test that the quenching was compatible with the competition experiment reaction conditions, reactions between bromide dimer **46** and hydroxide dimer **56** and boronic acid **37** and boronate **39** in a non-competitive transmetalation were performed and subsequently quenched by the same procedure (table 3.2).

Table 3.2. Non-competitive transmetalation between $\mu\text{-Br}$ and $\mu\text{-OH}$ complex **46** and **56** (16 μmol) and boronate **39** or boronic acid **37** (4 μmol). Yields are average of two measurements of the same sample.



entry	R	Boronate 39a		Boronate 39b		Boronic acid 37a		Boronic acid 37b	
		46 ($\mu\text{-Br}$)	yield 40ax [%]	yield 40bx [%]	56 ($\mu\text{-OH}$)	yield 40ax [%]	yield 40bx [%]		
1	OMe	46a	51	34	56a	83	79		
2	<i>t</i> -Bu	46b	21	68	56b	86	90		
3	Me	46c	53	73	56c	–	–		
4	H	46d	89	66	56d	89	102		
5	F	46e	33	66	56e	48	101		
6	CO ₂ Et	46f	85	75	56f	98	105		
7	CF ₃	46g	70	59	56g	100	72		
8	CN	46h	53	60	56h	79	93		

Unsubstituted phenylboron species **37a**, **39a** and 4-tolylboron species **37b** and **39b** were employed to determine which substrates resulted in the highest yield. A 4-fold excess of palladium complex to organoboron reactant was employed to create a pseudo-zero order reaction in palladium. Quantification of cross-coupled product **40** was performed with GC-FID. To a solution of **46** and **56** in DCM, boronate **39** or boronic acid **37** was added and stirred for 1 h. The crude reaction mixture was subsequently quenched with NH_4HCO_2 in MeOH and stirred for an additional 1 h. The solids were filtered off through a pipette with celite prior to injection in the GC-FID. Biaryl product **40a** from reactions with the unsubstituted organoboron species **37a** and **39a** were lower for some palladium complexes than the yield of biaryl **40b** formed from reactions with 4-tolyl organoboron species **37b** and **39b**. Therefore, the competition experiments were performed with the 4-tolyl substituted organoboron reagent.

3.3.5 Competition experiments with $[(\text{Ar})\text{Pd}(\mu\text{-X})(\text{P}(o\text{-tol})_3)_2]$

One transmetalation reaction each was set up with two bromide dimers **46** and tolyl boronate **39b** and the analogous reaction between two competing hydroxide dimers **56** and tolyl boronic acid **37b**. The competition experiments were set up in such manner that all possible combinations were investigated (table 3.3). To decrease instrumental error, each sample from the competition experiment was measured three times by GC-FID. Competition experiment between unsubstituted phenyl complex **46d/56d**, 4-fluorophenyl complex **46e/56e** and 4-trifluoromethyl phenyl complex **46g/56g** could not be performed because the peaks of the corresponding biaryls **40bd**, **40be** and **40bg** overlapped in the GC chromatogram.

Table 3.3. Possible combinations of bromide complex **46** and hydroxide complex **56** for competition experiments.

	OMe (46a/56a)	<i>t</i> -Bu (46b/56b)	Me (46c/56c)	F (46e/56e)	CO ₂ Et (46f/56f)	CF ₃ (46g/56g)	CN (46h/56h)
H (46d/56d)	A1	A2	A3	-	A5	-	A7
OMe (46a/56a)		B2	B3	B4	B5	B6	B7
<i>t</i> -Bu (46b/56b)			C3	C4	C5	C6	C7
Me (46c/56c)				D4	D5	D6	D7
F (46e/56e)					E5	-	E7
CO ₂ Et (46f/56f)						F6	F7
CF ₃ (46g/56g)							G7

Each combination of competing palladium complex gives rise to a biaryl product ratio **40bx/40by**. From this ratio, taking the small change in palladium concentration into account, the ratio $k(\text{R}^1)/k(\text{R}^2)$ of the rate constants of the two competing reactants was calculated and normalized to $k(\text{R}^1)/k(\text{H})$.^{42,205}

The logarithms of the obtained reaction rates k_{rel} were plotted versus σ in a Hammett plot. Obvious outliers were omitted.

Figure 3.3 shows the relative reaction rates for the competition experiment between bromide dimer **46** and tolyl boronate species **39b**. A reaction constant of $\rho = +0.81$ with a R^2 value of 0.75 was obtained. A relative large instrumental error was observed (see Experimental part 4.13.2). A positive reaction constant is indicating that the transmetalation is facilitated by electron-withdrawing substituents on the aryl group of the reacting palladium complex. Previous Hammett correlations of differently substituted aryl palladium complexes in the reaction with anionic aryl silanolates in Denmark-Hiyama cross-couplings also gave a positive slope ($\rho = +0.49$).⁷⁵ Their data is based on the measured absolute rates and therefore reflect the rate-limiting step of the reactions. Hammett correlations derived from competition experiments reflect all steps prior to the first irreversible step of the reaction. If there is an equilibrium prior to ligand transfer, it will affect the observed ρ -value.

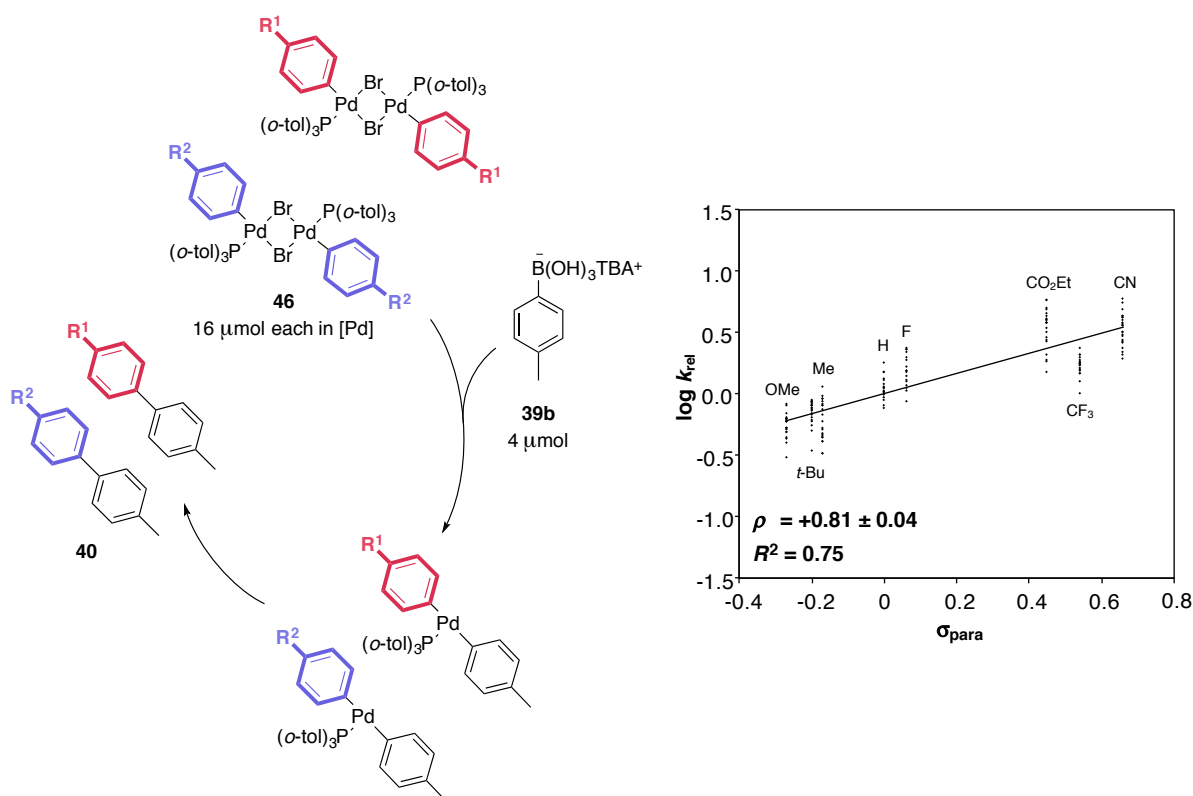


Figure 3.3. Competition experiment of bromide complexes **46** and TBA boronate **39b** and the resulting Hammett plot.

The analogous competition experiment between hydroxide complex **56** and tolylboronic acid **37b** was performed in the same manner and shown in figure 3.4. A reaction constant of $\rho = +0.52$, with a R^2 value of 0.65 was obtained. Similarly to the reaction shown above, a relatively large instrumental error was observed. Analogous to the reaction of bromide complexes **46**, a positive reaction constant for the reaction of hydroxide complexes **56** was obtained.

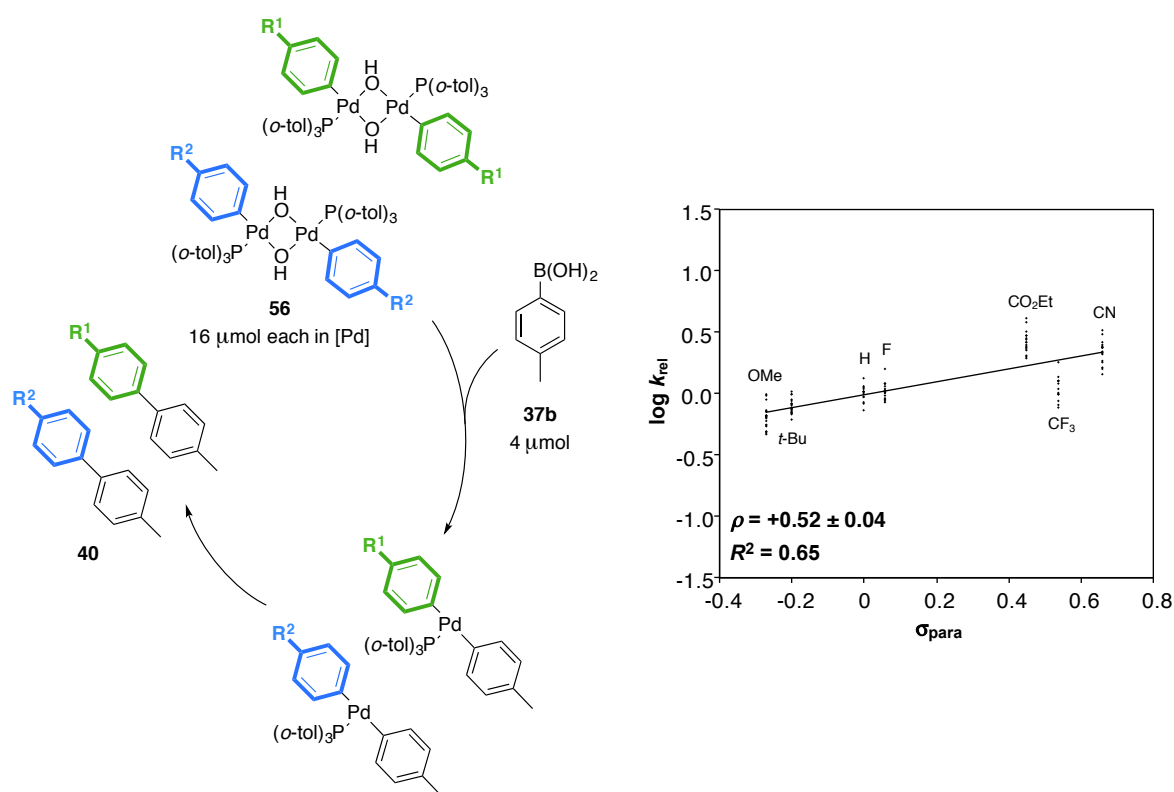


Figure 3.4. Competition experiment of hydroxide complexes **56** and boronic acid **37b** and the resulting Hammett plot.

The ρ -value for the reaction of bromide complex **46** is slightly larger than the one for the reaction of hydroxide complex **56**. This indicates that the reactions of bromide complexes **46** are more sensitive to the electronic influence of the aryl ligand than the corresponding hydroxide complex **56**. $P(o\text{-tol})_3$ palladium dimers **46** and **56** have a defined dimeric structure both in solution and in the solid-state. In contrast to the analogous PPh_3 dimer **42** or $P(i\text{-Pr})_3$ dimer **43**,¹⁸⁷ addition of excess ligand does not induce formation of a monomeric species.⁷⁷ Therefore, dimer **46** and **56** could form a monomeric species in solution with the open coordination site required for transmetalation. If the formation of the Pd–O–B intermediates shown above in scheme 3.6 is also occurring under the competition experiment reaction conditions, the presence of only one $P(o\text{-tol})_3$ ligand per palladium atom would exclude intermediates of type **I-5**, and rather suggest intermediates of type **I-6**. Sterically demanding $P(t\text{-Bu})_3$, which has a similar cone angle to $P(o\text{-tol})_3$, formed an intermediate of type **I-6** in the reaction of a palladium dimer and an organoboron species.^{118,119} However, these experiments were performed in coordinating THF. Because only two sets of competition experiments were performed, no extensive conclusions on the transmetalation step can be drawn. Additional experiments on the potential pre-transmetalation intermediates need to be performed.

3.4 Conclusion

Bromide-bridged P(*o*-tol)₃ palladium complexes **46** bearing an aryl ligand with substituents ranging from electron-donating to electron-withdrawing have been synthesized. These complexes undergo facile bromide displacement by the addition of KOH in a biphasic toluene/H₂O solvent system, resulting in the novel P(*o*-tol)₃ hydroxide-ligated palladium complexes **56**. The protocol is not sensitive to the substitution pattern on the aryl ligand and can therefore be applied on a wide range of bromide precursors. An advantage of this pathway is that no sacrificial phosphine ligand is required for the initial reduction of the palladium, circumventing the need to separate an oxidized phosphine species from the target complex in the purification step. X-ray analysis of the solid-state structures of three substituted aryl palladium hydroxide complexes **56** shows that the complexes adopt a dimeric structure with the hydroxide ligands bridging the two palladium atoms. In a similar manner as for bromide-bridging complex **46**, displacement of the P(*o*-tol)₃ ligand from hydroxide complex **56** with bidentate dppe or dppf ligand can be achieved at room temperature. Arguably, other ligands could be applied and a variety of monomeric hydroxide complexes would be accessible from complex **56** via similar processes.

Two anionic tetrabutylammonium boronate species **39a** and **39b** have been synthesized by displacing the potassium cation from the reported alkali boronate species **38**. The more lipophilic TBA counterion significantly increases the solubility of the boronate species in organic solvents, allowing investigations on the Suzuki-Miyaura cross-coupling to be performed in a wider variety of solvents. Previous mechanistic investigations on the transmetalation step employ mixed solvent systems and rely on the use of crown ethers as phase transfer agents to increase the solubility of alkali or thallium boronate species.^{118,119,151} A potential influence on the crown ether additive has not been investigated. With the anionic TBA boronate species **39**, investigations on the transmetalation step can be performed in a monophasic solvent system obviating the need for additives.

An initial study on the transmetalation step of the Suzuki-Miyaura cross-coupling reaction via the boronate or the oxo-palladium pathway has been performed. Competition experiments between differently substituted bromide complex **46** and TBA tolyl boronate **39b** resulted in a Hammett correlation with a ρ -value of +0.81. As comparison, the competition reaction between substituted hydroxide complexes **56** towards with a tolylboronic acid **37b** resulted in a Hammett correlation with a ρ -value of +0.52. As indicated by a positive ρ -values, both, reaction of bromide complex **46** and hydroxide complex **56**, are facilitated by electron-withdrawing substituents of the aryl ligand. These initial results indicate a higher sensitivity towards the substitution pattern of an aryl palladium complex bearing a bromide ligand in comparison to an aryl palladium complex bearing a hydroxide ligand. Additional experiments on the transmetalation reaction between bromide complex **46** or

hydroxide complex **56** with an organoboron species are required to investigate the presence of pre-transmetalation intermediates and potential pre-equilibrium reactions. Also, the influence on differently substituted organoboron species would give valuable information on the transmetalation step. No previous experiments on the reactivity of substituted aryl palladium complexes towards organoboron intermediates in the Suzuki-Miyaura cross-coupling have been performed. The previous analysis reported on the substitution pattern of the organoboron species only includes differently substituted boronic acid derivatives.^{150,175,177} With a soluble TBA boronate species **39**, additional experiments on the reactivity of the anionic nucleophile towards an electrophilic palladium complex can be carried out.

4 Experimental Section

4.1 General procedures and instrumentation

All air and moisture-sensitive reactions were set up in a glove box under argon atmosphere using oven-dried glassware. Heating of reactions was performed in a pre-heated oil bath or an aluminum well heating plate using a stirrer and heater with temperature control. Chemicals were purchased from commercial suppliers and used as received unless otherwise stated. Toluene, THF, benzene, Et₂O, pentane and dioxane were dried and distilled over sodium/benzophenone. Degassing of solvents was performed via freeze-pump-thaw techniques. CH₂Cl₂ was purchased from Sigma-Aldrich and dried via Solvent Purification System *MB-SPS 800* from *MBraun*. Dry DMF, MeOH, EtOH and pyridine were purchased from Acros in AcroSeal bottles. Column chromatography was done with *Merck Silica Gel 60* (230-400 mesh). Deactivation of silica gel was performed by flushing with 15% triethylamine in hexane. Thin layer chromatography was done using *Merck TLC Silica gel 60 F254*. Products were detected by using an UV/Vis lamp (254 nm).

¹H, ¹¹B, ¹³C, ¹⁹F and ³¹P NMR spectra were recorded on *Jeol ECX 400* or *Bruker Avance500* at room temperature unless otherwise stated. Data was processed by *MestReNova Version: 10.0.2-15465*. Chemical shifts (δ) are reported in parts per million (ppm) and referenced to residual solvent peak. Coupling constants (J) are reported in Hertz (Hz). Multiplicity of peaks is reported as s = singlet, d = doublet, t = triplet, q = quartet and m = multiplet. High-resolution ESI-MS spectra were recorded on an *Agilent 6210 ESI-TOF, Agilent Technologies*. The applied charge is reported as positive (+) or negative (-). The spray charge was set to 4 kV. Data is reported in mass to charge (m/z). IR spectra were recorded on a *Jasco FT/IR-4100 FT-IR* with a ZnSe optical window. The absorption bands are given in wave numbers (cm⁻¹) and the intensities are reported as follows: s = strong, m = medium, w = weak. Melting points (m.p.) were determined on a *BÜCHI 510* melting point apparatus and are uncorrected. Elemental analyses for carbon, nitrogen and hydrogen were performed on an elemental analyzer *VARIO EL, Elementar*, and results are reported in percentage (%). Gas chromatography measurements were performed on a *Varian CP-3800* equipped with a *Varian CP-8400* autosampler, a FID detector and WCOT column (fused silica, 30 m x 0.25 mm x 0.25 μ m film). Quantification of analytes was calculated from a calibration curve using an internal standard. The data was evaluated with *Varian Star Chromatography Workstation Version 6.41*.

4.2 Starting materials and reference compounds

4.2.1 Oxidations

Method A

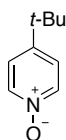
Pyridine or bipyridine substrate (1.0 equiv.) was dissolved in CH_2Cl_2 and *m*-CPBA (1.2-3.0 equiv.) was added to the solution. The reaction was stirred for 24 h or until the starting material was completely consumed. Removal of the solvent and purification of the product by column chromatography (deactivated silica gel, acetone/hexane) gave the substituted pyridine *N*-oxide or bipyridine *N,N'*-dioxide product.

Method B

Pyridine or bipyridine substrate (1.0 equiv.) was dissolved in acetic acid and H_2O_2 (30%, 1.2-10.0 equiv.) was added dropwise. The reaction was heated at 70 °C for 24 h or until complete consumption of substrate. The acetic acid was removed by evaporation and the solution was basified with an aqueous solution of saturated Na_2CO_3 . Extraction of the water phase with DCM and drying of the combined organic phases with Na_2SO_4 gave the pyridine *N*-oxide or bipyridine *N,N'*-dioxide product.

4-(*tert*-Butyl)pyridine *N*-oxide (**1a**)

[ES 3068]



Method B. 4-*tert*-Butylpyridine (3.30 g, 24.4 mmol) and H_2O_2 (6.0 mL, 2.4 equiv. in two portions) in acetic acid (8.0 mL) gave *N*-oxide **1a** (3.53 g, 23.3 mmol, 96%) as a colorless solid.

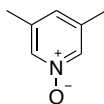
^1H NMR (400 MHz, CDCl_3): δ 8.09 (d, $J = 7.4$ Hz, 2H), 7.21 (d, $J = 7.3$ Hz, 2H), 1.27 (s, 9H) ppm.

$^{13}\text{C}\{^1\text{H}\}$ NMR (101 MHz, CDCl_3): δ 150.8, 138.6, 123.2, 34.6, 30.5 ppm.

The chemical shifts are in agreement with previously reported values.³

3,5-Dimethylpyridine *N*-oxide (**1i**)

[ES 3134]



Method B. 3,5-Dimethylpyridine (1.60 g, 15.0 mmol) and H_2O_2 (7.50 mL, 5.0 equiv.) in acetic acid (50 mL) gave *N*-oxide **1i** (1.56 g, 12.7 mmol, 85%) as a colorless solid.

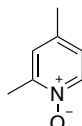
$^1\text{H NMR}$ (400 MHz, CDCl_3): δ 7.85 (s, 2H), 6.87 (s, 1H), 2.21 (s, 6H).

$^{13}\text{C}\{^1\text{H}\}$ NMR (101 MHz, CDCl_3): δ 136.7, 136.0, 128.6, 18.3 ppm.

The chemical shifts are in agreement with previously reported values.²⁰⁶

2,4-Dimethylpyridine *N*-oxide (**1j**)

[ES 4018]



Method B. 2,4-Dimethylpyridine (1.41 g, 13.2 mmol) and H_2O_2 (6.70 mL, 5.0 equiv.) in acetic acid (20 mL) gave *N*-oxide **1j** (0.98 g, 7.99 mmol, 61%) as an orange oil.

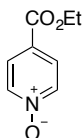
$^1\text{H NMR}$ (500 MHz, CDCl_3): δ 8.14 (d, $J = 6.6$ Hz, 1H), 7.05 (d, $J = 2.5$ Hz, 1H), 6.93 (dd, $J = 6.7$, 2.5 Hz, 1H), 2.48 (s, 3H), 2.30 (s, 3H) ppm.

$^{13}\text{C}\{^1\text{H}\}$ NMR (101 MHz, CDCl_3): δ 148.5, 138.9, 137.7, 127.3, 124.5, 20.4, 17.9 ppm.

The chemical shifts are in agreement with previously reported values.²⁰⁷

4-(Ethoxycarbonyl)pyridine *N*-oxide (**1d**)

[ES 1108]



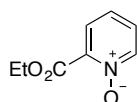
Method B. Ethyl isonicotinate (60.5 g, 0.40 mol), H_2O_2 (49 mL, 1.2 equiv.) in acetic acid (72 mL) gave *N*-oxide **1d** (60.1 g, 369 mmol, 90 %) as a colorless solid.

$^1\text{H NMR}$ (400 MHz, CDCl_3): δ 8.22 (d, $J = 6.2$ Hz, 2H), 7.88 (d, $J = 6.2$ Hz, 2H), 4.39 (q, $J = 7.1$ Hz, 2H), 1.39 (t, $J = 7.1$ Hz, 3H) ppm.

The chemical shifts are in agreement with previously reported values.³

2-(Ethoxycarbonyl)pyridine *N*-oxide (**1g**)

[KR 1011]



Method A. Ethyl picolinate (13.2 ml, 131.9 mmol), *m*-CPBA (32.9 g, 1.5 equiv.) in DCM (200 mL) gave *N*-oxide **1g** (10.8 g, 64.6 mmol, 49%) as a brown oil.

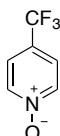
¹H NMR (400 MHz, CDCl₃): δ 8.23 (d, *J* = 7.1 Hz, 1H), 7.57 (dd, *J* = 7.7, 2.2 Hz, 1H), 7.32 (td, *J* = 7.1, 6.5, 2.3 Hz, 1H), 7.26 (td, *J* = 7.7, 1.1 Hz, 1H), 4.46 (q, *J* = 7.1 Hz, 2H), 1.40 (t, *J* = 7.1 Hz, 3H) ppm.

The chemical shifts are in agreement with previously reported values.³

HRESI-MS (+, MeOH, *m/z*): [M+Na]⁺ 190.0473, calc. 190.0475.

4-(Trifluoromethyl)pyridine *N*-oxide (**1e**)

[ES 1188]



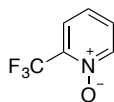
Method A. 4-(Trifluoromethyl)pyridine (4.87 g, 33.1 mmol), *m*-CPBA (6.85 g, 1.2 equiv.) in DCM (80 mL) gave *N*-oxide **1e** (4.79 g, 29.4 mmol, 89%) as an off-white solid.

¹H NMR (400 MHz, CDCl₃): δ 8.27 (d, *J* = 6.5 Hz, 2H), 7.50 (d, *J* = 6.7 Hz, 2H) ppm.

The chemical shifts are in agreement with previously reported values.³

2-(Trifluoromethyl)pyridine *N*-oxide (**1h**)

[ES 5125/ES 6014]



Method A. 2-(Trifluoromethyl)pyridine (5.70 g, 38.8 mmol) and *m*-CPBA (20.0 g, 3.0 equiv.) in DCM (50 mL) gave *N*-oxide **1h** (4.76 g, 29.2 mmol, 75%) as an orange oil.

¹H NMR (400 MHz, DMSO-*d*₆): δ 8.43 (d, *J* = 6.5 Hz, 1H), 7.92 (dd, *J* = 8.0, 2.0 Hz, 1H), 7.67 (td, *J* = 7.1, 6.4, 2.0 Hz, 1H), 7.47 (t, *J* = 7.9 Hz, 1H) ppm.

The chemical shifts are in agreement with previously reported values.²⁰⁸

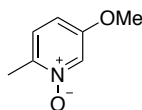
¹³C{¹H} NMR (101 MHz, CDCl₃): δ 141.6, 128.8, 125.2, 124.6, 121.3, 118.5 ppm.

¹⁹F{¹H} NMR (376 MHz, CDCl₃): δ -69.0 ppm.

HRESI-MS (+, *m/z*): [M+Na]⁺ 186.0152 calc. 186.0137.

5-Methoxy-2-methylpyridine *N*-oxide (**1k**)

[ES 3148/4006]



Method B. 5-Hydroxy-2-methyl pyridine (1.07 g, 8.68 mmol) and H₂O₂ (4.40 mL, 5.0 equiv.) in acetic acid (30 mL) gave *N*-oxide **1k** (1.01 g, 7.19 mmol, 86%) as a colorless solid.

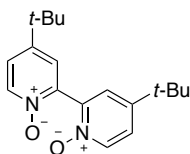
¹H NMR (400 MHz, CDCl₃): δ 7.99 (d, *J* = 2.4 Hz, 1H), 7.08 (d, *J* = 8.8 Hz, 1H), 6.79 (dd, *J* = 8.7, 2.4 Hz, 1H), 3.78 (s, 3H), 2.41 (s, 3H) ppm.

The chemical shifts are in agreement with previously reported values.²⁰⁹

¹³C{¹H} NMR (101 MHz, CDCl₃): δ 156.2, 141.7, 127.3, 125.8, 113.7, 56.2, 17.0 ppm.

4,4'-Di-*tert*-butyl-2,2'-bipyridine *N,N'*-dioxide (**10a**)

[ES 3048b]



Method B. 4,4'-Di-*tert*-butyl-2,2'-bipyridine (218.8 mg, 0.82 mmol) and H₂O₂ (0.42 mL, 5.0 equiv.) in acetic acid (8.0 mL) gave *N,N'*-dioxide **10a** (217.5 mg, 0.72 mmol, 88%) as a light yellow solid.

¹H NMR (400 MHz, CDCl₃): δ 8.25 (d, *J* = 6.9 Hz, 2H), 7.63 (d, *J* = 2.8 Hz, 2H), 7.33 (dd, *J* = 6.9, 2.8 Hz, 2H), 1.33 (s, 18H) ppm.

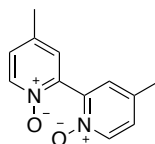
The chemical shifts are in agreement with previously reported values.⁵¹

¹³C{¹H} NMR (101 MHz, CDCl₃): δ 150.4, 141.6, 139.4, 125.6, 124.0, 34.8, 30.6 ppm.

HRESI-MS (+, MeOH, *m/z*): [M+H]⁺ 301.1905, calc. 301.1911, [M+Na]⁺ 323.1733, calc. 323.1730.

4,4'-Dimethyl-2,2'-bipyridine *N,N'*-dioxide (**10b**)

[ES 3048a]



Method B. 4,4'-Dimethyl-2,2'-bipyridine (150.2 mg, 0.82 mmol) and H₂O₂ (0.42 mL, 5.0 equiv.) in acetic acid (8.0 mL) *N,N'*-dioxide **10b** (123.9 mg, 0.57 mmol, 70%) as a colorless solid.

¹H NMR (400 MHz, CDCl₃): δ 8.22 (d, *J* = 6.7 Hz, 2H), 7.54 (d, *J* = 2.5 Hz, 2H), 7.15 (dd, *J* = 6.7, 2.6 Hz, 2H), 2.37 (s, 6H) ppm.

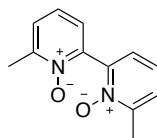
The chemical shifts are in agreement with previously reported values.⁵¹

¹³C{¹H} NMR (101 MHz, CDCl₃): δ 141.4, 139.5, 137.3, 129.2, 127.5, 20.5 ppm.

HRESI-MS (+, MeOH, *m/z*): [M+H]⁺ 217.0978, calc. 217.0972, [M+Na]⁺ 239.0802, calc. 239.0791.

6,6'-Dimethyl-2,2'-bipyridine *N,N'*-dioxide (10f)

[ES 3114]



Method B. 6,6'-Dimethyl-2,2'-bipyridine (103.9 mg, 0.56 mmol, 1.0 equiv.) and H₂O₂ (0.29 mL, 5.0 equiv.) in acetic acid (6.0 mL) gave *N,N'*-dioxide **10f** (109.1 mg, 0.50 mmol, 90%) as a light yellow solid.

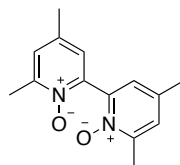
¹H NMR (400 MHz, CDCl₃): δ 7.37 – 7.28 (m, 4H), 7.21 (t, *J* = 7.7 Hz, 2H), 2.56 (s, 6H) ppm.

¹³C{¹H} NMR (101 MHz, CDCl₃): δ 149.8, 143.7, 126.9, 125.4, 124.2, 18.0 ppm.

The chemical shifts are in agreement with previously reported values.⁶²

4,4',6,6'-Tetramethyl-2,2'-bipyridine *N,N'*-dioxide (10j)

[ES 4060]



Method B. 4,4',6,6'-Tetramethyl-2,2'-bipyridine (242.0 mg, 1.14 mmol) and H₂O₂ (2.40 mL, 20 equiv. in 4 portions) in acetic acid (10 mL) gave *N,N'*-dioxide **10j** (176.6 mg, 0.72 mmol, 62%) as a yellow solid.

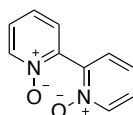
¹H NMR (400 MHz, CDCl₃): δ 7.20 (s, 2H), 7.14 (s, 2H), 2.52 (s, 6H), 2.32 (s, 6H) ppm.

The chemical shifts are in agreement with previously reported values.²¹⁰

HRESI-MS (+, MeOH, *m/z*): [M+H]⁺ 245.1298, calc. 245.1285.

2,2'-bipyridine *N,N'*-dioxide (10c)

[ES 3048d]



Method B. 2,2'-Bipyridine (128.1 mg, 0.82 mmol) and H₂O₂ (0.42 mL, 5.0 equiv.) in acetic acid (8.0 mL) gave *N,N'*-dioxide **10c** (83.6 mg, 0.44 mmol, 54%) as a colorless solid.

¹H NMR (400 MHz, D₂O): δ 8.36 (d, *J* = 6.6 Hz, 2H), 7.74 (t, *J* = 7.8 Hz, 2H), 7.69 – 7.63 (m, 4H) ppm.

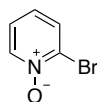
The chemical shifts are in agreement with previously reported values.²¹¹

$^{13}\text{C}\{^1\text{H}\}$ NMR (101 MHz, D_2O): δ 141.9, 139.8, 131.5, 128.9, 128.5 ppm.

HRESI-MS (+, MeOH, m/z): $[\text{M}+\text{H}]^+$ 189.0661, calc. 189.0659, $[\text{M}+\text{Na}]^+$ 211.0486, calc. 211.0478.

2-Bromopyridine *N*-oxide (11a)

[ES 3086]



Method A. 2-Bromopyridine (4.87 g, 30.8 mmol) and *m*-CPBA (6.38 g, 37.0 mmol, 1.2 equiv.) in DCM (60 mL) gave after column chromatography (deactivated silica gel, acetone/hexane) gave *N*-oxide **11a** (993.4 mg, 5.71 mmol, 19%) as a brown solid.

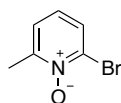
^1H NMR (400 MHz, CDCl_3): δ 8.36 (dd, $J = 6.6, 1.5$ Hz, 1H), 7.65 (dd, $J = 8.1, 2.0$ Hz, 1H), 7.24 – 7.21 (m, 1H), 7.09 (td, $J = 7.8, 1.5$ Hz, 1H) ppm.

$^{13}\text{C}\{^1\text{H}\}$ NMR (126 MHz, CDCl_3): δ 140.5, 133.2, 131.0, 125.6, 124.7 ppm.

The chemical shifts are in agreement with previously reported values.²¹²

2-Bromo-6-methylpyridine *N*-oxide (11b)

[ES 3094a/ES 3120]



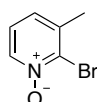
Method B. 2-Bromo-6-methylpyridine (685.0 mg, 3.98 mmol) and H_2O_2 (2.0 mL, 19.9 mmol, 5.0 equiv.) in acetic acid (40 mL) gave pyridine *N*-oxide **11b** (562.2 mg, 2.99 mmol, 75%) as a colorless solid.

^1H NMR (400 MHz, CDCl_3): δ 7.58 – 7.48 (m, 1H), 7.23 – 7.19 (m, 1H), 6.99 (t, $J = 7.9$ Hz, 1H), 2.56 (s, 3H) ppm.

The chemical shifts are in agreement with previously reported values.²¹³

2-Bromo-3-methylpyridine *N*-oxide (11c)

[ES 3104a]



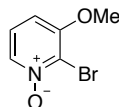
Method B. 2-Bromo-3-methylpyridine (739.9 mg, 4.30 mmol) and H_2O_2 (2.20 mL, 5.0 equiv.) in acetic acid (43 mL) gave *N*-oxide **11c** (675.8 mg, 3.59 mmol, 84%) as a light pink solid.

$^1\text{H NMR}$ (400 MHz, CDCl_3): δ 8.26 (d, $J = 6.6$ Hz, 1H), 7.17 – 6.99 (m, 2H), 2.45 (s, 3H) ppm.

The chemical shifts are in agreement with previously reported values.²¹³

2-Bromo-3-methoxypyridine *N*-oxide (**11d**)

[ES 3104b]



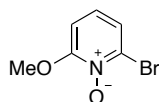
Method B. 2-Bromo-3-methoxypyridine (147.7 mg, 0.79 mmol) and H_2O_2 (0.40 mL, 5.0 equiv.) in acetic acid (8 mL) gave *N*-oxide **11d** (106.4 mg, 0.52 mmol, 66%) as a colorless solid.

$^1\text{H NMR}$ (500 MHz, CDCl_3): δ 8.11 (dd, $J = 6.6, 1.2$ Hz, 1H), 7.18 (dd, $J = 8.6, 6.6$ Hz, 1H), 6.81 (dd, $J = 8.6, 1.2$ Hz, 1H), 3.98 (s, 3H) ppm.

The chemical shifts are in agreement with previously reported values.²¹⁴

2-Bromo-6-methoxypyridine *N*-oxide (**11e**)

[ES 3098]



Method B. 2-Bromo-6-methoxypyridine (646.2 mg, 3.44 mmol) and H_2O_2 (3.50 mL, 10 equiv. in two portions) in acetic acid (35 mL) gave *N*-oxide **11e** (28.5 mg, 0.14 mmol, 4%) as a yellow solid.

$^1\text{H NMR}$ (500 MHz, CDCl_3): δ 7.35 (dd, $J = 8.1, 1.6$ Hz, 1H), 7.12 (t, $J = 8.2$ Hz, 1H), 6.88 (dd, $J = 8.3, 1.7$ Hz, 1H), 4.10 (s, 3H) ppm.

$^{13}\text{C}\{^1\text{H}\}$ NMR (126 MHz, CDCl_3): δ 160.2, 134.2, 126.3, 122.5, 106.5, 57.8 ppm.

The chemical shifts are in agreement with previously reported values.¹⁰⁹

Triethylphosphine oxide, $\text{O}=\text{PEt}_3$

[ES 4185a]



Method B. PEt_3 (100 mg, 0.84 mmol) and H_2O_2 (0.17 mL, 1.5 equiv.) in DCM (2.0 mL) gave $\text{O}=\text{PEt}_3$ as a colorless solid. No yield was determined.

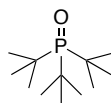
$^1\text{H NMR}$ (400 MHz, C_6D_6): δ 1.18 – 1.01 (m, 6H), 0.80 (dt, $J = 15.5, 7.6$ Hz, 9H) ppm.

$^{31}\text{P}\{^1\text{H}\}$ NMR (162 MHz, C_6D_6): δ 46.4 ppm.

The chemical shifts are in agreement with previously reported values.²¹⁵

Tri-*tert*-butylphosphine oxide, O=P(*t*-Bu)₃

[ES 4185b]



Method B. P(*t*-Bu)₃ (68.5 mg, 0.34 mmol) and H₂O₂ (0.05 mL, 1.5 equiv.) in DCM (1.0 mL) gave O=P(*t*-Bu)₃ (64.7 mg, 0.30 mmol, 87%) as a colorless solid.

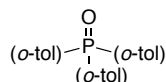
¹H NMR (400 MHz, C₆D₆): δ 1.15 (d, *J* = 12.1 Hz, 27H) ppm.

³¹P{¹H} NMR (162 MHz, C₆D₆): δ 63.1 ppm.

The chemical shifts are in agreement with previously reported values.¹²²

Tri-*ortho*-tolylphosphine oxide, O=P(*o*-tol)₃

[ES 6134]



Method B. P(*o*-tol)₃ (1.34 g, 4.42 mmol) and H₂O₂ (4.5 mL, 10 equiv.) in acetic acid (15 mL) gave O=P(*o*-tol)₃ (1.01 g, 3.15 mmol, 71%) as a colorless solid.

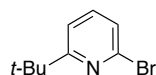
¹H NMR (400 MHz, CDCl₃): δ 7.42 (tt, *J* = 7.5, 1.6 Hz, 3H), 7.34 – 7.27 (m, 3H), 7.18 – 7.03 (m, 6H), 2.49 (s, 9H) ppm.

³¹P{¹H} NMR (162 MHz, CDCl₃): δ 37.8 ppm.

The chemical shifts are in agreement with previously reported values.²¹⁶

4.2.2 Substituted pyridines**2-Bromo-6-(*tert*-butyl)pyridine (2b)**

[ES 5168]



According to reported procedure,¹²¹ magnesium (6.32 g, 260 mmol, 1.3 equiv.) and a crystal of iodine were stirred vigorously under argon for 10 min. Dry Et₂O (20 mL) and *tert*-butylchloride (4.8 mL, 4.4 mmol) were added to initiate the Grignard reaction. The remaining *tert*-butylchloride (17.0 mL, 195.6 mmol) was dissolved in Et₂O (140 mL) and dropped into the reaction over a period of 1 h maintaining reflux temperature. Titration of the Grignard gave a concentration of *c* = 0.32 M. 2,6-Dibromopyridine (12.6 g, 53.3 mmol, 1.0 equiv.) and CuCl (158.3 mg, 1.56 mmol, 0.03 equiv.) were dissolved in dry THF (125 mL) and cooled to –78 °C. *tert*-BuMgCl (150 mL, 48.0 mmol, 0.9 equiv.) was added dropwise. After the addition was completed, the reaction was stirred at –78 °C for 30 min and at r.t.

for 2 h. The reaction was quenched with aqueous HCl and extracted with DCM. Subsequent drying the combined organic phases with Na₂SO₄ and purification of the crude product by column chromatography (deactivated silica gel, hexane) gave the title compound **2b** (9.18 g, 41.9 mmol, 89%) as a yellow oil.

¹H NMR (400 MHz, CDCl₃): δ 7.43 (ddd, *J* = 8.0, 7.5, 0.5 Hz, 1H), 7.28 – 7.22 (m, 2H), 1.33 (s, 9H) ppm.

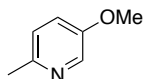
The chemical shifts are in agreement with previously reported values.¹²¹

¹³C{¹H} NMR (101 MHz, CDCl₃): δ 171.3, 141.3, 138.6, 125.0, 117.9, 37.7, 30.1 ppm.

HRESI-MS (+, MeOH, *m/z*): [M+H]⁺ 214.0247, calc. 214.0226.

5-Methoxy-2-methylpyridine

[ES 4004]



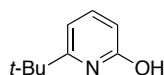
Similar to reported procedure,²⁰⁹ 5-hydroxy-2-methylpyridine (1.50 g, 13.8 mmol, 1.0 equiv.) was dissolved in THF (38 mL). In a separate flask, KO^t-Bu (2.01 g, 17.9 mmol, 1.3 equiv.) was dissolved in THF (14 mL) and the pyridine solution was slowly dropped into the base. After stirring for 1 h at room temperature, MeI (1.11 mL, 17.9 mmol, 1.3 equiv.) in THF (7.0 mL) was slowly added. The reaction was stirred for 2 h at room temperature and subsequently for 1 h at 50 °C. After quenching with aqueous HCl (100 mL), aqueous NaOH was added until pH = 14 and the water phase was extracted with DCM. Drying of the combined organic phases with Na₂SO₄ and removal of the solvent gave the title compound (750.2 mg, 6.09 mmol, 44%) as a red oil.

¹H NMR (400 MHz, CDCl₃): δ 8.17 (d, *J* = 2.7 Hz, 1H), 7.12 – 6.96 (m, 2H), 3.81 (s, 3H), 2.47 (s, 3H) ppm.

The chemical shifts are in agreement with previously reported values.²⁰⁹

6-*tert*-Butyl-2-hydroxypyridine

[ES 5111]



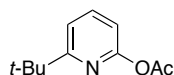
According to reported procedure,²¹⁷ 2-bromo-6-*tert*-butylpyridine (214.1 mg, 1.0 mmol, 1.0 equiv.) was dissolved in *tert*-amylalcohol (3.0 mL) and KO^t-Bu (1.12 g, 10.0 mmol, 10.0 equiv.) was added. After heating to 100 °C for 48 h, the reaction was cooled to ambient temperature and the solvent was removed. The residue was dissolved in formic acid (2.0 mL) and stirred at r.t. for 22 h. Aqueous NaOH was added until pH = 6 and the reaction was extracted with CHCl₃ and dried over Na₂SO₄. The

residue was purified by column chromatography (silica gel, MeOH/DCM), yielding the title compound (36.7 mg, 0.24 mmol, 24%) as a light yellow solid.

$^1\text{H NMR}$ (400 MHz, CDCl_3): δ 7.35 (dd, $J = 9.1, 7.0$ Hz, 1H), 6.40 (dd, $J = 9.1, 1.0$ Hz, 1H), 6.09 (dd, $J = 7.1, 0.9$ Hz, 1H), 1.34 (s, 9H) ppm.

6-*tert*-Butyl-2-acetopyridine

[ES 5120]



According to reported procedure,²¹⁸ 6-*tert*-butyl-2-hydroxypyridine (26.4 mg, 0.17 mmol) was dissolved in acetic anhydride (1.0 mL) and the reaction was heated to 100 °C for 4 h. Removal of the solvent resulted in the title compound (33.9 mg, 0.17 mmol, quant.) as a yellow oil.

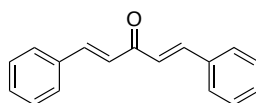
$^1\text{H NMR}$ (400 MHz, CDCl_3): δ 7.69 (t, $J = 7.9$ Hz, 1H), 7.23 (d, $J = 7.8$ Hz, 1H), 6.87 (d, $J = 8.0$ Hz, 1H), 2.34 (s, 3H), 1.34 (s, 9H) ppm.

4.3 Catalysts, ligands and precursors

4.3.1 Ligands

Dibenzylideneacetone, dba

[JR 1050]



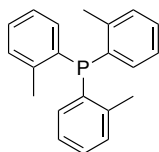
According to reported procedure,²¹⁹ a 2 L flask was charged with sodium hydroxide solution (2.5 M, 1.0 L, 2.5 mol) and ethanol (0.8 L). Keeping it at ambient temperature, half of a mixture of acetone (25.0 g, 1.0 mol, 1.0 equiv.) and benzaldehyde (105 g, 2.0 mol, 2.0 equiv.) was added and the mixture stirred for 15 min, resulting in a cloudy yellow solution. The second portion of the starting materials was added and the mixture stirred for another 30 min. Filtration of the formed solid and washing with water gave a yellow precipitate which was recrystallized from hot ethyl acetate giving the title compound (173 g, 0.73 mol, 73%).

$^1\text{H NMR}$ (400 MHz, CDCl_3): δ 7.74 (d, $J = 16.0$ Hz, 2H), 7.66 – 7.58 (m, 4H), 7.45 – 7.37 (m, 6H), 7.09 (d, $J = 16.0$ Hz, 2H) ppm.

HRESI-MS (+, MeOH, m/z): $[\text{M}+\text{Na}]^+$ 257.0939, calc. 257.0937.

Tri-ortho-tolylphosphine, P(*o*-tol)₃

[ES 6126]



Similar to the reported procedure,²²⁰ an oven-dried three-necked flask was charged with magnesium (15.5 g, 636 mmol), dry THF (100 mL) and a few crystals of iodine and set under argon. 2-Bromotoluene (1.50 mL, 12 mmol) was syringed into the flask and the reaction was heated to initiate the reaction. 2-Bromotoluene (70 mL, 582 mmol) and THF (200 mL) was added to a dropping funnel and dropped into the reaction maintaining reflux temperature. After refluxing for 2 h, the reaction was cooled down to 0 °C and PCl₃ (16.0 mL, 183 mmol, 0.31 equiv.) in THF (100 mL) was slowly dropped in. After the addition was completed, the reaction was stirred for 30 min at room temperature and an additional 3 h at reflux temperature. Aqueous NH₄Cl was added to quench the reaction. After stirring over night, the H₂O phase was extracted with Et₂O (2 L) and the combined organic phases dried over Na₂SO₄. Recrystallization from hot ethanol gave the title compound (22.0 g, 72.2 mmol, 39%) as a colorless solid.

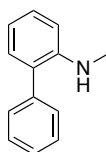
¹H NMR (400 MHz, CDCl₃): δ 7.38 – 7.16 (m, 6H), 7.13 – 7.00 (m, 3H), 6.81 – 6.65 (m, 3H), 2.41 (s, 9H) ppm.

³¹P{¹H} NMR (162 MHz, CDCl₃): δ –28.7 ppm.

The chemical shifts are in agreement with previously reported values.²²⁰

2-phenyl-*N*-methylaniline

[JR 1008]



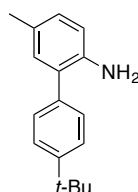
According to reported procedure,¹²⁷ LiAlH₄ (14.1 g, 373 mmol, 5.0 equiv.) was suspended in dry THF (300 mL) and 2-ethoxycarbonylaminobiphenyl (18.2 g, 75.0 mmol, 1.0 equiv.) in dry THF (100 mL) was added dropwise. After stirring the reaction for 1 h at room temperature, the mixture was refluxed for 3 h. The slurry was cooled to 0 °C and quenched with H₂O (28 mL) and NaOH (18 mL). The formed precipitate was filtered off and washed with Et₂O. Drying of the combined organic filtrates over Na₂SO₄ and removal of the solvent gave 2-phenyl-*N*-methylaniline (4.83 g, 26.4 mmol, 35%) as a yellow oil.

¹H NMR (400 MHz, CDCl₃): δ = 7.57 (d, J = 4.1 Hz, 4H), 7.51 – 7.45 (m, 1H), 7.44 – 7.39 (m, 1H), 7.29 – 7.22 (m, 1H), 6.93 (tt, J = 7.4, 1.1 Hz, 1H), 6.84 (d, J = 8.2 Hz, 1H), 4.10 (broad s, 1H), 2.90 (s, 3H) ppm.

The chemical shifts are in agreement with previously reported values.¹²⁵

2-(4-*tert*-butyl)phenyl-4-methylaniline

[ES 4098/5026]



According to reported procedure,¹²⁶ a Schlenk flask was charged with 4-*tert*-butyl boronic acid (2.00 g, 11.3 mmol, 1.2 equiv.), 2-bromo-4-methylaniline (1.17 mL, 9.38 mmol, 1.0 equiv.) and K₂CO₃ (5.83 g, 42.2 mmol, 4.5 equiv.) and dissolved in degassed H₂O:DME (1:1, 80 mL). After stirring at room temperature for 1 h, Pd(PPh₃)₂Cl₂ (131.7 mg, 0.19 mmol, 2 mol%) was added and the reaction was heated to 80 °C for 16 h. The reaction was cooled to ambient temperature and extracted with EtOAc (3x) and dried over Na₂SO₄. Purification by column chromatography (silica gel, EtOAc/hexane) gave the biphenyl product (2.05 g, 8.56 mmol, 91%) as a colorless solid.

¹H NMR (500 MHz, CDCl₃): δ 7.49 (d, J = 8.2 Hz, 2H), 7.43 (d, J = 8.1 Hz, 2H), 7.04 – 6.96 (m, 2H), 6.73 (d, J = 8.8 Hz, 1H), 3.70 (s, 2H), 2.32 (s, 3H), 1.41 (s, 9H) ppm.

¹³C{¹H} NMR (126 MHz, CDCl₃): δ 150.1, 141.1, 136.8, 131.2, 128.9, 128.8, 128.0, 127.9, 125.8, 116.0, 34.7, 31.5, 20.6 ppm.

The chemical shifts are in agreement with previously reported values.¹²⁶

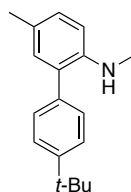
HRESI-MS (+, MeOH, m/z): [M+H]⁺ 240.1749, calc. 240.1752.

Elemental analysis (%): C 85.46, H 8.85, N 5.88, calc. C 85.30, H 8.84, N 5.85.

M.p.: 89-92 °C.

2-(4-*tert*-butyl)phenyl-*N*,4-dimethylaniline

[ES 4100/4102/5050]



2-(4-*tert*-Butyl)phenyl-4-methylaniline (1.80 g, 7.52 mmol, 1.0 equiv.) was dissolved in DCM (20 mL) and pyridine (4.12 mL, 51.2 mmol, 6.80 equiv.) was added. Ethyl chloroformate (0.97 mL, 10.2 mmol, 1.35 equiv.) was added dropwise and the reaction was stirred for 19 h at room temperature. The

reaction was quenched with NaOH (2 M, 8.0 mL) and extracted with DCM. Removal of the solvent gave the ethoxycarbonylaminobiphenyl a light yellow highly viscous oil that was used without further purification.

LiAlH₄ (15.8 g, 41.7 mmol, 5.2 equiv.) was suspended in THF (10 mL) in a Schlenk flask. The ethoxycarbonylaminobiphenyl was dissolved in THF (30 mL) in another Schlenk flask and dropped into the LiAlH₄ suspension. The reaction was stirred for 1 h at room temperature and subsequently refluxed for 3 h. After cooling to 0 °C, the reaction was quenched with H₂O (4 mL) and NaOH (6 mL). The formed precipitate was filtered off and washed with Et₂O. Drying of the organic phase with Na₂SO₄ gave the title compound (1.71 g, 6.75 mmol, 90%) as highly viscous yellow oil.

¹H NMR (500 MHz, CDCl₃): δ 7.45 (d, *J* = 8.4 Hz, 2H), 7.35 (d, *J* = 8.4 Hz, 2H), 7.07 (dd, *J* = 8.2, 2.0 Hz, 1H), 6.94 (d, *J* = 2.1 Hz, 1H), 6.62 (d, *J* = 8.2 Hz, 1H), 3.87 (s, 1H), 2.78 (s, 3H), 2.28 (s, 9H) ppm.

¹³C{¹H} NMR (126 MHz, CDCl₃): δ 150.0, 144.2, 136.6, 131.0, 129.1, 129.0, 127.7, 126.0, 125.8, 110.1, 34.7, 31.5, 31.2, 20.4 ppm.

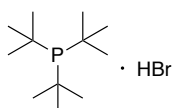
IR (solid, ν): 3426 (w), 2961 (m), 2868 (w), 2809 (w), 1615 (w), 1584 (w), 1508 (s), 1475 (w), 1394 (w), 1362 (w), 1308 (m), 1269 (w), 1243 (w), 1169 (m), 1109 (w), 1016 (w), 886 (w), 838 (m), 805 (m) cm⁻¹.

HRESI-MS (+, MeOH, *m/z*): [M+H]⁺ 254.1897, calc. 254.1908.

Elemental analysis (%): C 84.97, H 9.13, N 5.56, calc. C 85.32, H 9.15, N 5.53.

HBr·P(*t*-Bu)₃ (**28**)

[ES 4020]



According to reported procedure,⁷⁴ P(*t*-Bu)₃ (215.2 mg, 1.06 mmol, 1.0 equiv.) and pyridinium hydrobromide (150.0 mg, 0.94 mmol, 0.88 equiv.) were dissolved in MeCN (3.0 mL) in a glovebox. After stirring for 40 minutes, Et₂O was added and the formed precipitate was filtered off and washed with additional Et₂O. Drying of the precipitation gave the title compound **28** (209.3 mg, 0.73 mmol, 69%) as a colorless solid.

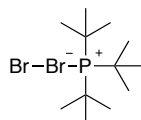
¹H NMR (400 MHz, MeCN-*d*₃) δ 6.54 (d, *J* = 453.6 Hz, 1H), 1.59 (dd, *J* = 15.3, 0.7 Hz, 27H) ppm.

³¹P{¹H} NMR (202 MHz, MeCN-*d*₃) δ 50.8 ppm.

The chemical shifts are in agreement with previously reported values.⁷⁴

Br[BrP(*t*-Bu)₃]

[ES 4185c]



In a glovebox, P(*t*-Bu)₃ (91.2 mg, 0.45 mmol, 1.0 equiv.) was weighed in a Schlenk tube and dry Et₂O (1.5 mL) was added. Outside of the glovebox, Br₂ (0.02 mL, 0.45 mmol, 1.0 equiv.) was dropped into the Schlenk flask. An orange precipitation was immediately formed. The solid was washed with Et₂O and dried on high vacuum, yielding the title compound (150.9 mg, 0.42 mmol, 93%) as an orange solid.

¹H NMR (400 MHz, CD₂Cl₂): δ 1.73 (d, *J* = 17.6 Hz, 27H) ppm.

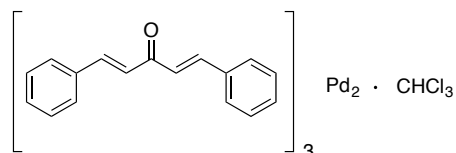
³¹P{¹H} NMR (162 MHz, CD₂Cl₂): δ 126.1 ppm.

The chemical shifts are in agreement with previously reported values.²²¹

HRESI-MS (+, MeOH, *m/z*): [M–Br]⁺ 281.1051, calc. 281.1028.

4.3.2 Palladium precursors and catalysts**Tris(dibenzylideneacetone)dipalladium(0) chloroform adduct, Pd₂dba₃·CHCl₃**

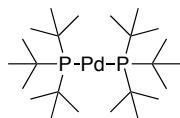
[ES 6093]



According to reported procedure,²²² in a 500 mL flask, palladium chloride (3.23 g, 18.2 mmol, 1.0 equiv.), dibenzylideneacetone (14.8 g, 63.2 mmol, 3.50 equiv.) and NaOAc (12.7 g, 154 mmol, 8.50 equiv.) were added. MeOH (300 mL) was added and the slurry was stirred at 40 °C for 3 h. After cooling to room temperature, the mixture was filtered through a glass frit. The formed solid was washed with H₂O until the filtrate was pH = 7 and thereafter with MeOH (2 times). The formed solid was washed off the frit with chloroform (3 L) and the solution was concentrated to 200 mL. Acetone (1 L) was added and the mixture was kept in the freezer over night. The formed precipitation was filtered off and dried on high vacuum giving the title compound (8.24 g, 8.0 mmol, 88%) as a purple solid. The compound was used without further purification.

Bis(tri-*tert*-butylphosphine)palladium(0) (32)

[ES 4150/6072]



According to reported procedure,²²³ a Schlenk flask was charged with Pd₂dba₃·CHCl₃ (4.57 g, 4.41 mmol, 1.0 equiv.) and P(*t*-Bu)₃ (4.00 g, 19.6 mmol, 4.5 equiv.) and DMF (50 mL) was added. The mixture was stirred under argon for 24 h and then filtered through a reversible glass frit. The solid was washed with degassed DMF (100 mL) and degassed MeOH (100 mL) and the grey solid was subsequently dissolved in degassed pentane (250 mL) and collected in a Schlenk flask. Removal of the solvent gave palladium complex **32** (3.50 g, 6.85 mmol, 78%) as a light brown solid.

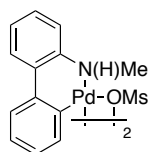
¹H NMR (400 MHz, C₆D₆): δ 1.49 – 1.41 (m, 54H) ppm.

³¹P{¹H} NMR (202 MHz, C₆D₆): δ 85.5 ppm.

The chemical shifts are in agreement with previously reported values.²²³

***N*-methyl-2-aminobiphenylpalladium methanesulfonate, Buchwald pre-catalyst G4**

[JR 1022]



According to reported procedure,¹²⁵ a Schlenk flask was charged with 2-phenyl-*N*-methyl aniline (4.11 g, 2.23 mmol, 1.0 equiv.) and methanesulfonic acid (0.14 mL, 2.23 mmol, 1.0 equiv.) in dry THF (10.0 mL). After stirring for 15 min, Pd(OAc)₂ (500.7 mg, 2.23 mmol, 1.0 equiv.) was added and the mixture was heated to 50 °C for 45 minutes. After cooling to ambient temperature, the reaction was filtered through celite to remove palladium black. The solvent was removed on the evaporator and pentane was added and the flask was kept at 4 °C over night. Drying of the precipitation gave the title complex (494.1 mg, 0.67 mmol, 60%) as a tan solid.

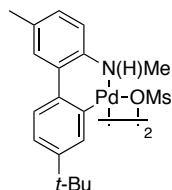
¹H NMR (400 MHz, CD₂Cl₂): δ 7.56 (d, *J* = 7.7 Hz, 1H), 7.35 (dd, *J* = 7.7, 1.6 Hz, 1H), 7.26 – 7.17 (m, 2H), 7.14 (d, *J* = 4.3 Hz, 2H), 7.08 (td, *J* = 7.3, 1.1 Hz, 1H), 7.03 – 6.90 (m, 1H), 6.78 (s, 1H), 2.73 (s, 3H), 2.55 (d, *J* = 5.2 Hz, 3H) ppm.

¹³C{¹H} NMR (101 MHz, CD₂Cl₂): δ 140.8, 139.1, 138.8, 134.6, 134.2, 128.8, 127.9, 127.4, 126.3, 125.8, 124.7, 120.6, 44.3, 39.3 ppm.

The chemical shifts are in agreement with previously reported values.¹²⁵

2-(4-*tert*-butyl)phenyl-N,4-dimethylaniline palladium methanesulfonate (complex H)

[ES 4104/5057]



A Schlenk flask was charged with 2-(4-*tert*-butyl)phenyl-N,4-dimethylaniline (503.2 mg, 1.99 mmol, 1.0 equiv.) and methanesulfonic acid (0.13 mL, 1.99 mmol, 1.0 equiv.) in dry THF (10.0 mL) and toluene (2.0 mL). The yellow mixture was stirred for 15 min and Pd(OAc)₂ (445.9 mg, 1.99 mmol, 1.0 equiv.) was added and the mixture was heated to 50 °C for 45 minutes. After cooling to ambient temperature, the reaction was filtered through celite to remove palladium black. The solvent was removed on the evaporator and pentane was added and the flask was kept at 4 °C over night. Drying of the precipitation gave the title complex (761.2 mg, 0.84 mmol, 84%) as a tan solid.

¹H NMR (500 MHz, CD₂Cl₂): δ 7.41 (s, 1H), 7.29 (d, *J* = 8.0 Hz, 1H), 7.27 – 7.21 (m, 1H), 7.12 (dd, *J* = 8.0, 1.9 Hz, 1H), 7.03 (d, *J* = 7.9 Hz, 1H), 6.95 (d, *J* = 7.7 Hz, 1H), 6.69 (s, 1H), 2.73 (s, 3H), 2.62 (s, 3H), 2.35 (s, 3H), 1.33 (s, 9H) ppm.

¹³C{¹H} NMR (126 MHz, CD₂Cl₂): δ 149.6, 138.8, 138.4, 137.1, 131.9, 130.9, 129.2, 127.9, 124.1, 122.7, 120.1, 44.5, 39.4, 34.6, 31.2, 20.9 ppm.

IR (solid, ν): 3195 (m), 3006 (w), 2961 (m), 2867 (w), 1583 (w), 1499 (w), 1477 (w), 1461 (m), 1381 (w), 1361 (w), 1327 (w), 1275 (m), 1260 (m), 1225 (m), 1141 (m), 1038 (m), 988 (w), 886 (w), 823 (m) 765 (s), 750 (s), 703 (w) cm⁻¹.

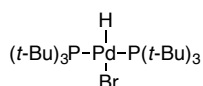
HRESI-MS (+, MeOH, *m/z*): [M-OMs]⁺ 813.1512, calc. 813.1381.

Elemental analysis (%): C 50.50, H 5.57 N 3.10, calc. C 50.28, H 5.55, N 3.09.

M.p.: decomposition > 146 °C.

(P(*t*-Bu)₃)₂Pd(Br)(H) (26)

[ES 6108]



According to reported procedure,¹³⁵ Pd(P(*t*-Bu)₃)₂ (50.0 mg, 0.098 mmol, 1.0 equiv.) was dissolved in toluene (2.50 mL). Py·HBr (31.3 mg, 0.20 mmol, 2.0 equiv.) was dissolved in MeCN (0.8 mL) and dropped into the toluene solution. After stirring for 10 minutes under argon, the solids were filtered off and the solvent evaporated. The residue was re-dissolved in toluene (2.0 mL) and filtered again. After removal of the solvent, complex **26** (40.1 mg, 0.068 mmol, 69%) was obtained as a light yellow solid.

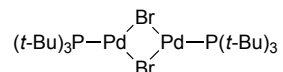
¹H NMR (400 MHz, C₆D₆): δ 1.51 – 1.41 (m, 54H) ppm.

$^{31}\text{P}\{^1\text{H}\}$ NMR (162 MHz, C_6D_6): δ 83.6 ppm.

The chemical shifts are in agreement with previously reported values.¹³⁵

[P(*t*-Bu)₃PdBr]₂ (27)

[ES 4106]



Similar to reported procedure,¹³⁶ in a glovebox Pd(P(*t*-Bu)₃)₂ (80.0 mg, 0.16 mmol, 1.0 equiv.) and CuBr₂ (35.0 mg, 0.16 mmol, 1.0 equiv.) were weighed in a vial and THF (1.0 mL) was added. The reaction was stirred for 25 min at room temperature and subsequently filtered through a short plug of celite. Pentane was added and the mixture was kept at -25 °C over night. Subsequently, the supernatant was pipetted off and the precipitation dried, yielding Pd(I)-dimer **27** (56.5 mg, 0.073 mmol, 45%) as a dark green solid.

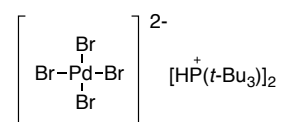
^1H NMR (400 MHz, C_6D_6): δ 1.29 – 1.22 (m, 54H) ppm.

$^{31}\text{P}\{^1\text{H}\}$ NMR (162 MHz C_6D_6): δ 86.8 ppm.

The chemical shifts are in agreement with previously reported values.²²⁴

(HP(*t*-Bu)₃)₂[PdBr₄] (31a)

[ES 5100]



According to reported procedure,⁷⁴ PdBr₂ (18.0 mg, 0.068 mmol, 1.0 equiv.) and HBr·P(*t*-Bu)₃ (42.3 mg, 0.15 mmol, 2.2 equiv.) were weighed in a vial. THF (2.0 mL) and MeCN (0.10 mL) were added and the mixture was stirred at room temperature for 1 h. The supernatant was pipetted off and the precipitate was washed with pentane and dried under vacuum, yielding complex **31a** (53.1 mg, 0.064 mmol, 94%) as a red solid.

^1H NMR (400 MHz, CD_2Cl_2): δ 8.22 (d, J = 466.4 Hz, 2H), 1.77 ppm (d, J = 15.1 Hz, 54H) ppm.

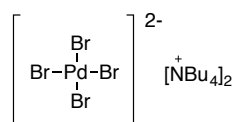
$^{31}\text{P}\{^1\text{H}\}$ NMR (162 MHz, CD_2Cl_2): δ 44.5 ppm.

The chemical shifts are in agreement with previously reported values.⁷⁴

HRESI-MS (-, MeCN, m/z): [PdBr₃]⁻ 346.6592, calc. 346.6544.

(NBu₄)₂[PdBr₄] (31b)

[ES 5101a]



In a glovebox, PdBr₂ (50.0 mg, 0.19 mmol, 1.0 equiv.) and NBu₄Br (133.8 mg, 0.42 mmol, 2.2 equiv.) were weighed in a vial. THF (2.0 mL) and MeCN (0.20 mL) were added and the mixture was stirred for 1 h at room temperature. Pentane was added and the vial was kept at -25 °C over night. Drying of the precipitation gave complex **31b** (186.0 mg, 0.20 mmol, quant.) as a red solid.

¹H NMR (400 MHz, MeCN-*d*₃): δ 3.16 – 3.09 (m, 16H), 1.60 (ddd, *J* = 12.0, 10.1, 6.4 Hz, 16H), 1.35 (h, *J* = 7.4 Hz, 16H), 0.94 (t, *J* = 7.3 Hz, 24H) ppm.

¹³C{¹H} NMR (101 MHz, MeCN-*d*₃) δ 58.5, 23.5, 19.5, 13.0 ppm.

IR (solid, ν): 3004 (w), 2958 (m), 2871 (m), 1470 (m), 1380 (w), 1276 (m), 1260 (m), 1151 (w), 1107 (w), 1065 (w), 1028 (w), 881 (m), 764 (s), 750 (s), 696 (w) cm⁻¹.

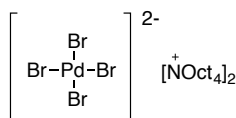
HRESI-MS (-, MeOH, *m/z*): [PdBr₃]⁻ 346.6569, calc. 346.6544.

Elemental analysis (%): C 43.70, H 8.12, N 3.12, calc. C 42.19, H 7.97, N 3.08.

M.p.: decomposition > 102 °C.

(NOct₄)₂[PdBr₄] (31c)

[ES 5101b/c]



In a glovebox, PdBr₂ (25.9 mg, 0.097 mmol, 1.0 equiv.) and NOct₄Br (145.9 mg, 0.27 mmol, 2.8 equiv.) were weighed in a vial. THF (1.0 mL) was added and the mixture was stirred at room temperature for 1 h. Pentane (1.0 mL) was added and the vial was kept at -25 °C over night. The precipitate was dried, yielding complex **31c** (132.4 mg, 0.097 mmol, quant.) as a sticky red solid.

¹H NMR (400 MHz, MeCN-*d*₃): δ 3.17 – 3.04 (m, 16H), 1.59 (dp, *J* = 10.3, 6.3 Hz, 16H), 1.35 – 1.18 (m, 80H), 0.91 – 0.81 (m, 24H) ppm.

¹³C{¹H} NMR (101 MHz, MeCN-*d*₃): δ 58.6, 31.5, 28.8, 28.7, 26.0, 22.4, 21.5, 13.5 ppm.

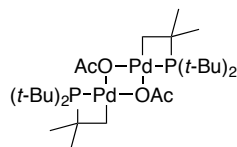
IR (solid, ν): 3005 (w), 2954 (w), 2922 (m), 2853 (m), 1466 (m), 1378 (w), 1276 (m), 1260 (m), 764 (s), 750 (s), 724 (w) cm⁻¹.

Elemental analysis (%): C 60.02, H 10.64, N 2.21, calc. C 56.53, H 10.08, N 2.06.

4.3.3 Cyclometalated catalysts

$[(\text{tert-Bu}_2\text{PC}(\text{CH}_3)_2\text{CH}_2)\text{Pd}(\text{OAc})]_2$ (complex A)

[ES 5014]



According to reported procedure,³⁹ Pd(OAc)₂ (2.13 g, 9.49 mmol) and P(*t*-Bu)₃ (2.15 g, 10.6 mmol, 1.12 equiv.) were weighed in a Schlenk flask. Toluene (70 mL) was added and the reaction was stirred at 90 °C for 30 minutes. The reaction mixture was concentrated and filtered through celite with Et₂O to remove palladium black. The Et₂O was removed on evaporator and pentane was added and the mixture was kept at -25 °C over night. Drying of the precipitation gave cyclometalated palladium complex **A** (1.52 g, 2.08 mmol, 44%) as a light yellow solid.

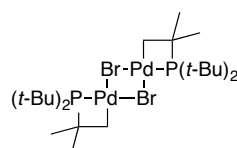
¹H NMR (400 MHz, CDCl₃): δ 1.92 (s, 6H), 1.55 (d, *J* = 13.8 Hz, 36H), 1.50 (d, *J* = 14.1 Hz, 12H), 1.09 (d, *J* = 3.1 Hz, 4H) ppm.

³¹P{¹H} NMR (162 MHz CDCl₃): δ -8.72 ppm.

The chemical shifts are in agreement with previously reported values.³⁹

$[(\text{tert-Bu}_2\text{PC}(\text{CH}_3)_2\text{CH}_2)\text{Pd}(\text{Br})]_2$ (complex B)

[ES 5015]



According to patented procedure,²²⁵ palladium complex **A** (1.16 g, 1.58 mmol) and tetrabutylammonium bromide (4.59 g, 14.2 mmol, 9.0 equiv.) were dissolved in DCM (50 mL) and stirred at room temperature for 1 h. The reaction mixture was concentrated and MeOH added resulting in a precipitation, which after drying gave cyclometalated palladium complex **B** (1.18 g, 1.52 mmol, 96%) as a light yellow solid.

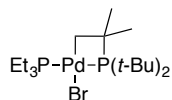
¹H NMR (400 MHz, CDCl₃): δ 1.56 (d, *J* = 14.0 Hz, 36H), 1.47 (d, *J* = 14.3 Hz, 12H), 1.19 (s, 4H) ppm.

³¹P{¹H} NMR (162 MHz, CDCl₃): δ -8.84 ppm.

The chemical shifts are in agreement with previously reported values.²²⁵

(*tert*-Bu₂PC(CH₃)₂CH₂)Pd(Br)(PEt₃) (complex C)

[ES 5028b]



Cyclometalated palladium complex **B** (1.04 g, 1.34 mmol) was added to a Schlenk flask containing PEt₃ (318 mg, 2.69 mmol, 2.0 equiv.) in THF (12 mL). The reaction was stirred at room temperature under argon for 1 h and the solvent was removed. Drying on high vacuum gave complex **C** (1.35 g, 2.67 mmol, 99%) as a light yellow solid.

¹H NMR (400 MHz, CDCl₃): δ 1.71 (pd, *J* = 7.7, 2.5 Hz, 6H), 1.54 (d, *J* = 13.0 Hz, 18H), 1.48 (d, *J* = 12.6 Hz, 6H), 1.10 (dt, *J* = 15.4, 7.6 Hz, 9H), 0.91 (dd, *J* = 7.3, 6.1 Hz, 2H) ppm.

¹³C{¹H} NMR (126 MHz, CDCl₃): δ 50.8 (d, *J* = 16.3 Hz), 37.8 (d, *J* = 6.9 Hz), 32.3, 32.3, 15.6 (d, *J* = 26.2 Hz), 14.5 (d, *J* = 21.3 Hz), 8.3 ppm.

³¹P{¹H} NMR (162 MHz, CDCl₃): δ 12.6 (d, *J*_{P-P} = 426.1 Hz), -10.7 (d, *J*_{P-P} = 426.2 Hz) ppm.

IR (solid, ν): 2959 (m), 2900 (m), 2871 (m), 1468 (m), 1415 (w), 1390 (m), 1376 (m), 1366 (m), 1253 (w), 1175 (m), 1036 (m), 987 (w), 930 (w), 809 (w), 766 (s), 725 (s) cm⁻¹.

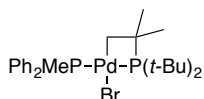
HRESI-MS (+, MeOH, *m/z*): [M-Br]⁺ 425.1798, calc. 425.1718.

Elemental analysis (%): C 42.82, H 8.18, calc. C 42.74, H 8.17.

m.p.: 112-116 °C.

(*tert*-Bu₂PC(CH₃)₂CH₂)Pd(Br)(PMePh₂) (complex D)

[ES 4014a]



In a glovebox, cyclometalated palladium complex **B** (54.3 mg, 0.070 mmol, 1.0 equiv.) was weighed in a Schlenk flask and THF (2.0 mL) and PMePh₂ (28.0 mg, 0.14 mmol, 2.0 equiv.) were added. The reaction was heated to 50 °C for 2 h and the solvent was removed in air. Drying on high vacuum gave palladium complex **D** (81.4 mg, 0.14 mmol, 99%) as a yellow solid.

¹H NMR (400 MHz, C₆D₆): δ 7.61 – 7.42 (m, 4H), 7.05 – 6.91 (m, 6H), 1.92 (dd, *J* = 8.1, 2.5 Hz, 3H), 1.42 (d, *J* = 13.1 Hz, 18H), 1.16 (d, *J* = 12.9 Hz, 6H), 0.64 (t, *J* = 6.6 Hz, 2H) ppm.

¹³C{¹H} NMR (101 MHz, CDCl₃): δ 134.5 (d, *J* = 2.3 Hz), 134.1 (d, *J* = 2.3 Hz), 132.9 (dd, *J* = 12.0, 1.3 Hz), 129.8 (d, *J* = 2.0 Hz), 128.4 (d, *J* = 9.4 Hz), 50.5 (dd, *J* = 17.3, 2.0 Hz), 37.9 (dd, *J* = 6.9, 3.1 Hz), 32.3, 32.1, 18.8 (d, *J* = 26.2 Hz), 13.5 (dd, *J* = 23.2, 2.8 Hz) ppm.

³¹P{¹H} NMR (162 MHz, C₆D₆): δ 6.89 (d, *J*_{P-P} = 436.7 Hz), -13.7 (d, *J*_{P-P} = 437.3 Hz) ppm.

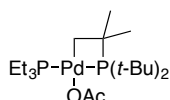
IR (solid, ν): 3006 (w), 2989 (w), 2908 (w), 2867 (w), 1471 (w), 1435 (w), 1276 (s), 1260 (s), 1176 (w), 1101 (w), 890 (w), 809 (w), 765 (s), 750 (s), 695 (w) cm^{-1} .

HRESI-MS (+, MeOH, m/z): $[\text{M}-\text{Br}]^+$ 507.1595, calc. 507.1562.

Elemental analysis (%): C 51.42, H 6.71, calc. C 51.08, H 6.69.

(*tert*-Bu₂PC(CH₃)₂CH₂)Pd(OAc)(PEt₃) (complex E)

[ES 4022a]



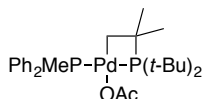
In a glovebox, cyclometalated palladium complex **A** (200 mg, 0.27 mmol, 1.0 equiv.) was weighed in a Schlenk flask and THF (10.0 mL) and PEt₃ (64 mg, 0.54 mmol, 2.0 equiv.) was added. The reaction was heated to 50 °C for 2.5 h and the solvent was removed in air. Recrystallization from EtOH/H₂O, removal of solvent and drying on high vacuum gave *trans* palladium complex **E** (261 mg, 0.54 mmol, quant.) as a yellow oil.

¹H NMR (400 MHz, C₆D₆): δ 2.21 (s, 3H), 1.48 – 1.33 (m, 24H, overlap.), 1.31 (d, $J = 12.4$ Hz, 6H), 0.95 (dt, $J = 15.4, 7.6$ Hz, 9H), 0.62 (dd, $J = 8.3, 6.2$ Hz, 2H) ppm.

³¹P{¹H} NMR (162 MHz, C₆D₆): δ 14.34 (d, $J_{\text{P-P}} = 419.9$ Hz), -3.74 (d, $J_{\text{P-P}} = 419.9$ Hz) ppm.

(*tert*-Bu₂PC(CH₃)₂CH₂)Pd(OAc)(PMePh₂) (complex F)

[ES 4014b]



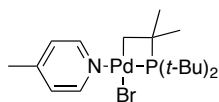
In a glovebox, cyclometalated palladium complex **A** (51.3 mg, 0.070 mmol, 1.0 equiv.) was weighed in a Schlenk flask and THF (2.0 mL) and PMePh₂ (28.0 mg, 0.14 mmol, 2.0 equiv.) were added. The reaction was heated to 50 °C for 2 h and the solvent was removed in air. Drying on high vacuum gave palladium complex **F** (85.2 mg, 0.14 mmol, quant.) as a yellow solid. The complex was obtained in a *cis/trans* mixture of 1:10.

¹H NMR (400 MHz, C₆D₆): δ 7.70 – 7.61 (m, 4H), 7.08 – 6.93 (m, 6H), 2.12 (s, 3H), 1.75 (dd, $J = 8.0, 2.5$ Hz, 3H), 1.37 (d, $J = 12.9$ Hz, 18H), 1.18 (d, $J = 12.7$ Hz, 6H), 0.53 (t, $J = 7.2$ Hz, 2H) ppm.

³¹P{¹H} NMR (162 MHz, C₆D₆): δ 7.57 (d, $J_{\text{P-P}} = 423.0$ Hz), -6.10 (d, $J_{\text{P-P}} = 423.2$ Hz) (*trans*), 6.66 (d, $J_{\text{P-P}} = 383.8$ Hz), -6.76 (d, $J_{\text{P-P}} = 383.7$ Hz) (*cis*) ppm.

(*tert*-Bu₂PC(CH₃)₂CH₂)Pd(Br)(4-picoline) (25a)

[ES 5099]



Palladium complex **B** (163.1 mg, 0.21 mmol) was dissolved in DCM (2.0 mL) and 4-picoline (2.5 mL) was added. The mixture was heated at 40 °C over night and the solvent was removed on high vacuum. After drying over night, complex **25a** (99.0 mg, 0.21 mmol, quant.) as obtained as a light brown solid.

¹H NMR (500 MHz, CDCl₃): δ 8.65 (broad s, 2H), 7.12 (d, *J* = 5.7 Hz, 2H), 2.35 (s, 3H), 1.62 (d, *J* = 13.8 Hz, 18H), 1.51 (d, *J* = 13.6 Hz, 6H), 1.01 (t, *J* = 7.6 Hz, 2H) ppm.

¹³C{¹H} NMR (126 MHz, CDCl₃): δ 150.8, 125.3, 49.0 (d, *J* = 21.1 Hz), 37.6, 32.2, 31.8, 21.2, 13.8 ppm.

³¹P{¹H} NMR (162 MHz, CDCl₃): δ -11.1 ppm.

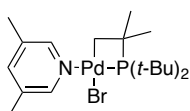
IR (solid, ν): 2991 (w), 2960 (m), 2898 (m), 2869 (m), 1617 (m), 1501 (w), 1469 (m), 1444 (m), 1390 (m), 1377 (m), 1365 (m), 1268 (w), 1230 (w), 1175 (m), 1069 (w), 1022 (m), 984 (w), 932 (w), 807 (s), 732 (s), 700 (m) cm⁻¹.

HRESI-MS (+, MeOH, *m/z*): [M-Br]⁺ 400.1429, calc. 400.1385.

Elemental analysis (%): C 45.54, H 6.99, N 3.25, calc. C 44.97, H 6.92, N 2.91.

(*tert*-Bu₂PC(CH₃)₂CH₂)Pd(Br)(3,5-lutidine) (25b)

[ES 5047d/5069]



In a glovebox, palladium complex **B** (109.5 mg, 0.14 mmol) was added to a Schlenk flask containing dried and distilled 3,5-lutidine (2.0 mL). The mixture was stirred for 4 h at room temperature and 20 min at 60 °C. While heating, the majority of lutidine was removed on high vacuum. Subsequent precipitation from THF/pentane yielded complex **25b** (115.3 mg, 0.23 mmol, 82%) as a light brown solid.

¹H NMR (400 MHz, CDCl₃): δ 8.43 (s, 2H), 7.31 (s, 1H), 2.27 (s, 6H), 1.61 (d, *J* = 13.8 Hz, 18H), 1.50 (d, *J* = 13.6 Hz, 6H), 0.95 (d, *J* = 3.5 Hz, 2H) ppm.

¹³C{¹H} NMR (101 MHz, CDCl₃): δ 148.8, 138.7, 133.7, 49.0 (d, *J* = 20.5 Hz), 37.6 (d, *J* = 10.1 Hz), 32.2 (d, *J* = 2.8 Hz), 31.8, 18.4, 16.9 (d, *J* = 29.6 Hz) ppm.

³¹P{¹H} NMR (162 MHz, CDCl₃): δ -10.7 ppm.

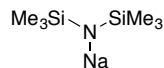
HRESI-MS (+, MeOH, *m/z*): [M-Br]⁺ 414.1565, calc. 414.1542.

Elemental analysis (%): C 46.29, H 7.15, N 2.84, calc. C 46.12, H 7.13, N 2.83.

4.3.4 Organometallic reagents

Sodium hexamethyldisilazide, NaHMDS

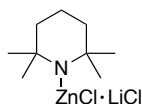
[ES 4131]



In a glovebox, NaH (3.53 g, 147.2 mmol, 1.0 equiv.) was weighed in a 250 mL Schlenk flask. Dry toluene (100 mL) was added and the flask was brought outside of the glovebox. Hexamethylsilazane (33.3 mL, 159.0 mmol, 1.08 equiv.) was syringed into the flask and the reaction was refluxed for 40 h under argon. The mixture was cooled down to ambient temperature and filtered through a reversible frit. Removal of the solvent and drying on high vacuum for 3 days yielded NaHMDS (21.32 g, 116.3 mmol, 79%) as a colorless solid that was used without further purification.

TMPZnCl·LiCl

[ES 3136]



According to reported procedure,¹⁰⁶ tetramethylpiperidine (876 mg, 6.20 mmol, 1.0 equiv.) and dry THF (6.0 mL) were added to a Schlenk flask under argon. After cooling to -40 °C in an ethanol/dry ice bath, *n*-BuLi (2.61 mL, 6.20 mmol, 1.0 equiv.) was added. The reaction was slowly warmed to -10 °C over the course of 1 h. ZnCl₂ (930 mg, 6.82 mmol, 1.1 equiv.) was weighed in the glovebox and dissolved in THF (6.0 mL) and added dropwise to the LiTMP solution. After stirring the reaction for 30 min at -10 °C, it was warmed to r.t. and stirred for an additional 40 min. After removal of the solvent on high vacuum, the yellow solid was dissolved in THF (5.0 mL) and titrated against salicylaldehyde hydrazone, yielding a 0.90 M solution of TMPZnCl·LiCl that was used directly in subsequent step.

4.4 Palladium-catalyzed direct arylation of pyridine *N*-oxides

4.4.1 Direct arylation with bromopyridines

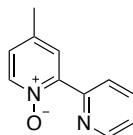
General procedure

In a glovebox, pyridine *N*-oxide **1** (2.0 equiv.), palladium complex **A** (0.025 equiv.) and K₃PO₄ (2.0 equiv.) were weighed in a Schlenk flask. Dry toluene (*c* = 1.0 M in *N*-oxide **1**) and aryl halide (1.0 equiv.) were added and the flask was sealed and brought outside of the glovebox. The reaction was

heated at 120 °C for 24 h. After cooling to room temperature, the crude reaction mixture was directly subjected to column chromatography (silica gel, acetone/hexane or MeOH/DCM).

4-Methyl-2,2'-bipyridine *N*-oxide (**4b**)

[ES 1172]



According to the general procedure, 4-methyl pyridine *N*-oxide **1b** (764 mg, 7.0 mmol), complex **A** (64.2 mg, 0.088 mmol), K₃PO₄ (1.49 g, 7.0 mmol) and 2-bromopyridine (553 mg, 3.5 mmol) in toluene (7.0 mL) were used for a kinetic reaction. The remaining reaction mixture was subjected to column chromatography (silica gel, MeOH/DCM) and gave bipyridine *N*-oxide **4b** (130 mg, 0.70 mmol, 20%) as a brown oil.

¹H NMR (400 MHz, CDCl₃): δ 8.89 (d, *J* = 8.1 Hz, 1H), 8.72 (d, *J* = 4.8 Hz, 1H), 8.20 (d, *J* = 6.6 Hz, 1H), 7.96 (d, *J* = 2.3 Hz, 1H), 7.82 (td, *J* = 7.8, 1.7 Hz, 1H), 7.34 (ddd, *J* = 7.6, 4.8, 1.1 Hz, 1H), 7.08 (dd, *J* = 6.7, 2.7 Hz, 1H), 2.41 (s, 3H) ppm.

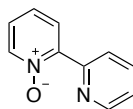
¹³C{¹H} NMR (126 MHz, CDCl₃): δ 149.8, 149.4, 146.5, 140.1, 137.7, 136.4, 128.3, 126.3, 125.8, 124.4, 20.5 ppm.

IR (solid, ν): 3006 (w), 2989 (w), 2924 (w), 2859 (w), 1716 (w), 1653 (w), 1583 (w), 1569 (w), 1454 (m), 1404 (w), 1276 (s), 1260 (s), 1235 (m), 1201 (w), 1150 (w), 1129 (w), 1093 (w), 1043 (w), 991 (w), 892 (w), 822 (w), 749 (s), 706 (w) cm⁻¹.

HRESI-MS (+, MeOH, *m/z*): [M+H]⁺ 187.0887, calc. 187.0866, [M+Na]⁺ 209.0703, calc. 209.0685.

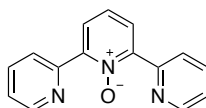
2,2'-Bipyridine *N*-oxide (**4c**)

[ES 1031]



According to the general procedure, pyridine *N*-oxide **1c** (190 mg, 2.0 mmol), Pd(OAc)₂ (11.2 mg, 0.050 mmol), P(*t*-Bu)₃ (12.1 mg, 0.060 mmol), K₃PO₄ (425 mg, 2.0 mmol) and 2-bromopyridine (158 mg, 1.0 mmol) in toluene (2.0 mL) after 24 h at 120 °C was subjected to column chromatography (silica gel, MeOH/DCM) and gave bipyridine *N*-oxide **4c** (42.0 mg, 0.24 mmol, 24%) and terpyridine *N*-oxide **6c** (19.0 mg, 0.076 mmol, 15%) as brown oils.

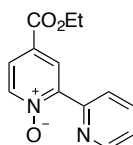
¹H NMR (500 MHz, CDCl₃): δ 8.89 (dt, *J* = 8.1, 1.1 Hz, 1H), 8.73 (ddd, *J* = 4.9, 1.8, 0.9 Hz, 1H), 8.33 (dd, *J* = 6.4, 1.2 Hz, 1H), 8.20 (dd, *J* = 8.0, 2.2 Hz, 1H), 7.85 (td, *J* = 7.9, 1.8 Hz, 1H), 7.42 – 7.33 (m, 2H), 7.29 (ddd, *J* = 7.4, 6.5, 2.2 Hz, 1H) ppm.

2,2':6,2''-terpyridine *N*-oxide (6c)

$^1\text{H NMR}$ (500 MHz, CDCl_3): δ 8.75 (ddd, $J = 4.8, 1.8, 0.9$ Hz, 2H), 8.69 (dt, $J = 8.1, 1.0$ Hz, 2H), 8.07 (d, $J = 7.9$ Hz, 2H), 7.82 (td, $J = 7.8, 1.8$ Hz, 2H), 7.47 (t, $J = 7.9$ Hz, 1H), 7.36 (ddd, $J = 7.5, 4.8, 1.1$ Hz, 2H) ppm.

4-Ethoxycarbonyl-2,2'-bipyridine *N*-oxide (4d)

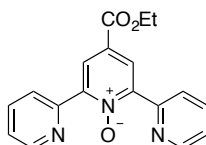
[ES 1023]



According to the general procedure, 4-ethoxycarbonyl pyridine *N*-oxide **1d** (1.95 g, 8.0 mmol), $\text{Pd}(\text{OAc})_2$ (44.9 mg, 0.20 mmol), $\text{P}(t\text{-Bu})_3$ (48.6 mg, 0.24 mmol), K_3PO_4 (1.70 g, 8.0 mmol) and 2-bromopyridine (632 mg, 4.0 mmol) in toluene (8.0 mL) after 24 h at 120 °C was subjected to column chromatography (deactivated silica gel, acetone/hexane) and gave bipyridine *N*-oxide **4d** (557 mg, 2.48 mmol, 62%) as a brown solid and terpyridine *N*-oxide **6d** (30.7 mg, 0.10 mmol, 5%) as a yellow solid.

$^1\text{H NMR}$ (400 MHz, CDCl_3): δ 8.82 – 8.69 (m, 3H), 8.31 (dd, $J = 6.8, 0.5$ Hz, 1H), 7.87 – 7.81 (m, 2H), 7.38 (ddd, $J = 7.6, 4.8, 1.2$ Hz, 1H), 4.41 (q, $J = 7.1$ Hz, 2H), 1.40 (t, $J = 7.1$ Hz, 3H) ppm.

The chemical shifts are in agreement with previously reported values.³

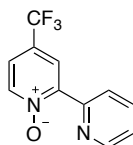
4-Ethoxycarbonyl-2,2':6,2''-terpyridine *N*-oxide (6d)

$^1\text{H NMR}$ (400 MHz, CDCl_3): δ 8.78 (ddd, $J = 4.8, 1.9, 1.0$ Hz, 2H), 8.64 (s, 2H), 8.59 (d, $J = 8.1$ Hz, 2H), 7.82 (td, $J = 7.8, 1.8$ Hz, 2H), 7.38 (ddd, $J = 7.6, 4.8, 1.2$ Hz, 2H), 4.43 (q, $J = 7.1$ Hz, 2H), 1.41 (t, $J = 7.1$ Hz, 3H) ppm.

The chemical shifts are in agreement with previously reported values.³

4-Trifluoromethyl-2,2'-bipyridine *N*-oxide (4e)

[ES 1160]

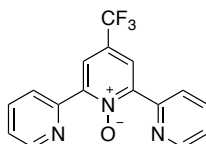


According to the general procedure, 4-trifluoromethyl pyridine *N*-oxide **1e** (1.14 g, 7.0 mmol), complex **A** (64.2 mg, 0.088 mmol), K₃PO₄ (1.49 g, 7.0 mmol) and 2-bromopyridine (553 mg, 3.5 mmol) in toluene (7.0 mL) was used for a kinetic reaction. The remaining reaction mixture was subjected to column chromatography (deactivated silica gel, acetone/hexane) and gave bipyridine *N*-oxide **4e** (377 mg, 1.57 mmol, 45%) and terpyridine *N*-oxide **6e** (63.0 mg, 0.20 mmol, 11%) as colorless solids.

¹H NMR (500 MHz, CDCl₃): δ 8.93 (dt, *J* = 8.0, 0.9 Hz, 1H), 8.75 (ddd, *J* = 4.7, 1.6, 0.8 Hz, 1H), 8.54 (d, *J* = 2.6 Hz, 1H), 8.37 (d, *J* = 6.8 Hz, 1H), 7.85 (td, *J* = 7.8, 1.8 Hz, 1H), 7.46 (dd, *J* = 6.8, 2.8 Hz, 1H), 7.39 (ddd, *J* = 7.5, 4.8, 1.1 Hz, 1H) ppm.

¹⁹F{¹H} NMR (471 MHz, CDCl₃): δ -63.4 ppm.

The chemical shifts are in agreement with previously reported values.³

4-Trifluoromethyl-2,2':6,2''-terpyridine *N*-oxide (6e)

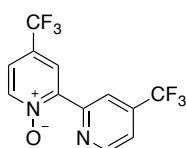
¹H NMR (500 MHz, CDCl₃): δ 8.76 (dt, *J* = 4.8, 1.3 Hz, 1H), 8.71 (dd, *J* = 8.0, 1.1 Hz, 1H), 8.37 (s, 1H), 7.82 (td, *J* = 7.8, 1.8 Hz, 1H), 7.38 (ddd, *J* = 7.6, 4.8, 1.2 Hz, 1H) ppm.

¹⁹F{¹H} NMR (471 MHz, CDCl₃): δ -63.4 ppm.

The chemical shifts are in agreement with previously reported values.³

4,4'-Di(trifluoromethyl)-2,2'-bipyridine *N*-oxide (4i)

[ES 2152]



According to the general procedure, 4-trifluoromethyl pyridine *N*-oxide **1e** (489 mg, 3.0 mmol), complex **A** (27.5 mg, 0.037 mmol), K₃PO₄ (637 g, 2.0 mmol) and 2-bromo-4-trifluoromethyl pyridine (339 mg, 1.5 mmol) in toluene (3.0 mL) gave after column chromatography (deactivated silica gel,

acetone/hexane) bipyridine *N*-oxide **4i** (257 mg, 1.16 mmol, 55%) and terpyridine *N*-oxide **6i** (57.3 mg, 0.13 mmol, 17%) as yellow solids.

$^1\text{H NMR}$ (400 MHz, CDCl_3): δ 9.32 (s, 1H), 8.93 (d, $J = 5.0$ Hz, 1H), 8.61 (d, $J = 2.7$ Hz, 1H), 8.39 (d, $J = 6.8$ Hz, 1H), 7.62 (dd, $J = 5.0, 1.5$ Hz, 1H), 7.52 (dd, $J = 6.9, 2.7$ Hz, 1H) ppm.

$^{13}\text{C}\{^1\text{H}\}$ NMR (101 MHz, CDCl_3): δ 150.4, 149.6, 146.5, 141.7, 139.3, 139.0, 127.2, 125.1 (d, $J = 4.0$ Hz), 123.9, 122.2 (d, $J = 3.4$ Hz), 121.2 (d, $J = 3.8$ Hz), 120.7 (d, $J = 3.5$ Hz) ppm.

$^{19}\text{F}\{^1\text{H}\}$ NMR (376 MHz, CDCl_3): δ -63.5, -64.6 ppm.

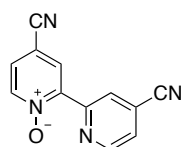
IR (solid, ν): 3121 (w), 3050 (w), 3006 (w), 2989 (w), 1471 (w), 1377 (m), 1321 (m), 1276 (s), 1260 (s), 1235 (w), 1170 (m), 1130 (m), 1084 (m), 1049 (w), 912 (w), 858 (m), 765 (s), 750 (s), 671 (w), 659 (w) cm^{-1} .

HRESI-MS (+, MeOH, m/z): $[\text{M}+\text{H}]^+$ 309.0448, calc. 309.0457, $[\text{M}+\text{Na}]^+$ 331.0265, calc. 331.0277.

Elemental analysis (%): C 46.79, H 2.13, N 9.10, calc. C 46.77, H 1.96, N 9.09.

4,4'-Dicyano-2,2'-bipyridine *N*-oxide (**4j**)

[ES 2154]

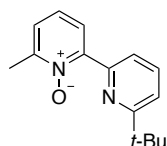


According to the general procedure, 4-cyanopyridine *N*-oxide (601 mg, 5.0 mmol), complex **A** (45.8 mg, 0.062 mmol), K_3PO_4 (1061 g, 5.0 mmol) and 2-chloro-4-cyano pyridine (346 mg, 2.5 mmol) in toluene (5.0 mL) gave after column chromatography (deactivated silica gel, acetone/hexane) bipyridine *N*-oxide **4j** (120 mg, 0.54 mmol, 22%) as a yellow solid.

$^1\text{H NMR}$ (400 MHz, CDCl_3): δ 9.33 – 9.25 (m, 1H), 8.92 (dd, $J = 4.9, 0.9$ Hz, 1H), 8.68 (d, $J = 2.5$ Hz, 1H), 8.35 (d, $J = 6.9$ Hz, 1H), 7.64 (dd, $J = 4.9, 1.5$ Hz, 1H), 7.54 (dd, $J = 6.9, 2.6$ Hz, 1H) ppm.

2-Methyl-6'-*tert*-butyl-2,2'-bipyridine *N*-oxide (**4f**)

[ES 4096/KR 1012]



According to the general procedure, 2-methylpyridine *N*-oxide **1f** (4.08 g, 37.4 mmol), complex **A** (344 mg, 0.47 mmol), K_3PO_4 (7.93 mg, 37.4 mmol) and 2-bromo-6-*tert*-butylpyridine (4.00 g, 18.7 mmol) in toluene (40 mL) gave after column chromatography (silica gel, MeOH/DCM) bipyridine *N*-oxide **4f** (665 mg, 2.74 mmol, 15%) as an orange oil and bipyridine **8m** (715 mg, 2.66 mmol, 29%) as a yellow solid.

¹H NMR (500 MHz, CDCl₃): δ 8.81 (d, *J* = 7.8 Hz, 1H), 8.23 – 8.18 (m, 1H), 7.75 (t, *J* = 7.9 Hz, 1H), 7.39 (dd, *J* = 7.9, 0.9 Hz, 1H), 7.27 – 7.23 (m, 2H), 2.61 (s, 3H), 1.42 (s, 9H) ppm.

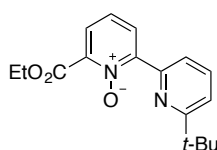
¹³C{¹H} NMR (126 MHz, CDCl₃): δ 168.7, 149.8, 148.6, 148.2, 136.3, 126.0, 125.5, 124.9, 122.4, 119.5, 37.8, 30.3, 18.6 ppm.

IR (neat, ν): 2955 (m), 2865 (w), 1697 (w), 1569 (m), 1477 (w), 1442 (m), 1385 (w), 1366 (m), 1319 (w), 1267 (m), 1257 (m), 1232 (w), 1218 (w), 1201 (w), 1165 (w), 1147 (w), 1088 (m), 1038 (w), 1000 (w), 967 (w), 849 (m), 819 (m), 770 (s), 747 (s), 661 (w) cm⁻¹.

HRESI-MS (+, MeOH, *m/z*): [M+H]⁺ 243.1479, calc. 243.1492, [M+Na]⁺ 265.1300, calc. 265.1311.

2-Ethoxycarbonyl-6'-*tert*-butyl-2,2'-bipyridine *N*-oxide (**4g**)

[KR 1018]



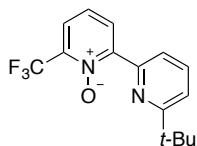
According to the general procedure, 2-ethoxycarbonyl pyridine *N*-oxide **1g** (6.25 g, 37.4 mmol), complex **A** (337 mg, 0.46 mmol), K₃PO₄ (7.93 g, 37.4 mmol) and 2-bromo-6-*tert*-butylpyridine (4.00 g, 18.7 mmol) in toluene (40 mL) gave after column chromatography (silica gel, acetone/hexane) bipyridine *N*-oxide **4g** (766 mg, 2.6 mmol, 14%) as a yellow solid.

¹H NMR (400 MHz, CDCl₃): δ 8.83 (dd, *J* = 8.0, 0.9 Hz, 1H), 8.42 (dd, *J* = 8.0, 2.3 Hz, 1H), 7.72 (t, *J* = 7.9 Hz, 1H), 7.44 (dd, *J* = 7.6, 2.3 Hz, 1H), 7.38 (dd, *J* = 2.8, 0.6 Hz, 1H), 7.10 (m, 1H), 4.50 (q, *J* = 7.1 Hz, 2H), 1.43 (t, *J* = 7.1 Hz, 3H), 1.39 (s, 9H) ppm.

HRESI-MS (+, MeOH, *m/z*): [M+H]⁺ 301.1577, calc. 301.1547, [M+Na]⁺ 323.1406, calc. 323.1366.

2-Trifluoromethyl-6'-*tert*-butyl-2,2'-bipyridine *N*-oxide (**4h**)

[ES 6034]



According to general procedure, 2-trifluoromethyl pyridine *N*-oxide **1h** (652.4 mg, 4.0 mmol), complex **A** (36.7 mg, 0.05 mmol), K₃PO₄ (849.1 mg, 4.0 mmol) and 2-bromo-6-*t*-butylpyridine (436.0 mg, 2.0 mmol) in toluene (4.0 mL) gave after column chromatography (deactivated silica gel, acetone/hexane) bipyridine *N*-oxide **4h** (259.1 mg, 0.87 mmol, 44%) as a light orange solid and bipyridine **8m** (94.3 mg, 0.35 mmol, 35%) as a yellow solid.

¹H NMR (400 MHz, CDCl₃): δ 8.81 (dd, *J* = 7.9, 0.9 Hz, 1H), 8.56 (dd, *J* = 8.2, 2.2 Hz, 1H), 7.74 (td, *J* = 7.9, 0.6 Hz, 1H), 7.69 (dd, *J* = 7.8, 2.2 Hz, 1H), 7.46 – 7.37 (m, 2H), 1.39 (s, 9H) ppm.

$^{13}\text{C}\{^1\text{H}\}$ NMR (101 MHz, CDCl_3): δ 169.0, 149.8, 146.5, 136.7, 130.9, 124.3, 124.2, 122.7, 121.7, 120.5, 119.0, 37.8, 30.2 ppm.

$^{19}\text{F}\{^1\text{H}\}$ NMR (376 MHz, CDCl_3): δ -68.6 ppm.

IR (solid, ν): 2962 (w), 2904 (w), 2869 (w), 1617 (w), 1581 (w), 1569 (w), 1479 (w), 1446 (w), 1417 (w), 1380 (m), 1333 (m), 1299 (m), 1274 (m), 1230 (w), 1213 (w), 1151 (s), 1127 (m), 1089 (m), 1077 (m), 990 (w), 889 (w), 850 (m), 821 (w), 791 (m), 764 (s), 750 (s), 692 (m) cm^{-1} .

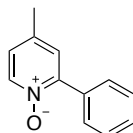
HRESI-MS (+, DCM/MeOH, m/z): $[\text{M}+\text{H}]^+$ 297.1229, calc. 297.1209.

m.p. 115-117 °C.

4.4.2 Direct arylation with bromobenzenes

2-Phenyl-4-methylpyridine *N*-oxide (**5b**)

[ES 2002F2]



According to the general procedure, 4-methyl pyridine *N*-oxide **1b** (764 g, 7.0 mmol), complex **A** (64.2 mg, 0.088 mmol), K_3PO_4 (1.49 g, 7.0 mmol) and bromobenzene (550 mg, 3.5 mmol) in toluene (7.0 mL) was used for a kinetic reaction. The remaining reaction mixture was subjected to column chromatography (silica gel, MeOH/DCM) and gave arylpyridine *N*-oxide **5b** (199 mg, 1.07 mmol, 31%) and biarylpyridine *N*-oxide **7b** (43.7 mg, 0.17 mmol, 10%) as brown oils.

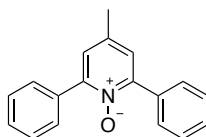
^1H NMR (500 MHz, CDCl_3): δ 8.25 (d, J = 6.6 Hz, 1H), 7.79 (dd, J = 8.1, 1.6 Hz, 2H), 7.50 – 7.39 (m, 3H), 7.23 (d, J = 2.6 Hz, 1H), 7.04 (dd, J = 6.6, 2.5 Hz, 1H), 2.38 (s, 3H) ppm.

$^{13}\text{C}\{^1\text{H}\}$ NMR (126 MHz, CDCl_3): δ 148.7, 140.0, 138.0, 132.67, 129.7, 129.4, 128.4, 128.1, 125.4, 20.5 ppm.

The chemical shifts are in agreement with previously reported values.²²⁶

Elemental analysis (%): C 77.85, H 5.99, N 7.64, calc. C 77.81, H 5.99, N 7.56.

2,6-Diphenyl-4-methylpyridine *N*-oxide (**7b**)

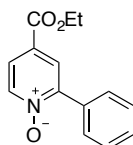


^1H NMR (500 MHz, CDCl_3): δ 7.86 – 7.76 (m, 4H), 7.51 – 7.38 (m, 6H), 7.22 (s, 2H), 2.40 (s, 3H) ppm.

The chemical shifts are in agreement with previously reported values.²²⁷

2-Phenyl-4-ethoxycarbonylpyridine *N*-oxide (5d)

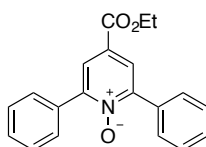
[ES 1036]



According to the general procedure, 4-ethoxycarbonyl pyridine *N*-oxide **1d** (2.34 g, 14.0 mmol), Pd(OAc)₂ (78.7 mg, 0.35 mmol), P(*t*-Bu)₃ (85.0 mg, 0.42 mmol), K₃PO₄ (2.97 g, 14.0 mmol) and bromobenzene (1.10 g, 7.0 mmol) in toluene (14.0 mL) after 24 h at 120 °C was subjected to column chromatography (deactivated silica gel, acetone/hexane) and gave arylpyridine *N*-oxide **5d** (956 mg, 3.93 mmol, 56%) and biarylpyridine *N*-oxide **7d** (144.7 mg, 0.45 mmol, 13%) as yellow solids.

¹H NMR (400 MHz, CDCl₃): δ 8.34 (dd, *J* = 6.8, 0.5 Hz, 1H), 8.04 (dd, *J* = 2.5, 0.5 Hz, 1H), 7.84 – 7.75 (m, 3H), 7.53 – 7.44 (m, 3H), 4.40 (q, *J* = 7.1 Hz, 2H), 1.40 (t, *J* = 7.1 Hz, 3H) ppm.

The chemical shifts are in agreement with previously reported values.³⁹

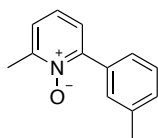
2,6-Diphenyl-4-ethoxycarbonylpyridine *N*-oxide (7d)

¹H NMR (400 MHz, CDCl₃): δ 8.01 (s, 2H), 7.83 – 7.80 (m, 4H), 7.51 – 7.43 (m, 6H), 4.41 (q, *J* = 7.1 Hz, 2H), 1.40 (t, *J* = 7.1 Hz, 3H) ppm.

The chemical shifts are in agreement with previously reported values.³⁹

2-(3-Tolyl)-6-methylpyridine *N*-oxide (5f)

[ES 4190/KR 1013]



According to the general procedure, 2-methyl pyridine *N*-oxide **1f** (4.07 g, 37.4 mmol), complex **A** (344 mg, 0.47 mmol), K₃PO₄ (7.93 mg, 37.4 mmol) and 3-bromotoluene (3.19 mg, 18.7 mmol) in toluene (40 mL) gave after column chromatography (silica gel, MeOH/DCM) gave biaryl **5f** *N*-oxide (750 mg, 3.76 mmol, 20%) as an orange oil and biphenyl **9c** (369 mg, 2.02 mmol, 22%) as a yellow oil.

¹H NMR (400 MHz, CDCl₃): δ 7.63 (s, 1H), 7.51 (d, *J* = 7.7 Hz, 1H), 7.35 (t, *J* = 7.7 Hz, 1H), 7.29 (dd, *J* = 7.6, 2.2 Hz, 1H), 7.24 (d, *J* = 7.8 Hz, 2H), 7.19 (t, *J* = 7.7 Hz, 1H), 2.57 (s, 3H), 2.40 (s, 3H) ppm.

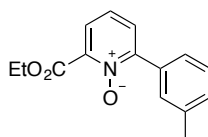
$^{13}\text{C}\{^1\text{H}\}$ NMR (126 MHz, CDCl_3): δ 150.0, 149.8, 137.8, 133.4, 130.2, 130.1, 128.2, 126.6, 125.1, 125.1, 124.8, 21.6, 18.7 ppm.

IR (neat, ν): 3021 (w), 2989 (w), 2953 (w), 2953 (w), 1676 (w), 1603 (w), 1584 (w), 1559 (w), 1475 (m), 1444 (m), 1425 (w), 1365 (m), 1309 (w), 1276 (m), 1259 (s), 1244 (s), 1207 (w), 1166 (w), 1100 (w), 1038 (w), 999 (w), 915 (w), 882 (w), 844 (m), 766 (s), 750 (s), 698 (s), 680 (w) cm^{-1} .

HRESI-MS (+, MeOH, m/z): $[\text{M}+\text{H}]^+$ 200.1069, calc. 200.1070, $[\text{M}+\text{Na}]^+$ 222.0884, calc. 222.0895.

2-(3-Tolyl)-6-ethoxycarbonylpyridine *N*-oxide (**5g**)

[KR 1020]



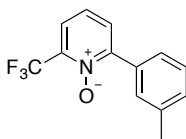
According to the general procedure, 2-ethoxycarbonyl pyridine *N*-oxide **1g** (6.25 g, 37.4 mmol), complex **A** (337 mg, 0.46 mmol), K_3PO_4 (7.93 g, 37.4 mmol) and 3-bromotoluene (3.19 mg, 18.7 mmol) in toluene (40 mL) gave after column chromatography (silica gel, acetone/hexane) arylpyridine *N*-oxide **5g** (221 mg, 0.9 mmol, 5%) as a yellow solid.

^1H NMR (400 MHz, CDCl_3): δ 7.67 (s, 1H), 7.54 (d, $J = 7.8$ Hz, 1H), 7.48 (dd, $J = 7.8, 2.1$ Hz, 1H), 7.43 (dd, $J = 7.8, 2.1$ Hz, 1H), 7.34 (m, 2H), 7.10 (m, 1H), 4.48 (q, $J = 7.1$ Hz, 2H), 2.40 (s, 3H), 1.41 (t, $J = 7.1$ Hz, 3H) ppm.

HRESI-MS (+, MeOH, m/z): $[\text{M}+\text{H}]^+$ 258.1147, calc. 258.1125, $[\text{M}+\text{Na}]^+$ 280.0983, calc. 280.0944.

2-(3-Tolyl)-6-trifluoromethylpyridine *N*-oxide (**5h**)

[ES 6036]



According to general procedure, 2-trifluoromethyl pyridine *N*-oxide **1h** (652.4 mg, 4.0 mmol), complex **A** (36.7 mg, 0.05 mmol), K_3PO_4 (849.1 mg, 4.0 mmol) and 3-bromotoluene (352.0 mg, 2.0 mmol) in toluene (4.0 mL) gave after column chromatography (deactivated silica gel, acetone/hexane) arylpyridine *N*-oxide **5h** (226.4 mg, 0.89 mmol, 45%) as a light yellow solid and biphenyl **9c** (47.6 mg, 0.26 mmol, 26%) as a yellow oil.

^1H NMR (500 MHz, CDCl_3): δ 7.68 – 7.62 (m, 2H), 7.59 (dd, $J = 8.0, 2.1$ Hz, 1H), 7.53 (d, $J = 7.7$ Hz, 1H), 7.35 (q, $J = 7.9$ Hz, 2H), 7.27 (d, $J = 7.6$ Hz, 1H), 2.40 (s, 3H) ppm.

$^{13}\text{C}\{^1\text{H}\}$ NMR (126 MHz, CDCl_3): δ 151.7, 138.1, 131.2, 131.02, 130.0, 130.0, 128.4, 126.6, 124.1, 123.8, 121.3, 119.1, 21.5 ppm.

$^{19}\text{F}\{^1\text{H}\}$ NMR (471 MHz, CDCl_3): δ -68.8 ppm.

IR (solid, ν): 3084 (w), 3006 (w), 2989 (w), 1616 (w), 1605 (w), 1585 (w), 1475 (w), 1385 (s), 1334 (s), 1297 (m), 1262 (s), 1227 (w), 1146 (s), 1123.33 (m), 1093 (m), 1058 (m), 997 (w), 892 (w), 849 (m), 776 (s), 765 (s), 751 (s), 713 (m), 698 (m) cm^{-1} .

HRESI-MS (+, DCM/MeOH, m/z): $[\text{M}+\text{H}]^+$ 254.0808, calc. 254.0787, $[\text{M}_2+\text{H}]^+$ 507.1537, calc. 507.1501.

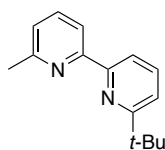
M.p. 85-87 °C.

4.4.3 Deoxygenation of cross-coupling products

According to reported procedure,³ *N*-oxide derivative (1.0 equiv.) was dissolved in DCM (0.1 M in *N*-oxide) and PCl_3 (3.0 equiv.) was added. The solution was stirred for 2 h at 80 °C and subsequently quenched with NaHCO_3 and NaOH was added until pH = 12. The mixture was extracted with DCM, dried over Na_2SO_4 and the solvent was removed.

2-Methyl-6'-*tert*-butyl-2,2'-bipyridine (16a)

[KR 1021]



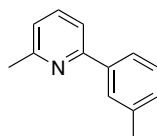
According to the general procedure, bipyridine *N*-oxide **4f** (688 mg, 2.84 mmol) and PCl_3 (0.74 mL, 8.52 mmol) in DCM (28 mL) gave bipyridine **16a** (641 mg, 2.83 mmol, quant.) as a brown oil.

^1H NMR (400 MHz, CDCl_3): δ 8.32 (d, J = 7.9 Hz, 1H), 8.22 (dd, J = 7.8, 0.8 Hz, 1H), 7.70 (dt, J = 14.0, 7.8 Hz, 2H), 7.32 (dd, J = 7.8, 1.0 Hz, 1H), 7.14 (d, J = 7.6 Hz, 1H), 2.62 (s, 3H), 1.43 (s, 9H) ppm.

HRESI-MS (+, MeOH, m/z): $[\text{M}+\text{H}]^+$ 227.1533, calc. 227.1543, $[\text{M}+\text{Na}]^+$ 249.1350, calc. 249.1362.

2-(3-Tolyl)-6-methylpyridine (16b)

[KR 1022]



According to the general procedure, arylpyridine *N*-oxide **5f** (377 mg, 1.89 mmol) and PCl_3 (0.49 mL, 5.60 mmol) gave biaryl **16b** (334 mg, 1.82 mmol, 95%) as a brown oil.

¹H NMR (500 MHz, CDCl₃): δ 7.81 (s, 1H), 7.73 (d, *J* = 7.7 Hz, 1H), 7.63 (t, *J* = 7.7 Hz, 1H), 7.50 (d, *J* = 7.8 Hz, 1H), 7.35 (t, *J* = 7.6 Hz, 1H), 7.21 (d, *J* = 7.5 Hz, 1H), 7.09 (d, *J* = 7.6 Hz, 1H), 2.64 (s, 3H), 2.44 (s, 3H) ppm.

HRESI-MS (+, MeOH, *m/z*): [M+H]⁺ 184.1119, calc. 184.1121, [M+Na]⁺ 206.0932, calc. 206.0940.

4.5 Homocoupling products

Method A

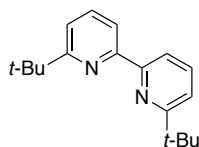
According to literature procedure,¹³⁴ a Schlenk flask was charged with magnesium powder (2.5 equiv.), anhydrous FeCl₃ (0.05 equiv.) and dry THF (0.2 M in aryl halide). Aryl halide (1.0 equiv.) and 1,2-dibromoethane (1.0 equiv.) and were syringed into the mixture. The reaction was refluxed under argon for 2 h and thereafter cooled to ambient temperature. After quenching with aqueous NaOH, the mixture was filtered through filter paper and the solution extracted with DCM. Subsequent drying over Na₂SO₄ and removal of the solvent gave the homocoupling product.

Method B

According to reported procedure,¹³³ NiCl₂·6H₂O (1.0 equiv.) and PPh₃ (4.0 equiv.) were dissolved in DMF (15 mL) and zinc powder (1.5 equiv.) was added. After heating at 50 °C for 1 h, aryl halide (1.0 equiv.) was added and the reaction was further heated at 50 °C over night. The reaction was quenched with aqueous NH₃ and extracted with DCM. Removal of the solvent gave a crude product that was dissolved in Et₂O. Iodine was added while stirring until the brown color persisted. Aqueous Na₂S₂O₃ was added and the solution was extracted with Et₂O. Drying of the combined organic phases with Na₂SO₄ and purification by column chromatography gave the homocoupling product.

6,6'-Di-*tert*-butyl-2,2'-bipyridine (8m)

[KR 1008]



Method B. 2-Bromo-6-*tert*-butylpyridine (1.00 g, 4.68 mmol), NiCl₂·6H₂O (1.11 g, 4.68 mmol), PPh₃ (4.93 g, 18.8 mmol), zinc powder (469 mg, 7.17 mmol) in DMF (15 mL) gave bipyridine **8m** (450 mg, 1.7 mmol, 72%) as a yellow solid.

¹H NMR (400 MHz, CDCl₃): δ 8.33 (d, *J* = 8.0 Hz, 2H), 7.72 (d, *J* = 8.0 Hz, 2H), 7.32 (d, *J* = 8.0 Hz, 2H), 1.43 (s, 18H) ppm.

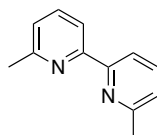
¹³C{¹H} NMR (101 MHz, CDCl₃): δ 168.3, 155.3, 136.9, 118.7, 117.8, 37.7, 30.4 ppm.

The chemical shifts are in agreement with previously reported values.¹³³

HRESI-MS (+, MeOH, m/z): = $[M+H]^+$ 269.2020, calc. 269.2012, $[M+Na]^+$ 291.1835, calc. 291.1832.

6,6'-Dimethyl-2,2'-bipyridine (**8f**)

[ES 4171/KR 1006]



Method A. 2-bromo-6-methylpyridine (756.0 mg, 4.39 mmol), Mg (267.4 mg, 11.0 mmol), 1,2-dibromoethane (0.38 mL, 4.39 mmol) and $FeCl_3$ (35.6 mg, 0.22 mmol) gave bipyridine **8f** (316.8 mg, 1.72 mmol, 78%) as a yellow oil.

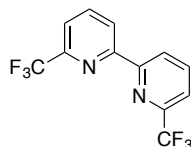
1H NMR (500 MHz, $CDCl_3$): δ 8.20 (d, $J = 7.8$ Hz, 2H), 7.70 (t, $J = 7.7$ Hz, 2H), 7.16 (d, $J = 7.6$ Hz, 2H), 2.64 (s, 6H) ppm.

The chemical shifts are in agreement with previously reported values.²²⁸

HRESI-MS (+, MeOH, m/z): = $[M+H]^+$ 185.1080, calc. 185.1073, $[M+Na]^+$ 229.0496, calc. 229.0485.

6,6'-Di(trifluoromethyl)-2,2'-bipyridine (**8h**)

[ES 6018]



Method A. 2-Bromo-6-trifluoromethylpyridine (486.6 mg, 2.15 mmol), magnesium (130.9 mg, 5.38 mmol), $FeCl_3$ (17.4 mg, 0.11 mmol) and 1,2-dibromoethane (0.19 mL, 2.15 mmol) gave bipyridine **8h** (36.7 mg, 0.13 mmol, 12%) as a light yellow solid after column chromatography (deactivated silica gel, EtOAc/hexane).

1H NMR (400 MHz, $CDCl_3$): δ 8.72 (d, $J = 8.0$ Hz, 2H), 8.02 (t, $J = 7.9$ Hz, 2H), 7.73 (d, $J = 7.7$ Hz, 2H) ppm.

$^{13}C\{^1H\}$ NMR (126 MHz, $CDCl_3$): δ 155.1, 148.0, 138.6, 124.1, 122.6, 120.9 ppm.

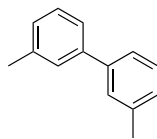
The chemical shifts are in agreement with previously reported values.²²⁹

$^{19}F\{^1H\}$ NMR (471 MHz, $CDCl_3$): δ -68.0 ppm.

HRESI-MS (+, DCM/MeOH, m/z): $[M+Na]^+$ 315.0327, calc. 315.0318.

3,3'-dimethyl-1,1'-biphenyl (9c)

[ES 4170a/KR 1004]



Method A. 3-Bromotoluene (0.25 mL, 2.06 mmol), Mg (125.2 mg, 5.15 mmol), 1,2-dibromoethane (0.18 mL, 2.06 mmol) and FeCl₃ (16.7 mg, 0.10 mmol) gave biphenyl **9c** (170.8 mg, 0.94 mmol, 91%) as a yellow oil.

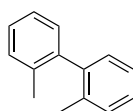
¹H NMR (400 MHz, CDCl₃): δ 7.39 (d, *J* = 8.8 Hz, 4H), 7.32 (t, *J* = 7.7 Hz, 2H), 7.16 (d, *J* = 7.2 Hz, 2H), 2.42 ppm (s, 6H) ppm.

¹³C{¹H} NMR (400 MHz, CDCl₃): δ 141.5, 138.4, 128.7, 128.1, 128.0, 124.4, 21.7 ppm.

The chemical shifts are in agreement with previously reported values.¹³⁴

2,2'-dimethyl-1,1'-biphenyl (9d)

[ES 4170b]



Method A. 2-Bromotoluene (0.25 mL, 2.06 mmol), Mg (125.2 mg, 5.15 mmol), 1,2-dibromoethane (0.18 mL, 2.06 mmol) and FeCl₃ (16.7 mg, 0.10 mmol) gave biphenyl **9d** (163.9 mg, 0.90 mmol, 87%) as a yellow oil.

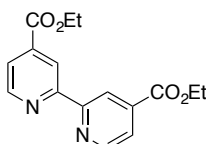
¹H NMR (400 MHz, CDCl₃): δ 7.26 (dd, *J* = 4.9, 1.3 Hz, 4H), 7.24 – 7.16 (m, 2H), 7.10 (d, *J* = 6.9 Hz, 2H), 2.05 (s, 6H) ppm.

¹³C{¹H} NMR (101 MHz, CDCl₃): δ 141.7, 135.9, 129.9, 129.4, 127.2, 125.6, 19.9 ppm.

The chemical shifts are in agreement with previously reported values.²³⁰

4,4'-Diethoxycarbonyl-2,2'-bipyridine (8d)

[ES 3056]



2,2'-Bipyridine-4,4'-dicarboxylic acid (200 mg, 0.82 mmol, 1.0 equiv.) was dissolved in EtOH (40 mL) and H₂SO₄ (0.3 mL) was added. The reaction was refluxed for 48 h and cooled to ambient temperature. Ice water was added and the formed precipitate was filtered and washed with H₂O. Drying of the precipitate gave **8d** (230.9 mg, 0.77 mmol, 94%) as a light pink solid.

¹H NMR (400 MHz, CDCl₃): δ 8.94 (s, 2H), 8.86 (d, *J* = 4.9 Hz, 2H), 7.91 (dd, *J* = 5.0, 1.6 Hz, 2H), 4.45 (q, *J* = 7.1 Hz, 4H), 1.44 (t, *J* = 7.1 Hz, 6H) ppm.

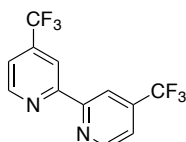
The chemical shifts are in agreement with previously reported values.²³¹

¹³C{¹H} NMR (101 MHz, CDCl₃): δ 165.2, 156.6, 150.2, 139.1, 123.4, 120.7, 62.0, 14.4 ppm.

HRESI-MS (+, MeOH, *m/z*): [M+H]⁺ 301.1195, calc. 301.1183, [M+Na]⁺ 323.1015, calc. 323.1002.

4,4'-Di(trifluoromethyl)-2,2'-bipyridine (**8e**)

[ES 2160]



4,4'-Di(trifluoromethyl)-2,2'-bipyridine *N*-oxide (125 mg, 0.41 mmol, 1.0 equiv.) was dissolved in CHCl₃ (10 mL) and PCl₃ (0.08 mL, 0.98 mmol, 2.4 equiv. in two portions) was added. The reaction was heated at 80 °C for 3 h and Na₂CO₃ was added to quench remaining PCl₃. After adjusting the pH to 12 with NaOH, the mixture was extracted with DCM and the solvent was removed, yielding bipyridine **8e** (112 mg, 0.38 mmol, 93%) as a light yellow solid.

¹H NMR: (400 MHz, CDCl₃): δ 8.88 (d, *J* = 5.1 Hz, 1H), 8.73 (s, 1H), 7.66 – 7.48 (m, 1H) ppm.

¹³C{¹H} NMR (101 MHz, CDCl₃): δ 156.1, 150.3, 139.7 (d, *J* = 34.3 Hz), 122.9 (d, *J* = 273.2 Hz), 120.0, 117.2 ppm.

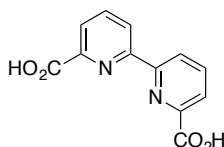
The chemical shifts are in agreement with previously reported values.²²⁹

¹⁹F{¹H} NMR (376 MHz, CDCl₃): δ -64.7 ppm.

HRESI-MS (+, MeOH, *m/z*): [M+H]⁺ 293.0507, calc. 293.0508, [M+Na]⁺ 315.0328, calc. 315.0327.

2,2'-Bipyridine-6,6'-dicarboxylic acid (**8ga**)

[KR 1014]



According to reported procedure,²³² 6,6'-dimethyl-2,2'-bipyridine (650 mg, 3.53 mmol, 1.0 equiv.) was added to concentrated H₂SO₄ (13 mL) under stirring. The solution was cooled in an ice bath and CrO₃ (2.10 g, 21.0 mmol, 6.0 equiv.) was slowly added while keeping the temperature under 40 °C. After stirring over night, the mixture was poured on crushed ice and the colorless precipitate was filtered off, washed with cold water and dried overnight at 40 °C. The title compound **8ga** (860 mg, 3.52 mmol, 97%) was obtained as a colorless solid.

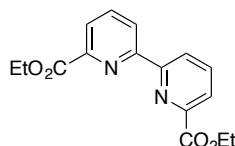
$^1\text{H NMR}$ (400 MHz, $\text{DMSO-}d_6$): δ 8.75 (d, $J = 7.7$ Hz, 2H), 8.17 (dt, $J = 7.6, 15.8$ Hz, 4H) ppm.

The chemical shifts are in agreement with previously reported values.²³²

HRESI-MS (+, MeOH, m/z): $[\text{M}+\text{H}]^+$ 245.0555, calc. 245.0557, $[\text{M}+\text{Na}]^+$ 267.0374, calc. 267.0376.

6,6'-Diethoxycarbonyl-2,2'-bipyridine (**8g**)

[KR 1015]



According to reported procedure,²³² 6,6'-bipicolinic acid (860 mg, 3.52 mmol) was dissolved in EtOH (70 mL) and H_2SO_4 (3.7 mL) was added. The solution was stirred for 30 min at room temperature and subsequently refluxed for 19 h. After cooling to 0 °C, a saturated NaHCO_3 was added and the mixture was extracted with DCM. Drying of the combined organic phases and drying on high vacuum yielded the title bipyridine **8g** (847 mg, 2.82 mmol, 80%) as a colorless solid.

$^1\text{H NMR}$ (400 MHz, CDCl_3): δ 8.77 (d, $J = 7.9$ Hz, 2H), 8.15 (d, $J = 7.7$ Hz, 2H), 7.99 (t, $J = 7.8$ Hz, 2H), 4.50 (q, $J = 7.1$ Hz, 4H), 1.48 (t, $J = 7.1$ Hz, 6H) ppm.

The chemical shifts are in agreement with previously reported values.²³²

$^{13}\text{C}\{^1\text{H}\}$ NMR (126 MHz, CDCl_3): δ 165.3, 155.6, 147.9, 138.1, 125.5, 124.9, 62.1, 14.5 ppm.

HRESI-MS (+, MeOH, m/z): $[\text{M}+\text{H}]^+$ 301.1237, calc. 301.1183, $[\text{M}+\text{Na}]^+$ 323.1012, calc. 323.1002.

4.6 Kinetic measurements of direct arylations

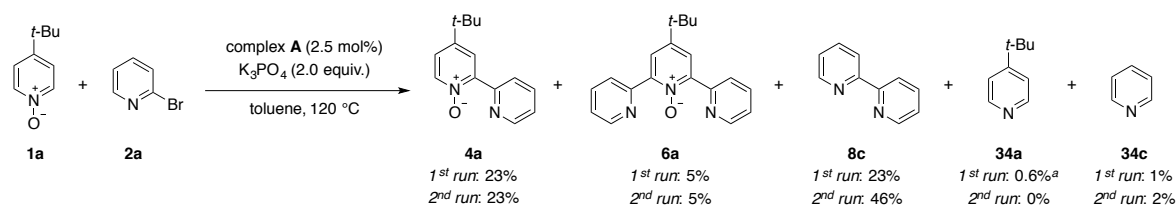
General procedure

In a glovebox, pyridine *N*-oxide derivative (7.0 mmol, 2.0 equiv.), bromoarene (3.50 mmol, 1.0 equiv.), cyclometalated palladium complex **A** (0.088 mmol, 0.025 equiv.), K_3PO_4 (7.0 mmol, 2.0 equiv.), decane (1.8 mmol, 0.5 equiv.) and 1,3,5-trimethoxybenene (1.8 mmol, 0.5 equiv.) were weighed into a 25 mL round-bottom Schlenk flask. Toluene (7.0 mL) was added and the mixture was stirred for 15 minutes at r.t. outside of the glovebox. The first aliquot (0.05 mL, $t = 0$ min) was withdrawn. The reaction mixture was to 120 °C and aliquots of 0.05 mL were withdrawn at $t = 5, 10, 20, 30, 40, 50, 60$ and 120 minutes. The samples were quenched with cold toluene (0.75 mL). A last aliquot was withdrawn at $t = 24$ h to verify that the reaction had reached completion.

Of each aliquot, 0.20 mL was measured by GC-FID to quantify aryl bromide **2a** or **3a** consumption and biaryl product **8** and **9** formation. The remains of the sample were evaporated and the residue dissolved in CDCl_3 (0.8 mL) and filtered through a pipette with celite. An $^1\text{H NMR}$ was measured to give the *N*-oxide **1** concentration when soluble at room temperature, arylpyridine *N*-oxide product **4**

and **5** and biarylpyridine *N*-oxide **6** and **7** product concentrations. Substrate consumption and product formation rates were determined from the initial linear rate during the first 60 minutes. Rate of biarylpyridine *N*-oxide formation was determined from when formed to $t = 120$ min. For overlapping peaks, the last ^1H NMR was recorded in an alternative solvent. Each reaction was run in duplicate. Formation of reduced *N*-oxide **34** and dehalogenated starting material **34c** or **35a** are not shown in plots.

4.6.1 Reactions with bromopyridine



^abased on pyridine *N*-oxide **1a**.

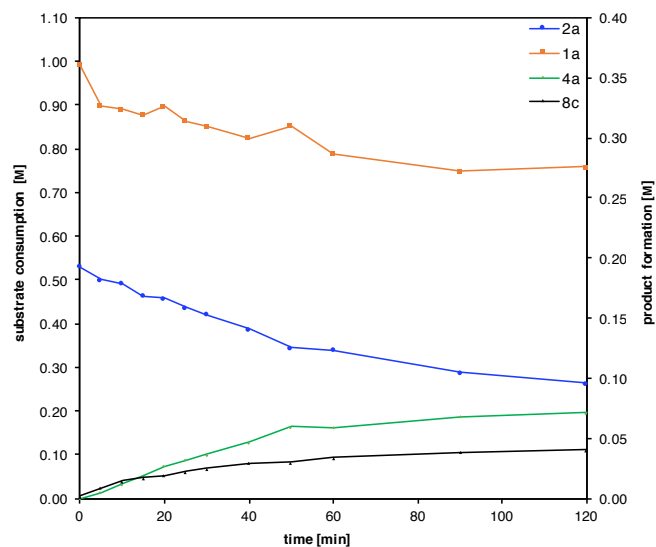
[ES 1166/ES 2024]

According to general procedure, *tert*-butyl pyridine *N*-oxide **1a** (1.06 g, 7.0 mmol), 2-bromopyridine **2a** (553 mg, 3.50 mmol), complex **A** (64.2 mg, 0.088 mmol), K_3PO_4 (1.49 mg, 7.0 mmol), decane (249 mg) and 1,3,5-trimethoxybenzene (294 mg) in toluene (7.0 mL) were monitored over 24 h.

1st run:

entry	time [min]	2a [M]	1a [M]	4a [M]	6a [M]	8c [M]	34a [M]	34c [M]
1	0	0.532	0.993			0.002	0.036	
2	5	0.501	0.899	0.005		0.009	0.035	0.001
3	10	0.491	0.890	0.012		0.014	0.037	0.003
4	15	0.463	0.877	0.018		0.018	0.037	0.003
5	20	0.458	0.897	0.027		0.019	0.037	0.003
6	25	0.437	0.863	0.032		0.023	0.039	0.004
7	30	0.421	0.851	0.037		0.025	0.039	0.004
8	40	0.388	0.824	0.047		0.030	0.040	0.004
9	50	0.346	0.852	0.060		0.030	0.039	0.004
10	60	0.340	0.789	0.059		0.034	0.041	0.005
11	90	0.288	0.749	0.068		0.038	0.043	0.006
12	120	0.264	0.759	0.072		0.040	0.043	0.006
13	1440	0.074	0.737	0.116	0.013	0.057	0.042	0.007

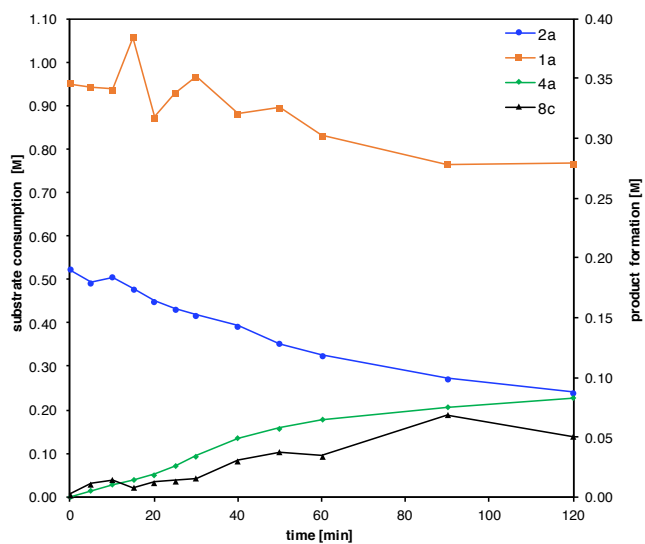
4 Experimental Section



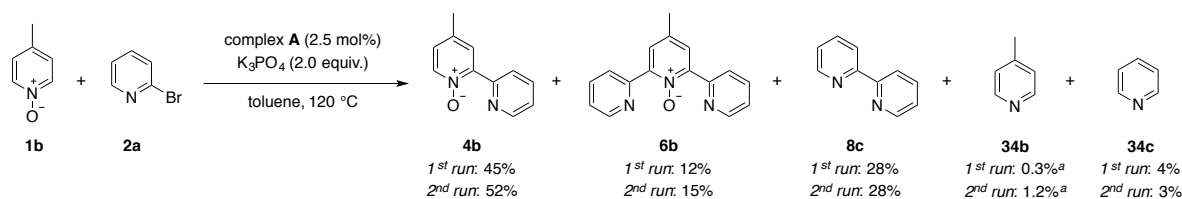
	k_{obs} [mM/min]	R^2
2a	-3.5	0.99
1a	-2.3	0.63
4a	+1.2	1.00
8c	+0.80	0.94

2nd run:

entry	time [min]	2a [M]	1a [M]	4a [M]	6a [M]	8c [M]	34a [M]	34c [M]
1	0	0.523	0.950			0.002	0.044	
2	5	0.492	0.944	0.005		0.011	0.042	0.002
3	10	0.506	0.938	0.010		0.014	0.046	0.003
4	15	0.479	1.057	0.014		0.008	0.043	0.003
5	20	0.450	0.874	0.019		0.012	0.039	0.004
6	25	0.432	0.929	0.026		0.013	0.038	0.005
7	30	0.418	0.967	0.034		0.016	0.039	0.006
8	40	0.394	0.881	0.049		0.031	0.043	0.006
9	50	0.352	0.896	0.058		0.038	0.037	0.007
10	60	0.326	0.831	0.065		0.035	0.038	0.007
11	90	0.272	0.765	0.075		0.068	0.040	0.008
12	120	0.240	0.767	0.083		0.050	0.040	0.008
13	1440	0.058	0.689	0.114	0.011	0.116	0.042	0.010



	k_{obs} [mM/min]	R^2
2a	-3.4	0.98
4a	+1.2	0.99
8c	+0.68	0.93



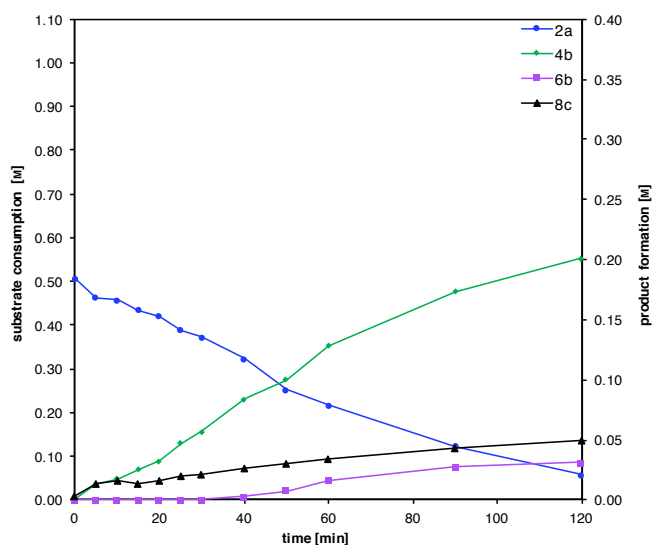
^abased on pyridine *N*-oxide **1b**.

[ES 1172/ES 2020]

According to general procedure, methyl pyridine *N*-oxide **1b** (764 mg, 7.0 mmol), 2-bromopyridine **2a** (553 mg, 3.50 mmol), complex **A** (64.2 mg, 0.088 mmol), K_3PO_4 (1.49 mg, 7.0 mmol), decane (249 mg) and 1,3,5-trimethoxybenzene (294 mg) in toluene (7.0 mL) were monitored over 24 h.

1st run:

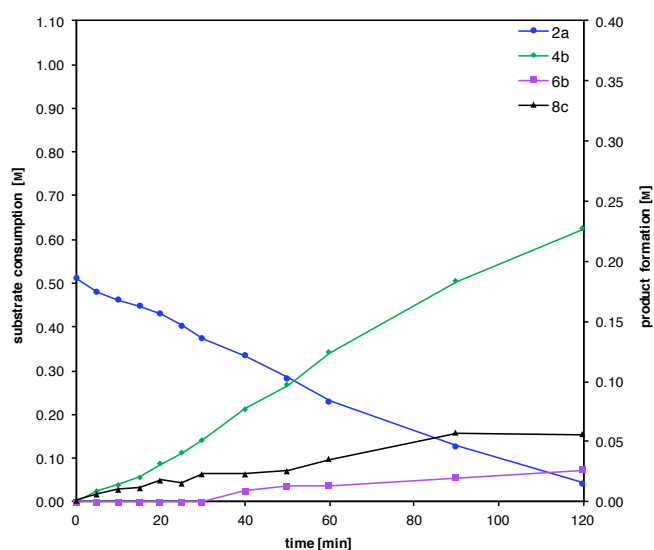
entry	time [min]	2a [M]	4b [M]	6b [M]	8c [M]	34b [M]	34c [M]
1	0	0.507			0.003	0.004	0.004
2	5	0.462	0.013		0.013	0.005	0.002
3	10	0.457	0.018		0.016	0.005	0.000
4	15	0.434	0.025		0.014	0.004	0.000
5	20	0.421	0.033		0.016	0.007	0.000
6	25	0.388	0.047		0.020	0.003	0.002
7	30	0.372	0.057		0.021	0.004	0.002
8	40	0.324	0.084	0.003	0.026	0.005	0.004
9	50	0.252	0.100	0.008	0.030	0.003	0.005
10	60	0.218	0.129	0.017	0.034	0.003	0.007
11	90	0.123	0.173	0.028	0.044	0.003	0.010
12	120	0.058	0.201	0.031	0.049	0.003	0.014
13	1440	0	0.227	0.030	0.070	0.007	0.020



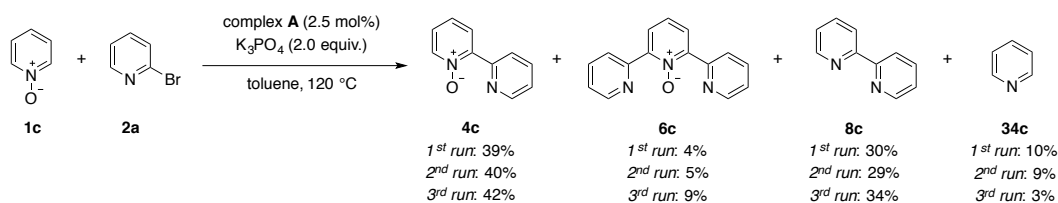
	k_{obs} [mM/min]	R^2
2a	-5.0	0.99
4b	+2.2	0.99
8c	+0.40	0.99

2nd run:

entry	time [min]	2a [M]	4b [M]	6b [M]	8c [M]	34b [M]	34c [M]
1	0	0.511			0.001	0.003	
2	5	0.480	0.009		0.006	0.011	0.002
3	10	0.463	0.014		0.010	0.019	0.003
4	15	0.448	0.021		0.012	0.007	0.003
5	20	0.429	0.031		0.018	0.013	0.004
6	25	0.404	0.041		0.015	0.007	0.005
7	30	0.373	0.052		0.023	0.015	0.006
8	40	0.335	0.077	0.009	0.023	0.007	0.007
9	50	0.283	0.097	0.013	0.026	0.007	0.008
10	60	0.230	0.124	0.013	0.035	0.009	0.010
11	90	0.127	0.183	0.020	0.058	0.013	0.013
12	120	0.043	0.227	0.026	0.056	0.009	0.016
13	1440	0	0.258	0.037	0.071	0.015	0.016



	k_{obs} [mM/min]	R^2
2a	-4.6	0.99
4b	+2.2	1.00
8c	+0.50	0.94

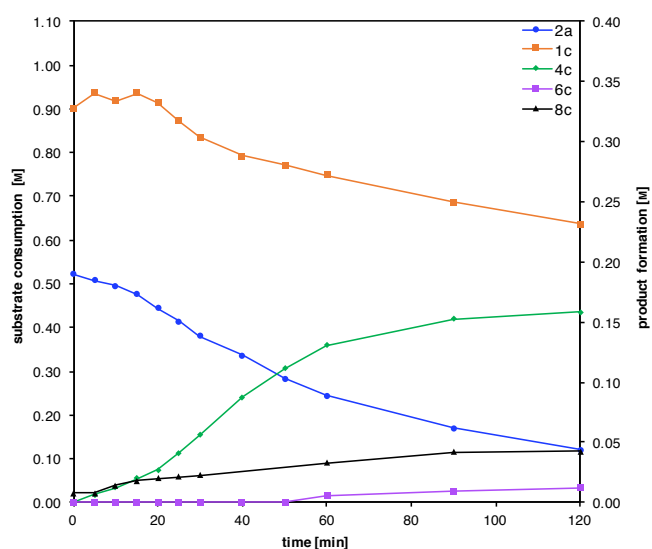


[ES 1164/ES 1176/ES 1184]

According to general procedure, pyridine *N*-oxide **1c** (666 mg, 7.0 mmol), 2-bromopyridine **2a** (553 mg, 3.50 mmol), complex **A** (64.2 mg, 0.088 mmol), K₃PO₄ (1.49 mg, 7.0 mmol), decane (248 mg) and 1,3,5-trimethoxybenzene (294 mg) in toluene (7.0 mL) were monitored over 24 h.

1st run:

entry	time [min]	2a [M]	1c [M]	4c [M]	6c [M]	8c [M]	34c [M]
1	0	0.523	0.903			0.008	0.003
2	5	0.509	0.936	0.006		0.008	0.002
3	10	0.496	0.919	0.013		0.014	0.004
4	15	0.475	0.936	0.020		0.018	0.005
5	20	0.443	0.915	0.027		0.020	0.005
6	25	0.414	0.873	0.041		0.021	0.005
7	30	0.380	0.836	0.056		0.023	0.005
8	40	0.336	0.793	0.088		0.053	0.007
9	50	0.284	0.772	0.111		0.036	0.009
10	60	0.243	0.749	0.131	0.006	0.033	0.010
11	90	0.171	0.686	0.153	0.009	0.042	0.018
12	120	0.121	0.638	0.159	0.012	0.042	0.024
13	1440	0	0.567	0.196	0.010	0.076	0.049



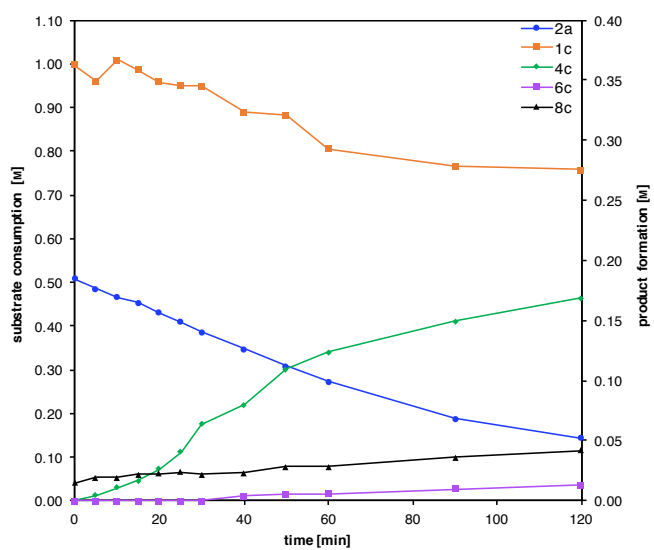
	k_{obs} [mM/min]	R^2
2a	-5.0	1.00
1c	-4.0	0.93
4c	+2.6	0.99
8c	+0.68	0.90

2nd run:

entry	time [min]	2a [M]	1c [M]	4c [M]	6c [M]	8c [M]	34c [M]
1	0	0.508	0.996			0.015	0.005
2	5	0.485	0.959	0.005		0.019	0.004
3	10	0.465	1.009	0.011		0.019	0.004
4	15	0.453	0.987	0.017		0.022	0.004
5	20	0.430	0.957	0.027		0.023	0.004
6	25	0.409	0.950	0.041		0.024	0.004
7	30	0.385	0.948	0.064		0.022	0.004
8	40	0.347	0.889	0.080	0.004	0.024	0.005
9	50	0.307	0.882	0.110	0.005	0.029	0.006
10	60	0.272	0.805	0.123	0.006	0.028	0.008
11	90	0.187	0.764	0.150	0.010	0.036	0.015

4 Experimental Section

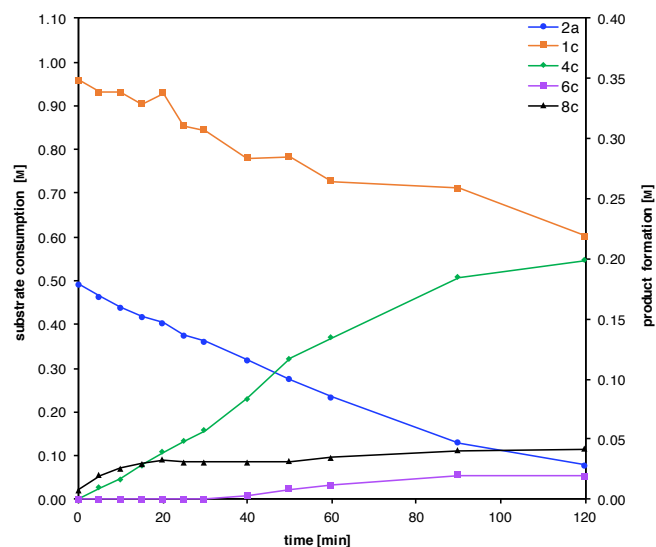
12	120	0.143	0.757	0.168	0.013	0.042	0.024
13	1440	0	0.589	0.199	0.013	0.073	0.044



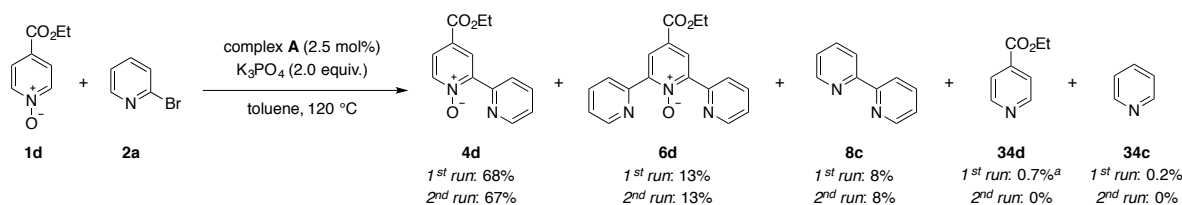
	k_{obs} [mM/min]	R^2
2a	-4.2	1.00
1c	-3.7	0.96
4c	+2.4	0.98
6c	+0.13	0.96

3rd run:

entry	time [min]	2a [M]	1c [M]	4c [M]	6c [M]	8c [M]	34c [M]
1	0	0.491	0.959			0.008	0.018
2	5	0.463	0.932	0.009		0.020	0.012
3	10	0.440	0.932	0.017		0.026	0.010
4	15	0.417	0.904	0.028		0.029	0.009
5	20	0.403	0.929	0.039		0.033	0.010
6	25	0.376	0.855	0.048		0.031	0.009
7	30	0.362	0.845	0.057		0.031	0.010
8	40	0.319	0.780	0.084	0.003	0.031	0.010
9	50	0.274	0.785	0.117	0.009	0.032	0.011
10	60	0.233	0.727	0.135	0.012	0.035	0.013
11	90	0.129	0.711	0.184	0.020	0.040	0.020
12	120	0.078	0.601	0.199	0.019	0.042	0.026
13	1440	0	0.448	0.208	0.023	0.085	0.018



	k_{obs} [mM/min]	R^2
2a	-4.2	1.00
1c	-3.9	0.91
4c	+2.4	0.99
6c	+0.34	0.98
8c	+1.2	0.92



^abased on pyridine *N*-oxide **1d**.

[ES 1180/ES 2018]

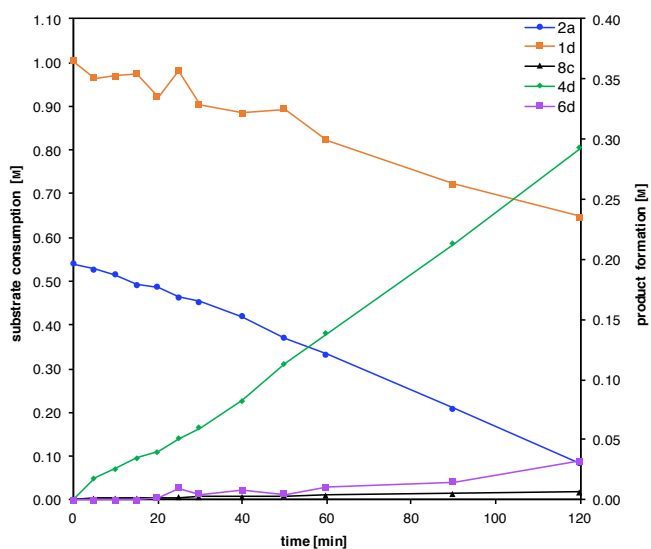
According to general procedure, ester pyridine *N*-oxide **1d** (1.17 g, 7.0 mmol), 2-bromopyridine **2a** (553 mg, 3.50 mmol), complex **A** (64.2 mg, 0.088 mmol), K_3PO_4 (1.49 mg, 7.0 mmol), decane (248 mg) and 1,3,5-trimethoxybenzene (294 mg) in toluene (7.0 mL) were monitored over 24 h. Due to overlap of peaks in the ^1H NMR spectra, [**4d**] was calculated by subtraction of [**6d**] from an overlapping peak.

1st run:

entry	time [min]	2a [M]	1d [M]	4d [M]	6d [M]	8c [M]	34d [M]	34c [M]
1	0	0.540	1.004			0.002	0.007	0.001
2	5	0.527	0.964	0.018		0.003	0.008	0.002
3	10	0.515	0.971	0.026		0.003	0.007	0.001
4	15	0.492	0.976	0.035		0.004	0.009	0.002
5	20	0.486	0.923	0.040	0.002	0.005	0.008	0.002
6	25	0.464	0.982	0.051	0.010	0.006	0.008	0.002
7	30	0.453	0.904	0.060	0.004	0.007	0.008	0.002
8	40	0.420	0.885	0.082	0.008	0.008	0.008	0.002
9	50	0.370	0.893	0.113	0.005	0.009	0.008	0.003
10	60	0.333	0.824	0.138	0.010	0.011	0.010	0.003
11	90	0.210	0.723	0.213	0.015	0.015	0.010	0.003

4 Experimental Section

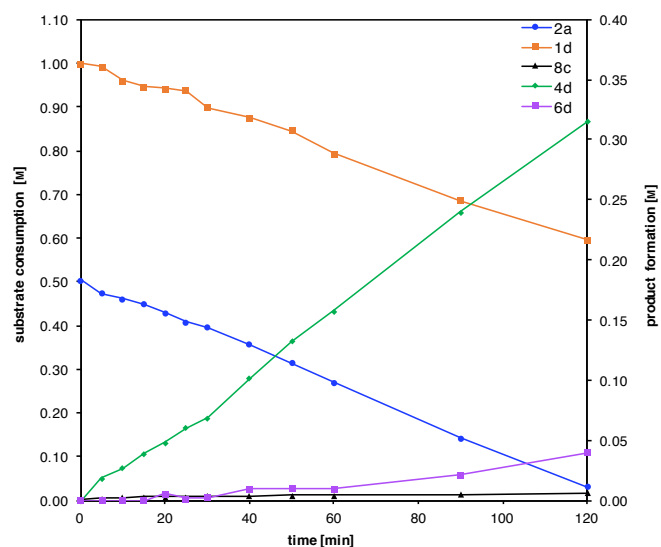
12	120	0.083	0.647	0.293	0.032	0.018	0.009	0.003
13	1440	0	0.476	0.339	0.033	0.020	0.014	0.003



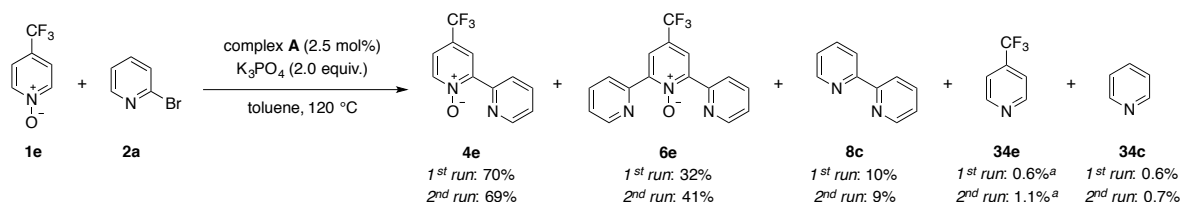
	k_{obs} [mM/min]	R^2
2a	-3.4	0.99
1d	-2.6	0.82
4d	+2.2	0.99
6d	+0.29	0.89
8c	+0.13	0.99

2nd run:

entry	time [min]	2a [M]	1d [M]	4d [M]	6d [M]	8c [M]	34d [M]	34c [M]
1	0	0.504	0.999			0.002	0.017	0.004
2	5	0.474	0.992	0.019		0.005	0.016	0.004
3	10	0.462	0.961	0.027		0.007	0.014	0.005
4	15	0.449	0.946	0.039		0.008	0.014	0.004
5	20	0.430	0.942	0.048	0.006	0.009	0.013	0.005
6	25	0.408	0.937	0.060	0.002	0.009	0.012	0.005
7	30	0.395	0.898	0.069	0.002	0.010	0.012	0.005
8	40	0.357	0.875	0.101	0.009	0.011	0.011	0.005
9	50	0.314	0.845	0.133	0.010	0.011	0.011	0.005
10	60	0.270	0.793	0.157	0.009	0.012	0.011	0.005
11	90	0.143	0.687	0.240	0.021	0.014	0.010	0.005
12	120	0.031	0.597	0.315	0.040	0.017	0.011	0.004
13	1440	0	0.475	0.333	0.032	0.020	0.017	0.004



	k_{obs} [mM/min]	R^2
2a	-3.8	1.00
1d	-3.3	0.98
4d	+2.6	0.99
6d	+0.38	0.95
8c	+0.35	0.93



^abased on pyridine *N*-oxide **1e**.

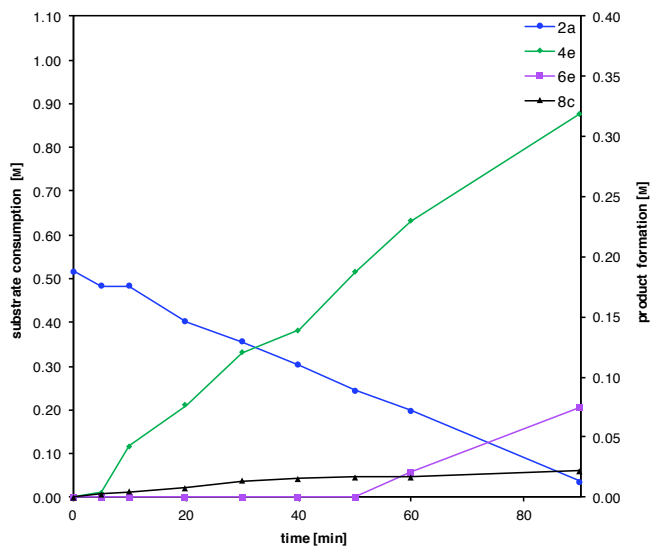
[ES 1160/ES 2030]

According to general procedure, trifluoromethyl pyridine *N*-oxide **1e** (1.14 g, 7.0 mmol), 2-bromopyridine **2a** (553 mg, 3.50 mmol), complex **A** (64.2 mg, 0.088 mmol), K_3PO_4 (1.49 mg, 7.0 mmol), decane (249 mg) and 1,3,5-trimethoxybenzene (294 mg) in toluene (7.0 mL) were monitored over 24 h. Due to overlap of peaks in the ^1H NMR spectra, **[6e]** was calculated by subtraction of **[4e]** from an overlapping peak. Rate of formation of **8c** was determined from $t = 0$ to $t = 30$ minutes.

1st run:

entry	time [min]	2a [M]	4e [M]	6e [M]	8c [M]	34e [M]	34c [M]
1	0	0.517				0.001	
2	5	0.483	0.004		0.003	0.000	
3	10	0.483	0.043		0.005	0.001	
4	20	0.401	0.077		0.008	0.000	
5	30	0.356	0.120		0.014	0.002	0.001
6	40	0.302	0.139		0.016	0.000	0.000
7	50	0.245	0.188		0.017	0.002	0.000
8	60	0.199	0.230	0.020	0.017	0.000	0.000
9	90	0.035	0.320	0.075	0.022	0.003	0.002
10	1440	0	0.350	0.079	0.025	0.007	0.003

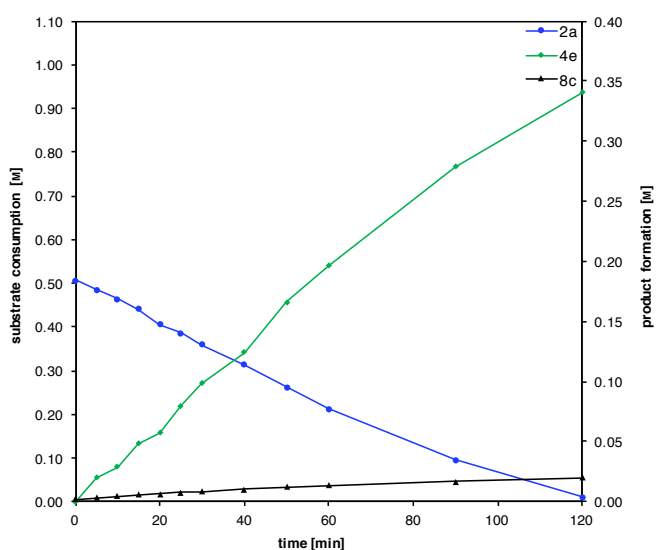
4 Experimental Section



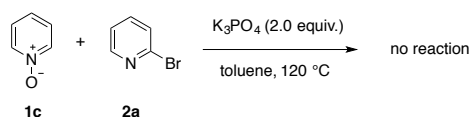
	k_{obs} [mM/min]	R^2
2a	-5.4	1.00
4e	+3.6	0.99
8c	+0.43	0.99

2nd run:

entry	time [min]	2a [M]	4e [M]	6e [M]	8c [M]	34e [M]	34c [M]
1	0	0.506			0.002		
2	5	0.485	0.020	0.032	0.004		
3	10	0.463	0.029	0.025	0.005	0.001	0.001
4	15	0.441	0.048	0.021	0.006	0.000	0.002
5	20	0.406	0.057	0.041	0.006	0.002	0.002
6	25	0.387	0.080	0.019	0.008	0.002	0.003
7	30	0.360	0.098	0.041	0.008	0.002	0.003
8	40	0.313	0.124	0.044	0.010	0.002	0.003
9	50	0.261	0.166	0.045	0.012	0.003	0.003
10	60	0.213	0.196	0.051	0.014	0.003	0.004
11	90	0.096	0.279	0.063	0.017	0.005	0.005
12	120	0.011	0.340	0.110	0.020	0.006	0.005
13	1440	0	0.347	0.103	0.021	0.011	0.004



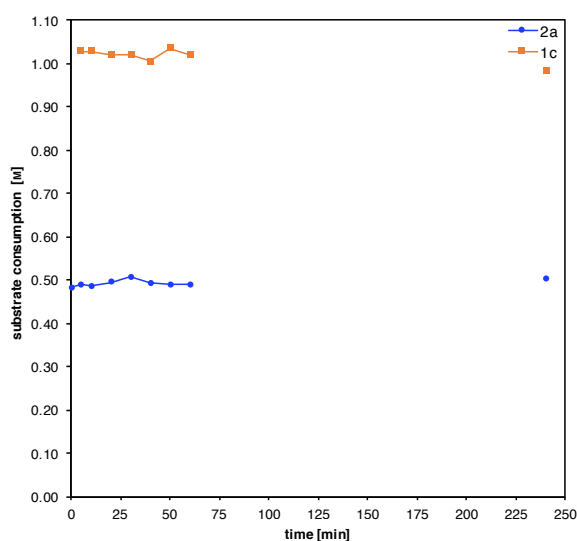
	k_{obs} [mM/min]	R^2
2a	-4.9	1.00
4e	+3.3	1.00
8c	+0.22	0.99



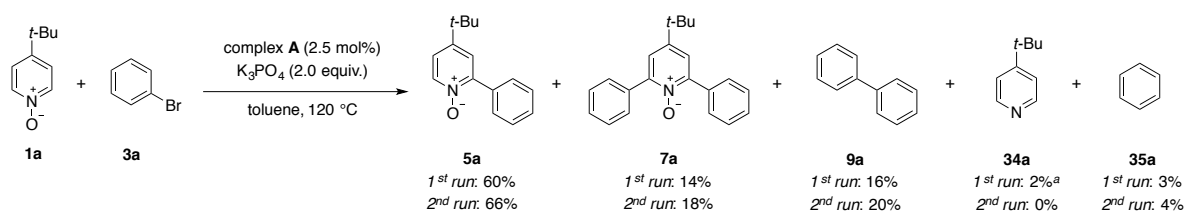
[ES 1156]

According to general procedure, pyridine *N*-oxide **1c** (666 mg, 7.0 mmol), 2-bromopyridine **2a** (553 mg, 3.50 mmol), K_3PO_4 (1.49 mg, 7.0 mmol), decane (249 mg) and 1,3,5-trimethoxybenzene (589 mg) in toluene (7.0 mL) were monitored over 24 h.

entry	time [min]	2a [M]	1c [M]
1	0	0.482	1.028
2	5	0.489	1.028
3	10	0.485	1.020
4	20	0.494	1.020
5	30	0.506	1.005
6	40	0.492	1.035
7	50	0.489	1.020
8	60	0.489	1.020
9	240	0.502	0.983
10	1440	0.487	1.020



4.6.2 Reactions with bromobenzene

^abased on pyridine *N*-oxide **1a**.

[ES 1168/ES 2022]

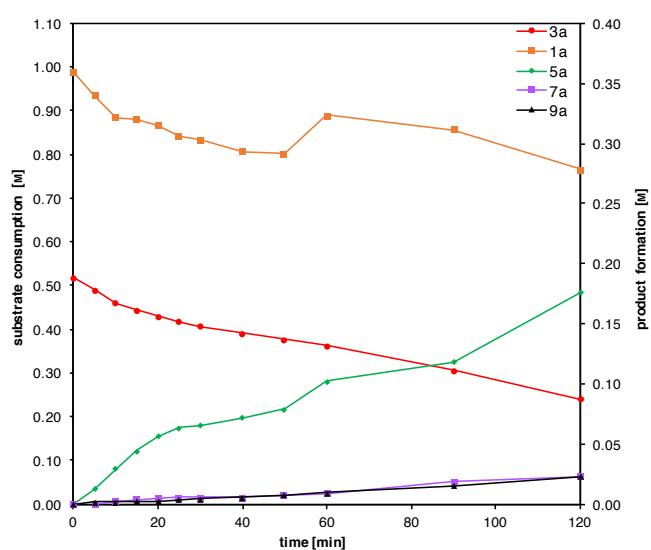
According to general procedure, *tert*-butyl pyridine *N*-oxide **1a** (1.06 g, 7.0 mmol), bromobenzene **3a** (550 mg, 3.50 mmol), complex **A** (64.2 mg, 0.088 mmol), K_3PO_4 (1.49 mg, 7.0 mmol), decane (249 mg) and 1,3,5-trimethoxybenzene (295 mg) in toluene (7.0 mL) were monitored over 24 h.

1st run:

entry	time [min]	3a [M]	1a [M]	5a [M]	7a [M]	9a [M]	34a [M]	35a [M]
1	0	0.518	0.989				0.039	0.004
2	5	0.489	0.934	0.012		0.002	0.036	0.006

4 Experimental Section

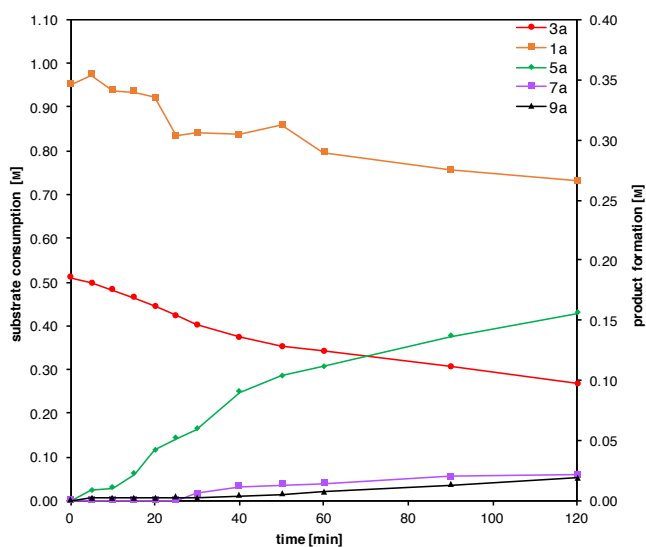
3	10	0.460	0.884	0.030	0.002	0.002	0.036	0.010
4	15	0.443	0.880	0.044	0.004	0.002	0.035	0.012
5	20	0.430	0.867	0.057	0.005	0.003	0.036	0.013
6	25	0.417	0.843	0.063	0.006	0.003	0.038	0.014
7	30	0.407	0.833	0.065	0.006	0.004	0.038	0.014
8	40	0.390	0.806	0.072	0.006	0.005	0.040	0.014
9	50	0.376	0.802	0.079	0.008	0.008	0.042	0.015
10	60	0.362	0.890	0.102	0.009	0.009	0.043	0.016
11	90	0.306	0.856	0.118	0.018	0.015	0.046	0.016
12	120	0.240	0.766	0.176	0.023	0.023	0.049	0.017
13	1440	0	0.545	0.299	0.036	0.040	0.055	0.018



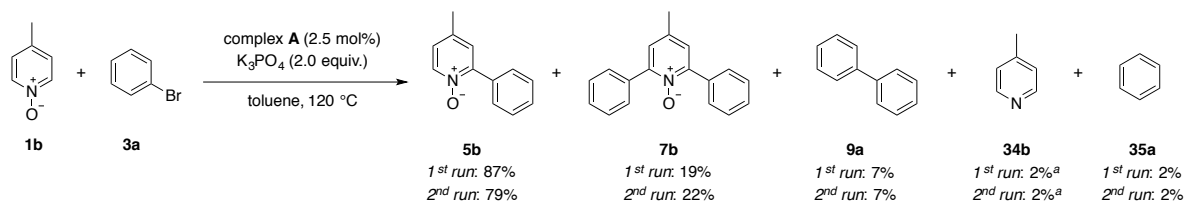
	k_{obs} [mM/min]	R^2
3a	-4.0	0.96
1a	-5.4	0.89
5a	+2.7	0.99
7a	+0.33	0.99
9a	+0.15	0.98

2nd run:

entry	time [min]	3a [M]	1a [M]	5a [M]	7a [M]	9a [M]	34a [M]	35a [M]
1	0	0.510	0.952				0.083	0.002
2	5	0.497	0.973	0.008		0.002	0.062	0.011
3	10	0.481	0.938	0.011		0.002	0.059	0.015
4	15	0.465	0.935	0.022		0.002	0.059	0.019
5	20	0.444	0.921	0.042		0.002	0.058	0.022
6	25	0.423	0.834	0.051		0.002	0.058	0.022
7	30	0.401	0.840	0.059	0.006	0.002	0.057	0.025
8	40	0.374	0.838	0.090	0.012	0.004	0.061	0.027
9	50	0.353	0.858	0.103	0.013	0.005	0.060	0.028
10	60	0.342	0.796	0.111	0.014	0.007	0.063	0.026
11	90	0.306	0.756	0.137	0.020	0.013	0.065	0.029
12	120	0.267	0.731	0.156	0.021	0.019	0.066	0.029
13	1440	0	0.554	0.331	0.046	0.051	0.075	0.021



	k_{obs} [mM/min]	R^2
3a	-3.6	0.99
1a	-3.8	0.81
5a	+2.3	0.98
7a	+0.39	0.84
9a	+0.19	1.00



^abased on pyridine *N*-oxide **1b**.

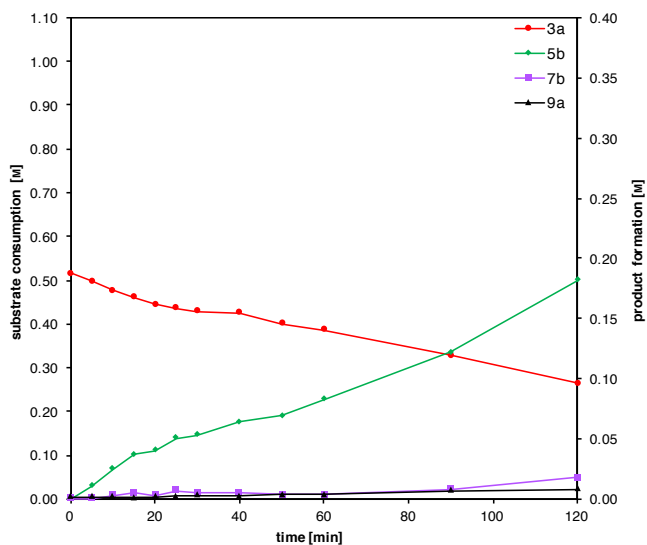
[ES 2002/ES 2028]

According to general procedure, methyl pyridine *N*-oxide **1b** (764 mg, 7.0 mmol), bromobenzene **3a** (550 mg, 3.50 mmol), complex **A** (64.2 mg, 0.088 mmol), K_3PO_4 (1.49 mg, 7.0 mmol), decane (249 mg) and 1,3,5-trimethoxybenzene (295 mg) in toluene (7.0 mL) were monitored over 24 h.

1st run:

entry	time [min]	3a [M]	5b [M]	7b [M]	9a [M]	34b [M]	35a [M]
1	0	0.514			0.001	0.002	0.005
2	5	0.498	0.010		0.001	0.005	0.010
3	10	0.477	0.025	0.002	0.001	0.006	0.013
4	15	0.461	0.037	0.004	0.001	0.006	0.015
5	20	0.444	0.040	0.003	0.001	0.006	0.015
6	25	0.436	0.050	0.007	0.002	0.006	0.015
7	30	0.428	0.053	0.004	0.003	0.007	0.015
8	40	0.425	0.064	0.004	0.002	0.006	0.013
9	50	0.399	0.069	0.003	0.003	0.008	0.015
10	60	0.386	0.082	0.003	0.003	0.006	0.018
11	90	0.328	0.122	0.008	0.006	0.009	0.017
12	120	0.263	0.181	0.018	0.007	0.009	0.015
13	1440	0	0.436	0.048	0.018	0.020	0.014

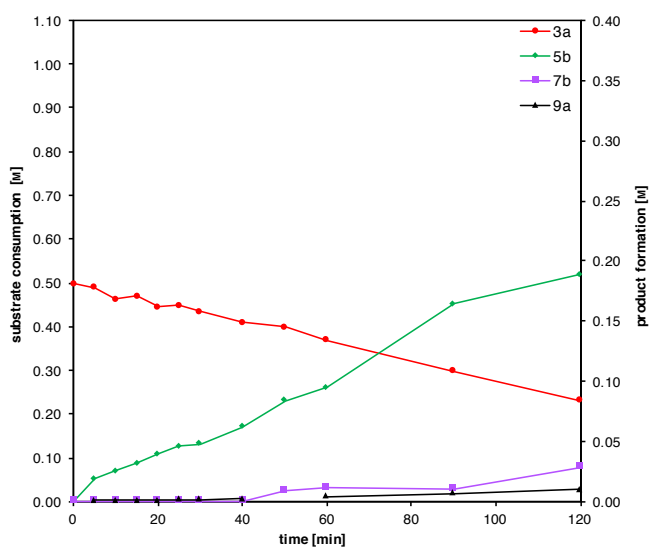
4 Experimental Section



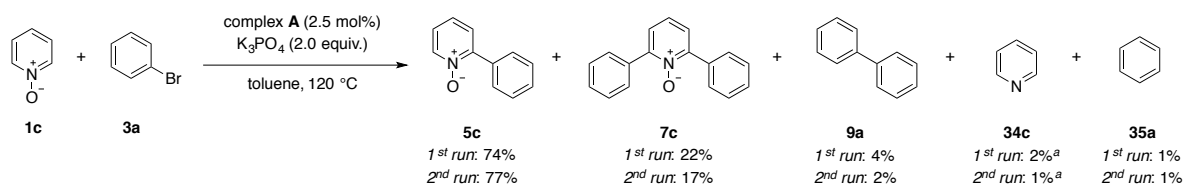
	k_{obs} [mM/min]	R^2
3a	-2.4	0.91
5b	+1.6	0.95
7b	+0.21	0.93
9a	+0.063	0.96

2nd run:

entry	time [min]	3a [M]	5b [M]	7b [M]	9a [M]	34b [M]	35a [M]
1	0	0.497			0.001	0.013	0.003
2	5	0.488	0.019		0.001	0.043	0.008
3	10	0.462	0.025		0.001	0.008	0.009
4	15	0.469	0.032		0.001	0.023	0.010
5	20	0.445	0.039		0.001	0.006	0.009
6	25	0.448	0.046		0.001	0.008	0.011
7	30	0.434	0.048		0.001	0.014	0.010
8	40	0.409	0.062		0.002	0.016	0.011
9	50	0.399	0.083	0.009	0.000	0.019	0.017
10	60	0.367	0.095	0.012	0.004	0.014	0.011
11	90	0.298	0.164	0.011	0.006	0.016	0.014
12	120	0.230	0.189	0.028	0.010	0.017	0.014
13	1440	0	0.396	0.055	0.017	0.033	0.011



	k_{obs} [mM/min]	R^2
3a	-2.0	0.98
5b	+1.5	0.98
7b	+0.28	0.81
9a	+0.084	0.99

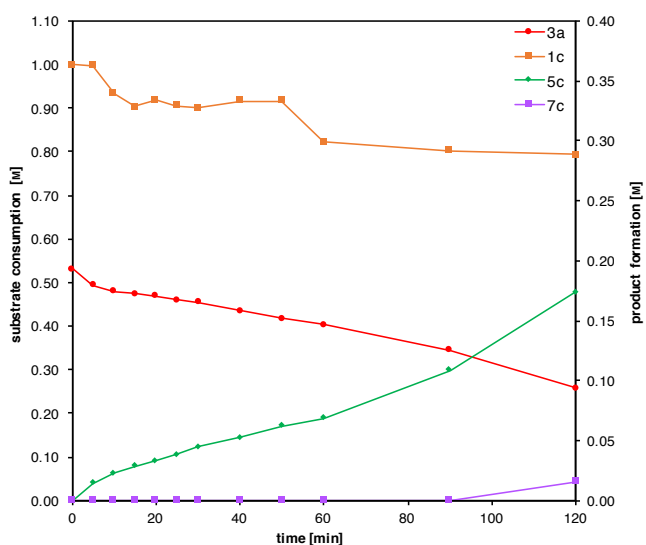


[ES 1182/ES 2006]

According to general procedure, pyridine *N*-oxide (**1c**) (666 mg, 7.0 mmol), bromobenzene **3a** (550 mg, 3.50 mmol), complex **A** (64.2 mg, 0.088 mmol), K_3PO_4 (1.49 mg, 7.0 mmol), decane (249 mg) and 1,3,5-trimethoxybenzene (295 mg) in toluene (7.0 mL) were monitored over 24 h. Rate of **9a** formation was not performed due to overlap in peaks with GC-FID.

1st run:

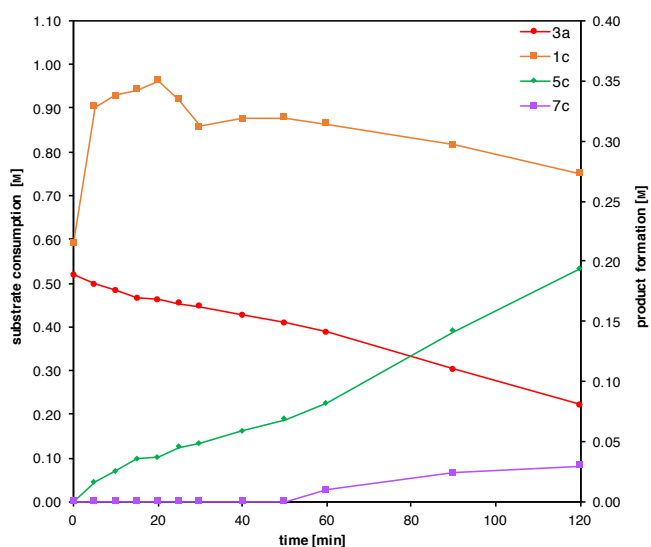
entry	time [min]	3a [M]	1c [M]	5c [M]	7c [M]	34c [M]	35a [M]
1	0	0.531	1,000			0.007	0.003
2	5	0.494	0.998	0.014		0.005	0.007
3	10	0.480	0.934	0.023		0.005	0.010
4	15	0.474	0.904	0.028		0.005	0.010
5	20	0.469	0.917	0.033		0.005	0.010
6	25	0.460	0.906	0.038		0.005	0.009
7	30	0.454	0.901	0.045		0.005	0.010
8	40	0.435	0.917	0.052		0.006	0.008
9	50	0.417	0.916	0.062		0.006	0.007
10	60	0.403	0.821	0.068		0.006	0.007
11	90	0.345	0.803	0.108		0.008	0.007
12	120	0.258	0.794	0.173	0.016	0.009	0.007
13	1440	0	0.545	0.371	0.054	0.022	0.007



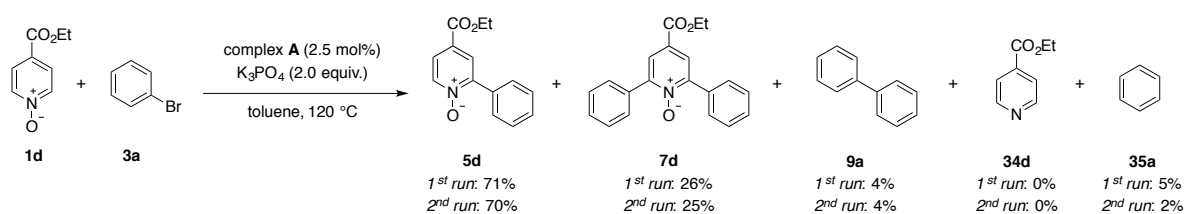
	k_{obs} [mM/min]	R^2
3a	-1.9	0.94
1c	-2.1	0.66
5c	+1.1	0.96

2nd run:

entry	time [min]	3a [M]	1c [M]	5c [M]	7c [M]	34c [M]	35a [M]
1	0	0.519	0.591			0.002	0.005
2	5	0.497	0.903	0.016		0.004	0.010
3	10	0.483	0.930	0.025		0.005	0.010
4	15	0.466	0.941	0.035		0.005	0.011
5	20	0.461	0.963	0.037		0.006	0.011
6	25	0.454	0.921	0.045		0.007	0.012
7	30	0.446	0.859	0.048		0.007	0.012
8	40	0.427	0.877	0.058		0.008	0.012
9	50	0.409	0.877	0.068		0.008	0.012
10	60	0.388	0.864	0.081	0.010	0.008	0.012
11	90	0.303	0.816	0.142	0.024	0.010	0.010
12	120	0.221	0.751	0.194	0.030	0.012	0.009
13	1440	0	0.548	0.386	0.043	0.016	0.006



	k_{obs} [mM/min]	R^2
3a	-2.0	0.98
5c	+1.2	0.96
7c	+0.41	0.92

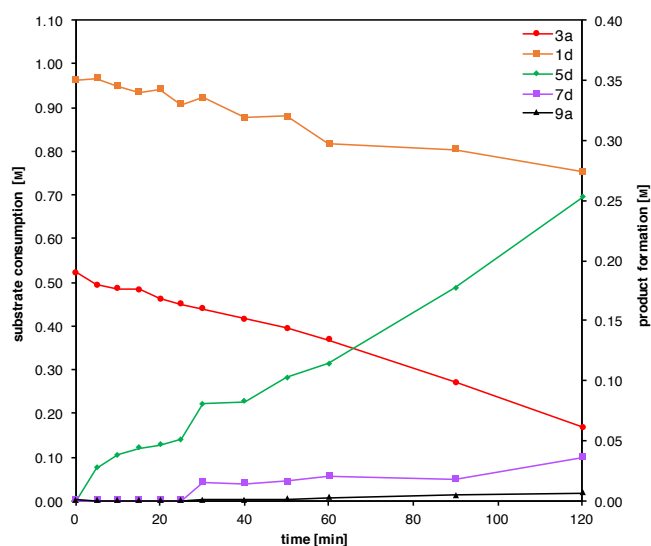
^abased on pyridine *N*-oxide **1d**.

[ES 1178/ES 2016]

According to general procedure, ester pyridine *N*-oxide **1d** (1.17 g, 7.0 mmol), bromobenzene **3a** (550 mg, 3.50 mmol), complex **A** (64.2 mg, 0.088 mmol), K₃PO₄ (1.49 mg, 7.0 mmol), decane (248 mg) and 1,3,5-trimethoxybenzene (294 mg) in toluene (7.0 mL) were monitored over 24 h.

1st run:

entry	time [min]	3a [M]	1d [M]	5d [M]	7d [M]	9a [M]	34d [M]	35a [M]
1	0	0.522	0.963			0.001	0.021	0.003
2	5	0.495	0.968	0.027		0.000	0.019	0.008
3	10	0.485	0.950	0.038		0.000	0.018	0.010
4	15	0.485	0.935	0.044		0.001	0.017	0.013
5	20	0.462	0.942	0.047		0.000	0.016	0.014
6	25	0.451	0.906	0.051		0.001	0.015	0.015
7	30	0.440	0.923	0.081	0.016	0.001	0.014	0.015
8	40	0.416	0.877	0.083	0.014	0.001	0.012	0.014
9	50	0.396	0.880	0.103	0.016	0.002	0.013	0.015
10	60	0.369	0.817	0.114	0.021	0.003	0.013	0.014
11	90	0.271	0.804	0.177	0.018	0.005	0.014	0.012
12	120	0.169	0.753	0.252	0.037	0.007	0.013	0.014
13	1440	0	0.558	0.353	0.066	0.009	0.014	0.028



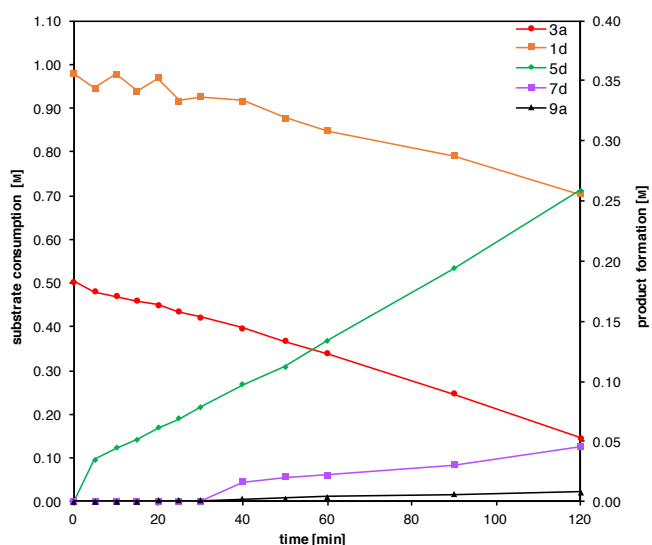
	k_{obs} [mM/min]	R^2
3a	-2.4	0.99
1c	-2.3	0.92
5d	+1.8	0.95
7d	+0.27	0.74
9a	+0.066	0.99

2nd run:

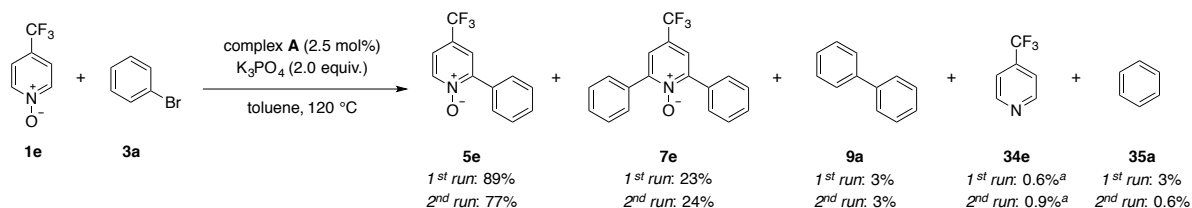
entry	time [min]	3a [M]	1d [M]	5d [M]	7d [M]	9a [M]	34d [M]	35a [M]
1	0	0.503	0.979				0.035	0.003
2	5	0.480	0.945	0.035			0.017	0.006
3	10	0.469	0.977	0.044			0.018	0.010
4	15	0.459	0.939	0.051			0.017	0.012
5	20	0.449	0.969	0.061		0.001	0.019	0.013
6	25	0.434	0.917	0.069		0.001	0.018	0.013
7	30	0.422	0.927	0.078		0.001	0.016	0.013
8	40	0.397	0.918	0.097	0.016	0.002	0.018	0.013
9	50	0.367	0.877	0.112	0.020	0.003	0.017	0.013
10	60	0.339	0.848	0.134	0.022	0.004	0.018	0.013

4 Experimental Section

11	90	0.247	0.791	0.194	0.030	0.006	0.017	0.011
12	120	0.146	0.703	0.259	0.046	0.008	0.016	0.012
13	1440	0	0.557	0.349	0.063	0.011	0.024	0.013



	k_{obs} [mM/min]	R^2
3a	-2.8	1.00
1c	-2.2	0.96
5d	+2.0	0.98
7d	+0.43	0.91
9a	+0.081	0.99



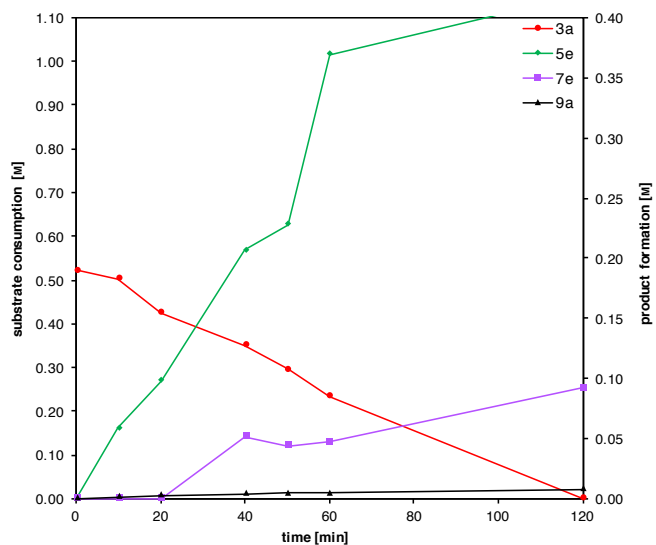
^abased on pyridine *N*-oxide **1e**.

[ES 1158/ES 1186]

According to general procedure, trifluoromethyl pyridine *N*-oxide **1e** (1.14 g, 7.0 mmol), bromobenzene **3a** (550 mg, 3.50 mmol), complex **A** (64.2 mg, 0.088 mmol), K_3PO_4 (1.49 mg, 7.0 mmol), decane (249 mg) and 1,3,5-trimethoxybenzene (295 mg) in toluene (7.0 mL) were monitored over 24 h.

1st run:

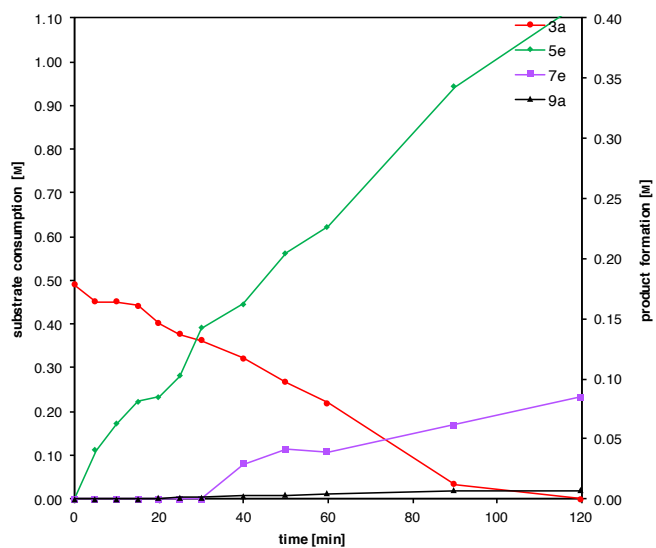
entry	time [min]	3a [M]	5e [M]	7e [M]	9a [M]	34e [M]	35a [M]
1	0	0.522				0.000	0.002
2	10	0.504	0.058		0.001	0.001	0.011
3	20	0.425	0.098		0.003	0.000	0.011
4	40	0.350	0.207	0.052	0.004	0.002	0.016
5	50	0.296	0.228	0.044	0.005	0.002	0.018
6	60	0.234	0.370	0.047	0.005	0.002	0.022
7	120	0	0.420	0.092	0.008	0.004	0.021
8	1440	0	0.446	0.100	0.007	0.006	0.018



	k_{obs} [mM/min]	R^2
3a	-4.5	0.99
5e	+3.7	0.88
7e	+0.79	0.84
9a	+0.077	0.95

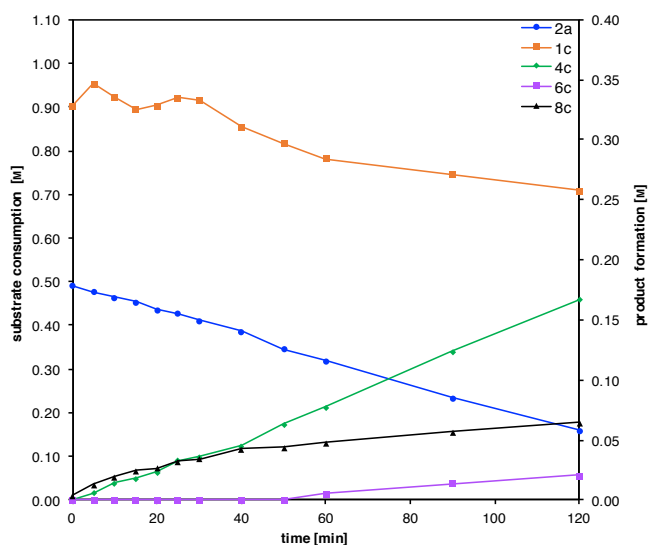
2nd run:

entry	time [min]	3a [M]	5e [M]	7e [M]	9a [M]	34e [M]	35a [M]
1	0	0.489					0.002
2	5	0.452	0.041				0.005
3	10	0.452	0.062				0.007
4	15	0.442	0.081				0.007
5	20	0.402	0.085		0.001		0.006
6	25	0.377	0.102		0.001	0.001	0.008
7	30	0.362	0.142		0.001	0.001	0.008
8	40	0.322	0.162	0.029	0.003	0.002	0.008
9	50	0.268	0.205	0.041	0.003	0.002	0.008
10	60	0.219	0.227	0.039	0.004	0.002	0.008
11	90	0.033	0.343	0.062	0.007	0.003	0.011
12	120	0	0.413	0.085	0.007	0.005	0.009
13	1440	0	0.383	0.081	0.007	0.009	0.005



	k_{obs} [mM/min]	R^2
3a	-4.4	0.99
5e	+3.6	0.98
7e	+0.81	0.91
9a	+0.10	0.99

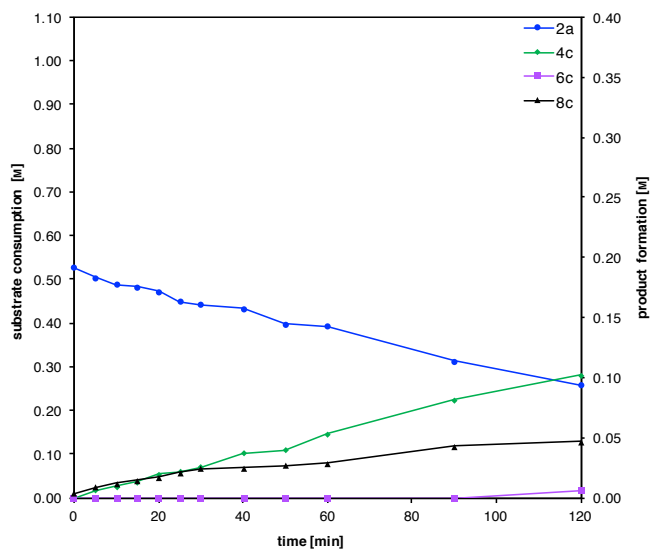
6	25	0.427	0.921	0.033		0.032
7	30	0.412	0.916	0.037		0.035
8	40	0.386	0.854	0.045		0.043
9	50	0.346	0.817	0.063		0.044
10	60	0.320	0.782	0.078	0.006	0.048
11	90	0.234	0.746	0.124	0.014	0.057
12	120	0.160	0.709	0.167	0.021	0.065
13	1440	0	0.543	0.209	0.025	0.091



	k_{obs} [mM/min]	R^2
2a	-2.8	1.00
1c	-2.4	0.78
4c	+1.3	0.99
6c	+0.29	0.98
8c	+0.91	0.97

2nd run:

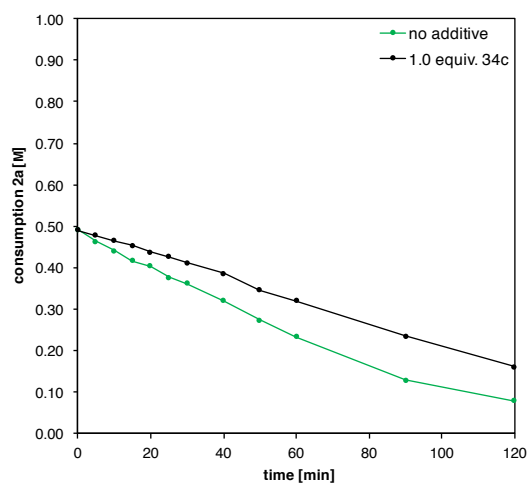
entry	time [min]	2a [M]	1c [M]	4c [M]	6c [M]	8c [M]
1	0	0.527	0.905			0.004
2	5	0.504	1.004	0.007		0.009
3	10	0.489	0.959	0.010		0.012
4	15	0.483	0.990	0.013		0.014
5	20	0.472	1.014	0.020		0.017
6	25	0.449	1.003	0.022		0.021
7	30	0.441	0.991	0.025		0.024
8	40	0.433	0.919	0.037		0.025
9	50	0.398	0.889	0.040		0.027
10	60	0.393	0.949	0.053		0.029
11	90	0.313	0.879	0.081		0.043
12	120	0.257	0.806	0.102	0.006	0.047
13	0	0,000	0.558	0.172	0.024	0.102



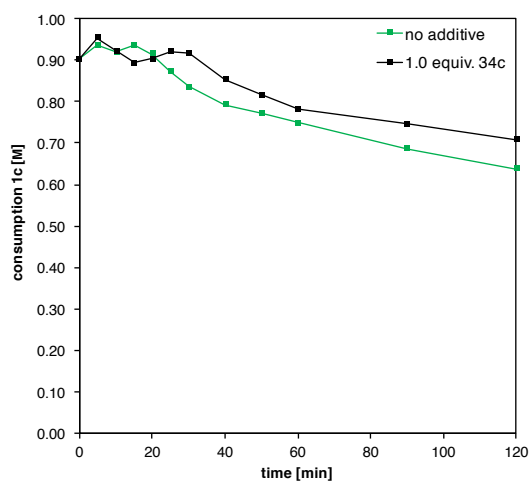
	k_{obs} [mM/min]	R^2
2a	-2.2	0.97
4c	+0.84	0.99
8c	+0.64	0.99

Comparison of rate for inhibition reactions with 2a

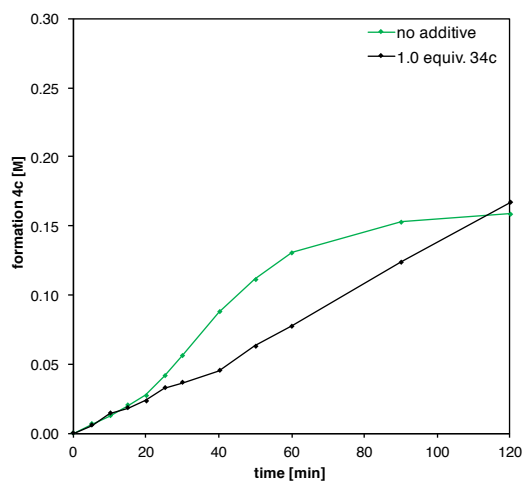
Consumption starting material **2a**



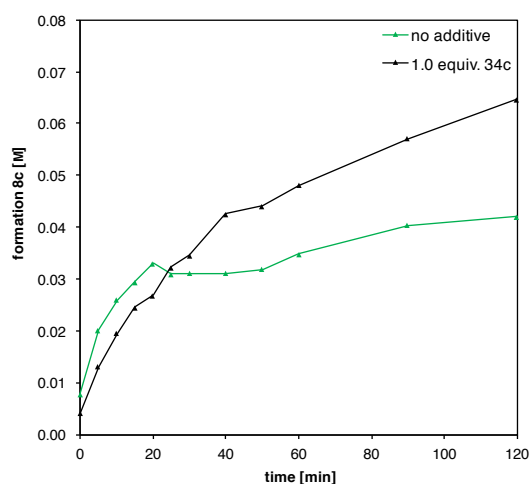
Consumption starting material **1c**

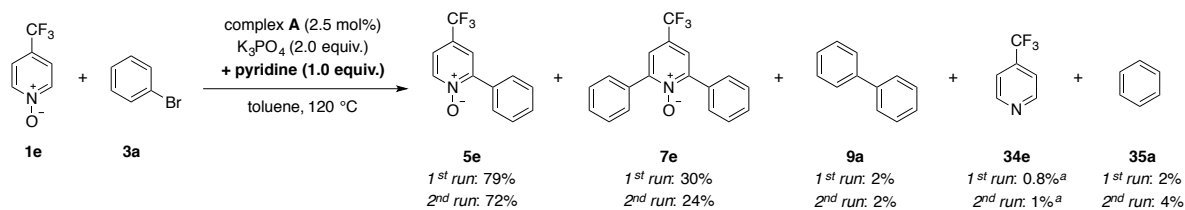


Formation product **4c**



Formation side-product **8c**





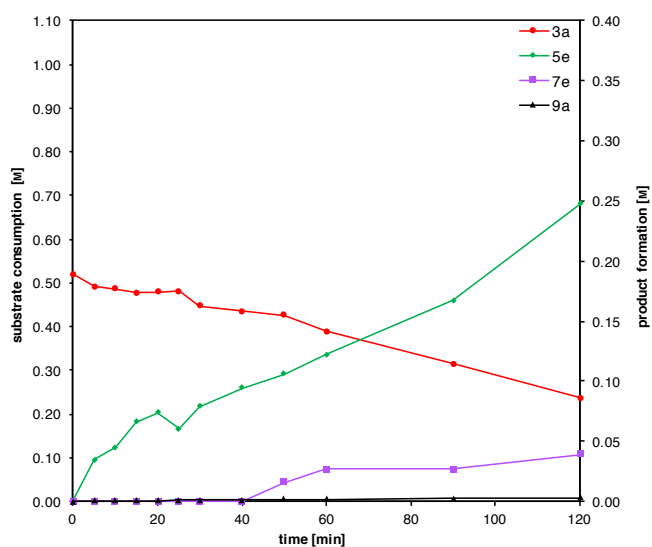
^abased on pyridine *N*-oxide **1e**.

[ES 2008/ES 2038]

According to general procedure, pyridine *N*-oxide **1e** (1.14 g, 7.0 mmol), bromobenzene **3a** (550 mg, 3.50 mmol), complex **A** (64.2 mg, 0.088 mmol), K_3PO_4 (1.49 mg, 7.0 mmol), pyridine (277 mg, 3.5 mmol), decane (249 mg) and 1,3,5-trimethoxybenzene (295 mg) in toluene (7.0 mL) were monitored over 24 h.

1st run:

entry	time [min]	3a [M]	5e [M]	7e [M]	9a [M]	34e [M]	35a [M]
1	0	0.520					0.002
2	5	0.491	0.035			0.001	0.005
3	10	0.486	0.045			0.001	0.006
4	15	0.476	0.066			0.001	0.006
5	20	0.480	0.074			0.001	0.007
6	25	0.480	0.061		0.001	0.001	0.008
7	30	0.448	0.079		0.001	0.001	0.006
8	40	0.434	0.095		0.001	0.002	0.008
9	50	0.425	0.106	0.016	0.001	0.002	0.010
10	60	0.390	0.122	0.027	0.002	0.002	0.009
11	90	0.314	0.167	0.027	0.002	0.003	0.011
12	120	0.237	0.247	0.039	0.003	0.003	0.013
13	1440	0	0.396	0.083	0.005	0.008	0.014

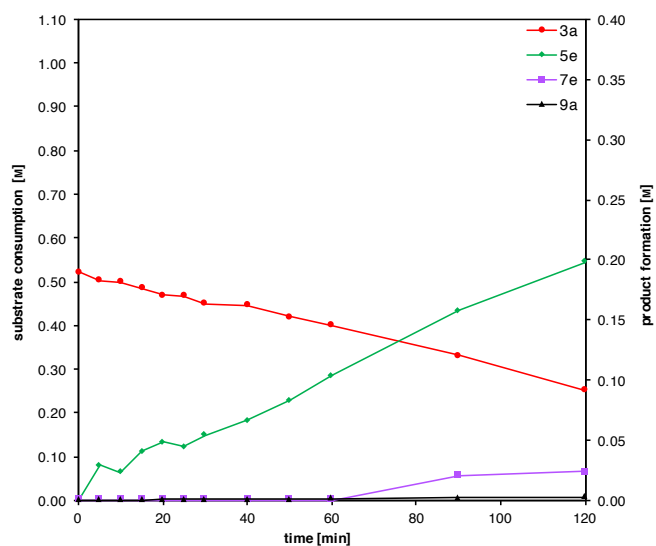


	k_{obs} [mM/min]	R^2
3a	-1.9	0.94
5e	+1.7	0.90
7e	+0.39	0.78
9a	+0.030	0.97

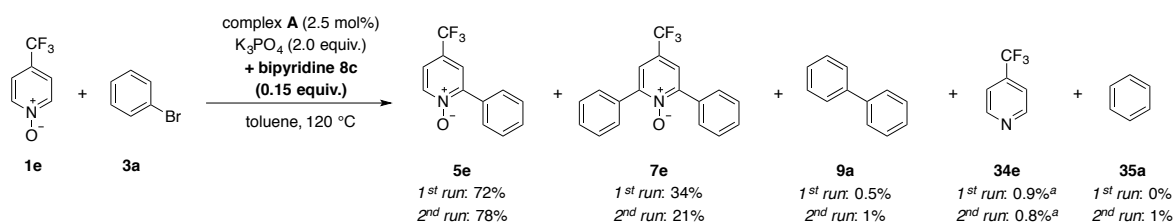
2nd run:

4 Experimental Section

entry	time [min]	3a [M]	5e [M]	7e [M]	9a [M]	34e [M]	35a [M]
1	0	0.522				0.001	0.002
2	5	0.502	0.029			0.000	0.005
3	10	0.499	0.023			0.003	0.006
4	15	0.484	0.040			0.000	0.006
5	20	0.470	0.048			0.002	0.007
6	25	0.467	0.045		0.001	0.002	0.007
7	30	0.450	0.054		0.001	0.002	0.008
8	40	0.445	0.067		0.001	0.003	0.009
9	50	0.420	0.083		0.001	0.003	0.009
10	60	0.400	0.104		0.001	0.003	0.010
11	90	0.331	0.158	0.020	0.002	0.004	0.014
12	120	0.252	0.198	0.024	0.002	0.004	0.016
13	1440	0	0.365	0.063	0.005	0.014	0.023



	k_{obs} [mM/min]	R^2
3a	-1.9	0.98
5e	+1.5	0.95
9a	+0.020	1.00



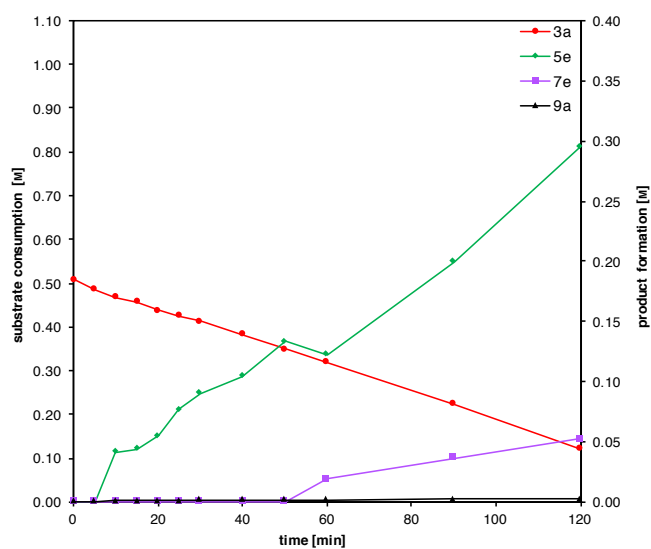
^abased on pyridine *N*-oxide **1e**.

[ES 2010/ES 2034]

According to general procedure, pyridine *N*-oxide **1e** (1.14 g, 7.0 mmol), bromobenzene **3a** (550 mg, 3.50 mmol), complex **A** (64.2 mg, 0.088 mmol), K₃PO₄ (1.49 mg, 7.0 mmol), bipyridine **8c** (82.2 mg, 0.53 mmol), decane (248 mg) and 1,3,5-trimethoxybenzene (295 mg) in toluene (7.0 mL) were monitored over 24 h.

1st run:

entry	time [min]	3a [M]	5e [M]	7e [M]	9a [M]	34e [M]	35a [M]
1	0	0.508					0.002
2	5	0.484					0.002
3	10	0.467	0.041		0.001	0.001	0.001
4	15	0.456	0.044		0.001	0.002	0.001
5	20	0.437	0.055		0.001	0.002	0.001
6	25	0.425	0.077		0.001	0.001	0.001
7	30	0.412	0.090		0.001	0.002	0.001
8	40	0.382	0.104		0.001	0.002	0.001
9	50	0.349	0.134		0.001	0.002	0.001
10	60	0.318	0.122	0.019	0.001	0.002	0.001
11	90	0.223	0.199	0.036	0.002	0.003	0.001
12	120	0.121	0.295	0.052	0.002	0.004	0.001
13	1440	0	0.359	0.085	0.001	0.009	0.001



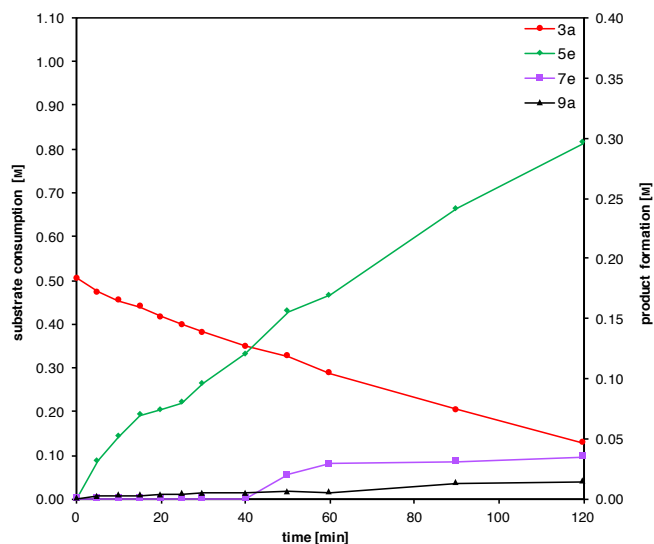
	k_{obs} [mM/min]	R^2
3a	-3.0	1.00
5e	+2.7	0.97
7e	+0.69	0.95
9a	+0.019	0.94

2nd run:

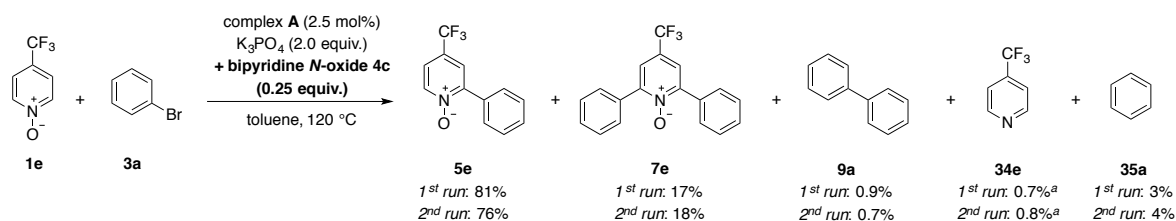
entry	time [min]	3a [M]	5e [M]	7e [M]	9a [M]	34e [M]	35a [M]
1	0	0.504					0.002
2	5	0.473	0.032		0.002		0.004
3	10	0.454	0.051		0.002		0.003
4	15	0.438	0.069		0.003		0.004
5	20	0.415	0.074		0.003		0.003
6	25	0.398	0.080		0.004	0.001	0.003
7	30	0.381	0.096		0.004	0.001	0.003
8	40	0.349	0.120		0.005	0.001	0.003
9	50	0.325	0.156	0.020	0.006	0.001	0.004
10	60	0.287	0.169	0.029	0.005	0.001	0.004

4 Experimental Section

11	90	0.204	0.242	0.031	0.013	0.002	0.005
12	120	0.127	0.296	0.035	0.014	0.009	0.004
13	1440	0	0.389	0.052	0.003	0.008	0.009



	k_{obs} [mM/min]	R^2
3a	-3.5	0.99
5e	+2.7	0.97
9a	+0.094	0.93



^abased on pyridine *N*-oxide **1e**.

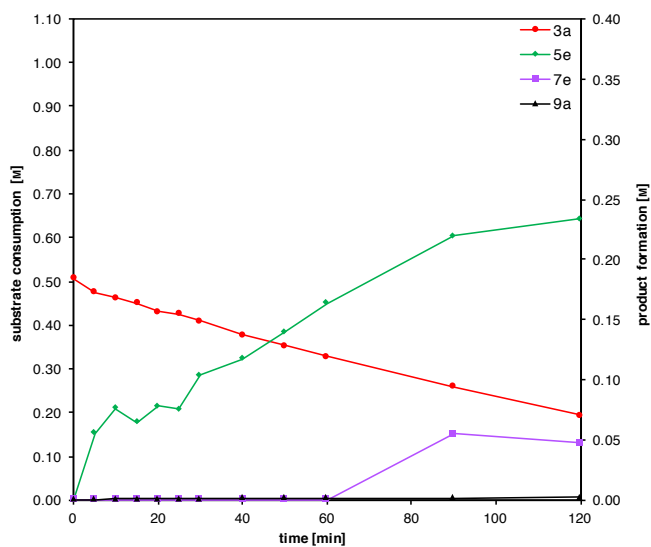
[ES 2012/ES 2036]

According to general procedure, pyridine *N*-oxide **1e** (1.14 g, 7.0 mmol), bromobenzene **3a** (550 mg, 3.50 mmol), complex **A** (64.2 mg, 0.088 mmol), K_3PO_4 (1.49 mg, 7.0 mmol), bipyridine *N*-oxide **4c** (151 mg, 0.88 mmol), decane (249 mg) and 1,3,5-trimethoxybenzene (294 mg) in toluene (7.0 mL) were monitored over 24 h.

1st run:

entry	time [min]	3a [M]	5e [M]	7e [M]	9a [M]	34e [M]	35a [M]
1	0	0.505					0.002
2	5	0.475	0.056			0.002	0.005
3	10	0.461	0.076		0.001	0.002	0.006
4	15	0.449	0.064		0.001	0.002	0.006
5	20	0.431	0.078		0.001	0.002	0.007
6	25	0.425	0.076		0.001	0.002	0.007
7	30	0.408	0.104		0.001	0.003	0.010

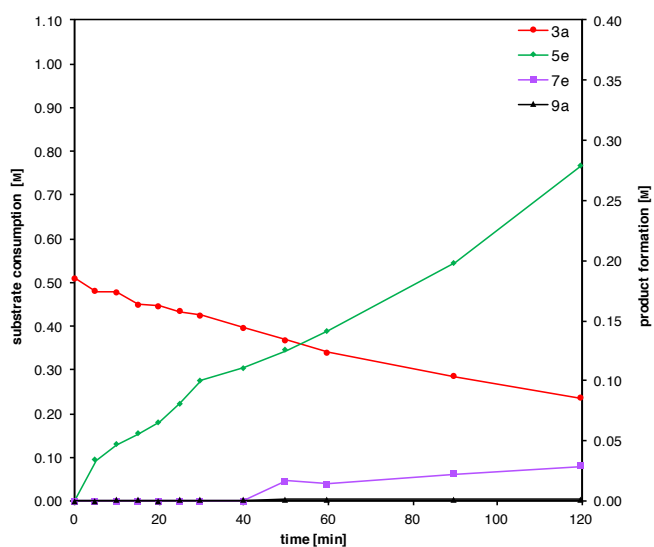
8	40	0.376	0.117		0.001	0.002	0.012
9	50	0.352	0.139		0.001	0.003	0.011
10	60	0.327	0.164		0.001	0.002	0.013
11	90	0.258	0.220	0.055	0.002	0.003	0.013
12	120	0.193	0.234	0.047	0.002	0.004	0.016
13	1440	0	0.405	0.085	0.002	0.007	0.016



	k_{obs} [mM/min]	R^2
3a	-2.8	0.99
5e	+2.2	0.90
9a	+0.021	0.87

2nd run:

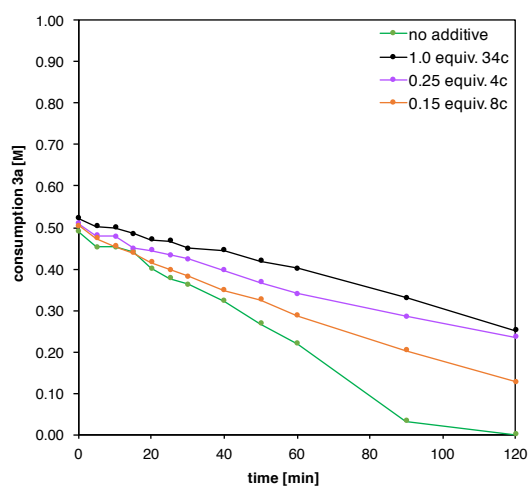
entry	time [min]	3a [M]	5e [M]	7e [M]	9a [M]	34e [M]	35a [M]
1	0	0.510				0.001	0.002
2	5	0.480	0.034			0.002	0.005
3	10	0.478	0.047			0.003	0.006
4	15	0.449	0.056			0.000	0.006
5	20	0.445	0.066			0.000	0.008
6	25	0.433	0.081		0.001	0.000	0.008
7	30	0.424	0.100		0.001	0.002	0.008
8	40	0.396	0.110		0.001	0.002	0.009
9	50	0.367	0.125	0.017	0.001	0.000	0.010
10	60	0.339	0.142	0.014	0.001	0.002	0.010
11	90	0.285	0.198	0.022	0.001	0.002	0.011
12	120	0.235	0.279	0.029	0.001	0.003	0.014
13	1440	0	0.381	0.065	0.002	0.009	0.022



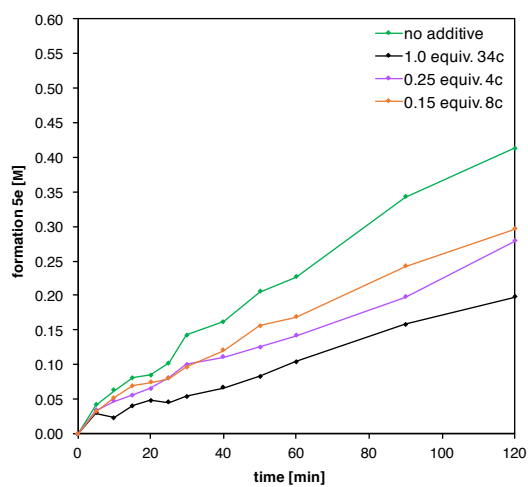
	k_{obs} [mM/min]	R^2
3a	-2.7	0.99
5e	+2.2	0.95
7e	+0.29	0.78

Comparison of rate for inhibition reactions with 3a

Consumption starting material 3a

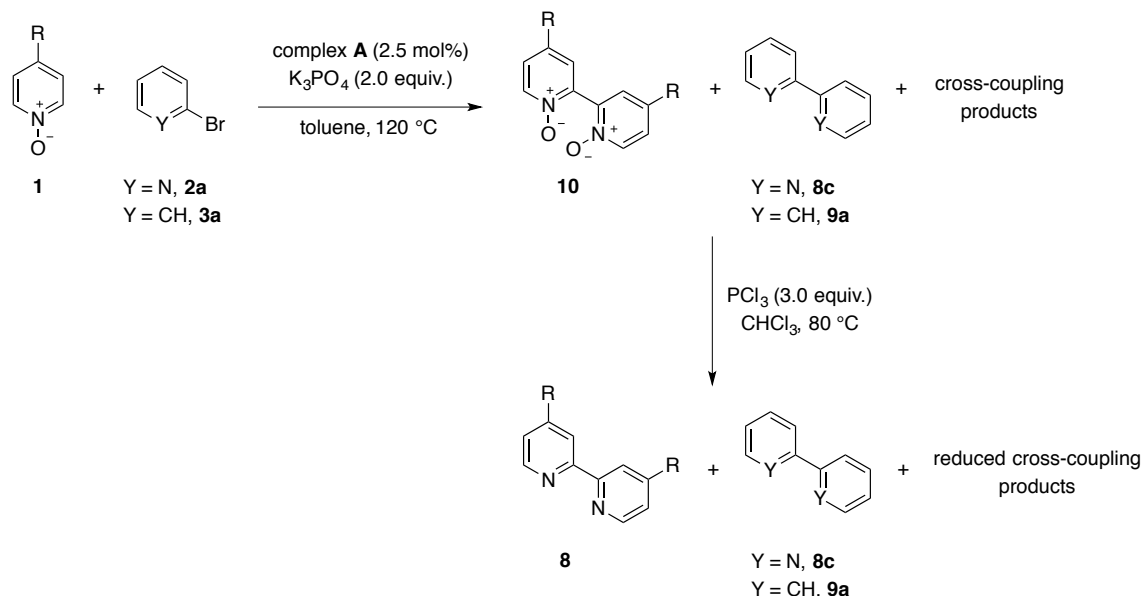


Formation product 5e

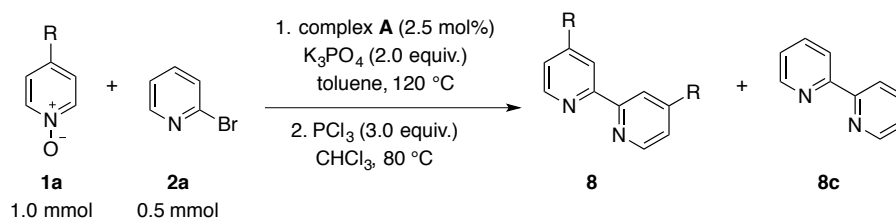


4.7 Quantification of homocoupling products **8c**, **9a**, **10**

General procedure reduction of bipyridine *N,N*-dioxide



The direct arylation reaction was set up on a 1.0 mmol scale in pyridine *N*-oxide **1**, 0.5 mmol aryl halide **2a** or **3a** and with decane (approx. 0.25 equiv. to *N*-oxide) as internal standard, according to the general procedure shown in section 4.6. After 24 h, 0.25 mL of the reaction mixture was filtered through a glass frit to remove insoluble base residues and the frit was washed with CHCl_3 (2.0 mL). PCl_3 (3.0 equiv. to *N*-oxide) was added and the reaction was heated at 80 °C for 3 h or until all *N,N*-dioxide **10** was consumed as judged by TLC. The remaining PCl_3 was quenched with Na_2CO_3 and extracted with 3 x 1.0 mL DCM. The yield of *N*-oxide homocoupling product **8** (reduced **10**) and aryl halide homocoupling product **8c** or **9a** was determined by GC-FID. The yields of cross-coupled products were not determined after reduction.

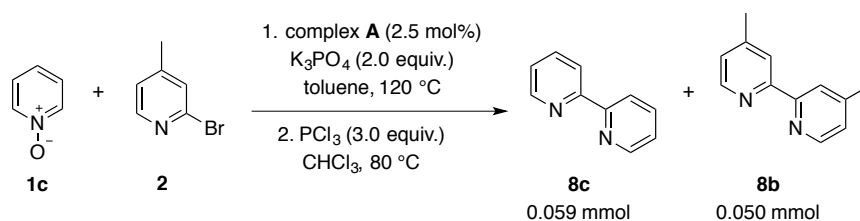


[ES 2090/ES 2104/ES 2106/ES 2130/ES 2164]

According to general procedure, pyridine *N*-oxide **1** (1.0 mmol) and 2-bromopyridine **2a** (0.5 mmol) gave after cross-coupling and deoxygenation bipyridines **8** as shown in table below.

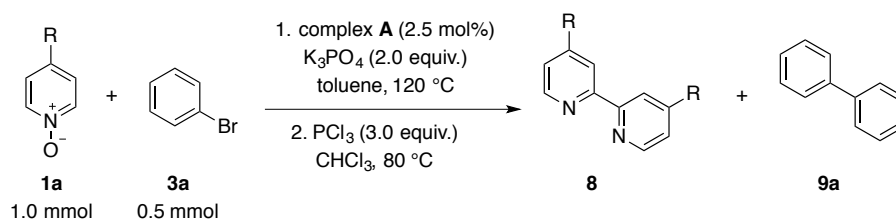
entry	R		8 [μmol]	8c [μmol]
1	<i>t</i> -Bu	a	33	58
2	Me	b	22	47
3 ^a	H	c	66	75
4	CO ₂ Et	d	29	22
5	CF ₃	e	28	23

^aHomocoupling of **1** calculated by subtraction of **4c** and **8c**.



[ES 2092]

According to general procedure, pyridine *N*-oxide **1c** (95.1 mg, 1.0 mmol) and 2-bromo-4-methylpyridine (86.3 mg, 0.5 mmol) gave bipyridine **8c** (0.059 mmol) and bipyridine **8b** (0.050 mmol) after cross-coupling and deoxygenation.



[ES 2094/ES 2096/ES 2108/ES 2132/ES 2166]

According to general procedure, pyridine *N*-oxide **1** (1.0 mmol) and bromobenzene **3a** (0.5 mmol) gave after cross-coupling and deoxygenation bipyridines **8** and biphenyl **9a** as shown in table below.

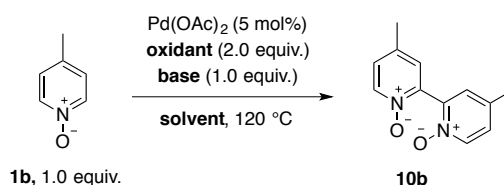
entry	R		8 [μmol]	9a [μmol]
1	<i>t</i> -Bu	a	17	35
2	Me	b	12	16
3	H	c	7	10
4	CO ₂ Et	d	13	8
5	CF ₃	e	26	7

4.8 Oxidative coupling of pyridine *N*-oxides

General procedure

Pyridine *N*-oxide **1b** (0.5 mmol, 1.0 equiv.), Pd(OAc)₂ (0.025 mmol, 0.05 equiv.), oxidant (1.0 mmol, 2.0 equiv.) and 1,3,5-trimethoxybenzene (0.25 mmol, 0.5 equiv.) as internal standard were added to a screw-cap vial. The solids were dissolved in solvent (1.0 mL) and pyridine (0.5 mmol, 1.0 equiv.) and stirred at 120 °C for 24-48 h. Subsequently, the solvent was removed on evaporator and the solids dissolved in MeOH-*d*₄ and filtered through a short pad of celite. Yield of bipyridine *N,N'*-dioxide **10b** was determined via ¹H NMR spectroscopy.

4.8.1 Screening of catalytic conditions

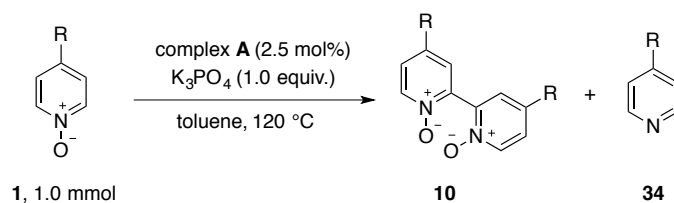


entry	oxidant (2.0 equiv.)	additive/base (1.0 equiv.)	solvent	10b [%]
1 [ES 2110]	Ag ₂ CO ₃	Py	dioxane	22
2 ^a [ES 2112]	Ag ₂ CO ₃	K ₃ PO ₄ (2.0 equiv.)	toluene	21
3 ^{b,c} [ES 3014f]	Ag ₂ CO ₃	-	DMSO	3
4 ^{b,c} [ES 3022a]	Ag ₂ CO ₃	Py (2.0 equiv.)	NMP	-
5 ^{b,c} [ES 3022b]	Ag ₂ CO ₃	Py (2.0 equiv.)	DMF	13
6 ^{b,c} [ES 3022c]	Ag ₂ CO ₃	Py (2.0 equiv.)	DMSO	10
7 ^b [ES 3010a]	AgOAc	Py	dioxane	15
8 ^b [ES 3010b]	AgNO ₃	Py	dioxane	-
9 ^b [ES 3010c]	Ag ₂ O	Py	dioxane	12
10 [ES 6094]	AgOPiv	Py	dioxane	traces
11 [ES 3012a]	Cu(OAc) ₂	Py	dioxane	-
12 ES [3038a]	Ag ₂ CO ₃	bipy (1.0 equiv)	dioxane	28

13 [ES 3038b]	Ag ₂ CO ₃	4-methyl Py (1.0 equiv.)	dioxane	23
14 ^b [ES 3002b]	PhI(OAc) ₂	K ₂ CO ₃ (2.0 equiv.)	dioxane	7
15 ^b [ES 3002d]	PhI(OAc) ₂	-	dioxane	-
16 ^{b,c} [ES 3014d]	PhI(OAc) ₂	K ₃ PO ₄ (2.0 equiv)	DMSO	traces
17 ^{b,c} [ES 3014c]	Oxone	K ₃ PO ₄ (2.0 equiv)	DMSO	traces
18 [ES 2116]	Cyanuric chloride	K ₃ PO ₄	toluene	-
19 [ES 3014]	Benzoquinone	K ₃ PO ₄	DMSO	-

^acomplex **A** used as catalyst. ^breaction performed under air. ^ctemperature = 140 °C. Py = pyridine, bipy = 2,2'-bipyridine **8c**.

4.8.2 Control experiments



[ES 3048]

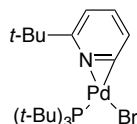
In a glovebox, pyridine *N*-oxide derivative (1.0 mmol), cyclometalated palladium complex **A** (0.013 mmol), K₃PO₄ (1.0 mmol) and 1,3,5-trimethoxybenzene (0.25 mmol) were weighed in a 10 mL Schlenk tube. Toluene (1.0 mL) was added and the mixture was heated for 24 h at 120 °C. The reaction mixture was evaporated and the residue dissolved in MeOH-*d*₄ and filtered through a plug of celite. ¹H NMR was used to calculate the yield of **10** and **34**. No reduced homocoupling product **8** was detected.

entry	R		10 [mmol]	34 [mmol]
1	<i>t</i> -Bu	a	0.052	0.049
2	Me	b	0.061	-
3	H	c	0.031	0.032
4	CO ₂ Et	d	-	-
5	CF ₃	e	-	-

4.9 Aryl palladium intermediates from the direct arylation reaction

4.9.1 (6-*tert*-Bu-2-pyridyl)Pd(Br)(P(*t*-Bu)₃) (12a)

[ES 4112/5020/5058]



In the glovebox, palladium methanesulfonate complex **H** (705.8 mg, 0.78 mmol, 1.0 equiv.) and P(*t*-Bu)₃ (330.3 mg, 1.63 mmol, 2.1 equiv.) was weighed in a Schlenk flask. Toluene (35 mL) and 2-*tert*-butyl-bromopyridine (1.66 g, 7.78 mmol, 10 equiv.) were added. In a separate flask, NaHMDS (299.4 mg, 1.63 mmol, 2.1 equiv.) was dissolved in toluene (10.0 mL) and THF (2.0 mL). The NaHMDS solution was slowly dropped into the bromopyridine flask and the reaction was stirred for 10 min at room temperature. The solution was concentrated to ~3 mL and dry pentane was added and the mixture was kept at -25 °C over night. Drying of the precipitate gave 2-pyridyl palladium complex **12a** (689.7 mg, 1.32 mmol, 86%) as a yellow solid.

¹H NMR (500 MHz, C₆D₆): δ 7.11 (dt, *J* = 7.7, 0.8 Hz, 1H, overlap.), 6.64 (ddd, *J* = 7.7, 7.1, 2.3 Hz, 1H), 6.39 (ddd, *J* = 7.2, 2.9, 0.6 Hz, 1H), 1.34 (s, 9H), 1.24 (d, *J* = 12.6 Hz, 27H) ppm.

¹³C{¹H} NMR (126 MHz, C₆D₆): δ 163.7, 145.1, 136.6, 123.7, 116.4, 39.2 (d, *J* = 9.8 Hz), 36.9, 32.1, 29.7 ppm.

³¹P{¹H} NMR (162 MHz, C₆D₆): δ 89.7 ppm.

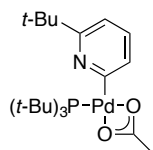
IR (solid, ν): 3005 (m), 2956 (m), 2903 (m), 2869 (m), 1577 (m), 1557 (m), 1542 (m), 1527 (m), 1472 (w), 1433 (w), 1393 (m), 1362 (w), 1276 (m), 1261 (m), 1171 (m), 1104 (w), 1076 (w), 1022 (w), 985 (w), 967 (w), 933 (w), 849 (w), 806 (w), 764 (s), 750 (s), 702 (w) cm⁻¹.

HRESI-MS (+, MeOH, *m/z*): [M-Br]⁺ 442.1858, calc. 442.1855.

Elemental analysis (%): C 48.27, H 7.67, N 2.75, calc. C 48.24, H 7.52, N 2.68.

4.9.2 (6-*tert*-Bu-2-pyridyl)Pd(OAc)(P(*t*-Bu)₃) (13a)

[ES 4148/5096]



In a glovebox, 2-pyridyl palladium complex **12a** (150 mg, 0.29 mmol, 1.0 equiv.) and AgOAc (239 mg, 1.43 mmol, 5.0 equiv.) were weighed in a vial and benzene (2.0 mL) was added. The reaction was

stirred for 1 h, followed by filtration through celite to remove the solids. Removal of the solvent gave acetate 2-pyridyl palladium complex **13a** (146 mg, 0.29 mmol, quant.) as a light yellow solid.

$^1\text{H NMR}$ (500 MHz, C_6D_6): δ 7.37 (dt, $J = 7.8, 0.7$ Hz, 1H), 6.69 – 6.64 (m, 1H), 6.55 (dt, $J = 7.5, 1.0$ Hz, 1H), 1.93 (s, 3H), 1.38 – 1.33 (m, 36H, overlap.) ppm.

$^{13}\text{C}\{^1\text{H}\}$ NMR (126 MHz, C_6D_6): δ 187.0, 166.3 (d, $J = 4.0$ Hz), 162.2 (d, $J = 7.2$ Hz), 133.2, 128.1, 114.2, 39.9 (d, $J = 11.2$ Hz), 37.5, 32.1, 30.2, 23.6 ppm.

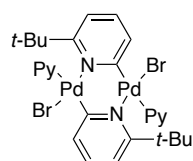
$^{31}\text{P}\{^1\text{H}\}$ NMR (162 MHz, C_6D_6): δ 76.6 ppm.

IR (solid, ν): 2953 (m), 2899 (m), 1544 (s), 1474 (w), 1441 (s), 1413 (s), 1393 (m), 1379 (w), 1341 (w), 1282 (w), 1205 (w), 1170 (m), 1138 (w), 1112 (m), 1083 (w), 1046 (w), 1023 (w), 972 (w), 934 (m), 853 (m), 806 (w), 790 (m), 758 (w), 734 (m), 700 (w), 677 (s) cm^{-1} .

HRESI-MS (+, MeOH, m/z): $[\text{M}-\text{OAc}]^+$ 442.1889, calc. 442.1855.

4.9.3 $[(\mu\text{-}(6\text{-tert-Bu-2-pyridyl})\text{-C}^2\text{,N})\text{Pd}(\text{Br})(\text{py})]_2$ (**17**)

[ES 4189/ES 5097]



In glovebox, palladium complex **12a** (34.0 mg, 0.065 mmol, 1.0 equiv.) was dissolved in benzene (1.0 mL) and pyridine (404 mg, 120 equiv.) was added. After stirring the reaction for 4 h under argon, the solvent was removed on high vacuum. Precipitation from benzene/pentane gave 2-pyridyl palladium complex **17** (24.0 mg, 0.030 mmol 93%) as an orange solid.

Alternative synthesis:

[ES 5187]

$\text{Pd}_2(\text{dba})_3\text{-CHCl}_3$ (404.6 mg, 0.39 mmol, 1.0 equiv.) and $\text{P}(o\text{-tol})_3$ (119.0 mg, 0.39 mmol, 1.0 equiv.) were dissolved in dry toluene (20 mL) and 2-bromo-6-tert-butylpyridine **2b** (1.26 g, 5.86 mmol, 15.0 equiv.) and pyridine (5.86 mmol, 0.47 mL, 15.0 equiv.) were successively added to the solution. The mixture was heated at 50 °C for 1 h until the purple color disappeared. The reaction was filtered through celite, concentrated and Et_2O was added. Rapid stirring at room temperature for 1 h resulted in precipitation, which was dried on high vacuum and resulted in palladium complex **17** (142.6 mg, 0.18 mmol 46%) as an orange solid.

$^1\text{H NMR}$ (500 MHz, $\text{DCM-}d_2$): δ 8.86 (dt, $J = 5.0, 1.6$ Hz, 4H), 7.68 (dd, $J = 7.8, 1.3$ Hz, 2H), 7.62 (tt, $J = 7.6, 1.7$ Hz, 2H), 7.18 (ddd, $J = 7.6, 4.9, 1.5$ Hz, 4H), 7.08 (t, $J = 7.8$ Hz, 2H), 6.82 (dd, $J = 7.8, 1.3$ Hz, 2H), 1.40 (s, 18H) ppm.

$^{13}\text{C}\{^1\text{H}\}$ NMR (126 MHz, $\text{DCM-}d_2$): δ 172.0, 167.9, 152.5, 137.6, 135.6, 132.7, 124.4, 117.1, 37.5, 30.9 ppm.

IR (solid, ν): 3060 (w), 2952 (w), 2865 (w), 1601 (w) 1572 (m), 1476 (w), 1443 (m), 1431 (m), 1415 (m), 1372 (w), 1359 (w), 1275 (m), 1266 (m), 1215 (m), 1182 (m), 1137 (w), 1099 (w), 1065 (w), 1041 (w), 1012 (w), 849 (w), 794 (m), 749 (s), 696 (s), 670 (w) cm^{-1} .

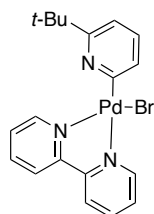
HRESI-MS (+, MeOH, m/z): $[\text{M}-2\text{Py}-\text{Br}]^+$ 560.9186, calc. 560.9197, $[\text{M}-2\text{Py}+\text{H}]^+$ 639.9602, calc. 639.8444.

Elemental analysis (%): C 42.37, H 4.08, N 7.04, calc. C 42.18, H 4.05, N 7.03.

M.p.: decomposition > 173 °C.

4.9.4 (6-*tert*-Bu-2-pyridyl)Pd(Br)(bipy) (**18**)

[ES 5192]



$\text{Pd}_2(\text{dba})_3\cdot\text{CHCl}_3$ (313.4 mg, 0.30 mmol) and $\text{P}(o\text{-tol})_3$ (92.2 mg, 0.30 mmol, 1.0 equiv.) were dissolved in dry toluene (20 mL) and 2-bromo-6-*tert*-butylpyridine (972.2 mg, 4.54 mmol, 15.0 equiv.) and 2,2'-bipyridine (236.6 mg, 1.52 mmol, 5.0 equiv.) were successively added to the solution. The mixture was heated at 50 °C for 30 min until the purple color disappeared. The mixture was filtered through celite, concentrated and Et_2O was added. Rapid stirring at room temperature for 1 h resulted in precipitation which after drying on high vacuum gave palladium complex **18** (259.7 mg, 0.54 mmol 91%) as a bright yellow solid.

^1H NMR (500 MHz, CD_2Cl_2): δ 9.32 (ddd, $J = 5.2, 1.7, 0.8$ Hz, 1H), 8.21 – 8.14 (m, 2H), 8.09 (td, $J = 7.8, 1.7$ Hz, 1H), 8.07 – 8.02 (m, 2H), 7.56 (ddd, $J = 7.6, 5.2, 1.2$ Hz, 1H), 7.41 – 7.33 (m, 2H), 7.07 (t, $J = 7.6$ Hz, 1H), 6.91 (dd, $J = 7.6, 0.9$ Hz, 1H), 1.42 (s, 9H) ppm.

$^{13}\text{C}\{^1\text{H}\}$ NMR (126 MHz, CD_2Cl_2): δ 167.6, 165.5, 155.4, 153.1, 150.7, 150.3, 138.9, 138.6, 132.0, 130.1, 126.1, 125.9, 121.9, 121.5, 113.5, 37.2, 29.9 ppm.

IR (solid, ν): 3026 (w), 2960 (w), 2899 (w), 2863 (w), 1598 (w), 1560 (w), 1543 (m), 1469 (w), 1442 (w), 1415 (m), 1376 (w), 1354 (w), 1313 (w), 1277 (m), 1261 (m), 1203 (w), 1159 (w), 1137 (w), 1118 (w), 1085 (w), 1025 (w), 975 (w), 931 (w), 888 (w), 852 (w), 794 (m), 751 (s), 729 (m), 701 (w), 658 (w) cm^{-1} .

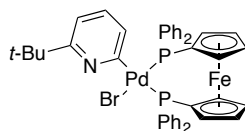
HRESI-MS (+, DCM/MeOH, m/z): $[\text{M}+\text{H}]^+$ 477.9965, calc. 477.9952, $[\text{M}-\text{Br}]^+$ 396.0715, calc. 396.0692.

Elemental analysis (%): C 47.97, H 4.29, N 8.83, calc. C 47.87, H 4.23, N 8.81.

M.p.: decomposition > 203 °C.

4.9.5 (6-*tert*-Bu-2-pyridyl)Pd(Br)(dppf) (**19**)

[ES 5034a]

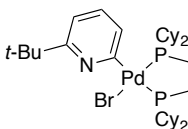


In the glovebox, a vial was charged with pyridyl palladium complex **12a** (5.0 mg, 9.6 μ mol, 1.0 equiv.) and dppf (5.3 mg, 9.6 μ mol, 1.0 equiv.). The solids were dissolved in benzene and stirred in the glovebox for 1 h at room temperature. Removal of the solvent and drying on high vacuum yielded an orange solid that was directly transferred to an NMR tube. No yield was calculated.

$^{31}\text{P}\{^1\text{H}\}$ NMR (162 MHz, C_6D_6): δ 26.3 (d, $J_{\text{P-P}} = 42.5$ Hz), 7.36 (d, $J_{\text{P-P}} = 42.5$ Hz) ppm.

4.9.6 (6-*tert*-Bu-2-pyridyl)Pd(Br)(dcpe) (**20**)

[ES 5034b]

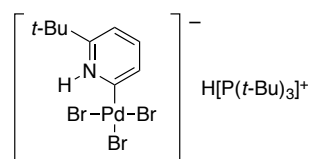


In the glovebox, a vial was charged with pyridyl palladium complex **12a** (5.0 mg, 9.6 μ mol, 1.0 equiv.) and dcpe (4.0 mg, 9.6 μ mol, 1.0 equiv.). The solids were dissolved in benzene and stirred in the glovebox for 1 h at room temperature. Removal of the solvent and drying on high vacuum yielded a light yellow solid that was directly transferred to an NMR tube. No yield was calculated.

$^{31}\text{P}\{^1\text{H}\}$ NMR (162 MHz, C_6D_6): δ 67.8 (d, $J_{\text{P-P}} = 24.4$ Hz), 56.9 (d, $J_{\text{P-P}} = 24.3$ Hz) ppm.

4.9.7 [(6-*tert*-Bu-2-pyridinium)Pd(Br)₃][HP(*t*-Bu)₃] (**30**)

[ES 5093/5160/6084]



In the glovebox, palladium complex **12a** (188.1 mg, 0.36 mmol, 1.0 equiv.) and $\text{HBr}\cdot\text{P}(\textit{t}\text{-Bu})_3$ (150 mg, 0.53 mmol, 1.5 equiv.) were weighed in a vial and dissolved in toluene (5.0 mL). The reaction was stirred for 1 h, during which a precipitate was formed. The precipitate was washed with toluene

and pentane and dried on high vacuum, yielding complex **30** (169.5 mg, 0.25 mmol, 68%) as a yellow solid.

$^1\text{H NMR}$ (400 MHz, MeCN- d_3): δ 11.90 (s, 1H), 7.81 (d, $J = 8.2$ Hz, 1H), 7.56 (t, $J = 8.0$ Hz, 1H), 7.15 (d, $J = 7.8$ Hz, 1H), 6.04 (d, $J_{\text{P-H}} = 449.5$ Hz, 1H), 1.59 (d, $J = 15.4$ Hz, 27H), 1.38 (s, 9H) ppm.

$^{13}\text{C}\{^1\text{H}\}$ NMR (101 MHz, MeCN- d_3): δ 170.0, 161.6, 138.2, 136.8, 116.7, 37.2, 36.9, 29.4, 28.2 ppm.

^{31}P NMR (162 MHz, MeCN- d_3): δ 53.0 (d, $J_{\text{P-H}} = 449.7$ Hz) ppm.

IR (solid, ν): 3437 (w), 2967 (w), 2873 (w), 1593 (w), 1572 (s), 1503 (m), 1471 (m), 1402 (w), 1379 (w), 1276 (w), 1238 (w), 1176 (m), 1072 (w), 1030 (w), 932 (w), 888 (w), 791 (m), 731 (m), 697 (w) cm^{-1} .

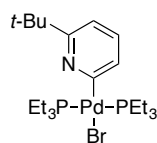
HRESI-MS (-, MeCN, m/z): [(*t*-Bu-pyridyl)PdBr $_2$] $^-$ 399.8353, calc. 399.8356, [(*t*-Bu-pyridyl)-PdBr $_2$] $_2$ +H]. 802.6783, calc. 802.6790.

Elemental analysis (%): C 36.65, H 6.25, N 2.04, calc. C 36.84, H 6.04, N 2.05.

M.p.: decomposition > 148 °C.

4.9.8 (6-*tert*-Bu-2-pyridyl)Pd(Br)(PEt $_3$) $_2$ (**23**)

[ES 6098]



In glovebox, pyridyl palladium complex **12a** (31.2 mg, 0.060 mmol, 1.0 equiv.) and PEt $_3$ (14.1 mg, 0.12 mmol, 2.0 equiv.) were dissolved in toluene (1.0 mL) and stirred under argon for 10 minutes. Removal of solvent and drying on high vacuum gave palladium complex **23** (30.3 mg, 0.054 mmol, 91%) as a colorless solid.

$^1\text{H NMR}$ (400 MHz, C $_6$ D $_6$): δ 6.92 (dd, $J = 7.6, 1.0$ Hz, 1H), 6.77 (tt, $J = 7.5, 1.1$ Hz, 1H), 6.53 (dd, $J = 7.6, 1.0$ Hz, 1H), 1.46 (tdt, $J = 13.9, 7.4, 3.6$ Hz, 12H), 1.34 (s, 9H), 0.92 (dt, $J = 15.5, 7.7$ Hz, 18H) ppm.

$^{13}\text{C}\{^1\text{H}\}$ NMR (101 MHz, C $_6$ D $_6$): δ 179.6, 167.8, 132.4, 130.4 (t, $J = 7.9$ Hz), 111.7, 37.3, 30.1, 14.9 (t, $J = 12.7$ Hz), 8.0 ppm.

$^{31}\text{P}\{^1\text{H}\}$ NMR (162 MHz, C $_6$ D $_6$): δ 12.8 ppm.

IR (solid, ν): 3006 (w), 2989 (w), 2961 (w), 2871 (w), 1558 (w), 1543 (w), 1456 (w), 1416 (w), 1372 (w), 1276 (s), 1260 (s), 1114 (w), 1034 (w), 1002 (w), 797 (w), 765 (s), 749 (s) cm^{-1} .

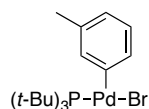
HRESI-MS (+, MeOH, m/z): [M+H] $^+$ 558.1078, calc. 558.1079.

Elemental analysis (%): C 45.50, H 7.80, N 2.56, calc. C 45.30, H 7.60, N 2.52.

M.p.: 135-137 °C.

4.9.9 (3-tolyl)Pd(Br)(P(*t*-Bu)₃) (14a)

[ES 4164/5060]



According to reported procedure,⁷⁵ a Schlenk tube was charged with Pd(P(*t*-Bu)₃)₂ (805 mg, 1.58 mmol, 1.0 equiv.) and HBr·P(*t*-Bu)₃ (13.3 mg, 0.05 mmol, 0.03 equiv.), dissolved in degassed MEK (20 mL) and 3-bromotoluene (7.6 mL, 40 equiv.) was added. The reaction was stirred under argon at 70 °C for 3 h. The solvent was concentrated, TMS was added and the reaction was kept at –25 °C over night. The precipitate was collected and dried, yielding 3-tolyl palladium complex **14a** (450 mg, 0.94 mmol, 59%) as a yellow solid.

¹H NMR (400 MHz, C₆D₆): δ 7.25 (s, 1H), 7.21 (d, *J* = 8.1 Hz, 1H), 6.71 (t, *J* = 7.6 Hz, 1H), 6.53 (d, *J* = 7.1 Hz, 1H), 2.02 (s, 3H), 0.98 (d, *J* = 12.5 Hz, 27H) ppm.

¹³C{¹H} NMR (126 MHz, C₆D₆ + 0.05 mL MeCN-*d*₃): δ 136.6 (d, *J* = 3.4 Hz), 136.5 (d, *J* = 2.2 Hz), 133.6 (d, *J* = 4.4 Hz), 133.2 (d, *J* = 3.4 Hz), 126.5 (d, *J* = 2.3 Hz), 124.7, 40.0 (d, *J* = 9.6 Hz), 31.4 (d, *J* = 3.1 Hz), 20.9 ppm.

³¹P{¹H} NMR (162 MHz, C₆D₆): δ 63.4 ppm.

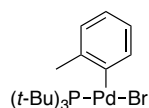
IR (solid, ν): 2973 (m), 2905 (m), 1581 (w), 1551 (m), 1462 (m), 1392 (m), 1370 (w), 1276 (m), 1261 (m), 1206 (w), 1168 (m), 1089 (w), 1060 (m), 1022 (m), 989 (m), 931 (w), 867 (w), 824 (m), 805 (w), 764 (s), 750 (s), 695 (w), 658 (w) cm⁻¹.

HRESI-MS (+, MeOH, *m/z*): [M–Br]⁺ 399.1465, calc. 399.1433.

Elemental analysis (%): C 47.56, H 7.15, calc. C 47.57, H 7.14.

4.9.10 (2-tolyl)Pd(Br)(P(*t*-Bu)₃) (14b)

[ES 5082]



According to reported procedure,²³³ Pd(P(*t*-Bu)₃)₂ (302.7 mg, 0.59 mmol, 1.0 equiv.) was weighed in a Schlenk flask and set under argon. Dry THF (3.7 mL) was added and the flask was removed from the glovebox. 2-Bromotoluene (3.7 mL, 30.5 mmol, 52 equiv.) was syringed into the mixture and the reaction was heated at 70 °C for 3 h. The solvent was removed on high vacuum and dry pentane was added. After keeping the mixture at –25 °C over night, the formed precipitate was washed with pentane and dried, yielding complex **14b** (76.8 mg, 0.16 mmol, 27%) as a yellow solid.

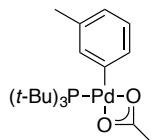
¹H NMR (400 MHz, C₆D₆): δ 7.31 (ddd, *J* = 7.8, 3.5, 1.1 Hz, 1H), 6.81 – 6.70 (m, 2H), 6.66 (t, *J* = 7.4 Hz, 1H), 3.03 (s, 3H), 1.02 (d, *J* = 12.5 Hz, 27H) ppm.

$^{31}\text{P}\{^1\text{H}\}$ NMR (162 MHz, C_6D_6): δ 64.9 ppm.

The chemical shifts are in agreement with previously reported values.⁴⁶

4.9.11 (3-tolyl)Pd(OAc)(P(*t*-Bu)₃) (15a)

[ES 4172]



In a glovebox, phenyl palladium complex **14a** (150 mg, 0.31 mmol, 1.0 equiv.) and AgOAc (252 mg, 1.51 mmol, 5.0 equiv.) were weighed in a vial and benzene (2.0 mL) was added. The reaction was stirred for 1 h and followed by filtration through celite to remove the solids. Removal of the solvent gave acetate palladium complex **15a** (132 mg, 0.29 mmol, 93%) as a yellow solid.

^1H NMR (400 MHz, C_6D_6): δ 7.38 (s, 1H), 7.32 (d, $J = 7.8$ Hz, 1H), 6.80 (t, $J = 7.6$ Hz, 1H), 6.66 (d, $J = 7.7$ Hz, 1H), 2.09 (s, 3H), 1.88 (s, 3H), 1.22 (d, $J = 12.6$ Hz, 27H) ppm.

$^{13}\text{C}\{^1\text{H}\}$ NMR (101 MHz, C_6D_6): δ 187.6, 142.5 (d, $J = 3.0$ Hz), 136.3 (d, $J = 2.6$ Hz), 136.2 (d, $J = 1.8$ Hz), 132.9 (d, $J = 2.7$ Hz), 126.7, 124.8, 40.2 (d, $J = 11.7$ Hz), 32.1 (d, $J = 3.0$ Hz), 23.7, 21.2 ppm.

$^{31}\text{P}\{^1\text{H}\}$ NMR (162 MHz, C_6D_6): δ 77.9 ppm.

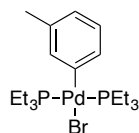
IR (solid, ν): 2976 (m), 2906 (m), 1577 (w), 1556 (m), 1526 (m), 1443 (s), 1393 (m), 1276 (m), 1260 (m), 1171 (m), 1063 (w), 1023 (w), 991 (w), 935 (m), 828 (w), 806 (w), 765 (s), 750 (s), 679 (s) cm^{-1} .

HRESI-MS (+, MeOH, m/z): $[\text{M}-\text{OAc}]^+$ 399.1437, calc. 399.1433, $[\text{M}+\text{Na}]^+$ 481.1464, calc. 481.1458.

Elemental analysis (%): C 54.96, H 8.18, calc. C 54.96, H 8.13.

4.9.12 (3-tolyl)Pd(Br)(PEt₃)₂ (24)

[ES 6099]



In glovebox, phenyl palladium complex **14a** (34.9 mg, 0.073 mmol, 1.0 equiv.) and PEt_3 (20.0 mg, 0.17 mmol, 2.3 equiv.) were dissolved in toluene (1.0 mL) and stirred under argon for 10 minutes. Removal of solvent and drying on high vacuum gave palladium complex **24** (36.8 mg, 0.072 mmol, 98%) as a colorless solid.

^1H NMR (400 MHz, C_6D_6): δ 7.23 (s, 1H), 7.14 (d, $J = 7.5$ Hz, 1H), 6.94 (t, $J = 7.5$ Hz, 1H), 6.69 (d, $J = 7.4$ Hz, 1H), 2.16 (s, 3H), 1.47 (qt, $J = 7.5, 3.2$ Hz, 12H), 0.87 (dt, $J = 15.6, 7.7$ Hz, 18H) ppm.

$^{13}\text{C}\{^1\text{H}\}$ NMR (101 MHz, C_6D_6): δ 155.3, 137.5 (t, $J = 4.0$ Hz), 136.4, 133.9, 123.2, 21.4, 15.0 (t, $J = 13.0$ Hz), 8.0 ppm.

$^{31}\text{P}\{^1\text{H}\}$ NMR (162 MHz, C_6D_6): δ 12.8 ppm.

IR (solid, ν): 2961 (w), 2930 (w), 2907 (w), 2874 (w), 1576 (w), 1556 (w), 1455 (w), 1413 (w), 1376 (w), 1276 (w), 1260 (w), 1033 (m), 799 (w), 765 (s), 725 (m), 703 (w) cm^{-1} .

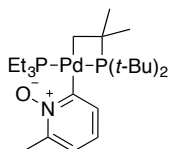
HRESI-MS (+, MeOH, m/z): $[\text{M}-\text{Br}]^+$ 433.1426, calc. 433.1406.

Elemental analysis (%): C 43.15, H 7.37, calc. C 44.42, H 7.26.

M.p.: 88-90 $^\circ\text{C}$.

4.9.13 (6-Me-2-pyridyl *N*-oxide) $\text{Pd}(\text{tert-Bu}_2\text{PC}(\text{CH}_3)_2\text{CH}_2)(\text{PEt}_3)$ (**21**)

[ES 5030/ES 6026]



Pyridine *N*-oxide **1f** (141.2 mg, 1.29 mmol) and THF (7.0 mL) was added to a Schlenk tube under argon and cooled to -78 $^\circ\text{C}$. Potassium *tert*-butoxide in THF (1.55 mL, 1.55 mmol, 1.2 equiv.) was added dropwise and the orange solution was stirred at -78 $^\circ\text{C}$ for 20 minutes. Cyclometalated palladium complex **C** (523.6 mg, 1.04 mmol, 0.8 equiv.) and Ag_2CO_3 (570.9 mg, 2.07 mmol, 1.6 equiv.) in THF (10.0 mL) was added to the metalated pyridine *N*-oxide solution. The reaction was stirred for 10 minutes at -78 $^\circ\text{C}$ and was then warmed to room temperature. After stirring at room temperature for 30 minutes, the solvent was removed and the remains were filtered under argon with pentane through a plug of celite. Removal of the pentane gave the pyridyl *N*-oxide complex **21** (498.3 mg, 0.93 mmol, 72%) as a colorless solid.

^1H NMR (500 MHz, C_6D_6): δ 7.41 (dd, $J = 6.8, 2.6$ Hz, 1H), 6.66 – 6.57 (m, 2H), 2.55 (s, 3H), 1.56 (d, $J = 12.6$ Hz, 6H), 1.46 – 1.32 (m, 26H, broad, overlap.), 0.99 (dt, $J = 15.3, 7.6$ Hz, 9H) ppm.

$^{13}\text{C}\{^1\text{H}\}$ NMR (101 MHz, C_6D_6): δ 183.8 (d, $J = 17.2$ Hz), 146.5, 135.4, 119.6, 119.3, 52.7 (d, $J = 18.1$ Hz), 37.0, 34.0, 31.8 (d, $J = 4.7$ Hz), 19.5, 16.0 (d, $J = 21.1$ Hz), 14.3 (d, $J = 31.4$ Hz), 8.11 ppm.

$^{31}\text{P}\{^1\text{H}\}$ NMR (162 MHz, C_6D_6): δ 16.6 (d, $J_{\text{P-P}} = 402.7$ Hz), 4.66 (d, $J_{\text{P-P}} = 402.2$ Hz) ppm.

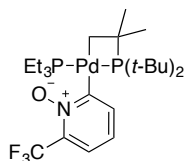
IR (solid, ν): 2959 (w), 2874 (w), 1532 (w), 1456 (w), 1351 (w), 1276 (m), 1260 (m), 1215 (w), 1175 (w), 1034 (w), 851 (w), 806 (w), 764 (s), 750 (s) cm^{-1} .

HRESI-MS (+, MeOH, m/z): $[\text{M}+\text{H}]^+$ 534.2249, calc. 534.2246.

Elemental analysis (%): C 54.00, H 8.90, N 2.77, calc. C 53.98, H 8.87, N 2.62.

4.9.14 (6-CF₃-2-pyridyl *N*-oxide)Pd(*tert*-Bu₂PC(CH₃)₂CH₂)(PEt₃) (22**)**

[ES 5134/6011]



Pyridine *N*-oxide **1h** (245.1 mg, 1.50 mmol) and THF (10.0 mL) was added to a Schlenk tube under argon and cooled to -78 °C. Potassium *tert*-butoxide in THF (1.80 mL, 1.80 mmol, 1.2 equiv.) was added dropwise and the solution was stirred at -78 °C for 20 minutes. Cyclometalated palladium complex **C** (608.0 mg, 1.20 mmol, 0.8 equiv.) and AgOTs (671.1 mg, 2.40 mmol, 1.6 equiv.) in THF (12.0 mL) was added to the metalated pyridine *N*-oxide solution. The reaction was stirred for 10 minutes at -78 °C and was then warmed to room temperature. After stirring at room temperature for 30 minutes, the solvent was removed and pentane (10.0 mL) was added. After stirring at room temperature for 5 minutes, the mixture was filtered under argon with pentane through a plug of celite and the solvent was removed, yielding pyridyl *N*-oxide complex **22** (526.3 mg, 0.90 mmol, 60%) as an orange solid.

¹H NMR (400 MHz, C₆D₆): δ 7.45 (d, $J = 7.3$ Hz, 1H), 6.97 (dd, $J = 7.8, 2.1$ Hz, 1H), 6.37 (t, $J = 7.5$ Hz, 1H), 1.44 (dd, $J = 12.7, 4.6$ Hz, 8H, overlap.), 1.26 (d, $J = 12.0$ Hz, 24H, broad, overlap.), 0.86 (dt, $J = 15.3, 7.6$ Hz, 9H) ppm.

¹³C{¹H} NMR (101 MHz, C₆D₆): δ 188.9 (d, $J = 15.5$ Hz), 140.1, 123.6, 120.9, 118.7, 118.0, 52.5 (dd, $J = 18.2, 1.8$ Hz), 36.9, 33.8, 31.7 (d, $J = 4.3$ Hz), 15.9 (d, $J = 21.3$ Hz), 14.3 (d, $J = 30.9$ Hz), 8.00 ppm.

³¹P{¹H} NMR (162 MHz, C₆D₆): δ 16.6 (d, $J_{P-P} = 395.7$ Hz), 3.33 (d, $J_{P-P} = 396.7$ Hz) ppm.

¹⁹F{¹H} NMR (376 MHz, C₆D₆): δ -68.6 ppm.

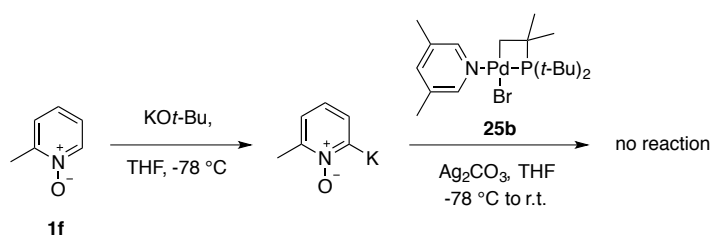
IR (solid, ν): 2961 (w), 2898 (w), 1590 (w), 1455 (w), 1372 (m), 1310 (s), 1276 (m), 1260 (m), 1211 (w), 1142 (s), 1057 (m), 1035 (w), 930 (w), 845 (w), 766 (s), 751 (s), 681 (m) cm⁻¹.

HRESI-MS (+, MeOH, m/z): [M+H]⁺ 588.1975, calc. 588.1958.

Elemental analysis (%): C 49.17, H 7.71, N 2.39, calc. C 49.03, H 7.54, N 2.38.

4.9.15 Attempted synthesis of a pyridine-ligated pyridyl *N*-oxide complex

[ES 5055/ES 5118]

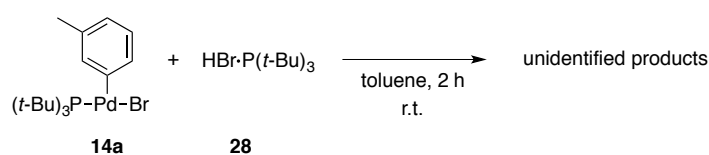


Pyridine *N*-oxide **1f** (8.3 mg, 0.076 mmol) and THF (0.15 mL) was added to a Schlenk tube under argon and cooled to -78 °C. Potassium *tert*-butoxide in THF (0.55 mL, 0.091 mmol, 1.2 equiv.) was added dropwise and the orange solution was stirred at -78 °C for 20 minutes. Cyclometalated pyridine palladium complex **25a** or **25b** (30.0 mg, 0.061 mmol, 0.8 equiv.) and Ag_2CO_3 (33.4 mg, 0.12 mmol, 1.6 equiv.) in THF (1.0 mL) were added to the metalated pyridine *N*-oxide solution. The reaction was stirred for 10 minutes at -78 °C and was then warmed to room temperature. After stirring at room temperature for 30 minutes, the solvent was removed and the remains were filtered with pentane through celite in the glovebox. Removal of the pentane gave an orange oil containing starting material **1f** and 3,5-dimethyl pyridine.

entry	percentage of <i>P</i> in [%]		
	shift δ [ppm]	with 25a	with 25b
1	85	5	1
2	62	5	
3	3.4	34	
4	1.5		58
5	1.1	6	
6	0.8		22
7	-3.1	50	7
8	-3.5		12

4.9.16 Attempted synthesis of an anionic phenyl dimer **29d**

[ES 5092]



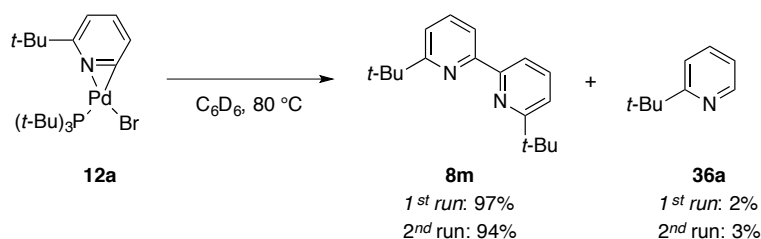
According to reported procedure,⁸¹ phenyl palladium complex **14a** (10.5 mg, 0.022 mmol, 1.0 equiv.) and $\text{HBr}\cdot\text{P}(t\text{-Bu})_3$ (3.1 mg, 0.011, 0.53 equiv.) were weighed in the glovebox and dissolved in toluene (1.0 mL). After stirring for 2 h, the supernatant was pipetted off and the residue dried on high vacuum. Decomposition peaks were observed via ^1H NMR.

4.10 Decomposition of aryl palladium complexes

General procedure

In a glovebox, aryl palladium complex (0.031 mmol) and additive were weighed in an NMR tube with a J Young screw cap. Deuterated or non-deuterated solvent was added (0.68 mL, $c = 0.045$ M) and the tube was sealed. The NMR tube was removed from the glovebox and immediately transferred to an ice bath where it was kept until put in the pre-heated NMR spectrometer. One ^1H or ^{31}P spectrum was recorded every 2 minutes and the reaction was heated until the starting complex was consumed. Thereafter, the NMR tube was opened to air and 1,3,5-trimethoxybenzene was added. An additional ^1H NMR spectrum was recorded to determine the yield.

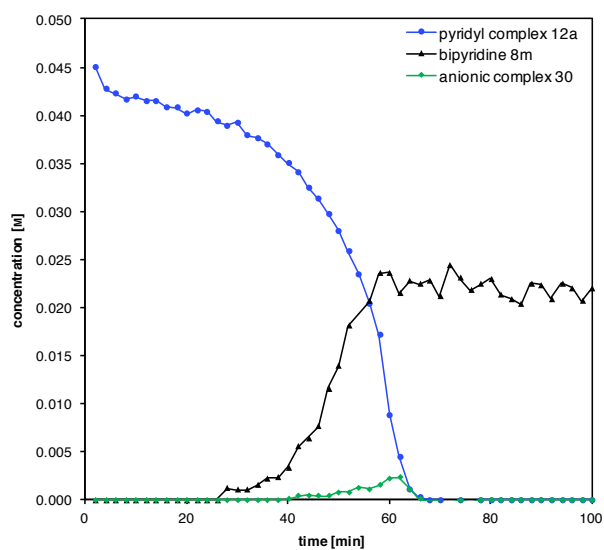
4.10.1 Pyridyl palladium bromide complex **12a**



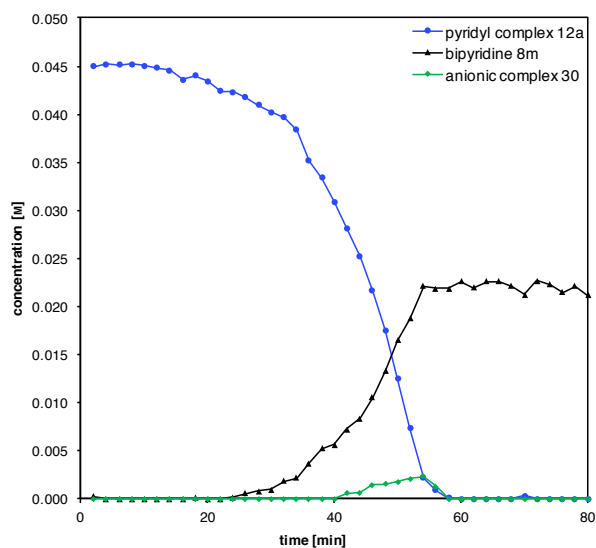
[ES 5108b/ES 5108f]

According to general procedure, pyridyl palladium complex **12a** (16.0 mg, 0.031 mmol) was dissolved in C_6D_6 (0.68 mL) and heated to 80 °C for 3 h while recording a ^1H NMR every 2 minutes. Rate of formation for **36a** not determined due to peak overlap at 80 °C.

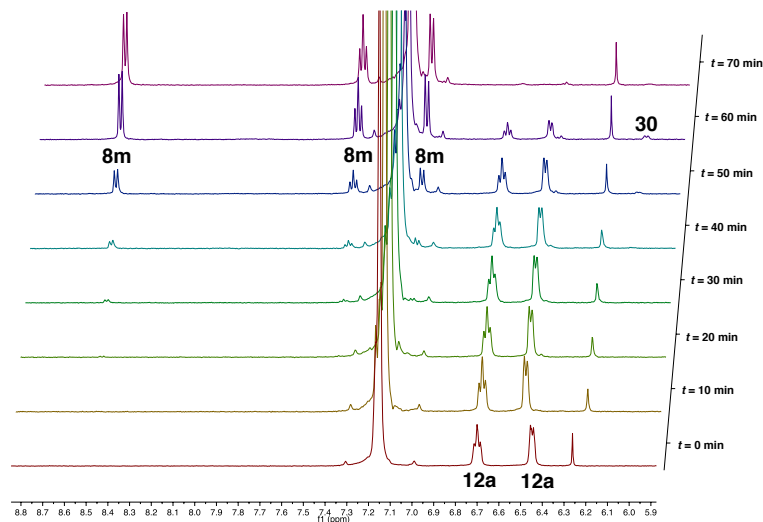
run	percentage of P in [%]					
	26	complex B	27	28	$\text{P}(t\text{-Bu})_3$	30
1 st	18	49	1	22	9	0
2 nd	24	46	8	14	8	0

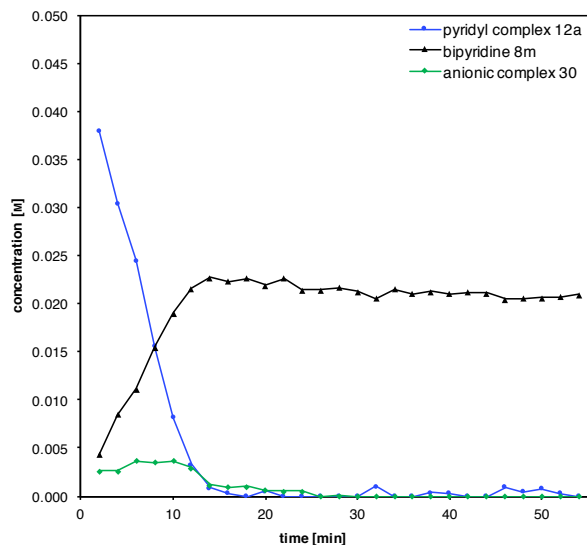
1st run:

	k_{obs} [mM/min]	R^2
12a	-1.8 (48-66 min)	0.96
8m	+1.1 (44-64 min)	0.97
30	+0.10 (40-62 min)	0.88

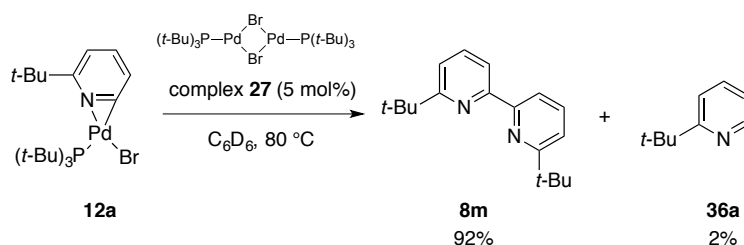
2nd run:

	k_{obs} [mM/min]	R^2
12a	-1.8 (34-54 min)	0.97
8m	+0.97 (34-54 min)	0.95
30	+0.16 (40-54 min)	0.97

Integrated peaks from ¹H NMR spectra ($t = 0$ to $t = 70$ min)



	k_{obs} [mM/min]	R^2
12a	-3.6 (0-12 min)	1.00
8m	+1.8 (0-12 min)	1.00
30	+0.14 (0-10 min)	0.73

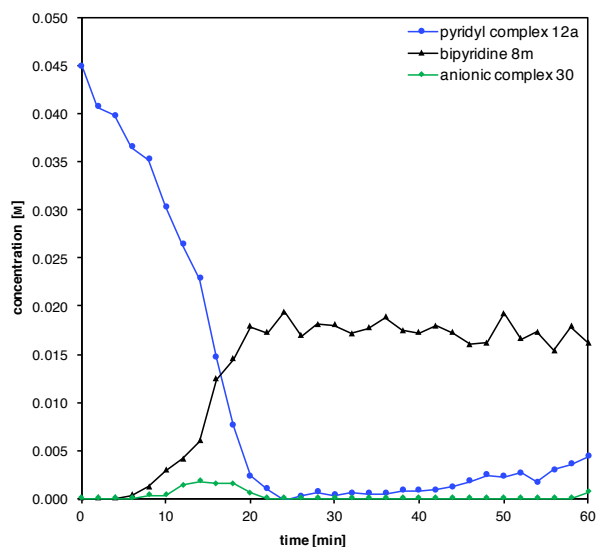


[ES 5108e]

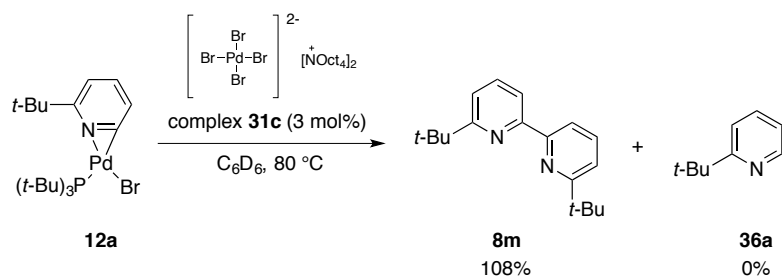
According to general procedure, pyridyl palladium complex **12a** (16.0 mg, 0.031 mmol) and palladium(I) dimer **27** (1.2 mg, 0.0015 mmol, 0.05 equiv.) were dissolved in C_6D_6 (0.68 mL) and heated to 80 °C for 1 h while recording a ^1H NMR every 2 minutes.

percentage of P in [%]

26	complex B	27	28	$\text{P}(t\text{-Bu})_3$	30
20	47	1	20	12	0



	k_{obs} [mM/min]	R^2
12a	-2.9 (12-22 min)	0.98
8m	+1.6 (12-22 min)	0.96
30	+0.23 (8-16 min)	0.90

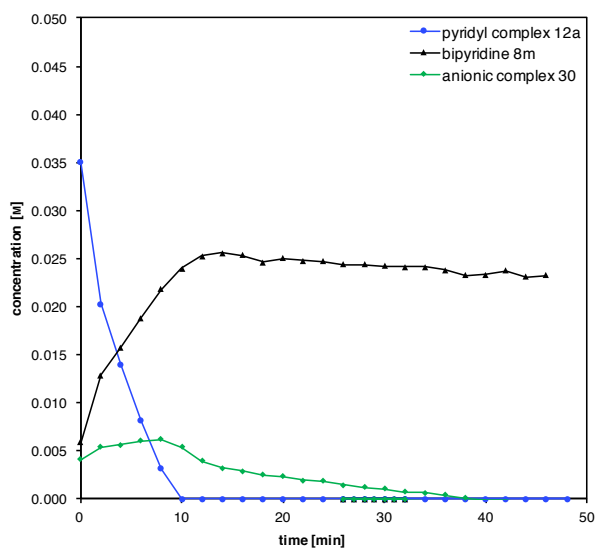


[ES 6057b]

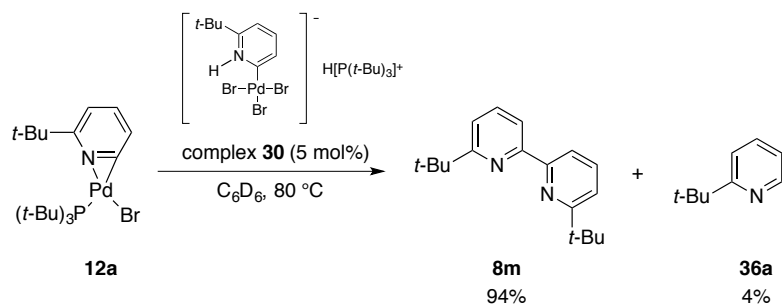
According to general procedure, pyridyl palladium complex **12a** (16.0 mg, 0.031 mmol) and anionic palladium complex **31c** (1.4 mg, 0.0010 mmol, 0.03 equiv.) were dissolved in C_6D_6 (0.68 mL) and heated to 80 °C for 1 h while recording a ^1H NMR every 2 minutes.

percentage of P in [%]

26	complex B	27	28	$\text{P}(\text{t-Bu})_3$	30
18	33	15	34	0	0

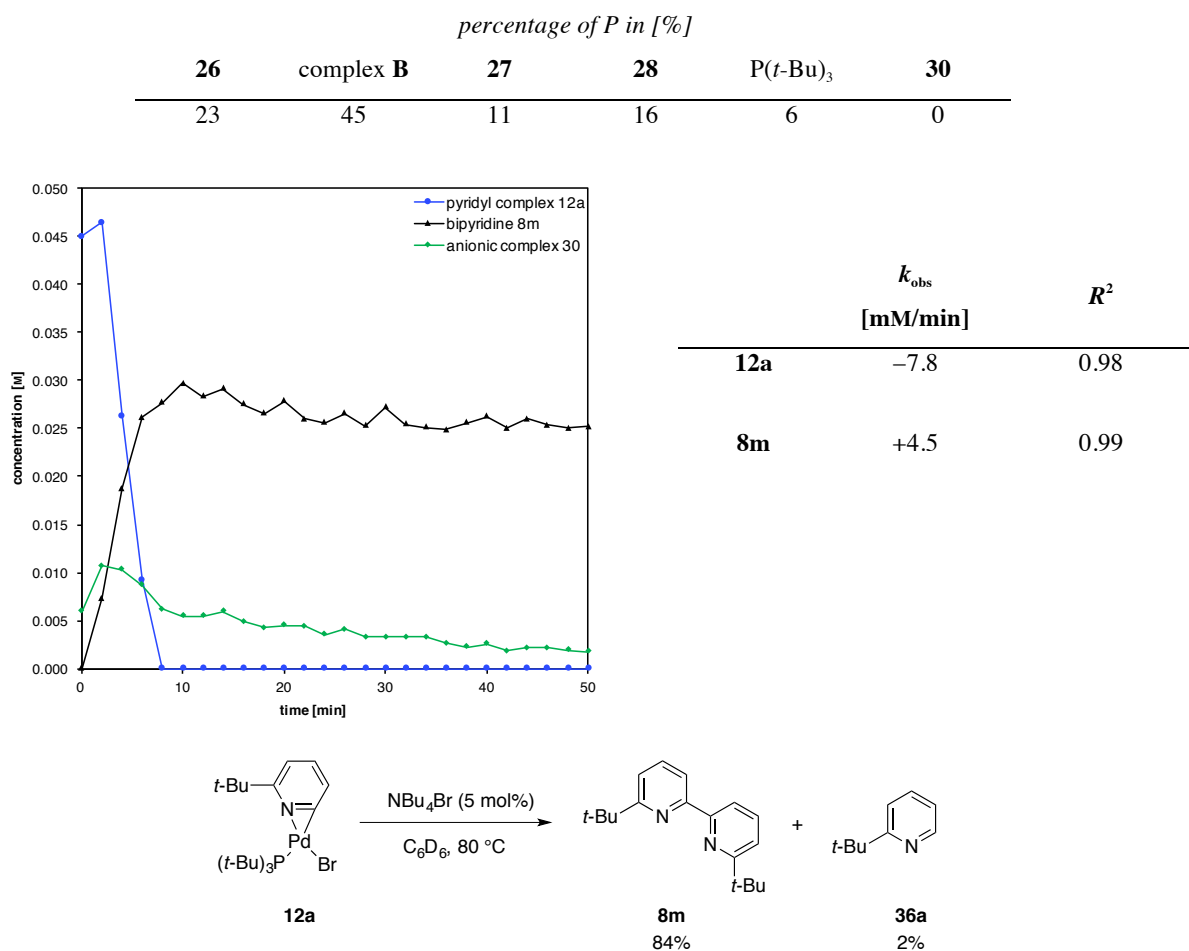


	k_{obs} [mM/min]	R^2
12a	-3.8	0.94
8m	+1.9	0.96
30	+0.24 (0-8 min)	0.84



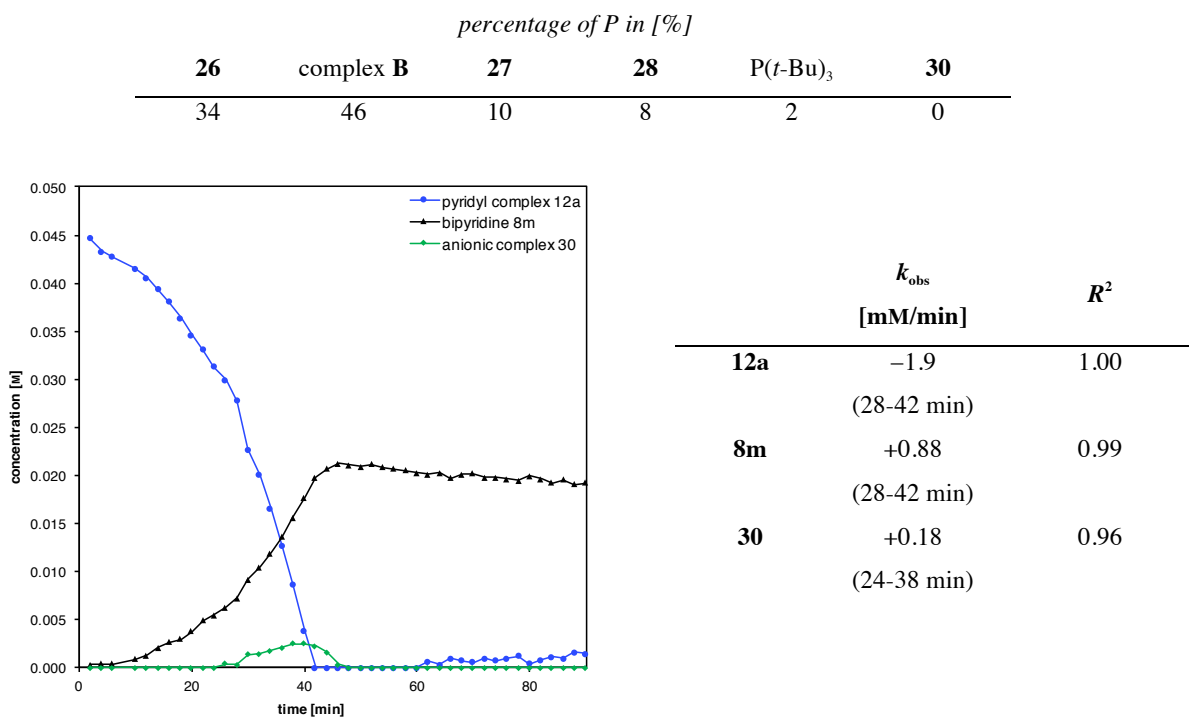
[ES 5178c]

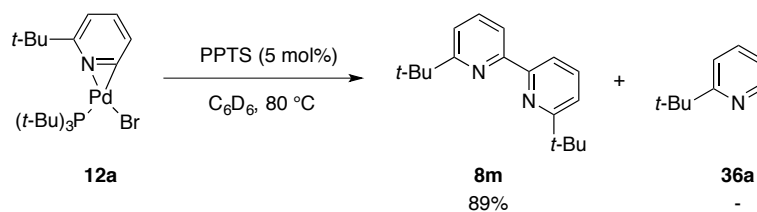
According to the general procedure, pyridyl palladium complex **12a** (16.0 mg, 0.031 mmol) and anionic pyridyl palladium complex **30** (1.0 mg, 0.0015 mmol, 0.05 equiv.) were dissolved in C_6D_6 (0.68 mL) and heated to 80 °C for 1 h while recording a ^1H NMR every 2 minutes.



[ES 5178a]

According to general procedure, pyridyl palladium complex **12a** (16.0 mg, 0.031 mmol) and NBu₄Br (0.5 mg, 0.0015 mmol, 0.05 equiv.) were dissolved in C₆D₆ (0.68 mL) and heated to 80 °C for 1 h while recording a ¹H NMR every 2 minutes.



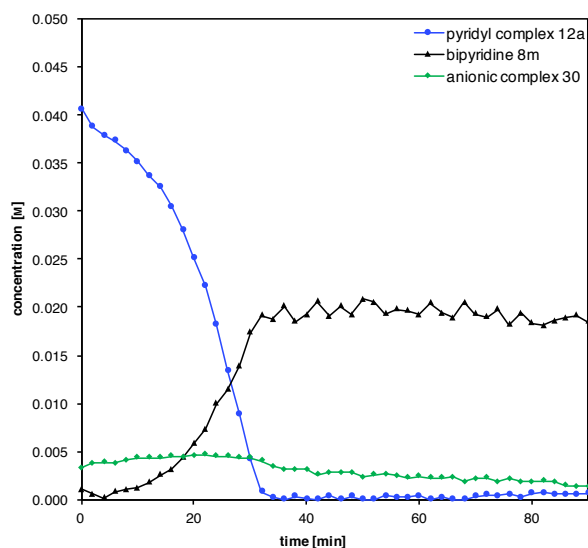


[ES 5178b]

According to general procedure, pyridyl palladium complex **12a** (16.0 mg, 0.031 mmol) and pyridinium *para*-toluenesulfonate (PPTS) (0.4 mg, 0.0015 mmol, 0.05 equiv.) were dissolved in C_6D_6 (0.68 mL) and heated to 80 °C for 1 h while recording a 1H NMR every 2 minutes. Compound **30**, **36a** not determined due to overlap with PPTS.

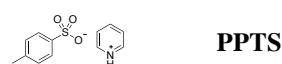
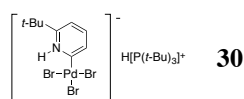
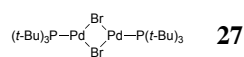
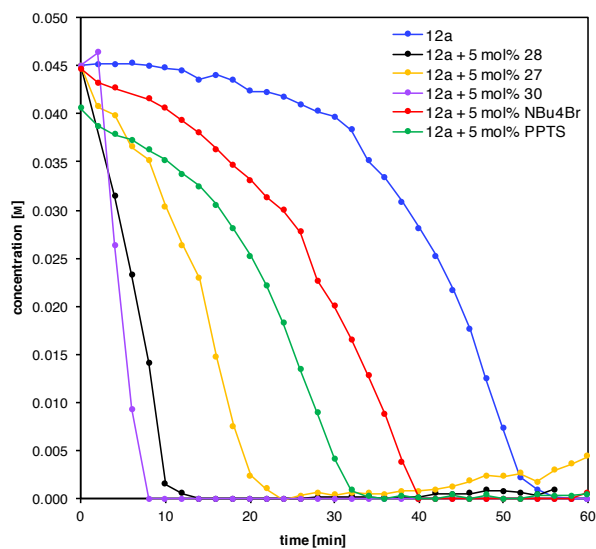
percentage of P in [%]

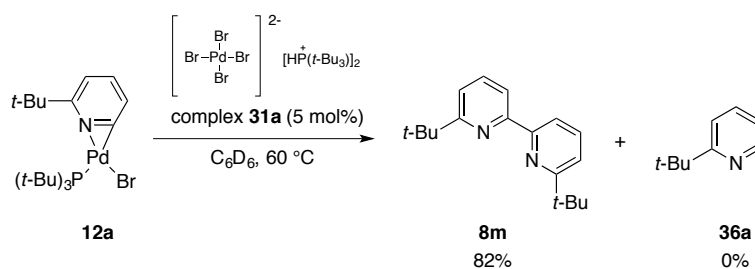
26	complex B	27	28	$P(t-Bu)_3$	30
9	27	1	54	9	0



	k_{obs} [mM/min]	R^2
12a	-1.9 (16-32 min)	0.99
8m	+1.0 (16-32 min)	0.98
30	+0.057 (0-22 min)	0.88

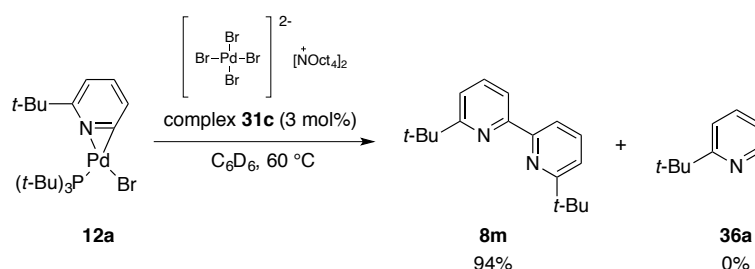
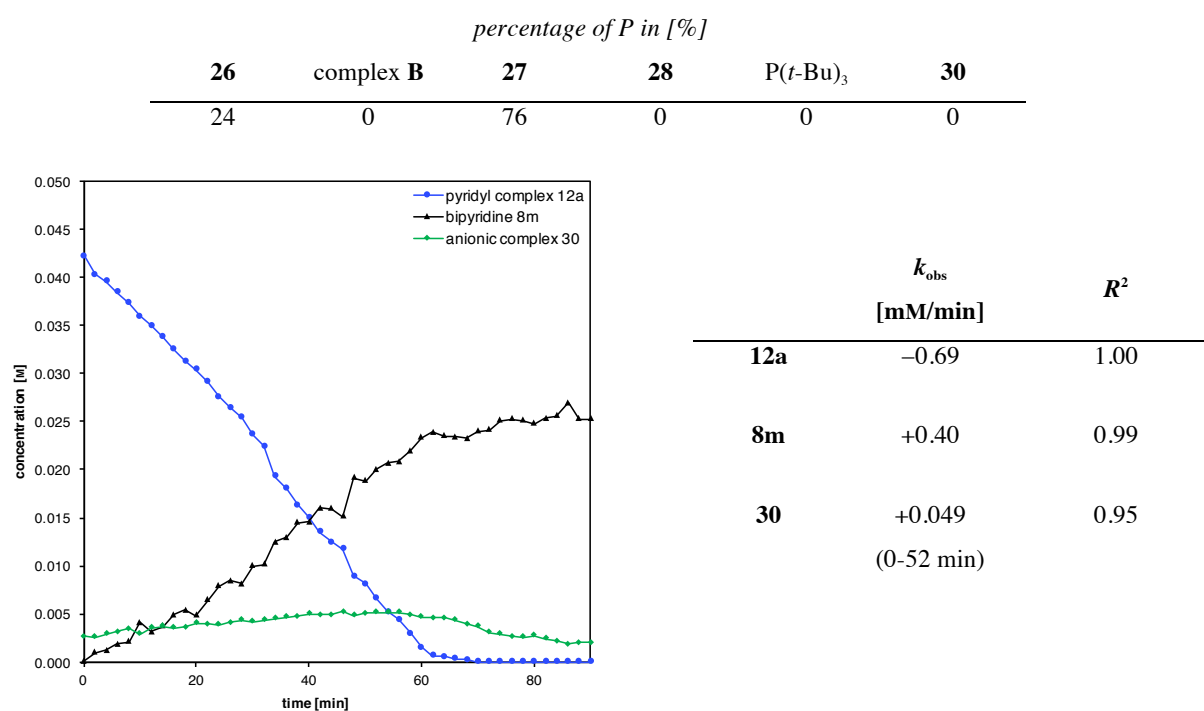
Comparison decomposition 12a with additives at 80 °C





[ES 6086a]

According to general procedure, pyridyl palladium complex **12a** (16.0 mg, 0.031 mmol) and anionic palladium complex **31a** (1.3 mg, 0.0015 mmol, 0.05 equiv.) were dissolved in C_6D_6 (0.68 mL) and heated to $60\text{ }^\circ\text{C}$ for 3 h while recording a ^1H NMR every 2 minutes.

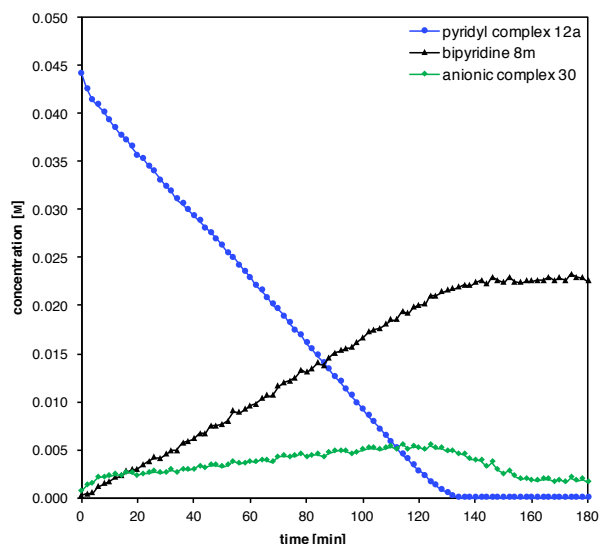


[ES 6057c]

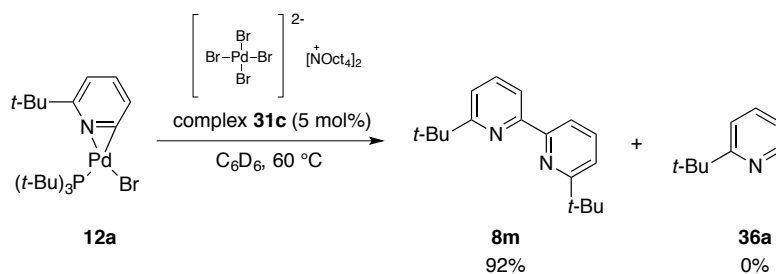
According to general procedure, pyridyl palladium complex **12a** (16.0 mg, 0.031 mmol) and anionic palladium complex **31c** (1.4 mg, 0.0010 mmol, 0.03 equiv.) were dissolved in C_6D_6 (0.68 mL) and heated to $60\text{ }^\circ\text{C}$ for 3 h while recording a ^1H NMR every 2 minutes.

percentage of P in [%]

26	complex B	27	28	$P(t\text{-Bu})_3$	30
22	22	51	1	4	0



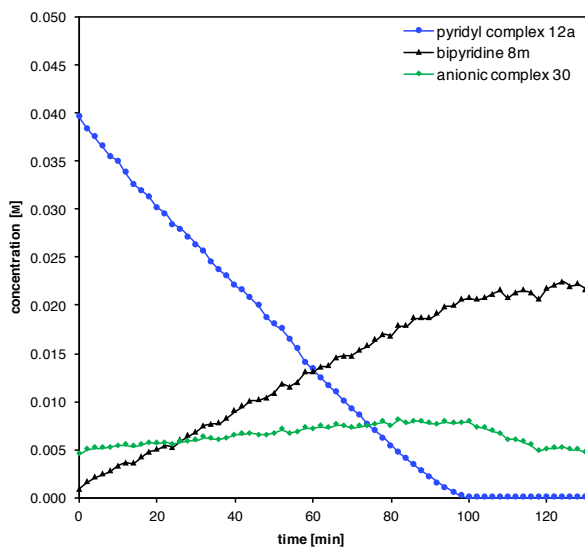
	k_{obs} [mM/min]	R^2
12a	-0.33	1.00
8m	+0.17	1.00
30	+0.031 (6-114 min)	0.98



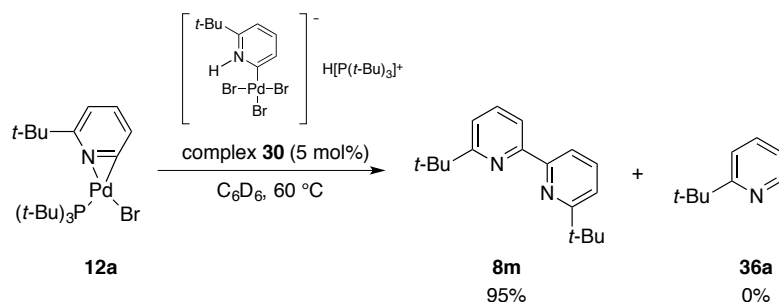
[ES 6074a]

According to general procedure, pyridyl palladium complex **12a** (16.0 mg, 0.031 mmol) and anionic palladium complex **31c** (2.1 mg, 0.0015 mmol, 0.05 equiv.) were dissolved in C_6D_6 (0.68 mL) and heated to 60 °C for 3 h while recording a ^1H NMR every 2 minutes.

percentage of P in [%]					
26	complex B	27	28	$\text{P}(t\text{-Bu})_3$	30
22	27	41	8	2	0

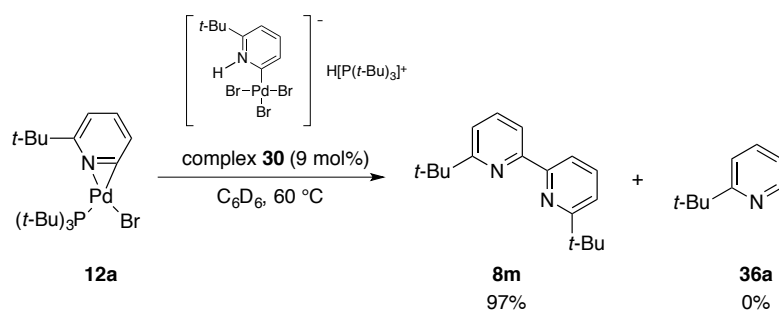
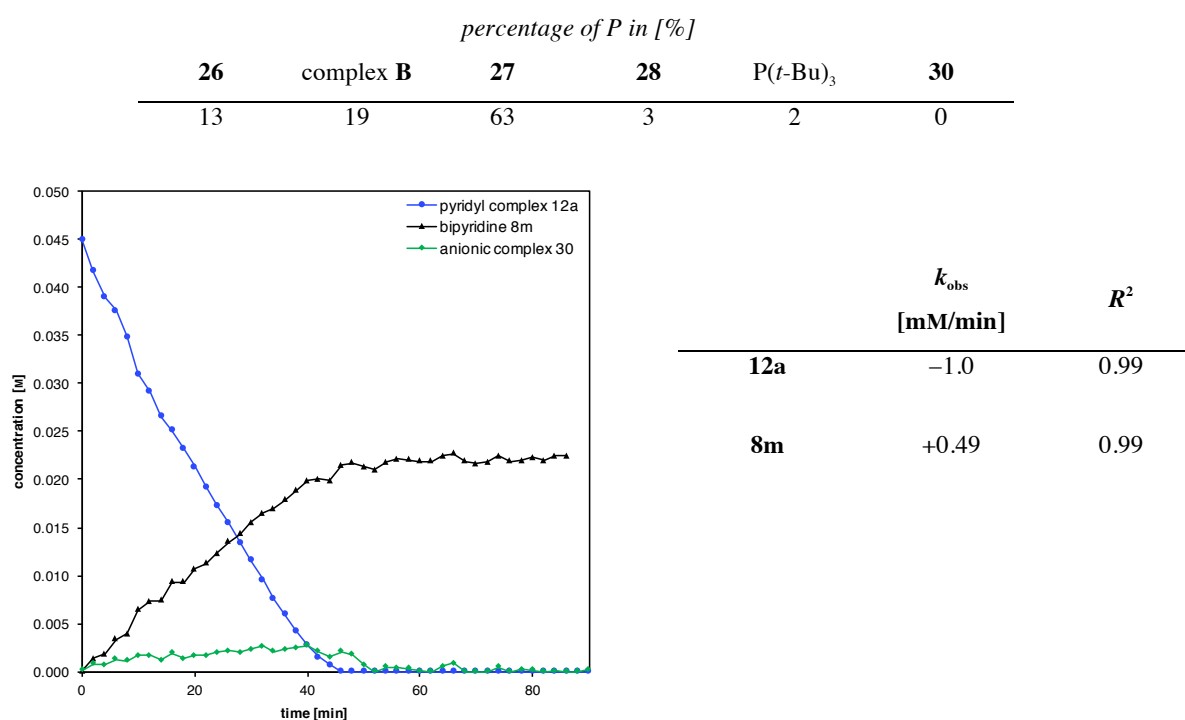


	k_{obs} [mM/min]	R^2
12a	-0.42	1.00
8m	+0.20	1.00
30	+0.036 (2-82 min)	0.97



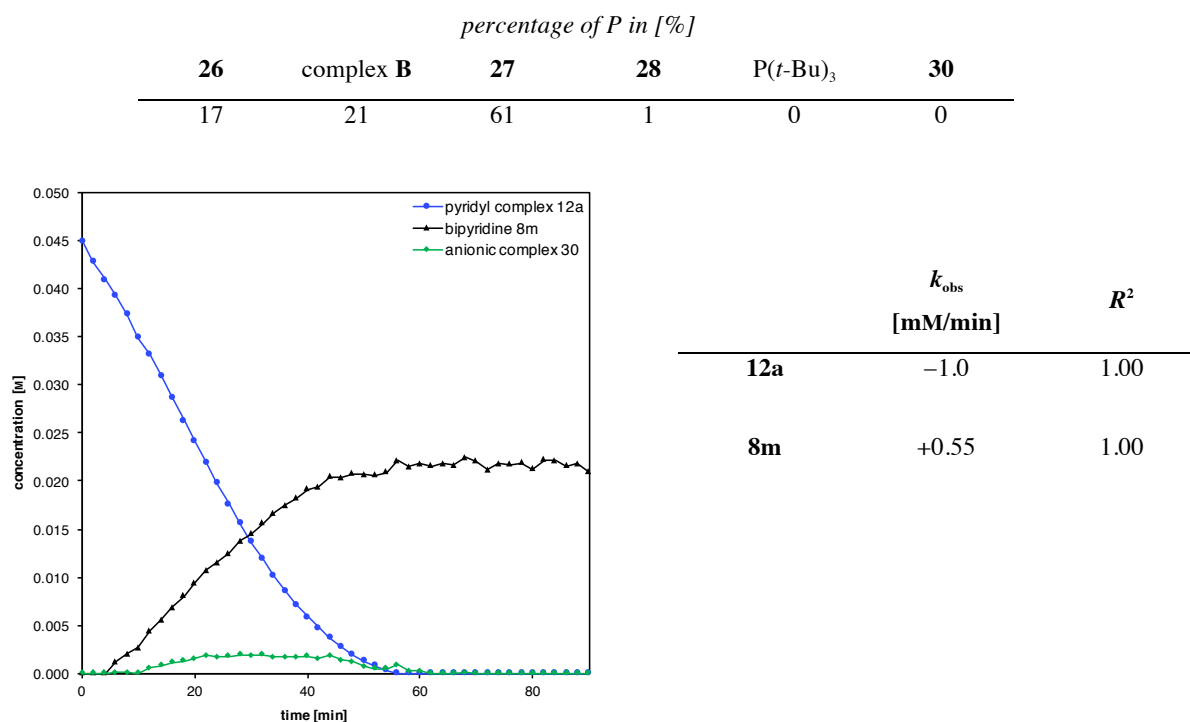
[ES 6122b]

According to general procedure, pyridyl palladium complex **12a** (16.0 mg, 0.031 mmol) and anionic pyridyl palladium complex **30** (1.0 mg, 0.0015 mmol, 0.05 equiv.) were dissolved in C_6D_6 (0.68 mL) and heated to 60 °C for 2 h while recording a ^1H NMR every 2 minutes.

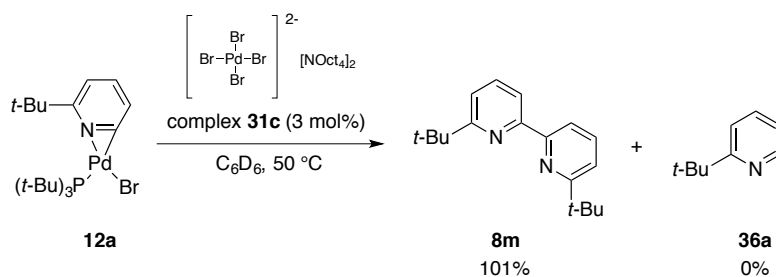
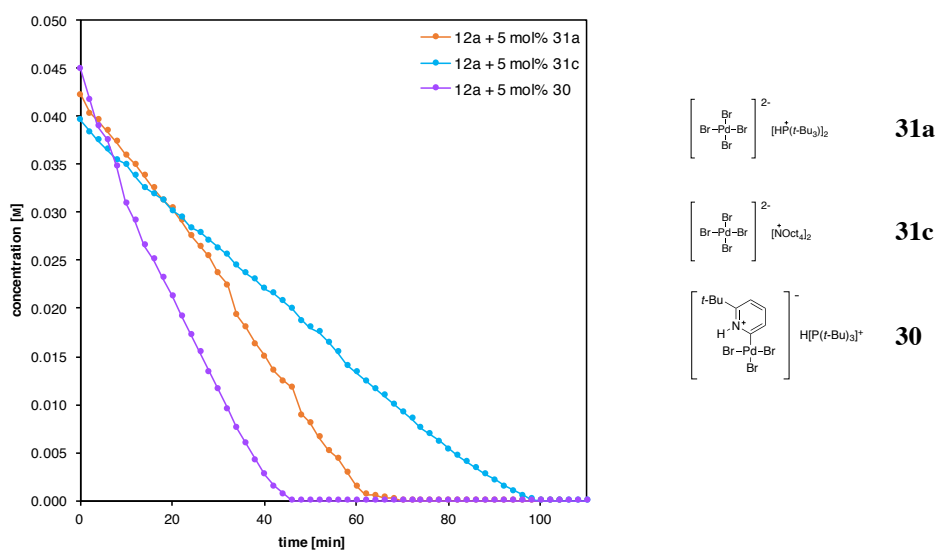


[ES 6122a]

According to general procedure, pyridyl palladium complex **12a** (16.0 mg, 0.031 mmol) and anionic pyridyl palladium complex **30** (1.8 mg, 0.0026 mmol, 0.09 equiv.) were dissolved in C_6D_6 (0.68 mL) and heated to 60 °C for 2 h while recording a ^1H NMR every 2 minutes.



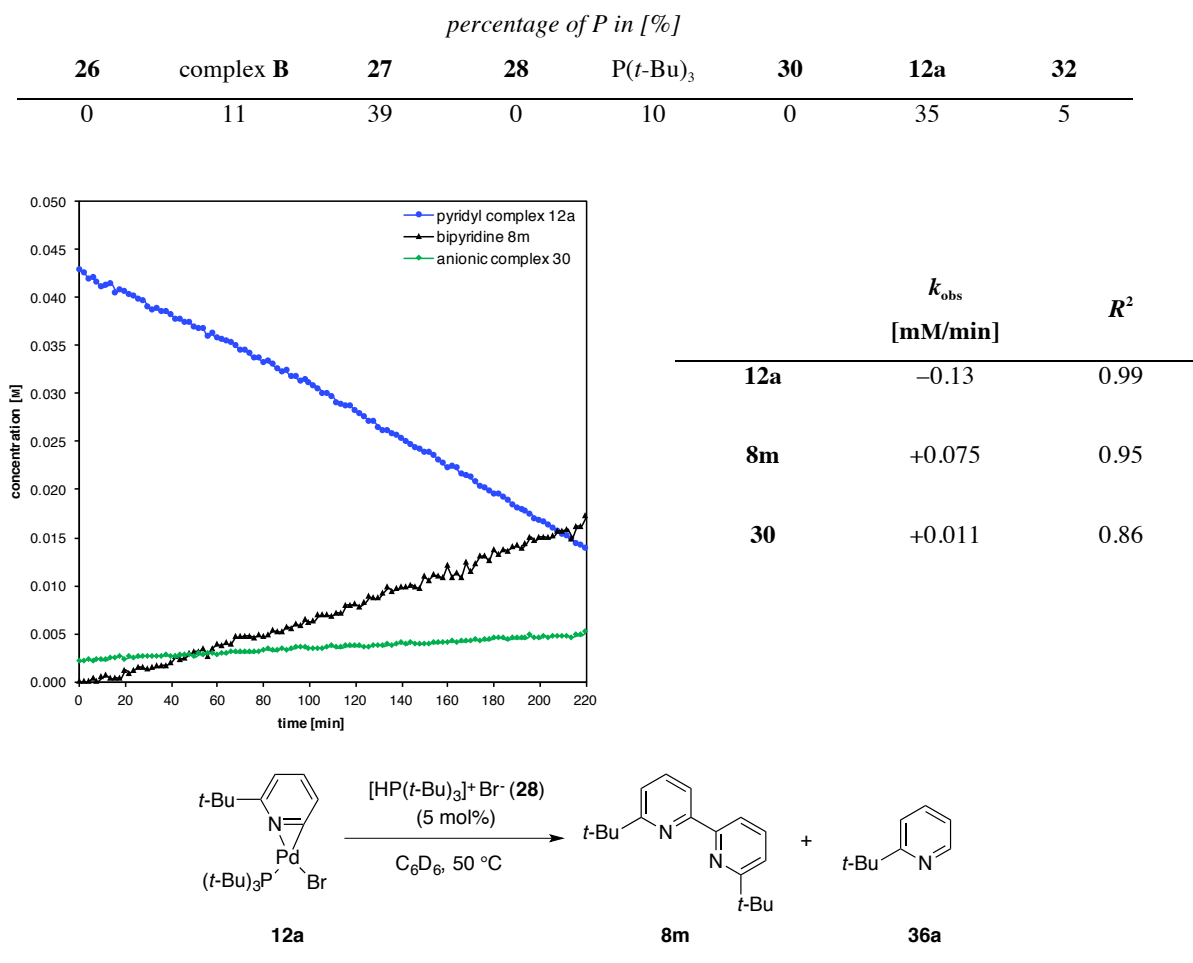
Comparison decomposition 12a with additives at 60 °C



[ES 6057a]

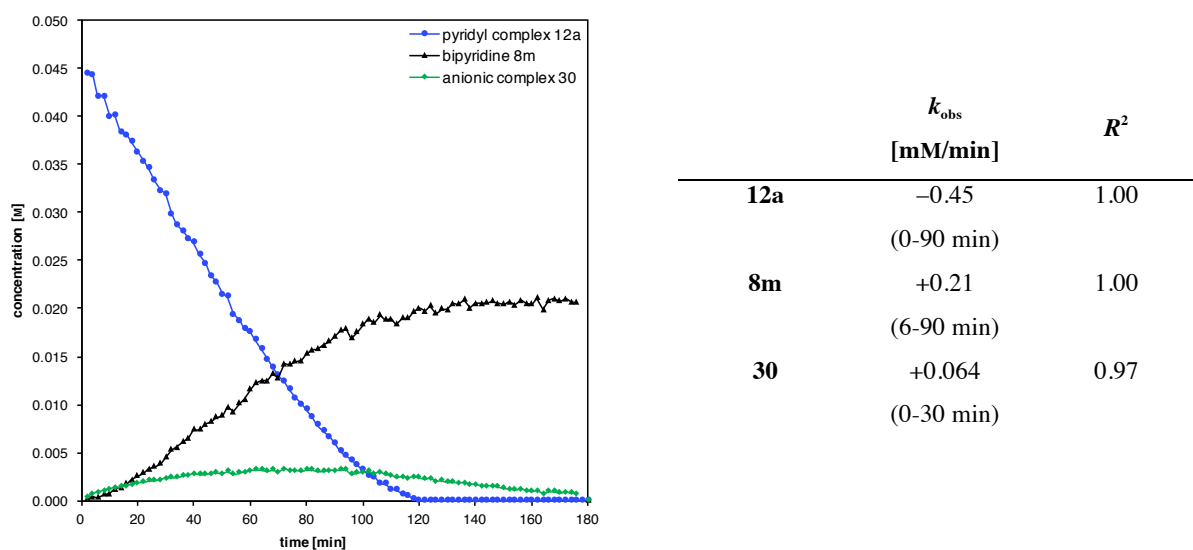
According to general procedure, pyridyl palladium complex **12a** (16.0 mg, 0.031 mmol) and anionic palladium complex **31c** (1.4 mg, 0.0010 mmol, 0.03 equiv.) were dissolved in C₆D₆ (0.68 mL) and

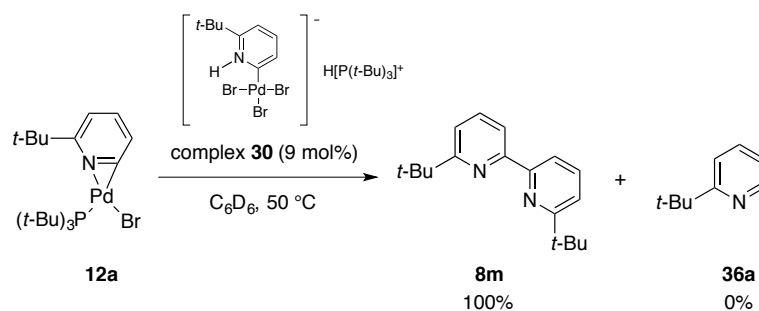
heated to 50 °C for 4 h while recording a ^1H NMR every 2 minutes. Starting material not completely consumed after 4 h.



[ES 5178e]

According to general procedure, pyridyl palladium complex **12a** (16.0 mg, 0.031 mmol) and phosphonium salt **28** (0.4 mg, 0.0015 mmol, 0.05 equiv.) were dissolved in C_6D_6 (0.68 mL) and heated to 50 °C for 3 h while recording a ^1H NMR every 2 minutes. No last NMR spectrum was measured.

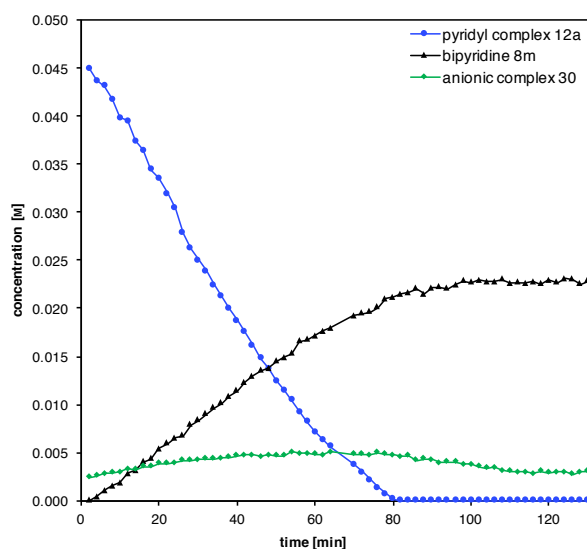




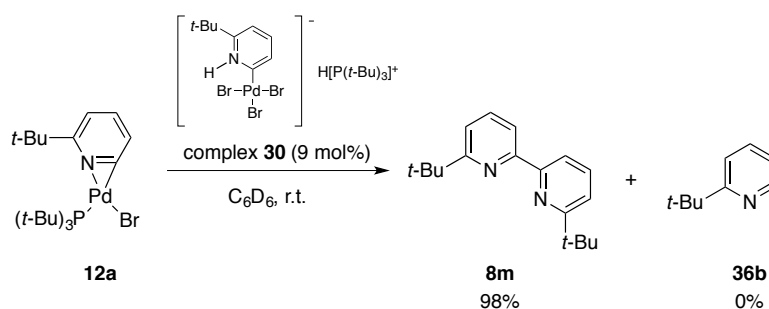
[ES 5178f]

According to general procedure, pyridyl palladium complex **12a** (16.0 mg, 0.031 mmol) and anionic pyridyl palladium complex **30** (1.8 mg, 0.0026 mmol, 0.09 equiv.) were dissolved in C_6D_6 (0.68 mL) and heated to $50\text{ }^\circ\text{C}$ for 4 h while recording a ^1H NMR every 2 minutes.

percentage of P in [%]					
26	complex B	27	28	$P(t\text{-Bu})_3$	30
11	7	67	1	0	15

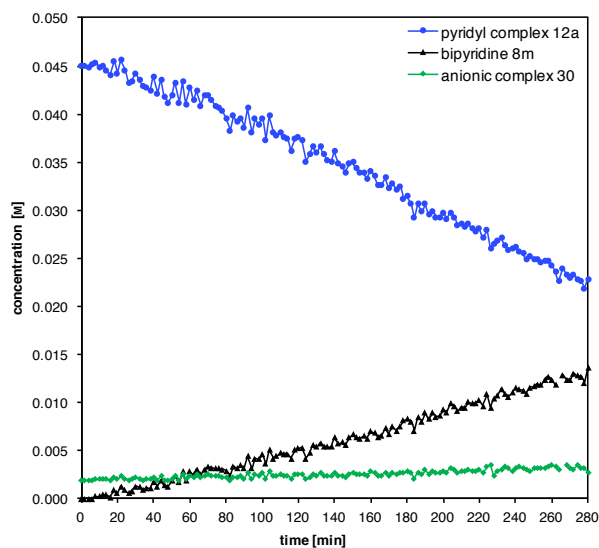


	k_{obs} [mM/min]	R^2
12a	-0.68 (0-60 min)	1.00
8m	+0.31	1.00



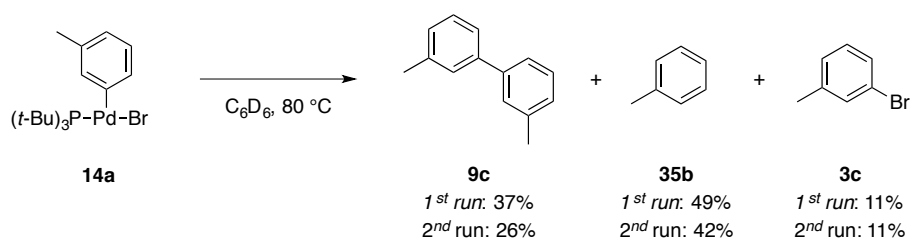
[ES 5178d]

According to general procedure, pyridyl palladium complex **12a** (16.0 mg, 0.031 mmol) and anionic pyridyl palladium complex **30** (1.8 mg, 0.0026 mmol, 0.09 equiv.) were dissolved in C_6D_6 (0.68 mL) and a ^1H NMR every 2 minutes at room temperature for 5 h was recorded. Starting material not completely consumed after 4 h. No last ^{31}P spectrum recorded.



	k_{obs} [mM/min]	R^2
12a	-0.086	0.99
8m	+0.048	0.99

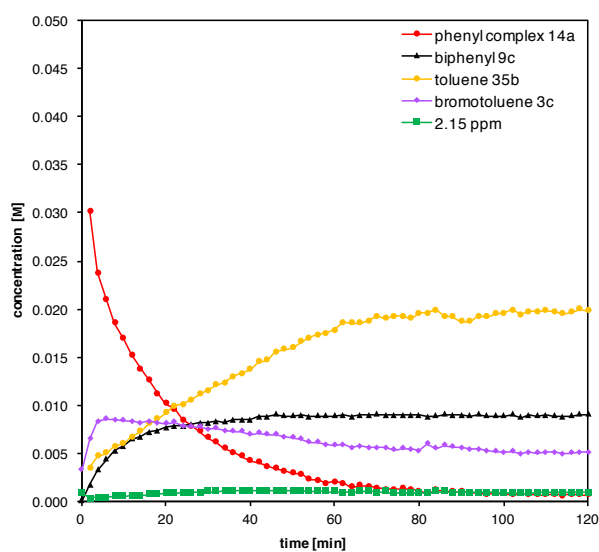
4.10.2 Phenyl palladium bromide complex **14a**



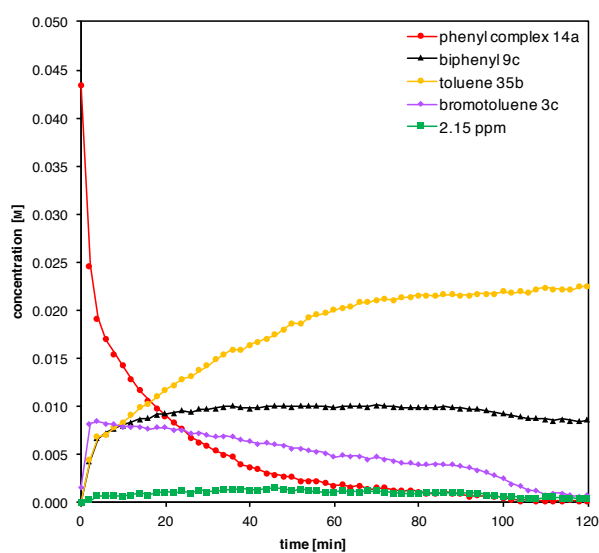
[ES 5074c/ES 5170b]

According to general procedure, phenyl palladium complex **14a** (14.7 mg, 0.031 mmol) was dissolved in C_6D_6 (0.68 mL) and heated to 80 °C for 3 h while recording a ^1H NMR every 2 minutes.

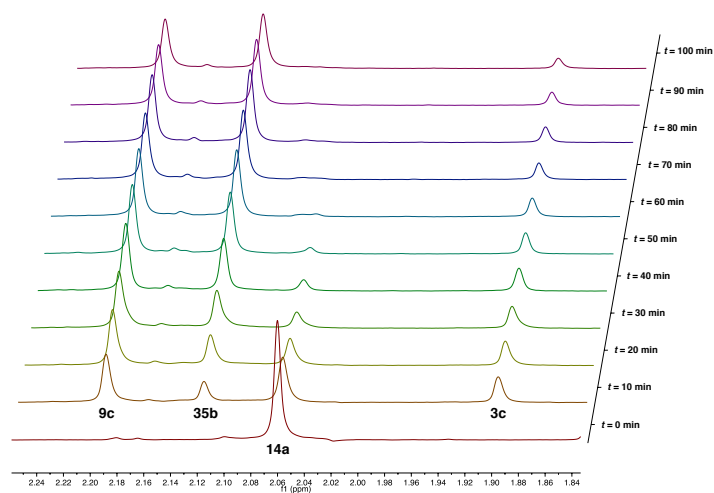
run	percentage of P in [%]				P(<i>t</i> -Bu) ₃
	26	complex B	27	28	
1 st	12	55	1	28	4
2 nd	18	57	5	18	2

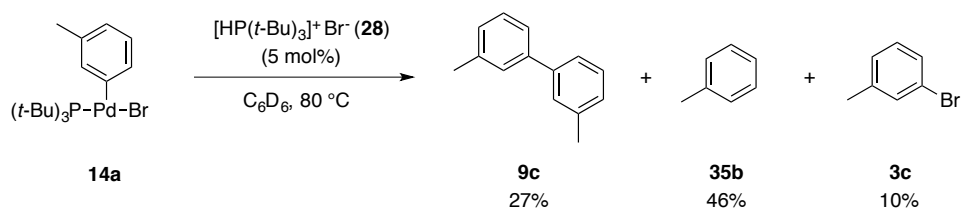
1st run:

	k_{obs} [min ⁻¹]	R^2
14a	-0.045	0.99

2nd run:

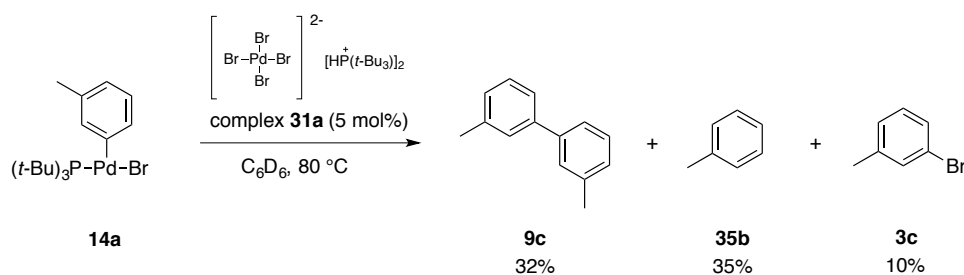
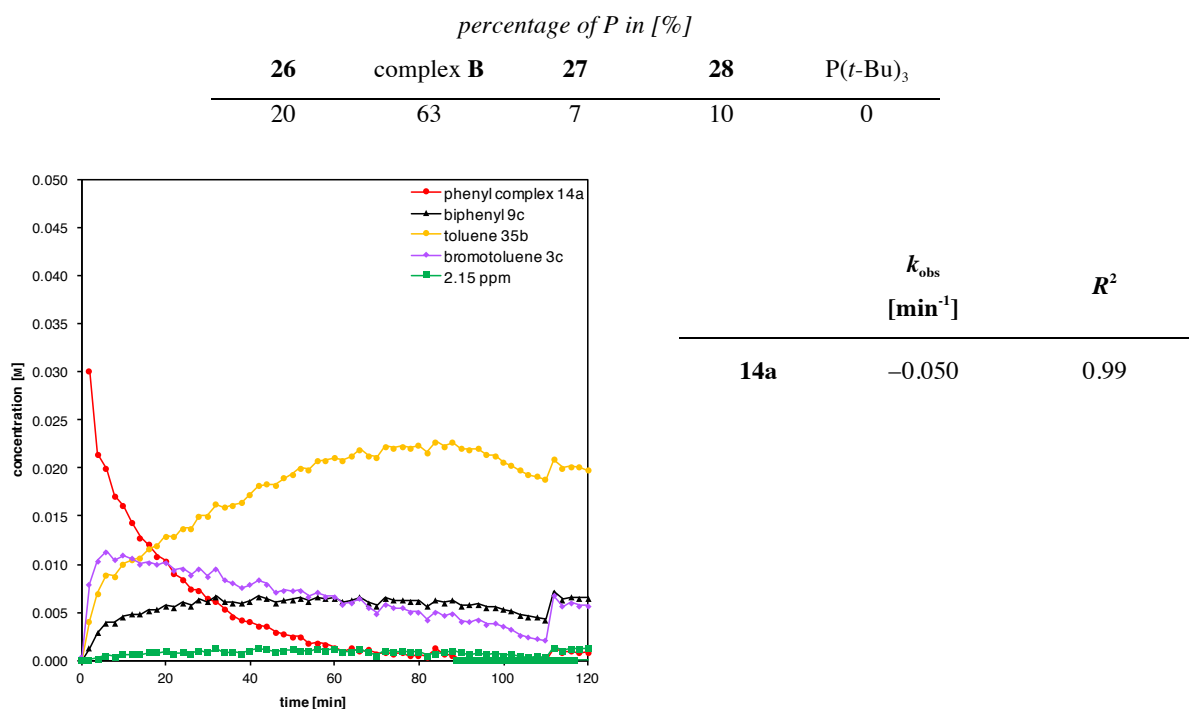
	k_{obs} [min ⁻¹]	R^2
14a	-0.045	0.98

Integrated peaks from ¹H NMR spectra ($t = 0$ to $t = 100$ min)



[ES 5170a]

According to general procedure, phenyl palladium complex **14a** (14.7 mg, 0.031 mmol) and phosphonium salt **28** (0.4 mg, 0.0015 mmol, 0.05 equiv.) were dissolved in C_6D_6 (0.68 mL) and heated to 80 °C for 3 h while recording a ^1H NMR every 2 minutes. Starting material was already consumed in the initial spectrum recorded.

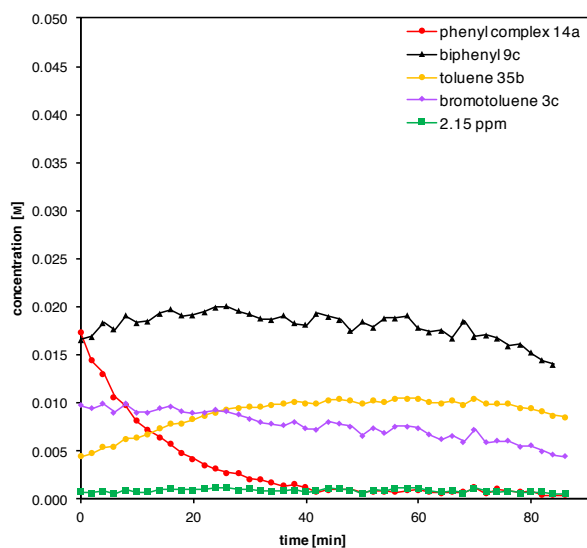


[ES 6087a]

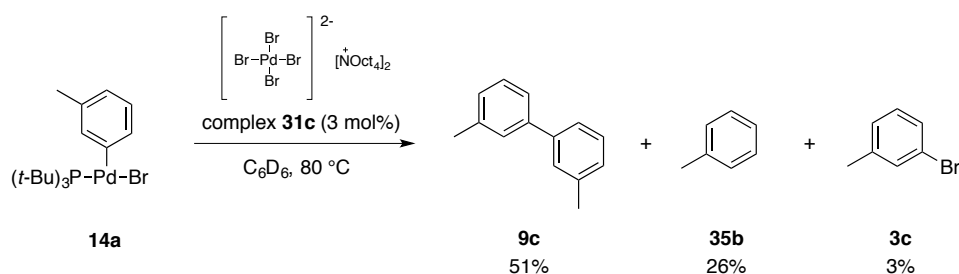
According to general procedure, phenyl palladium complex **14a** (14.7 mg, 0.031 mmol) and anionic palladium complex **31a** (1.3 mg, 0.0015 mmol, 0.05 equiv.) were dissolved in C_6D_6 (0.68 mL) and heated to 80 °C for 1.5 h while recording a ^1H NMR every 2 minutes.

percentage of P in [%]

26	complex B	27	28	$\text{P}(\text{t-Bu})_3$
21	55	11	13	0



	k_{obs} [min ⁻¹]	R^2
14a	-0.066	1.00

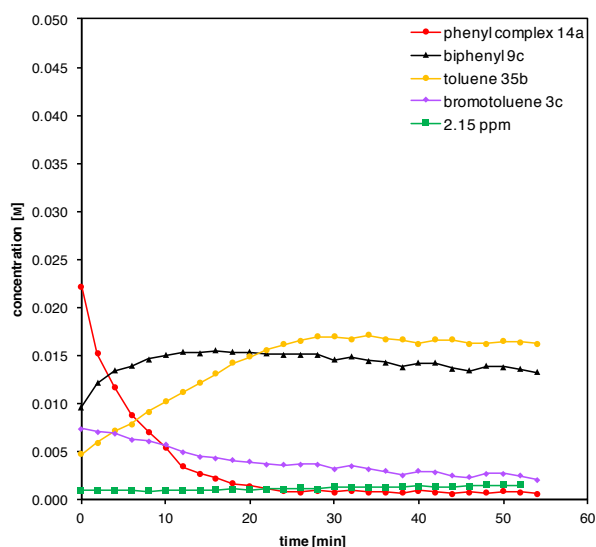


[ES 5171a]

According to general procedure, phenyl palladium complex **14a** (14.7 mg, 0.031 mmol) and anionic palladium complex **31c** (1.4 mg, 0.0010 mmol, 0.03 equiv.) were dissolved in C_6D_6 (0.68 mL) and heated to 80 °C for 1 h while recording a ^1H NMR every 2 minutes.

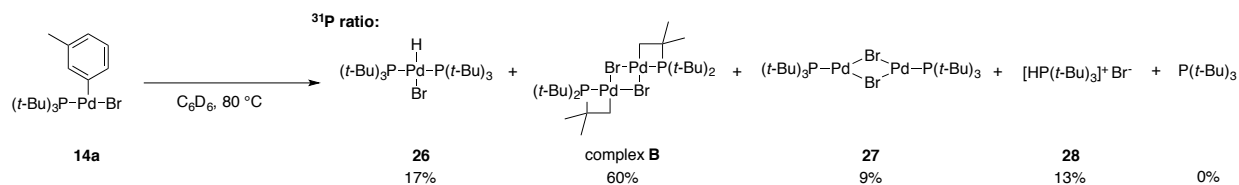
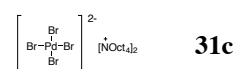
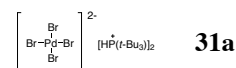
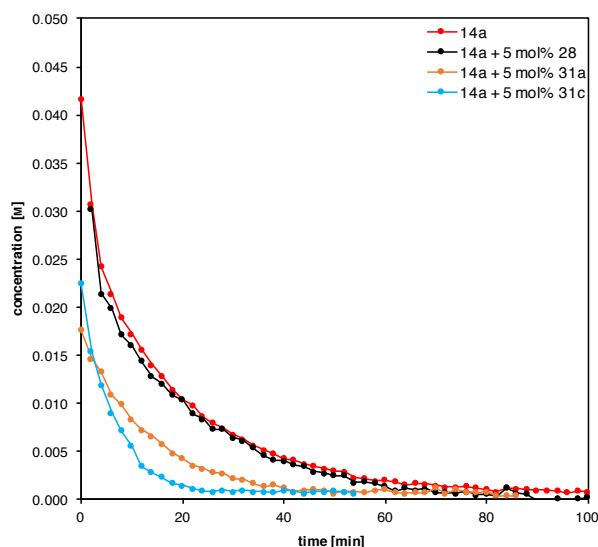
percentage of P in [%]

26	complex B	27	28	$\text{P}(t\text{-Bu})_3$
14	70	0	16	0



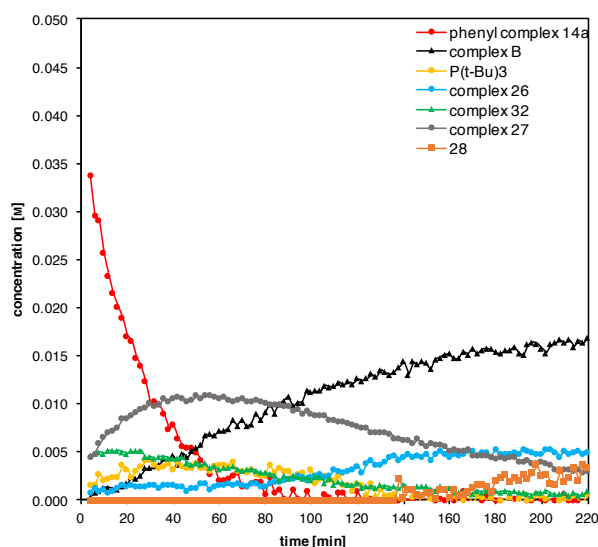
	k_{obs} [min ⁻¹]	R^2
14a	-0.13	1.00

Comparison decomposition 14a with additives



[ES 5074a]

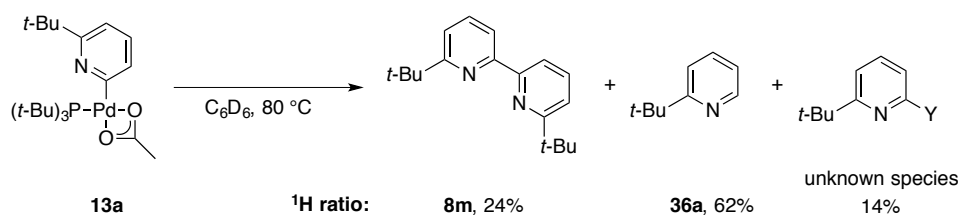
According to the general procedure, phenyl palladium complex **14a** (14.7 mg, 0.031 mmol) were dissolved in C_6D_6 (0.68 mL) and heated to 80°C for 4 h while recording a ^{31}P NMR every 2 minutes. Starting material was already consumed in the initial spectrum recorded. Formation of phosphonium species **28** not shown in plot.



	k_{obs} [min ⁻¹]	R^2
14a	-0.042	0.99

4.10.3 Pyridyl palladium acetate complex **13a**

[ES 4119a]

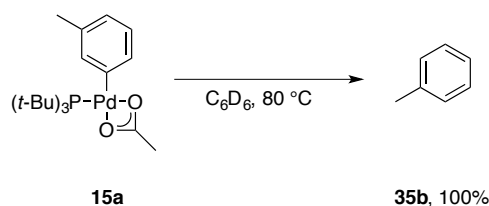


Pyridyl palladium complex **13a** (7.0 mg, 0.013 mmol) was dissolved in C_6D_6 (0.70 mL) and heated to 80 °C for ~80 h. The ratio of products was determined via 1H NMR and ^{31}P .

<i>percentage of P in [%]</i>		
32	P(<i>t</i> -Bu) ₃	O=P(<i>t</i> -Bu) ₃
27	24	49

4.10.4 Phenyl palladium acetate complex **15a**

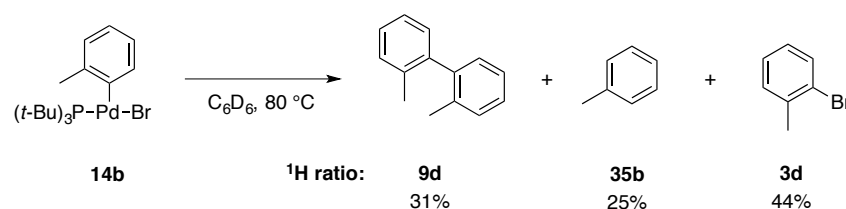
[ES 4127d]



Phenyl palladium complex **15a** (9.2 mg, 0.019 mmol) were dissolved in C_6D_6 (0.70 mL) and heated to 80 °C for ~80 h. The ratio of products was determined via 1H NMR and ^{31}P .

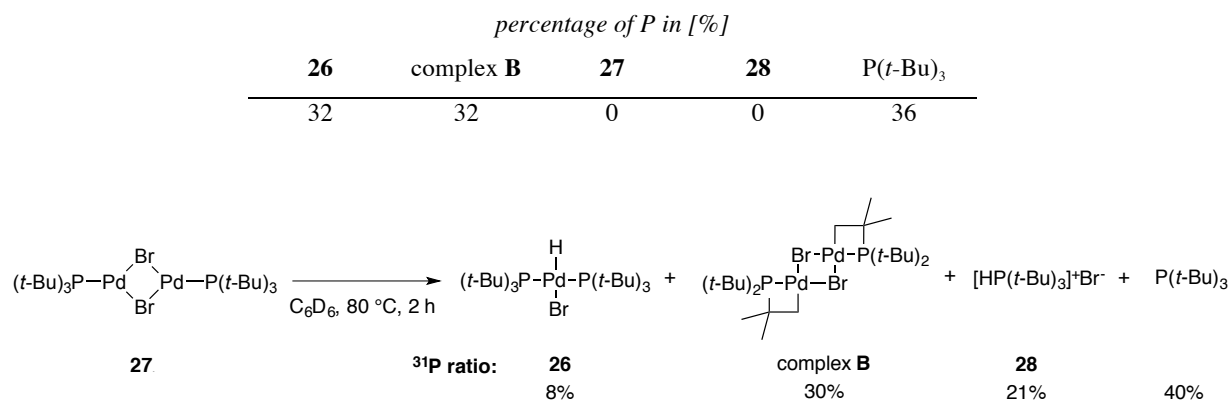
<i>percentage of P in [%]</i>		
complex A	32	O=P(<i>t</i> -Bu) ₃
80	6	14

4.10.5 Decomposition of other aryl palladium complexes



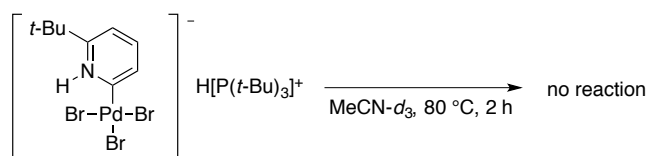
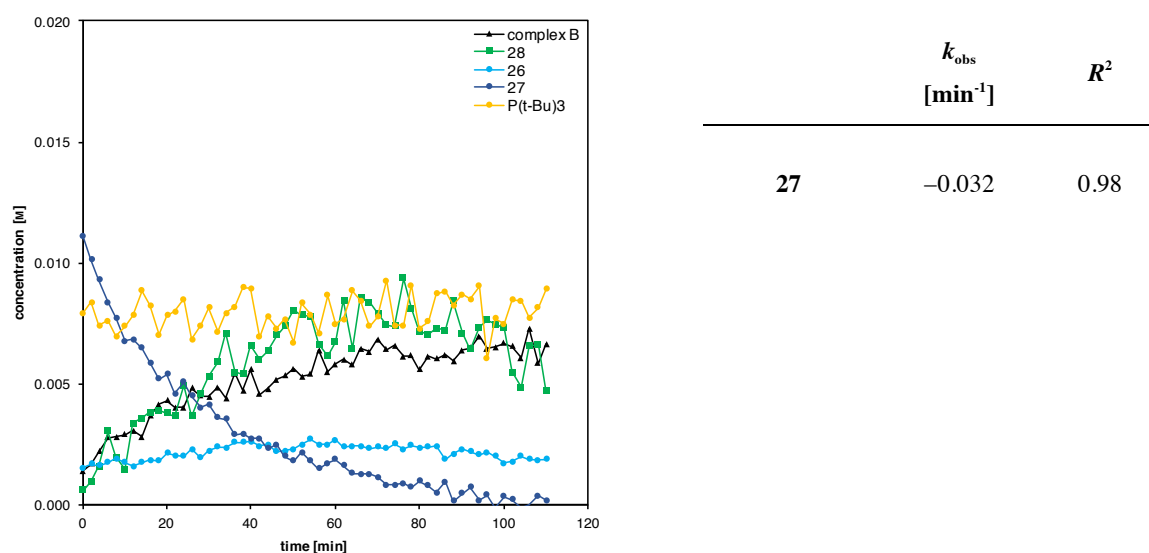
[ES 4072/ES 5075a]

Phenyl palladium complex **14b** (14.7 mg, 0.031 mmol) was dissolved in C_6D_6 (0.68 mL) and heated to 80 °C for 4 h. The ratio of products was determined via 1H NMR. No product formation was monitored due to poor solubility of **14b** in C_6D_6 .



[ES 6078]

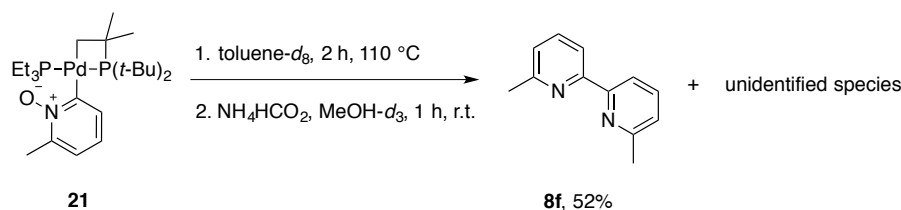
According to general procedure, palladium(I)-dimer **27** (11.9 mg, 0.0153 mmol) was in C₆D₆ (0.68 mL) was heated at 80 °C and a ³¹P NMR was recorded every 2 minutes for 2 h.



[ES 5093a]

Anionic palladium complex **30** (5.3 mg, 0.0077 mmol) was dissolved in MeCN-*d*₃ (0.70 mL) and heated to 80 °C for 2 h. No change was observed in the ¹H NMR or ³¹P NMR.

4.10.6 Methyl pyridyl *N*-oxide palladium complex **21**

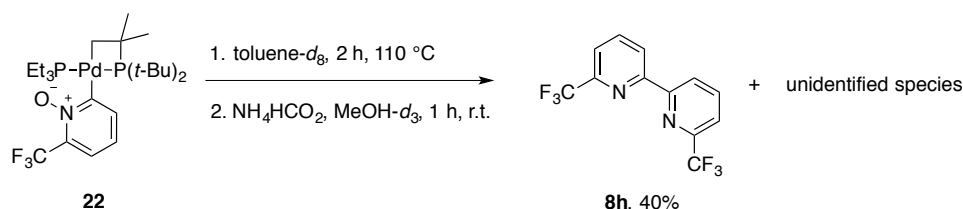


[ES 6172a]

In a glovebox, pyridyl *N*-oxide complex **21** (19.1 mg, 0.036 mmol) was weighed in an NMR tube with a J Young valve, dissolved in toluene-*d*₈ (0.65 mL) and heated to 110 °C for 2 h. A ³¹P NMR was recorded to verify complete consumption of starting material. The reaction mixture was opened to air and 1,3,5-trimethoxybenzene (3.3 mg, 0.020 mmol) in MeOH-*d*₃ (0.15 mL) was added. A spatula tip of NH₄HCO₂ was added and the reaction stirred at room temperature for 1 h. After filtering off the solids, the yield of bipyridine **8f** (0.0093 mmol, 52%) was determined via ¹H NMR and the phosphorus ratio via ³¹P NMR.

percentage of P in [%]			
entry	shift δ [ppm]	prior reduction	after reduction
1	218.9	10	9
2	123.3	10	9
3	122.0	25	22
4	58.2		6
5	52.6		9
6	47.3	8	
7	8.40	10	10
8	0.63	11	12
9	-2.23	26	23

4.10.7 Trifluoromethyl pyridyl *N*-oxide palladium complex **22**



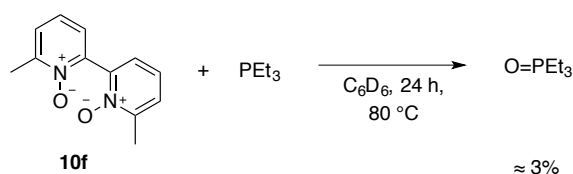
[ES 6172b]

In a glovebox, pyridyl *N*-oxide complex **22** (19.7 mg, 0.034 mmol) was weighed in an NMR tube with a J Young valve, dissolved in toluene-*d*₈ (0.65 mL) and heated to 110 °C for 2 h. A ³¹P NMR was recorded to verify complete consumption of starting material. The reaction mixture was opened to air and 1,3,5-trimethoxybenzene (3.3 mg, 0.020 mmol) in MeOH-*d*₃ (0.15 mL) was added. A spatula tip of NH₄HCO₂ was added and the reaction stirred at room temperature for 1 h. After filtering off the solids, the yield of bipyridine **8h** (0.0067 mmol, 40%) was determined via ¹H NMR and the phosphorus ratio via ³¹P NMR (minor peaks not shown).

percentage of P in [%]			
entry	shift δ [ppm]	prior reduction	after reduction
1	218.9	7	5
2	123.3	7	6

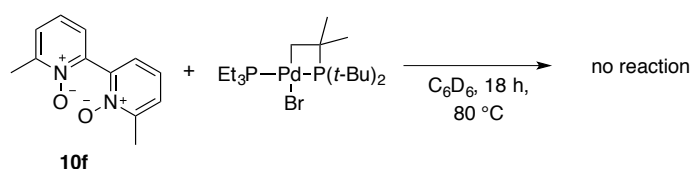
3	122.0	26	18
4	68.3		4
5	58.2		5
6	53.4		16
7	48.7	11	
8	12.8	3	4
9	8.39	6	6
10	0.57	7	10
11	-2.24	28	18

4.10.8 Control experiments



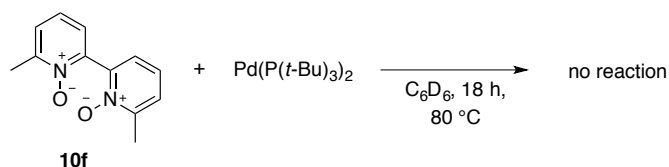
[ES 5042]

In a glovebox, bipyridine *N,N'*-dioxide **10f** (15.0 mg, 0.069 mmol, 1.0 equiv.) was weighed in an NMR tube with a J Young valve. CC(C)OP (16.4 mg, 0.14 mmol, 2.0 equiv.) and C6D6 (0.65 mL) were added and the reaction was heated at 80 °C outside of the glovebox for 24 h, resulting in ~3% oxidation of CC(C)OP to CC(C)OP=O. ^1H NMR indicated formation of new unidentified aromatic signals at low concentration.



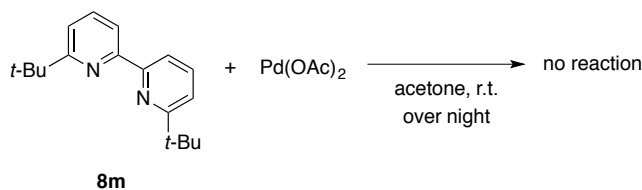
[ES 4186a]

In a glovebox, bipyridine *N,N'*-dioxide **10f** (4.1 mg, 0.019 mmol, 1.0 equiv.) and complex **C** (9.6 mg, 0.019 mmol, 1.0 equiv.) were weighed in an NMR tube with a J Young valve. C6D6 (0.65 mL) was added and the reaction was heated at 80 °C outside of the glovebox for 18 h. No change was observed via ^1H or ^{31}P NMR.



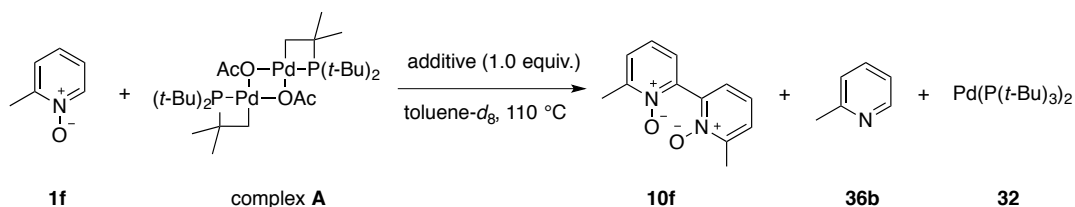
[ES 4186b]

In a glovebox, bipyridine *N,N'*-dioxide **10f** (4.1 mg, 0.019 mmol, 1.0 equiv.) and palladium(0) complex **32** (9.7 mg, 0.019 mmol, 1.0 equiv.) were weighed in an NMR tube with a J Young valve. C_6D_6 (0.65 mL) was added and the reaction was heated at 80 °C outside of the glovebox for 18 h. No change was observed via 1H or ^{31}P NMR.



[ES 5048]

According to reported procedure,²³⁴ bipyridine **8m** (10.0 mg, 0.037 mmol, 1.0 equiv.) and $Pd(OAc)_2$ (7.6 mg, 0.034 mmol, 0.9 equiv.) were weighed in a round-bottom flask and dissolved in acetone (1.0 mL). After stirring at room temperature over night, the precipitate was washed with acetone and hexane and dried on high vacuum. No new aromatic signals could be identified via 1H NMR.

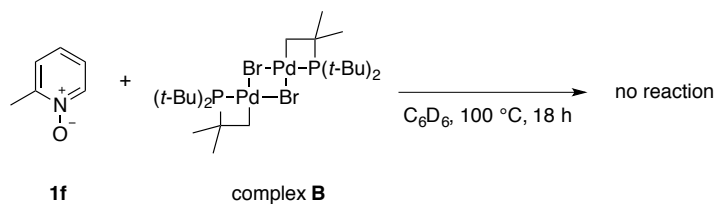


[ES 5148]

In a glovebox, pyridine *N*-oxide **1f** (11.5 mg, 0.011 mmol, 2.0 equiv.), palladium complex **A** (38.6 mg, 0.051 mmol, 1.0 equiv.) and additive were weighed in an NMR tube with a J Young valve and dissolved in toluene- d_8 (0.70 mL) and heated to 100 °C for 18 h. Homocoupling product **10f** and reduced starting material **36b** was observed via 1H NMR, however no yield was determined due to peak overlap. Minor ^{31}P peaks are not shown.

entry	shift δ [ppm]	percentage of P in [%]					
		w/o additive		+ K_3PO_4		+ pyridine (34c)	
		15 min	18 h	15 min	18 h	15 min	18 h
1	137			11			
2	129	7		48			
3	124		44	13	30		49
4	123		6		7		18

5	94		2		9
6	85	1	6		8
7	65		11		
8	62		19		19
9	61		7		11
10	32			4	
11	20			18	
12	-7.8	92			100



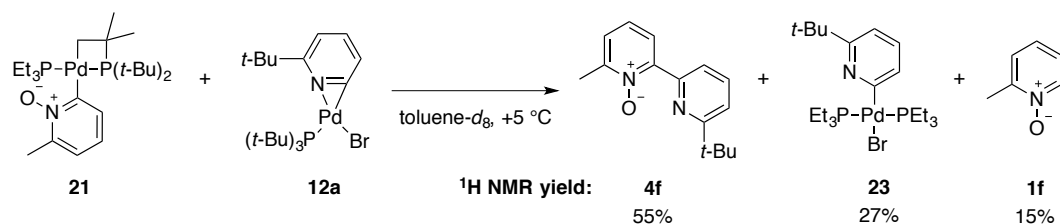
[ES 6045b]

In a glovebox, pyridine *N*-oxide **1f** (12.2 mg, 0.011 mmol, 2.0 equiv.) and palladium complex **B** (43.5 mg, 0.056 mmol, 1.0 equiv.) were weighed in an NMR tube with a J Young valve and dissolved in C_6D_6 (0.70 mL) and heated to 100 °C for 18 h. No homocoupling of *N*-oxide **1f** was observed via 1H NMR.

4.11 Transmetalation between aryl palladium complexes

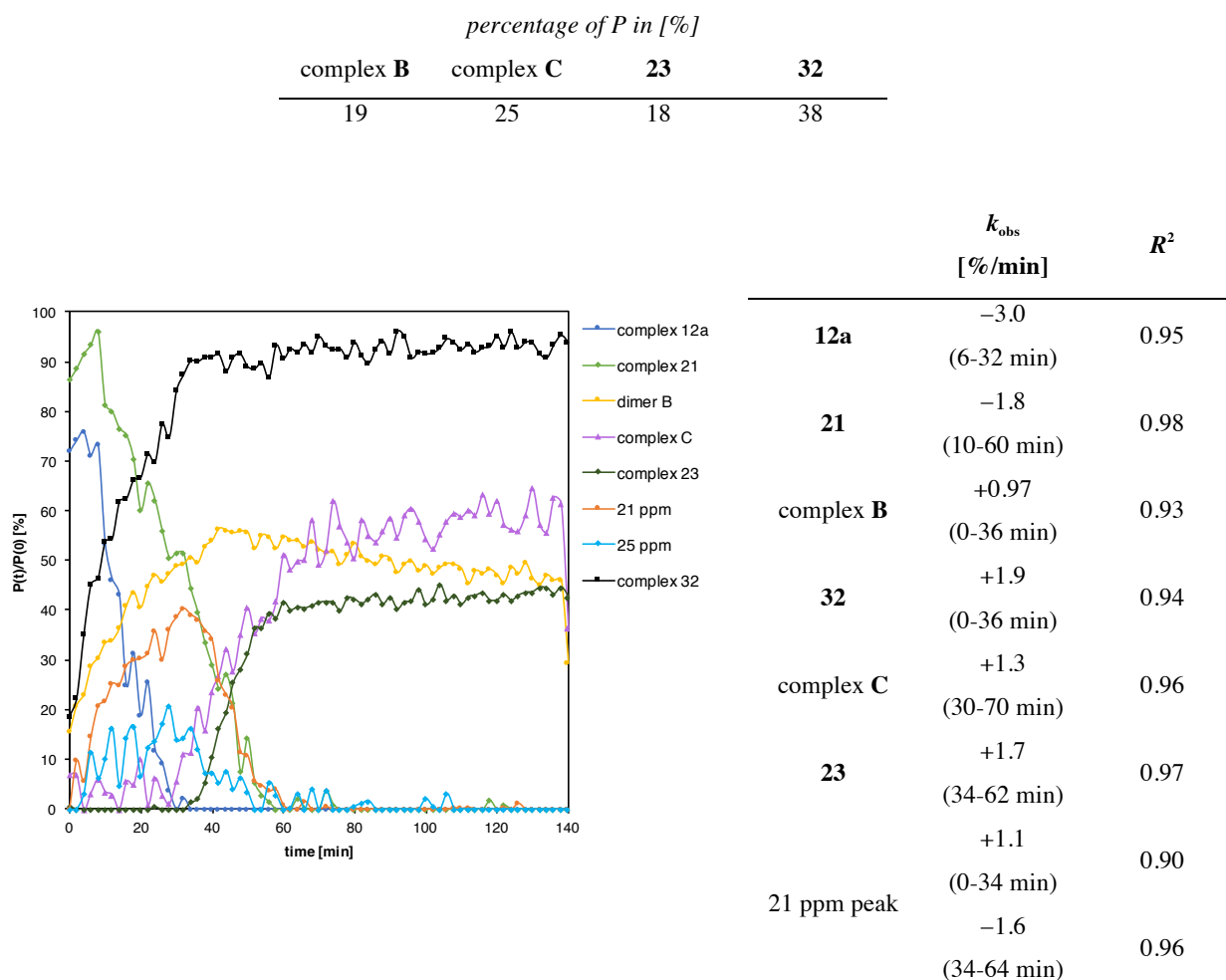
General procedure

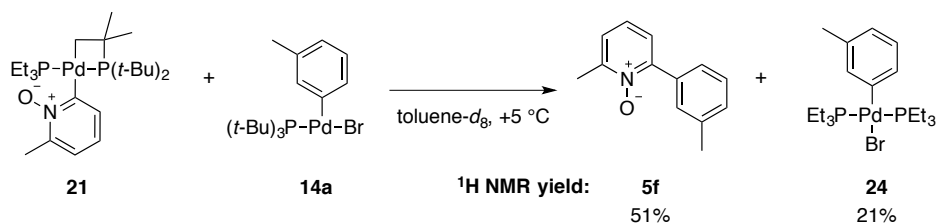
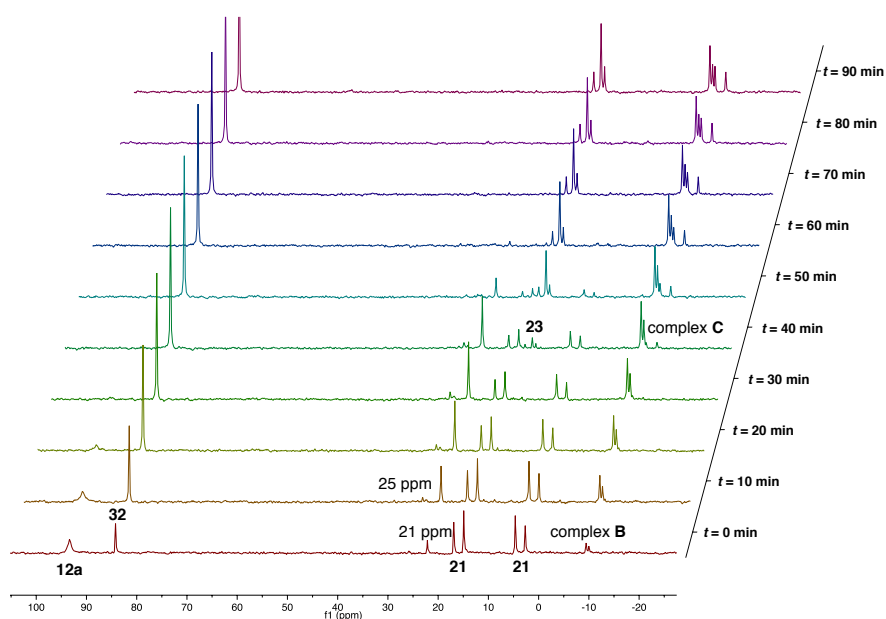
Pyridyl *N*-oxide palladium complex **21** or **22** (0.016 mmol, 1.0 equiv.) was weighed in an NMR tube in the glovebox and toluene- d_8 (0.35 mL, $c = 0.045$ M) was added. The NMR tube was sealed with a rubber septum and removed from the glovebox. After cooling the NMR tube to -78 °C, a stock solution of aryl palladium complex **12a** or **14a** in toluene- d_8 ($c = 0.045$ M, 0.35 mL, 1.0 equiv.) was added via syringe. The tube was kept at -78 °C until transferred to the pre-cooled NMR spectrometer. A spectrum was recorded every 2 minutes for a period of 3 or 4 h. The reaction was opened to air and 1,3,5-trimethoxybenzene was added and yield was determined via 1H NMR. Temperature-dependent change in chemical shift was determined for the isolated compounds. No internal standard was used over the course of reaction and the consumption and formation is given as percentage of phosphorus species in the initial sample.

4.11.1 Transmetalation with methyl pyridyl *N*-oxide complex **21**

[ES 6038a]

According to general procedure, pyridyl *N*-oxide complex **21** (8.4 mg, 0.016 mmol) and pyridyl complex **12a** (8.2 mg, 0.016 mmol) was monitored for 3 h at 5 °C with ³¹P NMR. With the addition of 1,3,5-trimethoxybenzene (3.8 mg, 0.023 mmol), bipyridine *N*-oxide **4f** (0.0087 mmol, 55%), complex **23** (0.043 mmol, 27%) and pyridine *N*-oxide **1f** (0.024 mmol, 15%) based on separate starting complex were obtained. No homocoupling product **8m** was observed.

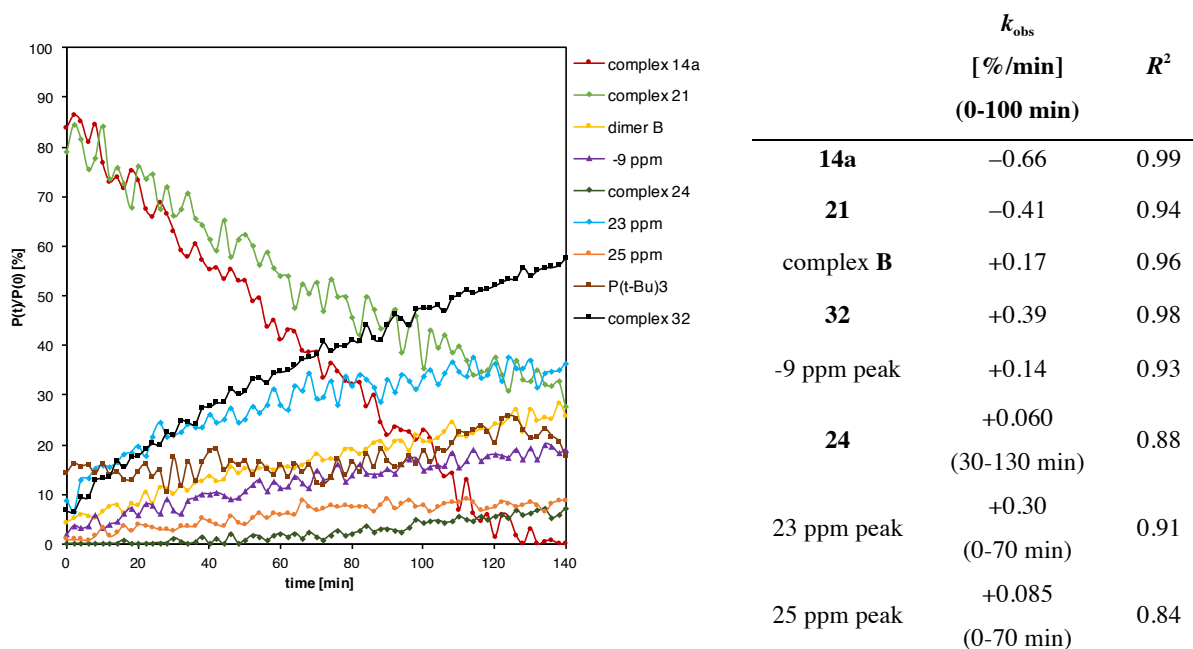
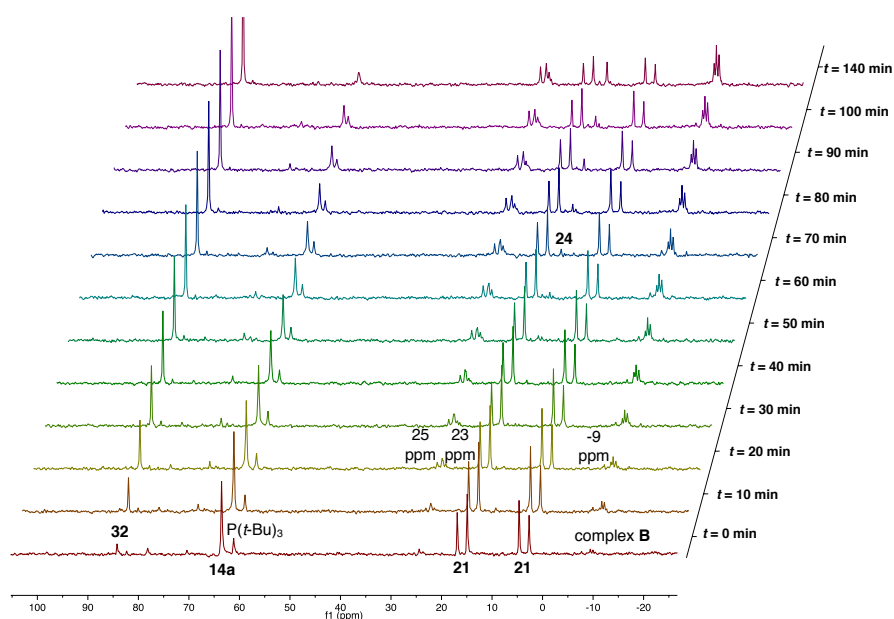
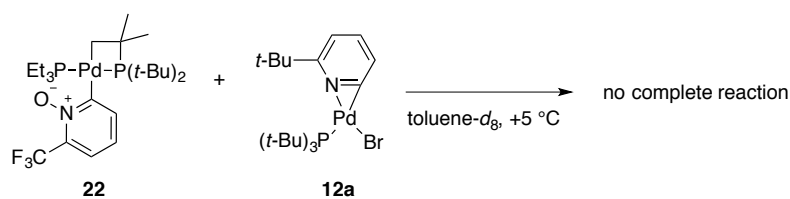


Integrated peaks from ^{31}P NMR spectra ($t = 0$ to $t = 90$ min)

[ES 5117c]

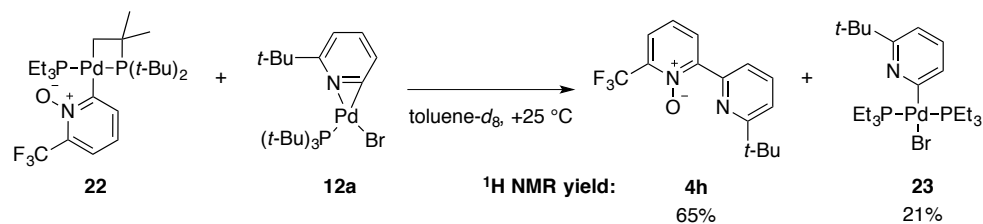
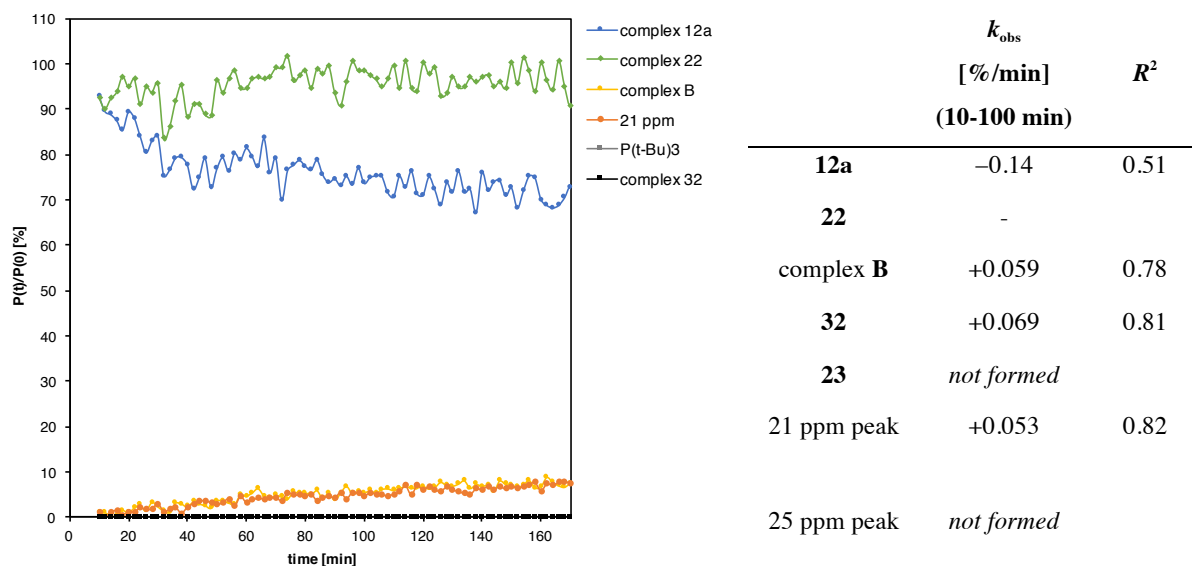
According to general procedure, pyridyl *N*-oxide complex **21** (8.4 mg, 0.016 mmol) and phenyl complex **14a** (7.6 mg, 0.016 mmol) was monitored for 3 h at 5 °C with ^{31}P NMR. With the addition of 1,3,5-trimethoxybenzene (3.6 mg, 0.021 mmol), arylpyridine *N*-oxide **5f** (0.0081 mmol, 51%) and complex **24** (0.033 mmol, 21%) were obtained. No pyridine *N*-oxide **1f** or homocoupling product **9c** was observed.

percentage of P in [%]							
21	complex B	-9 ppm	24	23 ppm	25 ppm	$\text{P}(\text{t-Bu})_3$	32
14	14	10	4	18	4	8	28

Integrated peaks from ^{31}P NMR spectra ($t = 0$ to $t = 140$ min)4.11.2 Transmetalation with trifluoromethyl pyridyl *N*-oxide complex **22**

[ES 6048b]

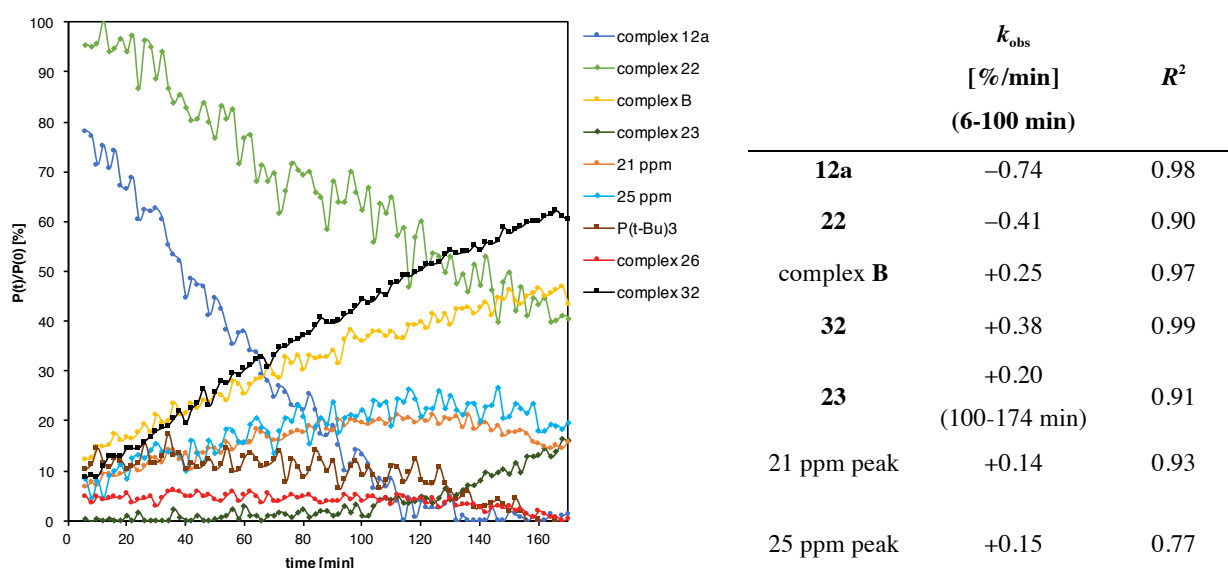
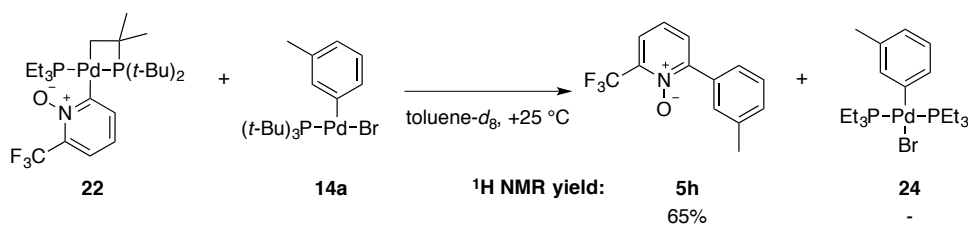
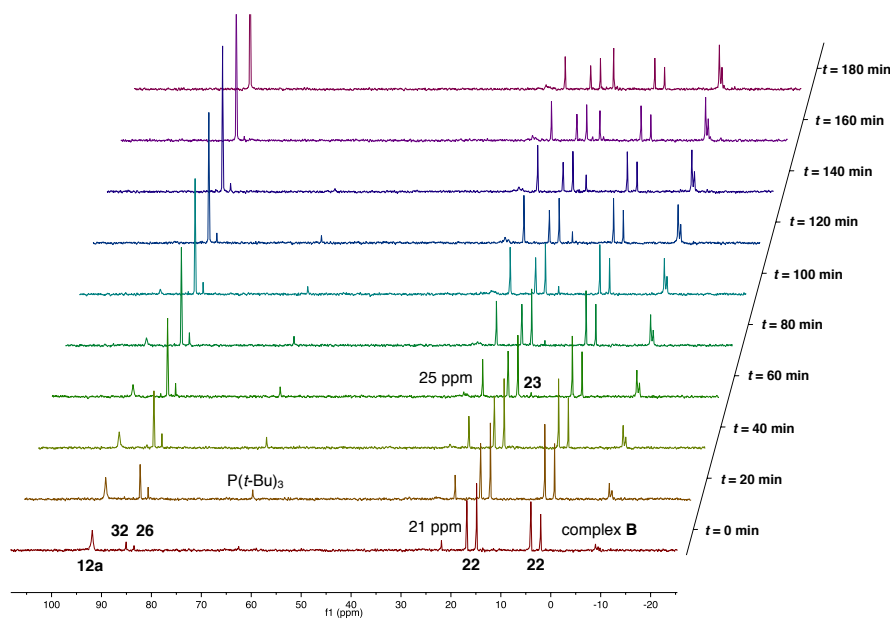
According to general procedure, pyridyl *N*-oxide complex **22** (9.2 mg, 0.016 mmol) and pyridyl complex **12a** (8.2 mg, 0.016 mmol) was monitored for 3 h at 5 °C with ³¹P NMR. No yield was determined due to incomplete consumption of starting materials.



[ES 6048c]

According to general procedure, pyridyl *N*-oxide complex **22** (9.2 mg, 0.016 mmol) and pyridyl complex **12a** (8.2 mg, 0.016 mmol) was monitored for 4 h at 25 °C via ³¹P NMR. With the addition of 1,3,5-trimethoxybenzene (4.9 mg, 0.029 mmol), bipyridine *N*-oxide **4h** (0.010 mmol, 65%) and complex **23** (0.0032 mmol, 21%) were obtained. No pyridine *N*-oxide **1h** was observed.

percentage of P in [%]						
22	complex B	23	21 ppm	25 ppm	32	
18	23	9	7	11	32	

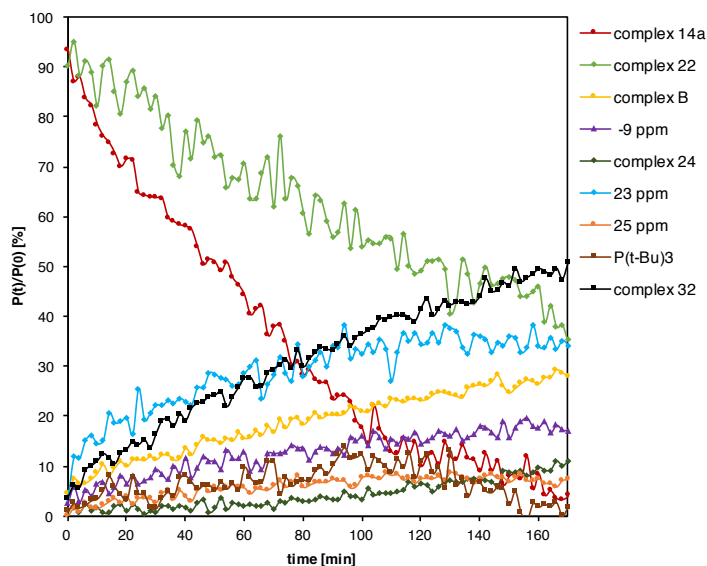
Integrated peaks from ^{31}P NMR spectra ($t = 0$ to $t = 180$ min)

[ES 6054a]

According to general procedure, pyridyl *N*-oxide complex **22** (9.2 mg, 0.016 mmol) and phenyl complex **14a** (7.5 mg, 0.016 mmol) was monitored for 4 h at 25 °C with ^{31}P NMR. With the addition of 1,3,5-trimethoxybenzene (6.9 mg, 0.041 mmol), arylpyridine *N*-oxide **5h** (0.010 mmol, 65%) was

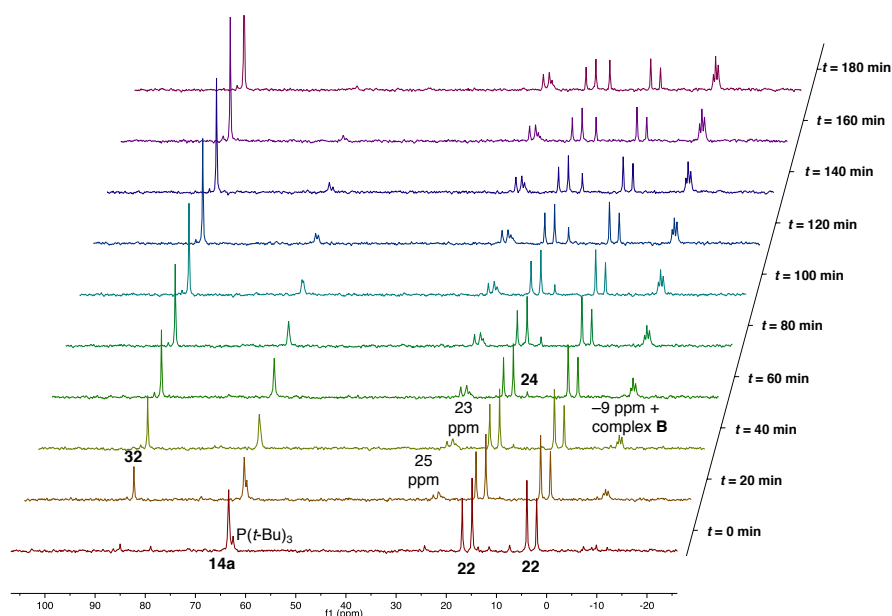
obtained. No isolated peak for **24** was present in ^1H NMR and no pyridine *N*-oxide **1h** or homocoupling product **9c** was observed.

percentage of <i>P</i> in [%]							
14	22	complex B	-9 ppm	24	23 ppm	25 ppm	32
4	21	14	8	5	19	4	25



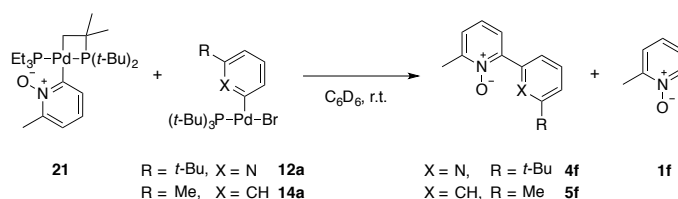
	k_{obs} [%/min]	R^2
(0-100 min)		
14a	-0.69	0.99
22	-0.36	0.87
complex B	+0.16	0.96
32	+0.31	0.97
-9 ppm peak	+0.11	0.84
24	+0.049	0.81
(30-130 min)		
23 ppm peak	+0.059	0.81
25 ppm peak	+0.22	0.84

Integrated peaks from ^{31}P NMR spectra ($t = 0$ to $t = 180$ min)

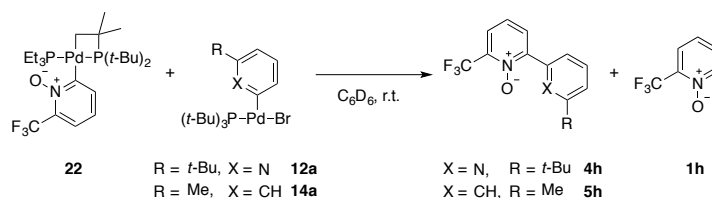


4.11.3 Yields of transmetalations

In a glovebox, pyridyl *N*-oxide palladium complex **21** or **22** (0.015 mmol) was weighed in a NMR tube with a J Young screw cap and dissolved in C₆D₆ (0.30 mL). Aryl palladium complex **12a** or **14a** (0.35 mL, 0.015 mmol in C₆D₆) was added and the NMR tube was removed from the glovebox. Consumption of starting materials was determined by ³¹P NMR (~ 18 h for complex **21** and ~ 48 h for complex **22**). The yield was calculated by addition of 1,3,5-trimethoxybenzene and recording a ¹H NMR. No homocoupling products were observed.



entry	12a,14a	time [min]	4,5 [%]	1 (recov.) [%]
1 [ES 6175b]	12a	18 h	4f , 90%	1f , 10%
2 [ES 6174b]	14a	18 h	5f , 85%	1f , 7%

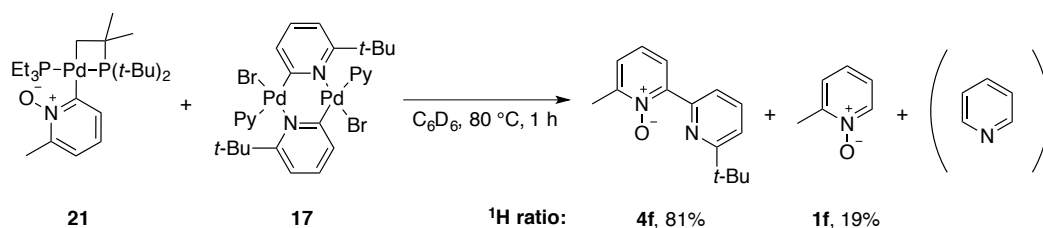


entry	12a,14a	time [min]	4,5 [%]	1 (recov.) [%]
3 [ES 6175a]	12a	>18 h	4h , 74%	1h , -
4 [ES 6174a]	14a	>18 h	5h , 85%	1h , -

percentage of P in [%]

entry	Aryl palladium		pyridyl <i>N</i> -oxide			
	complex	complex	32	P(<i>t</i> -Bu) ₃	O=PEt ₃	complex C
1	12a	21	25	5	3	67
2	14a	21	23	7	4	66
3	12a	22	19	16		65
4	14a	22	14	14	0	72

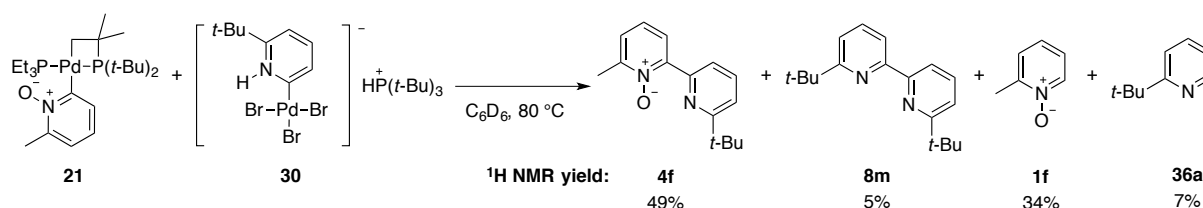
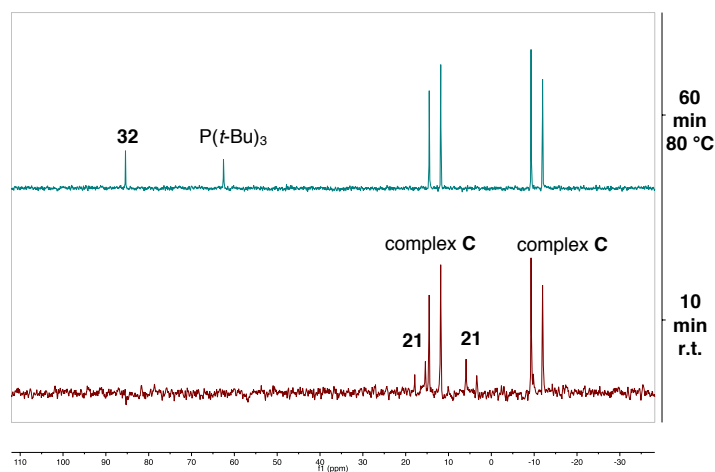
4.11.4 Transmetalation between other aryl palladium complexes



[ES 5018]

In a glovebox, pyridyl *N*-oxide palladium complex **21** (10.0 mg, 0.019 mmol, 2.0 equiv.) and pyridine pyridyl palladium dimer **17** (7.5 mg, 0.0094 mmol, 1.0 equiv.) were weighed in a NMR tube with a J Young valve and dissolved in C_6D_6 (0.65 mL). The color changed from yellow to brown within minutes and an 1H and ^{31}P NMR were recorded. The reaction was heated at 80 °C for 1 h and another 1H and ^{31}P NMR was recorded to determine the ratio of products.

time	percentage of P in [%]			complex C
	21	32	P(<i>t</i> -Bu) ₃	
10 minutes, r.t.	22			78
60 minutes, 80 °C		7	13	80

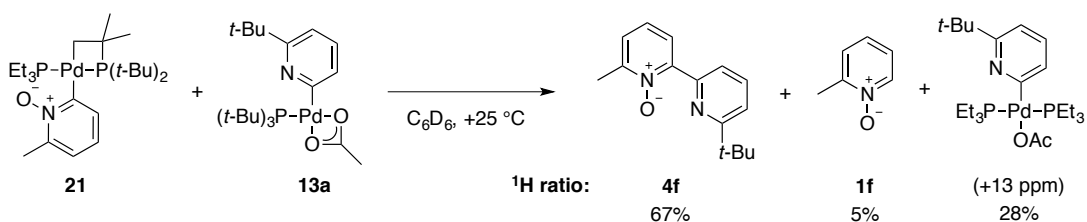
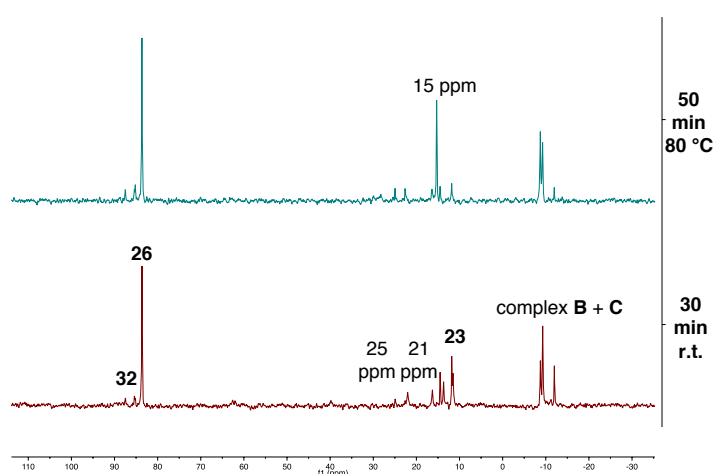
Integrated peaks from ^{31}P NMR spectra

[ES 6148]

In a glovebox, pyridyl *N*-oxide palladium complex **21** (4.2 mg, 0.0079 mmol) and anionic pyridyl palladium complex **30** (5.4 mg, 0.0079 mmol) were weighed in a NMR tube with a J Young screw cap

and dissolved in C_6D_6 (0.60 mL). The NMR tube was removed from the glovebox and after heated at 80 °C for 50 minutes and a ^{31}P spectrum was recorded. 1,3,5-TMB (5.2 mg, 0.031 mmol) was added and a 1H NMR spectrum was recorded to determine the yields of cross-coupled **4f** (0.0039 mmol, 49%), homocoupling product **8m** (0.00020 mmol, 5%), pyridine *N*-oxide **1f** (0.0027 mmol, 34%) and pyridine **36a** (0.00059 mmol, 7%).

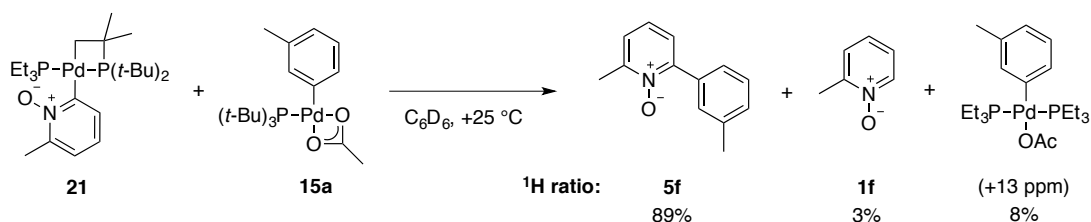
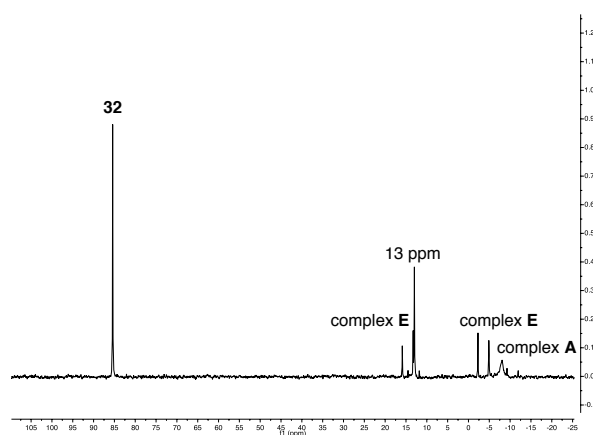
time	percentage of P in [%]					
	complex B	26	25 ppm	21 ppm	15 ppm	complex C
50 minutes, 80 °C	25	30	2	4	34	5

Integrated peaks from ^{31}P NMR spectra

[ES 4155a]

In a glovebox, pyridyl *N*-oxide palladium complex **21** (10.1 mg, 0.019 mmol) was weighed in an NMR tube with a J Young screw cap and dissolved in C_6D_6 (0.35 mL) and pyridyl palladium complex **13a** (9.5 mg, 0.019 mmol) in C_6D_6 (0.30 mL) was added. The NMR tube was removed from the glovebox and after 30 minutes in room temperature, the ratio of product species was determined via 1H NMR and ^{31}P NMR.

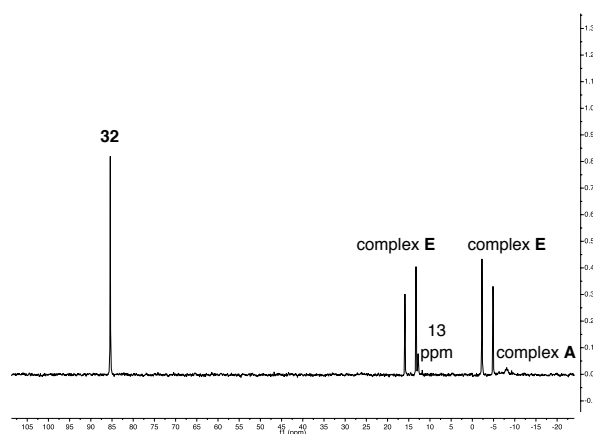
percentage of P in [%]			
complex A	complex E	13 ppm	32
18	24	20	38

Integrated peaks from ^{31}P NMR spectra

[ES 4194b]

In a glovebox, pyridyl *N*-oxide palladium complex **21** (10.1 mg, 0.019 mmol) was weighed in an NMR tube with a J Young valve and dissolved in C_6D_6 (0.35 mL) and phenyl palladium complex **15a** (9.1 mg, 0.019 mmol) in C_6D_6 (0.30 mL) was added. The NMR tube was removed from the glovebox and after 30 minutes in room temperature, the ratio of product species was determined via ^1H NMR and ^{31}P NMR.

percentage of P in [%]			
complex A	complex E	13 ppm	32
7	55	6	32

Integrated peaks from ^{31}P NMR spectra

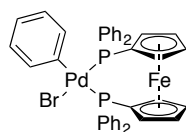
4.12 Intermediates in Suzuki-Miyaura cross-coupling reactions

4.12.1 (Pseudo)halogen-ligated palladium complexes

Monomeric (Ar)Pd(Br)(L) complexes

(phenyl)Pd(Br)(dppf) (**58d**)

[ES 5156]



Palladium bromide dimer **46d** (406.4 mg, 0.36 mmol, 1.0 equiv.) and dppf (396.8 mg, 0.72 mmol, 2.0 equiv.) were weighed in a round-bottom flask and dissolved in DCM (14 mL). The reaction was stirred at room temperature for 20 minutes and Et₂O (150 mL) was added. Rapid stirring for 1 h resulted in the precipitation of a solid that was washed with Et₂O and dried on high vacuum, resulting in dppf complex **58d** (471.0 mg, 0.57 mmol, 79%) as a yellow solid.

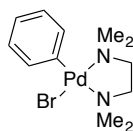
¹H NMR (400 MHz, CDCl₃): δ 8.06 (ddd, *J* = 9.9, 6.6, 3.0 Hz, 4H), 7.46 (dt, *J* = 3.9, 2.2 Hz, 6H), 7.36 (dd, *J* = 11.8, 7.7 Hz, 4H), 7.32 – 7.26 (m, 2H), 7.11 (td, *J* = 7.8, 2.5 Hz, 4H), 6.95 (td, *J* = 7.8, 2.9 Hz, 2H), 6.56 (td, *J* = 7.5, 2.7 Hz, 2H), 6.48 (t, *J* = 7.0 Hz, 1H), 4.67 (d, *J* = 2.1 Hz, 2H), 4.48 (d, *J* = 1.9 Hz, 2H), 4.13 (s, 2H), 3.63 (d, *J* = 2.0 Hz, 2H) ppm.

³¹P{¹H} NMR (162 MHz, CDCl₃): δ 30.8 (d, *J*_{P-P} = 33.8 Hz), 9.35 (d, *J*_{P-P} = 33.8 Hz) ppm.

The chemical shifts are in agreement with previously reported values.²⁰²

(phenyl)Pd(Br)(tmeda) (**55d**)

[ES 5190]



In a Schlenk flask, Pd₂dba₃·CHCl₃ (327.3 mg, 0.32 mmol, 1.0 equiv.) and P(*o*-tol)₃ (96.2 mg, 0.32 mmol, 1.0 equiv.) were added under argon. Dry toluene (10 mL) was added and bromobenzene (0.50 mL, 4.7 mmol, 15 equiv.) and tmeda (0.71 mL, 4.7 mmol, 15 equiv.) were syringed into the flask under an argon flow. The reaction was heated at 50 °C for 1 h and subsequently cooled to room temperature. The solids were filtered off and washed with DCM and the solvent was removed from the filtrate, resulting in tmeda complex **55d** (209.5 mg, 0.55 mmol, 86%) as a yellow solid.

^1H NMR (400 MHz, CDCl_3): δ 7.28 – 7.22 (m, 2H), 6.93 (t, $J = 7.3$ Hz, 2H), 6.82 (t, $J = 7.2$ Hz, 1H), 2.76 – 2.71 (dd, $J = 6.8, 4.3$ Hz, 2H), 2.63 (s, 6H), 2.57 (dd, $J = 6.6, 4.3$ Hz, 2H), 2.41 (s, 6H) ppm.

The chemical shifts are in agreement with previously reported values.¹²⁸

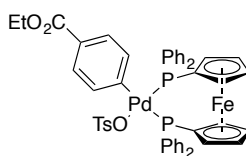
Monomeric (Ar)Pd(OTs)(L) complexes

General procedure

Bromide dppf palladium complex **58** (1.0 equiv.) was weighed in a round bottom flask and dissolved in toluene (1.0 mL) and DCM (1.0 mL). AgOTs (2.0 equiv.) was added and the reaction was stirred for 3 h at room temperature. Addition of Et_2O and rapid stirring resulted in a precipitation of tosylate complex **61**, which was filtered off and dried on high vacuum. Only ^{31}P was used for characterization of complex **61** and the complexes were used directly in subsequent reaction with a hydroxide source (see below 4.12.3).

(4-CO₂Et-phenyl)Pd(OTs)(dppf) (**61f**)

[ES 6042c]

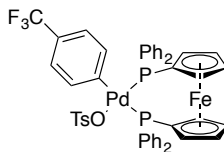


Palladium complex **58f** (39.8 mg, 0.045 mmol) and AgOTs (26.6 mg, 0.095 mmol) gave tosylate complex **61f** as a brown solid. No yield was determined.

$^{31}\text{P}\{^1\text{H}\}$ NMR (202 MHz, CDCl_3): δ 34.8 (d, $J_{\text{P-P}} = 32.1$ Hz), 12.6 (d, $J_{\text{P-P}} = 32.1$ Hz) ppm.

(4-CF₃-phenyl)Pd(OTs)(dppf) (**61g**)

[ES 6040b]



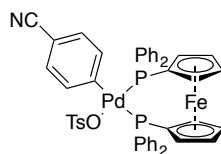
Palladium complex **58g** (36.0 mg, 0.041 mmol) and AgOTs (34.0 mg, 0.12 mmol) gave tosylate complex **61g** (37.7 mg, 0.039 mmol, 94%) as a tan solid.

^1H NMR (400 MHz, CDCl_3): δ 8.02 (ddd, $J = 10.1, 6.6, 3.0$ Hz, 4H), 7.50 (dt, $J = 4.6, 2.2$ Hz, 6H), 7.32 (dd, $J = 11.9, 7.7$ Hz, 6H), 7.24 – 7.07 (m, 8H), 6.70 (s, 2H), 6.65 – 6.57 (m, 2H), 4.74 (d, $J = 2.0$ Hz, 2H), 4.52 (d, $J = 2.0$ Hz, 2H), 4.20 (t, $J = 1.9$ Hz, 2H), 3.67 (q, $J = 1.9$ Hz, 2H), 2.35 (s, 3H) ppm.

$^{31}\text{P}\{^1\text{H}\}$ NMR (162 MHz, CDCl_3): δ 35.1 (d, $J_{\text{P-P}} = 31.9$ Hz), 12.7 (d, $J_{\text{P-P}} = 32.4$ Hz) ppm.

(4-CN-phenyl)Pd(OTs)(dppf) (61h)

[ES 6042d]



Palladium complex **58h** (28.6 mg, 0.034 mmol) and AgOTs (20.5 mg, 0.073 mmol) gave tosylate complex **61h** (31.1 mg, 0.033 mmol, 98%) as a yellow solid.

$^1\text{H NMR}$ (500 MHz CDCl_3): δ 7.93 (s, 4H), 7.49 (s, 6H), 7.38 – 7.29 (m, 6H), 7.23 – 7.09 (m, 8H), 6.77 (s, 2H), 6.65 (s, 2H), 4.76 (s, 2H), 4.56 (s, 2H), 4.22 (s, 2H), 3.63 (s, 2H), 2.20 (s, 3H) ppm.

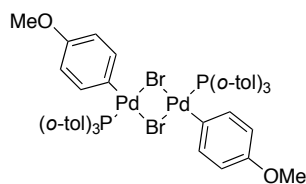
$^{31}\text{P}\{^1\text{H}\}$ NMR (202 MHz CDCl_3): δ 35.3 (d, $J_{\text{P-P}} = 30.3$ Hz), 13.5 (d, $J_{\text{P-P}} = 30.7$ Hz) ppm.

Dimeric [(Ar)Pd(μ -Br)(P(*o*-tol) $_3$)] $_2$ complexes**General procedure**

Similar to reported procedure, 130 $\text{Pd}_2\text{dba}_3\cdot\text{CHCl}_3$ (1.0 equiv.) and $\text{P}(\textit{o}\text{-tol})_3$ (~ 4 equiv.) were added to a dry Schlenk flask under argon. Dry toluene (60 mL) was added and the aryl halide (10-20 equiv.) was syringed into the reaction. The mixture was heated at 50 °C until the purple color vanished (30-120 min). The reaction was diluted with DCM and the solids filtered off through celite. Removal of the solvent gave an oily residue to which Et_2O was added. Stirring for 1 h at r.t. resulted in precipitation of the desired complex, which was collected on a glass frit (D4) and dried under high vacuum.

[(4-OMe-phenyl)Pd(μ -Br)(P(*o*-tol) $_3$)] $_2$ (46a**)**

[ES 6154b]



According to the general procedure, $\text{Pd}_2\text{dba}_3\cdot\text{CHCl}_3$ (1.32 g, 1.28 mmol), $\text{P}(\textit{o}\text{-tol})_3$ (1.59 g, 5.22 mmol) and 4-bromoanisole (3.20 mL, 25.6 mmol) gave palladium dimer **46a** (348.0 mg, 0.29 mmol, 23%) as a yellow solid.

$^{31}\text{P}\{^1\text{H}\}$ NMR (162 MHz, CD_2Cl_2): δ 28.5 (broad s) ppm.

The chemical shifts are in agreement with previously reported values. 130

IR (solid, ν): 3054 (w), 3006 (m), 2989 (m), 2831 (w), 2707 (w), 1590 (w), 1577 (w), 1561 (w), 1478 (m), 1447 (m), 1383 (w), 1276 (s), 1261 (s), 1232 (m), 1200 (w), 1174 (w), 1131 (w), 1097 (w), 1067 (w), 1030 (w), 1002 (w), 808 (m), 750 (s) cm^{-1} .

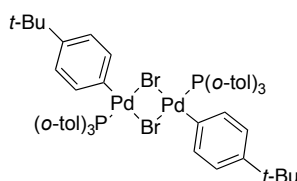
HRESI-MS (+, MeOH, m/z): [(4-OMe-phenyl)Pd(P(*o*-tol)₃)₂]⁺ 517.0983, calc. 517.0913.

Elemental analysis (%): C 56.26, H 4.73, calc. C 56.25, H 4.72.

M.p.: decomposition > 160 °C.

[(4-*tert*-Bu-phenyl)Pd(μ -Br)(P(*o*-tol)₃)₂] (46b)

[ES 6132h]



According to the general procedure, Pd₂dba₃·CHCl₃ (1.56 g, 1.50 mmol), P(*o*-tol)₃ (2.04 g, 6.72 mmol) and 1-bromo-4-*tert*-butylbenzene (5.20 mL, 30.0 mmol) gave palladium dimer **46b** (1.51 g, 1.20 mmol, 80%) as a yellow solid.

³¹P{¹H} NMR (162 MHz, CD₂Cl₂): δ 28.7 (broad s) ppm.

The chemical shifts are in agreement with previously reported values.¹³⁰

IR (solid, ν): 3056 (w), 2958 (w), 2864 (w), 1590 (w), 1576 (w), 1472 (m), 1445 (m), 1383 (w), 1361 (w), 1282 (w), 1268 (w), 1200 (w), 1164 (w), 1131 (w), 1113 (w), 1068 (w), 1032 (w), 1006 (m), 807 (m), 756 (m), 748 (s), 733 (m), 715 (m), 677 (w) cm^{-1} .

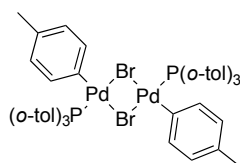
HRESI-MS (+, DCM/MeOH, m/z): [M-Br]⁺ 1167.1987, calc. 1167.2053; [(4-*tert*-Bu-phenyl)Pd(P(*o*-tol)₃)₂]⁺ 543.1429, calc. 543.1433.

Elemental analysis (%): C 59.66, H 5.52, calc. C 59.68, H 5.49.

M.p.: decomposition > 189 °C.

[(4-Me-phenyl)Pd(μ -Br)(P(*o*-tol)₃)₂] (46c)

[ES 6100/6154a]



According to the general procedure, Pd₂dba₃·CHCl₃ (1.13 g, 1.09 mmol), P(*o*-tol)₃ (1.43 g, 4.70 mmol) and 4-bromotoluene (2.70 mL, 21.8 mmol) gave palladium dimer **46c** (659.6 mg, 0.57 mmol, 52%) as a yellow solid.

$^{31}\text{P}\{^1\text{H}\}$ NMR (162 MHz, CD_2Cl_2): δ 28.0 (broad s) ppm.

The chemical shifts are in agreement with previously reported values.¹³⁰

IR (solid, ν): 3054 (m), 3006 (m), 2918 (m), 2864 (w), 2737 (w), 1589 (w), 1564 (w), 1477 (m), 1444 (m), 1381 (w), 1276 (m), 1263 (m), 1202 (w), 1164 (w), 1131 (w), 1068 (w), 1051 (w), 1032 (w), 1011 (m), 870 (w), 790 (m), 764 (s), 748 (s), 716 (m), 701 (m), 677 (w), 665 (w) cm^{-1} .

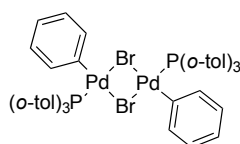
HRESI-MS (+, MeOH, m/z): $[\text{M}-\text{Br}]^+$ 1083.1108, calc. 1083.1114; $[(4\text{-Me-phenyl})\text{Pd}(\text{P}(o\text{-tol})_3)]^+$ 501.0967, calc. 501.0963.

Elemental analysis (%): C 57.88, H 4.88, calc. C 57.80, H 4.85.

M.p.: decomposition > 158 °C.

$[(\text{phenyl})\text{Pd}(\mu\text{-Br})(\text{P}(o\text{-tol})_3)]_2$ (46d**)**

[ES 6132a]



According to the general procedure, $\text{Pd}_2\text{dba}_3\cdot\text{CHCl}_3$ (1.52 g, 1.47 mmol), $\text{P}(o\text{-tol})_3$ (2.15 g, 7.06 mmol) and bromobenzene (3.10 mL, 29.5 mmol) gave palladium dimer **46d** (1.04 g, 0.92 mmol, 61%) as a light orange solid.

$^{31}\text{P}\{^1\text{H}\}$ NMR (162 MHz, CD_2Cl_2): δ 28.4 (broad s) ppm.

IR (solid, ν): 3053 (w), 3007 (w), 2967 (w), 2918 (w), 1929 (w), 1845 (w), 1816 (w), 1700 (w), 1623 (w), 1589 (w), 1589 (m), 1468 (m), 1444 (m), 1381 (m), 1265 (m), 1200 (m), 1163 (m), 1131 (m), 1067 (m), 1055 (m), 1031 (m), 1016 (m), 994 (m), 952 (w), 892 (w), 870 (w), 804 (m), 750 (s), 726 (s), 691 (m) cm^{-1} .

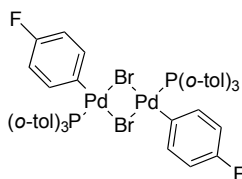
HRESI-MS (+, DCM/MeOH, m/z): $[\text{M}-\text{Br}]^+$ 1055.0710, calc. 1055.0801; $[(\text{phenyl})\text{Pd}(\text{P}(o\text{-tol})_3)]^+$ 487.0795, calc. 487.0807.

Elemental analysis (%): C 57.22, H 4.66, calc. C 57.11, H 4.62.

M.p.: decomposition > 186 °C.

$[(4\text{-F-phenyl})\text{Pd}(\mu\text{-Br})(\text{P}(o\text{-tol})_3)]_2$ (46e**)**

[ES 6132e]



According to the general procedure, Pd₂dba₃·CHCl₃ (1.59 g, 1.54 mmol), P(*o*-tol)₃ (1.98 g, 6.49 mmol) and 1-bromo-4-fluorobenzene (1.80 mL, 16.4 mmol) gave palladium dimer **46e** (1.61 g, 1.38 mmol, 90%) as a light yellow solid.

³¹P{¹H} NMR (162 MHz, CD₂Cl₂): δ 28.8 (broad s) ppm.

¹⁹F{¹H} NMR (376 MHz, CD₂Cl₂): δ -123.6 ppm.

The chemical shifts are in agreement with previously reported values.⁷⁷

IR (solid, ν): 3055 (w), 3008 (w), 2921 (w), 1590 (w), 1567 (w), 1474 (s), 1445 (m), 1382 (w), 1281 (w), 1266 (w), 1215 (s), 1155 (m), 1132 (w), 1083 (w), 1068 (w), 1045 (w), 1008 (m), 950 (w), 871 (w), 809 (m), 750 (s), 737 (m), 716 (m), 677 (w), 664 (w) cm⁻¹.

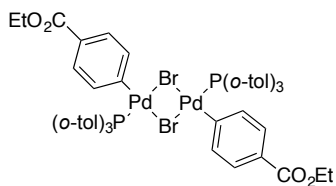
HRESI-MS (+, DCM/MeOH, *m/z*): [M-Br]⁺ 1091.0619, calc. 1091.0613; [(4-F-phenyl)Pd(P(*o*-tol)₃)]⁺ 505.0739, calc. 505.0713.

Elemental analysis (%): C 55.38, H 4.42, calc. C 55.36, H 4.30.

M.p.: decomposition > 169 °C.

[(4-CO₂Et-phenyl)Pd(μ-Br)(P(*o*-tol)₃)]₂ (**46f**)

[ES 6132d/6154c]



According to the general procedure, Pd₂dba₃·CHCl₃ (1.78 g, 1.72 mmol), P(*o*-tol)₃ (2.10 g, 6.90 mmol) and ethyl 4-bromobenzoate (2.90 mL, 17.8 mmol) gave palladium dimer **46f** (418.0 mg, 0.33 mmol, 19%) as a light yellow solid.

³¹P{¹H} NMR (162 MHz, CD₂Cl₂): δ 27.8 (broad s) ppm.

IR (solid, ν): 3056 (w), 2978 (w), 1709 (s), 1574 (s), 1470 (m), 1446 (m), 1382 (w), 1365 (w), 1274 (s), 1200 (w), 1176 (m), 1102 (s), 1068 (w), 1048 (w), 1011 (m), 838 (w), 804 (w), 753 (m), 735 (w), 716 (w), 699 (w), 678 (w) cm⁻¹.

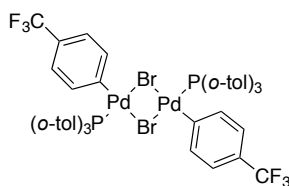
HRESI-MS (+, DCM/MeOH, *m/z*): [M-Br]⁺ 1199.1102, calc. 1199.1224; [(4-CO₂Et-phenyl)Pd(P(*o*-tol)₃)]⁺ 559.1003, calc. 559.1018.

Elemental analysis (%): C 56.31, H 4.85, calc. C 56.31, H 4.73.

M.p.: decomposition > 191 °C.

[(4-CF₃-phenyl)Pd(μ -Br)(P(*o*-tol)₃)₂] (46g)

[ES 6132b]



According to the general procedure, Pd₂dba₃·CHCl₃ (1.61 g, 1.56 mmol), P(*o*-tol)₃ (2.29 g, 7.52 mmol) and 4-bromobenzotrifluoride (2.20 mL, 15.7 mmol) gave palladium dimer **46g** (1.49 g, 1.17 mmol, 75%) as a light yellow solid.

³¹P{¹H} NMR (162 MHz, CD₂Cl₂): δ 28.3 ppm.

¹⁹F{¹H} NMR (376 MHz, CD₂Cl₂): δ -62.2 ppm.

IR (solid, ν): 3057 (w), 2920 (w), 1586 (m), 1563 (w), 1471 (w), 1446 (m), 1384 (m), 1323 (s), 1282 (w), 1269 (w), 1200 (w), 1157 (m), 1116 (m), 1099 (m), 1068 (s), 1032 (w), 1008 (m), 870 (w), 815 (m), 751 (m), 716 (m), 679 (w) cm⁻¹.

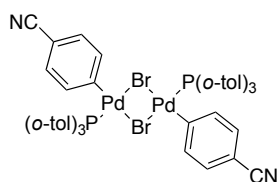
HRESI-MS (+, DCM/MeOH, m/z): [M-Br]⁺ 1191.0518, calc. 1191.0549; [(4-CF₃-phenyl)Pd(P(*o*-tol)₃)₂]⁺ 555.0690, calc. 555.0681.

Elemental analysis (%): C 52.95, H 4.01, calc. C 52.90, H 3.96.

M.p.: decomposition > 198 °C.

[(4-CN-phenyl)Pd(μ -Br)(P(*o*-tol)₃)₂] (46h)

[ES 6132c]



According to the general procedure, Pd₂dba₃·CHCl₃ (1.56 g, 1.51 mmol), P(*o*-tol)₃ (2.11 g, 6.94 mmol) and 4-bromobenzonitrile (2.85 g, 15.7 mmol) gave palladium dimer **46h** (962.6 g, 0.81 mmol, 54%) as a yellow solid.

³¹P{¹H} NMR (162 MHz, CD₂Cl₂): δ 28.2 ppm.

The chemical shifts are in agreement with previously reported values.¹³²

IR (solid, ν): 3056 (m), 3008 (w), 2920 (w), 2256 (w), 2221 (m), 1653 (w), 1621 (w), 1590 (w), 1573 (m), 1471 (m), 1446 (m), 1383 (w), 1338 (w), 1276 (m), 1200 (w), 1132 (w), 1095 (w), 1068 (w), 1049 (m), 1032 (w), 1011 (m), 872 (w), 809 (m), 751 (s), 736 (m), 715 (m), 678 (w), 664 (w) cm⁻¹.

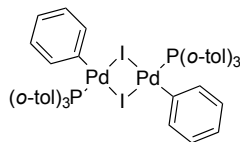
HRESI-MS (+, DCM/MeOH, m/z): [M-Br]⁺ 1105.0706, calc. 1105.0617; [(4-CN-phenyl)Pd(P(*o*-tol)₃)₂]⁺ 512.0765, calc. 512.0759.

Elemental analysis (%): C 56.70, H 4.29, N 2.30, calc. C 56.73, H 4.25, N 2.36.

M.p.: decomposition > 158 °C.

[(phenyl)Pd(μ -I)(P(*o*-tol)₃)₂] (47d)

[ES 6120]



According to the general procedure, Pd₂dba₃·CHCl₃ (530.1 mg, 0.51 mmol), P(*o*-tol)₃ (623.5 mg, 2.05 mmol) and iodobenzene (0.85 mL, 7.65 mmol) gave palladium dimer **47d** (42.8 mg, 0.035 mmol, 7%) as an orange insoluble solid.

IR (solid, ν): 3055 (w), 3006 (w), 2989 (w), 1589 (w), 1561 (w), 1466 (w), 1445 (w), 1381 (w), 1276 (m), 1260 (m), 1199 (w), 1164 (w), 1131 (w), 1068 (w), 1056 (w), 1033 (w), 1016 (w), 994 (w), 804 (w), 760 (s), 746 (s), 729 (m), 692 (w), 676 (w), 655 (w) cm⁻¹.

HRESI-MS (+, DCM/MeOH, m/z): [M-I]⁺ 1103.0628, calc. 1103.0663; [(phenyl)Pd(P(*o*-tol)₃)₂]⁺ 487.0806, calc. 487.0807.

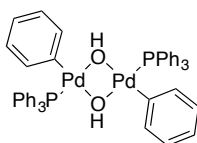
Elemental analysis (%): C 52.78, H 4.32, calc. C 52.75, H 4.26.

M.p.: decomposition > 186 °C.

4.12.2 Hydroxide-ligated palladium complexes

[(phenyl)Pd(μ -OH)(PPh₃)₂] (42d)

[ES 6023]



According to reported procedure,¹⁸⁶ (PPh₃)₂PdCl₂ (156.5 mg, 0.22 mmol, 1.0 equiv., prepared from (MeCN)₂Pd(Cl)₂) and PPh₃ in DCM/MeCN) and KOH (626.6 mg, 12.3 mmol, 55 equiv.) was added to a Schlenk flask and set under argon atmosphere. A degassed H₂O/toluene solvent mixture (1:3, 4 mL) and iodobenzene (0.05 mL, 0.47 mmol, 2.1 equiv.) were syringed into the solution. The reaction was heated to 80 °C and stirred vigorously for 3 hours under argon. After cooling to ambient temperature, the H₂O phase was extracted 3x with toluene and the solvent removed. After drying on high vacuum, a light yellow solid (134.2 mg) was obtained, containing complex **42d** and O=PPh₃. Washing the mixture with acetone resulted in a colorless solid containing a *cis/trans* mixture of 3:2 of title compound **42d** with only traces of O=PPh₃.

$^{31}\text{P}\{^1\text{H}\}$ NMR (202 MHz, CDCl_3): δ 34.2, 33.0 ppm.

The chemical shifts similar to the previously reported values for the analogous 4-fluorophenyl complex **42e**.¹¹⁹

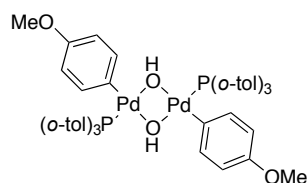
Dimeric $[(\text{Ar})\text{Pd}(\mu\text{-OH})(\text{P}(o\text{-tol})_3)]_2$ complexes

General procedure

To a Schlenk flask, dimeric $\mu\text{-Br}$ $\text{P}(o\text{-tol})_3$ palladium complex **46** (1.0 equiv.) and KOH (~180 equiv.) was added. The flask was set under argon by cycled evacuation and backfilling with argon. Degassed H_2O and degassed toluene (ratio 1:2) was added and the biphasic mixtures was rapidly stirred and heated to 40 °C over night. Thereafter, the organic phase was separated and the H_2O phase extracted with toluene twice. The combined organic phases were dried with Na_2SO_4 and concentrated. Et_2O was added and the reaction was rapidly stirred for 2 h, resulting in a precipitation that was washed with Et_2O or pentane to give the hydroxide complex **56**.

$[(4\text{-OMe-phenyl})\text{Pd}(\mu\text{-OH})(\text{P}(o\text{-tol})_3)]_2$ (**56a**)

[ES 6116a/6158a]



According to the general procedure, palladium complex **46a** (221.3 mg, 0.19 mmol) and KOH (1.89 g, 37.0 mmol) in toluene (10.0 mL) and H_2O (5.0 mL) gave hydroxide palladium complex **56a** (78.7 mg, 0.074 mmol, 39%) as a grey solid.

$^{31}\text{P}\{^1\text{H}\}$ NMR (162 MHz, CD_2Cl_2): δ 29.7 ppm.

IR (solid, ν): 3606 (w), 3054 (w), 3006 (w), 2830 (w), 1590 (w), 1577 (w), 1562 (w), 1480 (w), 1449 (w), 1383 (w), 1275 (m), 1264 (m), 1231 (m), 1175 (w), 1132 (w), 1096 (w), 1067 (w), 1030 (w), 1006 (w), 804 (w), 765 (m), 756 (s), 748 (s), 719 (w), 678 (w) cm^{-1} .

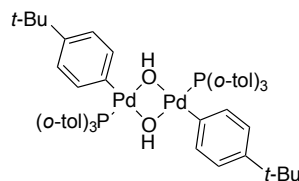
HRESI-MS (+, DCM/MeOH, m/z): $[\text{M}+\text{H}]^+$ 1071.1639, calc. 1071.1957; $[(4\text{-OMe-phenyl})\text{Pd}(\text{P}(o\text{-tol})_3)]^+$ 517.0964, calc. 517.0913.

Elemental analysis (%): C 62.75, H 5.72, calc. C 62.87, H 5.46.

M.p.: decomposition > 150 °C.

[(4-*tert*-Bu-phenyl)Pd(μ -OH)(P(*o*-tol)₃)₂]₂ (56b**)**

[ES 6158b]



According to the general procedure, palladium complex **46b** (907.0 mg, 0.73 mmol) and KOH (6.85 g, 134.0 mmol) in toluene (30.0 mL) and H₂O (15.0 mL) gave hydroxide palladium complex **56b** (444.0 mg, 0.40 mmol, 54%) as a light yellow solid.

³¹P{¹H} NMR (162 MHz, CD₂Cl₂): δ 30.3 ppm.

IR (solid, ν): 3607 (w), 3054 (w), 3006 (w), 2958 (w), 2900 (w), 2863 (w), 1590 (w), 1471 (m), 1447 (m), 1381 (w), 1360 (w), 1275 (m), 1200 (w), 1163 (w), 1131 (w), 1116 (w), 1068 (w), 1031 (w), 1009 (m), 869 (w), 805 (m), 750 (s), 730 (m) 716 (m), 677 (w) cm⁻¹.

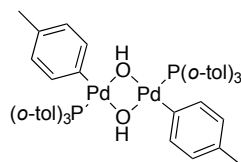
HRESI-MS (+, MeOH, m/z): [M+H]⁺ 1123.2562, calc. 1123.2998; [(4-*t*-Bu-phenyl)Pd(P(*o*-tol)₃)₂]⁺ 543.1448, calc. 543.1433.

Elemental analysis (%): C 65.73, H 6.40, calc. C 66.37, H 6.29.

M.p.: decomposition > 130 °C.

[(4-Me-phenyl)Pd(μ -OH)(P(*o*-tol)₃)₂]₂ (56c**)**

[ES 6106/6158c]



According to general procedure, palladium complex **46c** (726.4 mg, 0.64 mmol) and KOH (6.25 g, 122.2 mmol) in toluene (30.0 mL) and H₂O (15.0 mL) gave hydroxide palladium complex **56c** (292.5 mg, 0.28 mmol, 44%) as a light orange solid.

³¹P{¹H} NMR (162 MHz, CD₂Cl₂): δ 29.9 ppm.

IR (solid, ν): 3608 (w), 3052 (w), 3006 (m), 2990 (m), 2917 (w), 2862 (w), 1589 (w), 1560 (w), 1471 (m), 1447 (m), 1382 (w), 1276 (s), 1261 (s), 1201 (w), 1163 (w), 1131 (w), 1068 (w), 1054 (w), 1033 (w), 1013 (w), 897 (w), 872 (w), 792 (m), 749 (s), 678 (m) cm⁻¹.

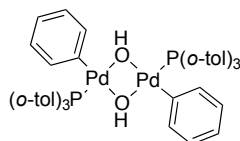
HRESI-MS (+, MeOH, m/z): [M+H]⁺ 1039.1752, calc. 1039.2059; [(4-Me-phenyl)Pd(P(*o*-tol)₃)₂]⁺ 501.1030, calc. 501.0963.

Elemental analysis (%): C 64.20, H 5.68, calc. C 64.81, H 5.63.

M.p.: decomposition > 145 °C.

[(phenyl)Pd(μ -OH)(P(*o*-tol)₃)₂] (56d)

[ES 6158d]



According to general procedure, palladium complex **46d** (566.1 mg, 0.50 mmol) and KOH (4.77 g, 93.4 mmol) in toluene (30.0 mL) and H₂O (15.0 mL) gave hydroxide palladium complex **56d** (379.3 mg, 0.38 mmol, 75%) as a light yellow solid.

³¹P{¹H} NMR (162 MHz, CD₂Cl₂): δ 29.7 ppm.

IR (solid, ν): 3605 (w), 3052 (w), 1563 (w), 1469, (m), 1446 (m), 1382 (w), 1265 (w), 1200 (w), 1163 (w), 1131 (m), 1062 (m), 1020 (m), 803 (m), 717 (s), 697 (s) cm⁻¹.

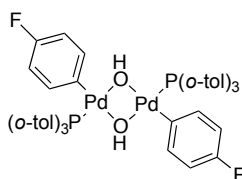
HRESI-MS (+, MeOH, m/z): [(phenyl)Pd(P(*o*-tol)₃)₂]⁺ 487.0890, calc. 487.0807.

Elemental analysis (%): C 64.33, H 5.62, calc. C 64.23, H 5.39.

M.p.: decomposition > 125 °C.

[(4-F-phenyl)Pd(μ -OH)(P(*o*-tol)₃)₂] (56e)

[ES 6116d/6158e]



According to the general procedure, palladium complex **46e** (909.8 mg, 0.78 mmol) and KOH (7.45 g, 145.8 mmol) in toluene (30.0 mL) and H₂O (15.0 mL) gave hydroxide palladium complex **56e** (610.6 mg, 0.58 mmol, 75%) as colorless solid.

³¹P{¹H} NMR (162 MHz, CD₂Cl₂): δ 29.3 ppm.

¹⁹F{¹H} NMR (376 MHz, CD₂Cl₂): δ -124.1 ppm.

IR (solid, ν): 3605 (w), 3054 (w), 3011 (w), 2962 (w), 2919 (w), 1590 (w), 1571 (m), 1474 (s), 1447 (m), 1383 (w), 1282 (w), 1210 (s), 1155 (m), 1132 (m), 1068 (w), 1049 (m), 1033 (m), 1010 (m), 804 (s), 751 (s), 734 (m), 717 (m), 678 (m), 666 (w) cm⁻¹.

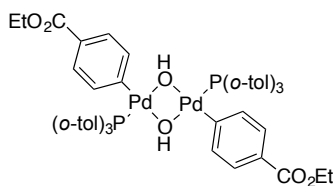
HRESI-MS (+, DCM/MeOH, m/z): [M+H]⁺ 1047.1167, calc. 1047.1557; [(4-F-phenyl)Pd(P(*o*-tol)₃)₂]⁺ 505.0749, calc. 505.0713.

Elemental analysis (%): C 59.17, H 5.09, calc. C 62.02, H 5.01.

M.p.: decomposition > 136 °C.

[(4-CO₂Et-phenyl)Pd(μ -OH)(P(*o*-tol)₃)₂] (56f)

[ES 6116b/6158f]



According to the general procedure, palladium complex **46f** (397.4 mg, 0.31 mmol) and KOH (3.28 g, 64.3 mmol) in toluene (20.0 mL) and H₂O (10.0 mL) gave hydroxide palladium complex **56f** (268.8 mg, 0.23 mmol, 75%) as light yellow solid.

³¹P{¹H} NMR (162 MHz, CD₂Cl₂): δ 29.3 ppm.

IR (solid, ν): 3606 (w), 3055 (w), 2977 (w), 1707 (s), 1577 (s), 1469 (w), 1446 (m), 1384 (w), 1365 (w), 1305 (w), 1272 (s), 1200 (w), 1176 (m), 1104 (s), 1069 (w), 1013 (m), 841 (w), 803 (w), 754 (m), 733 (m), 717 (m), 678 (w), 665 (w) cm⁻¹.

HRESI-MS (+, DCM/MeOH, m/z): [M+H]⁺ 1155.1756, calc. 1155.2168; [(4-CO₂Et-phenyl)Pd(P(*o*-tol)₃)₂]⁺ 559.1048, calc. 559.1018.

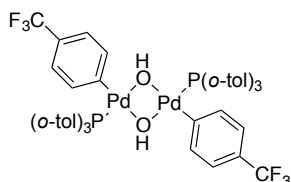
Elemental analysis (%): C 60.57, H 5.16, calc. C 62.45, H 5.42.

A better elemental analysis could not be obtained.

M.p.: decomposition > 128 °C.

[(4-CF₃-phenyl)Pd(μ -OH)(P(*o*-tol)₃)₂] (56g)

[ES 6158g]



According to the general procedure, palladium complex **46g** (910.7 mg, 0.72 mmol, 1.0 equiv.) and KOH (6.67 g, 130.6 mmol, 181 equiv.) in toluene (30.0 mL) and H₂O (15.0 mL) gave hydroxide palladium complex **56g** (736.7 mg, 0.64 mmol, 89%) as a light yellow solid.

³¹P{¹H} NMR (162 MHz, CD₂Cl₂): δ 29.3 ppm.

¹⁹F{¹H} NMR (376 MHz, CD₂Cl₂): δ -62.1 ppm.

IR (solid, ν): 3604 (w), 3056 (w), 2923 (w), 1588 (m), 1565 (w), 1469 (w), 1447 (m), 1385 (w), 1321 (s), 1283 (w), 1268 (w), 1200 (w), 1186 (w), 1156 (m), 1113 (s), 1098 (m), 1071 (s), 1045 (w), 1033 (w), 1011 (m), 950 (w), 871 (w), 819 (m), 804 (m), 753 (m), 730 (m), 717 (m), 680 (m), 665 (w) cm⁻¹.

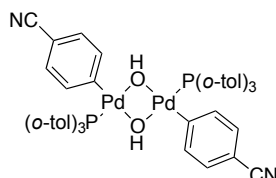
HRESI-MS (+, MeOH, m/z): [(4-CF₃-phenyl)Pd(P(*o*-tol)₃)₂]⁺ 555.0767, calc. 555.0681.

Elemental analysis (%): C 58.78, H 4.71, calc. C 58.70, H 4.57.

M.p.: decomposition > 131 °C.

[(4-CN-phenyl)Pd(μ -OH)(P(*o*-tol)₃)₂] (56h)

[ES 6158h]



According to the general procedure, palladium complex **46h** (888.8 mg, 0.75 mmol, 1.0 equiv.) and KOH (6.91 g, 135.2 mmol, 180 equiv.) in toluene (30.0 mL) and H₂O (15.0 mL) gave hydroxide palladium complex **56h** (613.5 mg, 0.58 mmol, 77%) as a light yellow solid.

³¹P{¹H} NMR (162 MHz, CD₂Cl₂): δ 28.9 ppm.

IR (solid, ν): 3607 (w), 3054 (w), 3006 (w), 2988 (w), 2921 (w), 2219 (m), 1573 (m), 1541 (w), 1472 (m), 1446 (m), 1381 (w), 1339 (w), 1276 (m), 1261 (m), 1200 (w), 1164 (w), 1131 (w), 1095 (w), 1068 (w), 1051 (w), 1032 (w), 1013 (w), 873 (w), 804 (m), 750 (s), 716 (m), 678 (w) cm⁻¹.

HRESI-MS (+, MeOH, m/z): [M+H]⁺ 1061.1368, calc. 1061.1651; [(4-CN-phenyl)Pd(P(*o*-tol)₃)₂]⁺ 512.0819, calc. 512.0759.

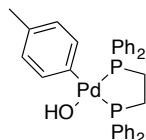
Elemental analysis (%): C 63.54, H 5.12, N 2.67 calc. C 63.46, H 4.95, N 2.64.

M.p.: decomposition > 139 °C.

Monomeric (Ar)Pd(OH)(L) complexes

(4-Me-phenyl)Pd(OH)(dppe) (62c)

[ES 6142b]



In the glovebox, hydroxide dimer **56c** (52.0 mg, 0.050 mmol, 1.0 equiv.) and dppe (39.9 mg, 0.10 mmol, 2.0 equiv.) were weighed in a Schlenk flask. Dry DCM (5 mL) was added and the reaction was stirred for 30 minutes at room temperature. Addition of Et₂O resulted in the precipitation of the title complex **62c** as a yellow solid. No yield was determined.

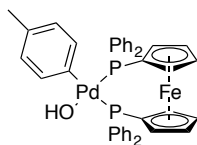
¹H NMR (400 MHz, CDCl₃): δ 7.96 (ddd, J = 10.0, 6.6, 3.0 Hz, 4H), 7.50 – 7.37 (m, 12H), 7.31 (td, J = 7.6, 2.5 Hz, 4H), 6.89 (td, J = 8.0, 2.8 Hz, 2H), 6.60 (d, J = 6.0 Hz, 2H), 2.56 – 2.39 (m, 2H), 2.18 (dq, J = 26.7, 7.4 Hz, 2H), 2.08 (s, 3H) ppm.

$^{31}\text{P}\{^1\text{H}\}$ NMR (162 MHz, CDCl_3): δ 51.6 (d, $J_{\text{P-P}} = 27.6$ Hz), 31.4 (d, $J_{\text{P-P}} = 27.4$ Hz) ppm.

HRESI-MS (+, MeOH, m/z): $[\text{M-OH}]^+$ 595.0975, calc. 595.0936.

(4-Me-phenyl)Pd(OH)(dppf) (**63c**)

[ES 6076b/ES 6142a]



In the glovebox, hydroxide dimer **56c** (33.4 mg, 0.032 mmol, 1.0 equiv.) and dppf (35.7 mg, 0.064 mmol, 2.0 equiv.) were weighed in a Schlenk flask. Dry DCM (8 mL) was added and the reaction was stirred for 30 minutes at room temperature. Addition of Et_2O resulted in the precipitation of the title complex **63c** (15.0 mg, 0.020 mmol, 30%) as a light orange solid.

^1H NMR (400 MHz, CDCl_3): δ 8.12 – 8.01 (m, 4H), 7.42 – 7.47 (m, 6H), 7.47 – 7.41 (m, 6H), 7.40 – 7.28 (m, 4H), 7.10 (td, $J = 7.7, 2.3$ Hz, 2H), 6.80 (td, $J = 7.9, 3.0$ Hz, 2H), 6.41 (d, $J = 6.6$ Hz, 2H), 4.65 (d, $J = 2.0$ Hz, 2H), 4.46 (s, 2H), 4.14 (d, $J = 1.9$ Hz, 2H), 3.60 (d, $J = 2.1$ Hz, 2H), 1.99 (s, 3H) ppm.

$^{31}\text{P}\{^1\text{H}\}$ NMR (162 MHz, CDCl_3): δ 31.4 (d, $J_{\text{P-P}} = 33.6$ Hz), 9.93 (d, $J_{\text{P-P}} = 33.6$ Hz) ppm.

HRESI-MS (+, MeOH, m/z): $[\text{M-OH}]^+$ 751.0664, calc. 751.0598.

4.12.3 Attempted direct displacement of halogen ligand

Direct displacement of (pseudo)halides on monomeric aryl palladium(II) complexes **55**, **58-61**, **64** was performed by addition of MOH in excess to a solution of the palladium complex. All hydroxide bases were pre-dried by heating under vacuum and all solvents (except entry 6) were distilled prior to use.

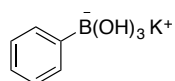
entry	complex	ligands	MOH	solvent	temperature [°C]	time [h]	conversion Br/I complex [%]
1 [ES 5080d+e]	60d	I/dppe	KOH, CsOH 5 equiv.	THF, benzene	r.t.	1	no reaction
2 [ES 5080f]	60d	I/dppe	CsOH 5 equiv.	THF	50 °C	1	decomposition
3 [ES 5081]	64d	I/tmeda	KOH, CsOH 5 equiv.	THF, benzene	r.t.	1-5 h	unidentified products
4 [ES 5191]	55d	Br/tmeda	NaOH (30 equiv.)	DCM	r.t.	1	no reaction

5 [ES 5128a2]	59d	I/dppf	CsOH (5 equiv.)	THF	r.t.	2.5	no reaction
6 [ES 6024/25]	59d	I/dppf	KOH (50 equiv.)	toluene/H ₂ O	40-80 °C	2	decomposition
7 [ES 5174]	58d	Br/dppf	KOH (20 equiv.)	DCM	r.t.	1	~40%
8 [ES 6043a]	61f	OTs/dppf	KOH (10 equiv.)	DCM	r.t.	1	decomposition
9 [ES 6041]	61g	OTs/dppf	KOH (100 equiv.)	DCM	r.t.	1	decomposition
10 [ES 6043b]	61h	OTs/dppf	KOH (10 equiv.)	DCM	r.t.	1	decomposition

4.12.4 Organoboron compounds

Potassium phenylboronate (**38a**)

[ES 6124]



Phenyl boronic acid (4.81 g, 39.5 mmol) was dissolved in toluene (150 mL) and THF was added until everything was dissolved (~ 25 mL). Saturated aqueous KOH was added drop wise until no more precipitation was formed. The solid was filtered off and washed with THF. Drying on high vacuum gave the title compound **38a** (5.63 g, 31.6 mmol, 80%) as a colorless solid.

¹H NMR (400 MHz, D₂O): δ 7.54 – 7.33 (m, 2H), 7.25 – 7.16 (m, 2H), 7.14 – 7.08 (m, 1H) ppm.

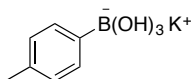
¹³C{¹H} NMR (101 MHz, D₂O): δ 131.4, 127.4, 126.0 ppm.

¹¹B{¹H} NMR (128 MHz, D₂O): δ 3.34 ppm.

The chemical shifts are in agreement with previously reported values.¹⁸⁹

Potassium 4-tolylboronate (**38b**)

[LCY 1138/ES 6160]



4-Tolyl boronic acid (1.30 g, 9.53 mmol) was dissolved in toluene (60 mL) and THF (50 mL). Saturated aqueous KOH was added drop wise until no more precipitation was formed. The solid was filtered off and washed with THF. Drying on high vacuum gave the title compound **38b** (1.20 g, 6.23 mmol, 65%) as an off-white solid.

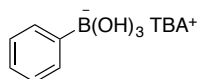
$^1\text{H NMR}$ (400 MHz, D_2O): δ 7.35 (d, $J = 7.7$ Hz, 2H), 7.03 (d, $J = 7.5$ Hz, 2H), 2.17 (s, 3H) ppm.

$^{11}\text{B}\{^1\text{H}\}$ NMR (128 MHz, D_2O): δ 1.87 ppm.

The chemical shifts are in agreement with previously reported values.¹⁵¹

Tetrabutylammonium phenylboronate (**39a**)

[LCY 1140/ES 6125]



Potassium phenylboronate **38a** (3.18 g, 17.9 mmol, 1.0 equiv.) was dissolved in EtOH (90 mL) and tetrabutylammonium chloride (4.72 g, 17.0 mmol, 0.95 equiv.) was dissolved in EtOH (15 mL) in a separate flask. Combining the two solutions resulted in immediate precipitation of KCl. The solid was removed by filtration through a glass frit and the solvent was removed from the filtrate. The oily residue was re-dissolved in Et_2O and the insoluble solids were filtered off. The solvent was removed and H_2O (3 mL) was added. Subsequent lyophilization gave the title compound **39a** (3.79 g, 9.94 mmol, 56%) as a colorless solid.

$^1\text{H NMR}$ (400 MHz, D_2O): δ 7.46 – 7.35 (m, 2H), 7.24 – 7.12 (m, 2H), 7.11 – 7.03 (m, 1H), 3.07 – 3.00 (m, 8H), 1.49 (td, $J = 11.6, 9.9, 6.1$ Hz, 8H), 1.21 (h, $J = 7.4$ Hz, 8H), 0.80 (t, $J = 7.4$ Hz, 12H) ppm.

$^{13}\text{C}\{^1\text{H}\}$ NMR (101 MHz, D_2O): δ 131.3, 127.3, 125.7, 58.1, 23.2, 19.2, 12.9 ppm.

The *ipso* carbon is not visible.

$^{11}\text{B}\{^1\text{H}\}$ NMR (128 MHz, D_2O): δ -5.52 ppm.

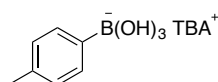
IR (solid, ν): 3005 (w), 2960 (w), 2873 (w), 1440 (m), 1398 (m), 1316 (w), 1276 (m), 1260 (m), 1172 (w), 1088 (w), 1025 (w), 969 (w), 925 (w), 886 (w), 764 (s), 750 (s), 704 (m), 671 (w), 655 (w) cm^{-1} .

Elemental analysis (%): C 69.30, H 11.61, N 3.70, calc. C 69.28, H 11.63, N 3.67.

M.p.: 72 °C.

Tetrabutylammonium 4-tolylboronate (**39b**)

[LCY 1142/ES 6161]



Potassium tolylboronate **38b** (728 mg, 3.79 mmol, 1.0 equiv.) was dissolved in EtOH (70 mL) and tetrabutylammonium chloride (1.00 g, 3.60 mmol, 0.95 equiv.) was dissolved in EtOH (10 mL) in a separate flask. The two solutions were combined and the formed solid was removed by filtration through a glass frit. Removal of the solvent from the filtrate resulted in an oily residue that was re-dissolved in Et_2O and the insoluble solids filtered off. The solvent was removed and H_2O (3 mL) was

added. Subsequent lyophilization for 48 h gave the title compound **39b** (1.02 g, 2.57 mmol, 71%) as a very hygroscopic colorless solid.

$^1\text{H NMR}$ (400 MHz, D_2O): δ 7.32 (d, $J = 7.6$ Hz, 2H), 7.00 (dd, $J = 7.9, 0.9$ Hz, 2H), 3.09 – 2.93 (m, 8H), 2.14 (s, 3H), 1.50 (p, $J = 7.9$ Hz, 8H), 1.21 (h, $J = 7.4$ Hz, 8H), 0.80 (t, $J = 7.4$ Hz, 12H) ppm.

$^{13}\text{C}\{^1\text{H}\}$ NMR (126 MHz, D_2O): δ 131.8, 128.1, 58.3, 23.3, 20.4, 19.3, 13.0 ppm.

The *ipso* and *para* carbon are not visible.

$^{11}\text{B}\{^1\text{H}\}$ NMR (128 MHz, D_2O): δ -4.64 ppm.

IR (solid, ν): 2960 (m), 2873 (m), 1605 (w), 1562 (w), 1456 (s), 1409 (s), 1383 (s), 1274 (m), 1175 (m), 1086 (m), 1061 (w), 1021 (m), 969 (m), 886 (m), 817 (m), 795 (m), 731 (s), 714 (w), 668 (w) cm^{-1} .

Elemental analysis (%): C 70.92, H 10.63, N 3.10, calc. C 69.86, H 11.73, N 3.54.

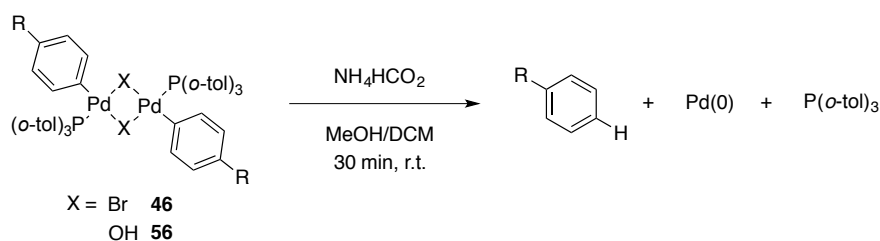
A better elemental analysis could not be obtained.

M.p.: 110-114 $^\circ\text{C}$.

4.13 Transmetalation reactions of the Suzuki-Miyaura reaction

Quenching protocol

Palladium complex **46** or **56** (16 μmol) was weighed in a vial and dissolved in DCM (1.0 mL). A stock solution of TMB in MeOH and a spatula tip of NH_4HCO_2 were added and the reaction was stirred for 30 minutes at room temperature. After the solids were filtered off through a short pad of celite, the sample was injected in a GC-FID to determine the conversion to substituted arene.



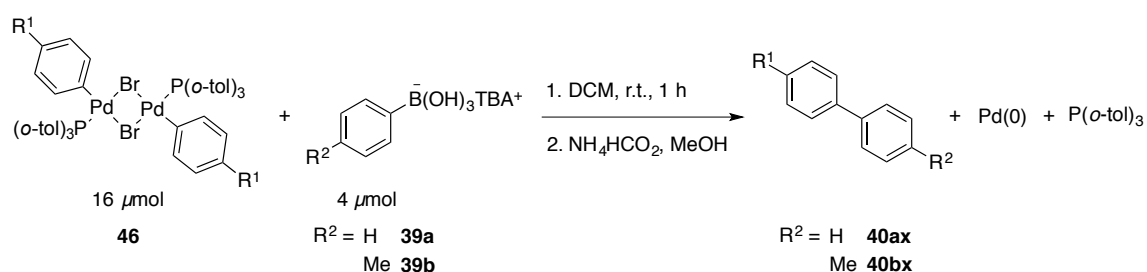
[ES 6144-ES 6147]

Entry	R	X		Yield [%]
1	OMe	OH	56a	76
2	OMe	Br	46a	99
3	CN	OH	56h	85
4	CN	Br	46h	87

General procedure for transmetalation reactions

Palladium complex **46** or **56** (16 μmol) was weighed in a 4 mL screw-cap vial with a septum. The vial was set under argon and DCM (0.20% H_2O , 1.5 mL) was added. After stirring for 15 min to ensure complete dissolution of the complex, a stock solution of boronate **39** or boronic acid **37** in DCM (0.20 mL, 4.0 μmol) was syringed into the solution. After stirring for 1 h at room temperature, the vial was opened to air and a stock solution of TMB internal standard in MeOH and a spatula tip of NH_4HCO_2 were added. The reaction was stirred for additionally 30 min and the solution was filtered through a short pad of celite into a GC vial. The yields are average values of two or three measurements of each sample.

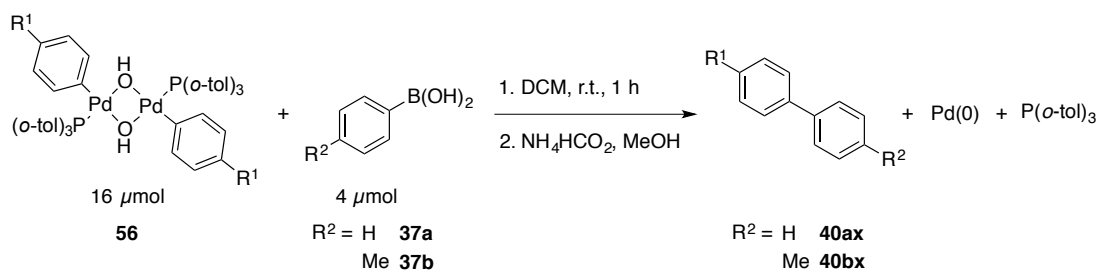
4.13.1 Non-competitive transmetalation reactions



[ES 6166a/ES 6162a]

According to the general procedure, complexes **46** (16 μmol) were treated with tolyl boronate **39** (1.6 mg, 4.0 μmol) in DCM (0.20 mL, $c[\mathbf{39}] = 20 \text{ mM}$). A stock solution of TMB ($c = 0.14 \text{ M}$, 0.20 mL, 0.028 mmol) was added for quantification via GC-FID.

entry	R		[ES 6166a]		[ES 6162a]	
			boronate	yield 40ax [%]	boronate	yield 40bx [%]
1	OMe	46a	39a	51	39b	34
2	<i>t</i> -Bu	46b	39a	21	39b	68
3	Me	46c	39a	53	39b	73
4	H	46d	39a	89	39b	66
5	F	46e	39a	33	39b	66
6	CO ₂ Et	46f	39a	85	39b	75
7	CF ₃	46g	39a	70	39b	59
8	CN	46h	39a	53	39b	60



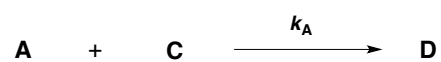
[ES 6166b/ES 6162b]

According to the general procedure, complexes **56** (16 μmol) was treated with tolyl boronic acid **37** (0.54 mg, 4.0 μmol) in DCM (0.20 mL, $c[\mathbf{37}] = 20 \text{ mM}$). A stock solution of TMB ($c = 0.15 \text{ M}$, 0.20 mL, 0.029 mmol) was added for quantification via GC-FID.

entry	R		[ES 6166b]		[ES 6162b]	
			boronic acid	yield 40ax [%]	boronic acid	yield 40bx [%]
1	OMe	56a	37a	83	37b	79
2	<i>t</i> -Bu	56b	37a	86	37b	90
3	Me	56c	37a	–	37b	–
4	H	56d	37a	89	37b	102
5	F	56e	37a	48	37b	101
6	CO ₂ Et	56f	37a	98	37b	105
7	CF ₃	56g	37a	100	37b	75
8	CN	56h	37a	79	37b	93

4.13.2 Competitive transmetalation reactions

For the competitive transmetalation reactions, the reaction equations are:



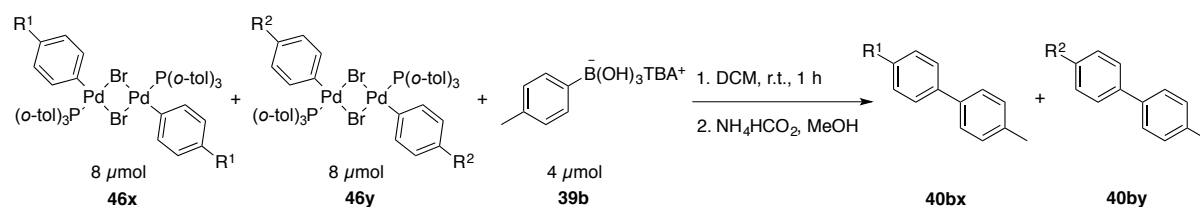
Under the assumptions that the reaction rates can be expressed as

$$\text{(eq. 1) } d[\mathbf{A}]/dt = -k_A[\mathbf{A}][\mathbf{C}]$$

$$\text{(eq. 2) } d[\mathbf{B}]/dt = -k_B[\mathbf{B}][\mathbf{C}]$$

Where **A** and **B** are the competing reagents to **C** and k_A and k_B are the observed reaction rates, the changes in concentration in reactants **A** and **B** over time are taken into account for the relative reaction rates as calculated by eq. 3, of which the derivation has previously been published.⁴²

$$\text{(eq. 3)} \quad k_{\text{rel}} = ((\log[\mathbf{A}_0] - [\mathbf{D}])(-\log[\mathbf{A}_0])) / ((\log[\mathbf{B}_0] - [\mathbf{E}])(-\log[\mathbf{B}_0]))$$

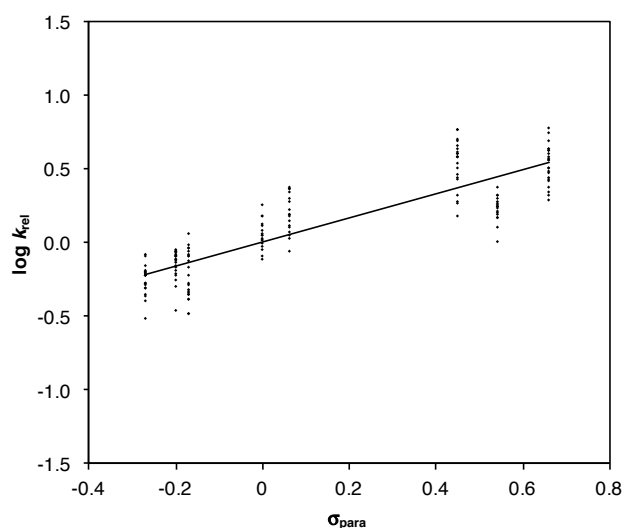


[ES 6180]

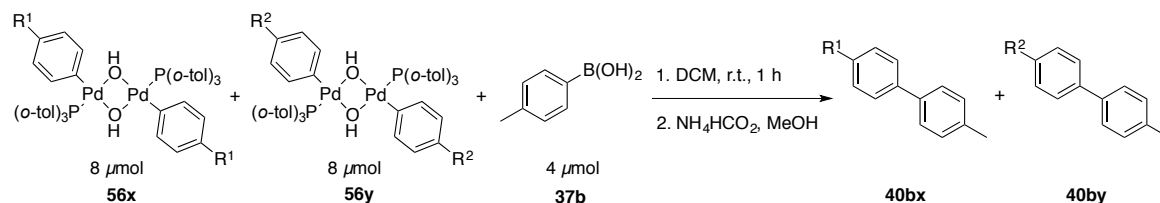
According to the general procedure, complexes **46x** and **46y** (8 μmol, 16 μmol in [Pd] each) were treated with tolyl boronate **39b** (1.6 mg, 4.0 μmol) in DCM (0.20 mL, $c[\mathbf{39b}] = 20$ mM). A stock solution of TMB ($c = 0.14$ M, 0.20 mL, 0.028 mmol) was added for quantification via GC-FID.

Sample	R ¹	46x	<i>m</i> [mg]	<i>n</i> [μmol]	R ²	46y	<i>m</i> [mg]	<i>n</i> [μmol]	40bx/ 40by	σ	yield 40b [%]	σ [%]
A1	OMe	a	9.6	8.0	H	d	9.4	8.3	0.40	0.06	46	5
A2	<i>t</i> -Bu	b	9.9	7.9	H	d	9.1	8.0	0.71	0.03	59	6
A3	Me	c	9.3	8.0	H	d	9.0	7.9	0.65	0.25	49	9
A4	F	e	9.4	8.0	H	d	9.2	8.1	-	-	-	-
A5	CO ₂ Et	f	10.1	7.9	H	d	9.3	8.2	2.34	1.15	76	9
A6	CF ₃	g	10.1	7.9	H	d	9.3	8.2	-	-	-	-
A7	CN	h	9.7	8.2	H	d	9.2	8.1	3.33	0.46	76	6
B2	<i>t</i> -Bu	b	10.0	8.0	OMe	a	9.6	8.0	1.35	0.07	59	5
B3	Me	c	9.2	7.9	OMe	a	9.5	7.9	1.59	0.28	49	3
B4	F	e	9.5	8.1	OMe	a	9.6	8.0	2.44	0.75	48	8
B5	CO ₂ Et	f	10.4	8.1	OMe	a	9.6	8.0	5.42	2.17	58	35
B6	CF ₃	g	10.2	8.0	OMe	a	9.4	7.9	3.05	0.20	43	4
B7	CN	h	9.4	7.9	OMe	a	9.6	8.0	3.68	0.40	85	5
C3	Me	c	9.4	8.1	<i>t</i> -Bu	b	10.1	8.1	0.60	0.32	43	3
C4	F	e	9.3	7.9	<i>t</i> -Bu	b	10.2	8.2	2.29	0.55	54	7
C5	CO ₂ Et	f	10.1	7.9	<i>t</i> -Bu	b	9.9	7.9	3.57	1.80	100	16
C6	CF ₃	g	10.2	8.0	<i>t</i> -Bu	b	10.3	8.3	2.18	0.06	55	4
C7	CN	h	9.5	8.0	<i>t</i> -Bu	b	10.1	8.1	5.14	0.21	68	14
D4	F	e	9.6	8.2	Me	c	9.2	7.9	2.76	0.74	80	13
D5	CO ₂ Et	f	10.3	8.0	Me	c	9.2	7.9	6.34	0	119	0
D6	CF ₃	g	10.3	8.1	Me	c	9.4	8.1	3.48	1.39	56	5
D7	CN	h	9.8	8.3	Me	c	9.5	8.2	4.55	1.80	89	8

E5	CO ₂ Et	f	10.3	8.0	F	e	9.6	8.2	3.65	1.79	93	1
E6	CF ₃	g	10.1	7.9	F	e	9.3	7.9	-	-	-	-
E7	CN	h	9.7	8.2	F	e	9.5	8.1	1.67	0.53	34	4
F6	CF ₃	g	10.3	8.1	CO ₂ Et	f	10.2	8.0	0.47	0.07	84	8
F7	CN	h	9.7	8.2	CO ₂ Et	f	10.2	8.0	1.24	0.22	83	15
G7	CN	h	9.6	8.1	CF ₃	g	10.3	8.1	2.38	0.47	67	8



	slope	R ²
	ρ	
[ES 6180]	+0.81 ± 0.04	0.75



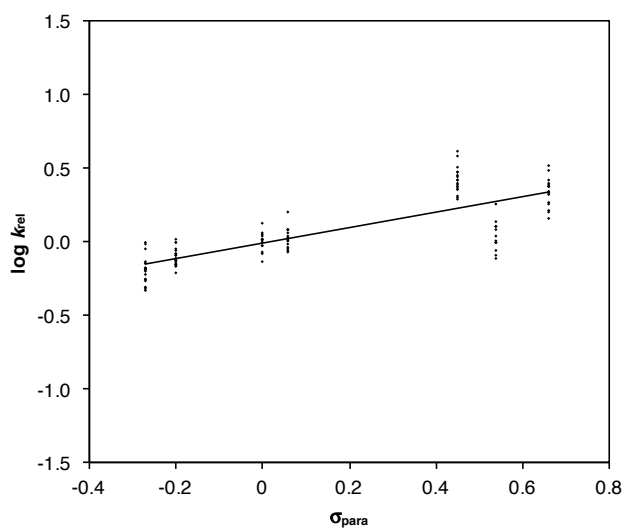
[ES 6178]

According to the general procedure, complexes **56x** and **56y** (8 μmol , 16 μmol in [Pd] each) were treated with tolyl boronic acid **37b** (0.54 mg, 4.0 μmol) in DCM (0.20 mL, $c[\mathbf{37b}] = 20 \text{ mM}$). A stock solution of TMB ($c = 0.15 \text{ M}$, 0.20 mL, 0.029 mmol) was added for quantification via GC-FID.

Sample	R ¹	56x	<i>m</i> [mg]	<i>n</i> [μmol]	R ²	56y	<i>m</i> [mg]	<i>n</i> [μmol]	40bx/ 40by	σ	yield 40b [%]	σ [%]
A1	OMe	a	9.2	8.6	H	d	8.2	8.1	0.59	0.14	73	10
A2	<i>t</i> -Bu	b	9.8	8.7	H	d	9.1	9.0	0.69	0.03	93	5
A4	F	e	8.6	8.2	H	d	8.0	7.9	-	-	-	-
A5	CO ₂ Et	f	9.7	8.4	H	d	8.0	7.9	2.55	0.39	118	16
A6	CF ₃	g	9.8	8.6	H	d	8.3	8.2	-	-	-	-
A7	CN	h	8.9	8.4	H	d	8.0	7.9	2.63	0.37	114	5
B2	<i>t</i> -Bu	b	9.5	8.5	OMe	a	8.8	8.2	1.31	0.20	84	16
B4	F	e	8.3	7.9	OMe	a	8.5	7.9	1.64	0.15	77	10

4 Experimental Section

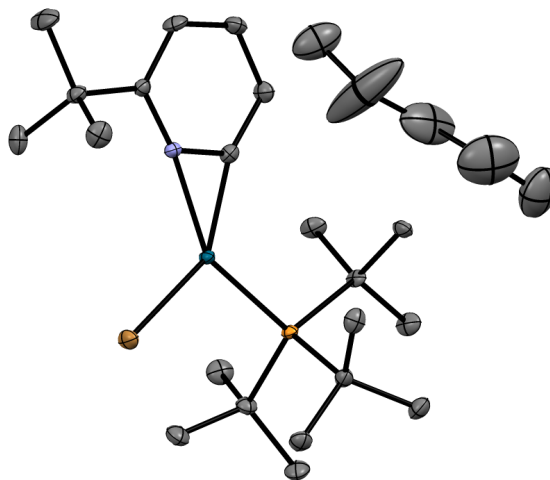
B5	CO ₂ Et	f	9.1	7.9	OMe	a	8.7	8.1	3.40	0.13	110	7
B6	CF ₃	g	9.3	8.1	OMe	a	8.8	8.2	2.05	0.32	76	12
B7	CN	h	8.8	8.3	OMe	a	8.6	8.0	2.33	0.19	87	16
C4	F	e	8.7	8.3	<i>t</i> -Bu	b	9.6	8.6	1.31	0.11	93	12
C5	CO ₂ Et	f	10.7	9.3	<i>t</i> -Bu	b	9.3	8.3	3.18	0.24	120	12
C6	CF ₃	g	9.7	8.5	<i>t</i> -Bu	b	9.4	8.4	1.34	0.30	96	9
C7	CN	h	10.2	9.6	<i>t</i> -Bu	b	10.8	9.6	2.65	0.33	104	4
E5	CO ₂ Et	f	11.3	9.8	F	e	10.5	10.0	2.17	0.29	117	7
E6	CF ₃	g	10.6	9.3	F	e	8.6	8.2	-	-	-	-
E7	CN	h	9.0	8.5	F	e	8.6	8.2	2.34	0.04	98	5
F6	CF ₃	g	9.4	8.9	CO ₂ Et	f	9.3	8.1	0.38	0.02	103	2
F7	CN	h	9.0	8.5	CO ₂ Et	f	9.1	7.9	0.90	0.13	110	38
G7	CN	h	9.0	8.5	CF ₃	g	9.6	8.4	2.12	0.20	97	6



	slope	R^2
	ρ	
[ES 6178]	$+0.52 \pm 0.04$	0.65

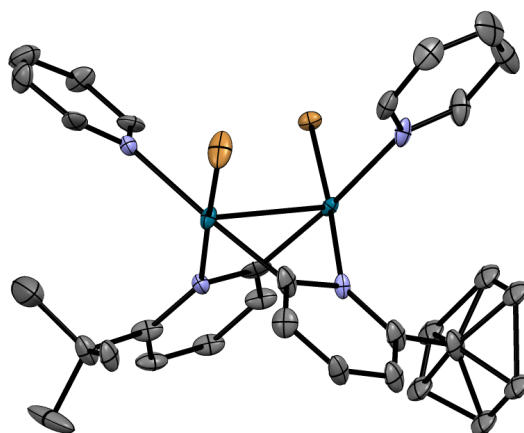
5 Crystallographic Data

(6-*tert*-Bu-2-pyridyl)Pd(Br)(P(*t*-Bu)₃) (12a)



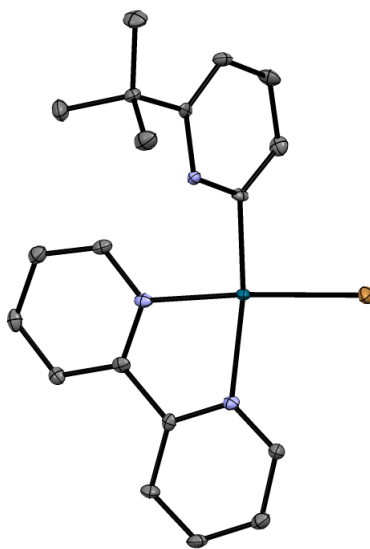
Sample number	ES 4082
Empirical formula	C ₂₁ H ₃₉ Br N P Pd, C ₅ H ₁₂
Formula weight	522.85
Temperature	100 K
Crystal system	monoclinic
Space group	P 21/c
Unit cell dimensions	a = 13.6988(3) Å α = 90° b = 13.3345(3) Å β = 108.221(1)° c = 16.7537(4) Å γ = 90°
Volume	2906.89(12) Å ³
Crystal color	yellow
Z	6
Density	1.353 g/cm ³
F(000)	1228
Radiation type	MoKα
Absorption coefficient	2.080
Crystal size	0.38 x 0.30 x 0.23 mm
Reflections collected	22325
Independent reflections	5934
Observed [I > 2σ(I)] reflections	4905
Goodness-to-fit on F ²	1.044
R (all data)	0.0521

CCDC-1819741 contains the crystallographic data for **12a**.

[(μ -6-*tert*-Bu-2-pyridyl)-C²,N]Pd(Br)(py)]₂ (17**)**

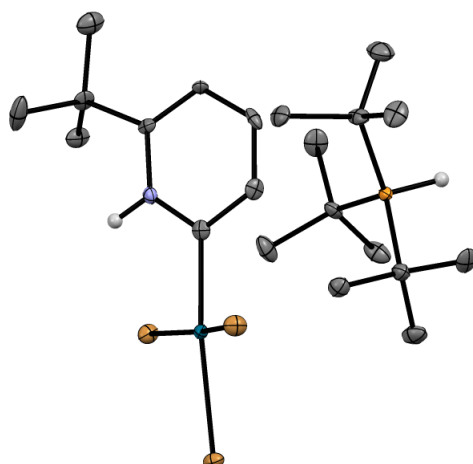
Sample number	ES 4189
Empirical formula	C ₂₈ H ₂₅ Br ₂ N ₄ Pd ₂
Formula weight	790.14
Temperature	100 K
Crystal system	monoclinic
Space group	P 21
Unit cell dimensions	a = 9.1934(2) Å $\alpha = 90^\circ$ b = 16.8864(4) Å $\beta = 94.7820(10)^\circ$ c = 9.3715(2) Å $\gamma = 90^\circ$
Volume	1449.80(6) Å ³
Crystal color	red
Z	2
Density	1.810 g/cm ³
F(000)	766
Radiation type	MoK α
Absorption coefficient	4.007
Crystal size	0.090 x 0.060 x 0.050 mm
Reflections collected	15137
Independent reflections	5079
Observed [I > 2 σ (I)] reflections	4770
Goodness-to-fit on F ²	1.095
R (all data)	0.0482

CCDC-1819819 contains the crystallographic data for **17**.

(6-*tert*-Bu-2-pyridyl)Pd(Br)(bipy) (18)

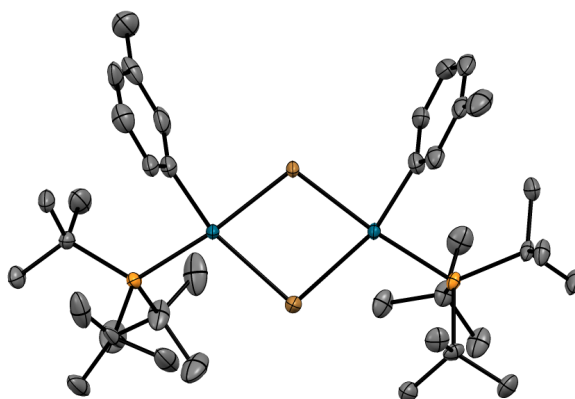
Sample number	ES 5192	
Empirical formula	C ₁₉ H ₂₀ Br N ₃ Pd	
Formula weight	476.69	
Temperature	100 K	
Crystal system	monoclinic	
Space group	C c	
Unit cell dimensions	a = 10.9359(2) Å	α = 90°
	b = 26.5588(5) Å	β = 122.2696(6)°
	c = 7.24790(10) Å	γ = 90°
Volume	1779.97(5) Å ³	
Crystal color	yellow	
Z	4	
Density	1.779 g/cm ³	
F(000)	944	
Radiation type	MoKα	
Absorption coefficient	3.292	
Crystal size	0.220 x 0.150 x 0.080 mm	
Reflections collected	10709	
Independent reflections	3429	
Observed [I > 2σ(I)] reflections	3304	
Goodness-to-fit on F ²	0.891	
R (all data)	0.0216	

CCDC-1819820 contains the crystallographic data for **18**.

[(6-*tert*-Bu-pyridinium)Pd(Br)₃][HP(*t*-Bu)₃] (30)

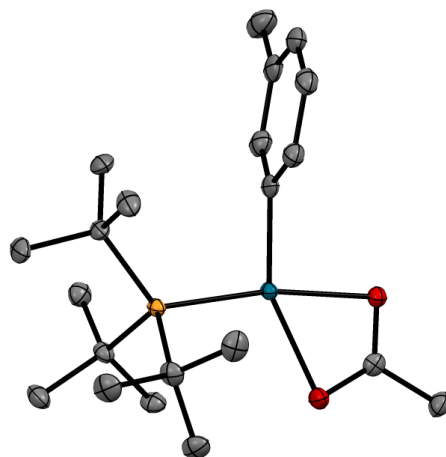
Sample number	ES5160	
Empirical formula	C ₂₁ H ₄₁ Br ₃ N P Pd	
Formula weight	684.67	
Temperature	100 K	
Crystal system	orthorhombic	
Space group	P c a 21	
Unit cell dimensions	a = 16.7639(6) Å	α = 90°
	b = 10.2855(3) Å	β = 90°
	c = 15.3622(4) Å	γ = 90°
Volume	2648.83(14) Å ³	
Crystal color	yellow	
Z	2	
Density	1.717 g/cm ³	
F(000)	1360	
Radiation type	MoKα	
Absorption coefficient	5.294	
Crystal size	0.27 x 0.06 x 0.03 mm	
Reflections collected	11378	
Independent reflections	4380	
Observed [I > 2σ(I)] reflections	3902	
Goodness-to-fit on F ²	0.858	
R (all data)	0.0383	

CCDC-1819821 contains the crystallographic data for **30**.

[(3-tolyl)Pd(Br)(P(*t*-Bu)₃)₂] (14a)

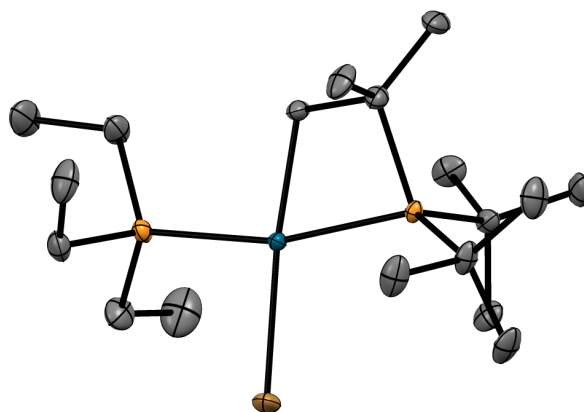
Sample number	ES 5060	
Empirical formula	C ₃₈ H ₆₈ Br ₂ P ₂ Pd ₂	
Formula weight	479.74	
Temperature	100 K	
Crystal system	monoclinic	
Space group	P 21/c	
Unit cell dimensions	a = 16.8382(3) Å	α = 90°
	b = 14.1942(3) Å	β = 115.4852(7)°
	c = 19.0215(4) Å	γ = 90°
Volume	4103.86(14) Å ³	
Crystal color	yellow	
Z	8	
Density	1.553 g/cm ³	
F(000)	1952	
Radiation type	MoKα	
Absorption coefficient	2.926	
Crystal size	0.170 x 0.150 x 0.030 mm	
Reflections collected	30403	
Independent reflections	7806	
Observed [I > 2σ(I)] reflections	6472	
Goodness-to-fit on F ²	1.056	
R (all data)	0.0557	

CCDC-1819822 contains the crystallographic data for **14a**.

(3-tolyl)Pd(OAc)(P(*t*-Bu)₃) (15a)

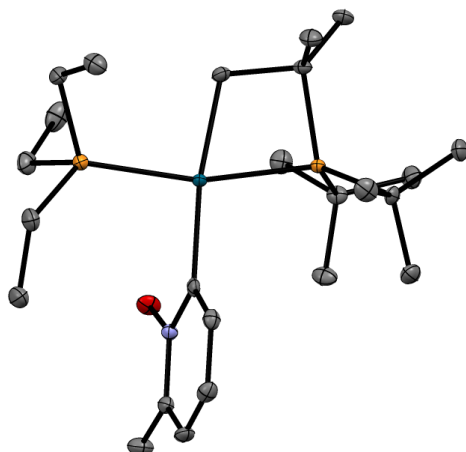
Sample number	ES 4172	
Empirical formula	C ₂₁ H ₃₇ O ₂ P Pd	
Formula weight	458.87	
Temperature	100 K	
Crystal system	monoclinic	
Space group	P 21/c	
Unit cell dimensions	a = 8.24780(10) Å	$\alpha = 90^\circ$
	b = 16.7056(3) Å	$\beta = 90.9469(6)^\circ$
	c = 15.6620(3) Å	$\gamma = 90^\circ$
Volume	2157.69(6) Å ³	
Crystal color	colorless	
Z	4	
Density	1.413 g/cm ³	
F(000)	960	
Radiation type	MoK α	
Absorption coefficient	0.945	
Crystal size	0.160 x 0.150 x 0.110 mm	
Reflections collected	13835	
Independent reflections	3783	
Observed [I > 2 σ (I)] reflections	3533	
Goodness-to-fit on F ²	1.056	
R (all data)	0.0285	

CCDC-1819823 contains the crystallographic data for **15a**.

(*tert*-Bu₂PC(CH₃)₂CH₂)Pd(Br)(PEt₃) (complex C)

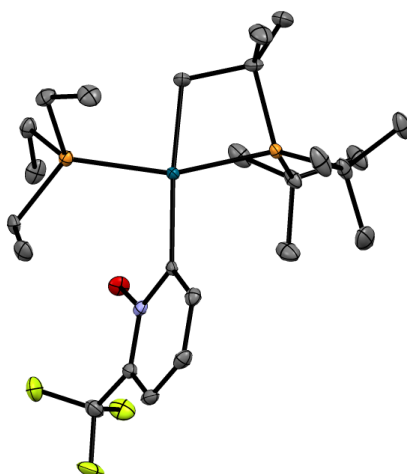
Sample number	ES 4166	
Empirical formula	C ₁₈ H ₄₁ Br P ₂ Pd	
Formula weight	505.76	
Temperature	100 K	
Crystal system	orthorhombic	
Space group	P b c a	
Unit cell dimensions	a = 16.5514(2) Å	α = 90°
	b = 14.8570(3) Å	β = 90°
	c = 18.9301(3) Å	γ = 90°
Volume	4654.99(13) Å ³	
Crystal color	yellow	
Z	8	
Density	1.443 g/cm ³	
F(000)	2080	
Radiation type	MoKα	
Absorption coefficient	2.649	
Crystal size	0.250 x 0.200 x 0.140 mm	
Reflections collected	27875	
Independent reflections	4126	
Observed [I > 2σ(I)] reflections	3589	
Goodness-to-fit on F ²	1.060	
R (all data)	0.0315	

CCDC-1819824 contains the crystallographic data for C.

(6-Me-2-pyridyl *N*-oxide)Pd(*tert*-Bu₂PC(CH₃)₂CH₂)(PEt₃) (21)

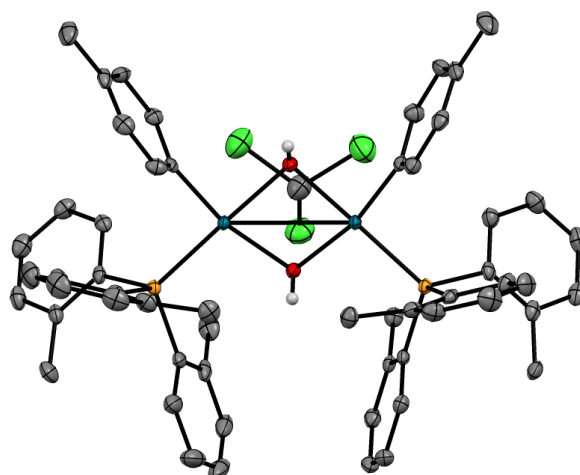
Sample number	ES 5030	
Empirical formula	C ₂₄ H ₄₇ N O P ₂ Pd	
Formula weight	533.96	
Temperature	100 K	
Crystal system	monoclinic	
Space group	P 21/c	
Unit cell dimensions	a = 14.9977(3) Å	α = 90°
	b = 13.2984(2) Å	β = 91.986(8)°
	c = 13.1884(2) Å	γ = 90°
Volume	2628.79(8) Å ³	
Crystal color	yellow	
Z	4	
Density	1.349 g/cm ³	
F(000)	1128	
Radiation type	MoKα	
Absorption coefficient	0.843	
Crystal size	0.220 x 0.100 x 0.060 mm	
Reflections collected	22445	
Independent reflections	4635	
Observed [I > 2σ(I)] reflections	4032	
Goodness-to-fit on F ²	1.032	
R (all data)	0.0311	

CCDC-1819825 contains the crystallographic data for **21**.

(6-CF₃-2-pyridyl *N*-oxide)Pd(*tert*-Bu₂PC(CH₃)₂CH₂)(PEt₃) (22)

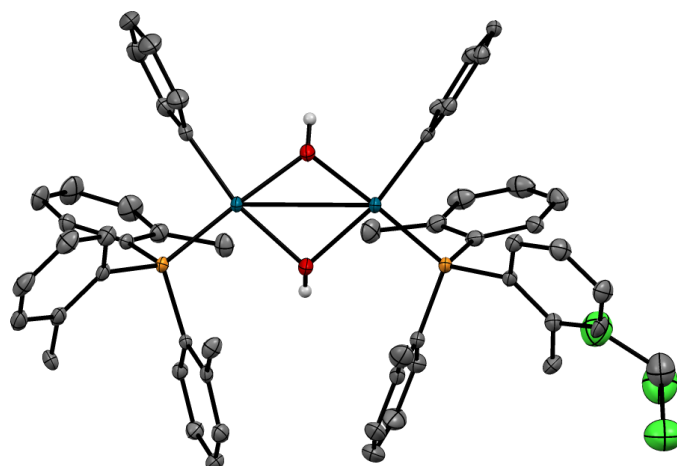
Sample number	ES 6011	
Empirical formula	C ₂₄ H ₄₄ F ₃ N O P ₂ Pd	
Formula weight	587.94	
Temperature	100 K	
Crystal system	monoclinic	
Space group	P 2 ₁ /n	
Unit cell dimensions	a = 8.9440(2) Å	α = 90°
	b = 15.2735(4) Å	β = 98.0290(10)°
	c = 20.2452(4) Å	γ = 90°
Volume	2738.51(11) Å ³	
Crystal color	yellow	
Z	4	
Density	1.426 g/cm ³	
F(000)	1224	
Radiation type	MoKα	
Absorption coefficient	0.831	
Crystal size	0.480 x 0.190 x 0.060 mm	
Reflections collected	20244	
Independent reflections	5208	
Observed [I > 2σ(I)] reflections	4207	
Goodness-to-fit on F ²	1.033	
R (all data)	0.0467	

CCDC-1819826 contains the crystallographic data for **22**.

[(4-Me-phenyl)Pd(μ -OH)(P(*o*-tol)₃)₂]₂ (46c**)**

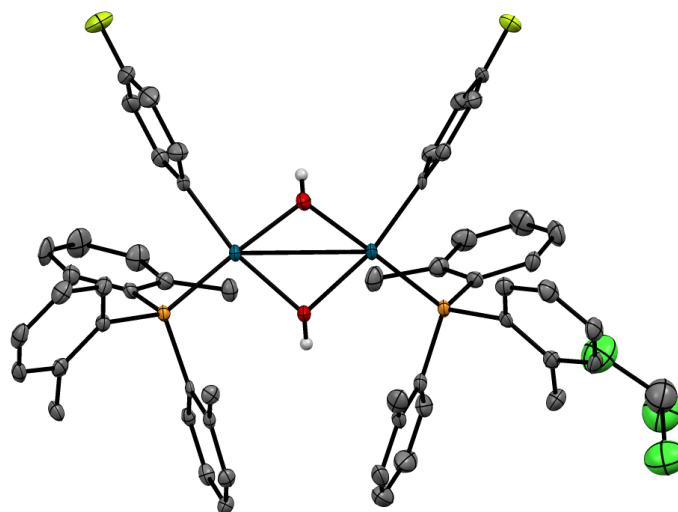
Sample number	ES 6106a	
Empirical formula	C ₅₆ H ₅₈ O ₂ P ₂ Pd ₂ , C H Cl ₃	
Formula weight	1157.13	
Temperature	100 K	
Crystal system	monoclinic	
Space group	P 2 ₁ /n	
Unit cell dimensions	a = 13.4270(10) Å	$\alpha = 90^\circ$
	b = 20.9564(13) Å	$\beta = 104.698(3)^\circ$
	c = 19.9451(14) Å	$\gamma = 90^\circ$
Volume	5428.5(7) Å ³	
Crystal color	yellow	
Z	4	
Density	1.416 g/cm ³	
F(000)	2360	
Radiation type	MoK α	
Absorption coefficient	0.909	
Crystal size	0.240 x 0.160 x 0.060 mm	
Reflections collected	55529	
Independent reflections	9965	
Observed [I > 2 σ (I)] reflections	8658	
Goodness-to-fit on F ²	1.047	
R (all data)	0.0405	

CCDC-1819827 contains the crystallographic data for **46c**.

[(phenyl)Pd(μ -OH)(P(*o*-tol)₃)₂]₂ (46d**)**

Sample number	ES 6158d	
Empirical formula	C ₅₄ H ₅₄ O ₂ P ₂ Pd ₂ , C H Cl ₃	
Formula weight	1129.08	
Temperature	112 K	
Crystal system	monoclinic	
Space group	P 21/n	
Unit cell dimensions	a = 13.4863(12) Å	$\alpha = 90^\circ$
	b = 20.5641(17) Å	$\beta = 105.260(3)^\circ$
	c = 19.6311(16) Å	$\gamma = 90^\circ$
Volume	5252.4(8) Å ³	
Crystal color	yellow	
Z	4	
Density	1.428 g/cm ³	
F(000)	2296	
Radiation type	MoK α	
Absorption coefficient	0.937	
Crystal size	0.380 x 0.300 x 0.200 mm	
Reflections collected	41581	
Independent reflections	9635	
Observed [I > 2 σ (I)] reflections	8812	
Goodness-to-fit on F ²	1.074	
R (all data)	0.0479	

CCDC-1819828 contains the crystallographic data for **46d**.

[(4-F-phenyl)Pd(μ -OH)(P(*o*-tol)₃)₂](46e**)**

Sample number	ES 6116d	
Empirical formula	C ₅₄ H ₅₂ F ₂ O ₂ P ₂ Pd ₂ , C H Cl ₃	
Formula weight	1165.06	
Temperature	101 K	
Crystal system	monoclinic	
Space group	P 2 ₁ /n	
Unit cell dimensions	a = 13.3973(6) Å	α = 90°
	b = 20.6491(11) Å	β = 105.462(2)°
	c = 19.7501(9) Å	γ = 90°
Volume	5266.0(4) Å ³	
Crystal color	orange	
Z	4	
Density	1.470 g/cm ³	
F(000)	2360	
Radiation type	MoKα	
Absorption coefficient	0.942	
Crystal size	0.240 x 0.170 x 0.060 mm	
Reflections collected	36373	
Independent reflections	9788	
Observed [I > 2σ(I)] reflections	8162	
Goodness-to-fit on F ²	1.057	
R (all data)	0.0696	

CCDC-1819829 contains the crystallographic data for **46e**.

6 References

- [1] J. A. Labinger, J. E. Bercaw, *Nature* **2002**, *417*, 507; D. Lapointe, K. Fagnou, *Chem. Lett.* **2010**, *39*, 1119; D. Balcells, E. Clot, O. Eisenstein, *Chem. Rev.* **2010**, *110*, 749; H. M. L. Davies, D. Morton, *J. Org. Chem.* **2016**, *81*, 343.
- [2] L. C. Campeau, S. Rousseaux, K. Fagnou, *J. Am. Chem. Soc.* **2005**, *127*, 18020.
- [3] S. Duric, C. C. Tzschucke, *Org. Lett.* **2011**, *13*, 2310.
- [4] Y. C. Tan, F. Barrios-Landeros, J. F. Hartwig, *J. Am. Chem. Soc.* **2012**, *134*, 3683.
- [5] H. Y. Sun, S. I. Gorelsky, D. R. Stuart, L. C. Campeau, K. Fagnou, *J. Org. Chem.* **2010**, *75*, 8180.
- [6] D. A. Horton, G. T. Bourne, M. L. Smythe, *Chem. Rev.* **2003**, *103*, 893.
- [7] G. Bringmann, R. Walter, R. Weirich, *Angew. Chem., Int. Ed.* **1990**, *29*, 977; M. C. Kozlowski, B. J. Morgan, E. C. Linton, *Chem. Soc. Rev.* **2009**, *38*, 3193.
- [8] L. Pu, *Chem. Rev.* **1998**, *98*, 2405.
- [9] U. S. Schubert, C. Eschbaumer, *Angew. Chem., Int. Ed.* **2002**, *41*, 2892.
- [10] B. Glover, K. A. Harvey, B. Liu, M. J. Sharp, M. F. Tymoschenko, *Org. Lett.* **2003**, *5*, 301; M. S. McClure, B. Glover, E. McSorley, A. Millar, M. H. Osterhout, F. Roschangar, *Org. Lett.* **2001**, *3*, 1677.
- [11] M. A. Campo, Q. H. Huang, T. L. Yao, Q. P. Tian, R. C. Larock, *J. Am. Chem. Soc.* **2003**, *125*, 11506.
- [12] B. S. Lane, M. A. Brown, D. Sames, *J. Am. Chem. Soc.* **2005**, *127*, 8050.
- [13] S. Yanagisawa, T. Sudo, R. Noyori, K. Itami, *J. Am. Chem. Soc.* **2006**, *128*, 11748.
- [14] M. Lafrance, C. N. Rowley, T. K. Woo, K. Fagnou, *J. Am. Chem. Soc.* **2006**, *128*, 8754.
- [15] D. Garcia-Cuadrado, A. A. C. Braga, F. Maseras, A. M. Echavarren, *J. Am. Chem. Soc.* **2006**, *128*, 1066.
- [16] S. I. Gorelsky, D. Lapointe, K. Fagnou, *J. Am. Chem. Soc.* **2008**, *130*, 10848.
- [17] D. Alberico, M. E. Scott, M. Lautens, *Chem. Rev.* **2007**, *107*, 174.
- [18] J. X. Wang, J. A. McCubbin, M. Z. Jin, R. S. Laufer, Y. Y. Mao, A. P. Crew, M. J. Mulvihill, V. Snieckus, *Org. Lett.* **2008**, *10*, 2923.
- [19] A. J. Mota, A. Dedieu, C. Bour, J. Suffert, *J. Am. Chem. Soc.* **2005**, *127*, 7171.
- [20] L. C. Campeau, K. Fagnou, *Chem. Soc. Rev.* **2007**, *36*, 1058.
- [21] D. J. Schipper, L. C. Campeau, K. Fagnou, *Tetrahedron* **2009**, *65*, 3155.
- [22] L. C. Campeau, D. R. Stuart, J. P. Leclerc, M. Bertrand-Laperle, E. Villemure, H. Y. Sun, S. Lasserre, N. Guimond, M. Lecavallier, K. Fagnou, *J. Am. Chem. Soc.* **2009**, *131*, 3291.
- [23] J. P. Leclerc, K. Fagnou, *Angew. Chem., Int. Ed.* **2006**, *45*, 7781.
- [24] M. P. Huestis, K. Fagnou, *Org. Lett.* **2009**, *11*, 1357.
- [25] D. J. Schipper, M. El-Salfiti, C. J. Whipp, K. Fagnou, *Tetrahedron* **2009**, *65*, 4977.
- [26] L. Ackermann, S. Fenner, *Chem. Comm.* **2011**, *47*, 430.
- [27] P. B. White, S. S. Stahl, *J. Am. Chem. Soc.* **2011**, *133*, 18594; D. Konning, T. Olbrisch, F. D. Sypaseuth, C. C. Tzschucke, M. Christmann, *Chem. Commun.* **2014**, *50*, 5014; F. D. Sypaseuth, C. Matlachowski, M. Weber, M. Schwalbe, C. C. Tzschucke, *Chem. Eur. J.* **2015**, *21*, 6564.
- [28] C. K. Prier, D. A. Rankic, D. W. C. MacMillan, *Chem. Rev.* **2013**, *113*, 5322; M. Gratzel, *Acc. Chem. Res.* **2009**, *42*, 1788.

- [29] C. Kaes, M. W. Hosseini, C. E. F. Rickard, B. W. Skelton, A. H. White, *Angew. Chem., Int. Ed.* **1998**, *37*, 920.
- [30] F. Krohnke, *Synthesis* **1976**, 1.
- [31] J. Dash, H. U. Reissig, *Chem. Eur. J.* **2009**, *15*, 6811.
- [32] M. Heller, U. S. Schubert, *J. Org. Chem.* **2002**, *67*, 8269; C. A. Panetta, H. J. Kumpaty, N. E. Heimer, M. C. Leavy, C. L. Hussey, *J. Org. Chem.* **1999**, *64*, 1015.
- [33] S. A. Savage, A. P. Smith, C. L. Fraser, *J. Org. Chem.* **1998**, *63*, 10048; A. Lutzen, M. Hapke, *Eur. J. Org. Chem.* **2002**, 2292.
- [34] K. Deshayes, R. D. Broene, I. Chao, C. B. Knobler, F. Diederich, *J. Org. Chem.* **1991**, *56*, 6787; N. A. Jones, J. W. Antoon, A. L. Bowie, J. B. Borak, E. P. Stevens, *J. Heterocycl. Chem.* **2007**, *44*, 363.
- [35] R. Balicki, *Synthesis* **1989**, 645.
- [36] D. Wenkert, R. B. Woodward, *J. Org. Chem.* **1983**, *48*, 283.
- [37] S. P. Zucker, F. Wossidlo, M. Weber, D. Lentz, C. C. Tzschucke, *J. Org. Chem.* **2017**, *82*, 5616.
- [38] Y. Aoyagi, T. Abe, A. Ohta, *Synthesis* **1997**, 891.
- [39] S. Duric, F. D. Sypaseuth, S. Hoof, E. Svensson, C. C. Tzschucke, *Chem. Eur. J.* **2013**, *19*, 17456.
- [40] J. P. Stambuli, M. Buhl, J. F. Hartwig, *J. Am. Chem. Soc.* **2002**, *124*, 9346.
- [41] L. Y. Wu, J. F. Hartwig, *J. Am. Chem. Soc.* **2005**, *127*, 15824.
- [42] S. P. Zucker, Ph.D. Thesis, Freie Universität Berlin, 2016.
- [43] W. H. Henderson, J. M. Alvarez, C. C. Eichman, J. P. Stambuli, *Organometallics* **2011**, *30*, 5038.
- [44] K. A. Connors, *Chemical kinetics: the study of reaction rates in solution*. 1st ed., VCH, New York, NY, 1990.
- [45] J. O. Schreck, *J. Chem. Educ.* **1971**, *48*, 103.
- [46] A. H. Roy, J. F. Hartwig, *J. Am. Chem. Soc.* **2003**, *125*, 13944.
- [47] K. M. Engle, J. Q. Yu, *J. Org. Chem.* **2013**, *78*, 8927.
- [48] V. V. Grushin, W. J. Marshall, *J. Am. Chem. Soc.* **2009**, *131*, 918.
- [49] A. Maleckis, M. S. Sanford, *Organometallics* **2011**, *30*, 6617.
- [50] A. B. Goel, S. Goel, H. C. Clark, *Inorg. Chem.* **1978**, *18*, 2803.
- [51] F. W. Lewis, L. M. Harwood, M. J. Hudson, P. Distler, J. John, K. Stamberg, A. Nunez, H. Galan, A. G. Espartero, *Eur. J. Org. Chem.* **2012**, 1509.
- [52] A. K. Jha, N. Jain, *Eur. J. Org. Chem.* **2017**, 4765.
- [53] B. V. Varun, J. Dhineshkumar, K. R. Bettadapur, Y. Siddaraju, K. Alagiri, K. R. Prabhu, *Tetrahedron Lett.* **2017**, *58*, 803.
- [54] S. S. Liu, C. C. Tzschucke, *Eur. J. Org. Chem.* **2016**, 3509.
- [55] D. E. Stephens, J. Lakey-Beitia, G. Chavez, C. Ilie, H. D. Arman, O. V. Larionov, *Chem. Commun.* **2015**, *51*, 9507.
- [56] M. D. Lotz, N. M. Camasso, A. J. Canty, M. S. Sanford, *Organometallics* **2017**, *36*, 165.
- [57] D. Monguchi, A. Yamamura, T. Fujiwara, T. Somete, A. Mori, *Tetrahedron Lett.* **2010**, *51*, 850; Y. Li, J. Jin, W. Qian, W. Bao, *Org. Biomol. Chem.* **2010**, *8*, 326.
- [58] T. Truong, J. Alvarado, L. D. Tran, O. Daugulis, *Org. Lett.* **2010**, *12*, 1200.
- [59] F. W. Patureau, F. Glorius, *Angew. Chem., Int. Ed.* **2011**, *50*, 1977.
- [60] Y. C. Tan, J. F. Hartwig, *J. Am. Chem. Soc.* **2010**, *132*, 3676.
- [61] J. L. Wu, X. L. Cui, L. M. Chen, G. J. Jiang, Y. J. Wu, *J. Am. Chem. Soc.* **2009**, *131*, 13888.
- [62] W. Liu, Y. Li, Y. Wang, C. Kuang, *Org. Lett.* **2013**, *15*, 4682.
- [63] X. J. Peng, P. P. Huang, L. L. Jiang, J. Y. Zhu, L. X. Liu, *Tetrahedron Lett.* **2016**, *57*, 5223.

- [64] B. Yao, C. L. Deng, Y. Liu, R. Y. Tang, X. G. Zhang, J. H. Li, *Chem. Commun.* **2015**, *51*, 4097.
- [65] J. P. Stambuli, C. D. Incarvito, M. Buhl, J. F. Hartwig, *J. Am. Chem. Soc.* **2004**, *126*, 1184.
- [66] K. H. Yih, G. H. Lee, *J. Chin. Chem. Soc.* **2008**, *55*, 109.
- [67] K. Nakatsu, K. Kinoshita, H. Kanda, K. Isobe, Y. Nakamura, S. Kawaguchi, *Chem. Lett.* **1980**, 913.
- [68] K. Isobe, Y. Nakamura, T. Miwa, S. Kawaguchi, *Bull. Chem. Soc. Jpn.* **1987**, *60*, 149.
- [69] C. Sicre, A. A. C. Braga, F. Maseras, M. M. Cid, *Tetrahedron* **2008**, *64*, 7437.
- [70] J. A. Pool, B. L. Scott, J. L. Kiplinger, *J. Am. Chem. Soc.* **2005**, *127*, 1338.
- [71] E. W. Zhou, W. S. Ren, G. H. Hou, G. F. Zi, D. C. Fang, M. D. Walter, *Organometallics* **2015**, *34*, 3637.
- [72] N. A. Siladke, J. LeDuc, J. W. Ziller, W. J. Evans, *Chem. Eur. J.* **2012**, *18*, 14820.
- [73] Y. L. Xu, S. W. Yang, L. J. Du, J. Li, *Eur. J. Org. Chem.* **2017**, 381.
- [74] F. Barrios-Landeros, B. P. Carrow, J. F. Hartwig, *J. Am. Chem. Soc.* **2008**, *130*, 5842.
- [75] S. E. Denmark, R. C. Smith, W. T. Chang, *Tetrahedron* **2011**, *67*, 4391.
- [76] F. Barrios-Landeros, B. P. Carrow, J. F. Hartwig, *J. Am. Chem. Soc.* **2009**, *131*, 8141.
- [77] P. Frederic, J. Patt, J. F. Hartwig, *Organometallics* **1995**, *14*, 3030.
- [78] A. H. Roy, J. F. Hartwig, *Organometallics* **2004**, *23*, 1533.
- [79] J. P. Flemming, M. C. Pilon, O. Y. Borbulevitch, M. Y. Antipin, V. V. Grushin, *Inorg. Chim. Acta* **1998**, *280*, 87.
- [80] Y. Tan, J. F. Hartwig, *J. Am. Chem. Soc.* **2011**, *133*, 3308.
- [81] B. P. Carrow, J. F. Hartwig, *J. Am. Chem. Soc.* **2010**, *132*, 79.
- [82] C. Amatore, A. Jutand, *Acc. Chem. Res.* **2000**, *33*, 314.
- [83] A. C. Albeniz, P. Espinet, B. Martin-Ruiz, D. Milstein, *J. Am. Chem. Soc.* **2001**, *123*, 11504.
- [84] F. Proutiere, F. Schoenebeck, *Angew. Chem., Int. Ed.* **2011**, *50*, 8192; M. Kolter, K. Boeck, K. Karaghiosoff, K. Koszinowski, *Angew. Chem., Int. Ed.* **2017**, *56*, 13244.
- [85] K. H. Yih, H. F. Wang, K. F. Huang, C. C. Kwan, G. H. Lee, *J. Chin. Chem. Soc.* **2009**, *56*, 1082.
- [86] B. Crociani, F. Dibianca, A. Fontana, R. Bertani, *J. Organomet. Chem.* **1992**, *425*, 155; L. Canovese, F. Visentin, P. Uguagliati, F. DiBianca, A. Fontana, B. Crociani, *J. Organomet. Chem.* **1996**, *525*, 43.
- [87] Q. L. Shen, J. F. Hartwig, *J. Am. Chem. Soc.* **2007**, *129*, 7734.
- [88] J. A. Pool, B. L. Scott, J. L. Kiplinger, *J. Alloys Compd.* **2006**, *418*, 178.
- [89] D. P. Krut'ko, R. S. Kirsanov, S. A. Belov, M. V. Borzov, A. V. Churakov, J. A. K. Howard, *Polyhedron* **2007**, *26*, 2864; R. F. Jordan, D. F. Taylor, *J. Am. Chem. Soc.* **1989**, *111*, 778; A. S. Guram, R. F. Jordan, *Organometallics* **1991**, *10*, 3470; B. Klei, J. H. Teuben, *J. Chem. Soc., Chem. Commun.* **1978**, 659.
- [90] K. C. Jantunen, B. L. Scott, J. C. Gordon, J. L. Kiplinger, *Organometallics* **2007**, *26*, 2777.
- [91] O. V. Ozerov, M. Pink, L. A. Watson, K. G. Caulton, *J. Am. Chem. Soc.* **2004**, *126*, 2105.
- [92] S. D. Gray, D. P. Smith, M. A. Bruck, D. E. Wigley, *J. Am. Chem. Soc.* **1992**, *114*, 5462; D. R. Neithamer, L. Parkanyi, J. F. Mitchell, P. T. Wolczanski, *J. Am. Chem. Soc.* **1988**, *110*, 4421.
- [93] M. W. Hooper, J. F. Hartwig, *Organometallics* **2003**, *22*, 3394.
- [94] A. Poulain, A. Neels, M. Albrecht, *Eur. J. Inorg. Chem.* **2009**, 1871.
- [95] B. Crociani, F. Dibianca, A. Giovenco, A. Scriveranti, *J. Organomet. Chem.* **1983**, *251*, 393.
- [96] E. Stander-Grobler, O. Schuster, G. Heydenrych, S. Cronje, E. Tosh, M. Albrecht, G. Frenking, H. G. Raubenheimer, *Organometallics* **2010**, *29*, 5821.
- [97] O. Schuster, L. R. Yang, H. G. Raubenheimer, M. Albrecht, *Chem. Rev.* **2009**, *109*, 3445.

- [98] J. S. Owen, J. A. Labinger, J. E. Bercaw, *J. Am. Chem. Soc.* **2004**, *126*, 8247; S. Wimmer, F. L. Wimmer, *J. Chem. Soc., Dalton Trans.* **1994**, 879.
- [99] J. C. Lewis, R. G. Bergman, J. A. Ellman, *J. Am. Chem. Soc.* **2007**, *129*, 5332.
- [100] E. Stander-Grobler, O. Schuster, C. E. Strasser, M. Albrecht, S. Cronje, H. G. Raubenheimer, *Polyhedron* **2011**, *30*, 2776; M. Albrecht, H. Stoeckli-Evans, *Chem. Commun.* **2005**, 4705.
- [101] O. Mongin, P. Rocca, L. Thomasditdumont, F. Trecourt, F. Marsais, A. Godard, G. Queguiner, *J. Chem. Soc., Perkin Trans. 1* **1995**, 2503.
- [102] E. M. Smith, E. E. Knaus, M. Saha, R. A. Abramovitch, *J. Org. Chem.* **1972**, *37*, 1690.
- [103] F. Trecourt, B. Gervais, O. Mongin, C. Le Gal, F. Mongin, G. Queguiner, *J. Org. Chem.* **1998**, *63*, 2892.
- [104] B. Koning, J. Buter, R. Hulst, R. Stroetinga, R. M. Kellogg, *Eur. J. Org. Chem.* **2000**, 2735.
- [105] F. Gosselin, S. J. Savage, N. Blaquiere, S. T. Staben, *Org. Lett.* **2012**, *14*, 862.
- [106] M. Mosrin, P. Knochel, *Org. Lett.* **2009**, *11*, 1837.
- [107] H. Andersson, M. Gustafsson, R. Olsson, F. Almqvist, *Tetrahedron Lett.* **2008**, *49*, 6901.
- [108] C. Najera, J. M. Sansano, M. Yus, *Tetrahedron* **2003**, *59*, 9255.
- [109] X. F. Duan, Z. Q. Ma, F. Zhang, Z. B. Zhang, *J. Org. Chem.* **2009**, *74*, 939.
- [110] M. Schnurch, M. Spina, A. F. Khan, M. D. Mihovilovic, P. Stanetty, *Chem. Soc. Rev.* **2007**, *36*, 1046.
- [111] L. M. Alcazar-Roman, J. F. Hartwig, *J. Am. Chem. Soc.* **2001**, *123*, 12905; S. Shekhar, J. F. Hartwig, *Organometallics* **2007**, *26*, 340.
- [112] A. Yahav-Levi, I. Goldberg, A. Vigalok, *J. Am. Chem. Soc.* **2006**, *128*, 8710; W. Oloo, P. Y. Zavalij, J. Zhang, E. Khaskin, A. N. Vedernikov, *J. Am. Chem. Soc.* **2010**, *132*, 14400.
- [113] A. H. Roy, J. F. Hartwig, *J. Am. Chem. Soc.* **2001**, *123*, 1232.
- [114] R. H. Crabtree, *The Organometallic Chemistry of the Transition Metals*. 5th ed., John Wiley & Sons, Inc., 2009.
- [115] R. J. Cross, *Chem. Soc. Rev.* **1985**, *14*, 197.
- [116] A. F. Littke, G. C. Fu, *Angew. Chem., Int. Ed.* **1998**, *37*, 3387; A. F. Littke, G. C. Fu, *J. Am. Chem. Soc.* **2001**, *123*, 6989.
- [117] S. E. Denmark, R. C. Smith, *J. Am. Chem. Soc.* **2010**, *132*, 1243.
- [118] A. A. Thomas, S. E. Denmark, *Science* **2016**, *352*, 329.
- [119] A. A. Thomas, H. Wang, A. F. Zahrt, S. E. Denmark, *J. Am. Chem. Soc.* **2017**, *139*, 3805.
- [120] K. Masui, H. Ikegami, A. Mori, *J. Am. Chem. Soc.* **2004**, *126*, 5074; M. Takahashi, K. Masui, H. Sekiguchi, N. Kobayashi, A. Mori, M. Funahashi, N. Tamaoki, *J. Am. Chem. Soc.* **2006**, *128*, 10930.
- [121] Z. J. Zheng, M. K. Elmekdem, C. Fischmeister, T. Roisnel, C. M. Thomas, J. F. Carpentier, J. L. Renaud, *New J. Chem.* **2008**, *32*, 2150.
- [122] A. Bowden, S. J. Coles, M. B. Pitak, A. W. G. Platt, *Inorg. Chem.* **2012**, *51*, 4379.
- [123] P. W. N. M. van Leeuwen, J. C. Chadwick, *Homogeneous Catalysts: Activity – Stability – Deactivation*. 1st ed., Wiley-VCH Verlag GmbH & Co. KGaA, 2011; C. Amatore, A. Jutand, A. Thuilliez, *Organometallics* **2001**, *20*, 3241.
- [124] N. C. Bruno, M. T. Tudge, S. L. Buchwald, *Chem. Sci.* **2013**, *4*, 916.
- [125] N. C. Bruno, N. Niljianskul, S. L. Buchwald, *J. Org. Chem.* **2014**, *79*, 4161.
- [126] M. Hartmann, C. G. Daniliuc, A. Studer, *Chem. Commun.* **2015**, *51*, 3121.
- [127] D. Selent, Boerner, A., Kadyrov, R., Borgmann, C., Hess, D., Wiese, K-D., Roettger, D., U.S. Patent 7,217,828 B2, 15 May, 2007.
- [128] B. A. Markies, A. J. Canty, W. Degraaf, J. Boersma, M. D. Janssen, M. P. Hogerheide, W. J. J. Smeets, A. L. Spek, G. Vankoten, *J. Organomet. Chem.* **1994**, *482*, 191.
- [129] T. M. Krygowski, H. Szatyłowicz, J. E. Zachara, *J. Org. Chem.* **2005**, *70*, 8859.
- [130] R. A. Widenhoefer, H. A. Zhong, S. L. Buchwald, *Organometallics* **1996**, *15*, 2745.

- [131] A. Montes, R. D. W. Kemmitt, J. Fawcett, D. R. Russeli, *Polyhedron* **1999**, *18*, 1141.
- [132] S. R. Zhang, Z. L. Zhang, H. W. Fu, X. Li, H. M. Zhan, Y. X. Cheng, *J. Organomet. Chem.* **2016**, *825*, 100.
- [133] L. Hintermann, L. Xiao, A. Labonne, *Angew. Chem., Int. Ed.* **2008**, *47*, 8246.
- [134] A. S. Y. Lee, P. L. Chen, Y. T. Chang, H. T. Tsai, *J. Chin. Chem. Soc.* **2012**, *59*, 452.
- [135] A. G. Sergeev, A. Spannenberg, M. Beller, *J. Am. Chem. Soc.* **2008**, *130*, 15549.
- [136] M. Aufiero, F. Proutiere, F. Schoenebeck, *Angew. Chem., Int. Ed.* **2012**, *51*, 7226.
- [137] B. P. Carrow, Ph.D. Thesis, University of Illinois at Urbana-Champaign, Illinois, 2011.
- [138] Y. Garcia, F. Schoenebeck, C. Y. Legault, C. A. Merlic, K. N. Houk, *J. Am. Chem. Soc.* **2009**, *131*, 6632.
- [139] O. Kühn, *Phosphorus-31 NMR Spectroscopy*. 1st ed., Springer-Verlag Berlin Heidelberg, 2008.
- [140] E. Alvarez, S. Conejero, M. Paneque, A. Petronilho, M. L. Poveda, O. Serrano, E. Carmona, *J. Am. Chem. Soc.* **2006**, *128*, 13060.
- [141] N. A. Piro, J. S. Owen, J. E. Bercaw, *Polyhedron* **2004**, *23*, 2797.
- [142] C. A. Tolman, *Chem. Rev.* **1977**, *77*, 313.
- [143] D. E. Stephens, J. Lakey-Beitia, J. E. Burch, H. D. Arman, O. V. Larionov, *Chem. Commun.* **2016**, *52*, 9945; H. Wang, Y. Pei, J. Bai, J. L. Zhang, Y. J. Wu, X. L. Cui, *Rsc. Adv.* **2014**, *4*, 26244.
- [144] I. P. Beletskaya, A. V. Cheprakov, *Chem. Rev.* **2000**, *100*, 3009.
- [145] S. H. Cho, S. J. Hwang, S. Chang, *J. Am. Chem. Soc.* **2008**, *130*, 9254.
- [146] S. K. Madan, W. E. Bull, *J. Inorg. Nucl. Chem.* **1964**, *26*, 2211.
- [147] K. R. Chaudhari, A. P. Wadawale, V. K. Jain, *J. Organomet. Chem.* **2012**, *698*, 15.
- [148] H. Rieger, *Magn. Reson. Chem.* **2004**, *42*, 814.
- [149] N. Miyaoura, K. Yamada, H. Suginome, A. Suzuki, *J. Am. Chem. Soc.* **1985**, *107*, 972.
- [150] V. R. Lando, A. L. Monteiro, *Org. Lett.* **2003**, *5*, 2891.
- [151] B. P. Carrow, J. F. Hartwig, *J. Am. Chem. Soc.* **2011**, *133*, 2116.
- [152] A. Suzuki, *J. Organomet. Chem.* **1999**, *576*, 147.
- [153] D. G. Hall, *Boronic Acids: Preparation and Applications in Organic Synthesis, Medicine and Materials*. 2nd ed., Wiley-VCH Verlag GmbH & Co. KGaA, 2011.
- [154] J. Magano, J. R. Dunetz, *Chem. Rev.* **2011**, *111*, 2177.
- [155] N. Miyaoura, K. Yamada, A. Suzuki, *Tetrahedron Lett.* **1979**, *20*, 3437; N. Miyaoura, A. Suzuki, *J. Chem. Soc., Chem. Commun.* **1979**, 866.
- [156] C. Amatore, A. Jutand, M. A. Mbarki, *Organometallics* **1992**, *11*, 3009; C. Amatore, A. Jutand, A. Suarez, *J. Am. Chem. Soc.* **1993**, *115*, 9531.
- [157] D. Gala, A. Stamford, J. Jenkins, M. Kugelman, *Org. Process Res. Dev.* **1997**, *1*, 163.
- [158] R. B. Bedford, U. G. Singh, R. I. Walton, R. T. Williams, S. A. Davis, *Chem. Mater.* **2005**, *17*, 701.
- [159] A. L. Casado, P. Espinet, *Organometallics* **1998**, *17*, 954.
- [160] P. Espinet, A. M. Echavarran, *Angew. Chem., Int. Ed.* **2004**, *43*, 4704.
- [161] G. B. Smith, G. C. Dezeny, D. L. Hughes, A. O. King, T. R. Verhoeven, *J. Org. Chem.* **1994**, *59*, 8151.
- [162] Z. Lu, G. C. Fu, *Angew. Chem., Int. Ed.* **2010**, *49*, 6676.
- [163] M. MorenoManas, M. Perez, R. Pleixats, *J. Org. Chem.* **1996**, *61*, 2346.
- [164] M. A. Aramendia, F. Lafont, M. Moreno-Manas, R. Pleixats, A. Roglans, *J. Org. Chem.* **1999**, *64*, 3592; M. S. Wong, X. L. Zhang, *Tetrahedron Lett.* **2001**, *42*, 4087.
- [165] C. Adamo, C. Amatore, I. Ciofini, A. Jutand, H. Lakmini, *J. Am. Chem. Soc.* **2006**, *128*, 6829.
- [166] W. D. Miller, A. H. Fray, J. T. Quatroche, C. D. Sturgill, *Org. Process Res. Dev.* **2007**, *11*, 359.

- [167] H. G. Kuivila, Mangravi, J. F. Reuwer, *J. Am. Chem. Soc.* **1964**, *86*, 2666.
- [168] A. Thakur, K. N. Zhang, J. Louie, *Chem. Commun.* **2012**, *48*, 203.
- [169] S. Darses, G. Michaud, J. P. Genet, *Eur. J. Org. Chem.* **1999**, 1875; G. A. Molander, N. Ellis, *Acc. Chem. Res.* **2007**, *40*, 275; M. Butters, J. N. Harvey, J. Jover, A. J. J. Lennox, G. C. Lloyd-Jones, P. M. Murray, *Angew. Chem., Int. Ed.* **2010**, *49*, 5156.
- [170] R. A. Batey, T. D. Quach, *Tetrahedron Lett.* **2001**, *42*, 9099.
- [171] A. J. J. Lennox, G. C. Lloyd-Jones, *J. Am. Chem. Soc.* **2012**, *134*, 7431.
- [172] T. D. Quach, R. A. Batey, A. J. Lough, *Acta Crystallogr. E* **2001**, *57*, O688.
- [173] S. W. Wright, D. L. Hageman, L. D. McClure, *J. Org. Chem.* **1994**, *59*, 6095; C. Amatore, A. Jutand, G. Le Duc, *Angew. Chem., Int. Ed.* **2012**, *51*, 1379.
- [174] A. O. Aliprantis, J. W. Canary, *J. Am. Chem. Soc.* **1994**, *116*, 6985.
- [175] C. M. Nunes, A. L. Monteiro, *J. Brazil. Chem. Soc.* **2007**, *18*, 1443.
- [176] K. Siegmann, P. S. Pregosin, L. M. Venanzi, *Organometallics* **1989**, *8*, 2659; I. Pantcheva, K. Osakada, *Organometallics* **2006**, *25*, 1735.
- [177] T. Moriya, N. Miyaura, A. Suzuki, *Synlett* **1994**, 149.
- [178] D. Zim, S. M. Nobre, A. L. Monteiro, *J. Mol. Catal. A: Chem.* **2008**, *287*, 16.
- [179] H. E. Bryndza, W. Tam, *Chem. Rev.* **1988**, *88*, 1163.
- [180] T. Yoshida, T. Okano, S. Otsuka, *J. Chem. Soc., Dalton Trans.* **1976**, 993.
- [181] D. D. Wick, K. I. Goldberg, *J. Am. Chem. Soc.* **1999**, *121*, 11900; S. Thyagarajan, C. D. Incarvito, A. L. Rheingold, K. H. Theopold, *Chem. Commun.* **2001**, 2198; S. S. Stahl, *Angew. Chem., Int. Ed.* **2004**, *43*, 3400.
- [182] M. C. Denney, N. A. Smythe, K. L. Cetto, R. A. Kemp, K. I. Goldberg, *J. Am. Chem. Soc.* **2006**, *128*, 2508.
- [183] Y. Hayashi, S. Wada, M. Yamashita, K. Nozaki, *Organometallics* **2012**, *31*, 1073.
- [184] G. Lopez, G. Garcia, J. Ruiz, G. Sanchez, J. Garcia, C. Vicente, *J. Chem. Soc., Chem. Commun.* **1989**, 1045.
- [185] J. Campora, P. Palma, D. del Rio, E. Alvarez, *Organometallics* **2004**, *23*, 1652; R. Johansson, L. Ohrstrom, O. F. Wendt, *Cryst. Growth Des.* **2007**, *7*, 1974.
- [186] V. V. Grushin, H. Alper, *Organometallics* **1993**, *12*, 1890.
- [187] V. V. Grushin, H. Alper, *Organometallics* **1996**, *15*, 5242.
- [188] V. V. Grushin, H. Alper, *J. Am. Chem. Soc.* **1995**, *117*, 4305.
- [189] A. Schumacher, M. G. Schrems, A. Pfaltz, *Chem. Eur. J.* **2011**, *17*, 13502.
- [190] A. N. Cammidge, V. H. M. Goddard, H. Gopee, N. L. Harrison, D. L. Hughes, C. J. Schubert, B. M. Sutton, G. L. Watts, A. J. Whitehead, *Org. Lett.* **2006**, *8*, 4071.
- [191] M. Sato, N. Miyaura, A. Suzuki, *Chem. Lett.* **1989**, 1405.
- [192] A. A. C. Braga, N. H. Morgon, G. Ujaque, A. Lledos, F. Maseras, *J. Organomet. Chem.* **2006**, *691*, 4459.
- [193] A. A. C. Braga, N. H. Morgon, G. Ujaque, F. Maseras, *J. Am. Chem. Soc.* **2005**, *127*, 9298.
- [194] C. Amatore, A. Jutand, G. Le Duc, *Chem. Eur. J.* **2011**, *17*, 2492.
- [195] K. Matos, J. A. Soderquist, *J. Org. Chem.* **1998**, *63*, 461.
- [196] L. P. Hammett, *Chem. Rev.* **1935**, *17*, 125.
- [197] C. Hansch, A. Leo, R. W. Taft, *Chem. Rev.* **1991**, *91*, 165.
- [198] M. an der Heiden, H. Plenio, *Chem. Commun.* **2007**, 972; M. R. an der Heiden, H. Plenio, S. Immel, E. Burello, G. Rothenberg, H. C. J. Hoefsloot, *Chem. Eur. J.* **2008**, *14*, 2857; C. He, J. Ke, H. Xu, A. W. Lei, *Angew. Chem., Int. Ed.* **2013**, *52*, 1527.
- [199] J. Jover, N. Fey, M. Purdie, G. C. Lloyd-Jones, J. N. Harvey, *J. Mol. Catal. A: Chem.* **2010**, *324*, 39.
- [200] A. Bouziane, M. Helou, B. Carboni, F. Carreaux, B. Demerseman, C. Bruneau, J. L. Renaud, *Chem. Eur. J.* **2008**, *14*, 5630.

- [201] M. Vaultier, S. Gmouh, U.S. Patent 2006/0128996 A1, 15 June, 2006.
- [202] J. D. Neukom, N. S. Perch, J. P. Wolfe, *Organometallics* **2011**, *30*, 1269.
- [203] M. Ludwig, S. Stromberg, M. Svensson, B. Akermark, *Organometallics* **1999**, *18*, 970.
- [204] M. S. Driver, J. F. Hartwig, *J. Am. Chem. Soc.* **1997**, *119*, 8232.
- [205] Z. B. Dong, G. Manolikakes, L. Shi, P. Knochel, H. Mayr, *Chem. Eur. J.* **2010**, *16*, 248.
- [206] V. Diemer, H. Chaumeil, A. Defoin, A. Fort, A. Boeglin, C. Carre, *Eur. J. Org. Chem.* **2008**, 1767.
- [207] D. Limnios, C. G. Kokotos, *J. Org. Chem.* **2014**, *79*, 4270.
- [208] Y. Oguro, N. Miyamoto, T. Takagi, K. Okada, Y. Awazu, H. Miki, A. Hori, K. Kamiyama, S. Imamura, *Biorg. Med. Chem.* **2010**, *18*, 7150.
- [209] G. Roelfes, V. V. K. Chen, R. Y. N. Ho, J. U. Rohde, C. Zondervan, R. M. la Crois, E. P. Schudde, M. Lutz, A. L. Spek, R. Hage, B. L. Feringa, E. Munck, L. Que, *Inorg. Chem.* **2003**, *42*, 2639.
- [210] V. M. Mukkala, J. J. Kankare, *Helv. Chim. Acta* **1992**, *75*, 1578.
- [211] S. Ladouceur, K. N. Swanick, S. Gallagher-Duval, Z. F. Ding, E. Zysman-Colman, *Eur. J. Inorg. Chem.* **2013**, *2013*, 5329.
- [212] J. Izquierdo, A. Landa, I. Bastida, R. Lopez, M. Oiarbide, C. Palomo, *J. Am. Chem. Soc.* **2016**, *138*, 3282.
- [213] D. P. Martin, P. G. Blachly, J. A. McCammon, S. M. Cohen, *J. Med. Chem.* **2014**, *57*, 7126.
- [214] M. Tiecco, M. Tingoli, L. Testaferri, D. Chianelli, E. Wenkert, *Tetrahedron* **1986**, *42*, 1475.
- [215] M. Bendle, K. Huynh, M. F. Haddow, I. Manners, *Inorg. Chem.* **2011**, *50*, 10292.
- [216] R. M. Denton, J. An, B. Adeniran, A. J. Blake, W. Lewis, A. M. Poulton, *J. Org. Chem.* **2011**, *76*, 6749.
- [217] J. Wysocki, C. Schlepfforst, F. Glorius, *Synlett* **2015**, *26*, 1557.
- [218] S. Kulyk, W. G. Dougherty, W. S. Kassel, M. J. Zdilla, S. M. Sieburth, *Org. Lett.* **2011**, *13*, 2180.
- [219] C. R. Conard, M. A. Dolliver, *Org. Synth.* **1943**, *2*, 167.
- [220] C. B. Ziegler, R. F. Heck, *J. Org. Chem.* **1978**, *43*, 2941.
- [221] W. W. DuMont, *Z. Anorg. Allg. Chem.* **1979**, *468*, 85.
- [222] S. S. Zalesskiy, V. P. Ananikov, *Organometallics* **2012**, *31*, 2302.
- [223] A. F. Littke, G. C. Fu, *Org. Synth.* **2005**, *81*, 63.
- [224] I. Kalvet, K. J. Bonney, F. Schoenebeck, *J. Org. Chem.* **2014**, *79*, 12041.
- [225] H. Geissler, P. Gross, B. Guckes, U.S. Patent 6,084,114, 4 July, 2000.
- [226] M. L. Li, X. Li, H. H. Chang, W. C. Gao, W. L. Wei, *Org. Biomol. Chem.* **2016**, *14*, 2421.
- [227] C. Uncuta, M. T. Caproiu, V. Campeanu, A. Petride, M. G. Danila, M. Plaveti, A. T. Balaban, *Tetrahedron* **1998**, *54*, 9747.
- [228] T. Yurino, Y. Ueda, Y. Shimizu, S. Tanaka, H. Nishiyama, H. Tsurugi, K. Sato, K. Mashima, *Angew. Chem., Int. Ed.* **2015**, *54*, 14437.
- [229] K. S. Chan, A. K. S. Tse, *Synth. Commun.* **1993**, *23*, 1929.
- [230] J. K. Laha, K. P. Jethava, S. Patel, K. V. Patel, *J. Org. Chem.* **2017**, *82*, 76.
- [231] I. Gillaizeau-Gauthier, F. Odobel, M. Alebbi, R. Argazzi, E. Costa, C. A. Bignozzi, P. Qu, G. J. Meyer, *Inorg. Chem.* **2001**, *40*, 6073.
- [232] G. Bozoklu, C. Marchal, C. Gateau, J. Pecaut, D. Imbert, M. Mazzanti, *Chem. Eur. J.* **2010**, *16*, 6159.
- [233] J. P. Stambuli, Z. Weng, C. D. Incarvito, J. F. Hartwig, *Angew. Chem., Int. Ed.* **2007**, *46*, 7674.
- [234] D. M. Pearson, N. R. Conley, R. M. Waymouth, *Adv. Synth. Catal.* **2011**, *353*, 3007.

Curriculum vitae

The curriculum vitae is not included in the online version due to data protection.

Acknowledgements

First of all, I would like to thank my advisor Prof. Dr. Christoph Tzschucke for giving me the opportunity to join his group and for his continuous support during my doctoral studies. The last five years have definitely been interesting and challenging and I have learnt a lot. Besides my supervisor, I would like to thank Prof. Dr. Christian Müller for being the second reviewer of this dissertation.

Thanks to the NMR and MS service for performing the analytics. A special thanks to Bettina Zeisig who helped me with all the temperature NMR measurements. I am very grateful to Manuela Weber and Massimo Rigo for the measurement and data analysis of the crystal structures reported in this dissertation. Also, my sincerest thanks to Frau Leo and Frau Nitschke from the MV who have always been extremely friendly and helpful.

Thanks to all my former colleagues and friends in the AG Tzschucke who has made working in the lab very pleasant. A special thanks to Sina for her guidance and translation of my abstract, Anja Svenssolowski for all the candy, Stefan for always being in the lab later than me and Fanni for being my favorite Hungarian princess. I'm very grateful to my students Meryem, Keerthana, Chunyu and Jan for contributing to the work presented in this dissertation. Thanks to the Mensa for always providing the most unthinkable combination of food for lunch and thanks to the nicest Mensa employee for always giving me a discount on coffee.

I am very grateful to my parents for their continuous support and for taking me to a lot of sunny places. Also, thanks to my sister who has made all those sunny places even better. Big up to my old laptop that survived my bachelor, master and half of my doctoral work (r.i.p.). These last years would have been horrible if Massimo had not introduced me to Jever. Thanks to Sofia for being reasonable and funny at the same time and Parasto for being incredibly supportive. My sincerest thanks to Emma Williams who has been my best friend for the last 15 years and will be for the next 150. Thanks to the remaining Italians, Germans, Scandinavians and the other Hungarian for making these last years spectacular. Last, thanks to Stefan Mattsson who is my absolute favorite person in the whole world (after Williams :-).